UNIVERSITAT POLITÈCNICA DE VALÈNCIA

DOCTORADO EN INGENIERÍA Y PRODUCCIÓN INDUSTRIAL

TESIS DOCTORAL

"Desarrollo y optimización de formulaciones industriales basadas en poli(3-hidroxibutirato) (PHB) mediante sistemas de mezclado y plastificación"

Autor:

Daniel García García

Dirigida por:

Dr. Rafael Antonio Balart Gimeno

Dr. Juan López Martínez

Fecha de presentación:

Junio de 2018

UNIVERSITAT POLITÈCNICA DE VALÈNCIA

DOCTORADO EN INGENIERÍA Y PRODUCCIÓN INDUSTRIAL

TESIS DOCTORAL

"Desarrollo y optimización de formulaciones industriales basadas en poli(3-hidroxibutirato) (PHB) mediante sistemas de mezclado y plastificación"

Daniel García García

El Dr. Rafael Antonio Balart Gimeno y el Dr. Juan López Martínez, Catedráticos de Universidad del Departamento de Ingeniería Mecánica y de Materiales de la Universitat Politècnica de València en calidad de directores de la Tesis Doctoral (modalidad Doctorado Internacional) presentada por D. Daniel García García, con el título "**Desarrollo y optimización de formulaciones industriales basadas en poli(3-hidroxibutirato) (PHB) mediante sistemas de mezclado y plastificación**".

CERTIFICAN

Que la presente memoria, "**Desarrollo y optimización de formulaciones industriales basadas en poli(3-hidroxibutirato) (PHB) mediante sistemas de mezclado y plastificación**", para aspirar al grado de Doctor por la Universitat Politècnica de València reúne las condiciones adecuadas para constituir la tesis doctoral de D. Daniel García García (modalidad Doctorado Internacional).

Asimismo, certifican que la citada tesis doctoral se ha realizado en el Instituto de Tecnología de Materiales de la Universitat Politècnica de València y en el Departamento de Fibra y Tecnología de Polímeros del Royal Institute of Technology – KTH (Suecia).

Y para que conste a los efectos oportunos, firman la presente en Alcoy a 18 de abril de 2018.

Fdo. Dr. Rafael Antonio Balart Gimeno

Fdo. Dr. Juan López Martínez

A mis padres

“El hombre nunca sabe de lo que es capaz hasta que lo intenta”

Charles Dickens

AGRADECIMIENTOS

En primer lugar, quiero dar las gracias, de forma muy especial, a mis directores de tesis, los catedráticos Rafael Balart Gimeno y Juan López Martínez. Gracias por haberme dado la oportunidad de trabajar con vosotros durante todos estos años. He crecido científicamente de vuestra mano y gracias a vuestra forma de ser habéis conseguido que me apasione la investigación. Muchas gracias por enseñarme tantas cosas, por todos vuestros consejos y por confiar en mí. Muchas gracias "Rafa" por toda la ayuda prestada en la realización de la presente tesis, por guiarme en todo este camino, por estar ahí siempre que he necesitado de tu ayuda y por tu apoyo y positividad cuando las cosas no salían bien. Muchas gracias "Juan" por tus consejos, por tu motivación cuando me has visto flaquear y por todo tu apoyo durante estos años. Sois y seréis un referente para mí. ¡MUCHAS GRACIAS!

Al ministerio de Educación Cultura y Deporte por el apoyo financiero a través de la ayuda otorgada (FPU13/06011).

Al Ministerio de Economía y Competitividad (MINECO) por el soporte financiero de este trabajo (MAT2014-59242-C2-1-R/MAT2017-84909-C2-2-R).

A la Conselleria d'Educació, Cultura i Esport de la Generalitat Valenciana por el soporte financiero de este trabajo (GV/2014/008).

Al Instituto de Tecnología de Materiales (ITM) de la Universitat Politècnica de València, donde se llevó a cabo el presente trabajo.

A las profesoras Monica Ek y Emma Strömberg del Royal Institute of Technology (KTH) de Estocolmo por permitirme realizar las estancias en vuestras instalaciones. ¡Tack så mycket!

A los profesores Lourdes Sánchez Nácher, David García Sanoguera, Octavio Fenollar, Emilio Rayón, Teodomiro Boronat y Néstor Montañés quiero agradecerles todos los consejos y la ayuda prestada durante estos años ¡Muchas gracias a tod@s!

A los técnicos de laboratorio Matías, Javi y Rafa por su ayuda con todos aquellos problemas técnicos que han ido surgiendo durante el trabajo.

Al grupo de investigación del profesor Alfonso Jiménez de la Universidad de Alicante por permitirme el uso de sus instalaciones. En especial a Nuria Burgos por su ayuda y amabilidad.

A la Profesora Rosana Moriana del Royal Institute of Technology (KTH) de Estocolmo por su ayuda en la realización de esta tesis, pero, principalmente, por cuidarme cada vez que he realizado una estancia en Suecia. Gracias por tratarme como a uno más de tu familia y hacerme sentir en casa a más de 2000 km. ¡Muchas gracias!

A mi familia del laboratorio: Mado, Pelayo, Alfredo, Vicent y Marina. Sois los mejores compañeros que uno puede tener. Gracias por ser como sois, por toda vuestra ayuda y por estar siempre que os he necesitado. Sin vosotros todos estos años no hubieran sido lo mismo. Lo mejor que me llevo de esta experiencia es haberos conocido y los buenos momentos que hemos pasado dentro y fuera de la universidad. ¡Muchísimas gracias amig@s!

A todos los compañeros que durante este tiempo han formado parte del laboratorio en especial a Miguel, Luís, David, Jennifer, Ivet y Alondra. Ha sido un gran placer conoceros y compartir con vosotros grandes momentos que nunca olvidaré.

A todos mis amig@s, que han sabido hacerme desconectar cuando lo he necesitado. En especial quiero agradecer a Alberto y a María por su apoyo durante todo este tiempo. ¡Gracias a tod@s!

A toda mi familia, en especial a mi "iaia" Carmen, Antonio, Rosa, Manolo, Miriam y Jose por ser como sois y por estar siempre ahí.

A mi hermano y mi cuñada, Andrés y Ana, gracias por todo vuestro apoyo, por preocuparos por mí y por darme lo mejor de este mundo, mis sobrinos, Xavi y Carlos, que han sido mi dosis de alegría diaria.

Por último, quiero dar las gracias a mis padres, Andrés y Ascensión, por apoyarme y animarme en todo lo que he querido hacer, sin vuestra ayuda nada de esto hubiera sido posible. Gracias por ser los mejores profesores que he tenido y por haberme guiado en todo este camino. ¡MUCHÍSIMAS GRACIAS!

RESUMEN

"Desarrollo y optimización de formulaciones industriales basadas en poli(3-hidroxibutirato) (PHB) mediante sistemas de mezclado y plastificación"

El principal objetivo de la presente tesis ha sido el desarrollo y caracterización de diferentes formulaciones a partir de poli(3-hidroxibutirato) (PHB) con el fin de mejorar sus propiedades.

El PHB es un polímero sintetizado mediante fermentación bacteriana por diferentes tipos de bacterias, que se caracteriza por ser biodegradable, biocompatible y por presentar unas propiedades mecánicas que lo hacen un polímero interesante como sustituto de los polímeros de uso común obtenidos a partir del petróleo. Sin embargo, a día de hoy, el PHB presenta una serie de inconvenientes que hacen que no sea competitivo con los polímeros de uso común y, por tanto, dificultan su introducción a nivel industrial. Entre dichos inconvenientes se encuentra su elevado coste, su elevada fragilidad debida a su alta cristalinidad y su estrecha ventana de procesado, ya que su degradación térmica se inicia a temperaturas cercanas a la de su fusión. Por ello, en la presente tesis se han llevado a cabo diferentes tecnologías de modificación del PHB, todas ellas encaminadas a reducir sus inconvenientes con el objetivo de mejorar su funcionalidad y ampliar su uso a nivel industrial. Una de dichas estrategias de mejora ha consistido en la plastificación del polímero biodegradable mediante el empleo de plastificantes derivados de aceites vegetales, como son el aceite de linaza epoxidado (ELO), el aceite de soja epoxidado (ESBO), el aceite de linaza maleinizado (MLO) y los ésteres de ácidos grasos epoxidados (EFAE). La segunda de las estrategias empleadas ha sido el desarrollo de formulaciones mediante la mezcla física o "*blending*" del PHB con otro polímero biodegradable como es la poli(ε-caprolactona) (PCL), así como la mejora de la miscibilidad entre ambos polímeros mediante el empleo de un agente compatibilizante, el peróxido de dicumilo (DCP). La última de las estrategias seguidas ha consistido en la incorporación de pequeñas cantidades de nanocargas en la mezcla de PHB/PCL sin compatibilizar y compatibilizada con DCP. Concretamente, se ha estudiado el efecto de la incorporación de nanotubos de haloisita sin tratar y tratados superficialmente con silano (3-glicidoxipropiltrimetoxisilano) y con ácido cafeico en la mezcla de PHB/PCL compatibilizada con DCP. Además, también se ha analizado el efecto de diferentes cantidades de nanocristales de celulosa obtenidos y optimizados a

partir de un residuo forestal, como son las piñas de los pinos, en la mezcla de PHB/PCL sin compatibilizar.

La incorporación de pequeñas cantidades (5-10 phr) de derivados de aceites vegetales en el PHB dio lugar a un aumento de la ductilidad y una reducción de la fragilidad del PHB como consecuencia de una menor cristalinidad. Además, los plastificantes proporcionaron una mejora en la estabilidad térmica del polímero, disminuyendo su temperatura de fusión y aumentando considerablemente su temperatura de inicio de degradación, reduciendo así el riesgo de degradación térmica y aumentando su ventana de procesado. Los mejores resultados fueron obtenidos tras la incorporación de 5 phr de EFAE. Por tanto, el empleo de plastificantes de origen natural representa una alternativa sostenible, económica y efectiva para la mejora de las propiedades mecánicas y térmicas del PHB.

La mezcla física de PHB con un 25 % en peso de PCL redujo la rigidez del PHB puro aumentando su flexibilidad y su ductilidad, obteniendo un material con una mayor capacidad de absorción de energía a impacto y un mayor alargamiento a la rotura. También se observó un importante aumento de la temperatura de inicio de degradación tras la incorporación de la PCL, aumentando el rango de temperaturas de procesado. Sin embargo, la falta de miscibilidad existente entre ambos polímeros restringe su posibilidad de mejora. La incorporación de un 1 phr de DCP a la mezcla de PHB/PCL mejoró significativamente su miscibilidad, dando lugar a un notable aumento de las propiedades dúctiles, como el alargamiento a la rotura y la absorción de energía a impacto, sin afectar significativamente a las propiedades resistentes ni a las propiedades térmicas. Por tanto, la mezcla física de PHB con PCL y el empleo de un compatibilizante, permite obtener formulaciones con mejores propiedades dúctiles y térmicas que el PHB puro de una forma sencilla, económica y eficaz.

La incorporación de un 3% en peso de nanocristales de celulosa, previamente sintetizados y optimizados, en la mezcla de PHB/PCL mejoró la miscibilidad entre ambos polímeros, dando lugar a un aumento de la transparencia y de la humectabilidad de los films, además, aceleró considerablemente el proceso de degradación en condiciones de compost de la mezcla. Por otro lado, el aumento de la hidrofobicidad y la mejor dispersión de los nanotubos de haloisita en la mezcla de PHB/PCL compatibilizada con DCP tras el tratamiento con ácido cafeico dio lugar a un aumento de la compatibilidad entre el refuerzo y la matriz, que se reflejó en un aumento de las propiedades dúctiles y resistentes de la mezcla con respecto a la mezcla reforzada con HNTs sin tratar y tratados con silano. Además, los HNTs redujeron la temperatura de fusión de la mezcla y aumentaron

ligeramente su temperatura de inicio de degradación, permitiendo ampliar su ventana de procesado. Por tanto, la incorporación de nanocargas es otra alternativa eficaz y sostenible que permite moldear las propiedades de la mezcla de PHB/PCL con el fin de adaptarlas a diferentes aplicaciones.

De forma general, la presente tesis muestra diferentes alternativas para la mejora de las propiedades del PHB. Estas alternativas permiten obtener formulaciones más económicas y con propiedades mejoradas, aumentando así su competitividad a nivel industrial. Además, dichas modificaciones amplían el rango de aplicaciones del polímero biodegradable en sectores como el del envase y el embalaje o el sector médico.

RESUM

"Desenvolupament i optimització de formulacions industrials derivades de poli(3-hidroxibutirat) (PHB) mitjançant sistemes de mescla i plastificació"

El principal objectiu de la present tesi ha sigut el desenvolupament i caracterització de diferents formulacions a partir de poli(3-hidroxibutirat) (PHB) amb la finalitat de millorar les seues propietats.

El PHB és un polímer sintetitzat mitjançant fermentació bacteriana per diferents bacteris, que es caracteritza per ser biodegradable, biocompatible i per presentar unes propietats mecàniques que el fan molt atractiu com a substitut dels anomenats "plàstics d´ús comú" obtinguts del petroli. Malgrat això, a dia de hui, el PHB presenta una sèrie d'inconvenients que fan que no siga competitiu amb aquests "plàstics d´ús comú" i, per tant, dificulten la seua introducció a nivell industrial. Entre aquests inconvenients destaca el seu elevat cost, la seua elevada fragilitat deguda a una elevada cristal·linitat i una estreta finestra de processat, ja que la seua degradació tèrmica comença a temperatures molt properes a la de fusió. És per això, que en aquesta tesi s'han dut a terme diferents tecnologies de modificació de PHB, totes elles encaminades a reduir els seus inconvenients amb l'objectiu de millorar la seua funcionalitat i ampliar el seu ús a nivell industrial. Una de les esmentades estratègies de millora ha consistit en la plastificació del polímer biodegradable mitjançant la utilització de plastificants derivats d'olis vegetals, com són l'oli de lli epoxidat (ELO), l'oli de soja epoxidat (ESBO), l'oli de lli maleinitzat (MLO) i els ésters d'àcids grassos epoxidats (EFAE). La segona de les estratègies empleades ha sigut el desenvolupament de formulacions mitjançant la mescla física o "*blending*" del PHB amb altre polímer biodegradable com és la poli(ε-caprolactona) (PCL), així com la millora de la miscibilitat entre ambdós polímers mitjançant la utilització d'un agent compatibilitzant, el peròxid de dicumil (DCP). L´última de les estratègies seguides ha consistit en la incorporació de petites quantitats de nanocàrregues en la mescla de PHB/PCL sense compatibilitzar i compatibilitzada amb DCP. En particular, s'ha estudiat l'efecte de la incorporació de nanotubs d'hal·loysita sense tractar i tractats superficialment amb un silà (3-glicidoxipropiltrimetoxisilà) i amb àcid cafeic a la mescla de PHB/PCL compatibilitzada amb DCP. A més a més, també s'ha considerat l'efecte de diferents quantitats de nanocristalls de cel·lulosa obtinguts i optimitzats a partir d'un residu forestal, com ara les pinyes dels pins, en la mescla de PHB/PCL sense compatibilitzar.

La incorporació de petites quantitats (5-10 phr) de derivats d'olis vegetals al PHB va donar lloc a un augment de la ductilitat i una reducció de la fragilitat del PHB com a conseqüència d'una menor cristal·linitat. A més a més, els plastificants van proporcionar una millora en l'estabilitat tèrmica del polímer amb una disminució de la temperatura de fusió i un augment considerable de la temperatura d'inici de la degradació, reduint, així, el risc de degradació tèrmica i augmentant la seua finestra de processat. Els millors resultats van ser obtinguts després de la incorporació de 5 phr d'EFAE. Per tant, la utilització de plastificants d'origen natural representa una alternativa sostenible, econòmica i efectiva per a la millora de les propietats mecàniques i tèrmiques del PHB.

La mescla física de PHB amb un 25% en pes de PCL va reduir la rigidesa del PHB pur augmentant la seua flexibilitat i la seua ductilitat, obtenint, d'aquesta manera, un material amb una major capacitat d'absorció d'energia a impacte i un major allargament al trencament. També es va observar un important augment de la temperatura d'inici de degradació després de la incorporació de PCL, fet que dona lloc a un augment del rang de temperatures de processat. Malgrat això, la falta de miscibilitat existent entre ambdós polímers restringeix les possibilitats de millora. La incorporació d'un 1 phr de DCP a la mescla de PHB/PCL va millorar significativament la miscibilitat, fet que va donar lloc a un notable augment de les propietats dúctils, com ara l'allargament al trencament i l'absorció d'energia a impacte, sense afectar significativament a les propietats resistents ni a les propietats tèrmiques. Per tant, la mescla física de PHB amb PCL i la utilització d'un agent compatibilitzant, permet obtenir formulacions amb millors propietats dúctils i tèrmiques que el PHB pur d'una forma senzilla, econòmica i eficaç.

La incorporació d'un 3% en pes de nanocristalls de cel·lulosa, prèviament sintetitzats i optimitzats, en la mescla de PHB/PCL va millorar la miscibilitat entre ambdós polímers, donant lloc a un augment de la transparència i de la humectabilitat dels films i, a més a més, va accelerar considerablement el procés de degradació en condicions de compost de la mescla. Per altre costat, l'augment de la hidrofobicitat i la millor dispersió dels nanotubs d'hal·loysita en la mescla de PHB/PCL compatibilitzada amb DCP després del tractament amb àcid cafeic va donar lloc a un augment de la compatibilitat entre el reforç i la matriu, que es va reflectir en un augment de les propietats dúctils i resistents de la mescla en relació a la mescla reforçada amb HNTs sense tractar i tractats amb silà. A més a més, els HNTs van reduir la temperatura de fusió de la mescla i van augmentar lleugerament la temperatura d'inici de degradació, permetent ampliar la finestra de processat. Per tant, la incorporació de nanocàrregues és una altra alternativa eficaç i sostenible que permet adaptar les propietats de la mescla PHB/PCL amb el fi d'adaptar-les a diferents aplicacions.

De forma general, la present tesi mostra diferents alternatives per a la millora de les propietats del PHB. Aquestes alternatives permeten obtenir formulacions més econòmiques i amb propietats millorades, augmentant així la seua competitivitat a nivell industrial. A més a més, les esmentades modificacions amplien el rang d'aplicacions del polímer biodegradable en sectors com ara l'envàs i embalatge o bé, el sector mèdic.

ABSTRACT

"Development and optimization of industrial formulations based on poly(3-hydroxybutyrate) (PHB) by blending and plasticization"

The main aim of the present doctoral thesis is the development and characterization of several formulations from poly(3-hydroxybutyrate) (PHB) with the main purpose of improving its properties.

PHB is synthesized from bacterial fermentation by several bacteria. It is characterized by being biodegradable, biocompatible and it also shows interesting mechanical properties that make it an interesting alternative to commodity plastics derived from petroleum. Nevertheless, up today, PHB still shows some drawbacks that are responsible for its low competitiveness versus commodity plastics thus restricting its industrial applications. Among these drawbacks, it is worthy to note its high cost, its high brittleness due to high crystallinity and its extremely narrow processing window. In fact, thermal degradation starts at a temperature near the end of the melt process. For these reasons, several technologies to modify PHB have been addressed in this doctoral thesis, with the main aim of overcoming the above-mentioned drawbacks and, hence, improve its functionality and potential industrial applications. The first strategy has consisted on plasticization of the biodegradable polymer by using several vegetable oil-derived plasticizers such as epoxidized linseed oil (ELO), epoxidized soybean oil (ESBO), maleinized linseed oil (MLO) and epoxidized fatty acid esters (EFAE). The second strategy has been the development of industrial formulations by physical blending PHB with other biodegradable polymer, *i.e.*, poly(ε-caprolactone) (PCL), as well as the improvement of the miscibility between these two polymers by reactive extrusion with dicumyl peroxide (DCP) which produces compatibilization. The last strategy has consisted on the addition of small amounts of nanofillers into the PHB/PCL blend both non-compatibilized and compatibilized with DCP. In particular, the effect of the addition of halloysite nanotubes (HNTs), without treatment and with a silane (3-glycidoxypropyltrimethoxysilane) and caffeic acid surface treatment, to the PHB/PCL blend compatibilized with DCP has been studied. In addition, the effect of different cellulose nanocrystals (CNCs) obtained and optimized from forestry wastes, *i.e.*, pine cones, on the PHB/PCL blend has been studied.

The addition of small amounts (5-10 phr) of vegetable oil-derived plasticizers led to a remarkable increase in ductility and a noticeable reduction of the PHB intrinsic brittleness

due to a decrease in the overall crystallinity. Moreover, these plasticizers provided an improvement on the thermal stability by decreasing the melt peak temperature and increasing the thermal degradation onset temperature. This has a positive effect on thermal stability and broadens the processing window. The best results were obtained after addition of 5 phr EFAE. Therefore, the use of vegetable oil-derived plasticizers from natural resources is a sustainable, cost-effective and technically viable alternative to improve mechanical and thermal performance of PHB.

The physical blend with 25 weight% PCL led to a clear decrease in brittleness and, subsequently, both flexibility and ductility were improved. The obtained material showed an increased ability to absorb energy and increased elongation at break values. In addition, a remarkable increase in the thermal degradation onset temperature was observed, with the subsequent improvement on processing window. Despite this, the lack of miscibility between these two polymers restricted higher improvements. Addition of 1 phr DCP to the PHB/PCL blend during a reactive extrusion process, led to a remarkable increase in ductile properties such as elongation at break and the impact-absorbed energy (Charpy test), without compromising other mechanical resistant or thermal properties. Therefore, the physical blend between PHB and PCL, together with the use of a compatibilizing agent, allows obtaining industrial formulations with improved ductile and thermal properties with regard to neat PHB in a simple, cost-effective and technically viable way.

On the other hand, addition of 3 weight% cellulose nanocrystals (CNCs), previously synthesized and optimized, to the PHB/PCL blend improved their miscibility thus leading to an increase in transparency and the wetting behavior of films. Moreover, these CNCs accelerated the disintegration rate in controlled compost soil. On the other hand, caffeic acid treatment contributed to an increase in hydrophobicity and a better particle dispersion of the halloysite nanotubes into the PHB/PCL blend compatibilized with DCP. Caffeic acid treated-HNTs were responsible for an increase in both ductile and resistant properties and gave better results than untreated and silanized HNTs. Furthermore, HNTs provided a decrease in the melt peak and promoted a slight increase in the onset degradation temperature thus broadening the processing window. So, the addition of nanofillers is another efficient and sustainable way to tailor the properties of PHB/PCL blends for industrial applications.

As a general conclusion, this doctoral thesis shows different approaches to improve the overall properties of PHB. These approaches allow to obtain cost-effective formulations with improved properties, thus increasing their competitiveness at industrial scale. These formulations broadens the potential use of PHB in sectors such as packing or medical.

TABLA DE CONTENIDOS

LISTADO DE ARTÍCULOS

La presente tesis consta de un compendio de los siguientes artículos y manuscritos:

I. Plasticization effects of epoxidized vegetable oils on mechanical properties of poly(3-hydroxybutyrate).

II. Improvement of mechanical ductile properties of poly(3-hydroxybutyrate) by using vegetable oil derivatives.

III. Processing and characterization of binary poly(hydroxybutyrate) (PHB) and poly(caprolactone) (PCL) blends with improved impact properties.

IV. Improvement of the compatibility between poly(3-hydroxybutyrate) and poly(ε-caprolactone) by reactive extrusion with dicumyl peroxide.

V. Optimizing the yield and physico-chemical properties of pine cone cellulose nanocrystals by different hydrolysis time.

VI. Reinforcing capability of cellulose nanocrystals obtained from pine cones in a biodegradable poly(3-hydroxybutyrate)/poly(ε-caprolactone) (PHB/PCL) thermoplastic blend.

VII. Characterization of selectively etched halloysite nanotubes by acid treatment.

VIII. Improvement of mechanical and thermal properties of poly(3-hydroxybutyrate) (PHB) blends with surface-modified halloysite nanotubes (HNTs).

Los artículos realizados relacionados con los estudios previos llevados a cabo en la presente tesis han sido:

I. Green composites based on polypropylene matrix and hydrophobized spend coffee ground (SCG) powder.

II. Development and characterization of green composites from bio-based polyethylene and peanut shell.

III. Manufacturing and characterization of composite fiberboards with Posidonia oceanica wastes with an environmentally friendly binder from epoxy resin.

ECUACIONES

$X_c = \left[\frac{\Delta H_m}{\Delta H_0 \cdot w}\right] \times 100$	**X_c =** grado de cristalinidad **ΔH_m =** entalpía de fusión **ΔH_0 =** entalpía de fusión teórica para el polímero 100% cristalino **w =** fracción en peso del polímero
$WU = \frac{(m_f - m_i)}{m_i} \times 100$	**WU =** absorción de agua **m_f =** masa final tras la inmersión **m_i =** masa inicial antes de la inmersión
$\sigma_f = \frac{3FL}{2bh^2}$	**σ_f =** tensión máxima a flexión **F =** fuerza máxima **L =** distancia entre puntos de apoyo **b =** ancho de la muestra **h =** espesor de la muestra
$E_f = \frac{\sigma_{f2} - \sigma_{f1}}{\varepsilon_{f2} - \varepsilon_{f1}}$	**E_f =** módulo a flexión **σ_{fi} =** tensión a flexión en un punto **ε_{fi} =** deformación unitaria en un punto
$s_i = \frac{\varepsilon_{fi} L^2}{6h}$	**S_i =** flecha **ε_{fi} =** deformación unitaria **L =** distancia entre puntos de apoyo **h =** espesor de la muestra
$[\eta] = K \times M_V^a$	**[η] =** viscosidad intrínseca **K/a=** constantes dependientes del sistema polímero-disolvente **M_v=** peso molecular

$\delta = \frac{\rho \sum G}{M}$	**δ =** parámetro de solubilidad **ρ =** densidad **G =** constante de atracción molar **M =** peso molecular promedio por unidad repetitiva
$GF = \frac{m_1}{m_0} \times 100$	**GF =** fracción de gel $\mathbf{m_0}$ **=** masa seca inicial $\mathbf{m_1}$ **=** masa seca final
$F_{\text{tip}} = F - F_{\text{adh}} = \frac{4}{3} E_{\text{r}} \sqrt{R(d - d_0)^3}$	$\mathbf{F_{tip}}$ **=** fuerza en la punta del AFM $\mathbf{F - F_{adh}}$ **=** fuerza de adhesión $\mathbf{E_r}$ **=** módulo elástico reducido **R =** radio de la punta del AFM $\mathbf{d - d_0}$ **=** deformación de la muestra
$CrI = \frac{I_{002} - I_{\text{am}}}{I_{002}} \times 100$	**CrI =** índice de cristalinidad $\mathbf{I_{002}}$ **=** intensidad máxima en el plano 002 $\mathbf{I_{am}}$ **=** intensidad mínima de la parte amorfa

ABREVIATURAS Y TÉRMINOS

AA	ácido acrílico
ABS	acrilonitrilo butadieno estireno
AESO	aceite de soja epoxidado acrilado
AEVO	aceite vegetal epoxidado acrilado
AFM	microscopía de fuerza atómica
APTES	3-aminopropiltrietoxisilano
APTMS	3-aminopropiltrimetoxisilano
ATBC	acetil tributil citrato
ATR	reflectancia total atenuada
BET	método Brunauer-Emmett-Teller
Bio-PA	poliamida de origen renovable
Bio-PC	policarbonato de origen renovable
Bio-PE	polietileno de origen renovable
Bio-PET	polietilén tereftalato de origen renovable
Bio-PP	polipropileno de origen renovable
Bio-PU	poliuretano de origen renovable
Bio-PVC	policloruro de vinilo de origen renovable
BJH	método Barret-Joyner-Halenda
CA	acetato de celulosa
CAB	acetato-butirato de celulosa
CAP	acetato-propionato de celulosa
CEN	comité europeo de normalización
CNCs	nanocristales de celulosa
CNTs	nanotubos de carbono
CoA	coenzima A
CrI	índice de cristalinidad
CSR	residuos celulósicos sólidos
D/d	diámetro
DBP	dibutil ftalato
DCP	peróxido de dicumilo
DMT	modelo Derjaguin-Muller-Toporov
DMTA	análisis térmico dinámico-mecánico
DOA	dioctil adipato
DOP	dioctil ftalato

DOS	dioctil sebacato
DPPH	técnica de captación de radicales libres con difenilpicrilhidrazilo
DSC	calorimetría diferencial de barrido
DTG	derivada de la masa frente a la temperatura
e	espesor
E	módulo elástico o de Young
ECO	aceite de ricino epoxidado
EDS	espectrometría por dispersión de energías de rayos X
EFAE	ésteres de ácidos grasos epoxidados
ELO	aceite de linaza epoxidado
EPO	aceite de palma epoxidado
EPSO	mezcla de aceite de palma epoxidado y aceite de soja
ESO/ESBO	aceite de soja epoxidado
EVO	aceite vegetal epoxidado
FESEM	microscopía electrónica de barrido de emisión de campo
FRAP	poder antioxidante de reducción férrica
FS	resistencia a flexión
FTIR	espectroscopía infrarroja por transformada de Fourier
G'	módulo de almacenamiento
G''	módulo de pérdidas
GLYMO	3-glicidoxipropiltrimetoxisilano
H	dureza
HA	ácido hidroxialcanoico
HDPE	polietileno de alta densidad
HDT	temperatura de flexión bajo carga
HNTs	nanotubos de haloisita
HPAEC-PAD	cromatografía de intercambio aniónico a alto pH con detección amperométrica pulsada
IR	infrarrojos
IUPAC	unión internacional de química pura y aplicada
L	longitud
LCNF	nanofibras lignocelulósicas
LDH	hidróxidos de doble capa
LDPE	polietileno de baja densidad
LIBS	espectroscopia de plasma inducido por láser
LOI	pérdida por ignición

MA	anhídrido maleico
mcl-PHAs	polihidroxialcanoatos con longitud de cadena media
MCSO	aceite de semilla de algodón maleinizado
MLO	aceite de linaza maleinizado
MOFs	compuestos organometálicos
MSO	aceite de soja maleinizado
MUF	resina de melamina-urea-formaldehído
MVO	aceite vegetal maleinizado
M_w	peso molecular
MWCNTs	nanotubos de carbono multicapa
NFRPs	plásticos reforzados con fibras naturales
P(3HB-*co*-3HHx)	poli(3-hidroxibutirato-*co*-3-hidroxihexanoato)
P(3HB-*co*-4HB)	poli(3-hidroxibutirato-*co*-4-hidroxibutirato)
P(3HHx)	poli(3-hidroxihexanoato)
P(3HHx-*co*-3HO)	poli(3-hidroxihexanoato-*co*-3-hidroxioctanoato)
P(3HO)	poli(3-hidroxioctanoato)
P(3HV)	poli(3-hidroxivalerato)
P(4HB)	poli(4-hidroxibutirato)
PA 11	poliamida 11
PA 4	poliamida 4
PA 6.10	poliamida 6.10
PA	poliamida
PBA	polibutilén adipato
PBAT	poli(butilén adipato-*co*-tereftalato)
PBAT-*g*-MA	poli(butilén adipato-*co*-tereftalato) funcionalizado con anhídrido maleico
PBS	polibutilén succinato
PBSA	poli(butilén succinato-*co*-adipato)
PBST	poli(butilén succinato-*co*-tereftalato)
PBT	polibutilén tereftalato
PC	policarbonato
PCL	poli(ε-caprolactona)
PCs	piñas de pino
PDLA	poli(D-ácido láctico)
PDLLA	poli(D,L-ácido láctico)
PE	polietileno

PEEK	polieteretercetona
PEG	polietilenglicol
PE-*g*-MA	polietileno funcionalizado con anhídrido maleico
PEK	polietercetona
PES	polietilén succinato
PET	polietilén tereftalato
PF	resina de fenol-formaldehído
PGA	poli(ácido glicólico)
PHAs	polihidroxialcanoatos
PHB/P(3HB)	poli(3-hidroxibutirato)
PHBV	poli(3-hidroxibutirato-*co*-3-hidroxivalerato)
phr	partes por cien de resina
PI	poliimida
PLA	poli(ácido láctico)
PLLA	poli(L-ácido láctico)
PNS	cáscara de cacahuete
PO	posidonia oceánica
POM	polioximetileno
PP	polipropileno
PPD	poli(p-dioxanona)
PP-*g*-MA	polipropileno funcionalizado con anhídrido maleico
PS	poliestireno
PU	poliuretano
PVA	polialcohol vinílico
PVC	policloruro de vinilo
QNM	mapeo cuantitativo de propiedades nanomecánicas
RH	humedad relativa
ROP	polimerización por apertura de anillo
RSD	desviación estándar relativa
SCG	posos de café
scl-PHAs	polihidroxialcanoatos con longitud de cadena corta
SEBS-*g*-MA	estireno-etileno-butileno-estireno funcionalizado con anhídrido maleico
SEM	microscopía electrónica de barrido
SWCNTs	nanotubos de carbono monocapa
T_0	temperatura de inicio de degradación

TAG	triacetil glicerol
Tan δ	factor de pérdidas
TBC	tributil citrato
TEC	trietil citrato
TEGB	trietilenglicol-di-(2-etilhexanoato)
TEM	microscopía electrónica de transmisión
T_g	temperatura de transición vítrea
TGA	análisis termogravimétrico
T_m	temperatura de fusión
T_{max}	temperatura de degradación máxima
TPA	ácido tereftálico
TPS	almidón termoplástico
TS	resistencia a tracción
UF	resina de urea formaldehído
UV	ultravioleta
UV-Vis	ultravioleta-visible
VO	aceite vegetal
VST	temperatura de reblandecimiento Vicat
WPCs	materiales compuestos de madera y plástico
wt%	porcentaje en peso
X_c	grado de cristalinidad
XRD	difracción de rayos X
XRF	fluorescencia de rayos X
1D	nanomateriales con una dimensión en la escala nano
2D	nanomateriales con dos dimensiones en la escala nano
3D	nanomateriales con tres dimensiones en la escala nano
3HB	3-hidroxibutirato
3HHx	3-hidroxihexanoato
3HV	3-hidroxivalerato
4HB	4-hidroxibutirato
ΔH_m	entalpía de fusión
γ	máxima deformación en ensayo DMTA
δ	parámetro de solubilidad
ε_b	alargamiento a la rotura
υ	coeficiente de Poisson
θ	ángulo de contacto

I. INTRODUCCIÓN

I.1. BIOPOLÍMEROS EN INGENIERÍA

Los plásticos obtenidos a partir del petróleo son unos de los materiales más presentes en nuestra sociedad. Propiedades como su ligereza, su bajo coste de obtención, su durabilidad, su facilidad de procesado, su capacidad de ser moldeado en multitud de formas y sus propiedades físicas y mecánicas han hecho que los plásticos se utilicen en la gran mayoría de sectores, como por ejemplo el sector de la agricultura, de la automoción, de la construcción o el sector eléctrico y electrónico, aunque es el sector del envase y el embalaje el que concentra el mayor consumo de este tipo de material. Durante las últimas décadas ha habido un aumento en la producción de polímeros de origen petroquímico. Según la asociación de fabricantes de plásticos (PlasticsEurope), en 2016 se estimó una producción mundial de 335 millones de toneladas, produciéndose un aumento de 13 millones de toneladas con respecto a la producción mundial de 2015; además se prevé una tendencia al alza en la producción de plásticos del 2,5% para el año 2017 y del 1,5% para el año 2018 [1].

Sin embargo, el consumo masivo de plásticos lleva asociadas una serie de consecuencias negativas para el medio ambiente. Por un lado, para la producción de estos materiales son necesarios recursos fósiles limitados, y el aumento de la producción acelera su agotamiento. Esto conlleva a un continuo aumento del precio del petróleo y, por tanto, a un encarecimiento de los plásticos. Además, la producción de plásticos a partir del petróleo genera una serie de problemas ambientales, entre ellos la emisión a la atmosfera de grandes cantidades de gases nocivos para el medio ambiente como el CO_2. Sin embargo, el mayor problema se genera tras el final del ciclo de vida de los productos fabricados con este tipo de material, ya que la gran mayoría de plásticos sintéticos no son biodegradables, y una vez usados acaban depositados, en el mejor de los casos, en vertederos legales, generando graves problemas medioambientales, además de un considerable impacto visual.

Con el objetivo de reducir la cantidad de residuos plásticos destinados a los vertederos, existen diferentes alternativas para su gestión, entre las que se encuentra el reciclado. Esta alternativa es una de las más respetuosas con el medio ambiente. Sin embargo, existen una serie de limitaciones tecnológicas y económicas que dificultan el proceso, como es la presencia de cargas y aditivos en los polímeros, la gran variedad de grados de un mismo polímero, el elevado coste y la dificultad de la separación de los diferentes tipos de polímeros o la pérdida de propiedades mecánicas del material tras varios procesos de reciclado [2]. Otra de las principales alternativas al depósito de los residuos plásticos en el vertedero es la incineración para la recuperación de energía. Esto es posible gracias al elevado poder calorífico de los polímeros; sin embargo, este proceso

puede generar una serie de productos tóxicos perjudiciales para el medio ambiente y el ser humano. Según la asociación de fabricantes de plásticos (PlasticsEurope), de los 27,1 millones de toneladas de residuos plásticos que se recogieron en Europa a través de los cauces oficiales en el año 2016, un 41,6% fue incinerado para la recuperación de energía, un 31,1% fue reciclado y un 27,3% fue depositado en vertederos, lo cual sigue indicando que una cantidad muy elevada de residuos plásticos acaba su vida en vertederos sin posibilidad de tratamiento [1].

Todos los problemas medioambientales generados por los plásticos obtenidos a partir de recursos fósiles, así como el aumento de la concienciación medioambiental por parte de la sociedad ha dado lugar a un incremento en la investigación, el desarrollo y la producción de materiales poliméricos más respetuosos con el medio ambiente. Esta nueva generación de materiales más sostenibles y con un menor impacto medioambiental se conocen comúnmente como "bioplásticos o biopolímeros". Según la Asociación Europea de Bioplásticos (European Bioplastics), los bioplásticos son aquellos polímeros de origen bio o "biobasados", que son biodegradables o que presentan ambas características [3].

Según el Comité Europeo de Normalización (CEN), un producto "biobasado" o de origen bio es aquel que se deriva total o parcialmente de la biomasa, como son las plantas, los árboles o lo animales [4]. Por tanto, el término "biobasado" hace referencia al origen del polímero y no al final de su ciclo de vida; es por esto que un polímero obtenido a partir de fuentes renovables no tiene que ser necesariamente biodegradable, ya que la propiedad de biodegradación no depende de la fuente de origen del material, sino que está vinculada a su estructura química. Por esta razón existen materiales obtenidos a partir de fuentes no renovables como el petróleo que son totalmente biodegradables. Según la norma europea EN 13432:2001 [5], para que un polímero sea biodegradable tiene que ser capaz de descomponerse mediante la acción de microorganismos naturales tales como bacterias, hongos o algas, dando lugar a sustancias tales como dióxido de carbono, agua, sales minerales y nueva biomasa. Desde el punto de vista medioambiental e industrial es interesante que un polímero además de ser biodegradable sea compostable, y para que así sea, éste debe cumplir una serie de condiciones. La principal es que el polímero debe alcanzar un nivel de degradación superior al 90% en menos de 6 meses sin dejar residuos visibles, distinguibles o tóxicos en el compost final.

Los biopolímeros se pueden clasificar según su procedencia (origen renovable o no renovable) y su capacidad de biodegradación o no. Atendiendo a dicha clasificación, existen tres grandes grupos de biopolímeros. Un grupo que engloba aquellos polímeros obtenidos a partir de fuentes renovables pero que no son biodegradables; otro grupo que recoge

aquellos polímeros que provienen de recursos no renovables, como el petróleo, pero que son biodegradables y, por último, un tercer grupo que abarca a todos aquellos polímeros que además de proceder de fuentes renovables son biodegradables. Como se observa en la Figura I.1, hay un cuarto grupo en el que se engloban todos aquellos polímeros que provienen de fuentes no renovables y que no son biodegradables; por tanto, no se consideran biopolímeros. En este grupo se encuentran los plásticos de uso común o "*commodities*", como es el caso del polipropileno (PP), el polietileno (PE), el poliestireno (PS) o el policloruro de vinilo (PVC). Dicho grupo también abarca a los plásticos técnicos como es el caso de las poliamidas (PA) o el policarbonato (PC) y los plásticos de altas prestaciones como la polietercetona (PEK) [6]. Este tipo de plásticos son los más empleados en la actualidad y los que generan un mayor impacto medioambiental. Por tanto, el reto actual de la industria es ir sustituyendo progresivamente los polímeros pertenecientes a este grupo por biopolímeros más respetuosos con el medio ambiente.

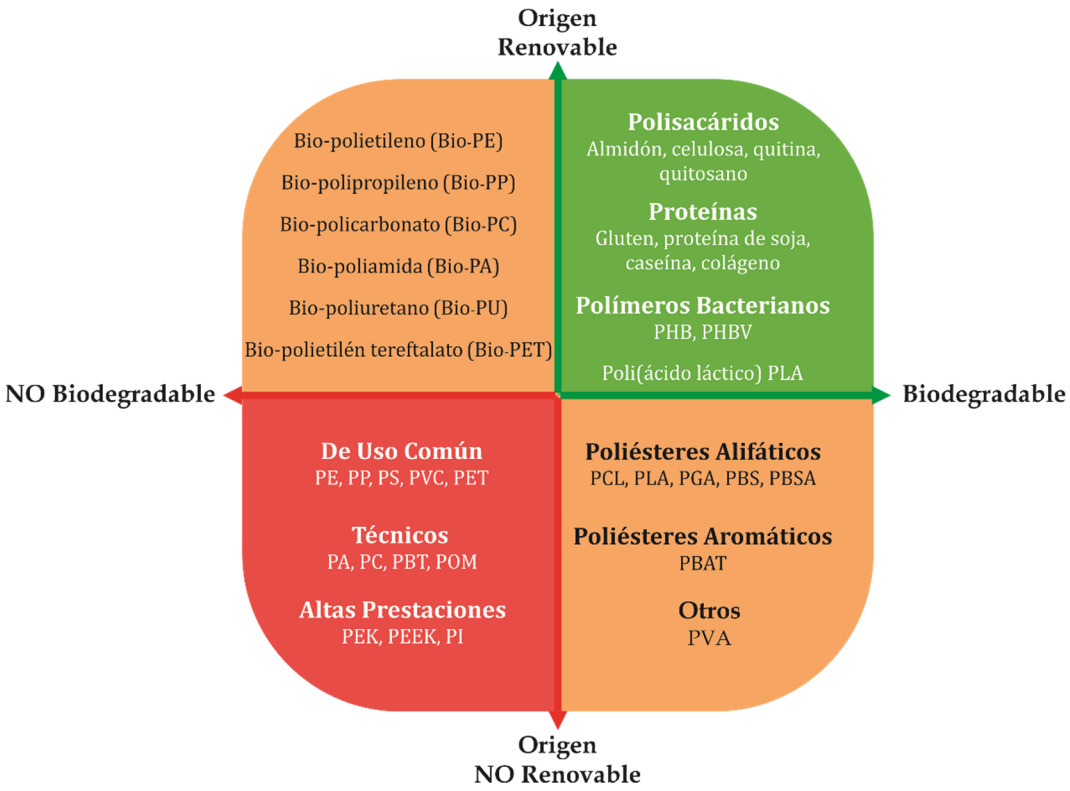

Figura I.1. Clasificación de polímeros según su origen (renovable o no renovable) y su capacidad de biodegradación.

De los tres grupos de biopolímeros descritos anteriormente, aquellos cuya procedencia es de origen renovable y son biodegradables son los que presentan un mayor

interés, ya que se tratan de los polímeros más respetuosos con el medio ambiente. Este tipo de biopolímeros se puede clasificar dependiendo de su origen en tres grandes grupos, como se observa en la Figura I.2 [7]. Estos tres grupos engloban a aquellos polímeros obtenidos a partir de la biomasa, como es el caso de algunos polisacáridos (almidón, celulosa, quitina o quitosano) o proteínas (gluten, caseína, proteína de soja o colágeno), a los polímeros sintetizados a partir de monómeros obtenidos de fuentes renovables, entre los que destaca el poli(ácido láctico) (PLA) y, por último, a aquellos polímeros sintetizados por microorganismos, compuesto principalmente por los polihidroxialcanoatos (PHAs).

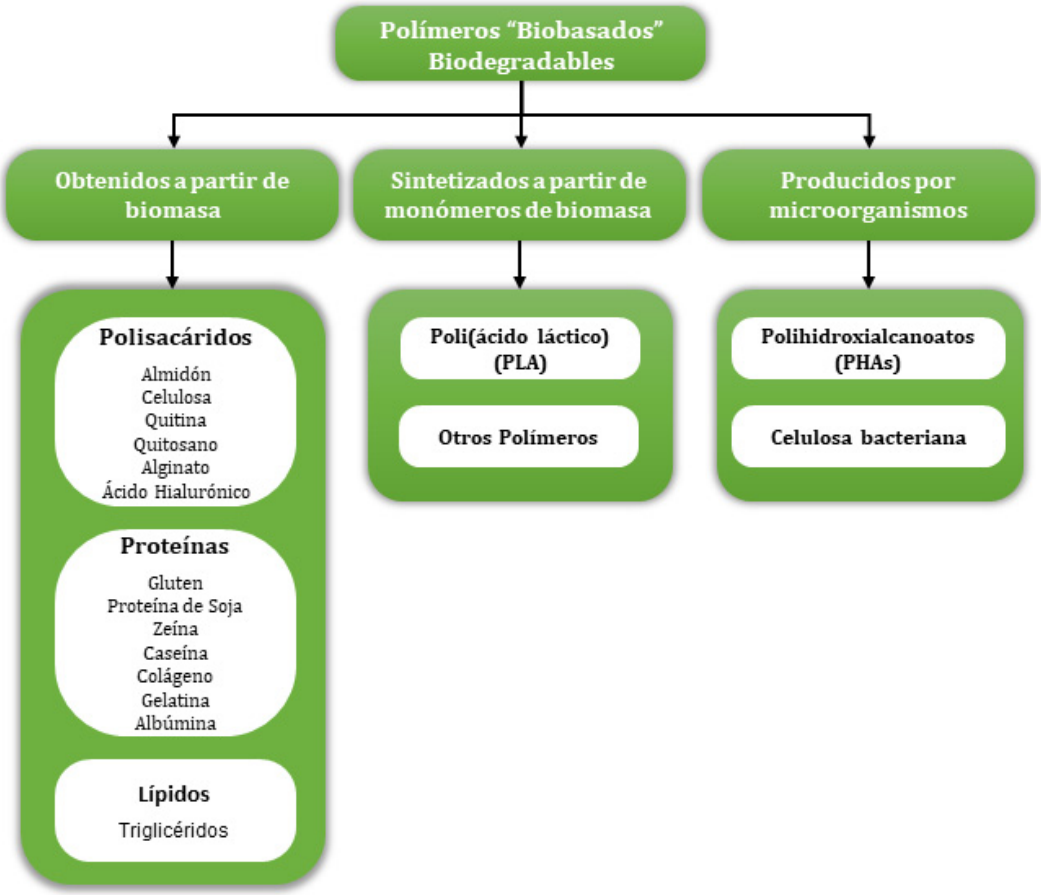

Figura I.2. Clasificación de los biopolímeros de origen renovable y biodegradables según su proceso de síntesis.

El bajo impacto medioambiental de los biopolímeros, junto con la reducción de los costes de obtención, debido al aumento en la investigación y desarrollo de técnicas de síntesis más sencillas, efectivas y baratas, ha dado lugar a un crecimiento considerable de la producción de este tipo de polímeros en los últimos años. Según el último estudio de mercado realizado por European Bioplastics [8], la producción global de biopolímeros en el

año 2017 fue de 2,05 millones de toneladas, y se espera que para el año 2022 dicha capacidad de producción incremente hasta los 2,44 millones de toneladas, como se puede observar en la Figura I.3.

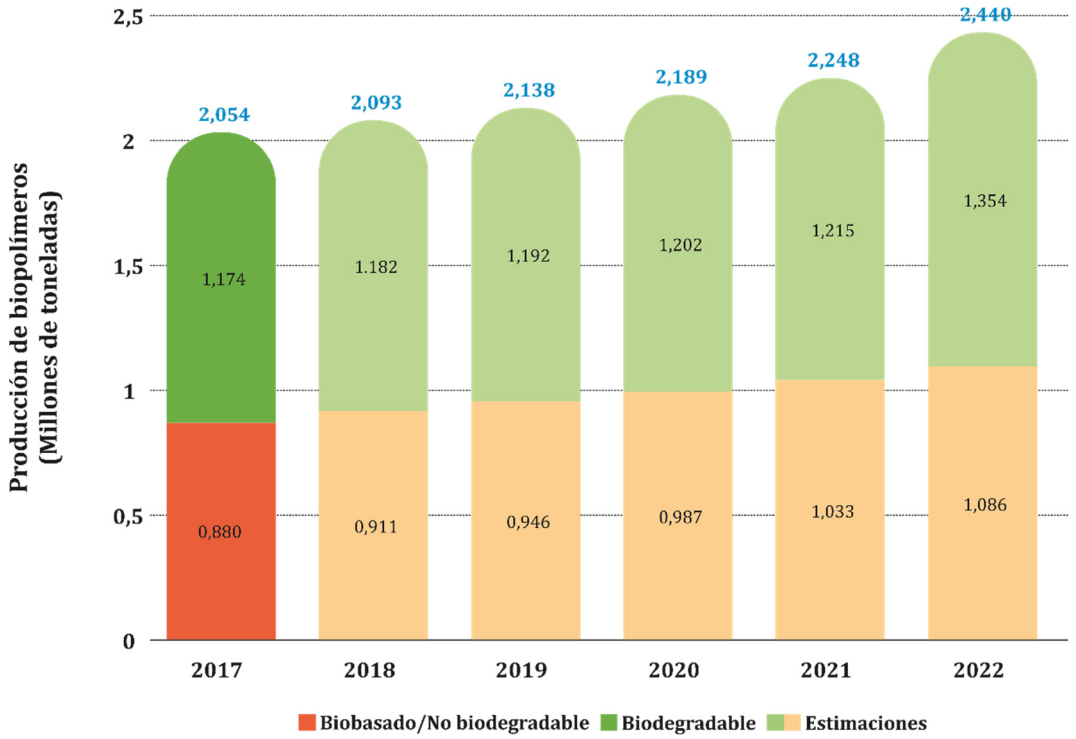

Figura I.3. Proyección de la capacidad de producción de biopolímeros a nivel mundial entre 2017-2022 [8].

Los biopolímeros como el PLA y los PHAs son los que han experimentado un mayor crecimiento dentro del grupo de polímeros de origen renovable y biodegradables. Los PHAs han estado bajo investigación y desarrollo durante un tiempo y ahora comienzan a introducirse en el mercado, con una producción en 2017 cercana a las 50.000 toneladas y se estima que dicha producción se triplique en los próximos cinco años. Por otro lado, el PLA es uno de los biopolímeros más consolidados a nivel comercial y con un creciente aumento de su producción. Se estima que para 2022 la producción de PLA incremente un 50% en comparación con la de 2017, que fue cercana a las 212.000 toneladas.

I.2. TIPOS DE BIOPOLÍMEROS

Como se ha visto anteriormente, los biopolímeros se clasifican en tres grandes grupos dependiendo de su origen y de su capacidad de biodegradación. En el presente apartado se comentan las propiedades más destacadas de los principales biopolímeros pertenecientes a cada uno de los grupos.

I.2.1. Polímeros de origen renovable no biodegradables

Dentro de este grupo se encuentran aquellos polímeros con estructuras idénticas a la de los polímeros de uso común, pero a diferencia de estos, se obtienen parcial o totalmente a partir de fuentes renovables. Este tipo de polímeros se caracteriza por presentar propiedades mecánicas y térmicas similares o idénticas a la de sus grados petroquímicos, sin embargo, su impacto medioambiental es mucho menor [3]. Algunos ejemplos incluidos en este grupo de biopolímeros son el polietileno (Bio-PE), el polietilén tereftalato (Bio-PET), las poliamidas (Bio-PA), el policloruro de vinilo (Bio-PVC) o el poliuretano (Bio-PU) obtenidos total o parcialmente a partir de fuentes renovables. En la Figura I.4 se muestran las estructuras químicas de algunos de los biopolímeros pertenecientes a este grupo.

Dentro de este grupo de biopolímeros, el Bio-polietileno (Bio-PE) es uno de los más empleados en la actualidad a nivel industrial. En este caso, el Bio-PE se produce a partir del bioetanol obtenido mediante fermentación microbiana de recursos naturales como la caña de azúcar, la remolacha azucarera o el almidón de maíz. En el proceso de producción, el etanol se destila con el objetivo de eliminar el agua y obtener una mezcla azeotrópica de etanol hidratado, que posteriormente se deshidrata a altas temperaturas sobre un catalizador sólido para producir el etileno que se polimeriza para obtener Bio-PE [7]. El Bio-PE obtenido a partir de fuentes renovables presenta las mismas propiedades químicas, físicas y mecánicas que el polietileno de origen petroquímico. Es por ello, que este biopolímero puede sustituir al PE petroquímico en todas aquellas aplicaciones en las que se emplea a día de hoy [7]. Además, el proceso de producción de Bio-PE reduce considerablemente las emisiones de CO_2 a la atmosfera con respecto a la producción del PE de origen petroquímico. Se estima que la producción de una tonelada de Bio-PE captura y elimina de la atmosfera 2,5 toneladas de dióxido de carbono, mientras que el proceso de producción tradicional del PE genera unas emisiones cercanas a las 3,5 toneladas [9]. En la actualidad, la compañía brasileña Braskem es la principal productora de Bio-PE a nivel

mundial. Dicha compañía obtiene el polímero a partir del bioetanol derivado de la caña de azúcar [7].

Otro de los polímeros de uso común que también puede obtenerse parcialmente a partir de recursos renovables es el polietilén tereftalato (PET). El PET es uno de los materiales más utilizados hoy en día, y se obtiene principalmente a partir de la poliesterificación del ácido tereftálico (TPA) y un dialcohol (etilenglicol). En el caso del polietilén tereftalato de origen bio (Bio-PET), el etilenglicol utilizado se obtiene a partir de recursos naturales, más concretamente, a partir de bioetanol obtenido de cultivos agrícolas. Para producir bioetilenglicol, el etileno obtenido mediante la deshidratación del etanol se oxida a óxido de etileno y se hidroliza a etilenglicol, obteniéndose así el componente "bio" del PET [10]. Como ocurre con este tipo de materiales, el Bio-PET presenta propiedades idénticas a las del PET tradicional. Esto ha dado lugar a que grandes compañías de refrescos hayan decidido sustituir el PET tradicional por Bio-PET en sus botellas. Actualmente el Bio-PET comercializado es parcialmente obtenido a partir de fuentes renovables, sin embargo, existen investigaciones para obtener TPA a partir de recursos renovables, por ejemplo a partir del xileno producido mediante la despolimerización de la lignina, con el objetivo de poder obtener Bio-PET totalmente "bio" [11].

Otros polímeros petroquímicos como el policloruro de vinilo (PVC), las poliamidas (PA) o los poliuretanos (PU) también pueden obtenerse a partir de fuentes renovables. El policloruro de vinilo de origen bio (Bio-PVC) puede sintetizarse a partir del etileno derivado de bioetanol, obteniéndose así un material parcialmente obtenido a partir de recursos renovables. Como ocurre con este tipo de materiales, el Bio-PVC puede sustituir al PVC convencional en todas sus aplicaciones [12]. También existen poliamidas comerciales obtenidas total o parcialmente a partir de recursos naturales, como es el caso de la poliamida 11, la cual se sintetiza a partir del aceite de ricino y se emplea en multitud de aplicaciones, como piezas para automóviles, molduras de precisión para usos de ingeniería, artículos deportivos, etc. [13], o la poliamida 6.10, en la que uno de sus componentes (el ácido sebácico) también se obtiene a partir de aceite de ricino. En la actualidad existen numerosas investigaciones para producir poliamidas a partir de fuentes totalmente renovables, como es el caso de la poliamida 4, que se obtiene a partir del glutamato monosódico, un aditivo alimentario producido a través de microorganismos [14]. Los poliuretanos de origen bio (Bio-PU), se sintetizan de la misma forma que el PU tradicional, es decir, mediante la reacción de poliol con isocianato, pero en el caso del Bio-PU uno o ambos componentes provienen de fuentes renovables [15].

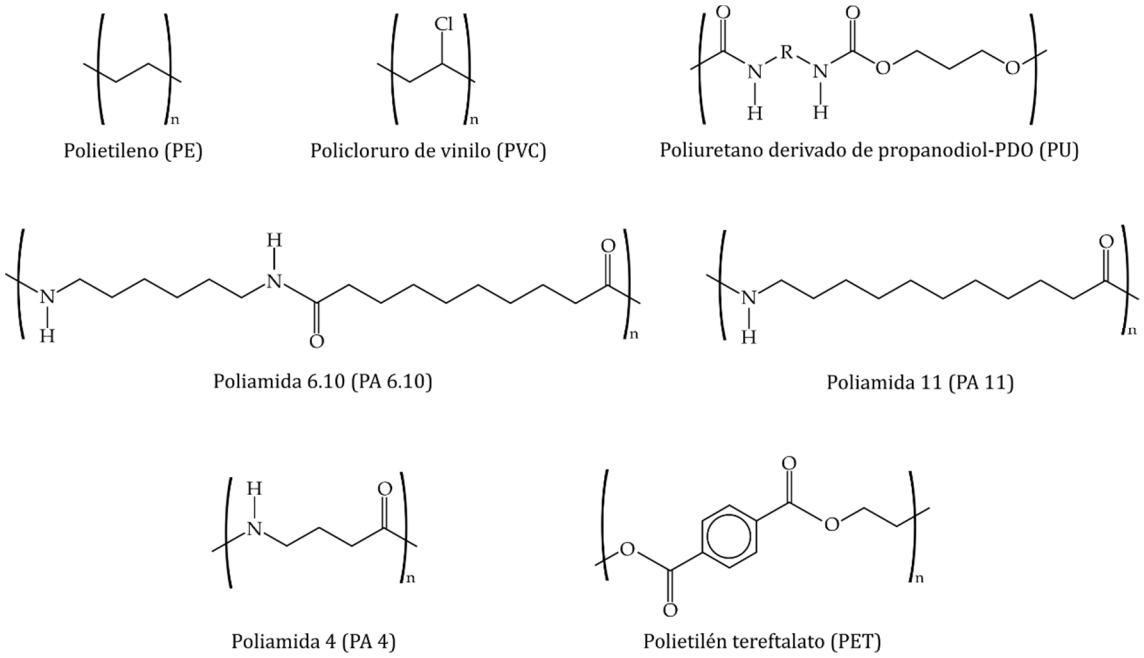

Figura I.4. Representación esquemática de la unidad monomérica de diferentes tipos de biopolímero de origen renovable no biodegradables.

I.2.2. Polímeros de origen no renovable biodegradables

Este grupo de biopolímeros abarca a todos aquellos polímeros sintetizados químicamente mediante la polimerización de monómeros obtenidos de recursos no renovables y que tienen la capacidad de biodegradarse. Dentro de este grupo, tienen especial relevancia los poliésteres alifáticos como la poli(ε-caprolactona) (PCL), el poli(butilén adipato) (PBA), el poli(ácido glicólico) (PGA) o el poli(butilén succinato) (PBS) y su copoliéster, el poli(butilén succinato-*co*-adipato) (PBSA). Dentro de este grupo de polímeros también se encuentran copoliésteres que presentan componentes alifáticos y aromáticos en su estructura, como es el caso del poli(butilén adipato-*co*-tereftalato) (PBAT) o el poli(butilen succinato-*co*-tereftalato) (PBST). La capacidad de biodegradación de este tipo de poliésteres se debe a que el grupo éster presente en sus estructuras es fácilmente hidrolizable, lo cual contribuye a su biodegradabilidad [16].

Entre los poliésteres alifáticos biodegradables más estudiados y empleados en la actualidad se encuentra la poli(ε-caprolactona) (PCL), Figura I.5. La PCL es un polímero termoplástico semicristalino que se obtiene mediante la polimerización por apertura de anillo (ROP) de la unidad monomérica ε-caprolactona en presencia de alcóxidos metálicos como octoato de estaño o isopropóxido de aluminio [9]. La PCL se caracteriza por presentar un grado de cristalinidad en torno al 50% y una temperatura de fusión muy baja, cercana a

60 °C, lo cual dificulta su procesado y limita sus aplicaciones. También presenta una temperatura de transición vítrea muy baja, alrededor de los −60 °C, y una temperatura de degradación superior a la mayoría de poliésteres alifáticos, la cual se encuentra en torno a los 350 °C [17]. En cuanto a sus propiedades mecánicas, la PCL presenta una baja resistencia a tracción y un bajo módulo elástico, pero se caracteriza principalmente por ser un polímero muy dúctil, con un elevado alargamiento a la rotura y una elevada tenacidad. Otra de las características de la PCL es que presenta una elevada compatibilidad con numerosos polímeros [18]; esto, unido a sus elevadas propiedades dúctiles y su elevada resistencia térmica hacen de este biopolímero un buen candidato para la mejora de las propiedades de otros polímeros mediante la mezcla física. Existen numerosas investigaciones en las que se ha empleado PCL con el objetivo de disminuir la rigidez y aumentar la estabilidad térmica de polímeros biodegradables como el PLA [19-21], PHAs [22, 23] o el TPS [24, 25], obteniéndose nuevas formulaciones totalmente biodegradables con mejores propiedades mecánicas y térmicas que posibilitan ampliar el campo de aplicación de estos polímeros. Además de ser biodegradable, la PCL se caracteriza por ser biocompatible, con un grado de bioabsorción lento, lo que resulta interesante en el sector médico para aplicaciones que necesiten durabilidad. Por tanto, la PCL y sus mezclas son de especial interés en el sector médico para su uso en sistemas de liberación controlada, en filamentos para suturas, en placas de fijación o en odontología [26-28], así como en el sector del envase y el embalaje para alimentos [29, 30].

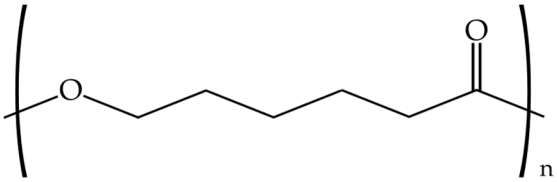

Poli(ε-caprolactona) (PCL)

Figura I.5. Representación esquemática de la unidad monomérica de la poli(ε-caprolactona).

Otro de los poliésteres alifáticos más empleados hoy en día es el poli(butilén succinato) (PBS), Figura I.6. El PBS se sintetiza químicamente por policondensación de 1,4-butanodiol y ácido succínico en presencia de un catalizador [31]. En la actualidad, el ácido succínico empleado en la obtención del PBS se obtiene principalmente de forma química a partir de recursos fósiles, pero existen numerosas investigaciones que demuestran cómo

dicho componente puede obtenerse mediante fermentación microbiana de fuentes renovables como el almidón de maíz, el suero lácteo, la melaza de caña o lignocelulosa [32]. El PBS es un poliéster semicristalino, con un grado de cristalinidad entre el 20−35%, cuyas propiedades mecánicas son comparables a las de los polímeros de uso común como el polipropileno o el polietileno [33]. En cuanto a las propiedades térmicas, dicho biopolímero se caracteriza por presentar una temperatura de transición vítrea en torno a los −30 °C, una temperatura de fusión entre los 110−115 °C y una temperatura de inicio de degradación superior a los 300 °C, aunque, tanto sus propiedades térmicas como sus propiedades mecánicas, de transparencia y de biodegradabilidad dependen principalmente del grado de cristalinidad del polímero.

La incorporación de ácido adípico durante la síntesis del PBS da lugar al poli(butilén succinato-*co*-adipato) (PBSA) [31], Figura I.6. Este polímero biodegradable se caracteriza por presentar una mayor velocidad de degradación que el PBS, así como un menor grado de cristalinidad y una mayor ductilidad. Ambos polímeros se pueden procesar mediante las técnicas convencionales de moldeo de polímeros como la inyección, extrusión o soplado, y, actualmente, se están empezando a utilizar en sectores como el del envase y el embalaje, en films de envasado o bolsas, o en el sector de la agricultura para su uso como films para cultivos [32].

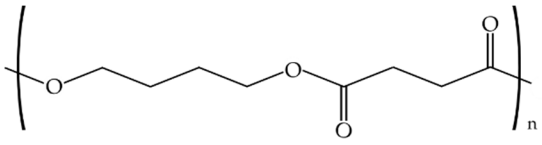

Poli(butilén succinato) (PBS)

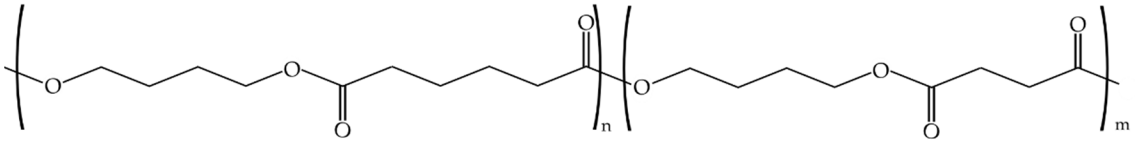

Poli(butilén succinato-*co*-adipato) (PBSA)

Figura I.6. Representación esquemática de la unidad monomérica del poli(butilén succinato) y del poli(butilén succinato-*co*-adipato).

El poli(ácido glicólico) (PGA), Figura I.7, es otro de los polímeros más estudiados dentro de este grupo de biopolímeros. El PGA se obtiene principalmente mediante la polimerización por apertura de anillo del monómero glicólido, el cual se sintetiza mediante

dimerización del ácido glicólico, aunque existen otros métodos de síntesis, como es el caso de la policondensación del ácido glicólico. El PGA se trata de un polímero altamente cristalino (45−55%), lo cual le confiere unas elevadas propiedades barrera; además presenta una elevada rigidez y módulo elástico, así como una elevada temperatura de fusión, en torno a 225 °C [9]. Gracias a su biocompatibilidad, el PGA es de gran interés en el campo de la medicina, empleándose en la fabricación de suturas absorbibles, como dispositivo de fijación ósea en forma de placas o tornillos o en sistemas de liberación controlada de medicamentos [34-36]. Además, gracias a sus elevadas propiedades barrera, se suele emplear en el sector del envase como capas intermedias en films de polímeros comerciales con el objetivo de aumentar la protección de los alimentos [9].

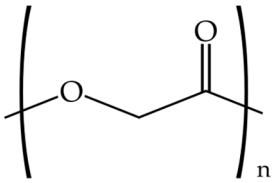

Poli(ácido glicólico) (PGA)

Figura I.7. Representación esquemática de la unidad monomérica del poli(ácido glicólico).

La copolimerización entre monómeros alifáticos y aromáticos sintéticos también puede dar lugar a copolímeros biodegradables como es el caso del poli(butilén adipato-*co*-tereftalato) (PBAT), Figura I.8, el cual se obtiene a partir de policondensación de 1,4-butanodiol, dimetil tereftalato y ácido adípico, utilizando como catalizador tetrabutilortotitanato [37]. El PBAT es otro de los polímeros pertenecientes al grupo de polímeros biodegradables obtenidos de fuentes no renovables que más interés despierta a nivel industrial, ya que se trata de un material flexible que presenta una elevada resistencia a la fractura y un elevado alargamiento a la rotura, similar al del polietileno de baja densidad (LDPE), con una buena estabilidad térmica, procesabilidad y resistencia al agua y al aceite. Todas estas propiedades hacen que el PBAT sea una buena alternativa para su aplicación en films para envases de alimentos y agricultura [38].

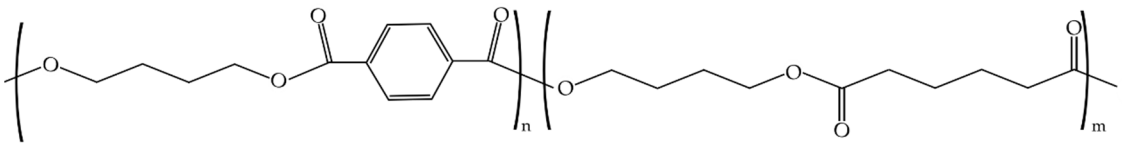

Figura I.8. Representación esquemática de la unidad monomérica del poli(butilén adipato-*co*-tereftalato).

La capacidad de biodegradación de este grupo de polímeros reduce considerablemente los problemas medioambientales generados al final de su ciclo de vida con respecto a los polímeros de uso común; sin embargo, y aunque actualmente se investiga en la posibilidad de síntesis de estos materiales a partir de fuentes renovables, lo cierto es que hoy en día estos polímeros se obtienen a partir de recursos no renovables como el petróleo, lo que hace que estos biopolímeros presenten un elevado impacto medioambiental en su origen, contribuyendo a aumentar la huella de carbono.

I.2.3. Polímeros de origen renovable biodegradables

Los biopolímeros vistos anteriormente son de gran interés científico e industrial ya que en todos ellos se consigue reducir los problemas medioambientales derivados de los polímeros sintéticos tradicionales. Sin embargo, ambos grupos de biopolímeros siguen presentando un cierto impacto ambiental, bien en el origen, al ser sintetizados a partir de recursos no renovables como el petróleo, o bien en su final de ciclo de vida, ante la imposibilidad de biodegradarse. A diferencia de los biopolímeros anteriores, el presente grupo de biopolímeros presentan ambas cualidades, es decir, proceden de recursos renovables y son biodegradables, siendo materiales capaces de cerrar el ciclo de vida de un producto. Este hecho hace que dichos biopolímeros resulten de gran interés gracias al bajo impacto medioambiental que ocasionan. Sin embargo, este tipo de materiales presentan todavía una serie de limitaciones físicas, mecánicas y económicas que no los hacen competitivos con el resto de polímeros, lo cual limita su utilización a nivel industrial. Es por ello que, actualmente, las investigaciones realizadas sobre estos biopolímeros están encaminadas a mejorar sus propiedades y a hacer más eficientes los procesos de obtención con el objetivo final de obtener materiales más competitivos industrialmente capaces de sustituir, en un futuro cercano, a los polímeros más contaminantes.

Como se ha comentado anteriormente, los polímeros obtenidos a partir de fuentes renovables y biodegradables se pueden clasificar en tres grandes grupos según su proceso

de síntesis. A continuación, se realiza una breve descripción de los principales polímeros pertenecientes a cada uno de los grupos.

I.2.3.1. Polímeros derivados de la biomasa

Los principales polímeros que engloba este grupo son polisacáridos y proteínas. Este grupo de polímeros se obtienen directamente a partir de la biomasa, principalmente de la agricultura; es por ello que también son conocidos como agropolímeros.

Polímeros derivados de polisacáridos

Los polisacáridos son las macromoléculas más abundantes en la biosfera. Estos carbohidratos complejos constituidos por enlaces glicosídicos, presentan dos funciones, una como elementos estructurales del exoesqueleto de plantas y animales, y otra como material de almacenamiento de energía. Algunos de los polisacáridos más importantes a nivel industrial son el almidón, la celulosa, la quitina, el quitosano y las pectinas.

El almidón es la principal reserva de energía de las plantas y, tradicionalmente, es la mayor fuente de carbohidratos en la dieta humana. Éste se encuentra en forma de gránulos y se extrae principalmente de cereales como el trigo, el maíz o el arroz, y de tubérculos como la patata o la mandioca. Su estructura está compuesta por una mezcla de dos homopolímeros de α-D-glucopiranosa como son la amilosa (polisacárido lineal basado en enlaces α-(1−4) glicosídicos) y la amilopectina (polisacárido ramificado basado en enlaces α-(1−4) glicosídicos y α-(1−6) glicosídicos), Figura I.9, cuya proporción en el almidón depende del origen botánico, aunque de forma general, los almidones contienen alrededor de un 80−90% de amilopectina y un 10−20% de amilosa, a parte de otros compuestos en pequeñas proporciones como proteínas, lípidos y minerales [9]. Los gránulos de almidón son semicristalinos, y su grado de cristalinidad suele variar entre el 20 y el 45%, dependiendo del origen botánico. Debido a la presencia de numerosos enlaces de hidrógeno intra- e intermoleculares entre las cadenas de almidón, su inicio de degradación térmica tiene lugar antes que la fusión, imposibilitando su procesado en su forma nativa. Es por ello que para poder procesar el almidón es necesario incorporarle agua y/o algún plastificante no volátil como el glicerol o el sorbitol, en presencia de calor y presión. Con ello se consigue eliminar la estructura cristalina del almidón produciendo una mayor fluidez, así como una disminución de la temperatura de transición vítrea (T_g) y de la temperatura de fusión (T_m), dando lugar a un material procesable denominado almidón termoplástico (TPS). El proceso de transformación del almidón a TPS se conoce como gelatinización, en el cual, los gránulos

se rompen y la estructura cristalina se pierde bajo la influencia de plastificantes, calor y presión, pasando de una estructura ordenada a una estructura desordenada [39, 40].

Las propiedades térmicas y mecánicas del TPS varían considerablemente dependiendo de la cantidad de plastificante empleado. Además, dichas propiedades también se ven considerablemente afectadas durante el almacenamiento y la vida útil del material debido a múltiples factores como la absorción de agua, el envejecimiento físico o la difusión del plastificante. Al tratarse de un material altamente hidrofílico, la absorción de agua afecta a sus propiedades térmicas y mecánicas, disminuyendo su T_g y reduciendo su resistencia a tracción. Además, la susceptibilidad del TPS al agua también provoca que el material tenga una baja estabilidad dimensional, limitando aún más sus aplicaciones. Por otro lado, el TPS se caracteriza por presentar envejecimiento físico, mediante el cual se produce un aumento de su cristalinidad con el tiempo, durante su almacenamiento o vida en servicio, dando lugar a una variación de sus propiedades mecánicas, que se refleja en una fragilización del material. Por tanto, las propiedades del TPS varían durante su almacenamiento y vida útil dependiendo de diferentes factores, los cuales son difíciles de controlar. Por eso, este polímero no se suele utilizar sólo, sino que suele emplearse en mezclas físicas con otros polímeros, principalmente hidrofóbicos y biodegradables, como el PLA [41, 42], PHAs [43] o la PCL [24, 44] dando lugar a formulaciones de TPS con un mejor rendimiento mecánico, mayor resistencia a la humedad y mejor estabilidad térmica.

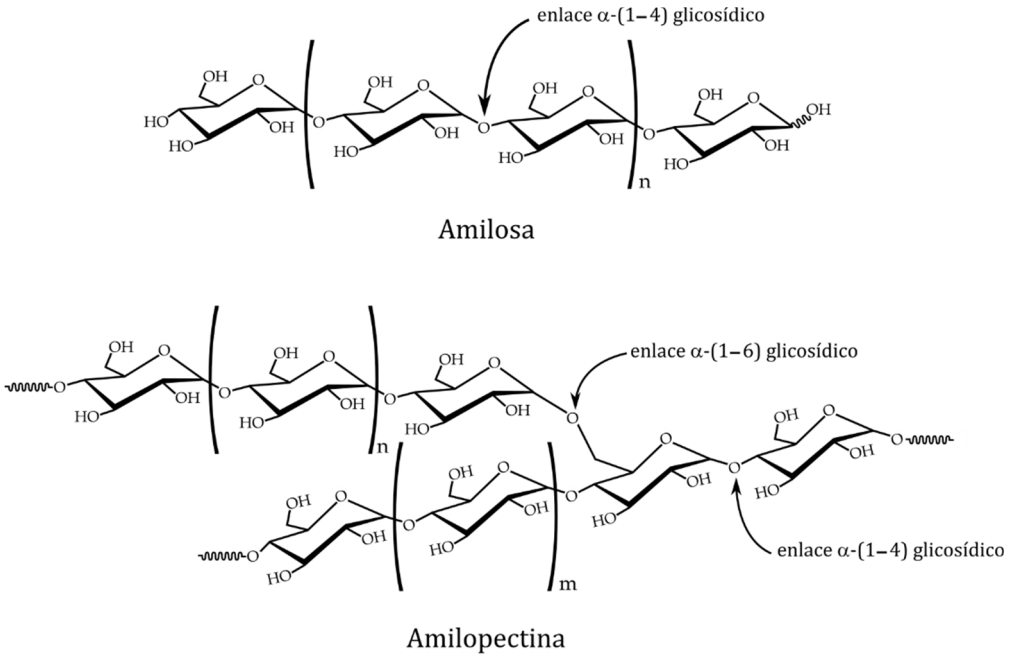

Figura I.9. Representación esquemática de las cadenas poliméricas de amilosa y amilopectina que constituyen el almidón.

Otro polisacárido extensamente utilizado a nivel industrial es la celulosa, que se trata del principal componente estructural de las células vegetales y es el biopolímero más abundante en la Tierra. La celulosa presenta una estructura molecular similar a la del almidón; sin embargo, las unidades de β-D-glucopiranosa están unidas por enlaces β-(1−4) glicosídicos en lugar de enlaces α-glicosídicos como ocurre en el almidón, Figura I.10. La gran cantidad de grupos hidroxilo presentes en las cadenas de celulosa da lugar a la formación de enlaces de hidrógeno con las cadenas adyacentes haciendo que éstas se sitúen unas al lado de otras formando fibrillas elementales, las cuales se agrupan en unidades más grandes llamadas microfibrillas, que a su vez se ensamblan formando fibras. Por tanto, cada fibra se trata esencialmente de un material compuesto en el que microfibrillas rígidas de celulosa se encuentran embebidas en una matriz blanda, compuesta principalmente de lignina y hemicelulosa [45, 46]. En las plantas superiores, la celulosa, junto con la hemicelulosa y la lignina, desempeña un papel fundamental como elemento de refuerzo en la pared celular. Estos tres elementos están estrechamente asociados dando lugar a la biomasa lignocelulósica [47]. Actualmente, la celulosa se utiliza de dos formas a escala industrial; una es la celulosa regenerada o mercerizada, que no es moldeable y se utiliza para la producción de fibras y películas, y la celulosa modificada químicamente, compuesta principalmente por los ésteres de celulosa, los cuales se utilizan en una amplia variedad de aplicaciones como recubrimientos, usos biomédicos u otras aplicaciones. Los ésteres de celulosa son materiales termoplásticos que se obtienen a partir de la esterificación de celulosa, Figura I.10. Entre los tipos más comunes se encuentran el acetato de celulosa (CA), producto de la reacción de esterificación entre celulosa y anhídrido acético, que se trata de un material barato que puede ser transparente y que se emplea en una gran cantidad de aplicaciones como en films para envases, recubrimiento para películas fotográficas, así como para la fabricación de utensilios de uso cotidiano como peines, mangos de cepillos o monturas de gafas. Los otros dos tipos de ésteres de celulosa más empleados a nivel industrial son el acetato-propionato de celulosa (CAP) y el acetato-butirato de celulosa (CAB) que se obtienen mediante la reacción de esterificación con los ácidos y anhídridos apropiados. El CAP se caracteriza por presentar una elevada transparencia, una baja dispersión de la luz y una buena resistencia a impacto y se suele utilizar en la fabricación de monturas de gafas, para equipos de protección personal y en gafas deportivas. Por otro lado, el CAB se caracteriza por presentar una buena estabilidad dimensional, una alta dureza y una elevada resistencia a la humedad y se emplea en diferentes aplicaciones como tiradores de puertas, mangos de herramientas, en envases, cubiertas de máquinas, etc. [9, 48].

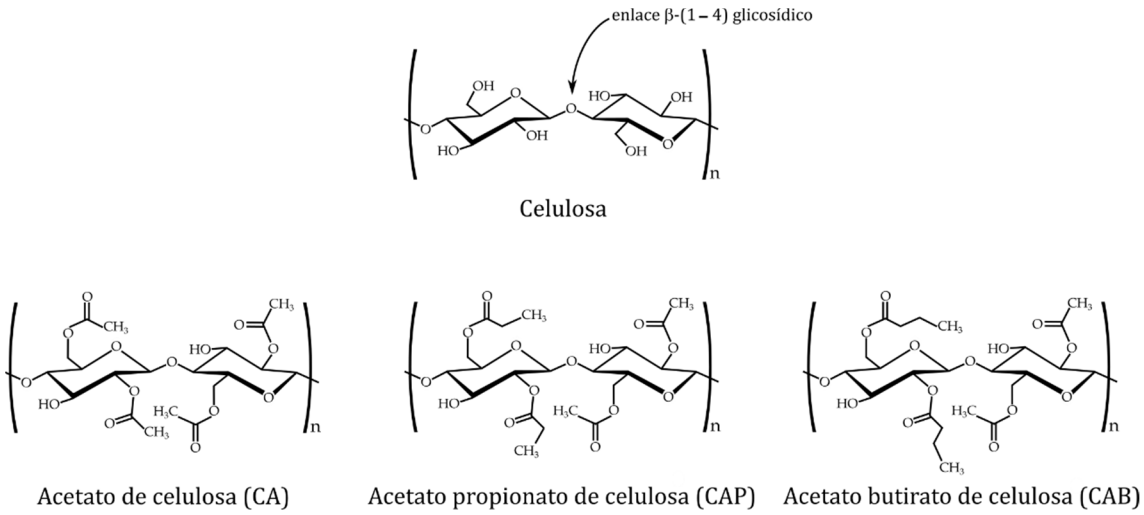

Figura I.10. Representación esquemática de la unidad monomérica de la celulosa y de diversos ésteres de celulosa.

Dentro de este grupo de materiales también se encuentra la quitina, que se trata del segundo polímero biodegradable más abundante producido en la naturaleza después de la celulosa. Este biopolímero se sintetiza por una amplia variedad de organismos vivos, pero su principal fuente de obtención es el exoesqueleto (caparazón) de varios crustáceos como las gambas, las langostas o los cangrejos, aunque también puede obtenerse de las paredes celulares de diversos hongos o algas [49]. La quitina se trata de un polisacárido acetilado que se encuentra en forma de microfibrillas cristalinas ordenadas y está formado por grupos N-acetil-D-glucosamina unidos mediante enlaces β-(1-4) glicosídicos, Figura I.11. Ésta se caracteriza por ser altamente insoluble en agua y presentar baja reactividad. Mediante la desacetilación parcial de la quitina se obtiene el quitosano, Figura I.11, el cual presenta unas mejores propiedades de reactividad y solubilidad [50]. Ambos polímeros son biodegradables y biocompatibles, además poseen propiedades antibacterianas, así como la capacidad de absorber iones de metales pesados. Gracias a sus propiedades, la quitina y el quitosano son utilizados en un amplio rango de sectores como es el de la alimentación, donde se usan como agentes espesantes, gelificantes o emulsificantes. Estos biopolímeros también se emplean como material para el envasado de alimentos, para el tratamiento de aguas residuales, así como en el sector de la medicina, para su uso en fibras para suturas reabsorbibles y apósitos para heridas. En el caso particular del quitosano se ha estudiado su aplicación como piel artificial, como material para encapsulación y sistema de liberación controlada de fármacos o para la fabricación de lentes de contacto [51].

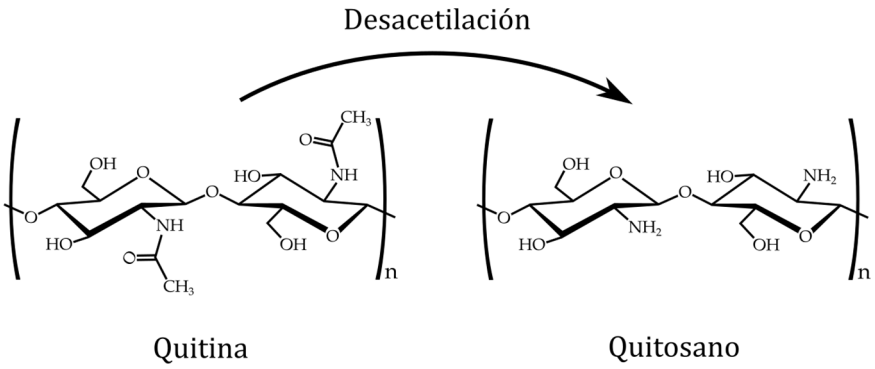

Figura I.11. Representación esquemática de la unidad monomérica de la quitina y del quitosano.

La pectina es un compuesto natural de alto peso molecular y es uno de los principales componentes de la pared celular de todas las plantas superiores. Se trata de un polisacárido complejo formado por una cadena de unidades de ácido galacturónico parcialmente esterificados con metanol (metoxilados) unidos por enlaces α-(1,4)-glicosídicos, Figura I.12, y que a menudo se interrumpen por la presencia de unidades de L-ramnosa que presenta ramificaciones laterales de azúcares neutros como L-arabinosa o D-galactosa [52]. Durante los últimos años, la pectina ha ganado un especial interés industrial gracias a propiedades como su biodegradabilidad y su biocompatibilidad. Además, la pectina es comestible y puede ser gelificada, lo cual le permite ser utilizada en un amplio rango de sectores como la alimentación, donde se utiliza como agente gelificante, estabilizante o espesante en productos alimenticios como mermeladas, bebidas de yogur o helados. La pectina también se emplea en el sector del envase para la elaboración de películas comestibles destinadas al envasado de alimentos [53] o en medicina en forma de hidrogeles para la administración de fármacos, para ingeniería de tejidos o para la curación de heridas [54].

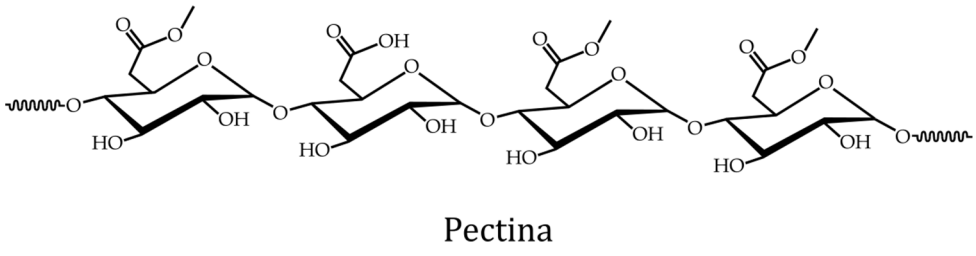

Figura I.12. Representación esquemática de las cadenas poliméricas de pectina.

Polímeros derivados de proteínas

El otro grupo de los considerados agropolímeros son las proteínas, las cuales son producidas por animales, plantas y bacterias. Entre las proteínas más importantes empleadas a nivel industrial como polímeros biodegradables se encuentran proteínas vegetales como la proteína de soja, de maíz o de trigo y proteínas animales como la caseína, el colágeno (gelatina) o la queratina.

Entre las proteínas vegetales que más interés despiertan a nivel industrial destacan la proteína de soja y el gluten. La proteína de soja se extrae de la semilla de soja, que se utiliza para obtener aceite. Dichas proteínas se componen de una mezcla de albúminas y globulinas, siendo estas últimas el principal componente, en torno a un 90% [55]. Debido a su abundancia, a su bajo coste y a su biodegradabilidad y biocompatibilidad resulta un material muy interesante a nivel científico e industrial para su uso en diferentes sectores como el de alimentación o el sector médico. Sin embargo, la baja resistencia y la elevada absorción de agua que presenta este material, limitan su aplicabilidad industrial. Es por ello que para mejorar sus propiedades y aumentar la utilidad de este polímero se han estudiado diferentes procedimientos como la plastificación, la mezcla física con otros polímeros biodegradables o tratamientos químicos para disminuir su hidrofilidad. Los materiales basados en proteína de soja tienen una amplia aplicación industrial abarcando diferentes sectores como el sector del envase y embalaje, donde se utiliza como film para envases de alimentos, o el sector biomédico, donde puede emplearse como sistema de liberación controlada de fármacos o en la fabricación de matrices para la ingeniería de tejidos [56, 57].

Otra proteína de origen vegetal de gran interés es el gluten, que se trata de la principal proteína de almacenamiento en el trigo, y se obtiene como subproducto de la industria del almidón. El gluten es una mezcla compleja de cientos de proteínas relacionadas pero distintas, siendo la gliadina y la glutenina las principales proteínas. Se trata de un material con una elevada disponibilidad, bajo coste, buena biodegradabilidad, propiedades viscoelásticas únicas y presenta la capacidad de entrecruzamiento cuando se le aplica calor. El gluten es fácilmente procesable mediante procesos convencionales de procesado de polímeros como la extrusión o el moldeo por compresión [58]. Sin embargo, al igual que ocurre con la proteína de soja, los bioplásticos a base de gluten son frágiles debido a las fuertes interacciones inter- e intramoleculares que existen entre las cadenas de proteínas. Además, también presenta una elevada sensibilidad al agua, haciendo que se trate de un material con una baja estabilidad dimensional y mecánica a largo plazo, ya que sus propiedades mecánicas dependen del contenido de humedad y del tiempo de almacenamiento. Estos inconvenientes limitan de forma significativa las aplicaciones de los

polímeros basados en gluten. Una de las principales técnicas empleadas para mejorar sus propiedades es el empleo de elevadas cantidades de plastificantes como agua, glicerol o sorbitol. Con ello se consigue disminuir la fragilidad del gluten y mejorar su procesado [59]. En la actualidad, el gluten de trigo se utiliza en numerosas aplicaciones en la industria alimenticia, aunque también se emplea en otras aplicaciones no alimentarias como en films de envasado de alimentos [60].

Entre las proteínas animales más utilizadas a nivel industrial se encuentra la gelatina, que se trata de un polímero natural de uso común que se obtiene por la hidrólisis parcial del colágeno, que es el pilar estructural y la proteína más común en el reino animal y se encuentra principalmente en tejidos fibrosos como el tendón, el ligamento y la piel. Gracias a su biodegradabilidad, su biocompatibilidad y sus propiedades gelificantes y viscoelásticas, la gelatina se utiliza en un amplio rango de sectores, siendo el sector de la alimentación uno de los más importantes, donde la gelatina se utiliza como agente emulsionante, espumante o estabilizante. También se utiliza en el sector del envase para la fabricación de films biodegradables. Otros sectores en los que el empleo de la gelatina está extendido son la fotografía, la cosmética y la medicina [61].

Otra de las proteínas animales extensamente utilizada es la caseína, que se trata de la principal proteína de la leche. Debido a su elevada disponibilidad, a su bajo coste y a sus excelentes propiedades mecánicas y propiedades barrera, la caseína se utiliza industrialmente en un amplio rango de sectores y en aplicaciones tan diversas como adhesivos, pinturas, films para envase de alimentos, fibras, productos moldeados o como sistema de liberación controlada de medicamentos en el sector biomédico [62].

I.2.3.2. Polímeros sintetizados a partir de monómeros obtenidos de la biomasa

También existen polímeros biodegradables que no se encuentran directamente en la naturaleza, como los vistos en el punto anterior, pero que pueden sintetizarse mediante la intervención humana a partir de recursos naturales biológicos. El principal polímero perteneciente a este grupo de biopolímeros es el poli(ácido láctico) (PLA), Figura I.13. El PLA es el polímero de origen renovable y biodegradable más estudiado y utilizado a nivel industrial en una amplia variedad de aplicaciones.

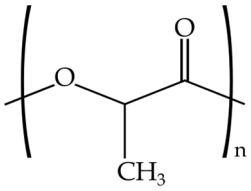

Poli(ácido láctico) (PLA)

Figura I.13. Representación esquemática de la unidad monomérica del poli(ácido láctico).

El PLA es un poliéster alifático biodegradable y biocompatible, cuyo monómero, el ácido láctico, puede obtenerse mediante síntesis química o a partir de la fermentación de fuentes renovables como el almidón de maíz, la caña de azúcar, la remolacha azucarera, el almidón de patata u otros azúcares obtenidos de la biomasa, siendo éste procedimiento el más respetuoso con el medio ambiente y el más empleado en la actualidad. El monómero de ácido láctico es una molécula quiral y existe en forma de isómeros D-ácido láctico o L-ácido láctico, Figura I.14, los cuales pueden obtenerse biológicamente, dependiendo de la cepa microbiana utilizada durante el proceso de fermentación [63].

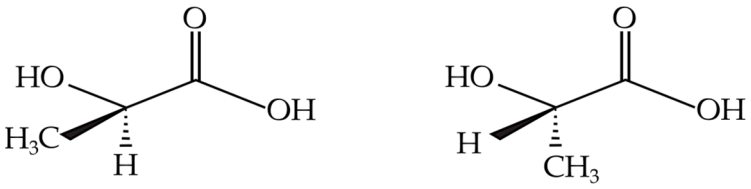

D-ácido láctico L-ácido láctico

Figura I.14. Representación esquemática de la estructura química de los isómeros del ácido láctico.

El PLA puede sintetizarse principalmente mediante tres procesos: a través de la reacción de policondensación del ácido láctico, mediante condensación deshidratante azeotrópica o por la polimerización de apertura del anillo (ROP) del monómero de lactida (un dímero cíclico de ácido láctico), siendo este último método el más empleado. Aunque el proceso de policondensación es el método menos costoso, sólo permite obtener PLA de bajo peso molecular. En cambio, el proceso de polimerización mediante ROP permite obtener PLA de alto peso molecular, además de un mayor control del proceso de síntesis, pudiendo modificar las propiedades del polímero resultante de una forma más controlada [63]. En la Figura I.15 se puede observar la representación esquemática de la síntesis del PLA mediante los diferentes procesos.

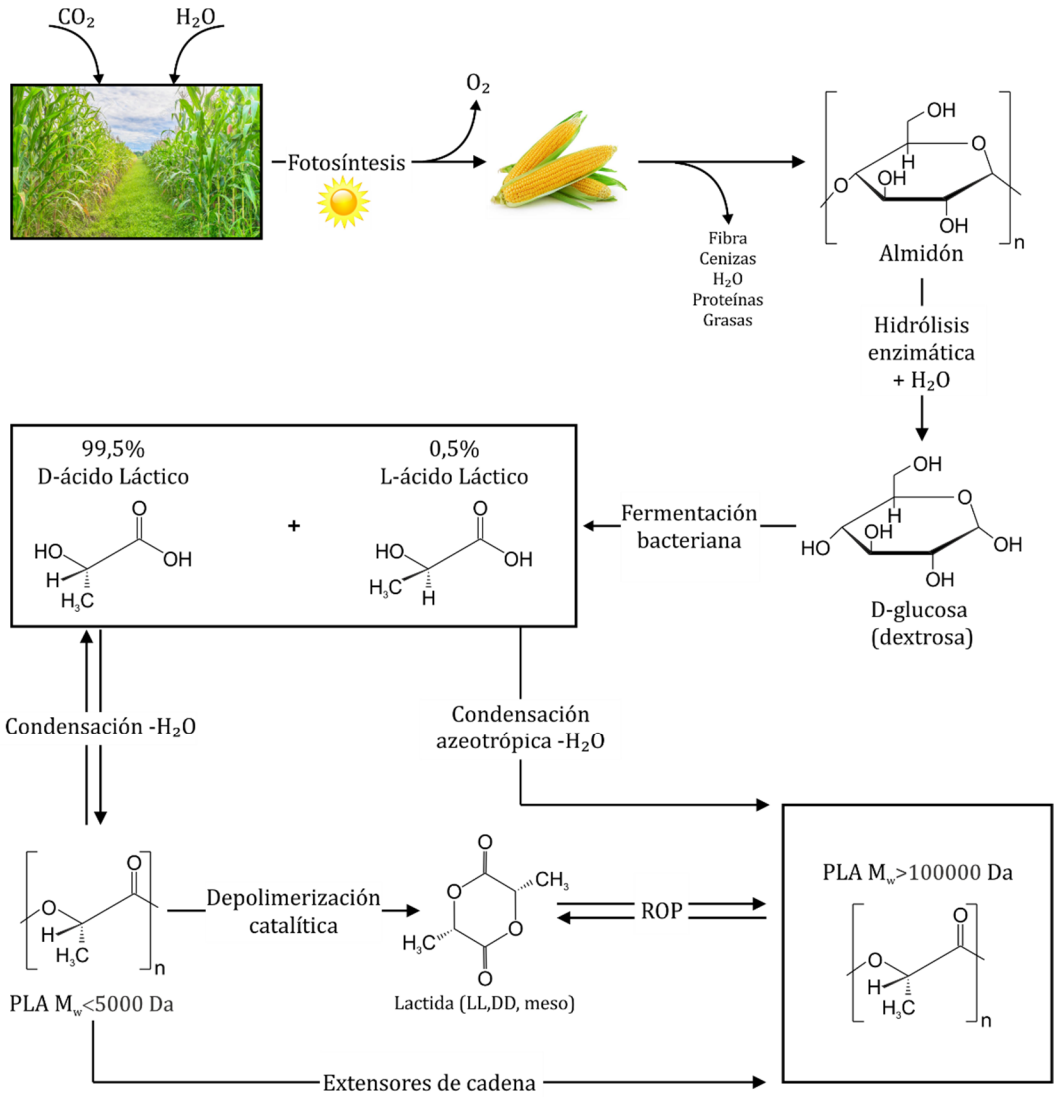

Figura I.15. Representación esquemática de las principales rutas de síntesis del PLA.

La estructura interna del PLA puede presentar tres formas estereoquímicas que dependerán del monómero utilizado en la síntesis, pudiéndose obtener poli L-láctico (PLLA), poli D-láctico (PDLA) y poli D-,L-láctico (PDLLA). Por tanto, las propiedades del PLA dependerán en gran medida de la cantidad y de la naturaleza estereoquímica del monómero (L- o D-). Por ejemplo, el homopolímero de isómero L- (PLLA) es un polímero semicristalino, con una elevada cristalinidad, caracterizado por presentar una alta resistencia a tracción y módulo, pero muy bajo alargamiento a la rotura. Por otro lado, el copolímero aleatorio de isómeros D-,L- (PDLLA) se trata de un polímero amorfo con una menor resistencia a tracción y un mayor alargamiento a la rotura, así como una mayor velocidad de degradación [64]. Por tanto, las propiedades mecánicas del PLA dependerán en gran medida de la estereoquímica, aunque otros factores como la masa molar y el porcentaje de cristalinidad también influirán en las mismas. De forma general, el PLA se trata de un polímero frágil y

rígido, con muy poco alargamiento a la rotura y baja resistencia al impacto, aunque se pueden conseguir ciertas mejoras en su ductilidad mediante la variación de la estereoquímica, la masa molar y el porcentaje de cristalinidad, esta mejora resulta insuficiente para satisfacer los requisitos de muchas aplicaciones [65]; es por ello que en la actualidad existen numerosos estudios centrados en la mejora de las propiedades del PLA mediante el empleo de plastificantes [66-68] o la mezcla física con otros polímeros biodegradables más dúctiles como la PCL [69, 70], el PBAT [71, 72] o el PBS [73].

En cuanto a la degradación del PLA, ésta se produce en dos etapas: en primer lugar, el PLA comienza a degradarse por hidrólisis, produciéndose la ruptura aleatoria de los grupos éster de las cadenas poliméricas, dando lugar a una reducción del peso molecular y fragilizando el material. En segundo lugar, el PLA de bajo peso molecular es metabolizado por microorganismos, produciendo dióxido de carbono, agua y compost [74].

El PLA presenta una serie de ventajas que lo hacen muy atractivo a nivel industrial. Además, la caída continua del precio del polímero hace que éste gane cada día más cuota de mercado. El PLA se trata de un material biodegradable, reciclable y biocompatible que puede ser fácilmente procesado por técnicas convencionales de procesado de polímeros como el moldeo por inyección, moldeo por soplado, termoconformado, extrusión o hilado de fibras. Actualmente, la mayoría de las aplicaciones del PLA se encuentran en el sector del envase y el embalaje gracias a sus propiedades mecánicas, a su elevada transparencia y a sus buenas propiedades barrera, empleándose en la fabricación de botellas, en recipientes de comida o como embalaje de alimentos. Su propiedad de biocompatibilidad hace que también sea utilizado en el sector médico como hilo de sutura, fijaciones como tornillos o alfileres, implantes reabsorbibles o como dispositivo de liberación controlada de medicamentos. Aunque el campo de aplicación del PLA abarca una gran cantidad de sectores y aplicaciones como, por ejemplo, la producción de fibras para ropa, alfombras o toallas, telas no tejidas para la fabricación de toallitas húmedas o relleno de almohadas. Además, durante los últimos años, el PLA se ha establecido como uno de los materiales más empleados en impresoras 3D [75, 76].

I.2.3.3. Polímeros producidos por microorganismos

Dentro de este grupo de biopolímeros se encuentran aquellos materiales producidos a partir de microorganismos, siendo los polihidroxialcanoatos (PHAs) los que presentan un mayor interés científico e industrial. Las principales características de este tipo de polímeros se desarrollan más extensamente en el siguiente apartado.

I.3. GENERALIDADES DE LOS POLIHIDROXIALCANOATOS

A diferencia de otros polímeros biodegradables obtenidos de fuentes renovables como el PLA, los PHAs son completamente biosintetizados y biopolimerizados por microorganismos. Además, pueden presentar propiedades mecánicas y térmicas similares a las de los polímeros de uso común obtenidos a partir de recursos fósiles, lo que los hacen potenciales candidatos como futuros sustitutos de estos. Dentro de los PHAs, el poli(3-hidroxibutirato) (PHB) y el poli(3-hidroxibutirato-*co*-3-hidroxivalerato) (PHBV) son los biopolímeros más estudiados y empleados en la actualidad, aunque su uso a nivel industrial no está todavía generalizado.

Los PHAs son poliésteres termoplásticos o elastómeros de monómeros de ácido R-hidroxialcanoicos ((R)-HA) que son sintetizados por una amplia variedad de bacterias Gram-positivas y Gram-negativas (más de 300 tipos), aunque existen estudios en los que se han sintetizado PHAs a partir de plantas. Las bacterias productoras de PHAs acumulan dicho polímero en su citoplasma como gránulos de reserva de carbono y energía, utilizándolo como reserva de nutrientes que pueden ser requeridos ante la ausencia de estos con el fin de mantener su metabolismo [77]. La acumulación de PHA tiene lugar cuando las bacterias experimentan un desequilibrio de nutrientes, como la falta de nitrógeno, fósforo, magnesio, azufre u oxígeno y un exceso de fuentes de carbono. Aunque también existen bacterias que no requieren limitación de nutrientes para la síntesis del PHA como es el caso de *Escherichia coli* recombinante [78]. La cantidad acumulada de este biopolímero puede llegar a representar más del 90% del peso seco de la célula, aunque dicha cantidad depende del tipo de bacteria y de las condiciones en las que se cultiva [79]. Como se observa en la Figura I.16, las inclusiones de PHAs en el interior de las bacterias presentan una forma de gránulos esféricos de diferentes tamaños, cuyo diámetro puede variar entre los 0,2 y 0,5 μm.

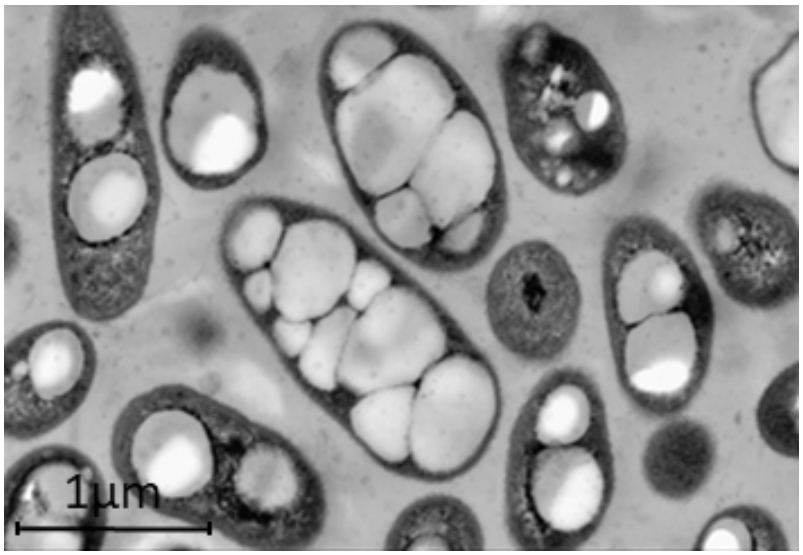

Figura I.16. Imagen de microscopia electrónica de células de *C. necator* DSM 545 con inclusiones de PHB (Fuente de la imagen: [80]).

I.3.1. Estructura y clasificación de los polihidroxialcanoatos

Estructuralmente, los PHAs son un tipo de poliésteres lineales que consisten en monómeros de ácido R-hidroxialcanoico conectados entre sí mediante un enlace éster. La polimerización de los ácidos hidroxialcanoicos, por acción de las enzimas intracelulares, tiene lugar mediante condensación del grupo carboxílico de un monómero con el grupo hidroxilo de otro monómero, formándose un enlace tipo éster; es por ello que estos polímeros también se conocen como biopoliésteres [81]. Existen una gran variedad de PHAs diferentes, cuya composición del monómero y las propiedades fisicoquímicas varían según la cepa bacteriana, la fuente de carbono y las condiciones de cultivo empleadas. Actualmente se tiene constancia de la existencia de más de 150 unidades monoméricas diferentes de PHAs, siendo el 3-hidroxibutirato (3HB) y el 3-hidroxivalerato (3HV) los dos monómeros de PHA más comunes y más ampliamente estudiados [82]. La Figura I.17 muestra la estructura química general de la unidad repetitiva de los polihidroxialcanoatos y algunos de los PHAs más conocidos.

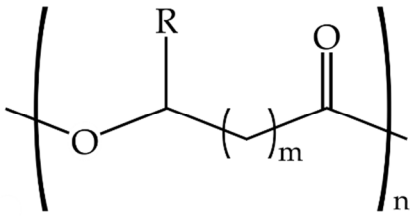

m	R	Polímero	Abreviatura
1	Hidrógeno	Poli(3-hidroxipropionato)	P(3HP)
1	Metilo	Poli(3-hidroxibutirato)	P(3HB)
1	Etilo	Poli(3-hidroxivalerato)	P(3HV)
1	Propilo	Poli(3-hidroxihexanoato)	P(3HHx)
1	Pentilo	Poli(3-hidroxioctanoato)	P(3HO)
1	Nonilo	Poli(3-hidroxidodecanoato)	P(3HDD)
2	Hidrógeno	Poli(4-hidroxibutirato)	P(4HB)
2	Metilo	Poli(4-hidroxivalerato)	P(4HV)
3	Hidrógeno	Poli(5-hidroxivalerato)	P(5HV)
3	Metilo	Poli(5-hidroxihexanoato)	P(5HHx)
4	Hexilo	Poli(6-hidroxidodecanoato)	P(6HDD)

Figura I.17. Representación esquemática de la unidad monomérica repetitiva general de los polihidroxialcanoatos y los principales polímeros obtenidos en función de la unidad de repetición "m" y del radical "R".

Los PHAs pueden ser homopolímeros, si están constituidos por un solo tipo de ácido hidroxialcanoico como unidad monomérica, o heteropolímeros (copolímeros), si están constituidos por más de un ácido hidroxialcanoico como unidad monomérica. Los PHAs se pueden clasificar de forma general en dos grupos dependiendo del número de átomos de carbono presente en su unidad monomérica. Según esto, se encuentran los PHAs con longitud de cadena corta (scl-PHAs), los cuales presentan entre 3 y 5 átomos de carbono en su unidad monomérica, y los PHAs con longitud de cadena media (mcl-PHAs), los cuales contienen entre 6 y 14 átomos de carbono [83]. Existe un tercer grupo denominado PHAs híbridos o mixtos que se compone de una mezcla de monómeros de cadena corta y de cadena media. La formación de los diferentes tipos de PHAs, así como la formación de homopolímeros o heteropolímeros dependerá principalmente del tipo de microorganismo empleado. En la Figura I.18 se puede observar la clasificación de diferentes PHAs dependiendo del número de átomos de carbono de su unidad monomérica.

Las propiedades de los PHAs varían considerablemente dependiendo de su estructura. Los scl-PHAs presentan un amplio rango de propiedades dependiendo de su composición monomérica. Sin embargo, de forma general, este tipo de biopolímeros se caracterizan por presentar un elevado grado de cristalinidad, llegando a alcanzar hasta un 80%. Esto hace que se trate de materiales que presentan una elevada rigidez y fragilidad. Las propiedades térmicas también varían considerablemente entre los diferentes scl-PHAs, pero se suelen caracterizar por presentar temperaturas de fusión elevadas, entre los 175 y

los 180 °C, y temperaturas de transición vítrea bajas, entre los 5 y los 10 °C. Entre los PHAs de longitud de cadena corta más conocidos se encuentran homopolímeros como el poli(3-hidroxibutirato) P(3HB) o PHB, el poli(4-hidroxibutirato) P(4HB) o el poli(3-hidroxivalerato) P(3HV), y el copolímero poli(3-hidroxibutirato-*co*-3-hidroxivalerato) P(3HB-*co*-3HV) o PHBV, obtenido a partir de la copolimerización de los monómeros 3HB y 3HV [81, 84].

Por otra parte, los mcl-PHAs se tratan de elastómeros que presentan una baja cristalinidad, en torno al 25 %, una baja resistencia a tracción, un bajo módulo elástico y un elevado alargamiento a la rotura. En cuanto a sus propiedades térmicas, este tipo de PHAs se caracterizan por presentar muy bajas temperaturas de transición vítrea, entre −50 y −25 °C, así como bajas temperaturas de fusión, entre 40 y 60 °C. Dentro de los PHAs de longitud de cadena media más conocidos se encuentran los homopolímeros poli(3-hidroxihexanoato) P(3HHx) y poli(3-hidroxioctanoato) P(3HO), y el copolímero poli(3-hidroxihexanoato-*co*-3-hidroxioctanoato) P(3HHx-*co*-3HO) [81, 84].

Como se ha comentado, existe un tercer grupo denominado PHAs híbridos o PHAs mixtos, que están comprendidos por unidades monoméricas de cadena corta y de cadena media. Estos copolímeros presentan un amplio rango de propiedades, las cuales dependerán de la fracción molar de cada uno de los monómeros en el copolímero. Uno de los PHAs híbridos más estudiados es el poli(3-hidroxibutirato-*co*-3-hidroxihexanoato) P(3HB-*co*-3HHx) [84].

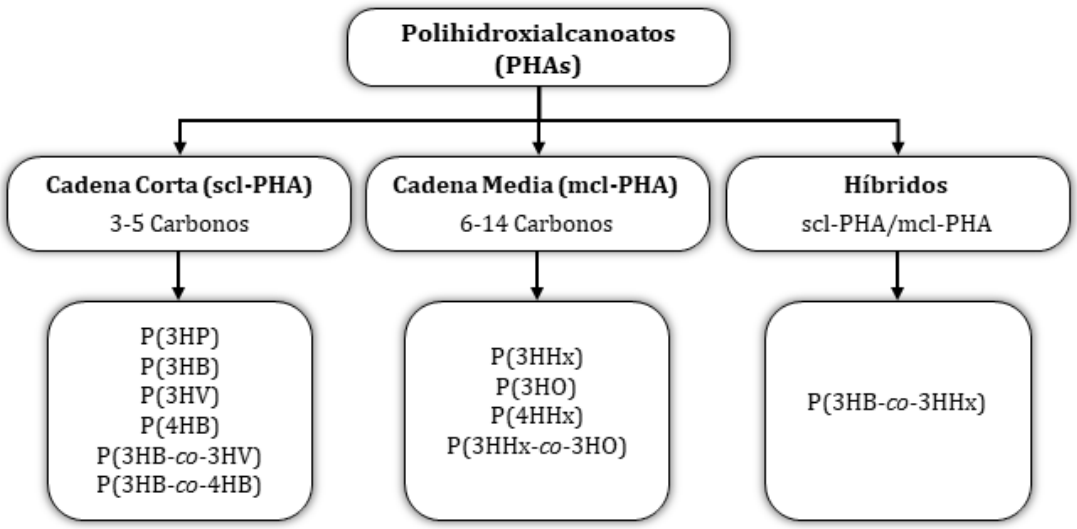

Figura I.18. Clasificación de PHAs según el número de átomos de carbono presente en su unidad monomérica.

I.3.2. Producción de polihidroxialcanoatos

Existe una gran cantidad de bacterias capaces de sintetizar PHAs, más de 300 tipos; sin embargo, solamente unas pocas son capaces de sintetizar PHAs para su producción a escala industrial, como es el caso de las bacterias *Pseudomonas olovorans*, *Azotobacter vinelandii* o *Escherichia coli* recombinante [85]. La gran mayoría de bacterias presentan una serie de inconvenientes que no las hacen adecuadas para la producción en masa de PHAs, como, por ejemplo, un crecimiento lento durante el proceso de fermentación o la necesidad de utilizar fuentes de carbono concretas. En la actualidad existen numerosos estudios de modificación genética de microorganismos con el objetivo de incrementar la producción de PHAs, disminuyendo así sus costes. Este es el caso de una de las cepas más empleadas en la producción de PHAs, la *Escherichia coli* recombinante, la cual se obtiene mediante modificación genética a partir de *Escherichia coli,* que se trata de una cepa no productora de PHAs pero que puede alcanzar una elevada densidad celular en poco tiempo y que puede usar una gran variedad de fuentes de carbono, tras introducirle genes de biosíntesis de PHAs de una cepa productora como *Cupriavidus necator* o *Alcaligenes latus*. Esto da lugar a cepas de *Escherichia coli* recombinante, las cuales presentan un elevado rendimiento de producción de PHAs, ya que presenta un crecimiento rápido y una alta densidad celular, pudiendo acumular grandes cantidades de biopolímero en poco tiempo. Además, tienen la capacidad de usar varias fuentes de carbono renovable y baratas [86-88].

Las bacterias empleadas en la producción de PHAs se pueden dividir en dos grandes grupos según las condiciones de cultivo requeridas para la síntesis del biopolímero. Un primer grupo abarca a todas aquellas bacterias que requieren de la limitación de nutrientes, como nitrógeno, fósforo, azufre o magnesio, y un exceso de fuente de carbono para la producción de PHAs. Dentro de este grupo se encuentran bacterias como *Ralstonia eutropha*, *Pseudomonas oleovorans* o *Pseudomonas putida*. Al segundo grupo pertenecen aquellas bacterias que no requieren de limitación de nutrientes para la síntesis de PHAs y son capaces de acumular el polímero durante su crecimiento, como es el caso de las bacterias *Alcaligenes latus*, *Azotobacter vinelandii* recombinante o *Escherichia coli* recombinante [89]. Por tanto, dependiendo del tipo de bacterias empleadas se realizará un tipo de fermentación diferente.

El proceso de obtención industrial de PHAs se lleva a cabo en tres etapas fundamentales: fermentación, extracción y purificación, como se puede observar en la Figura I.19. Existen diferentes tipos de fermentación para la producción industrial de PHAs, entre las que se encuentran el cultivo continuo o el cultivo por lotes alimentados, siendo este último método uno de los más empleados. El cultivo por lotes alimentados de las

bacterias que necesitan limitación de nutrientes se suele realizar en dos etapas separadas. Una primera etapa en la que no hay limitación de nutrientes, donde se produce el crecimiento celular en un sustrato enriquecido con nutrientes, y una segunda etapa en la que se utiliza un sustrato donde existe una limitación de nutrientes, pero que mantiene un nutriente esencial para permitir la síntesis de PHAs en los microorganismos. En esta segunda etapa, las células no pueden multiplicarse y permanecen prácticamente constantes, sin embargo, se produce un crecimiento de la concentración celular debido a que las células comienzan a aumentar de tamaño y de peso por la acumulación intracelular de PHA como producto de almacenamiento. Para los microorganismos que no necesitan limitación de nutrientes para sintetizar PHAs se suele utilizar un cultivo por lotes alimentados en una sola etapa, en la cual se aporta un sustrato enriquecido de nutrientes [77, 89].

La elección del sustrato para la fermentación, es decir, la fuente de nutrientes, es de gran importancia en la producción de PHAs, ya que éste debe proporcionar las condiciones óptimas para la producción de un determinado tipo de PHA en diferentes bacterias, así como permitir hacerlo con una alta productividad. Por tanto, la elección del sustrato dependerá del tipo de microorganismo empleado, así como del tipo de PHA que se desee producir. El sustrato supone uno de los principales costes en la producción de PHAs. En la actualidad se emplean sustratos como sacarosa y glucosa para la producción de estos biopolímeros a escala industrial, pero se está estudiando el uso de sustratos más económicos con el objetivo de reducir el coste del proceso productivo y, por tanto, del polímero. También se está explorando el empleo de materiales de desecho agrícolas o de la industria de la alimentación como melaza, suero lácteo, salvado de trigo y arroz, aceites vegetales y residuos de aceites vegetales, almidón, aguas residuales de almazaras, aguas residuales porcinas, etc., como sustratos económicos para la producción de PHAs [90]. Otras estrategias seguidas para abaratar los costes productivos son el desarrollo de cepas modificadas genéticamente que permitan la producción de PHAs con fuentes de carbono baratas en vez de con sustratos de carbono purificados, así como el desarrollo de estrategias de fermentación más eficientes [77, 91, 92].

Tras la fermentación, las células que contienen PHAs se han de separar del caldo de cultivo. Para ello se emplean diferentes métodos como la sedimentación, la centrifugación, la filtración o, con menor frecuencia, la floculación. Una vez recogido, y antes del proceso de recuperación, se suelen realizar uno o varios pretratamientos para debilitar la membrana celular y facilitar así su disrupción. Dichos pretratamientos se suelen llevar a cabo mediante calor, tratamiento alcalino, mediante sales o por congelación [93]. Tras dichos pretratamientos, se procede a la extracción del polímero del interior de las células, para ello

se pueden emplear diferentes métodos de recuperación. Uno de los métodos de recuperación más utilizado actualmente es el empleo de disolventes tales como hidrocarburos clorados (cloroformo o 1,2-dicloroetano) o carbonatos cíclicos (carbonato de etileno o carbonato de 1,2-propileno). Durante este proceso, los disolventes actúan en un primer lugar modificando la permeabilidad de la membrana celular y posteriormente disolviendo el polímero. Este método de recuperación consta de una segunda etapa en la que se realiza la precipitación de los PHAs mediante metanol o etanol. Este proceso es el más ampliamente utilizado debido a su simplicidad, rapidez y eficiencia. Además, este método causa muy poca degradación en los polímeros, permitiendo obtener PHAs con una elevada pureza y altos pesos moleculares; sin embargo, debido al carácter dañino de algunos disolventes y a la gran cantidad necesaria para la extracción, este método es poco respetuoso con el medio ambiente. Otro de los métodos de recuperación comúnmente empleados es mediante procesos de digestión química o enzimática con los que se produce la liberación del polímero mediante la destrucción de los componentes de la membrana celular que rodean los gránulos de PHA, como lípidos, carbohidratos, proteínas y enzimas. Los gránulos de PHA liberados son posteriormente separados mediante filtración, flotación o centrifugación. Este método presenta un menor impacto medioambiental que la extracción con disolventes, sin embargo, el rendimiento de recuperación es menor. La disrupción celular mecánica es otro de los métodos más empleados. Al igual que el método anterior, también se produce la desintegración de la membrana celular con el fin de liberar el polímero, pero en este caso el proceso se realiza de forma mecánica. Existen diferentes procesos mecánicos para la recuperación de PHAs, como la homogeneización a alta presión, la disrupción con ultrasonido o la disrupción con molino de bolas. Al no utilizar productos químicos, estos procesos reducen la contaminación ambiental, así como la contaminación en el polímero, sin embargo, se trata de métodos de extracción costosos debido a la elevada inversión en equipos y a los largos tiempos de procesado necesarios. Existen más métodos de extracción como la flotación por aire disuelto o la extracción mediante CO_2 supercrítico. Sin embargo, ninguno de estos procedimientos de recuperación posee todos los requisitos necesarios para ser un proceso eficiente y económico a gran escala, siendo los principales inconvenientes el coste, la seguridad medioambiental y su escalabilidad a nivel industrial. Por tanto, en la actualidad, el proceso de recuperación sigue siendo un proceso costoso, que repercute de forma significativa en el precio final de los PHAs [77, 89, 94].

Tras la recuperación, los PHAs pueden ser sometidos a un proceso de purificación mediante un tratamiento con peróxido de hidrógeno, combinado con la acción de enzimas o agentes quelantes, o mediante el empleo de ozono con el fin de aumentar la pureza del polímero [93].

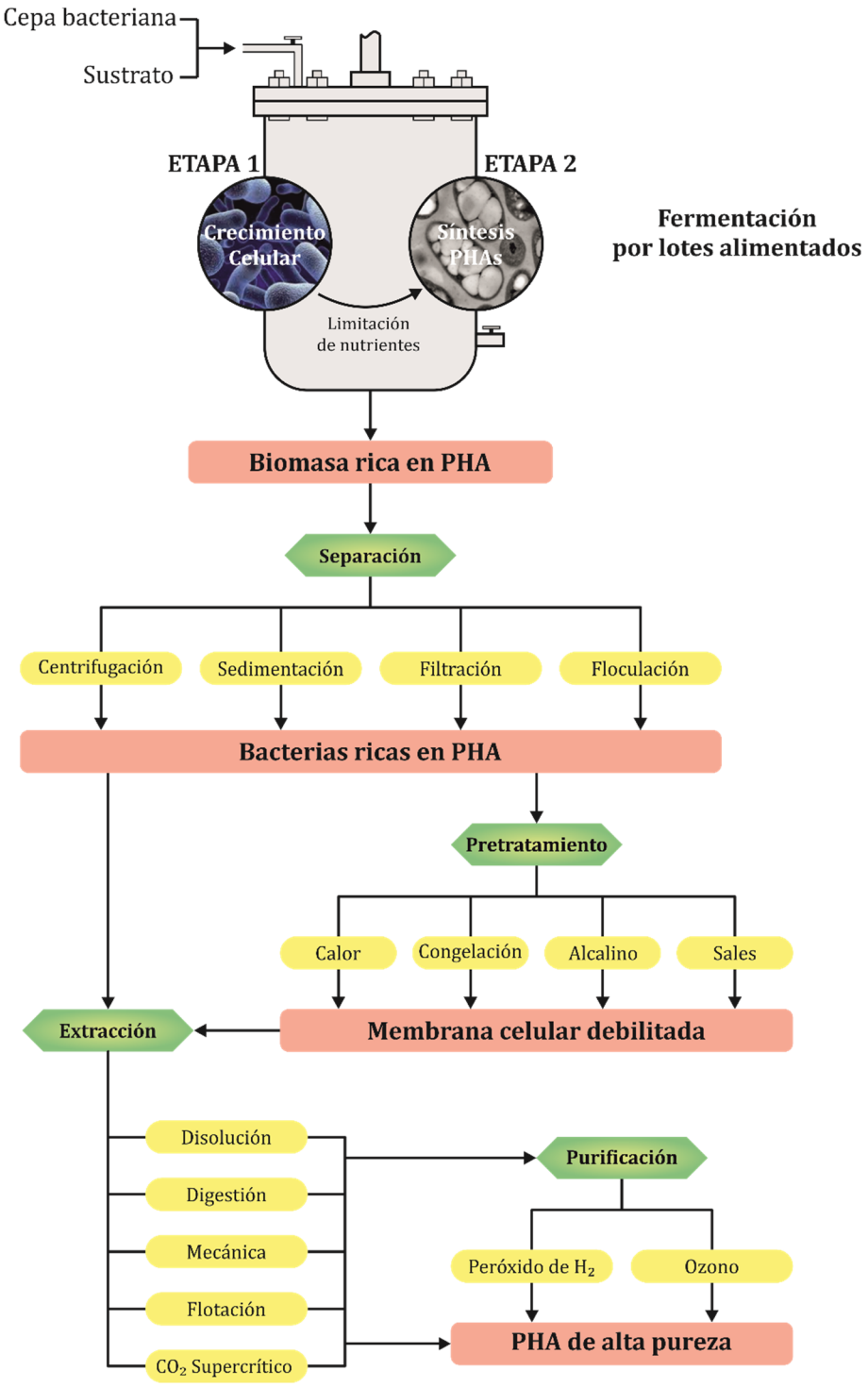

Figura I.19. Esquema general del proceso de obtención de PHAs.

Como se ha observado, la producción de PHAs resulta un proceso complejo en el que el rendimiento se ve afectado por una serie de factores como el tipo de microorganismo, el tipo de sustrato, las condiciones y el tipo de fermentación y el proceso de recuperación. Esto hace que a día de hoy el proceso de producción de PHAs sea todavía un proceso costoso y con una baja eficiencia, lo cual repercute en un mayor precio del material. El elevado precio

actual de este tipo de biopolímeros es una de las principales limitaciones de su uso a nivel industrial. Este elevado coste, ha llevado a la investigación de otros sistemas de producción más económicos. Una de las alternativas más estudiadas es la producción de PHAs a partir de plantas modificadas genéticamente que son capaces de utilizar el CO_2 atmosférico y la luz solar para la síntesis del biopolímero [95-99]. Las plantas permiten obtener PHAs de una forma más económica y respetuosa con el medio ambiente, sin embargo, la síntesis a partir de plantas no es tan versátil como la síntesis microbiana en términos de tipos de PHAs que pueden producirse [100].

I.3.3. Degradación de los polihidroxialcanoatos

Los PHAs son eficientemente degradados por una gran cantidad de microorganismos y hongos presentes en la naturaleza, es por ello que este tipo de polímeros pueden ser degradados en diferentes entornos como en el suelo, en compost, en sedimento marino, en agua salada (mar), en agua dulce (lago) o en lodos de aguas residuales, aunque la velocidad de degradación dependerá de varios factores ambientales como la actividad microbiana, la humedad, la temperatura, el pH y los nutrientes del medio, así como factores propios del material, como su peso molecular, la composición del PHA, la cristalinidad y el área superficial expuesta [89].

Los microorganismos que producen PHAs bajo condiciones de limitación de nutrientes, son capaces de degradarlo y metabolizarlo intracelularmente cuando no existe dicha limitación. Sin embargo, la capacidad de producir y almacenar PHAs no garantiza la capacidad de degradarlo en el medio ambiente. En la degradación de los PHAs los microorganismos colonizan la superficie de los polímeros. Como los polímeros son demasiado grandes para ser transportados directamente a través de la pared celular, dichos microorganismos secretan depolimerasas extracelulares de PHAs que hidrolizan los enlaces éster de las cadenas poliméricas convirtiendo el polímero en los correspondientes monómeros de ácido hidroxialcanoico. Por ejemplo, el producto de la hidrólisis del PHB es el ácido R-3-hidroxibutírico o en el caso del PHBV se produce tanto 3-hidroxibutirato como 3-hidroxivalerato. Estos monómeros producidos por la hidrólisis son solubles en agua y lo suficientemente pequeños para difundirse a través de la pared celular de los microorganismos, donde son metabolizados por β-oxidación y ciclo de los ácidos tricarboxílicos (ciclo de Krebs) produciendo dióxido de carbono y agua en condiciones aeróbicas, mientras que en condiciones anaerobias también se produce metano. Generalmente, durante la degradación microbiana de los PHAs no se genera ningún subproducto dañino para el medio ambiente [101].

Los PHAs también son susceptibles a la degradación hidrolítica, es decir, la degradación producida debido al contacto del material con un medio acuoso. En la degradación hidrolítica el agua se difunde en el material produciendo la hidrólisis de grupos éster al azar en las cadenas poliméricas, dando lugar a oligómeros de menor peso molecular y al monómero principal [102]. Generalmente, la degradación hidrolítica de los PHAs es un proceso lento, aunque la velocidad de degradación dependerá de diferentes factores del medio, como el pH o la temperatura, y de factores inherentes al material, como la porosidad, el área superficial, el peso molecular, la cristalinidad o su hidrofobicidad [103, 104]. Una forma de aumentar la velocidad de degradación hidrolítica de este tipo de materiales es mediante la incorporación de aditivos amorfos o hidrofílicos al polímero, los cuales dan lugar a una mayor absorción de agua y aceleran la hidrólisis [105]. Algunos PHAs, como es el caso del PHB, presentan una elevada resistencia a la hidrólisis. En el caso particular del PHB esta resistencia relativa a la hidrólisis se debe principalmente a su elevado grado de cristalinidad que dificulta la difusión del agua a la matriz ralentizando considerablemente la degradación hidrolítica. Esto hace que dicho polímero presente una elevada estabilidad en condiciones normales de uso.

I.3.4. Aplicaciones de los polihidroxialcanoatos

Debido a las propiedades que presentan los PHAs tales como su biodegradabilidad, biocompatibilidad, no toxicidad, piezoelectricidad, insolubilidad en agua, resistencia a los rayos UV, buenas propiedades barrera, variedad de propiedades mecánicas debido a su elevada diversidad estructural y buena procesabilidad en equipos convencionales de procesado, este tipo de biopolímeros están llamados a ser los sustitutos de los polímeros de uso común. Estas propiedades hacen que los PHAs se empleen en una amplia variedad de sectores como el sector del envase para la fabricación de botellas de bebidas, en films para envases de alimentos o como recubrimiento de hojas de papel destinadas a proteger productos alimentarios, así como en el sector agrícola para la fabricación de films para el mantillo o como sistema de liberación controlada de insecticidas o herbicidas. Pero es en el sector médico y farmacéutico donde los PHAs han experimentado un mayor desarrollo, empleándose en multitud de aplicaciones como en la fabricación de productos cardiovasculares (válvulas cardíacas, stents coronarios, injertos vasculares, vasos sanguíneos), en sistemas de liberación controlada de medicamentos, para la cura de heridas (suturas, manguitos, bastoncillos, apósitos) o en ortopedia (tornillos, matrices para ingeniería de tejidos, sustitutos de injertos óseos) [83].

I.4. TECNOLOGÍA DE POLI(3-HIDROXIBUTIRATO)

I.4.1. Estructura y propiedades generales del poli(3-hidroxibutirato)

El poli(3-hidroxibutirato), P(3HB) o PHB, fue el primer PHA en ser descubierto y también es el PHA mejor estudiado y caracterizado. El PHB es un poliéster lineal de 3-hidroxibutirato producido por una gran cantidad de bacterias de la familia de los *Alcaligenes*, *Azobacter*, *Bacillus* y *Pseudomonas*, siendo la *Alcaligenes eutrophus* (o *Ralstonia eutrophus*) la más ampliamente utilizada debido a su tasa de reproducción y a la capacidad de acumulación de grandes cantidades de polímero [106]. Como se ha comentado anteriormente, el polímero se produce y acumula por microorganismos como respuesta a una limitación de nutrientes en el medio, utilizándolo como almacenamiento de energía para evitar la inanición si un elemento esencial deja de estar disponible [107]. La biosíntesis del PHB comienza con la condensación de dos moléculas de acetil-CoA para dar acetoacetil-CoA, que posteriormente es reducida al monómero hidroxibutiril-CoA que polimeriza formando PHB [108].

El PHB producido biológicamente, cuya estructura química se muestra en la Figura I.20, es un poliéster estereoregular semicristalino con una configuración R, una densidad de 1,26 g cm^{-3} y un peso molecular que varía en el rango de 1×10^{4}–3×10^{6} g mol^{-1} con una polidispersidad en torno a dos [89]. Dicho peso molecular dependerá de diversos factores como el microorganismo productor, las condiciones de cultivo y el método de extracción empleado [109]. Además, el PHB se caracteriza por presentar un elevado grado de cristalinidad que puede variar entre el 55 y 80% [110].

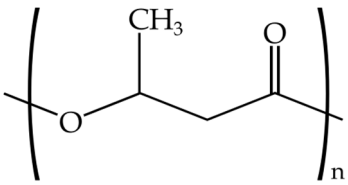

Poli(3-hidroxibutirato) (PHB)

Figura I.20. Representación esquemática de la unidad monomérica del poli(3-hidroxibutirato).

Este biopolímero termoplástico se caracteriza por ser completamente biodegradable y biocompatible; también presenta buenas propiedades barrera, es insoluble en agua, presenta resistencia a los rayos UV, tiene propiedades piezoeléctricas, actividad

óptica, así como propiedades térmicas y mecánicas similares a las de polímeros de naturaleza sintética como el polipropileno, lo que hacen que sea un material muy interesante a nivel industrial en sectores como el del envase de alimentos, el sector agrícola o el sector biomédico [111]. Además, el PHB puede moldearse por extrusión, inyección e inyección soplado u obtener fibras y films mediante los equipos convencionales empleados en la transformación de polímeros sintéticos [89]. Sin embargo, a pesar de sus numerosas ventajas, su aplicación generalizada a nivel industrial es muy reducida debido a que presenta una serie de inconvenientes que limitan su uso, entre los que se encuentra su elevada fragilidad, su baja estabilidad térmica durante el procesado y su elevado coste.

I.4.2. Propiedades mecánicas del poli(3-hidroxibutirato)

El PHB se caracteriza por presentar una resistencia a tracción y un módulo elástico similar o superior al de otros polímeros termoplásticos sintéticos como el polipropileno (PP). Sin embargo, a diferencia de éste, el PHB presenta una elevada rigidez y fragilidad con un bajo alargamiento a la rotura, en torno al 5%, y una baja absorción de energía a impacto. En la Tabla I.1 se puede observar una comparativa de las propiedades físicas del PHB con la de otros polímeros de origen sintético como el PP y el LDPE.

Tabla I.1. Propiedades físicas del PHB y de polímeros sintéticos de uso común como el PP y el LDPE [108].

Propiedad	**Polímero**		
	PHB	**PP**	**LDPE**
Resistencia a tracción (MPa)	40	38	10
Módulo elástico (GPa)	3,5	1,5	0,2
Alargamiento a la rotura (%)	5	400	620
Temperatura de fusión (°C)	175	176	110
Temperatura de transición vítrea (°C)	4	-10	-30
Densidad (g cm^{-3})	1,26	0,91	0,92

La elevada fragilidad del PHB es uno de los principales inconvenientes que limita su aplicabilidad industrial. Existen diferentes factores que contribuyen a dicha fragilidad, todos ellos relacionados con la cristalinidad del material. Por un lado, la baja densidad de

nucleación debido a la elevada pureza del polímero, junto con el alto grado de cristalinidad y la baja velocidad de cristalización, hacen que el PHB cristalice lentamente formando grandes esferulitas, las cuales pueden presentar grietas internas, tanto circunferenciales como radiales, debidas a las tensiones térmicas que se producen durante el enfriamiento de las mismas desde las altas temperaturas de cristalización hasta la temperatura ambiente. Estas grietas pueden actuar como punto de concentración de tensiones, fragilizando el material [112-114]. Otros factores que afectan de forma significativa a la fragilidad del PHB son el proceso de cristalización secundaria de la fase amorfa durante el almacenamiento a temperatura ambiente del polímero y el envejecimiento físico debido a la cercanía de la temperatura de transición vítrea (T_g) del polímero con la temperatura ambiente [115]. Ambos procesos están englobados dentro del envejecimiento del PHB, que es el principal factor que afecta a la fragilidad del polímero.

I.4.2.1. Envejecimiento del poli(3-hidroxibutirato)

El envejecimiento del PHB provoca una fragilidad progresiva del material durante su almacenamiento a temperatura ambiente o su vida en servicio. Dicho aumento de la fragilidad con el tiempo es uno de los principales inconvenientes del PHB que limita notablemente sus posibles aplicaciones industriales.

El PHB recién procesado presenta un comportamiento dúctil, pero cuando el producto moldeado se almacena a temperatura ambiente sufre un proceso de envejecimiento progresivo que da lugar a una fragilización del material, provocando una drástica disminución del alargamiento a la rotura [116]. En la actualidad se proponen principalmente dos fenómenos que pueden contribuir a dicho envejecimiento: la cristalización secundaria y el envejecimiento físico, aunque no existe un consenso sobre el origen físico de la fragilización del PHB [117].

La teoría de la cristalización secundaria propuesta por De Koning *et al.* [118], atribuye la fragilidad a la cristalización progresiva de la fase amorfa durante el almacenamiento a temperatura ambiente. Durante la cristalización secundaria se forman pequeños cristales que restringen el movimiento de la fase amorfa, lo cual conlleva un aumento de la fragilización del material que reduce notablemente su rendimiento mecánico. El impacto negativo de la cristalización secundaria puede minimizarse mediante un proceso de recocido a altas temperaturas, con el que se consigue aliviar las restricciones impuestas por los cristales a las cadenas amorfas, mejorando la tenacidad y la ductilidad del material;

además, se evita en gran medida la posterior cristalización secundaria, manteniendo gran parte de la tenacidad y ductilidad alcanzada tras el recocido [118, 119].

El fenómeno del envejecimiento físico fue estudiado por Struik [120, 121] para polímeros amorfos y semicristalinos, y posteriormente fue investigado por Scandola *et al.* [122] para el PHB. Esta teoría atribuye la fragilización a una disminución del volumen libre por la reorganización de las cadenas poliméricas cuando el material se almacena a temperaturas cercanas a las de su T_g. Según esta teoría, cuando un polímero se enfría rápidamente a temperaturas inferiores a su T_g, la parte amorfa no se encuentra en un estado de equilibrio, ya que el calor ha sido extraído tan rápido que las cadenas no han alcanzado su volumen libre de equilibrio. Si el material se almacena a temperaturas cercanas pero inferiores a la de su T_g, las cadenas poliméricas se reorganizan lentamente debido a la movilidad residual de las mismas, reduciendo el volumen libre disponible hacia el valor de equilibrio. Esta disminución del volumen libre da lugar a una menor movilidad de las cadenas poliméricas, aumentando así la fragilidad del material. La diferencia entre los polímeros amorfos y semicristalinos es que en estos últimos los cristales pueden restringir el movimiento de la parte amorfa, aumentando la T_g con respecto a la del material completamente amorfo, por lo que la temperatura a la que puede producirse el envejecimiento físico se eleva ligeramente [123]. Algunos autores como Biddlestone *et al.* [124] o De Koning *et al.* [118] argumentaron que el envejecimiento físico no influía en la fragilización del PHB ya que su T_g es demasiado baja para que se produzca el fenómeno de envejecimiento físico a temperatura ambiente, lo cual sería cierto en un modelo de dos fases (amorfo-cristalino) de la morfología del PHB. Sin embargo, existen estudios que desvelan una morfología del PHB con tres fases: una fase cristalina, una fase amorfa móvil y una tercera fase amorfa rígida cuya movilidad es mucho más reducida y, por tanto, su T_g es más elevada, permitiendo el proceso de envejecimiento físico [125].

Por tanto, el proceso de fragilización del PHB podría ser debido a la presencia de ambos fenómenos, tanto el de envejecimiento físico como la cristalización secundaria [117, 126].

I.4.3. Propiedades térmicas del poli(3-hidroxibutirato)

El PHB es un material termoplástico altamente cristalino que presenta una temperatura de fusión relativamente alta, entre los 170 y 180 °C, y una temperatura de transición vítrea baja, entre 0 y 5 °C [127]. Sin embargo, el PHB se caracteriza por presentar una baja estabilidad térmica durante el procesado, ya que su degradación térmica comienza

a temperaturas cercanas a la de su fusión, entre los 170 y 200 °C; esto provoca que la ventana de procesado del PHB sea muy estrecha [128]. La reducida ventana de procesado que presenta el PHB es otra de sus principales limitaciones.

La degradación térmica del PHB se produce casi exclusivamente mediante una reacción de escisión aleatoria de cadenas no radicalaria (*cis*-eliminación). La escisión aleatoria de la cadena tiene lugar en los grupos éster, ocasionando un estado de transición de un anillo éster de seis miembros, el cual se descompone dando lugar a la formación de ácido crotónico y oligómeros de PHB [129, 130]. El mecanismo de degradación térmica se observa en la Figura I.21. La degradación térmica del PHB provoca una reducción del peso molecular del biopolímero, lo cual afecta significativamente a sus propiedades mecánicas, así como a su viscosidad en estado fundido [131, 132].

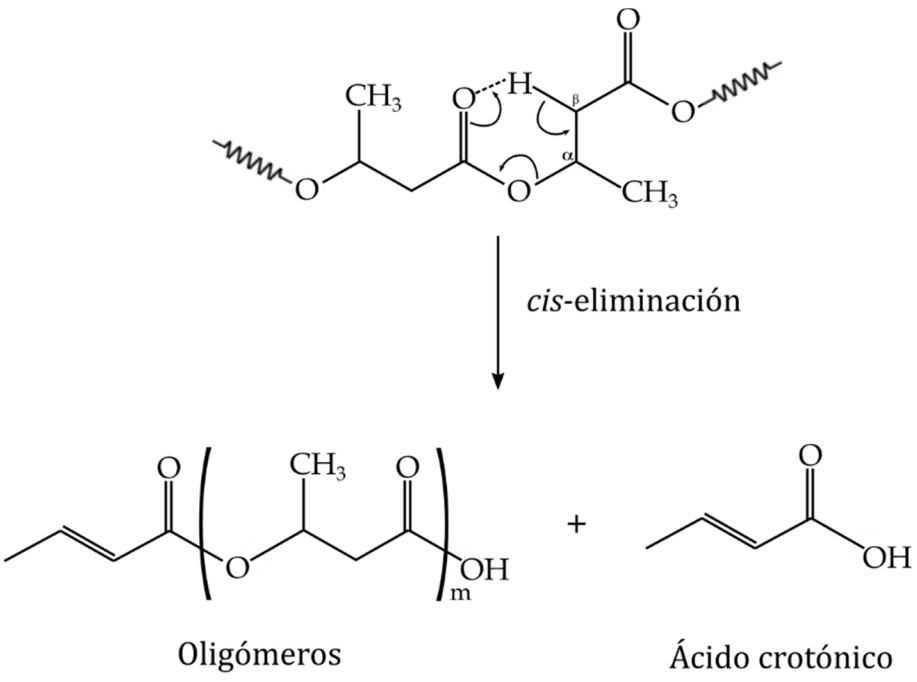

Figura I.21. Representación esquemática del mecanismo de degradación térmica del poli(3-hidroxibutirato) mediante *cis*-eliminación.

I.4.4. Propiedades barrera del poli(3-hidroxibutirato)

Las propiedades barrera son importantes en muchas aplicaciones, pero tienen especial relevancia en el sector del envase y embalaje de alimentos. El vapor de agua, el oxígeno y el dióxido de carbono son tres de los principales permeantes estudiados para las aplicaciones de envasado de alimentos, ya que estos pueden transferirse desde el exterior

al interior del envase, o viceversa, a través de la pared del envase polimérico, produciendo cambios en la calidad del producto envasado y en su vida útil [133].

La barrera de un polímero al oxígeno es de gran importancia en el envasado de alimentos, una mala propiedad barrera al oxígeno acelerará la degradación oxidativa del alimento, afectando a su sabor, a su color y a su estabilidad microbiana. Por tanto, en el sector del envase es interesante que el polímero presente un bajo coeficiente de permeabilidad al oxígeno con el principal objetivo de retrasar la oxidación y alargar la vida útil del producto. Generalmente, los polímeros biodegradables presentan una menor permeabilidad que los polímeros sintéticos usados en aplicaciones de envase como el PET. Existen numerosos estudios en los que se demuestra la menor permeabilidad al oxígeno del PHB con respecto a polímeros petroquímicos empleados en envases como el PET, el PP o el HDPE [134, 135]. Además, la permeabilidad al oxígeno del PHB también es muy inferior a la de otros polímeros biodegradables como el PLA [136].

La propiedad barrera al vapor de agua también es de gran importancia en el sector del envase, principalmente en aquellos productos cuyo deterioro físico está relacionado con su equilibrio de humedad, por ejemplo, en el caso de los productos frescos es importante evitar su deshidratación, mientras que en otros productos, por ejemplo, los productos de panadería, es importante evitar la penetración de agua. El PHB presenta una buena propiedad barrera frente al vapor de agua, con valores de permeabilidad similares a los de otros polímeros termoplásticos convencionales de origen petroquímico como el PET o el PVC [137].

El PHB también presenta una baja permeabilidad al CO_2, con valores de permeabilidad inferiores a los del PET y el PVC no plastificado, los cuales son considerados materiales poco permeables al CO_2, y muy inferiores a los de otros polímeros biodegradables como el PLA [137]. También se ha observado que el PHB presenta una menor permeabilidad a los compuestos aromáticos en comparación con el PET, lo cual es importante a la hora de preservar el sabor de los alimentos envasados [138].

En la Tabla I.2. se muestra una comparativa de los valores de permeabilidad al agua, al oxígeno y al dióxido de carbono del PHB con respecto a otros polímeros biodegradables como el PHBV, el PLA y la PCL, y no biodegradables como el LDPE, el PET, el PP, el PS y el PVC.

Tabla I.2. Permeabilidad al vapor de agua, al oxígeno y al dióxido de carbono de diferentes biopolímeros y polímeros de uso común [139].

Polímero	Permeabilidad		
	H_2O[a] (g mm m^{-2} dia^{-1})	O_2[b] (ml mm m^{-2} dia^{-1} atm^{-1})	CO_2[b] (ml mm m^{-2} dia^{-1} atm^{-1})
PHB	1–5	2–10	3
PHBV	1–3	5–14	-
PLA	5–7	15–25	35–70
PCL	300	20–200	-
LDPE	0,5–2	50–200	800–1000
PET	0,5–2	1–5	15–20
PP	0,2–0,4	50–100	200–400
PS	1–4	100–150	250–500
PVC	1-2	2–8	10-15

[a] 23–38°C, 50–90% RH.

[b] 23°C, 0–50% RH.

La cristalinidad de los polímeros tiene una gran influencia en las propiedades barrera del mismo [140]. Se cree que los dominios cristalinos alteran la ruta de difusión de las moléculas, ya que se supone que la permeabilidad no se produce dentro ni a través de un cristal, dando lugar a una mejora de las propiedades barrera del material. Por tanto, la elevada cristalinidad del PHB hace que se trate de un material con buenas propiedades barrera, comparable a la de polímeros sintéticos como el PVC o el PET; esto, unido a otras propiedades inherentes al polímero como su biodegradabilidad, hacen que se trate de un material muy interesante para su uso en aplicaciones como las de envases de alimentos.

I.4.5. Usos del poli(3-hidroxibutirato) en ingeniería

Como se ha comentado, el PHB es un polímero biodegradable y biocompatible, ya que su degradación no genera ningún compuesto tóxico. Además, los productos de su degradación, como el ácido R-3-hidroxibutírico, están presentes de forma natural en la sangre humana [102]. Todo esto, unido a sus propiedades piezoeléctricas, que le proporcionan osteoconductividad, y su baja respuesta inflamatoria, hacen que dicho

material sea un potencial candidato para su uso en el sector biomédico. El PHB ha encontrado exitosas aplicaciones en ingeniería de tejidos para la regeneración o reparación de tejidos óseos, cardiovasculares, subcutáneos, nerviosos o de válvulas cardiacas. Otras aplicaciones biomédicas en las que se emplea el PHB son los implantes ortopédicos, las suturas y mallas quirúrgicas, en apósitos para heridas o como material para la liberación controlada de fármacos [141-144].

Otro sector donde el PHB puede llegar a ser de gran interés es el sector del envasado de productos. Gracias a propiedades como su biodegradabilidad, sus buenas propiedades barrera y su resistencia a la luz UV, el PHB es un potencial sustituto de los plásticos sintéticos en aplicaciones de envasado. Algunas investigaciones, como las realizadas por Bucci *et al.* [106, 145] han demostrado que el PHB puede ser un buen sustituto del PP en el envasado de alimentos. Sin embargo, hoy en día, a pesar de emplearse en algunos productos desechables como botellas o material de embalaje [146], su uso no está extendido en dicho sector debido principalmente a sus limitaciones, como son su elevada fragilidad y su elevado coste, que hacen que no resulte un material competitivo mecánica y económicamente en un sector donde la ductilidad y el precio del material son de gran importancia. Es por ello, que la gran mayoría de los estudios realizados sobre el PHB están centrados en disminuir los costes de producción del polímero, utilizando microorganismos con mayor capacidad productora o introduciendo substratos más económicos, y en la mejora de las propiedades dúctiles del material mediante sistemas de plastificación o mediante la mezcla física con otros polímeros más dúctiles. Todo ello con el objetivo de obtener formulaciones basadas en PHB que pueda llegar a ser competitivas mecánica y económicamente con los actuales materiales sintéticos empleados en el sector del envase.

Gracias a sus propiedades, el PHB también puede ser de gran importancia en el sector de la agricultura para su uso en films biodegradables, como sustitutos de los actuales films de PE empleados para proteger los cultivos del sol, de los animales e insectos y para mantener la humedad. Además, la capacidad del PHB para ser procesado en múltiples formas junto con su degradación enzimática relativamente lenta, hacen que este biopolímero resulte de especial interés en el sector agrícola como matriz (en forma de "*pellets*", de films o macropartículas) para la carga y la posterior liberación lenta, dirigida y controlada de compuestos químicos como insecticidas, fungicidas, herbicidas o fertilizantes [147-149].

I.5. TECNOLOGÍAS DE MODIFICACIÓN DE FORMULACIONES DE POLÍMEROS

Como se ha podido ver en el anterior apartado, el PHB presenta una serie de limitaciones, como son su elevada fragilidad y su baja estabilidad térmica, que, junto a su elevado coste, impiden a día de hoy que dicho biopolímero sea utilizado ampliamente a nivel industrial. Con el fin de mejorar dichas limitaciones y aumentar la competitividad de dicho polímero es necesario llevar a cabo una serie de metodologías de actuación para la modificación de las propiedades del PHB.

A continuación se describen de forma general las metodologías más empleadas para mejorar las propiedades de los polímeros, como son la plastificación, la mezcla física con otros polímeros y la incorporación de nanocargas.

I.5.1. Plastificación

Uno de los métodos más empleados para la mejora de las propiedades de los polímeros es el empleo de plastificantes. Según la Unión Internacional de Química Pura y Aplicada (IUPAC), un plastificante es una sustancia o material que se incorpora en un material (generalmente un plástico o elastómero) con el objetivo de aumentar su flexibilidad, su procesabilidad o su distensibilidad [150]. Por tanto, el principal objetivo de la plastificación es mejorar la flexibilidad y la procesabilidad de un polímero.

La incorporación de plastificantes en los polímeros provoca una disminución de las propiedades mecánicas resistentes como la dureza, la resistencia a tracción o el módulo elástico y aumenta las propiedades mecánicas dúctiles como el alargamiento a la rotura o la absorción de energía a impacto. Por otra parte, da lugar a un aumento de la flexibilidad de las cadenas poliméricas provocando una disminución de la viscosidad del material y un aumento del índice de fluidez, lo cual facilita su procesabilidad. Las propiedades térmicas de los polímeros también se ven afectadas por la incorporación de plastificantes, obteniéndose generalmente menores temperaturas de fusión y de transición vítrea, lo que implica un menor gasto energético durante su procesado. Otras de las propiedades de los polímeros que se ven afectadas tras la incorporación de plastificantes son el grado de cristalización, la humectabilidad, la transparencia, la permeabilidad al gas, la conductividad eléctrica o la velocidad de degradación en polímeros biodegradables [151].

Existen diferentes teorías clásicas que intentan explicar el efecto de la plastificación en los polímeros. Entre ellas, las principales son: la teoría de la lubricación, la teoría de gel y la teoría del volumen libre [152]. De forma general, sostienen que el bajo peso molecular de los plastificantes permite que estos ocupen espacios intermoleculares entre las cadenas

poliméricas reduciendo las fuerzas de atracción secundaria entre ellas y modificando la organización tridimensional de los polímeros, dando lugar a una disminución de la energía requerida para el movimiento molecular [153]. La Figura I.22 muestra una representación del efecto de la plastificación en polímeros según las diferentes teorías clásicas.

La teoría de la lubricación considera que el plastificante actúa como un lubricante de las cadenas poliméricas, es decir, se inserta entre las cadenas del polímero reduciendo la fricción intermolecular y facilitando el movimiento de las moléculas cuando el polímero plastificado se somete a un esfuerzo. Este modelo supone que las macromoléculas se deslizan unas sobre otras cuando el material plastificado se somete a un esfuerzo. Por tanto, según esta teoría, la rigidez del polímero viene dada por las fricciones internas de las moléculas debidas a las irregularidades de la superficie y el plastificante actúa como lubricante.

La teoría de gel considera que el polímero plastificado consiste en una red tridimensional con moléculas de plastificante unidas a las cadenas poliméricas mediante fuerzas secundarias débiles. En este caso, el plastificante actúa rompiendo los enlaces y las interacciones entre las cadenas del polímero haciendo que una proporción de estos centros activos queden enmascarados detrás de las moléculas de plastificante, deshabilitándolos como potencial punto de entrecruzamiento con otras cadenas colindantes. Al presentar menos cantidad de enlaces, las cadenas presentan una mayor movilidad, haciendo que el material sea más dúctil. Según esta teoría, la rigidez del polímero viene dada por las uniones existente entre las cadenas del polímero y el plastificante actúa reduciendo el número de sitios activos capaces de formar enlace.

La teoría del volumen libre es la más aceptada hoy en día y supone que existe un espacio libre entre las moléculas poliméricas que permite su movimiento, por tanto, los polímeros rígidos presentan poco espacio libre. Tras la incorporación del plastificante al polímero se consigue aumentar el volumen libre, obteniéndose un mayor espacio que permite un mayor movimiento de las cadenas poliméricas, mejorando así su ductilidad y disminuyendo su temperatura de transición vítrea.

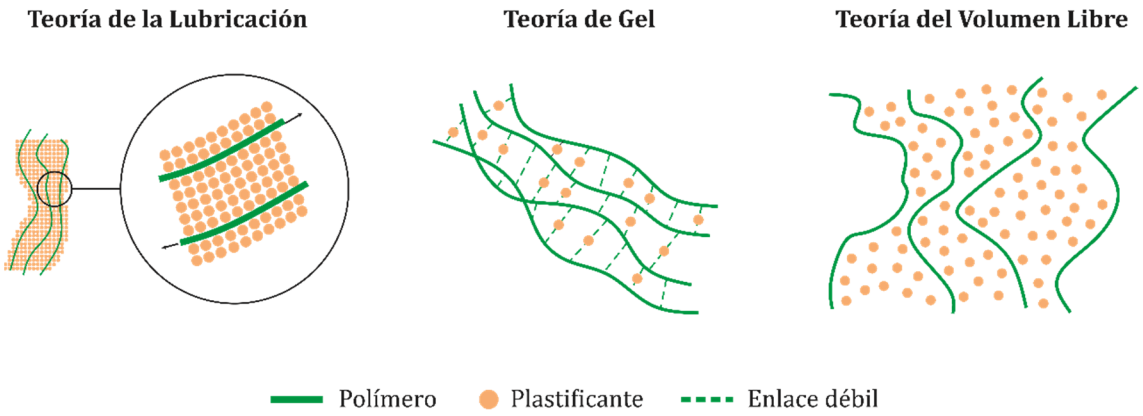

Figura I.22. Representación del efecto de la plastificación según las diferentes teorías clásicas [153].

La compatibilidad entre el plastificante y el polímero es un factor fundamental para que se produzca una plastificación efectiva y obtener así las propiedades deseadas en el material. Son numerosos los parámetros que pueden influir en la compatibilidad del sistema, como la polaridad, los enlaces de hidrógeno, los grupos químicos, el peso molecular, la longitud de las cadenas, la cristalinidad, la constante dieléctrica o los parámetros de solubilidad.

Existen diferentes maneras de estimar la compatibilidad entre el plastificante y el polímero. Una de las más empleadas es comparando los parámetros de solubilidad (δ) de ambos componentes. Se ha observado que cuanto más cerca estén los valores del parámetro de solubilidad del plastificante y del polímero, mayor será la miscibilidad entre ambos y, por tanto, se obtendrá una mayor compatibilidad [154]. Aunque el parámetro de solubilidad puede ser de gran ayuda para la elección del plastificante adecuado, un valor de solubilidad cercano no siempre es indicativo de una plastificación efectiva, ya que puede ocurrir que ambos componentes sean incompatibles produciéndose una mala o nula plastificación, afectando a las propiedades del material. Por tanto, conocer el parámetro de solubilidad no es suficiente para estimar la eficacia de la plastificación.

I.5.1.1. Clasificación de los plastificantes

Los plastificantes pueden clasificarse de diferente forma atendiendo a varias de características como el peso molecular, la compatibilidad con el polímero, etc. Una de las principales clasificaciones de los plastificantes está relacionada con su estructura y peso molecular, obteniéndose principalmente dos grandes grupos: los plastificantes monoméricos y los plastificantes poliméricos [155]:

- Los plastificante monoméricos se caracterizan por presentar una estructura molecular simple y única. Su peso molecular varía de forma general entre los 300 y los 600 g mol^{-1}. Suelen ser líquidos, con un alto punto de ebullición, baja viscosidad y buena solubilidad en la mayoría de los polímeros. Además, poseen buena estabilidad térmica y química. Sin embargo, este tipo de plastificantes se caracteriza por presentar una alta volatilidad y una baja resistencia a la migración, por lo que su permanencia en el polímero es limitada. Este tipo de plastificantes es el más empleado a nivel industrial, excepto en aquellas aplicaciones donde la permanencia del plastificante en el polímero es importante, como en el sector de la alimentación.

- Los plastificantes poliméricos están formados mediante la repetición de unidades moleculares y se caracterizan por presentar un amplio rango de especies moleculares, con una distribución del peso molecular que varía de un producto a otro. El peso molecular de los plastificantes poliméricos es elevado y puede variar entre los 1000 y los 10.000 g mol^{-1}, lo que contribuye a aumentar su permanencia en el polímero. Este tipo de plastificantes poseen una baja volatilidad y migración, por lo que presentan una buena permanencia en el polímero en comparación con los plastificante monoméricos. Sin embargo, presentan alta viscosidad lo que dificultan su procesado y, generalmente, son más caros, limitando su uso únicamente a aquellas aplicaciones donde la permanencia del plastificante en el polímero es imprescindible.

Los plastificantes también se pueden clasificar como primarios o secundarios dependiendo de su compatibilidad con el polímero [153]:

- Los plastificantes primarios son aquellos totalmente solubles en el polímero, incluso a altas concentraciones; es decir, presentan buena compatibilidad con el polímero. Este tipo de plastificantes no suelen exudar del material final debido a la buena compatibilidad y gelifican el polímero rápidamente en el rango de temperaturas de procesado. A diferencia de los plastificantes secundarios, estos suelen emplearse en solitario en el proceso de plastificación del polímero.

- Los plastificantes secundarios se caracterizan por presentar una compatibilidad limitada con el polímero. Este tipo de plastificantes suele exudar, provocando que la superficie del material sea pegajosa si se emplean en exceso. Además, presentan una capacidad de gelificación baja y, normalmente, se usan conjuntamente con

plastificantes primarios con el objetivo de mejorar una cierta propiedad o para reducir costes.

I.5.1.2. Aceites vegetales como plastificantes

A medida que la industria del plástico crece, aumenta la demanda de plastificantes. Sin embargo, durante los últimos años ha habido un aumento de la preocupación por los efectos en la salud humana y en el medio ambiente por el uso de plastificantes de origen petroquímico como los ftalatos, trimelitatos, dicarboxilatos o adipatos. Estos plastificantes son cuestionados por problemas de toxicidad asociados a la migración de los mismos. Además, la gran mayoría de los plastificantes tradicionales de origen petroquímico que se emplean en el procesado de polímeros sintéticos no son efectivos en algunos polímeros biodegradables, como es el caso del PHB. Es por ello que, actualmente, existe un creciente interés en el estudio y uso de plastificantes obtenidos a partir de recursos naturales, los cuales se caracterizan por presentar una baja toxicidad y baja migración. Además, este interés por el desarrollo y empleo de plastificantes naturales también se ha visto positivamente afectado por el aumento del empleo de polímeros biodegradables a nivel industrial, ya que es importante e interesante que los plastificantes utilizados en este grupo de biopolímeros presenten biodegradabilidad con el objetivo de no modificar la sostenibilidad de los materiales.

Entre los plastificantes de origen renovable, los aceites vegetales presentan un especial interés, ya que estos ofrecen una ruta prometedora para su uso a nivel industrial debido a que son fáciles de obtener, baratos, biodegradables, no presentan toxicidad y su migración es inferior a la de otros plastificantes. Los aceites vegetales se extraen de plantas y árboles oleaginosos y se encuentran en abundancia en todo el planeta, lo que los hace ideales como materia prima para su uso como plastificantes. Algunos de los aceites vegetales más empleados como plastificantes son el aceite de palma, el aceite de soja, el aceite de canola, el aceite de girasol, el aceite de maíz, el aceite de oliva, el aceite de semilla de algodón, el aceite de linaza o el aceite de colza. Químicamente, los aceites vegetales consisten principalmente en triglicéridos, que son el producto de la esterificación del glicerol (una cadena de tres átomos de carbono que están unidos a tres grupos hidroxilo) y tres cadenas de ácidos grasos [156]. En la Figura I.23 se puede observar la estructura genérica de los triglicéridos.

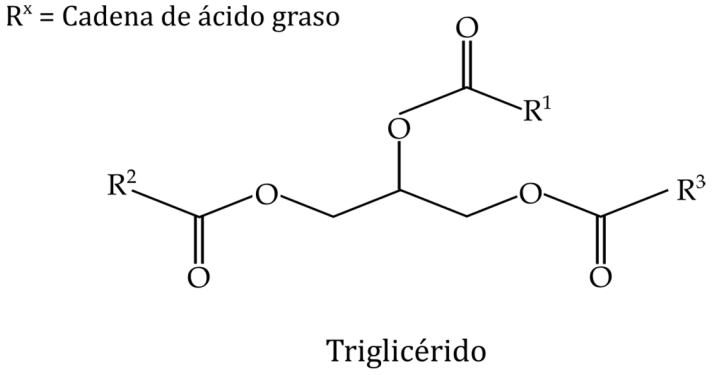

Figura I.23. Representación esquemática de la estructura química genérica de los triglicéridos.

Un ácido graso es un ácido carboxílico unido a una larga cadena alifática de carbono no ramificada. La mayoría de los ácidos grasos que se encuentran en los aceites vegetales comunes presentan una longitud entre 14 y 22 átomos de carbono, y en algunos de ellos aparecen uno o varios dobles enlaces carbono–carbono o insaturaciones. Cada aceite vegetal contiene diferentes composiciones de ácidos grasos que dependerán del tipo de planta y de las condiciones de crecimiento de la misma. La Tabla I.3 muestra la fórmula química y la estructura de los ácidos grasos más comunes presentes en los aceites vegetales, mientras que la Tabla I.4 muestra la distribución de ácidos grasos en los aceites vegetales más comunes.

Tabla I.3. Fórmula, contenido de carbono y representación gráfica de la estructura de los ácidos grasos más comunes presentes en aceites vegetales.

Ácido graso	Fórmula	C_T:C=C[a]	Estructura
Mirístico	$C_{14}H_{28}O_2$	14:0	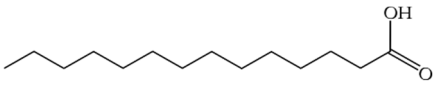
Miristoleico	$C_{14}H_{26}O_2$	14:1	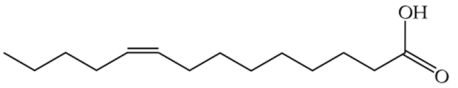
Palmítico	$C_{16}H_{32}O_2$	16:0	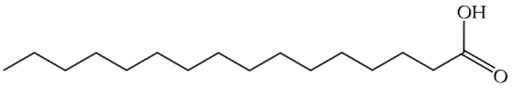
Palmitoleico	$C_{16}H_{30}O_2$	16:1	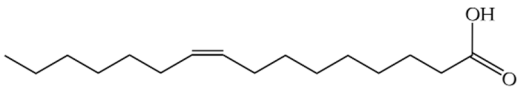
Margárico	$C_{17}H_{34}O_2$	17:0	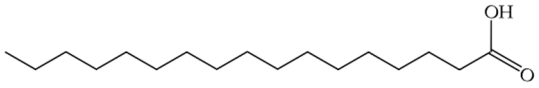
Margaroleico	$C_{17}H_{32}O_2$	17:1	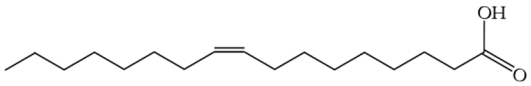
Esteárico	$C_{18}H_{36}O_2$	18:0	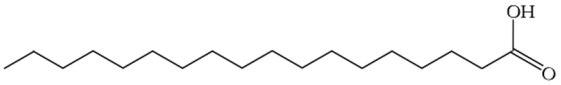
Oleico	$C_{18}H_{34}O_2$	18:1	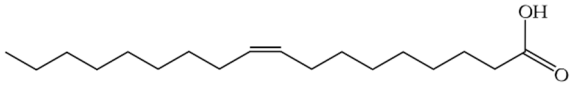
Linoleico	$C_{18}H_{32}O_2$	18:2	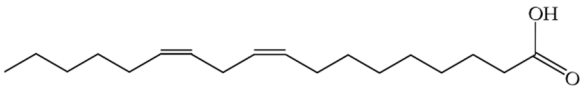
Linolénico	$C_{18}H_{30}O_2$	18:3	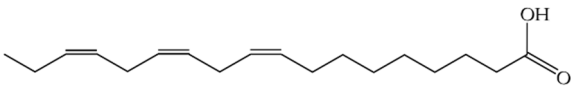
Araquídico	$C_{20}H_{40}O_2$	20:0	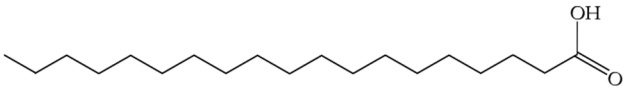

[a] Número total de carbonos (C_T):Número de dobles enlaces (C=C).

Tabla I.4. Distribución en porcentaje de ácidos grasos en varios aceites vegetales [157].

Ácido graso	Canola	Maíz	Algodón	Linaza	Oliva	Palma	Colza	Soja
Mirístico	0,1	0,1	0,7	0,0	0,0	1,0	0,1	0,1
Miristoleico	0,0	0,0	0,0	0,0	0,0	0,0	0,0	0,0
Palmítico	4,1	10,9	21,6	5,5	13,7	44,0	3,0	11,0
Palmitoleico	0,3	0,2	0,6	0,0	1,2	0,2	0,2	0,1
Margárico	0,1	0,1	0,1	0,0	0,0	0,1	0,0	0,0
Margaroleico	0,0	0,0	0,1	0,0	0,0	0,0	0,0	0,0
Esteárico	1,8	2,0	2,6	3,5	2,5	4,1	1,0	4,0
Oleico	60,9	25,4	18,6	19,1	71,1	39,3	13,2	23,4
Linoleico	21,0	59,6	54,4	15,3	10,0	10,0	13,2	53,2
Linolénico	8,8	1,2	0,7	56,6	0,6	0,4	9,0	7,8
Araquídico	0,7	0,4	0,3	0,0	0,9	0,3	0,5	0,3
Gadoleico	1,0	0,0	0,0	0,0	0,0	0,0	9,0	0,0
Eicosadienoico	0,0	0,0	0,0	0,0	0,0	0,0	0,7	0,0
Behénico	0,3	0,1	0,2	0,0	0,0	0,1	0,5	0,1
Erúcico	0,7	0,0	0,0	0,0	0,0	0,0	49,2	0,0
Lignocérico	0,2	0,0	0,0	0,0	0,0	0,0	1,2	0,0

Los aceites vegetales presentan dos características químicas que los sitúan como buenos plastificantes. La primera es que las cadenas de ácidos grasos pueden mezclarse e intercalarse entre las cadenas poliméricas, aumentando el espacio intermolecular y facilitando la movilidad. La segunda es que los grupos éster pueden interactuar con las cadenas poliméricas mejorando la compatibilidad. Además de los grupos éster, la estructura de triglicéridos de los aceites vegetales presentan otros sitios reactivos como son los dobles enlaces de los ácidos grasos insaturados, entre los que destacan el oleico, el linoleico y el linolénico con uno, dos y tres dobles enlaces carbono-carbono respectivamente, y que son los que están más presentes en los aceites vegetales más comunes, como se observa en la Tabla I.4. Es precisamente la reactividad de dichas insaturaciones, la que permite realizar modificaciones para obtener nuevas estructuras que incrementen la compatibilidad de los aceites vegetales con el polímero a plastificar [153].

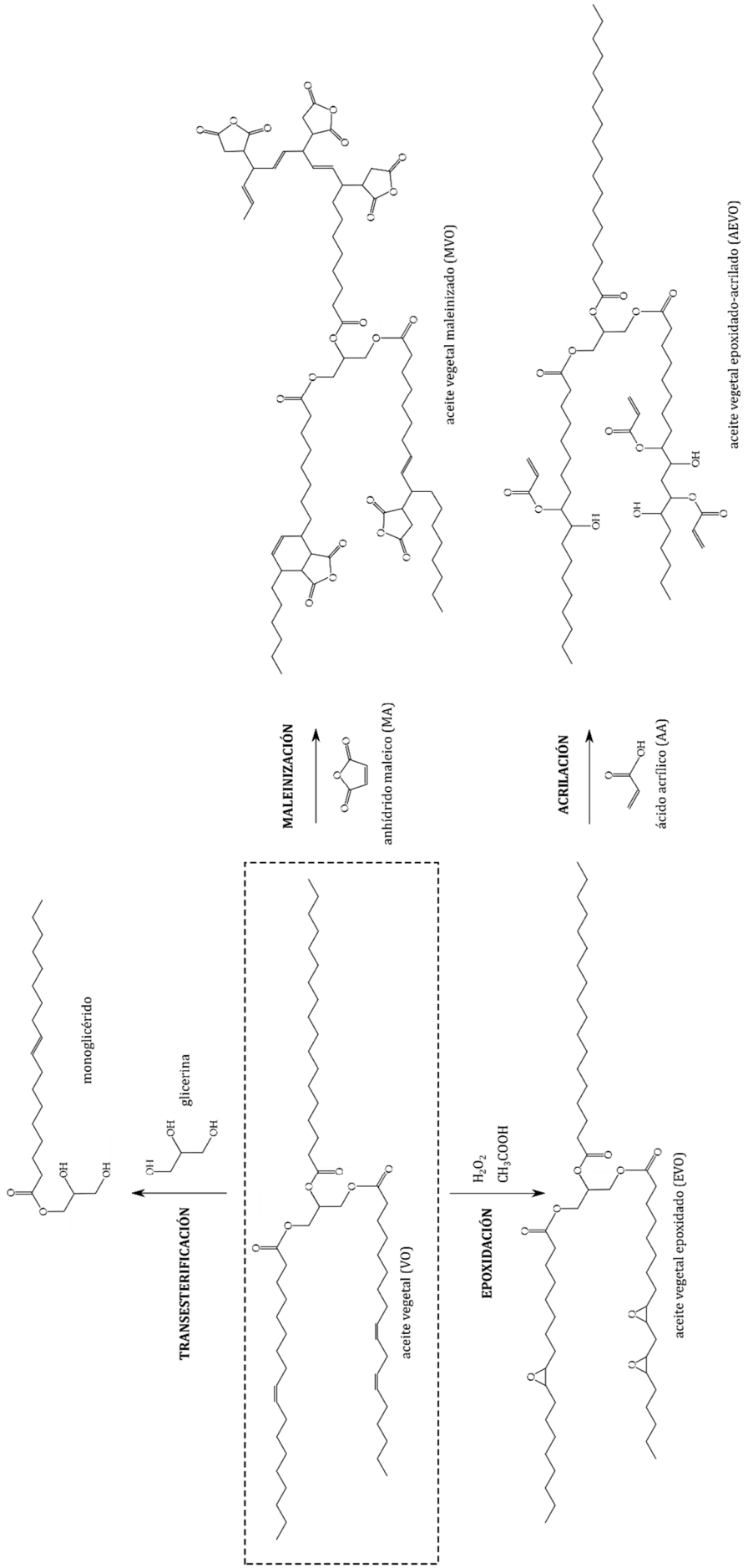

Figura I.24. Representación esquemática de la estructura de un triglicérido tras diferentes modificaciones químicas.

La epoxidación, la acrilación o la maleinización son solo algunas de las modificaciones químicas que se pueden realizar a los triglicéridos de los aceites vegetales, mediante las cuales se consiguen modificar los dobles enlaces con el objetivo de aumentar su reactividad y mejorar así su interacción con las cadenas poliméricas. El grado de funcionalización alcanzado tras la modificación química, está directamente relacionado con el número de instauraciones que contienen los aceites. También puede realizarse un proceso de transesterificación mediante el cual se obtiene glicerol y ésteres de ácidos grasos que pueden ser modificados para su uso como plastificantes [153]. La Figura I.24 muestra la estructura química obtenida tras diferentes modificaciones realizadas a los triglicéridos.

El empleo de aceites vegetales epoxidados (EVO) ha sido ampliamente estudiado para su uso como plastificantes en biopolímeros; entre ellos destacan el aceite de linaza epoxidado (ELO), el aceite de soja epoxidado (ESO) y el aceite de ricino epoxidado (ECO), siendo los dos primeros los que suelen presentar una mayor eficacia como plastificantes. Esto se debe a que el aceite de linaza y el aceite de soja presentan un elevado número de insaturaciones que permiten obtener un mayor grado de epoxidación y, por tanto, pueden presentar una mayor reactividad con el polímero a plastificar. Existen numerosos estudios en los que aceites vegetales epoxidados se han utilizado con éxito en la plastificación de polímeros biodegradables. Seydibeyoğlu *et al*. [158] estudiaron el efecto del ELO y del ESO como plastificantes del PHBV, observando cómo la incorporación de un 10% en peso de ambos plastificantes aumentó las propiedades dúctiles del material, como el alargamiento a la rotura, y disminuyó la resistencia a tracción y el módulo elástico, demostrando la eficacia de ambos aceites vegetales epoxidados como agentes plastificantes. También observaron cambios en las propiedades térmicas del PHBV tras la incorporación de los aceites, produciéndose una ligera disminución de la temperatura de fusión, entre 4–5 °C, con respecto al PHBV puro. Choi *et al.* [159] observaron el mismo comportamiento tras plastificar el PHBV con ESO; además, evidenciaron la mayor efectividad del ESO con respecto al aceite de soja sin epoxidar. Por otro lado, Chieng *et al.* [160] estudiaron el efecto de plastificación del aceite de palma epoxidado (EPO) y una mezcla de aceite de palma epoxidado y aceite de soja (EPSO) en las propiedades mecánicas y térmicas del PLA, observando cómo ambos aceites aumentaron la ductilidad del PLA y disminuyeron su temperatura de fusión y de transición vítrea.

Los aceites vegetales maleinizados (MVO) también han sido utilizados con éxito como plastificantes en polímeros biodegradables, principalmente en el PLA. Carbonell-Verdu *et al.* [161] estudiaron el efecto del aceite de semilla de algodón maleinizado (MCSO) como plastificante del PLA, observando un incremento del alargamiento a la rotura tras la

incorporación de un 7,5% en peso de aceite. Además, en dicho estudio se observó cómo la presencia de aceite en el PLA, aceleró su desintegración en compost. Actualmente, no se tiene constancia de estudios sobre el efecto de aceites vegetales maleinizados en las propiedades térmicas y mecánicas del PHB.

Además del efecto plastificante de los derivados de aceites vegetales, existen estudios que han demostrado un efecto compatibilizante de dichos aceites en mezclas de polímeros inmiscibles. Garcia-Campo *et al.* [162] observaron cómo la incorporación por separado de aceite de soja epoxidado (ESO), aceite de soja epoxidado acrilado (AESO) y aceite de soja maleinizado (MSO) mejoró la compatibilidad en mezclas inmiscibles de PLA/PHB/PCL (60/10/30), obteniendo formulaciones con propiedades dúctiles mejoradas en todos los casos. Ferri *et al.* [163] también observaron un efecto de plastificación-compatibilización del aceite de linaza maleinizado (MLO) en las mezclas de PLA con almidón termoplástico (TPS).

I.5.2. Mezclado físico o "*Blending*"

La mezcla física o "*blending"* es el proceso mediante el cual se mezclan dos o más polímeros en estado fundido, sin producirse reacciones químicas, para crear un nuevo material con propiedades físicas diferentes. Durante dicho proceso, los polímeros se funden conjuntamente y se mezclan mecánicamente dando lugar a un nuevo material, que, tras enfriarse, presenta unas propiedades diferentes a las de los polímeros utilizados en la mezcla. Dicho proceso puede realizarse mediante el empleo de técnicas convencionales de procesado de polímeros, siendo la más extendida industrialmente la extrusión, por lo que dicho sistema de modificación no necesita de grandes inversiones. Resumiendo, el mezclado físico se trata de un proceso que permite obtener nuevos materiales con una combinación deseada de propiedades para que puedan cumplir con los requisitos de aplicaciones específicas. Además, estos pueden obtenerse en un tiempo relativamente corto y con un bajo coste en comparación con el desarrollo de nuevos monómeros y técnicas de polimerización. Por tanto, la mezcla física en estado fundido de polímeros es uno de los métodos más sencillos y económicos para la mejora de las propiedades de los polímeros y, por ello, es uno de los sistemas de modificación más empleados a nivel industrial.

El objetivo general de las mezclas de polímeros es mejorar las propiedades físico-químicas de un determinado material, o adaptarlas a una determinada aplicación mediante la correcta selección de los componentes poliméricos. Aunque también se realiza la mezcla en fundido de varios polímeros para alcanzar ciertos objetivos más específicos como, por

ejemplo, la mejora de la resistencia a impacto, la disminución de la sensibilidad al agua o el abaratamiento de costes. El mezclado físico de polímeros para abaratar costes es un proceso ampliamente empleado, especialmente en el campo de los polímeros biodegradables donde todavía, polímeros como los PHAs o el PLA presentan un elevado coste. Es por ello, que este tipo de biopolímeros se suelen mezclar con otros polímeros biodegradables más económicos, como el almidón termoplástico (TPS), con el objetivo de disminuir el precio final y obtener productos con un rendimiento similar al material de partida pero más competitivos económicamente [164-166].

Dependiendo de la estructura y de la naturaleza de los polímeros que componen la mezcla se pueden obtener diferentes fenómenos de compatibilidad, que afectan de forma decisiva a las propiedades finales del material resultante. La compatibilidad entre las diferentes fases en los sistemas poliméricos depende principalmente de la polaridad intrínseca de cada uno de los polímeros, las interacciones entre ellos, las propiedades de la entrecara formada durante la mezcla, así como la estructura de la mezcla. Teniendo en cuenta la compatibilidad entre los polímeros, se dan tres tipos de mezclas: las mezclas miscibles, las mezclas parcialmente miscibles y las mezclas inmiscibles [167, 168].

Cuando entre los polímeros que constituyen la mezcla hay compatibilidad se obtiene una mezcla miscible. Este tipo de mezcla tiene lugar cuando existen fuertes interacciones moleculares entre los polímeros y, por tanto, la tensión interfacial en la entrecara de los polímeros es prácticamente inexistente. Las mezclas miscibles presentan una única fase más o menos homogénea, obteniéndose un material cuyas propiedades resultan de la combinación de las características de los polímeros que constituyen la mezcla. En este tipo de sistemas poliméricos las proporciones de los polímeros en la mezcla son las que varían las propiedades mecánicas y térmicas de la mezcla final. Por otro lado, la ausencia de compatibilidad, o lo que es lo mismo, la ausencia de interacciones entre los segmentos moleculares de los componentes da lugar a mezclas inmiscibles. En este tipo de mezclas, existen elevadas tensiones interfaciales en la entrecara de los polímeros, produciéndose una separación de fases, dando lugar a un sistema multifase en el que el polímero mayoritario actúa como fase matriz y el resto como fase dispersa. En este tipo de sistemas, las partículas de la fase dispersa pueden experimentar coalescencia incrementando su tamaño en la matriz y dando lugar a unas peores propiedades mecánicas. Este tipo de mezclas presenta generalmente malas propiedades mecánicas, empeorando incluso las propiedades de los polímeros que forman la mezcla, ya que la cohesión entre las distintas fases es muy pobre o nula. Otra de las posibilidades es que la mezcla de polímeros dé lugar a un sistema parcialmente miscible, en el que existe cierta interacción entre los segmentos

moleculares de los componentes. En este sistema también se distinguen varias fases y suele presentar unas propiedades intermedias pero inferiores a las esperadas. Por tanto, las propiedades generales de las mezclas, como son las propiedades mecánicas o térmicas, dependen fundamentalmente de la compatibilidad/interacciones de los polímeros utilizados en las mismas, aunque también influyen otros factores como las propiedades de los polímeros, la composición de la mezcla y la estructura [167, 168].

Aunque existen mezclas de polímeros totalmente miscibles, la situación más habitual que se produce en la mezcla de polímeros es la miscibilidad parcial o la inmiscibilidad total [167]. Es por ello que, durante los últimos años, se han desarrollado una gran cantidad de investigaciones dirigidas a la mejora de la compatibilidad de mezclas parcialmente miscibles o inmiscibles mediante el empleo de agentes compatibilizantes, con el objetivo de mejorar sus propiedades finales. Los agentes compatibilizantes se emplean para mejorar la compatibilidad de mezclas inmiscibles o parcialmente miscibles con el objetivo de mejorar propiedades como la resistencia al impacto, la resistencia a tracción, el alargamiento a la rotura, la permeabilidad, la resistencia al calor, la cristalización, etc. Dichos compuestos actúan reduciendo la tensión interfacial en la entrecara de las distintas fases de la mezcla, promoviendo su adhesión, evitando la coalescencia y reduciendo el tamaño de las partículas dispersas. La combinación de todos estos efectos da lugar a un aumento de la compatibilidad y, como consecuencia, una mejora de las propiedades generales [169]. De forma general, las mezclas compatibilizadas presentan fases separadas, pero con una mejor dispersión y un menor tamaño de la fase dispersa en la matriz.

La compatibilización de mezclas poliméricas inmiscibles o parcialmente miscibles puede llevarse a cabo de diferentes maneras, entre las que destacan la compatibilización no reactiva y la compatibilización reactiva. En el caso de la compatibilización no reactiva se suelen añadir a la mezcla compuestos anfifílicos prefabricados, como copolímeros en bloque o de injerto. Estos consisten en moléculas que contienen un segmento miscible con uno de los componentes de la mezcla y el otro segmento miscible con el otro componente de la mezcla. Estos copolímeros se acumulan a lo largo de la interfase entre los polímeros de la mezcla inmiscible reduciendo la tensión superficial y el tamaño de la fase dispersa, consiguiendo una mejora de la compatibilidad. En este tipo de compatibilización no se producen reacciones químicas, como en el caso de la compatibilización reactiva, pero el compatibilizante sí que presenta miscibilidad con los componentes de la mezcla. La efectividad del copolímero empleado en este tipo de compatibilización depende de varios factores, como su estructura, su peso molecular, la concentración empleada y su localización en la interfase [167].

En la compatibilización reactiva, también conocida como compatibilización "*in situ*", las estructuras en bloque o injerto que actúan como compatibilizantes se forman "*in situ*" durante la mezcla; es decir, durante la mezcla en fundido de los polímeros se forman copolímeros en bloque o de injerto en varias concentraciones a través de enlaces covalentes o iónicos de los polímeros adecuadamente funcionalizados. Los compatibilizantes formados presentan segmentos que son químicamente idénticos a los de los polímeros de la mezcla, por tanto, completamente miscibles, y se localizan preferentemente en la interfase de los polímeros, reduciendo la tensión interfacial y mejorando la compatibilidad. Para que la compatibilización reactiva tenga lugar, es necesario que al menos uno de los polímeros presentes en la mezcla posea grupos funcionales reactivos. Existen dos métodos principales de compatibilización reactiva. Uno es la compatibilización de mezclas poliméricas a través de la formación de copolímeros mediante la incorporación de compuestos reactivos de bajo peso molecular, como peróxidos, que actúan como iniciadores de radicales libres favoreciendo las reacciones entre los polímeros. El segundo método es la compatibilización reactiva de mezclas poliméricas por la adición de polímeros con grupos reactivos como compatibilizantes, tales como el polímero injertado con anhídrido maleico. En este tipo de compatibilización reactiva, generalmente, una fase polimérica presenta grupos reactivos en sus cadenas, inherentes al polímero, mientras que la otra fase no tiene ninguna funcionalidad inherente. Los grupos reactivos se pueden incorporar en esta segunda fase añadiendo un polímero funcionalizado que es miscible con él y reactivo con los grupos funcionales del otro polímero, dando como resultado la formación "*in situ*" de copolímeros de injerto o de bloque que actúan como compatibilizantes, disminuyendo la tensión interfacial y mejorando la dispersión de la fase minoritaria. Dentro de la compatibilización reactiva también se puede realizar la modificación química de uno de los polímeros para crear grupos reactivos en él y no tener la necesidad de incorporar un tercer componente [168, 170].

El sistema de compatibilización reactiva es más efectivo que la compatibilización no reactiva, ya que los copolímeros compatibilizantes se forman directamente en la interfase de los componentes inmiscibles de la mezcla mientras que en la compatibilización no reactiva los copolímeros incorporados por separado deben difundirse hasta la interfase para que la compatibilización sea efectiva. Además, en la compatibilización reactiva el peso molecular de los dos segmentos de polímero en el copolímero generado es el mismo que el de las fases poliméricas donde se han de disolver. Otra de las ventajas de la compatibilización reactiva, es que se puede controlar la estructura y las propiedades de la mezcla de una forma relativamente fácil mediante la selección adecuada de los agentes, la composición de la mezcla y las condiciones de procesado [167, 168].

I.5.2.1. Peróxido de dicumilo como compatibilizante

El peróxido de dicumilo (DCP) es uno de los compuestos reactivos de bajo peso molecular más utilizados en la compatibilización reactiva de mezclas inmiscibles. El DCP se somete durante la mezcla física de los polímeros (compatibilización reactiva) a elevadas temperaturas, lo que posibilita su ruptura hemolítica, dando lugar a dos radicales cumiloxi que presentan una alta capacidad de extracción de átomos de hidrógeno de cualquier grupo –CH de las cadenas poliméricas, generando de esta manera un radical polimérico (reacción de abstracción). Posteriormente, los radicales poliméricos son capaces de combinarse generando enlaces carbono-carbono entre las cadenas poliméricas, dando lugar a la formación de diferentes productos de reacción como, por ejemplo, copolímeros de injerto (A-*g*-B), que actúan como compatibilizantes entre ambas fases, la ramificación o entrecruzamiento entre el mismo polímero o el entrecruzamiento entre los polímeros que componen la mezcla. Todos estos productos dan como resultado un aumento de la compatibilidad de los polímeros, mejorando el rendimiento general de la mezcla [171, 172]. El DCP también puede presentar otro tipo de reacción de extracción alternativa, ya que los fragmentos radicales cumiloxi pueden sufrir la escisión beta generando acetofenona y radicales metilo, que también son capaces de arrancar átomos de hidrógeno de las cadenas poliméricas. Además de las reacciones de entrecruzamiento, durante la compatibilización reactiva se pueden producir otro tipo de reacciones secundarias que pueden dar lugar a una disminución de la eficacia del peróxido como agente reticulante, entre las que se encuentran la adición del radical al doble enlace, la reacción de escisión del radical polimérico, la transferencia del radical o la oxigenación [173]. En la Figura I.25 se puede observar de forma esquemática las reacciones que se producen entre el DCP y las cadenas poliméricas durante la compatibilización reactiva.

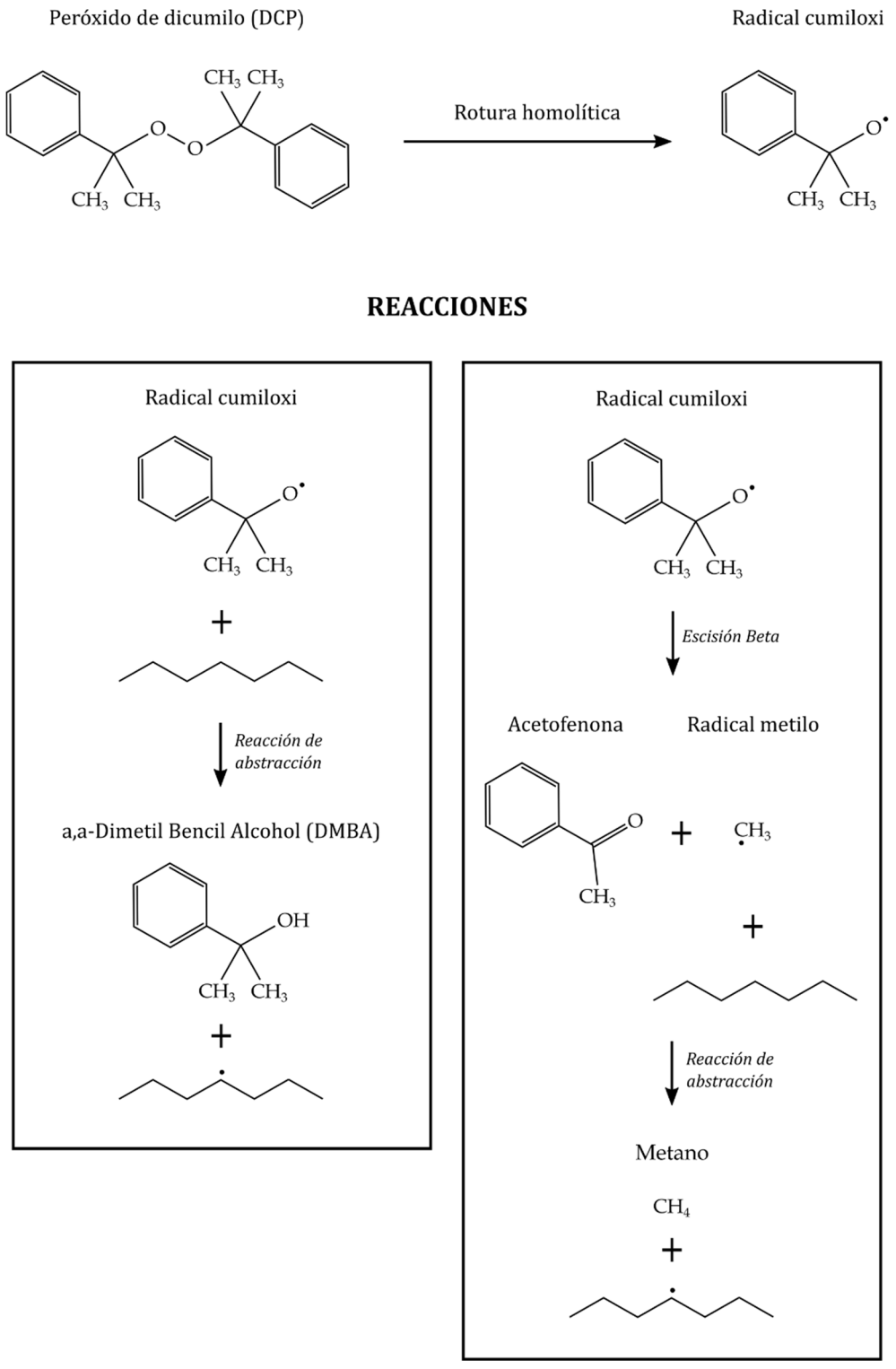

Figura I.25. Representación esquemática de la descomposición hemolítica del peróxido de dicumilo y su reacción con las cadenas poliméricas.

El DCP ha sido ampliamente empleado para mejorar la compatibilidad de mezclas inmiscibles o parcialmente miscibles de polímeros biodegradables, como es el caso de las

mezclas de PLA con otros biopolímeros como la PCL [174], el PBS [175, 176] o el PBAT [171]. En todas estas mezclas, el empleo de DCP como compatibilizante dio lugar a una reducción considerable del tamaño de las partículas dispersas y se obtuvo una mejor adhesión interfacial entre ambos polímeros, mejorando su compatibilidad y obteniendo como resultado una mejora de las propiedades mecánicas dúctiles de las mezclas. El DCP también ha sido empleado para mejorar la compatibilidad de las mezclas de PHB. Ma *et al.* [172] estudiaron el efecto de diferentes cantidades de DCP en las mezclas inmiscibles de PHBV/PBS (80/20) y la incorporación de 0,5 % en peso de DCP en la mezcla inmiscible de PHB/PBS con diferentes contenidos de PBS. En ambos casos se observó una reducción del tamaño de los dominios de PBS en la matriz, acompañado de una mejora de la adhesión interfacial entre ambos polímeros. Este aumento de la compatibilidad provocó una mejora de las propiedades dúctiles en las mezclas, concretamente, en el caso de la mezcla de PHBV/PBS se observó cómo, tras la incorporación de un 0,5% de DCP, el alargamiento a la rotura aumentó de un 10 a un 400%, mientras que en el caso de la mezcla de PHB/PBS (70/30), la incorporación de DCP incrementó la absorción de energía a impacto de 10 a 50 kJ m^{-2}. Dong *et al.* [177] estudiaron el efecto de diferentes cantidades de DCP en mezclas de PHB/PDLLA (70/30), observando también una disminución del tamaño de la fase minoritaria de PDLLA y una mejora de la compatibilidad, que dio lugar a un aumento de las propiedades mecánicas, alcanzándose el mayor aumento de la resistencia a tracción y de la absorción de energía a impacto para un contenido de DCP del 0,5% en peso. Además, debido a la reticulación/ramificación producida por la presencia de DCP en la mezcla, la cristalización del PHB se vio significativamente restringida, reduciéndose su porcentaje de cristalinidad. En este caso, también estudiaron el efecto del DCP en las propiedades térmicas de estas mezclas, observando cómo el aumento de la compatibilidad entre ambos polímeros dio lugar a una ligera disminución de la temperatura de fusión.

I.5.3. Incorporación de nanocargas

Otra de las técnicas extensamente estudiadas en la actualidad para la modificación de ciertas propiedades de los polímeros es la incorporación de nanopartículas, también conocidas como nanocargas o nanorefuerzos, al polímero para dar lugar a nanocompuestos o bionanocompuestos en el caso de que la matriz polimérica se trate de un biopolímero. Los nanocompuestos son materiales sólidos formados por múltiples fases, donde al menos una de las ellas tiene una, dos o tres dimensiones en la escala nanométrica, es decir, entre 1 y 100 nm [178]. Estas nanopartículas se caracterizan por presentar una elevada superficie específica (relación entre el área y el volumen) y una elevada reactividad superficial, lo que

da lugar a buenas interacciones moleculares con la matriz polimérica, proporcionando propiedades inusuales e incrementadas que no se alcanzan con los materiales compuestos tradicionales. La incorporación de nanocargas a los polímeros puede dar lugar a la mejora de las propiedades mecánicas, térmicas, barrera, ópticas, eléctricas, magnéticas, reológicas, etc., y esto se consigue con unas cantidades de refuerzo muy bajas (entre 1 y 10% en peso), lo que permite conservar la procesabilidad del polímero y hace que los nanocompuestos sean más ligeros que los materiales compuestos convencionales [179]. Existen multitud de investigaciones sobre los efectos de diferentes nanopartículas en las propiedades de los polímeros. Sin embargo, en la actualidad, estos nanomateriales están resultando de gran interés científico en el campo de las mezclas físicas de polímeros inmiscibles o parcialmente miscibles, ya que se ha demostrado que la incorporación de nanopartículas en mezclas inmiscibles da lugar a una mejora de la compatibilidad, lo que repercute en unas mejores propiedades globales de las mezclas [180, 181].

El principal problema del empleo de nanocargas en matrices poliméricas es que éstas tienden a formar aglomerados. La elevada superficie específica de las nanopartículas da lugar a una fuerte atracción entre ellas provocando la formación de aglomerados de partículas que permanecen unidas a través de fuerzas atractivas, como, por ejemplo, fuerzas de van der Waals. La formación de aglomerados impide una buena dispersión de las nanocargas en la matriz, reduciéndose considerablemente la mejora de las propiedades de los nanocompuestos. Además, la presencia de aglomerados en el polímero reduce la interacción entre la partícula y la matriz, que puede dar lugar a una separación de la entrecara entre ambas fases, llegando incluso a empeorar las propiedades mecánicas del polímero [182]. Con el objetivo de evitar la formación de aglomerados, suele realizarse la modificación química superficial de las nanopartículas, consiguiéndose un aumento de su dispersión en la matriz y mejorando la interacción entre las diferentes fases, dando como resultado un aumento del rendimiento del nanocompuesto resultante [183, 184].

Hoy en día existen multitud de nanocargas disponibles para su uso como refuerzo en materiales poliméricos. Estas nanocargas pueden clasificarse de diferentes formas dependiendo de sus características. Una de las clasificaciones se realiza según su naturaleza química, pudiendo ser nanocargas orgánicas, como es el caso de las nanofibrillas de celulosa y de quitina, los nanocristales de celulosa y de almidón o los nanotubos de carbono, o nanocargas inorgánicas, que incluyen nanopartículas metálicas u óxidos metálicos y nanoarcillas como la montmorillonita o la bentonita [185]. Otra de las clasificaciones de los nanomateriales se realiza según su origen, obteniéndose nanomateriales naturales, semi-sintéticos o sintéticos [186]. Sin embargo, la clasificación más extendida de las nanocargas

es la que se realiza dependiendo de su geometría y del número de dimensiones que se encuentran dentro de la escala nanométrica. Según esta clasificación, existen tres grandes grupos de nanomateriales: nanomateriales unidimensionales, bidimensionales y tridimensionales [186, 187]:

- Nanomateriales unidimensionales (1D): son aquellos que presentan una única dimensión en el orden nano. Este tipo de cargas presentan forma de láminas, y se hace referencia a ellas como como nanocapas ("*nanolayers"*), nanoláminas ("*nanosheets"*), nanoescamas ("*nanoflakes"*) o nanoplaquetas ("*nanoplatelets"*). Dentro de este grupo se encuentran nanomateriales como el grafeno o la montmorillonita.

- Nanomateriales bidimensionales (2D): son aquellos que presentan dos de sus dimensiones en la escala nano y la tercera dimensión puede estar en la escala micro o macro. Estos materiales presentan una estructura alargada en forma de aguja y generalmente se hace referencia a ellos como nanotubos ("*nanotubes*"), nanofibras ("*nanofibers*"), nanovarillas ("*nanorods*") o "*whiskers*". Dentro de este grupo se encuentran algunos nanomateriales como los nanotubos de carbono, los nanotubos de haloisita o los nanocristales de celulosa.

- Nanomateriales tridimensionales (3D): son aquellos materiales cuyas tres dimensiones se encuentran en la escala nano. Este tipo de materiales presentan forma esférica y se hace referencia a ellos como nanopartículas ("*nanoparticles"*). Dentro de este grupo se encuentran nanomateriales como las nanopartículas cerámicas o metálicas.

En la Tabla I.5 se puede observar un resumen de cada uno de los grupos de nanomateriales clasificados según su geometría, así como algunos de los nanomateriales disponibles pertenecientes a cada uno de los grupos.

Tabla I.5. Clasificación de nanomateriales según su geometría.

Tipo	Forma	Dimensiones	Ejemplos
1D	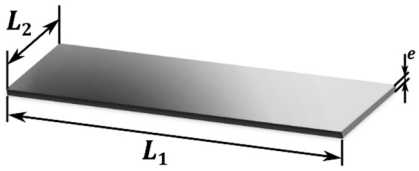	e = 0,1–100 nm L_1 > 100 nm L_2 > 100 nm	Grafeno Nanoarcillas
2D	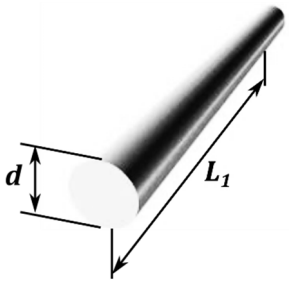	d = 0,1–100 nm L_1 > 100 nm	Nanotubos de haloisita Nanotubos de carbono Nanocristales de celulosa
3D	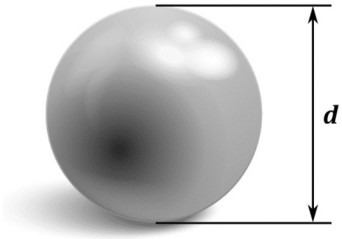	d = 0,1–100 nm	Fullereno Nanopartículas cerámicas o metálicas

I.5.3.1. Nanotubos de haloisita (HNTs)

Una de las nanopartículas que más interés científico ha despertado en los últimos años para su uso como nanorefuerzo en nanocompuestos son los nanotubos de haloisita (HNTs), gracias, principalmente, a su geometría nanotubular, su naturaleza química, su elevada relación de aspecto, su disponibilidad en la naturaleza, su alta funcionalidad, su buena biocompatibilidad, su alta resistencia mecánica, su capacidad de almacenar aditivos en su lumen y su bajo coste. La haloisita consiste en un mineral arcilloso de color blanco que se extrae de depósitos naturales y que se somete a molienda para obtener polvo. Dependiendo de las diferentes condiciones de cristalización y de los acontecimientos geológicos, la haloisita puede presentar forma tubular, forma de placas o incluso esferoidales; sin embargo, la forma tubular es la más común y la más valiosa a nivel científico [188]. Los HNTs son aluminosilicatos de origen natural cuya fórmula molecular es similar a la de la caolinita, excepto por la presencia de una monocapa de agua entre las capas de arcilla adyacentes ($Al_2Si_2O_5(OH)_4 \cdot nH_2O$). Además, a diferencia de la caolinita, cuya

estructura es en forma de placas apiladas, la haloisita se caracteriza por presentar una forma tubular con la presencia de múltiples capas separadas entre sí, como se observa en la Figura I.26. La forma característica de la haloisita es obtenida geológicamente tras enrollarse una lámina de caolinita con preferencia a la rotación tetraédrica [189]. Estructuralmente, dicha lámina está formada por dos capas, una de ellas se trata de una capa octaédrica de alúmina y la otra se trata de una capa tetraédrica de sílice, en una relación estequiométrica 1:1. Por tanto, la morfología tubular de los HNTs hace que exista una diferencia química entre la superficie interior, formada por grupos aluminol (Al−OH), y la superficie exterior del nanotubo, formada por grupos siloxano (Si−O−Si) con algunos grupos silanol (Si−OH) y aluminol en los bordes. Esta diferencia química entre la superficie interna y externa del nanotubo da lugar a la presencia de diferentes cargas en el interior (negativa) y el exterior (positiva). Además, posibilita la funcionalización selectiva de los HNTs. Todo esto unido a su disponibilidad natural, a su estructura tubular y a su bajo coste hacen que los HNTs sean de gran interés en un amplio rango de sectores para su uso en aplicaciones como nanoreactor, como agente adsorbente de contaminantes o como catalizador en la industria de refinado del petróleo [188]. Sin embargo, gracias a la capacidad de almacenar compuestos en su lumen, los HNTs han adquirido especial relevancia como sistemas de liberación controlada de diferentes sustancias, como fármacos [190-193], insecticidas [194], herbicidas [195], antioxidantes [196], agentes antimicrobianos [197], etc., lo cual resulta de gran interés en sectores como la medicina, la agricultura o en el sector de envases de alimentos.

Los HNT se presentan principalmente en dos polimorfos diferentes, dependiendo de su estado de hidratación. La forma hidratada de los HNTs (n=2) presenta una capa de moléculas de agua entre las múltiples capas del nanotubo, existiendo un espaciado entre ellas de 10 Å. Debido a esto, este tipo de haloisita es conocida como haloisita-10Å. La forma deshidratada de la haloisita (n=0) se obtiene tras calentar los HNTs a bajas temperaturas (30-100°C); con ello se consigue eliminar el agua adsorbida entre las capas, reduciéndose el espacio entre ellas a 7 Å. Este tipo de haloisita se conoce como haloisita-7Å [198]. Dimensionalmente, y de forma general, los HNTs presentan una longitud entre 0,5 y 2 μm, un diámetro interno entre 10−15 nm y un diámetro externo entre 50−70 nm [199].

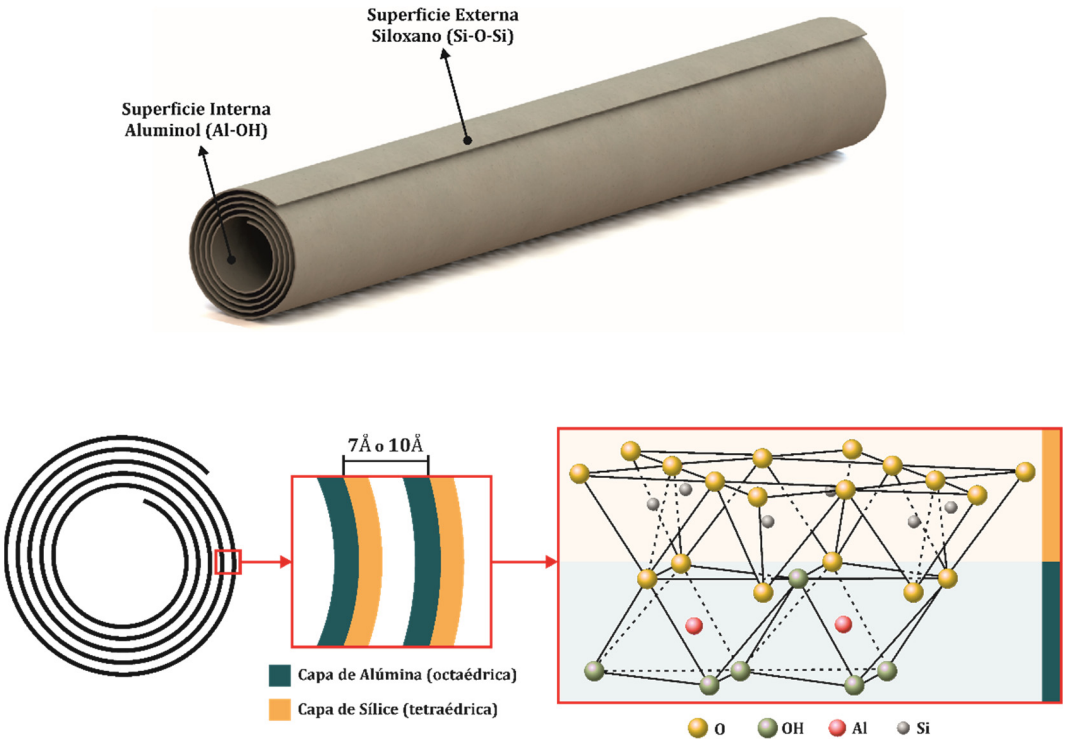

Figura I.26. Representación de la estructura química y física de los nanotubos de haloisita.

En el campo de los nanocompuestos se ha observado cómo la incorporación de HNTs en matrices poliméricas ha dado lugar a la mejora de ciertas propiedades como, por ejemplo, el aumento de propiedades mecánicas como la resistencia a tracción, el módulo elástico o la resistencia a impacto de los polímeros. También se ha demostrado la capacidad de los HNTs para mejorar la estabilidad térmica de los polímeros, gracias, en parte, al atrapamiento de los productos de descomposición en el lumen de los nanotubos; así como a su efecto como agente retardarte de llama. Además, se ha observado que los HNTs pueden actuar como agentes nucleantes en polímeros semicristalinos acelerando la velocidad de cristalización e influyendo en la cristalinidad del polímero [200]. En el campo de los biopolímeros, el empleo de HNTs como agente de refuerzo ha sido ampliamente estudiado. Existen investigaciones que demuestran cómo la incorporación de HNTs a biopolímeros como el PLA [201-203], el PHBV [204, 205] o la PCL [206] da lugar a un aumento de sus propiedades resistentes y/o la mejora de su estabilidad térmica.

Además de mejorar las propiedades de los polímeros, también se ha observado la capacidad de los HNTs como agente compatibilizante en mezclas de polímeros inmiscibles. Pal *et al.* [207] estudiaron el efecto de la incorporación de un 1% en peso de HNTs sin modificar y de HNTs modificados con silano en la compatibilidad de la mezcla inmiscible de polioximetileno (POM)/polipropileno (PP) (50/50), observando una disminución del

tamaño de los dominios de la fase dispersa (POM), así como una mejora de la adhesión interfacial entre ambas fases con respecto a la mezcla sin reforzar, demostrando el efecto compatibilizante de los HNTs. Además, la presencia de HNTs en la mezcla, principalmente los HNTs modificados, mejoraron sus propiedades mecánicas, aumentando la resistencia a tracción y el módulo elástico, sin afectar al alargamiento a la rotura.

Uno de los principales problemas del empleo de HNTs en nanocompuestos es la formación de agregados, aunque el bajo contenido de grupos hidroxilo en la superficie de los HNTs hace que estos sean relativamente hidrofóbicos, dicha hidrofobicidad no es suficiente para evitar la formación de agregados y conseguir una buena dispersión e interacción con la matriz [208]. Es por ello, que en la mayoría de los casos se debe realizar un tratamiento superficial adicional de los HNTs antes de incorporarlos al polímero, con el objetivo de aumentar su hidrofobicidad y conseguir así una mayor dispersión e interacción con la matriz. Uno de los tratamientos químicos más empleados en la modificación superficial de los HNTs es la silanización mediante el injerto de silano a través de la condensación entre los grupos silanos hidrolizados y los grupos hidroxilo disponibles en la superficie de los HNTs, aumentando de esta forma la hidrofobicidad de los HNTs y mejorando su dispersión e interacción con la matriz. Krishnaiah *et al.* [209] estudiaron el efecto de la incorporación de diferentes cantidades de HNTs sin modificar y modificadas con 3-aminopropiltrietoxisilano (APTES) en el PLA, observando cómo las formulaciones con HNTs modificados presentaban mejor dispersión en la matriz que las formulaciones con HNTs sin modificar. Esto dio lugar a que el aumento de la resistencia a tracción, del módulo elástico y de la resistencia a impacto obtenido tras la incorporación de los HNTs fuese superior en el caso de las formulaciones con HNTs modificados. Además, la incorporación de HNTs en el PLA aumentó su temperatura de inicio de degradación, siendo dicho aumento superior a los 17 °C para la muestra reforzada con 4% en peso de HNTs modificado con silano. También observaron cómo los HNTs aumentaron la cristalinidad del PLA; sin embargo, dicho aumento fue menor en el caso de los HNTs modificados. Otros estudios, como el realizado por Carli *et al.* [205], analizaron la influencia del tipo de silano empleado en el tratamiento de los HNTs en las propiedades térmicas y mecánicas del material, en este caso el PHBV, observando notables diferencias según el tipo de silano empleado.

I.5.3.2. Nanocristales de celulosa (CNCs)

Los nanocristales de celulosa (CNCs) son una de las cargas orgánicas más empleadas como nanorefuerzo en nanocompuestos, principalmente en bionanocompuestos. Los CNCs se caracterizan por presentar biodegradabilidad, biocompatibilidad, baja densidad, alta

relación de aspecto, alta superficie específica, buenas propiedades mecánicas (alta rigidez y módulo elástico), baja expansión térmica, baja toxicidad, estabilidad en medios agresivos, permeabilidad al gas, transparencia óptica y facilidad de funcionalización química debido a la presencia de grupos hidroxilo en su superficie. Estas propiedades permiten obtener nanocompuestos con propiedades mejoradas que se emplean en una gran variedad de sectores, como el sector biomédico, el sector del envase o el sector agrícola.

Como se ha comentado anteriormente, la celulosa es el biopolímero más abundante en la naturaleza y se caracteriza por ser renovable, biodegradable y no tóxico. La celulosa es un homopolisacárido lineal formado por unidades de β-D-glucopiranosa unidas mediante enlaces β-(1-4) glicosídicos [210]. Dichas cadenas poliméricas se empaquetan a través de fuerzas de van de Waals y enlaces de hidrógeno intra- e intermoleculares formando fibrillas elementales, que se agrupan en unidades más grandes llamadas microfibrillas, que presentan unas dimensiones entre 5−50 nm de diámetro y varias micras de longitud. Estas microfibrillas a su vez se ensamblan formando fibras de celulosa [47]. Los enlaces de hidrógeno hacen que la celulosa sea un polímero relativamente estable y proporcionan a las fibrillas de celulosa una gran rigidez axial, siendo estas el principal refuerzo en árboles y plantas. Dentro de las fibrillas de celulosa, hay regiones con un elevado orden (cristalinas) y regiones que están desordenadas (amorfas). Dichas regiones cristalinas contenidas dentro de las microfibrillas de celulosa son conocidas como nanocristales de celulosa o "*nanowhiskers*" [46, 211].

La extracción de los CNCs a partir de materiales celulósico se realiza principalmente en dos etapas; una primera etapa consistente en un pretratamiento que implica la eliminación total o parcial de los materiales de la matriz celulósica, como son la hemicelulosa y la lignina, consiguiendo de esta manera aislar las fibras celulósicas, y una segunda etapa que implica la obtención de los CNCs mediante la eliminación de las regiones amorfas de las microfibrillas. Esta segunda etapa puede llevarse a cabo mediante diferentes métodos, como son la hidrólisis ácida con diferentes ácidos [212-215], la hidrólisis enzimática [216, 217] o mediante procesos mecánicos [218-220]; sin embargo, la hidrólisis ácida con ácido sulfúrico (H_2SO_4) es el método de extracción más conocido, el más eficiente y el más ampliamente utilizado en la actualidad. Durante dicho proceso, las regiones amorfas se hidrolizan, liberando los cristales individuales, los cuales presentan una mayor resistencia al ataque químico. El procedimiento comúnmente empleado en la extracción de CNCs se resume en la Figura I.27. Dicho procedimiento implica la hidrólisis del material celulósico bajo condiciones de agitación, tiempo y temperatura controladas. Después de la hidrólisis, la mezcla ácida se diluye con agua para detener la reacción y se realiza un lavado

mediante varias centrifugaciones y una posterior diálisis con agua ultrapura, con el objetivo de eliminar el ácido residual y las impurezas. Tras la diálisis, la suspensión se somete a un tratamiento mecánico de ultrasonido con el fin de mejorar la dispersión de los nanocristales. Finalmente, la suspensión puede ser liofilizada para obtener CNCs en estado sólido. Las propiedades de los CNCs resultantes, como sus dimensiones, su morfología, su estabilidad térmica y su grado de cristalinidad, dependerán de la fuente del material celulósico, así como de las condiciones de la hidrólisis ácida (concentración, tiempo y temperatura) y de la intensidad de la irradiación ultrasónica [221]. De forma general, los CNCs obtenidos a partir de la mayoría de fibras celulósicas mediante hidrólisis ácida presentan una geometría de varilla (2D), con unas dimensiones entre los 100–250 nm de largo y unos 5–15 nm de diámetro [222].

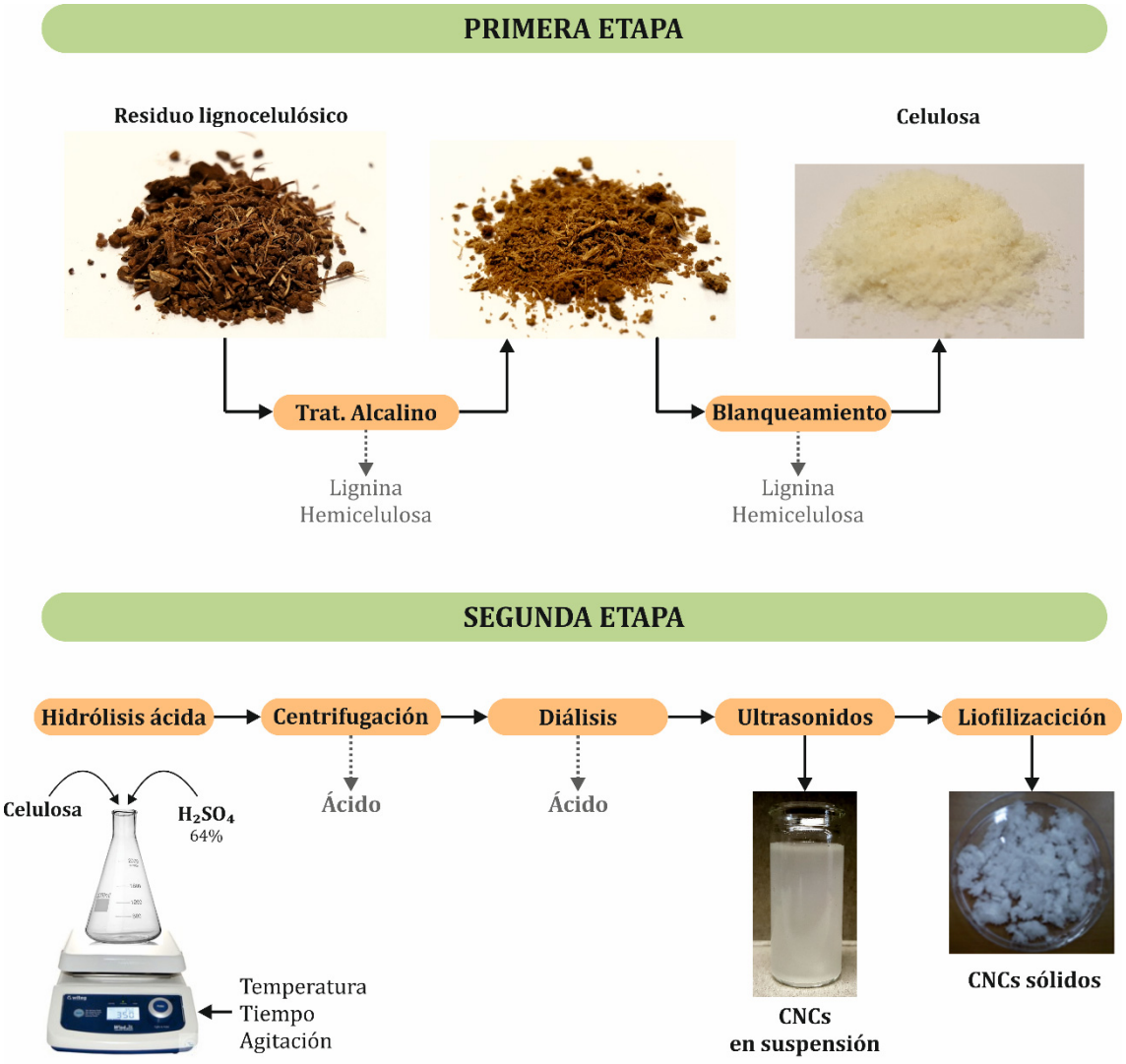

Figura I.27. Esquema del proceso de obtención de nanocristales de celulosa mediante hidrólisis ácida.

Las propiedades físicas y químicas intrínsecas de los CNCs, hacen que estos tengan un gran potencial para su uso como refuerzo en biopolímeros. Gran parte de los estudios realizados han demostrado cómo la incorporación de CNCs en matrices poliméricas da lugar a un aumento de las propiedades mecánicas y de las propiedades barrera del polímero [223]. Algunas investigaciones también han observado el efecto de los CNCs en la mejora de las propiedades ópticas de los polímeros [224, 225]. Incluso, se ha demostrado cómo los CNCs pueden dar lugar a una mejora de la adhesión interfacial y, por tanto, de la compatibilidad de mezclas físicas de polímeros inmiscibles o parcialmente miscibles. Luzi *et al.* [226] observaron un aumento de la compatibilidad en mezclas de PLA/PBS tras la incorporación de CNCs. Dicha mejora de la compatibilidad también fue demostrada por Arrieta *et al.* [227] tras incorporar CNCs en mezclas de PLA/PHB.

Sin embargo, el principal problema del empleo de CNCs como refuerzo en nanocompuestos es la baja dispersión y compatibilidad que éstos presentan en matrices poliméricas hidrofóbicas, lo cual puede llegar a limitar las propiedades mecánicas y térmicas del nanocompuesto obtenido. El elevado carácter hidrofílico de los CNCs, por la gran cantidad de grupos hidroxilo en su superficie, hace que estos tiendan a formar agregados; además, dicho carácter hidrofílico dificulta su compatibilidad con las matrices poliméricas hidrofóbicas. Todo ello da lugar a una baja dispersión de los CNCs en el nanocompuesto, así como a una pobre interacción con la matriz [228]. Una de las estrategias más empleadas para evitar dichos problemas es la modificación química de los grupos funcionales superficiales de los CNCs, con el objetivo de aumentar su hidrofobicidad y evitar así la formación de agregados, mejorando de esta manera su dispersión y su compatibilidad con la matriz polimérica, lo cual se verá reflejado en un mejor rendimiento del nanocompuesto obtenido. Otro de los problemas del empleo de CNCs como refuerzo en nanocompuestos termoplásticos está relacionado con su baja estabilidad térmica, la cual podría verse comprometida durante el procesado del polímero, produciéndose una degradación parcial que influiría negativamente en las propiedades finales del material obtenido [229].

Actualmente existe una gran cantidad de estudios sobre el efecto de los CNCs, obtenidos de diferentes fuentes lignocelulósicas, en las propiedades de biopolímero como el PLA [230, 231], la PCL [232, 233] o el PHBV [234-236]. Sin embargo, el efecto de los CNCs en las propiedades del PHB ha sido escasamente investigado. Algunos autores como Seoane *et al.* [237] observaron cómo la incorporación de CNCs al PHB dio lugar a una mejora de sus propiedades mecánicas resistentes, aumentando su resistencia a tracción y módulo elástico en torno al 50 y al 35% respectivamente tras incorporar un 6% en peso de CNCs. Las

pruebas de nanoindentación realizadas también mostraron un aumento de la dureza en las formulaciones reforzadas con CNCs. Las propiedades térmicas del polímero también fueron evaluadas por los autores, observando cómo la incorporación de los nanorefuerzos al PHB provocó un ligero aumento de la temperatura de fusión, así como una disminución de su temperatura de degradación máxima, lo cual atribuyeron a la presencia de grupos sulfato e hidroxilo en la superficie de los CNCs, que actúan como sitios de nucleación para la escisión de las cadenas poliméricas a altas temperaturas. Además, pudieron comprobar cómo la incorporación de CNCs en el PHB mejoró notablemente su permeabilidad al vapor de agua y aumentó la transparencia de los films. Seoane *et al.* [225] también estudiaron el efecto de los CNCs en la desintegración en condiciones de compost del PHB, observando cómo en los primeros días de compostaje, la presencia de pequeñas cantidades de CNCs en el polímero (2% en peso), ralentiza la degradación debido a la menor permeabilidad al vapor de agua obtenida para dicha formulación. Esto dificulta la difusión del agua al interior de las muestras impidiendo la hidrólisis del material. Para la formulación con mayor cantidad de CNCs (4% en peso) se observó un aumento de la velocidad de degradación con respecto al PHB puro, lo cual atribuyeron a que un mayor contenido de CNCs hidrofílicos permite una mayor absorción de agua, favoreciendo así la hidrólisis del material. Dhar *et al.* [238] estudiaron el efecto de diferentes cantidades de CNCs en la cristalinidad, las propiedades térmicas y las propiedades barrera de films de PHB, así como en la migración de dos simulantes alimentarios, observando cómo la incorporación de pequeñas cantidades CNCs al PHB (2% en peso) dio lugar a una disminución de la cristalinidad del polímero, permitiendo obtener films con una mejor transparencia y flexibilidad, y redujo notablemente la permeabilidad al oxígeno del film reforzado con respecto al PHB, cerca de un 65%. Además, observaron que la migración de los simulantes se encontraba dentro de los límites de las normativas. Por tanto, dichos autores demostraron cómo la incorporación de CNCs al PHB puede dar lugar a bionanocompuestos que pueden resultar de gran interés en el campo del envasado de alimentos.

I.5.4. Otras modificaciones

Existen otros tipos de métodos para modificar las propiedades físicas de los polímeros, entre las que se encuentran la copolimerización y la aditivación del polímero con agentes específicos para la mejora de propiedades concretas, como es el caso de antioxidantes, estabilizantes a la luz UV, pigmentos, retardantes de llama, modificadores de impacto, espumantes, etc. [6].

La copolimerización es una reacción química de polimerización en la que se emplean dos o más monómeros diferentes a la vez, dando lugar a cadenas poliméricas en las que aparecen ambos monómeros con diferente ordenación. A este tipo de polímeros se les conoce como copolímeros (en el caso de emplear tres monómeros distintos se les denomina terpolímeros). Dependiendo de la disposición de los monómeros en la cadena polimérica se pueden distinguir cuatro tipos de copolímeros, entre los que se encuentran los copolímeros aleatorios (el más habitual), alternantes, en bloque o de injerto. La copolimerización permite combinar las características de los diferentes monómeros empleados, dando lugar a polímeros con excelentes prestaciones. Dichas propiedades dependerán en gran medida de la composición del copolímero, es decir, de la proporción relativa de cada monómero en el copolímero. Aunque este proceso es más costoso que la mezcla física, las características mecánicas obtenidas son superiores [6].

En el caso del PHB, los copolímeros también son biosintetizados por determinados microorganismos y mediante el empleo de diferentes condiciones de cultivo como, por ejemplo, el empleo de sustratos mixtos. Generalmente, cuando se usa una mezcla de sustratos, los copolímeros resultantes son copolímeros aleatorios; sin embargo, es posible obtener copolímeros de bloque sintetizados por bacterias alternando los sustratos con el tiempo [239]. Algunos de los copolímeros de PHB más estudiados en la actualidad son el poli(3-hidroxibutirato-*co*-3-hidroxivalerato) P(3HB-*co*-3HV) o PHBV, el poli(3-hidroxibutirato-*co*-4-hidroxibutirato) P(3HB-*co*-4HB) o el poli(3-hidroxibutirato-*co*-3-hidroxihexanoato) P(3HB-*co*-3HHx), cuyas estructuras químicas se pueden observar en la Figura I.28.

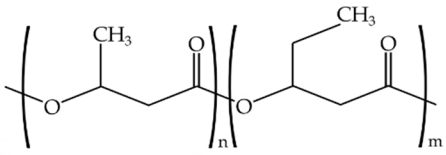

Poli(3-hidroxibutirato-*co*-3-hidroxivalerato) (PHBV)

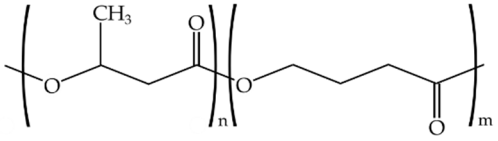

Poli(3-hidroxibutirato-*co*-4-hidroxibutirato) P(3HB-*co*-4HB)

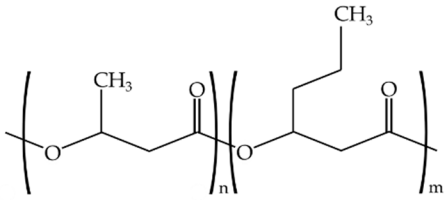

Poli(3-hidroxibutirato-*co*-3-hidroxihexanoato) P(3HB-*co*-3HHx)

Figura I.28. Representación esquemática de la unidad monomérica de diferentes copolímeros de poli(3-hidroxibutirato).

La Tabla I.6 muestra las principales propiedades mecánicas y térmicas, así como el porcentaje de cristalinidad de algunos copolímeros de PHB. Como se puede observar, la presencia de monómeros secundarios diferentes al 3-hidroxibutirato en la cadena polimérica, como es el caso del 3-hidroxivalerato (3HV), el 4-hidroxibutirato (4HB) o el 3-hidroxihexanoato (3HHx), da lugar a copolímeros con un menor grado de cristalinidad, propiedades dúctiles mejoradas y una menor temperatura de fusión y de transición vítrea que el PHB puro. Hay que tener en cuenta que las propiedades finales de los copolímeros dependerán, principalmente, del contenido de monómero secundario presente en el mismo, lo cual también dependerá de las condiciones de cultivo.

Tabla I.6. Propiedades físicas del PHB y sus principales copolímeros [240].

Parámetro	**Polímero/Copolímero**			
	PHB	**PHBV[a]**	**P(3HB-*co*-4HB)[b]**	**P(3HB-*co*-HHx)[c]**
Resistencia a tracción (MPa)	40	20	26	21
Alargamiento a la rotura (%)	5	50	444	400
Cristalinidad (%)	60	56	45	34
Fusión (°C)	175	145	150	127
Transición vítrea (°C)	4	-1	-7	-1

[a] 20% molar de 3HV.

[b] 16% molar de 4HB.

[c] 10% molar de 3HHx.

Además de la formación de copolímeros por síntesis bacteriana, también se ha investigado el desarrollo de copolímeros de PHB mediante síntesis química con el objetivo de obtener nuevos polímeros con mejores rendimientos que el PHB puro [241-243].

I.6. PLASTIFICACIÓN DE POLI(3-HIDROXIBUTIRATO)

El PHB es uno de los biopolímeros con mayor perspectiva de futuro a nivel industrial, ya que se trata de un termoplástico biodegradable y biocompatible, con buenas propiedades mecánicas resistentes y buenas propiedades barrera. Sin embargo, como se ha podido ver, este biopolímero presenta una serie de inconvenientes que hacen que no sea competitivo y que limitan su inclusión a nivel industrial. El elevado precio de producción, su elevada fragilidad y su estrecha ventana de procesado, debido a su baja estabilidad térmica, son las principales desventajas que presenta este material. Como se ha comprobado, la plastificación es uno de los procesos más eficientes, simples y económicos para la modificación de propiedades de los polímeros, así como para disminuir su coste. Mediante este sistema se consigue una mejora de las propiedades mecánicas dúctiles de los polímeros, disminuyendo la fragilidad, así como una disminución de la temperatura de fusión (T_m) y de la temperatura de transición vítrea (T_g), entre otras propiedades.

Debido a los problemas de migración y toxicidad generados por algunos de los plastificantes de origen petroquímico más utilizados hoy en día en la plastificación de polímeros de uso común, se está produciendo un aumento en la investigación y desarrollo de plastificantes más respetuosos con el medio ambiente, que no presenten toxicidad y que sean biodegradables. Estas características son de especial interés en el campo de los biopolímeros, ya que es interesante que los plastificantes empleados en este tipo de materiales no influyan negativamente en su capacidad de biodegradación.

Los estudios realizados sobre la plastificación del PHB se han centrado principalmente en el empleo de plastificantes, tanto de origen natural como petroquímico, capaces de biodegradarse. La Tabla I.7 recoge los principales plastificantes empleados para la mejora de las propiedades del PHB, los cuales han sido clasificados, dependiendo de su peso molecular, en plastificantes monoméricos o poliméricos. En la gran mayoría de las investigaciones realizadas se analizó el efecto de la concentración de plastificante en las propiedades del PHB, empleándose en todas ellas concentraciones relativamente elevadas, que van desde el 2 al 50 % en peso de plastificante. La gran mayoría de los plastificantes utilizados mejoraron las propiedades dúctiles del PHB, como el alargamiento a la rotura, reduciendo así su fragilidad. Además, algunos de los plastificantes estudiados también mejoraron su estabilidad térmica, aumentando su ventana de procesado.

Tabla I.7. Recopilación de los plastificantes empleados en la plastificación de poli(3-hidroxibutirato) clasificados según su peso molecular en plastificantes monoméricos y plastificantes poliméricos.

Plastificantes Monoméricos		**Plastificantes Poliméricos**	
Aceite de soja epoxidado (ESO)	[244]	Adipato de dietilenglicol	[245]
Acetil tributil citrato (ATBC)	[244, 246-248]	Glicerina oxipropilada	[249]
Ácido láurico	[250]	Poliadipato	[251]
Dibutil ftalato (DBP)	[252]	Polietilenglicol (PEG)	[244]
Dioctil adipato (DOA)	[251]		
Dioctil ftalato (DOP)	[248, 251]		
Dioctil sebacato (DOS)	[248, 253]		
Dodecanol	[250]		
Glicerina	[254, 256]		
Lapol 108	[255]		
Pentaeritritol	[256]		
Polietilenglicol (PEG)	[249, 256-258]		
Triacetato de glicerina (TAG)	[251, 254]		
Tributil citrato (TBC)	[247]		
Tributirina	[245, 250]		
Trietil citrato (TEC)	[247]		
Trietilenglicol-di-(2-etilhexanoato) (TEGB)	[256]		
Trilaurina	[250]		

Como se observa en la Tabla I.7, entre los plastificantes más estudiados y efectivos para mejorar las propiedades del PHB se encuentra el polietilenglicol (PEG) de bajo peso molecular y el acetil tributil citrato (ATBC). Parra *et al.* [257] estudiaron el efecto de diferentes cantidades (2, 5, 10, 20 y 40% en peso) de PEG en films de PHB obtenidos mediante disolución en cloroformo, observando cómo las muestras plastificadas presentaban una menor resistencia a tracción y un mayor alargamiento a la rotura con respecto al PHB puro, obteniéndose el mayor alargamiento a la rotura en la muestra de PHB plastificada con un 20% de PEG, con un valor del 32%, lo cual supuso un aumento en torno al 255% con respecto al PHB puro. En cuanto a las propiedades térmicas, los autores

observaron cómo la presencia de PEG en el PHB dio lugar a una disminución considerable de la temperatura de fusión, siendo dicha disminución cercana a los 21 °C para la muestra plastificada con 10% en peso de PEG. Además, el plastificante provocó una disminución de la cristalinidad del material. Esto, unido a su naturaleza hidrofílica, dio lugar a un aumento de la permeabilidad al vapor de agua en las muestras plastificadas, favoreciendo la degradación hidrolítica. Por tanto, la presencia de PEG en las muestras aumentó la velocidad de degradación del material, degradándose más rápido las muestras con mayor cantidad de plastificante. Fernandes *et al.* [256] estudiaron el efecto en las propiedades del PHB de diferentes polioles con distinta cantidad de grupos hidroxilo, como el PEG200, la glicerina, el trietilenglicol-di-(2-etilhexanoato) y el pentaeritritol, en dos concentraciones diferentes de cada uno de ellos, 5 y 20% en peso. Los autores observaron cómo la incorporación de glicerina y PEG provocó una disminución de la estabilidad térmica del PHB, reduciendo su temperatura de inicio de degradación en 3 y 9 °C respectivamente para una concentración del 20% en peso de cada uno de ellos. Sin embargo, observaron cómo para dicha concentración de PEG se produjo una disminución de la temperatura de fusión y de la temperatura de transición vítrea con respecto al PHB en torno a 16 y 24 °C respectivamente. En cuanto a las propiedades mecánicas, los autores observaron cómo la glicerina, en una concentración del 20% en peso, fue el plastificante que dio lugar a una mayor reducción de las propiedades resistentes del PHB, como la resistencia a tracción y el módulo de elástico.

La compatibilidad y la eficacia del acetil tributil citrato (ATBC) como plastificante del PHB también ha sido estudiada por algunos autores. El ATBC es un plastificante que se deriva del ácido cítrico natural, no presenta toxicidad y es biodegradable; por tanto, resulta de especial interés a nivel industrial para su uso en diferentes sectores como el del envase de alimentos. Wang *et al.* [248] estudiaron el efecto de la incorporación de diferentes cantidades de ATBC (10, 20, 25 y 30% en peso) en las propiedades mecánicas y térmicas del PHB, observando cómo las muestras plastificadas presentaban una menor rigidez y una mayor ductilidad que el PHB puro, lo cual quedó plasmado en una menor resistencia a tracción, un menor módulo elástico y un mayor alargamiento a la rotura de las muestras plastificadas. En cuanto a las propiedades térmicas, observaron cómo la incorporación de ATBC al PHB provocó una disminución de la temperatura de fusión y de la temperatura de transición vítrea, pasando de los 169 y 6,1 °C del PHB puro a los 156,8 y −30,7 °C respectivamente para la muestra plastificada con un 30% en peso de ATBC. Sin embargo, dicho plastificante redujo considerablemente la estabilidad térmica del PHB, reduciendo su temperatura de inicio de degradación a medida que aumentaba el contenido de plastificante en la matriz, pasando de 224 °C del PHB puro a 189 °C para la muestra plastificada con 30% en peso de ATBC; no obstante, la temperatura de degradación máxima del PHB no se vio

afectada. Esto fue atribuido a la existencia de impurezas de bajo punto de ebullición presentes en el plastificante. Panaitescu *et al.* [244] también analizaron el efecto del ATBC en dos concentraciones diferentes, 5 y 10% en peso, en las propiedades del PHB. Al igual que Wang *et al.* [248], los autores observaron una disminución de la temperatura de inicio de degradación y de la temperatura de fusión del PHB tras la incorporación del ATBC, siendo dicha disminución en torno a 20 y 6 °C respectivamente para la muestra con un contenido de ATBC del 10% en peso, lo cual supuso una reducción de la ventana de procesado del PHB. Los resultados también mostraron como la incorporación de ATBC (10% en peso) al PHB redujo su grado de cristalinidad y su fragilidad, aumentando su alargamiento a la rotura.

El efecto de aceites vegetales sin modificar y modificados químicamente en las propiedades del PHB ha sido escasamente estudiado hasta el momento. En el mismo trabajo, Panaitescu *et al.* [244] estudiaron el efecto del aceite de soja epoxidado (ESO) en las propiedades del PHB. Los resultados demostraron cómo la incorporación de un 5% en peso de aceite aumentó el alargamiento a la rotura del PHB un 45% y redujo ligeramente su resistencia a tracción y su módulo elástico. En dicho trabajo, los autores también estudiaron el efecto de otros plastificantes como el ATBC y dos PEGs con un peso molecular medio, el PEG4000 y el PEG6000, siendo el ESO el plastificante que mejores propiedades dúctiles proporcionó al PHB. En cuanto a las propiedades térmicas observaron cómo, a diferencia del ATBC, la incorporación del 5% en peso de ESO aumentó ligeramente la temperatura de inicio de degradación del PHB, sin afectar a la temperatura de fusión, manteniendo así su estabilidad térmica. Sin embargo, de los plastificantes estudiados por los autores, el ATBC fue el que indujo el efecto plastificante más notable, reflejándose en una mayor disminución de la temperatura de fusión, de la viscosidad y de la cristalinidad, y en un aumento de alargamiento a la rotura similar al alcanzado por el ESO, pero con una mayor disminución de la resistencia a tracción y del módulo elástico.

I.7. MEZCLAS FÍSICAS CON BASE POLI(3-HIDROXIBUTIRATO)

La mezcla física en fundido o "*blending*" es uno de los métodos más eficaces, económicos y sencillos de llevar a cabo para obtener formulaciones con propiedades físicas mejoradas. Dicho método, mediante la correcta elección de los polímeros a mezclar y el contenido de los mismos en la mezcla, permite obtener formulaciones con un mejor rendimiento que los polímeros individuales, pudiendo ser adaptadas a diferentes aplicaciones.

La mezcla física del PHB con otros polímeros ha sido de gran interés científico con el fin de mejorar sus principales limitaciones, como su elevada fragilidad, su inestabilidad térmica y su elevado coste. Algunas investigaciones realizadas han estudiado el efecto de la mezcla del PHB con polímeros de origen petroquímico como el polipropileno [259] o el polietileno de baja densidad [260], no obstante, son las mezclas con otros polímeros biodegradables las que despiertan un mayor aliciente, debido al interés en no alterar la biodegradabilidad del PHB y obtener formulaciones que mantengan el concepto de sostenibilidad y ecología tras la mezcla. Sin embargo, la mayoría de las mezclas de PHB con otros biopolímeros no resultan exitosas a consecuencia de su inmiscibilidad; es por ello que en gran parte de las investigaciones realizadas se ha recurrido al empleo de compatibilizantes con el objetivo de aumentar la miscibilidad entre los polímeros y obtener mezclas con mejores propiedades.

Uno de los polímeros biodegradables empleados en la mezcla física con el PHB ha sido el PLA. Zhang *et al.* [261] estudiaron la morfología, la estructura química, la cristalización, las propiedades térmicas, las propiedades mecánicas y la biodegradación de la mezcla física inmiscible de PHB/PLA con diferentes proporciones (100/0, 75/25, 50/50, 25/75, 0/100). Los autores observaron cómo en las formulaciones en las que el PHB actúa como matriz (50/50, 25/75, 0/100), la presencia de PLA mejoró las propiedades mecánicas, como la resistencia a tracción y el alargamiento a la rotura, y disminuyó significativamente el tamaño de las esferulitas de PHB, obteniéndose una distribución de tamaños más uniforme a medida que aumentaba el contenido de PLA. Además, térmicamente, observaron un aumento de la temperatura de fusión con respecto al PHB puro. La biodegradabilidad del PHB también se vio afectada por la presencia de PLA, reduciéndose la velocidad de degradación a medida que aumentaba el contenido de PLA en la mezcla. Dong *et al.* [177] estudiaron las propiedades de la mezcla física de PHB/PDLLA (70/30) sin compatibilizar y compatibilizada con diferentes cantidades (0, 0,2, 0,5 y 1% en peso) de peróxido de dicumilo (DCP). Los autores observaron cómo la incorporación de PDLLA en la mezcla mejoró notablemente las propiedades mecánicas resistentes del PHB puro, como la resistencia a

tracción y a flexión, así como su tenacidad, aumentando la absorción de energía a impacto. Tras la incorporación de un 0,5% en peso de DCP a la mezcla se obtuvo una mejor adhesión interfacial entre ambos polímeros, mejorando su compatibilidad e incrementando, aún más, las propiedades mecánicas alcanzadas en la mezcla sin compatibilizar. La presencia de DCP en la mezcla también dio lugar a una considerable disminución de la cristalinidad y de la temperatura de cristalización, y redujo ligeramente su temperatura de fusión. Sin embargo, debido a que el PLA también es un material frágil, las mezclas de PHB/PLA tienden a presentar una fragilidad elevada; es por ello que algunos autores como D'Amico *et al.* [262] estudiaron el efecto de la incorporación de un plastificante natural (tributirina), con una concentración fija del 20% en peso, en mezclas físicas de PHB/PLA con diferentes proporciones (100/0, 70/30, 60/40, 50/50, 40/60, 30/70 y 0/100), obteniendo formulaciones con mejores propiedades dúctiles que el PHB y el PLA puros. Como se ha comentado, la incorporación de PLA al PHB suele dar lugar a formulaciones que presentan una elevada fragilidad, lo cual ha provocado que este tipo de mezcla haya sido escasamente estudiada; sin embargo, existen numerosas investigaciones en las que se han empleado pequeñas cantidades de PHB para mejorar ciertas propiedades del PLA como las propiedades barrera.

La ductilidad del PHB se ha visto mejorada tras ser mezclado con otros biopolímeros como el PBS [172] o el almidón, mediante el cual también se obtuvo una mejora de la estabilidad térmica y de la viscosidad del PHB, así como una notable reducción del coste final del material [164]. Sin embargo, uno de los biopolímeros que más interés ha generado científicamente para mejorar las propiedades del PHB mediante la mezcla física ha sido la poli(ε-caprolactona) (PCL), debido principalmente a sus excelentes propiedades dúctiles y a su elevada estabilidad térmica. Dichas propiedades hacen que la PCL sea un material atractivo para mejorar los inconvenientes que presenta el PHB, manteniendo su biodegradabilidad y su biocompatibilidad.

La PCL es miscible con una amplia variedad de polímeros en los que actúa como plastificante, mejorando la procesabilidad de la mezcla, aumentando su ductilidad y disminuyendo su temperatura de fusión y de transición vítrea. Sin embargo, algunos autores han observado que las mezclas de PHB/PCL presentan inmiscibilidad o una miscibilidad muy reducida, lo que impide una mejora efectiva de las propiedades de las mezclas. Kumagai *et al.* [263] investigaron la miscibilidad, la morfología y la biodegradabilidad de mezclas de PHB/PCL. En dicho trabajo, al igual que trabajos posteriores como el realizado por Antunes *et al.* [264], observaron la inmiscibilidad total entre ambos polímeros. Sin embargo, otros autores como Gassner *et al.* [22] observaron una ligera reducción de la

temperatura de fusión de los dos componentes, lo cual se atribuyó a la existencia de una pequeña solubilidad entre ambos polímeros. Autores como Hinüber *et al.* [265] o Cavalcante *et al.* [266] también defienden la existencia de cierta compatibilidad entre ambos polímeros para determinadas concentraciones.

La mejora de la compatibilidad entre ambos polímeros, con el objetivo de obtener formulaciones con mejores rendimientos que el de los componentes individuales, es uno de los principales retos científicos. Lovera *et al.* [267] estudiaron el efecto de la PCL con diferentes pesos moleculares, una PCL de alto peso molecular y dos PCL de bajo peso molecular modificadas químicamente, en la morfología y la estabilidad térmica de mezclas de PHB/PCL con diferente composición. Los autores observaron cómo la mezcla de PHB/PCL que contenía PCL de alto peso molecular daba lugar a mezclas inmiscibles en todo el rango de composiciones estudiado. Sin embargo, cuando mezclaron el PHB con las PCL de bajo peso molecular modificadas químicamente obtuvieron mezclas parcialmente miscibles, observando un menor tamaño y una mejor dispersión de los dominios de PCL en la matriz de PHB. El aumento de la compatibilidad entre ambos polímeros dio lugar a una disminución de la temperatura de fusión y la temperatura de transición vítrea del PHB en las mezclas, dicho descenso se vio influenciado por el peso molecular de la PCL empleada (siendo mayor en el caso de la PCL con menor peso molecular) y por el contenido de PCL en las mezclas. El aumento de la miscibilidad en las mezclas de PHB/PCL con bajo peso molecular también influyó en su degradación enzimática, reduciendo su velocidad de degradación. Por otro lado, Liau *et al.* [268] mejoraron la compatibilidad de films de PHB/PCL (80/20) obtenidos mediante disolución tras la incorporación de pequeñas cantidades de nanopartículas modificadas (estearato de hidróxidos de doble capa de Mg-Al), obteniendo formulaciones con mayor resistencia a tracción, módulo elástico y alargamiento a la rotura. Los autores observaron cómo la presencia de un 1% en peso de nanopartículas en la mezcla aumentó la resistencia a tracción y el alargamiento a la rotura cerca de un 66% y un 300% respectivamente con respecto a la mezcla sin reforzar. Kim *et al.* [269] también mejoraron la miscibilidad entre ambos polímeros utilizando un copoliéster de PHB/PCL, sintetizado mediante transesterificación, como compatibilizante en mezclas de PHB/PCL.

I.8. CARGAS FUNCIONALES EN FORMULACIONES DE POLI(3-HIDROXIBUTIRATO)

Otro de los enfoques empleados para mejorar las propiedades del PHB, es la incorporación de un refuerzo secundario, como fibras naturales o nanocargas en la matriz del biopolímero. Generalmente, dicha incorporación se realiza con el objetivo de aumentar las propiedades mecánicas resistentes, las propiedades térmicas y, principalmente, para que actúen como agentes nucleantes aumentando la densidad de nucleación, la velocidad de cristalización y disminuyendo el tamaño medio de las esferulitas, ya que, como se ha comentado anteriormente, las esferulitas grandes pueden dar lugar a grietas internas fragilizando el material [270]. Sin embargo, dependiendo de las propiedades específicas del refuerzo empleado, pueden dar lugar a una mejora de otro tipo de propiedades como las ópticas, las propiedades barrera, la conductividad, la velocidad de biodegradación, etc.

La relativa baja hidrofobicidad que presenta el PHB permite una mejor adhesión con las fibras naturales en comparación con otros termoplásticos altamente hidrofóbicos; es por ello, que el empleo de fibras naturales como refuerzo del PHB ha sido ampliamente estudiado. Fibras de lino [271-273], kenaf [274], agave [275], de bagazo de caña de azúcar [276], cáñamo [273, 277], yute [277], carnauba [278], lyocell [274] o curauá [279] han sido incorporadas en elevadas cantidades a la matriz de PHB, dando lugar a materiales compuestos con un mejor rendimiento mecánico resistente y una mayor tenacidad que el biopolímero puro, sin afectar al carácter biodegradable del mismo y reduciendo considerablemente el coste final de la formulación, gracias a la elevada cantidad de fibras utilizadas como refuerzo y a su bajo coste con respecto al del PHB.

Sin embargo, durante los últimos años, el empleo de nanocargas orgánicas e inorgánicas como refuerzo del PHB ha llamado especialmente la atención de los científicos debido a las propiedades únicas que estas aportan al polímero con el empleo de pequeñas cantidades. Nanorefuerzos como nanotubos de carbono, nanoarcillas o nanocristales de celulosa (ver apartado I.5.3.2), entre otros, han sido incorporados al PHB de forma exitosa para mejorar propiedades como las propiedades barrera, la estabilidad térmica, las propiedades mecánicas, la cristalización o la velocidad de degradación. Una de las nanocargas más estudiadas como refuerzo del PHB han sido las nanoarcillas montmorillonita sin modificar y/u orgánicamente modificadas. Las propiedades del PHB reforzado con montmorillonita varían dependiendo de un gran número de factores como el nivel de dispersión de la carga en la matriz, el contenido de nanopartículas, la estructura de la carga en la matriz (estructura exfoliada o intercalada) o la naturaleza química del modificador. De forma general, este tipo de nanocarga aumenta las propiedades mecánicas

del PHB, como la resistencia y el módulo elástico a tracción y flexión, así como mejora su estabilidad térmica mediante la disminución de la temperatura de fusión y un aumento de la temperatura de inicio de degradación. Además, dichas nanopartículas actúan como agente nucleante acelerando la cristalización y disminuyendo el tamaño de los cristales, e incluso pueden obstaculizar el crecimiento de los cristales dando lugar a nanocompuestos con un menor grado de cristalinidad. También se ha demostrado que la forma laminar del nanorefuerzo aumenta la tortuosidad de la ruta de difusión de los gases, mejorando notablemente las propiedades barrera del PHB. Incluso se ha observado que este tipo de nanocarga puede retrasar la velocidad de biodegradación del material [134, 280-287]. El aumento de la estabilidad térmica del PHB tras la incorporación de nanoarcillas también quedó demostrado por Gardolinski *et al.* [288] después de la incorporación de caolinita modificada.

El efecto de los nanotubos de carbono (monocapa-SWCNTs y multicapa-MWCNTs), sin funcionalizar y funcionalizados, en las propiedades del PHB también ha sido estudiado. De forma general, se ha observado cómo la incorporación de nanotubos de carbono en el PHB ofrece mejoras en las propiedades mecánicas resistentes, como la resistencia a tracción o el módulo elástico, en las propiedades térmicas, aumentando la temperatura de inicio de degradación, así como en la conductividad eléctrica. Además, esta nanocarga también actúa como agente nucleante, acelerando la velocidad de cristalización e influyendo en el tamaño y la morfología cristalina del PHB [289-293]. Zarei *et al.* [290] demostraron cómo la incorporación de CNTs en el PHB permite la obtención de formulaciones capaces de ser utilizadas en medicina como soporte o estructura para la regeneración de tejidos gracias al aumento de la humectabilidad, la bioactividad y la viabilidad celular obtenidos tras la incorporación de nanotubos de carbono en el PHB.

Otro tipo de nanocargas como el óxido de zinc, dióxido de titanio, sulfuro de plata o hidróxidos de doble capa han sido incorporadas al PHB con el fin de mejorar ciertas propiedades. Díez-Pascual *et al.* [294] observaron cómo la incorporación de pequeñas cantidades de nanopartículas de óxido de zinc (ZnO) al PHB aumentaron su rigidez, su resistencia y su tenacidad. La estabilidad térmica del PHB también se vio afectada significativamente por la presencia de esta nanocarga, incrementando su temperatura de inicio de degradación en más de 23 °C tras incorporar un 10% en peso de ZnO en la matriz. En este caso, las partículas de ZnO también actuaron como agente nucleante acelerando la cristalización y aumentaron el grado de cristalinidad del polímero, dando lugar a una mejora de las propiedades barrera del PHB, disminuyendo su permeabilidad al vapor de agua y al oxígeno. Además, los nanocompuestos de PHB/ZnO obtenidos mostraron actividad

antibacteriana. El aumento de la temperatura de inicio de degradación y el efecto nucleante del refuerzo también fueron observados por Iulianellia *et al.* [295] tras incorporar diferentes cantidades (0,5, 0,75 y 1% en peso) de nanopartículas de dióxido de titanio (TiO_2) en la matriz de PHB. En este caso se observó cómo la incorporación de un 1% en peso de nanorefuerzo en la matriz de PHB dio lugar a un aumento de la temperatura de inicio de degradación de 56 °C y a un aumento de la temperatura de degradación máxima de 46 °C. Por el contrario, Yeo *et al.* [296] observaron una disminución de la temperatura de inicio de degradación del PHB tras la incorporación de sulfuro de plata (Ag_2S), así como una diminución de la temperatura de fusión, de la temperatura de cristalización, de la temperatura de transición vítrea y de la cristalinidad del PHB a medida que aumentaba el contenido de Ag_2S en la matriz. Hsu *et al.* [297, 298] y Wu *et al.* [299] estudiaron el efecto de hidróxidos de doble capa (LDH) modificados en la cristalinidad del PHB y en su estabilidad térmica, observando un aumento de la velocidad de cristalización debido al efecto nucleante de la carga y una disminución de la temperatura de inicio de degradación del PHB tras la incorporación del nanorefuerzo modificado. Ciou *et al.* [300] también observaron cómo la incorporación de LDH aumentaba las propiedades mecánicas del PHB sin afectar de forma significativa a la velocidad de biodegradación del polímero.

REFERENCIAS

[1] PlasticsEurope. *Plastics – The Facts 2017: An analysis of European plastics production, demand and waste data.* 2017. Disponible en: *"https://www.plasticseurope.org"* [Consulta: 03 de abril de 2018].

[2] Siddique R, Khatib J y Kaur I. *Use of recycled plastic in concrete: A review.* Waste Management, 2008. **28**(10):1835-1852.

[3] European Bioplastics. "*https://www.european-bioplastics.org"* [Consulta: 03 de abril de 2018].

[4] European Committee for Standarization (CEN). *Bio-based products – Vocabulary*. EN 16575:2014. 2014, Bruselas: CEN.

[5] Asociación Española de Normalización (AENOR). *Envases y embalajes. Requisitos de los envases y embalajes valorizables mediante compostaje y biodegradación. Programa de ensayo y criterios de evaluación para la aceptación final del envase o embalaje*. UNE-EN 13432:2001. 2001, Madrid: AENOR.

[6] Balart R, López J, Sánchez L y Nadal A. *Introducción a la ciencia e ingeniería de polímeros.* 2001, Alcoy.

[7] Babu RP, O'connor K y Seeram R. *Current progress on bio-based polymers and their future trends.* Progress in Biomaterials, 2013. **2**(1):8.

[8] European Bioplastics. *Bioplastics market data 2017.* 2017. Disponible en: "*https://www.european-bioplastics.org"* [Consulta: 03 de abril de 2018].

[9] Ashter SA. *5 – Types of Biodegradable Polymers*, en *Introduction to Bioplastics Engineering*. 2016, Oxford: William Andrew. p. 81-151.

[10] Reddy MM, Vivekanandhan S, Misra M, Bhatia SK y Mohanty AK. *Biobased plastics and bionanocomposites: Current status and future opportunities.* Progress in Polymer Science, 2013. **38**(10-11):1653-1689.

[11] Collias DI, Harris AM, Nagpal V, Cottrell IW y Schultheis MW. *Biobased terephthalic acid technologies: A literature review.* Industrial Biotechnology, 2014. **10**(2):91-105.

[12] Fernandez MF, Ozkalustyan MLV, Camargo AS, Nascimento PT y Yu ASO. *Bio-based plastics evolution and the challenges to achieve dominance,* en *2013 Proceedings of PICMET'13: Technology Management in the IT-Driven Services (PICMET)*. 2013, San José: IEEE. p. 2726-2734.

[13] Martino L, Basilissi L, Farina H, Ortenzi MA, Zini E, Silvestro GD y Scandola M. *Bio-based polyamide 11: Synthesis, rheology and solid-state properties of star structures.* European Polymer Journal, 2014. **59**:69-77.

[14] Park SJ, Kim EY, Noh W, Oh YH, Kim HY, Song BK, Cho KM, Hong SH, Lee SH y Jegal J. *Synthesis of nylon 4 from gamma-aminobutyrate (GABA) produced by recombinant Escherichia coli.* Bioprocess and Biosystems Engineering, 2013. **36**(7):885-892.

[15] Miao S, Wang P, Su Z y Zhang S. *Vegetable-oil-based polymers as future polymeric biomaterials.* Acta Biomaterialia, 2014. **10**(4):1692-1704.

[16] Tokiwa Y y Calabia BP. *Biodegradability and biodegradation of polyesters.* Journal of Polymers and the Environment, 2007. **15**(4):259-267.

[17] Shor L, Güçeri S y Sun W. *Precision extrusion deposition of polycaprolactone/hydroxyapatite tissue scaffolds*, en *Solid Freeform Fabrication Proceedings*. 2006, Austin: University of Texas at Austin. p. 96-101.

[18] Eastmond GC. *Poly(ε-caprolactone) blends*, en *Biomedical Applications Polymer Blends,* Eastmond GC, Höcker H y Klee D. 2000, Heidelberg: Springer. p. 59-223.

[19] Mittal V, Akhtar T y Matsko N. *Mechanical, thermal, rheological and morphological properties of binary and ternary blends of PLA, TPS and PCL.* Macromolecular Materials and Engineering, 2015. **300**(4):423-435.

[20] Ostafinska A, Fortelny I, Nevoralova M, Hodan J, Kredatusova J y Slouf M. *Synergistic effects in mechanical properties of PLA/PCL blends with optimized composition, processing, and morphology.* RSC Advances, 2015. **5**(120):98971-98982.

[21] Patrício T y Bártolo P. *Thermal stability of PCL/PLA blends produced by physical blending process.* Procedia Engineering, 2013. **59**:292-297.

[22] Gassner F y Owen AJ. *Physical properties of poly(β-hydroxybutyrate)-poly(ε-caprolactone) blends.* Polymer, 1994. **35**(10):2233-2236.

[23] Chun YS y Kim WN. *Thermal properties of poly(hydroxybutyrate-co-hydroxyvalerate) and poly(ϵ-caprolactone) blends.* Polymer, 2000. **41**(6):2305-2308.

[24] Averous L, Moro L, Dole P y Fringant C. *Properties of thermoplastic blends: Starch-polycaprolactone.* Polymer, 2000. **41**(11):4157-4167.

[25] Ninago MD, López OV, Lencina MMS, García MA, Andreucetti NA, Ciolino AE y Villar MA. *Enhancement of thermoplastic starch final properties by blending with poly(ε-caprolactone).* Carbohydrate Polymers, 2015. **134**:205-212.

[26] Williams JM, Adewunmi A, Schek RM, Flanagan CL, Krebsbach PH, Feinberg SE, Hollister SJ y Das S. *Bone tissue engineering using polycaprolactone scaffolds fabricated via selective laser sintering.* Biomaterials, 2005. **26**(23):4817-4827.

[27] Dash TK y Konkimalla VB. *Poly-ε-caprolactone based formulations for drug delivery and tissue engineering: A review.* Journal of Controlled Release, 2012. **158**(1):15-33.

[28] Abedalwafa M, Wang F, Wang L y Li C. *Biodegradable poly-epsilon-caprolactone (PCL) for tissue engineering applications: A review.* Review on Advanced Materials Science, 2013. **34**(2):123-140.

[29] Joseph CS, Prashanth KVH, Rastogi NK, Indiramma AR, Reddy SY y Raghavarao KSMS. *Optimum blend of chitosan and poly-(ε-caprolactone) for fabrication of films for food packaging applications.* Food and Bioprocess Technology, 2011. **4**(7):1179-1185.

[30] Wu Y, Qin Y, Yuan M, Li L, Chen H, Cao J y Yang J. *Characterization of an antimicrobial poly(lactic acid) film prepared with poly(ε-caprolactone) and thymol for active packaging.* Polymers for Advanced Technologies, 2014. **25**(9):948-954.

[31] Xu J y Guo BH. *Poly(butylene succinate) and its copolymers: Research, development and industrialization.* Biotechnology Journal, 2010. **5**(11):1149-1163.

[32] Xu J y Guo BH. *Microbial succinic acid, its polymer poly(butylene succinate), and applications*, en *Plastics from Bacteria,* Chen GQ. 2010, Heidelberg: Springer. p. 347-388.

[33] Han SO, Lee SM, Park WH y Cho D. *Mechanical and thermal properties of waste silk fiber-reinforced poly(butylene succinate) biocomposites.* Journal of Applied Polymer Science, 2006. **100**(6):4972-4980.

[34] Grayson ACR, Voskerician G, Lynn A, Anderson JM, Cima MJ y Langer R. *Differential degradation rates in vivo and in vitro of biocompatible poly(lactic acid) and poly(glycolic acid) homo- and co-polymers for a polymeric drug-delivery microchip.* Journal of Biomaterials Science, Polymer Edition, 2004. **15**(10):1281-1304.

[35] Mackinnon SE y Dellon AL. *Clinical nerve reconstruction with a bioabsorbable polyglycolic acid tube.* Plastic and Reconstructive Surgery, 1990. **85**(3):419-424.

[36] Herrmann JB, Kelly RJ y Higgins GA. *Polyglycolic acid sutures: Laboratory and clinical evaluation of a new absorbable suture material.* Archives of Surgery, 1970. **100**(4):486-490.

[37] Zhang N, Wang Q, Ren J y Wang L. *Preparation and properties of biodegradable poly(lactic acid)/poly(butylene adipate-co-terephthalate) blend with glycidyl methacrylate as reactive processing agent.* Journal of Materials Science, 2009. **44**(1):250-256.

[38] Chieng BW, Ibrahim NA y Yunus WMZW. *Effect of organo-modified montmorillonite on poly(butylene succinate)/poly(butylene adipate-co-terephthalate) nanocomposites.* Express Polymer Letters, 2010. **4**(7):404-414.

[39] Nafchi AM, Moradpour M, Saeidi M y Alias AK. *Thermoplastic starches: Properties, challenges, and prospects.* Starch-Stärke, 2013. **65**(1-2):61-72.

[40] Liu H, Xie F, Yu L, Chen L y Li L. *Thermal processing of starch-based polymers.* Progress in Polymer Science, 2009. **34**(12):1348-1368.

[41] Li H y Huneault MA. *Comparison of sorbitol and glycerol as plasticizers for thermoplastic starch in TPS/PLA blends.* Journal of Applied Polymer Science, 2011. **119**(4):2439-2448.

[42] Yang Y, Tang Z, Xiong Z y Zhu J. *Preparation and characterization of thermoplastic starches and their blends with poly(lactic acid).* International Journal of Biological Macromolecules, 2015. **77**:273-279.

[43] Lai SM, Don TM y Huang YC. *Preparation and properties of biodegradable thermoplastic starch/poly(hydroxy butyrate) blends.* Journal of Applied Polymer Science, 2006. **100**(3):2371-2379.

[44] Shin BY, Lee SI, Shin YS, Balakrishnan S y Narayan R. *Rheological, mechanical and biodegradation studies on blends of thermoplastic starch and polycaprolactone.* Polymer Engineering & Science, 2004. **44**(8):1429-1438.

[45] Siqueira G, Bras J y Dufresne A. *Cellulosic bionanocomposites: A review of preparation, properties and applications.* Polymers, 2010. **2**(4):728-765.

[46] Moon RJ, Martini A, Nairn J, Simonsen J y Youngblood J. *Cellulose nanomaterials review: Structure, properties and nanocomposites.* Chemical Society Reviews, 2011. **40**(7):3941-3994.

[47] Brinchi L, Cotana F, Fortunati E y Kenny JM. *Production of nanocrystalline cellulose from lignocellulosic biomass: Technology and applications.* Carbohydrate Polymers, 2013. **94**(1):154-169.

[48] Reddy MM, Vivekanandhan S, Misra M, Bhatia SK y Mohanty AK. *Biobased plastics and bionanocomposites: Current status and future opportunities.* Progress in Polymer Science, 2013. **38**(10-11):1653-1689.

[49] Hamed I, Özogul F y Regenstein JM. *Industrial applications of crustacean by-products (chitin, chitosan, and chitooligosaccharides): A review.* Trends in Food Science & Technology, 2016. **48**:40-50.

[50] Kumar MNVR. *A review of chitin and chitosan applications.* Reactive and Functional Polymers, 2000. **46**(1):1-27.

[51] Zargar V, Asghari M y Dashti A. *A review on chitin and chitosan polymers: Structure, chemistry, solubility, derivatives, and applications.* ChemBioEng Reviews, 2015. **2**(3):204-226.

[52] Wang X, Chen Q y Lü X. *Pectin extracted from apple pomace and citrus peel by subcritical water.* Food Hydrocolloids, 2014. **38**:129-137.

[53] Espitia PJP, Du WX, Avena-Bustillos RJ, Soares NFF y McHugh TH. *Edible films from pectin: Physical-mechanical and antimicrobial properties – A review.* Food Hydrocolloids, 2014. **35**:287-296.

[54] Munarin F, Tanzi MC y Petrini P. *Advances in biomedical applications of pectin gels.* International Journal of Biological Macromolecules, 2012. **51**(4):681-689.

[55] Koshy RR, Mary SK, Thomas S y Pothan LA. *Environment friendly green composites based on soy protein isolate – A review.* Food Hydrocolloids, 2015. **50**:174-192.

[56] Fernández-Espada L, Bengoechea C, Cordobés F y Guerrero A. *Protein/glycerol blends and injection-molded bioplastic matrices: Soybean versus egg albumen.* Journal of Applied Polymer Science, 2016. **133**(6):42980.

[57] Tansaz S y Boccaccini AR. *Biomedical applications of soy protein: A brief overview.* Journal of Biomedical Materials Research Part A, 2016. **104**(2):553-569.

[58] Flambeau M, Redl A y Respondek F. *Chapter 4 – Proteins from wheat: Sustainable production and new developments in nutrition – Based and functional applications,* en *Sustainable Protein Sources,* Nadathur S, Wanasundara JPD y Scanlin L. 2017, Academic Press. p. 67-78.

[59] Thammahiwes S, Riyajan SA y Kaewtatip K. *Preparation and properties of wheat gluten based bioplastics with fish scale.* Journal of Cereal Science, 2017. **75**:186-191.

[60] Martin O, Schwach E, Avérous L y Couturier Y. *Properties of biodegradable multilayer films based on plasticized wheat starch.* Starch-Stärke, 2001. **53**(8):372-380.

[61] Gómez-Guillén MC, Giménez B, López-Caballero ME y Montero MP. *Functional and bioactive properties of collagen and gelatin from alternative sources: A review.* Food Hydrocolloids, 2011. **25**(8):1813-1827.

[62] Elzoghby AO, El-Fotoh WSA y Elgindy NA. *Casein-based formulations as promising controlled release drug delivery systems.* Journal of Controlled Release, 2011. **153**(3):206-216.

[63] Auras R, Harte B y Selke S. *An overview of polylactides as packaging materials.* Macromolecular Bioscience, 2004. **4**(9):835-864.

[64] Jiang L y Zhang J. *7 – Biodegradable and biobased polymers*, en *Applied Plastics Engineering Handbook (Second Edition),* Kutz M. 2017, William Andrew. p. 127-143.

[65] Liu H y Zhang J. *Research progress in toughening modification of poly(lactic acid).* Journal of Polymer Science Part B: Polymer Physics, 2011. **49**(15):1051-1083.

[66] Chieng BW, Ibrahim NA, Then YY y Loo YY. *Mechanical, thermal, and morphology properties of poly(lactic acid) plasticized with poly(ethylene glycol) and epoxidized palm oil hybrid plasticizer.* Polymer Engineering & Science, 2016. **56**(10):1169-1174.

[67] Rapa M, Darie-Nita RN y Vasile C. *Influence of plasticizers over some physico-chemical properties of PLA.* Materiale Plastice, 2017. **54**(1):73-78.

[68] Darie-Niţă RN, Vasile C, Irimia A, Lipşa R y Râpă M. *Evaluation of some eco-friendly plasticizers for PLA films processing.* Journal of Applied Polymer Science, 2016. **133**(13):43223.

[69] Matta AK, Rao RU, Suman KNS y Rambabu V. *Preparation and characterization of biodegradable PLA/PCL polymeric blends.* Procedia Materials Science, 2014. **6**:1266-1270.

[70] Urquijo J, Guerrica-Echevarría G y Eguiazábal JI. *Melt processed PLA/PCL blends: Effect of processing method on phase structure, morphology, and mechanical properties.* Journal of Applied Polymer Science, 2015. **132**(41):42641.

[71] Kumar M, Mohanty S, Nayak SK y Parvaiz MR. *Effect of glycidyl methacrylate (GMA) on the thermal, mechanical and morphological property of biodegradable PLA/PBAT blend and its nanocomposites.* Bioresource Technology, 2010. **101**(21):8406-8415.

[72] Lin S, Guo W, Chen C, Ma J y Wang B. *Mechanical properties and morphology of biodegradable poly(lactic acid)/poly(butylene adipate-co-terephthalate) blends compatibilized by transesterification.* Materials & Design (1980-2015), 2012. **36**:604-608.

[73] Hassan E, Wei Y, Jiao H y Muhuo Y. *Dynamic mechanical properties and thermal stability of poly(lactic acid) and poly(butylene succinate) blends composites.* Journal of Fiber Bioengineering and Informatics, 2013. **6**(1):85-94.

[74] Nampoothiri KM, Nair NR y John RP. *An overview of the recent developments in polylactide (PLA) research.* Bioresource Technology, 2010. **101**(22):8493-8501.

[75] Jem KJ, van der Pol JF y de Vos S. *Microbial lactic acid, its polymer poly(lactic acid), and their industrial applications*, en *Plastics from Bacteria,* Chen GQ. 2010, Heidelberg: Springer. p. 323-346.

[76] Castro-Aguirre E, Iñiguez-Franco F, Samsudin H, Fang X y Auras R. *Poly(lactic acid) – Mass production, processing, industrial applications, and end of life.* Advanced Drug Delivery Reviews, 2016. **107**:333-366.

[77] Keshavarz T y Roy I. *Polyhydroxyalkanoates: Bioplastics with a green agenda.* Current Opinion in Microbiology, 2010. **13**(3):321-326.

[78] Anjum A, Zuber M, Zia KM, Noreen A, Anjum MN y Tabasum S. *Microbial production of polyhydroxyalkanoates (PHAs) and its copolymers: A review of recent advancements.* International Journal of Biological Macromolecules, 2016. **89**:161-174.

[79] Reddy CSK, Ghai R, Rashmi y Kalia VC. *Polyhydroxyalkanoates: An overview.* Bioresource Technology, 2003. **87**(2):137-146.

[80] Koller M, Gasser I, Schmid F y Berg G. *Linking ecology with economy: Insights into polyhydroxyalkanoate-producing microorganisms.* Engineering in Life Sciences, 2011. **11**(3):222-237.

[81] Możejko-Ciesielska J y Kiewisz R. *Bacterial polyhydroxyalkanoates: Still fabulous?.* Microbiological Research, 2016. **192**:271-282.

[82] Urtuvia V, Villegas P, González M y Seeger M. *Bacterial production of the biodegradable plastics polyhydroxyalkanoates.* International Journal of Biological Macromolecules, 2014. **70**:208-213.

[83] Philip S, Keshavarz T y Roy I. *Polyhydroxyalkanoates: Biodegradable polymers with a range of applications.* Journal of Chemical Technology and Biotechnology, 2007. **82**(3):233-247.

[84] Pillai AB y Kumarapillai HK. *Bacterial polyhydroxyalkanoates: Recent trends in production and applications*, en *Recent Advances in Applied Microbiology,* Shukla P. 2017, Singapur: Springer. p. 19-53.

[85] Leong YK, Show PL, Ooi CW, Ling TC y Lan JCW. *Current trends in polyhydroxyalkanoates (PHAs) biosynthesis: Insights from the recombinant Escherichia coli.* Journal of Biotechnology, 2014. **180**:52-65.

[86] Kim BS, Lee SY y Chang HN. *Production of poly-β-hydroxybutyrate by fed-batch culture of recombinant Escherichia coli.* Biotechnology Letters, 1992. **14**(9):811-816.

[87] Liu F, Li W, Ridgway D, Gu T y Shen Z. *Production of poly-β-hydroxybutyrate on molasses by recombinant Escherichia coli.* Biotechnology Letters, 1998. **20**(4):345-348.

[88] Ahn WS, Park SJ y Lee SY. *Production of poly(3-hydroxybutyrate) from whey by cell recycle fed-batch culture of recombinant Escherichia coli.* Biotechnology Letters, 2001. **23**(3):235-240.

[89] Khanna S y Srivastava AK. *Recent advances in microbial polyhydroxyalkanoates.* Process Biochemistry, 2005. **40**(2):607-619.

[90] Akaraonye E, Keshavarz T y Roy I. *Production of polyhydroxyalkanoates: The future green materials of choice.* Journal of Chemical Technology and Biotechnology, 2010. **85**(6):732-743.

[91] Chee JY, Yoga SS, Lau NS, Ling SC, Abed RMM y Sudesh K. *Bacterially produced polyhydroxyalkanoate (PHA): Converting renewable resources into bioplastics.* Current Research, Technology and Education Topics in Applied Microbiology and Microbial Biotechnology, 2010. **2**:1395-1404.

[92] Ciesielski S, Możejko J y Pisutpaisal N. *Plant oils as promising substrates for polyhydroxyalkanoates production.* Journal of Cleaner Production, 2015. **106**:408-421.

[93] Jacquel N, Lo CW, Wei YH, Wu HS y Wang SS. *Isolation and purification of bacterial poly(3-hydroxyalkanoates).* Biochemical Engineering Journal, 2008. **39**(1):15-27.

[94] Kunasundari B y Sudesh K. *Isolation and recovery of microbial polyhydroxyalkanoates.* Express Polymer Letters, 2011. **5**(7):620-634.

[95] Dalton DA, Ma C, Shrestha S, Kitin P y Strauss SH. *Trade-offs between biomass growth and inducible biosynthesis of polyhydroxybutyrate in transgenic poplar.* Plant Biotechnology Journal, 2011. **9**(7):759-767.

[96] McQualter RB, Petrasovits LA, Gebbie LK, Schweitzer D, Blackman DM, Chrysanthopoulos P, Hodson MP, Plan MR, Riches JD, Snell KD, Brumbley SM y Nielsen LK. *The use of an acetoacetyl-CoA synthase in place of a β-ketothiolase enhances poly-3-hydroxybutyrate production in sugarcane mesophyll cells.* Plant Biotechnology Journal, 2015. **13**(5):700-707.

[97] Parveez GKA, Bahariah B, Ayub NH, Masani MYA, Rasid OA, Tarmizi AH y Ishak Z. *Production of polyhydroxybutyrate in oil palm (Elaeis guineensis Jacq.) mediated by microprojectile bombardment of PHB biosynthesis genes into embryogenic calli.* Frontiers in Plant Science, 2015. **6**:598.

[98] Tilbrook K, Gebbie L, Schenk PM, Poirier Y y Brumbley SM. *Peroxisomal polyhydroxyalkanoate biosynthesis is a promising strategy for bioplastic production in high biomass crops.* Plant Biotechnology Journal, 2011. **9**(9):958-969.

[99] Bohmert-Tatarev K, McAvoy S, Daughtry S, Peoples OP y Snell KD. *High levels of bioplastic are produced in fertile transplastomic tobacco plants engineered with a synthetic operon for production of polyhydroxybutyrate.* Plant Physiology, 2011. **155**(4):1690-1708.

[100] Gumel AM, Annuar MSM y Chisti Y. *Recent advances in the production, recovery and applications of polyhydroxyalkanoates.* Journal of Polymers and the Environment, 2013. **21**(2):580-605.

[101] Shah AA, Hasan F, Hameed A y Ahmed S. *Biological degradation of plastics: A comprehensive review.* Biotechnology Advances, 2008. **26**(3):246-265.

[102] Polyák P, Szemerszki D, Vörös G y Pukánszky B. *Mechanism and kinetics of the hydrolytic degradation of amorphous poly(3-hydroxybutyrate).* Polymer Degradation and Stability, 2017. **140**:1-8.

[103] Leimann FV, Biz MH, Musyanovych A, Sayer C, Landfester K y de Araújo PHH. *Hydrolysis of poly(hydroxybutyrate-co-hydroxyvalerate) nanoparticles.* Journal of Applied Polymer Science, 2013. **128**(5):3093-3098.

[104] Nigmatullin R, Thomas P, Lukasiewicz B, Puthussery H y Roy I. *Polyhydroxyalkanoates, a family of natural polymers, and their applications in drug delivery.* Journal of Chemical Technology and Biotechnology, 2015. **90**(7):1209-1221.

[105] Renard E, Walls M, Guérin P y Langlois V. *Hydrolytic degradation of blends of polyhydroxyalkanoates and functionalized polyhydroxyalkanoates.* Polymer Degradation and Stability, 2004. **85**(2):779-787.

[106] Bucci DZ, Tavares LBB y Sell I. *Biodegradation and physical evaluation of PHB packaging.* Polymer Testing, 2007. **26**(7):908-915.

[107] Lenz RW y Marchessault RH. *Bacterial polyesters: Biosynthesis, biodegradable plastics and biotechnology.* Biomacromolecules, 2005. **6**(1):1-8.

[108] Chodak I. *Chapter 22 – Polyhydroxyalkanoates: Origin, properties and applications*, en *Monomers, Polymers and Composites from Renewable Resources,* Belgacem MN y Gandini A. 2008, Amsterdam: Elsevier. p. 451-477.

[109] Bugnicourt E, Cinelli P, Lazzeri A y Alvarez VA. *Polyhydroxyalkanoate (PHA): Review of synthesis, characteristics, processing and potential applications in packaging.* Express Polymer Letters, 2014. **8**(11):791-808.

[110] Sudesh K, Abe H y Doi Y. *Synthesis, structure and properties of polyhydroxyalkanoates: Biological polyesters.* Progress in Polymer Science, 2000. **25**(10):1503-1555.

[111] Fan X, Jiang Q, Sun Z, Li G, Ren X, Liang J y Huang TS. *Preparation and characterization of electrospun antimicrobial fibrous membranes based on polyhydroxybutyrate (PHB).* Fibers and Polymers, 2015. **16**(8):1751-1758.

[112] Barham PJ y Keller A. *The relationship between microstructure and mode of fracture in polyhydroxybutyrate.* Journal of Polymer Science Part B: Polymer Physics, 1986. **24**(1):69-77.

[113] Hobbs JK, McMaster TJ, Miles MJ y Barham PJ. *Cracking in spherulites of poly(hydroxybutyrate).* Polymer, 1996. **37**(15):3241-3246.

[114] Di Lorenzo ML y Righetti MC. *Evolution of crystal and amorphous fractions of poly [(R)-3-hydroxybutyrate] upon storage.* Journal of Thermal Analysis and Calorimetry, 2013. **112**(3):1439-1446.

[115] El-Hadi A, Schnabel R, Straube E, Müller G y Henning S. *Correlation between degree of crystallinity, morphology, glass temperature, mechanical properties and biodegradation of poly(3-hydroxyalkanoate) PHAs and their blends.* Polymer Testing, 2002. **21**(6):665-674.

[116] dos Santos AJ, Valentina OD, Veriano L, Schulz H, Alayo A y Duarte MAT. *From obtaining to degradation of PHB: Material properties. Part I.* Ingeniería y Ciencia, 2017. **13**(26):269-298.

[117] Crétois R, Chenal JM, Sheibat-Othman N, Monnier A, Martin C, Astruz O, Kurusu R y Demarquette NR. *Physical explanations about the improvement of polyhydroxybutyrate ductility: Hidden effect of plasticizer on physical ageing.* Polymer, 2016. **102**:176-182.

[118] De Koning GJM y Lemstra PJ. *Crystallization phenomena in bacterial poly[(R)-3-hydroxybutyrate]: 2. Embrittlement and rejuvenation.* Polymer, 1993. **34**(19):4089-4094.

[119] Hobbs JK y Barham PJ. *The fracture of poly(hydroxybutyrate) Part II Fracture mechanics study after annealing.* Journal of Materials Science, 1998. **33**(10):2515-2518.

[120] Struik LCE. *Physical Aging in Amorphous Polymers and Other Materials*. 1978, Amsterdam: Elsevier.

[121] Struik LCE. *The mechanical behaviour and physical ageing of semicrystalline polymers: 2.* Polymer, 1987. **28**(9):1534-1542.

[122] Scandola M, Ceccorulli G y Pizzoli M. *The physical aging of bacterial poly(D-β-hydroxybutyrate).* Macromolecular Rapid Communications, 1989. **10**(2):47-50.

[123] Hurrell BL y Cameron RE. *Physical ageing and the embrittlement of poly(hydroxybutyrate) on storage: A time resolved small angle X-ray scattering study.* Polymer International, 1998. **45**(3):308-312.

[124] Biddlestone F, Harris A, Hay JN y Hammond T. *The physical ageing of amorphous poly(hydroxybutyrate).* Polymer International, 1996. **39**(3):221-229.

[125] Di Lorenzo ML, Gazzano M y Righetti MC. *The role of the rigid amorphous fraction on cold crystallization of poly(3-hydroxybutyrate).* Macromolecules, 2012. **45**(14):5684-5691.

[126] Daly JH, Hayward D, Liggat JJ y Mackintosh AR. *Ageing and rejuvenation of Biopol™, [poly(3-hydroxybutyrate-co-3-hydroxyvalerate)] copolymers: A dielectric study.* Journal of Materials Science, 2004. **39**(3):925-931.

[127] Gunaratne LMWK, Shanks RA y Amarasinghe G. *Thermal history effects on crystallisation and melting of poly(3-hydroxybutyrate).* Thermochimica Acta, 2004. **423**(1-2):127-135.

[128] Yamaguchi M y Arakawa K. *Effect of thermal degradation on rheological properties for poly(3-hydroxybutyrate).* European Polymer Journal, 2006. **42**(7):1479-1486.

[129] Aoyagi Y, Yamashita K y Doi Y. *Thermal degradation of poly[(R)-3-hydroxybutyrate], poly[ε-caprolactone], and poly[(S)-lactide].* Polymer Degradation and Stability, 2002. **76**(1):53-59.

[130] Grassie N, Murray EJ y Holmes PA. *The thermal degradation of poly(-(d)-β-hydroxybutyric acid): Part 1 – Identification and quantitative analysis of products.* Polymer Degradation and Stability, 1984. **6**(1):47-61.

[131] Pachekoski WM, Dalmolin C y Agnelli JAM. *The influence of the industrial processing on the degradation of poly(hidroxybutyrate)-PHB.* Materials Research, 2013. **16**(2):327-332.

[132] Grassie N, Murray EJ y Holmes PA. *The thermal degradation of poly(-(d)-β-hydroxybutyric acid): Part 2 – Changes in molecular weight.* Polymer Degradation and Stability, 1984. **6**(2):95-103.

[133] Siracusa V, Rocculi P, Romani S y Rosa MD. *Biodegradable polymers for food packaging: A review.* Trends in Food Science & Technology, 2008. **19**(12):634-643.

[134] Sanchez-Garcia MD, Gimenez E y Lagaron JM. *Novel PET nanocomposites of interest in food packaging applications and comparative barrier performance with biopolyester nanocomposites.* Journal of Plastic Film & Sheeting, 2007. **23**(2):133-148.

[135] Haugaard VK, Danielsen B y Bertelsen G. *Impact of polylactate and poly(hydroxybutyrate) on food quality.* European Food Research and Technology, 2003. **216**(3):233-240.

[136] Arrieta MP, López J, Hernández A y Rayón E. *Ternary PLA-PHB-Limonene blends intended for biodegradable food packaging applications.* European Polymer Journal, 2014. **50**:255-270.

[137] Miguel O y Iruin JJ. *Water transport properties in poly(3-hydroxybutyrate) and poly(3-hydroxybutyrate-co-3-hydroxyvalerate) biopolymers.* Journal of Applied Polymer Science, 1999. **73**(4):455-468.

[138] Koller M. *Poly(hydroxyalkanoates) for food packaging: Application and attempts towards implementation.* Applied Food Biotechnology, 2014. **1**(1):3-15.

[139] Plackett D y Siró I. *18 – Polyhydroxyalkanoates (PHAs) for food packaging*, en *Multifunctional and Nanoreinforced Polymers for Food Packaging,* Lagarón JM. 2011, Sawston: Woodhead Publishing. p. 498-526.

[140] Lagaron JM, Catalá R y Gavara R. *Structural characteristics defining high barrier properties in polymeric materials.* Materials Science and Technology, 2004. **20**(1):1-7.

[141] Yeo JCC, Muiruri JK, Thitsartarn W, Li Z y He C. *Recent advances in the development of biodegradable PHB-based toughening materials: Approaches, advantages and applications.* Materials Science and Engineering: C, 2017. 10.1016/j.msec.2017.11.006.

[142] Raza ZA, Abid S y Banat IM. *Polyhydroxyalkanoates: Characteristics, production, recent developments and applications.* International Biodeterioration & Biodegradation, 2018. **126**:45-56.

[143] Ke Y, Zhang XY, Ramakrishna S, He LM y Wu G. *Reactive blends based on polyhydroxyalkanoates: Preparation and biomedical application.* Materials Science and Engineering: C, 2017. **70**:1107-1119.

[144] Hazer DB, Kılıçay E y Hazer B. *Poly(3-hydroxyalkanoate)s: Diversification and biomedical applications: A state of the art review.* Materials Science and Engineering: C, 2012. **32**(4):637-647.

[145] Bucci DZ, Tavares LBB y Sell I. *PHB packaging for the storage of food products.* Polymer Testing, 2005. **24**(5):564-571.

[146] Rosa DS, Lotto NT, Lopes DR y Guedes CGF. *The use of roughness for evaluating the biodegradation of poly-β-(hydroxybutyrate) and poly-β-(hydroxybutyrate-co-β-valerate).* Polymer Testing, 2004. **23**(1):3-8.

[147] Volova T, Zhila N, Vinogradova O, Shumilova A, Prudnikova S y Shishatskaya E. *Characterization of biodegradable poly-3-hydroxybutyrate films and pellets loaded with the fungicide tebuconazole.* Environmental Science and Pollution Research, 2016. **23**(6):5243-5254.

[148] Boyandin AN, Zhila NO, Kiselev EG y Volova TG. *Constructing slow-release formulations of metribuzin based on degradable poly(3-hydroxybutyrate).* Journal of Agricultural and Food Chemistry, 2016. **64**(28):5625-5632.

[149] Volova TG, Prudnikova SV y Boyandin AN. *Biodegradable poly-3-hydroxybutyrate as a fertiliser carrier.* Journal of the Science of Food and Agriculture, 2016. **96**(12):4183-4193.

[150] Wilkes CE, Summers JW y Daniels CA. *PVC handbook*. 2005, Hanser.

[151] Vieira MGA, da Silva MA, dos Santos LO y Beppu MM. *Natural-based plasticizers and biopolymer films: A review.* European Polymer Journal, 2011. **47**(3):254-263.

[152] Daniels PH. *A brief overview of theories of PVC plasticization and methods used to evaluate PVC-plasticizer interaction.* Journal of Vinyl and Additive Technology, 2009. **15**(4):219-223.

[153] Bocqué M, Voirin C, Lapinte V, Caillol S y Robin JJ. *Petro-based and bio-based plasticizers: Chemical structures to plasticizing properties.* Journal of Polymer Science Part A: Polymer Chemistry, 2016. **54**(1):11-33.

[154] Arrieta MP, Samper MD, López J y Jiménez A. *Combined effect of poly(hydroxybutyrate) and plasticizers on polylactic acid properties for film intended for food packaging.* Journal of Polymers and the Environment, 2014. **22**(4):460-470.

[155] Godwin AD y Krauskopf LG. *Monomeric plasticizers, e*n *Handbook of Vinyl Formulating,* Grossman RF. 2008, Hoboken: John Wiley & Sons. p. 173-238.

[156] Lligadas G, Ronda JC, Galià M y Cádiz V. *Renewable polymeric materials from vegetable oils: A perspective.* Materials Today, 2013. **16**(9):337-343.

[157] Khot SN, Lascala JJ, Can E, Morye SS, Williams GI, Palmese GR, Kusefoglu SH y Wool RP. *Development and application of triglyceride-based polymers and composites.* Journal of Applied Polymer Science, 2001. **82**(3):703-723.

[158] Seydibeyoğlu MÖ, Misra M y Mohanty A. *Synergistic improvements in the impact strength and % elongation of polyhydroxybutyrate-co-valerate copolymers with functionalized soybean oils and POSS.* International Journal of Plastics Technology, 2010. **14**(1):1-16.

[159] Choi JS y Park WH. *Effect of biodegradable plasticizers on thermal and mechanical properties of poly(3-hydroxybutyrate).* Polymer Testing, 2004. **23**(4):455-460.

[160] Chieng BW, Ibrahim NA, Then YY y Loo YY. *Epoxidized vegetable oils plasticized poly(lactic acid) biocomposites: Mechanical, thermal and morphology properties.* Molecules, 2014. **19**(10):16024-16038.

[161] Carbonell-Verdu A, Garcia-Garcia D, Dominici F, Torre L, Sanchez-Nacher L y Balart R. *PLA films with improved flexibility properties by using maleinized cottonseed oil.* European Polymer Journal, 2017. **91**:248-259.

[162] Garcia-Campo MJ, Quiles-Carrillo L, Masia J, Reig-Pérez MJ, Montanes N y Balart R. *Environmentally friendly compatibilizers from soybean oil for ternary blends of poly(lactic acid)-PLA, poly(ε-caprolactone)-PCL and poly(3-hydroxybutyrate)-PHB.* Materials, 2017. **10**(11):1339.

[163] Ferri JM, Garcia-Garcia D, Sánchez-Nacher L, Fenollar O y Balart R. *The effect of maleinized linseed oil (MLO) on mechanical performance of poly(lactic acid)-thermoplastic starch (PLA-TPS) blends.* Carbohydrate Polymers, 2016. **147**:60-68.

[164] Zhang M y Thomas NL. *Preparation and properties of polyhydroxybutyrate blended with different types of starch.* Journal of Applied Polymer Science, 2010. **116**(2):688-694.

[165] Parulekar Y y Mohanty AK. *Extruded biodegradable cast films from polyhydroxyalkanoate and thermoplastic starch blends: Fabrication and characterization.* Macromolecular Materials and Engineering, 2007. **292**(12):1218-1228.

[166] Ferri JM, Garcia-Garcia D, Carbonell-Verdu A, Fenollar O y Balart R. *Poly(lactic acid) formulations with improved toughness by physical blending with thermoplastic starch.* Journal of Applied Polymer Science, 2018. **135**(4):45751.

[167] Imre B y Pukánszky B. *Compatibilization in bio-based and biodegradable polymer blends.* European Polymer Journal, 2013. **49**(6):1215-1233.

[168] Pracella M. *7 – Blends and alloys*, en *Modification of Polymer Properties,* Jasso-Gastinel CF y Kenny JM. 2017, William Andrew. p. 155-184.

[169] Thomas S, Grohens Y y Jyotishkumar P. *Characterization of Polymer Blends: Miscibility, Morphology and Interfaces*. 2014, Weinheim: Wiley-VCH.

[170] Isayev AI. *Encyclopedia of Polymer Blends, Volume 3: Structure*. 2016, Weinheim: Wiley-VCH.

[171] Ma P, Cai X, Zhang Y, Wang S, Dong W, Chen M y Lemstra PJ. *In-situ compatibilization of poly(lactic acid) and poly(butylene adipate-co-terephthalate) blends by using dicumyl peroxide as a free-radical initiator.* Polymer Degradation and Stability, 2014. **102**:145-151.

[172] Ma P, Hristova-Bogaerds DG, Lemstra PJ, Zhang Y y Wang S. *Toughening of PHBV/PBS and PHB/PBS blends via in situ compatibilization using dicumyl peroxide as a free-radical grafting initiator.* Macromolecular Materials and Engineering, 2012. **297**(5):402-410.

[173] Cruz BAS, Martínez AMM, de la Garza AE, Espiricueto SM y Armenta JLR, E*valuation of crosslinking reaction in adhesive based styrene-butadiene elastomers using infrared spectroscopy*, en *Infrared Spectroscopy – Anharmonicity of Biomolecules, Crosslinking of Biopolymers, Food Quality and Medical Applications,* Theophile T. 2015, InTech. p. 117-135.

[174] Semba T, Kitagawa K, Ishiaku US y Hamada H. *The effect of crosslinking on the mechanical properties of polylactic acid/polycaprolactone blends.* Journal of Applied Polymer Science, 2006. **101**(3):1816-1825.

[175] Ji D, Liu Z, Lan X, Wu F, Xie B y Yang M. *Morphology, rheology, crystallization behavior, and mechanical properties of poly(lactic acid)/poly(butylene succinate)/dicumyl peroxide reactive blends.* Journal of Applied Polymer Science, 2014. **131**(3):39580.

[176] Wang R, Wang S, Zhang Y, Wan C y Ma P. *Toughening modification of PLLA/PBS blends via in situ compatibilization.* Polymer Engineering & Science, 2009. **49**(1):26-33.

[177] Dong W, Ma P, Wang S, Chen M, Cai X y Zhang Y. *Effect of partial crosslinking on morphology and properties of the poly(β-hydroxybutyrate)/poly(D,L-lactic acid) blends.* Polymer Degradation and Stability, 2013. **98**(9):1549-1555.

[178] Lamouroux E y Fort Y. *Chapter 2 – An overview of nanocomposite nanofillers and their functionalization*, en *Spectroscopy of Polymer Nanocomposites,* Thomas S, Rouxel D y Ponnamma D. 2016, William Andrew. p. 15-64.

[179] Rallini M y Kenny JM. *3 – Nanofillers in polymers*, en *Modification of Polymer Properties,* Jasso-Gastinel CF y Kenny JM. 2017, William Andrew. p. 47-86.

[180] de Luna MS y Filippone G. *Effects of nanoparticles on the morphology of immiscible polymer blends – Challenges and opportunities.* European Polymer Journal, 2016. **79**:198-218.

[181] Taguet A, Cassagnau P y Lopez-Cuesta JM. *Structuration, selective dispersion and compatibilizing effect of (nano)fillers in polymer blends.* Progress in Polymer Science, 2014. **39**(8):1526-1563.

[182] Zare Y, Rhee KY y Hui D. *Influences of nanoparticles aggregation/agglomeration on the interfacial/interphase and tensile properties of nanocomposites.* Composites Part B: Engineering, 2017. **122**:41-46.

[183] Kango S, Kalia S, Celli A, Njuguna J, Habibi Y y Kumar R. *Surface modification of inorganic nanoparticles for development of organic-inorganic nanocomposites – A review.* Progress in Polymer Science, 2013. **38**(8):1232-1261.

[184] Eyley S y Thielemans W. *Surface modification of cellulose nanocrystals.* Nanoscale, 2014. **6**(14):7764-7779.

[185] Dasari A y Njuguna J. *Functional and Physical Properties of Polymer Nanocomposites*. 2016, Chichester: John Wiley & Sons.

[186] Raquez JM, Habibi Y, Murariu M y Dubois P. *Polylactide (PLA)-based nanocomposites.* Progress in Polymer Science, 2013. **38**(10-11):1504-1542.

[187] Buzea C, Pacheco II y Robbie K. *Nanomaterials and nanoparticles: Sources and toxicity.* Biointerphases, 2007. **2**(4):MR17-MR71.

[188] Du M, Guo B y Jia D. *Newly emerging applications of halloysite nanotubes: A review.* Polymer International, 2010. **59**(5):574-582.

[189] Singh B. *Why does halloysite roll? – A new model.* Clays and Clay Minerals, 1996. **44**(2):191-196.

[190] Tan D, Yuan P, Annabi-Bergaya F, Liu D, Wang L, Liu H y He H. *Loading and in vitro release of ibuprofen in tubular halloysite.* Applied Clay Science, 2014. **96**:50-55.

[191] Hemmatpour H, Haddadi-Asl V y Roghani-Mamaqani H. *Synthesis of pH-sensitive poly(N,N-dimethylaminoethyl methacrylate)-grafted halloysite nanotubes for adsorption and controlled release of DPH and DS drugs.* Polymer, 2015. **65**:143-153.

[192] Vergaro V, Lvov YM y Leporatti S. *Halloysite clay nanotubes for resveratrol delivery to cancer cells.* Macromolecular Bioscience, 2012. **12**(9):1265-1271.

[193] Wang Q, Zhang J, Zheng Y y Wang A. *Adsorption and release of ofloxacin from acid- and heat-treated halloysite.* Colloids and Surfaces B: Biointerfaces, 2014. **113**:51-58.

[194] Kim J, Park NH, Na JH y Han J. *Development of natural insect-repellent loaded halloysite nanotubes and their application to food packaging to prevent Plodia interpunctella infestation.* Journal of Food Science, 2016. **81**(8):E1956-E1965.

[195] Zhong B, Wang S, Dong H, Luo Y, Jia Z, Zhou X, Chen M, Xie D y Jia D. *Halloysite tubes as nanocontainers for herbicide and its controlled release in biodegradable poly(vinyl alcohol)/starch film.* Journal of Agricultural and Food Chemistry, 2017. **65**(48):10445-10451.

[196] Jang SH, Jang SR, Lee GM, Ryu JH, Park SI y Park NH. *Halloysite nanocapsules containing thyme essential oil: Preparation, characterization, and application in packaging materials.* Journal of Food Science, 2017. **82**(9):2113-2120.

[197] Shemesh R, Krepker M, Natan M, Danin-Poleg Y, Banin E, Kashi Y, Nitzan N, Vaxman A y Segal E. *Novel LDPE/halloysite nanotube films with sustained carvacrol release for broad-spectrum antimicrobial activity.* RSC Advances, 2015. **5**(106):87108-87117.

[198] Liu M, Jia Z, Jia D y Zhou C. *Recent advance in research on halloysite nanotubes-polymer nanocomposite.* Progress in Polymer Science, 2014. **39**(8):1498-1525.

[199] Zhong B, Jia Z, Hu D, Luo Y, Guo B y Jia D. *Surface modification of halloysite nanotubes by vulcanization accelerator and properties of styrene-butadiene rubber nanocomposites with modified halloysite nanotubes.* Applied Surface Science, 2016. **366**:193-201.

[200] Yuan P, Tan D y Annabi-Bergaya F. *Properties and applications of halloysite nanotubes: Recent research advances and future prospects.* Applied Clay Science, 2015. **112-113**:75-93.

[201] Liu M, Zhang Y y Zhou C. *Nanocomposites of halloysite and polylactide.* Applied Clay Science, 2013. **75-76**:52-59.

[202] Dong Y, Marshall J, Haroosh HJ, Mohammadzadehmoghadam S, Liu D, Qi X y Lau KT. *Polylactic acid (PLA)/halloysite nanotube (HNT) composite mats: Influence of HNT content and modification.* Composites Part A: Applied Science and Manufacturing, 2015. **76**:28-36.

[203] De Silva RT, Pasbakhsh P, Goh KL, Chai SP y Chen J. *Synthesis and characterisation of poly(lactic acid)/halloysite bionanocomposite films.* Journal of Composite Materials, 2014. **48**(30):3705-3717.

[204] Carli LN, Crespo JS y Mauler RS. *PHBV nanocomposites based on organomodified montmorillonite and halloysite: The effect of clay type on the morphology and thermal and mechanical properties.* Composites Part A: Applied Science and Manufacturing, 2011. **42**(11):1601-1608.

[205] Carli LN, Daitx TS, Soares GV, Crespo JS y Mauler RS. *The effects of silane coupling agents on the properties of PHBV/halloysite nanocomposites.* Applied Clay Science, 2014. **87**:311-319.

[206] Lee KS y Chang YW. *Thermal, mechanical, and rheological properties of poly(ε-caprolactone)/halloysite nanotube nanocomposites.* Journal of Applied Polymer Science, 2013. **128**(5):2807-2816.

[207] Pal P, Kundu MK, Malas A y Das CK. *Compatibilizing effect of halloysite nanotubes in polar-nonpolar hybrid system.* Journal of Applied Polymer Science, 2014. **131**(1):39587.

[208] Terzopoulou Z, Papageorgiou DG, Papageorgiou GZ y Bikiaris DN. *Effect of surface functionalization of halloysite nanotubes on synthesis and thermal properties of poly(ε-caprolactone).* Journal of Materials Science, 2018. **53**(9):6519-6541.

[209] Krishnaiah P, Ratnam CT y Manickam S. *Development of silane grafted halloysite nanotube reinforced polylactide nanocomposites for the enhancement of mechanical, thermal and dynamic-mechanical properties.* Applied Clay Science, 2017. **135**:583-595.

[210] Luzi F, Fortunati E, Puglia D, Petrucci R, Kenny JM y Torre L. *Modulation of acid hydrolysis reaction time for the extraction of cellulose nanocrystals from Posidonia oceanica leaves.* Journal of Renewable Materials, 2016. **4**(3):190-198.

[211] Fernandes EM, Pires RA, Mano JF y Reis RL. *Bionanocomposites from lignocellulosic resources: Properties, applications and future trends for their use in the biomedical field.* Progress in Polymer Science, 2013. **38**(10-11):1415-1441.

[212] Espinosa SC, Kuhnt T, Foster EJ y Weder C. *Isolation of thermally stable cellulose nanocrystals by phosphoric acid hydrolysis.* Biomacromolecules, 2013. **14**(4):1223-1230.

[213] Neto WPF, Silvério HA, Dantas NO y Pasquini D. *Extraction and characterization of cellulose nanocrystals from agro-industrial residue – Soy hulls.* Industrial Crops and Products, 2013. **42**:480-488.

[214] Yu H, Qin Z, Liang B, Liu N, Zhou Z y Chen L. *Facile extraction of thermally stable cellulose nanocrystals with a high yield of 93% through hydrochloric acid hydrolysis under hydrothermal conditions.* Journal of Materials Chemistry A, 2013. **1**(12):3938-3944.

[215] Sadeghifar H, Filpponen I, Clarke SP, Brougham DF y Argyropoulos DS. *Production of cellulose nanocrystals using hydrobromic acid and click reactions on their surface.* Journal of Materials Science, 2011. **46**(22):7344-7355.

[216] Siqueira G, Tapin-Lingua S, Bras J, Perez DS y Dufresne A. *Morphological investigation of nanoparticles obtained from combined mechanical shearing, and enzymatic and acid hydrolysis of sisal fibers.* Cellulose, 2010. **17**(6):1147-1158.

[217] Satyamurthy P, Jain P, Balasubramanya RH y Vigneshwaran N. *Preparation and characterization of cellulose nanowhiskers from cotton fibres by controlled microbial hydrolysis.* Carbohydrate Polymers, 2011. **83**(1):122-129.

[218] Filson PB y Dawson-Andoh BE. *Sono-chemical preparation of cellulose nanocrystals from lignocellulose derived materials.* Bioresource Technology, 2009. **100**(7):2259-2264.

[219] Chen W, Yu H, Liu Y, Chen P, Zhang M y Hai Y. *Individualization of cellulose nanofibers from wood using high-intensity ultrasonication combined with chemical pretreatments.* Carbohydrate Polymers, 2011. **83**(4):1804-1811.

[220] Zimmermann T, Bordeanu N y Strub E. *Properties of nanofibrillated cellulose from different raw materials and its reinforcement potential.* Carbohydrate Polymers, 2010. **79**(4):1086-1093.

[221] Klemm D, Kramer F, Moritz S, Lindström T, Ankerfors M, Gray D y Dorris A. *Nanocelluloses: A new family of nature-based materials.* Angewandte Chemie International Edition, 2011. **50**(24):5438-5466.

[222] Patrício PSO, Pereira FV, dos Santos MC, de Souza PP, Roa JPB y Orefice RL. *Increasing the elongation at break of polyhydroxybutyrate biopolymer: Effect of cellulose nanowhiskers on mechanical and thermal properties.* Journal of Applied Polymer Science, 2013. **127**(5):3613-3621.

[223] Fortunati E, Peltzer M, Armentano I, Torre L, Jiménez A y Kenny JM. *Effects of modified cellulose nanocrystals on the barrier and migration properties of PLA nano-biocomposites.* Carbohydrate Polymers, 2012. **90**(2):948-956.

[224] Chen Y, Liu C, Chang PR, Cao X y Anderson DP. *Bionanocomposites based on pea starch and cellulose nanowhiskers hydrolyzed from pea hull fibre: Effect of hydrolysis time.* Carbohydrate Polymers, 2009. **76**(4):607-615.

[225] Seoane IT, Manfredi LB, Cyras VP, Torre L, Fortunati E y Puglia D. *Effect of cellulose nanocrystals and bacterial cellulose on disintegrability in composting conditions of plasticized PHB nanocomposites.* Polymers, 2017. **9**(11):561.

[226] Luzi F, Fortunati E, Jiménez A, Puglia D, Pezzolla D, Gigliotti G, Kenny JM, Chiralt A y Torre L. *Production and characterization of PLA_PBS biodegradable blends reinforced with cellulose nanocrystals extracted from hemp fibres.* Industrial Crops and Products, 2016. **93**:276-289.

[227] Arrieta MP, Fortunati E, Dominici F, Rayón E, López J y Kenny JM. *Multifunctional PLA–PHB/cellulose nanocrystal films: Processing, structural and thermal properties.* Carbohydrate Polymers, 2014. **107**:16-24.

[228] Arrieta MP, Fortunati E, Dominici F, Rayón E, López J y Kenny JM. *PLA-PHB/cellulose based films: Mechanical, barrier and disintegration properties.* Polymer Degradation and Stability, 2014. **107**:139-149.

[229] Siqueira G, Bras J y Dufresne A. *Cellulose whiskers versus microfibrils: Influence of the nature of the nanoparticle and its surface functionalization on the thermal and mechanical properties of nanocomposites.* Biomacromolecules, 2009. **10**(2):425-432.

[230] Dhar P, Tarafder D, Kumar A y Katiyar V. *Effect of cellulose nanocrystal polymorphs on mechanical, barrier and thermal properties of poly(lactic acid) based bionanocomposites.* RSC Advances, 2015. **5**(74):60426-60440.

[231] Fortunati E, Luzi F, Puglia D, Petrucci R, Kenny JM y Torre L. *Processing of PLA nanocomposites with cellulose nanocrystals extracted from Posidonia oceanica waste: Innovative reuse of coastal plant.* Industrial Crops and Products, 2015. **67**:439-447.

[232] Zoppe JO, Peresin MS, Habibi Y, Venditti RA y Rojas OJ. *Reinforcing poly(ε-caprolactone) nanofibers with cellulose nanocrystals.* ACS Applied Materials & Interfaces, 2009. **1**(9):1996-2004.

[233] Sheng L, Jiang R, Zhu Y y Ji Y. *Electrospun cellulose nanocrystals/polycaprolactone nanocomposite fiber mats.* Journal of Macromolecular Science, Part B, 2014. **53**(5):820-828.

[234] Yu HY, Qin ZY, Liu YN, Chen L, Liu N y Zhou Z. *Simultaneous improvement of mechanical properties and thermal stability of bacterial polyester by cellulose nanocrystals.* Carbohydrate Polymers, 2012. **89**(3):971-978.

[235] Yu HY, Qin ZY, Liu L, Yang XG, Zhou Y y Yao JM. *Comparison of the reinforcing effects for cellulose nanocrystals obtained by sulfuric and hydrochloric acid hydrolysis on the mechanical and thermal properties of bacterial polyester.* Composites Science and Technology, 2013. **87**:22-28.

[236] Ten E, Bahr DF, Li B, Jiang L y Wolcott MP. *Effects of cellulose nanowhiskers on mechanical, dielectric, and rheological properties of poly(3-hydroxybutyrate-co-3-hydroxyvalerate)/cellulose nanowhisker composites.* Industrial & Engineering Chemistry Research, 2012. **51**(7):2941-2951.

[237] Seoane IT, Fortunati E, Puglia D, Cyras VP y Manfredi LB. *Development and characterization of bionanocomposites based on poly(3-hydroxybutyrate) and cellulose nanocrystals for packaging applications.* Polymer International, 2016. **65**(9):1046-1053.

[238] Dhar P, Bhardwaj U, Kumar A y Katiyar V. *Poly(3-hydroxybutyrate)/cellulose nanocrystal films for food packaging applications: Barrier and migration studies.* Polymer Engineering & Science, 2015. **55**(10):2388-2395.

[239] Verlinden RAJ, Hill DJ, Kenward MA, Williams CD y Radecka I. *Bacterial synthesis of biodegradable polyhydroxyalkanoates.* Journal of Applied Microbiology, 2007. **102**(6):1437-1449.

[240] Tsuge T. *Metabolic improvements and use of inexpensive carbon sources in microbial production of polyhydroxyalkanoates.* Journal of Bioscience and Bioengineering, 2002. **94**(6):579-584.

[241] Liu KL, Choo ESG, Wong SY, Li X, He CB, Wang J y Li J. *Designing poly[(R)-3-hydroxybutyrate]-based polyurethane block copolymers for electrospun nanofiber scaffolds with improved mechanical properties and enhanced mineralization capability.* The Journal of Physical Chemistry B, 2010. **114**(22):7489-7498.

[242] Wu L, Wang L, Wang X y Xu K. *Synthesis, characterizations and biocompatibility of novel biodegradable star block copolymers based on poly[(R)-3-hydroxybutyrate] and poly(ε-caprolactone).* Acta Biomaterialia, 2010. **6**(3):1079-1089.

[243] Aluthge DC, Xu C, Othman N, Noroozi N, Hatzikiriakos SG y Mehrkhodavandi P. *PLA-PHB-PLA triblock copolymers: Synthesis by sequential addition and investigation of mechanical and rheological properties.* Macromolecules, 2013. **46**(10):3965-3974.

[244] Panaitescu DM, Nicolae CA, Frone AN, Chiulan I, Stanescu PO, Draghici C, Iorga M y Mihailescu M. *Plasticized poly(3-hydroxybutyrate) with improved melt processing and balanced properties.* Journal of Applied Polymer Science, 2017. **134**(19):44810.

[245] Seoane IT, Manfredi LB y Cyras VP. *Effect of two different plasticizers on the properties of poly(3-hydroxybutyrate) binary and ternary blends.* Journal of Applied Polymer Science, 2018. **135**(12):46016.

[246] Erceg M, Kovačić T y Klarić I. *Thermal degradation of poly(3-hydroxybutyrate) plasticized with acetyl tributyl citrate.* Polymer Degradation and Stability, 2005. **90**(2):313-318.

[247] Râpă M, Darie-Niţă RN, Grosu E, Tănase EE, Trifoi AR, Pap T y Vasile C. *Effect of plasticizers on melt processability and properties of PHB.* Journal of Optoelectronics and Advanced Materials, 2015. **17**(11-12):1778-1784.

[248] Wang L, Zhu W, Wang X, Chen X, Chen GQ y Xu K. *Processability modifications of poly(3-hydroxybutyrate) by plasticizing, blending, and stabilizing.* Journal of Applied Polymer Science, 2008. **107**(1):166-173.

[249] Bibers I, Tupureina V, Dzene A, Savenkova L y Kalnins M. *Biodegradable materials from plasticized PHB biomass*. Macromolecular Symposia, 2001. **170**(1):61-72.

[250] Yoshie N, Nakasato K, Fujiwara M, Kasuya K, Abe H, Doi Y y Inoue Y. *Effect of low molecular weight additives on enzymatic degradation of poly(3-hydroxybutyrate).* Polymer, 2000. **41**(9):3227-3234.

[251] Baltieri RC, Mei LHI y Bartoli J. *Study of the influence of plasticizers on the thermal and mechanical properties of poly(3-hydroxybutyrate) compounds*. Macromolecular Symposia, 2003. **197**(1):33-44.

[252] Pizzoli M, Scandola M y Ceccorulli G. *Crystallization and melting of isotactic poly(3-hydroxy butyrate) in the presence of a low molecular weight diluent.* Macromolecules, 2002. **35**(10):3937-3941.

[253] Muizniece-Brasava S y Dukalska L. *Impact of biodegradable PHB packaging composite materials on dairy product quality.* Proceedings of the Latvia University of Agriculture, 2006. **16**(311):79-87.

[254] Janigová I, Lacík I y Chodák I. *Thermal degradation of plasticized poly(3-hydroxybutyrate) investigated by DSC.* Polymer Degradation and Stability, 2002. **77**(1):35-41.

[255] Abdelwahab MA, Flynn A, Chiou BS, Imam S, Orts W y Chiellini E. *Thermal, mechanical and morphological characterization of plasticized PLA-PHB blends.* Polymer Degradation and Stability, 2012. **97**(9):1822-1828.

[256] Fernandes EG, Pietrini M y Chiellini E. *Thermo-mechanical and morphological characterization of plasticized poly[(R)-3-hydroxybutyric acid]*. Macromolecular Symposia, 2004. **218**(1):157-164.

[257] Parra DF, Fusaro J, Gaboardi F y Rosa DS. *Influence of poly(ethylene glycol) on the thermal, mechanical, morphological, physical-chemical and biodegradation properties of poly(3-hydroxybutyrate).* Polymer Degradation and Stability, 2006. **91**(9):1954-1959.

[258] Hong SG, Hsu HW y Ye MT. *Thermal properties and applications of low molecular weight polyhydroxybutyrate.* Journal of Thermal Analysis and Calorimetry, 2013. **111**(2):1243-1250.

[259] Pachekoski WM, Agnelli JAM y Belem LP. *Thermal, mechanical and morphological properties of poly(hydroxybutyrate) and polypropylene blends after processing.* Materials Research, 2009. **12**(2):159-164.

[260] Ol'Khov AA, Iordanskii AL, Zaikov GE, Shibryaeva LS, Litvinov IA y Vlasov SV. *Morphologically special features of poly(3-hydroxybutyrate)/low-density polyethylene blends.* Polymer-Plastics Technology and Engineering, 2000. **39**(5):783-792.

[261] Zhang M y Thomas NL. *Blending polylactic acid with polyhydroxybutyrate: The effect on thermal, mechanical, and biodegradation properties.* Advances in Polymer Technology, 2011. **30**(2):67-79.

[262] D'Amico DA, Montes MLI, Manfredi LB y Cyras VP. *Fully bio-based and biodegradable polylactic acid/poly(3-hydroxybutirate) blends: Use of a common plasticizer as performance improvement strategy.* Polymer Testing, 2016. **49**:22-28.

[263] Kumagai Y y Doi Y. *Enzymatic degradation and morphologies of binary blends of microbial poly(3-hydroxy butyrate) with poly(ε-caprolactone), poly(1,4-butylene adipate) and poly(vinyl acetate).* Polymer Degradation and Stability, 1992. **36**(3):241-248.

[264] Antunes MCM y Felisberti MI. *Blends of poly(hydroxybutyrate) and poly(ε-caprolactone) obtained from melting mixture.* Polímeros, 2005. **15**(2):134-138.

[265] Hinüber C, Häussler L, Vogel R, Brünig H, Heinrich G y Werner C. *Hollow fibers made from a poly(3-hydroxybutyrate)/poly-ε-caprolactone blend.* Express Polymer Letters, 2011. **5**(7):643-652.

[266] Cavalcante MP, Toledo ALMM, Rodrigues EJR, Neto RPC y Tavares MIB. *Correlation between traditional techniques and TD-NMR to determine the morphology of PHB/PCL blends.* Polymer Testing, 2017. **58**:159-165.

[267] Lovera D, Márquez L, Balsamo V, Taddei A, Castelli C y Müller AJ. *Crystallization, morphology, and enzymatic degradation of polyhydroxybutyrate/polycaprolactone (PHB/PCL) blends.* Macromolecular Chemistry and Physics, 2007. **208**(9):924-937.

[268] Liau CP, Ahmad MB, Shameli K, Yunus WMZW, Ibrahim NA, Zainuddin N y Then YY. *Preparation and characterization of polyhydroxybutyrate/polycaprolactone nanocomposites.* The Scientific World Journal, 2014. **2014**:572726.

[269] Kim BO y Woo SI. *Compatibilizing capability of poly(β-hydroxybutyrate-co-ε-caprolactone) in the blend of poly(β-hydroxybutyrate) and poly(ε-caprolactone).* Polymer Bulletin, 1998. **41**(6):707-712.

[270] Briassoulis D. *An overview on the mechanical behaviour of biodegradable agricultural films.* Journal of Polymers and the Environment, 2004. **12**(2):65-81.

[271] Bodros E, Pillin I, Montrelay N y Baley C. *Could biopolymers reinforced by randomly scattered flax fibre be used in structural applications?.* Composites Science and Technology, 2007. **67**(3-4):462-470.

[272] Barkoula NM, Garkhail SK y Peijs T. *Biodegradable composites based on flax/polyhydroxybutyrate and its copolymer with hydroxyvalerate.* Industrial Crops and Products, 2010. **31**(1):34-42.

[273] Taha I y Ziegmann G. *A comparison of mechanical properties of natural fiber filled biodegradable and polyolefin polymers.* Journal of Composite Materials, 2006. **40**(21):1933-1946.

[274] Graupner N y Müssig J. *A comparison of the mechanical characteristics of kenaf and lyocell fibre reinforced poly(lactic acid) (PLA) and poly(3-hydroxybutyrate) (PHB) composites.* Composites Part A: Applied Science and Manufacturing, 2011. **42**(12):2010-2019.

[275] Torres-Tello EV, Robledo-Ortíz JR, González-García Y, Pérez-Fonseca AA, Jasso-Gastinel CF y Mendizábal E. *Effect of agave fiber content in the thermal and mechanical properties of green composites based on polyhydroxybutyrate or poly(hydroxybutyrate-co-hydroxyvalerate).* Industrial Crops and Products, 2017. **99**:117-125.

[276] Hodzic A, Coakley R, Curro R, Berndt CC y Shanks RA. *Design and optimization of biopolyester bagasse fiber composites.* Journal of Biobased Materials and Bioenergy, 2007. **1**(1):46-55.

[277] Gunning MA, Geever LM, Killion JA, Lyons JG y Higginbotham CL. *Melt processing of bioplastic composites via twin screw extrusion and injection molding.* Polymer-Plastics Technology and Engineering, 2014. **53**(4):379-386.

[278] Melo JDD, Carvalho LFM, Medeiros AM, Souto CRO y Paskocimas CA. *A biodegradable composite material based on polyhydroxybutyrate (PHB) and carnauba fibers.* Composites Part B: Engineering, 2012. **43**(7):2827-2835.

[279] Scalioni LV, Gutiérrez MC y Felisberti MI. *Green composites of poly(3-hydroxybutyrate) and curaua fibers: Morphology and physical, thermal, and mechanical properties.* Journal of Applied Polymer Science, 2017. **134**(14):44676.

[280] Prakalathan K, Mohanty S y Nayak SK. *Reinforcing effect and isothermal crystallization kinetics of poly(3-hydroxybutyrate) nanocomposites blended with organically modified montmorillonite.* Polymer Composites, 2014. **35**(5):999-1012.

[281] Maiti P, Batt CA y Giannelis EP. *New biodegradable polyhydroxybutyrate/layered silicate nanocomposites.* Biomacromolecules, 2007. **8**(11):3393-3400.

[282] Bordes P, Pollet E, Bourbigot S y Avérous L. *Structure and properties of PHA/clay nano-biocomposites prepared by melt intercalation.* Macromolecular Chemistry and Physics, 2008. **209**(14):1473-1484.

[283] Botana A, Mollo M, Eisenberg P y Sanchez RMT. *Effect of modified montmorillonite on biodegradable PHB nanocomposites.* Applied Clay Science, 2010. **47**(3-4):263-270.

[284] Akin O y Tihminlioglu F. *Effects of organo-modified clay addition and temperature on the water vapor barrier properties of polyhydroxy butyrate homo and copolymer nanocomposite films for packaging applications.* Journal of Polymers and the Environment, 2018. **26**(3):1121-1132.

[285] Puglia D, Fortunati E, D'Amico DA, Manfredi LB, Cyras VP y Kenny JM. *Influence of organically modified clays on the properties and disintegrability in compost of solution cast poly(3-hydroxybutyrate) films.* Polymer Degradation and Stability, 2014. **99**:127-135.

[286] Achilias DS, Panayotidou E y Zuburtikudis I. *Thermal degradation kinetics and isoconversional analysis of biodegradable poly(3-hydroxybutyrate)/organomodified montmorillonite nanocomposites.* Thermochimica Acta, 2011. **514**(1-2):58-66.

[287] Lim ST, Hyun YH, Lee CH y Choi HJ. *Preparation and characterization of microbial biodegradable poly(3-hydroxybutyrate)/organoclay nanocomposite.* Journal of Materials Science Letters, 2003. **22**(4):299-302.

[288] Gardolinski JE, Carrera LCM, Cantão MP y Wypych F. *Layered polymer-kaolinite nanocomposites.* Journal of Materials Science, 2000. **35**(12):3113-3119.

[289] Yun SI, Gadd GE, Latella BA, Lo V, Russell RA y Holden PJ. *Mechanical properties of biodegradable polyhydroxyalkanoates/single wall carbon nanotube nanocomposite films.* Polymer Bulletin, 2008. **61**(2):267-275.

[290] Zarei M y Karbasi S. *Evaluation of the effects of multiwalled carbon nanotubes on electrospun poly(3-hydroxybutirate) scaffold for tissue engineering applications.* Journal of Porous Materials, 2018. **25**(1):259-272.

[291] Huh M, Jung MH, Park YS, Kim BJ, Kang MS, Holden PJ y Yun SI. *Effect of carbon nanotube functionalization on the structure and properties of poly(3-hydroxybutyrate)/MWCNTs biocomposites.* Macromolecular Research, 2014. **22**(7):765-772.

[292] Xu C y Qiu Z. *Crystallization behavior and thermal property of biodegradable poly(3-hydroxybutyrate)/multi-walled carbon nanotubes nanocomposite.* Polymers for Advanced Technologies, 2011. **22**(5):538-544.

[293] Valentini L, Fabbri P, Messori M, Esposti MD y Bon SB. *Multilayer films composed of conductive poly(3-hydroxybutyrate)/carbon nanotubes bionanocomposites and a photoresponsive conducting polymer.* Journal of Polymer Science Part B: Polymer Physics, 2014. **52**(8):596-602.

[294] Díez-Pascual AM y Díez-Vicente AL. *Poly(3-hydroxybutyrate)/ZnO bionanocomposites with improved mechanical, barrier and antibacterial properties.* International Journal of Molecular Sciences, 2014. **15**(6):10950-10973.

[295] Iulianelli GCV, David GS, dos Santos TN, Sebastião PJO y Tavares MIB. *Influence of TiO_2 nanoparticle on the thermal, morphological and molecular characteristics of PHB matrix.* Polymer Testing, 2018. **65**:156-162.

[296] Yeo SY, Tan WL, Bakar MA y Ismail J. *Silver sulfide/poly(3-hydroxybutyrate) nanocomposites: Thermal stability and kinetic analysis of thermal degradation.* Polymer Degradation and Stability, 2010. **95**(8):1299-1304.

[297] Hsu SF, Wu TM y Liao CS. *Isothermal crystallization kinetics of poly(3-hydroxybutyrate)/layered double hydroxide nanocomposites.* Journal of Polymer Science Part B: Polymer Physics, 2006. **44**(23):3337-3347.

[298] Hsu SF, Wu TM y Liao CS. *Nonisothermal crystallization behavior and crystalline structure of poly(3-hydroxybutyrate)/layered double hydroxide nanocomposites.* Journal of Polymer Science Part B: Polymer Physics, 2007. **45**(9):995-1002.

[299] Wu TM, Hsu SF, Shih YF y Liao CS. *Thermal degradation kinetics of biodegradable poly(3-hydroxybutyrate)/layered double hydroxide nanocomposites.* Journal of Polymer Science Part B: Polymer Physics, 2008. **46**(12):1207-1213.

[300] Ciou CY, Li SY y Wu TM. *Morphology and degradation behavior of poly(3-hydroxybutyrate-co-3-hydroxyvalerate)/layered double hydroxides composites.* European Polymer Journal, 2014. **59**:136-143.

II. ESTUDIOS PREVIOS

Previamente a la realización de la investigación en poliésteres de origen bacteriano y optimización de las formulaciones, se llevó a cabo una serie de estudios preliminares centrados en el campo de los compuestos ecológicos, que permitió abordar el sector de los materiales compuestos bajo dos perspectivas: empleo de matrices poliméricas y, por otro lado, utilización de residuos lignocelulósicos como cargas reforzantes. El análisis de este sector permitió identificar las tendencias más importantes en los desarrollos actuales y para un futuro inmediato. Es precisamente el recorrido a través de estos trabajos previos el que permite identificar los grandes retos que se plantean en la tesis doctoral. Por un lado, el desarrollo y optimización de formulaciones derivadas de poliésteres de origen bacteriano, con potencial en un amplio campo de aplicaciones que puedan abarcar sectores como el del envase-embalaje, agricultura, medicina, etc. y, lógicamente el sector de los materiales compuestos. Por otro lado, si bien los residuos lignocelulósicos pueden incorporarse de forma directa en matrices poliméricas, a partir de los resultados previos, se decide abordar el aprovechamiento integral de residuos agroforestales. Este aprovechamiento integral se centra en la obtención de compuestos naturales con actividad antioxidante y, fundamentalmente, la obtención de nanopartículas con un efecto reforzante para matrices poliméricas.

A través de este capítulo de resultados previos, se lleva a cabo un recorrido de diversos aspectos ligados a las tecnologías de materiales sostenibles y de bajo impacto medioambiental. A lo largo de este capítulo se va incrementando el contenido medioambiental de los materiales desarrollados, que desemboca en un análisis de los polímeros con mayor potencial industrial para los próximos años.

El capítulo comienza con un trabajo que se centra en el desarrollo de compuestos con matrices de polipropileno (PP) de origen petroquímico. Estos compuestos integran en sus formulaciones residuos lignocelulósicos de posos de café. El trabajo aborda la mejora en propiedades que se consigue con la incorporación de estos residuos en formato polvo. En particular, la propiedad de estabilidad térmica a temperaturas moderadas se mejora notablemente debido al contenido en compuestos antioxidantes remanentes en el residuo de café. Además, el trabajo aborda, de forma novedosa, uno de los problemas más importantes de los compuestos con partículas lignocelulósicas, que es la falta de compatibilidad entre ambos componentes debido a la fuerte hidrofobicidad de la matriz y la altísima hidrofilidad del residuo de refuerzo. Para ello, y siempre con un planteamiento medioambiental, se desarrolla un tratamiento con ácidos grasos derivados de aceites vegetales que permite mejorar la interacción entre ambos componentes y, en consecuencia, reducir los efectos de absorción de agua en los materiales desarrollados. La reactividad de

estos aceites vegetales y su capacidad de compatibilización, claramente identificada en este trabajo, sirvió de base para trabajos posteriores en la optimización de poliésteres mediante aceites epoxidados, aceites maleinizados y ácidos grasos epoxidados.

Con el segundo trabajo mostrado en este capítulo se avanza en el contenido medioambiental y se contempla el desarrollo de compuestos ecológicos obtenidos con matrices de polietileno de origen renovable (derivado del bioetanol de la caña de azúcar) y refuerzos lignocelulósicos derivados de la cáscara de cacahuete. Concretamente, se aborda el procesado y la mejora de las propiedades generales con la incorporación de diversos agentes compatibilizantes. Con este trabajo se demuestra la viabilidad de materiales de origen completamente renovable capaces de competir industrialmente con el grupo de los plásticos que imitan la madera o "*wood plastic composites (WPCs)*".

Finalmente, el capítulo contempla un trabajo centrado en el empleo de resinas derivadas de aceites vegetales, dada su alta reactividad, como matrices para la fabricación de materiales compuestos con residuos de plantas acuáticas de *Posidonia oceánica*. Este trabajo explora el desarrollo de tableros de partículas con elevado contenido en residuos de esta planta acuática, con alto contenido en celulosa. Se demuestra la viabilidad de estos materiales a través del conjunto de propiedades mecánicas, térmicas y termomecánicas, y se valida la alta reactividad de los aceites vegetales.

Con este trabajo se cierra el bloque correspondiente a los resultados preliminares. A partir de un mayor conocimiento del sector de los materiales poliméricos y compuestos y, en un esfuerzo por desarrollar materiales con potencial uso industrial, se identifican diferentes candidatos en el ámbito de los poliésteres para el desarrollo de nuevas formulaciones con potencial uso en envase-embalaje, agricultura, medicina, automoción, etc., tanto en forma de polímeros como de compuesto con refuerzos lignocelulósicos. El sector de los poliésteres ofrece grandes expectativas para los polímeros de origen bacteriano, entre los que se contempla el poli(3-hidroxibutirato) (PHB). El PHB se trata de un material que, actualmente, todavía ofrece un coste alto debido a los elevados costes de producción, y, por otro lado, presenta una serie de dificultades que limitan su uso masivo en el sector de los plásticos y materiales compuestos. Entre estas limitaciones, destaca su estrecha ventana de procesado, debida a su baja estabilidad térmica, y su alta fragilidad, ligada a su alta cristalinidad. Considerando que el conjunto de los plásticos de uso común (polietileno, polipropileno, policloruro de vinilo, poliestireno, etc.) han sido extensamente estudiados tanto a nivel de formulaciones así como matrices para compuestos y, por otro lado, teniendo en cuenta que el poli(ácido láctico) (PLA) es uno de los poliésteres con mayor uso en la industria y sobre el que se ha trabajado intensamente en la última década, se

considera oportuno abordar los retos que plantea el PHB para convertirse en un poliéster de uso masivo.

II.1

"Green composites based on polypropylene matrix and hydrophobized spend coffee ground (SCG) powder"

Daniel García García[a], *Alfredo Carbonell Verdú*[a], *María Dolores Samper*[a], *David García Sanoguera*[a], *Rafael Balart*[a]

[a] Instituto de Tecnología de Materiales (ITM)
Universitat Politècnica de València (UPV)
Plaza Ferrándiz y Carbonell 1, 03801 Alcoy, Alicante, Spain.

Composites Part B: Engineering

2015, 78:256-265

Green composites based on polypropylene matrix and hydrophobized spend coffee ground (SCG) powder

Abstract

Green composites were prepared with polypropylene matrix and 20 wt% spent coffee ground (SCG) powder for uses as a wood plastic composite (WPC). The effects of hydrophobic treatment with palmitoyl chloride on SCG powder is compared with conventional surface treatment based on silanization with (3-glycidyloxypropyl) trimethoxysilane and the use of a maleated copolymer compatibilizer (polypropylene-*graft*-maleic anhydride, PP-*g*-MA) in terms of mechanical properties, morphology, thermal properties and water uptake. Composites were previously mixed in a twin-screw co-rotating extruder and subsequently subjected to injection molding. The comparative effect of the different surface treatments and or compatibilizers on mechanical performance was studied by flexural, impact tests and dynamic mechanical thermal analysis (DMTA-torsion); in addition, the stabilizing effect of SCG was revealed by differential scanning calorimetry (DSC) and thermogravimetric analysis (TGA). As one of the main drawbacks of wood plastic composites and natural fiber reinforced plastics is the moisture gain, water uptake tests were carried out in order to quantify the effectiveness of the hydrophobization process with palmitoyl chloride. Results show a slight increase in flexural modulus for composites with both untreated and treated/compatibilized SCG powder (20 wt%). As expected, thermal stability is improved as indicated by an increase of more than 8% in the onset degradation temperature by DSC if compared to unfilled polypropylene. Fracture analysis by scanning electron microscopy (SEM) shows better particle dispersion for PP/SCG composites with hydrophobized SCG with palmitoyl chloride treatment; in addition a remarkable decrease in water uptake is observed for composites with hydrophobized SCG.

Keywords: Polymer-matrix composites (PMCs); adhesion; wettability; thermal analysis; spent coffee ground (SCG).

INTRODUCTION

Today, ecological concerns and issues such as recycling and environmental care are increasingly important. As a consequence of such environmental awareness we are witnessing a great interest in the research on more environmentally friendly materials as it is the case of polymer composites reinforced with natural fibers (natural fiber reinforced plastics-NFRPs and wood plastic composites-WPCs) [1-3]. Natural fillers are acquiring increasing importance as reinforcing materials in composites due to some advantages they provide such as low cost, low density, no toxicity, balanced mechanical properties and a clear lower environmental impact [3, 4]. The main problem related to the use of natural fillers is their low compatibility with most polymer matrices. Most natural fillers are lignocellulosic-based materials and, consequently, highly hydrophilic, while most polymer matrices are intrinsically hydrophobic. This fact leads to low polymer-filler interactions which lead to poor mechanical properties thus making necessary the use of surface treatments on fillers (*i.e.*, silanization) or addition of compatibilizer agents (maleated copolymers). In addition to the lack of compatibility between the two main components, moisture gain is another big drawback when using natural fiber reinforcements. Hydrophilicity in natural fiber reinforcements is provided by the high amount of cellulose and hemicelluloses with hydroxyl groups which are also responsible for high water absorption capacity. Moisture gain in NFRPs and WPCs is a critical issue as the water uptake leads to dimensional instability [4-6]. With the aim of improving polymer-filler interactions and reduce the water uptake, different physical or chemical modifications have been proposed (silanization, esterification, etherification, benzylation, etc.) as well as the use of compatibilizer agents (mainly maleated copolymers) [6-10].

Coffee is one of the most consumed beverages and the second most traded product in the world after petroleum [11], so that the coffee industry generates a lot of waste. A major waste generated by this industry is spent coffee ground (SCG), which is obtained from the treatment of the coffee powder with hot water to prepare instant coffee. About 6 million tons of SCG are generated annually worldwide [11, 12]. In general terms, 650 kg of SCG are obtained during processing one ton green coffee and 2 kg of wet SCG are obtained from one kg soluble coffee [11, 13]. Nowadays most of the SCG wastes are poured into the environment or burned in order to remove them, being these techniques highly disrespectful with the environment [13]. In the literature there are different researches focused on providing an alternative to the residue of SCG to reduce its environmental impact [11]. Some of these proposals are the use of SCG for animal feed [14], for producing organic compost [15], as fuel pellets [16] or the production of active carbon [17]. In addition, the

potential of SCG as raw material for the extraction of natural antioxidants [18] the production of ethanol [19], biodiesel [20] or polyhydroxyalkanoates (PHAs) [21] have been investigated in the last years. The novelty of this work is the use of SCG as functional reinforcement in polypropylene for wood plastic composites (WPCs); SCG provides a typical dark brown color. It could be possible to bleach SCG by environmentally friendly processes using enzymes due to its lignocellulosic nature but its natural color could be attracting as it is similar to some dark or black woods such as: Gaboon Ebony, Ziricote, African Blackwood, Wenge, Panga-Panga, among others.

The main objective of this study is to investigate the effect of a hydrophobic surface treatment of SCG powder with palmitoyl chloride and compare it with conventional treatments on SCG such as silanization with (3-Glycidyloxypropyl) trimethoxysilane (GLYMO) and/or use of compatibilizers (polypropylene-*graft*-maleic copolymer, PP-*g*-MA) in terms of mechanical, morphological and thermal properties as well as the effects on water absorption of PP/SCG composites. Manufacturing of PP/SCG composites was performed using a twin screw extruder and subsequent injection molding. PP/SCG composites containing 20 wt% SCG with the different treatments and formulations were compared in terms of mechanical properties (flexural an impact tests) as well as dynamic mechanical thermal analysis (DMTA) in torsion mode. Particle dispersion and particle-matrix were qualitatively assessed by scanning electron microscopy (SEM) and the effect of SCG on thermal stability of composites was evaluated with differential scanning calorimetry (DSC) and thermogravimetric analysis (TGA). The effect of the different treatments on the chemical composition of SCG was analyzed by FTIR spectroscopy. Finally, the effect of the hydrophobic treatment with palmitoyl chloride is compared with conventional treatments/compatibilizers in terms of the water uptake and dynamic contact angle measurements.

EXPERIMENTAL

Materials

A commercial polypropylene (PP) grade PR290 P1M supplied by REPSOL (REPSOL, Madrid, Spain) was used as matrix. This PP grade is characterized by a density of 0.905 g cm^{-3} and a melt flow index of 35 g $(10\ min)^{-1}$ at 230 °C.

Spent coffee grounds (SCG) were collected from local bars in the form of a wet cake as a consequence of extraction with hot water. This raw material was dried in an oven at 80 °C for 5 h.

The remaining antioxidant capacity of spent coffee grounds (SCG) after the extraction with hot water was determined by DPPH and FRAP methods. In addition polyphenol and flavonoid total content was measured by the Folin-Ciocalteu method. Table II.1.1 summarizes the main properties of spent coffee grounds (SCG) regarding the remaining antioxidant capacity.

Table II.1.1. Characterization of the antioxidant capacity and polyphenol and flavonoid total content of spent coffee ground.

Property	Value
Antioxidant capacity, DPPH (%RSA)	86 ± 1
Antioxidant capacity, FRAP (mg Trolox/g sample)	1.63 ± 0.16
Flavonoids (mg quercetin/g sample)	0.96 ± 0.05
Polyphenols FOLIN (mg quercetin/g sample)	5.10 ± 0.41

The compatibilizer used was a polypropylene-*graft*-maleic anhydride (PP-*g*-MA) copolymer with a density of 0.934 g cm^{-3} at 25 °C (Sigma Aldrich, Madrid, Spain). The silane used for surface treatment of SCG was (3-Glycidyloxypropyl) trimethoxysilane (GLYMO) supplied by Sigma Aldrich. The hydrophobic treatment of SCG was carried out with palmitoyl chloride in presence of pyridine and 1,2-dichloroethane; all they were supplied by Sigma Aldrich.

Surface treatments on spent coffee grounds (SCG)

Hydrophobization of SCG was done by esterification with palmitoyl chloride. The procedure was carried out as follows: initially, SCG was dried overnight at 80 °C and subsequently dropped into 1,2-dichloroethane solution; after this, palmitoyl chloride and equimolar amount of pyridine were added at a temperature of 70 °C as described by Zini *et al.* [22]. After a reaction time of 60 min, SCG was collected by filtration and washed with 1,2-dichloroethane and water respectively. Finally, SCG was dried at 80 °C overnight and was ready for further processing.

Silanization with GLYMO was carried out in a water-methanol (50/50, v/v) containing 1 wt% silane (referred to the total amount of SCG). The solution was subjected

to magnetic stirring for 2 h and subsequently SGC was collected, washed with distilled water and dried at room temperature for 48 h and then it was ready for composite manufacturing.

Conventional maleated polypropylene (PP-*g*-MA) was used to compare the effects of the different surface treatments. PP-*g*-MA (2 wt% referred to the total weight of the composite) was manually mixed in a zip bag prior to the extrusion process.

PP/SCG composite manufacturing

Four different formulations with constant SCG content (20 wt%) were manufactured and labeled as follows:

SCG: 80 wt% PP + 20 wt% untreated SCG.

SCG-SIL: 80 wt% PP + 20 wt% silanized SCG with GLYMO.

SCG-PALM: 80 wt% PP + 20 wt% hydrophobized SCG with palmitoyl chloride.

SCG-MAPP: 78 wt% PP + 2 wt% PP-*g*-MA + 20 wt% untreated SCG.

All four formulations were mixed in a twin screw co-rotating extruder with a temperature profile of 180 °C, 185 °C, 190 °C and 195 °C (from the hopper to the extruder die) at a rate of 40 rpm to allow good mixing. The extruded material was pelletized in a mill and subsequently processed in an injection molding machine Meteor 270/75 (Mateu & Solé, Barcelona, Spain) at a temperature of 200 °C to obtain standard samples for tests. Due to the typical dark brown color of SCG after the roasting process, it provides similar appearance to dark/black wood, which is an attracting feature for furniture and automotive applications.

Characterization techniques

Mechanical characterization of PP/SCG composites

Flexural properties were obtained at room temperature using a universal test machine Ibertest ELIB 30 (S.A.E. Ibertest, Madrid, Spain) equipped with a 5 kN load cell. Flexural tests were carried out by following the guidelines of the ISO 178 at a crosshead rate of 5 mm min^{-1}. Five different samples were subjected to flexural test and average values of flexural modulus and strength were calculated.

In addition, impact properties were evaluated with a 1 J Charpy pendulum (Metrotec S.A., San Sebastián, Spain) according to ISO 179:1993 with notched samples ("V" type at 45° and 0.25 mm notch radius). Five different samples were subjected to impact test and average values of absorbed energy were calculated.

Scanning electron microscopy (SEM) of fractured surfaces of PP/SCG composites

Fractured surfaces from impact tests were observed by scanning electron microscopy (SEM) in a Phenom (FEI Company, Eindhoven, the Netherlands). Before observation, samples were covered with a thin layer of aurum-palladium alloy in a sputter-coater EMITECH mod. SC7620 (Quorum Technologies Ltd., East Sussex, UK).

Dynamic mechanical thermal analysis (DMTA) of PP/SCG composites

Evolution of storage modulus (G'), loss modulus (G'') and tan δ of all four composites with temperature was obtained with an oscillatory rheometer AR G2 (TA Instruments, New Castle, USA) equipped with a clamp system for solid samples (torsion mode). Samples sizing 40×10×4 mm^3 were subjected to a heating program from –50 up to 100 °C at a heating rate of 2 °C min^{-1}, at a frequency of 1 Hz and constant deformation (γ) of 0.1%.

Thermal analysis of PP/SCG composites

Thermal stability of PP/SCG composites at moderate temperatures (initial oxidation stages) was obtained by differential scanning calorimetry (DSC) in a Mettler-Toledo 821 (Mettler-Toledo Inc., Schwerzenbach, Switzerland). Samples with an average weight of 7–10 mg were placed in standard aluminum crucibles and subjected to a temperature ramp from 30 to 300 °C at a heating rate of 10 °C min^{-1} in air atmosphere. Air atmosphere was selected to evaluate the stabilizing effect of natural phenols in SCG in oxidizing conditions. During the test the melting temperature (T_m) of different composites was determined. Degree of crystallinity (X_c) of PP in each composite was calculated by Equation II.1.1.

$$\boldsymbol{X_c}\,(\%) = \left[\frac{\Delta \boldsymbol{H_m}}{\Delta \boldsymbol{H_0} \cdot \boldsymbol{w}}\right] \times \mathbf{100} \qquad \textbf{Equation II.1.1}$$

where ΔH_m is the heat of fusion of PP/SCG composites, ΔH_0 is the theoretical heat of fusion of purely crystalline isotactic PP, considering this value as 138 J g^{-1} [23] and w is the weight fraction of PP in the PP/SCG composites.

Thermal degradation of PP/SCG composites at high temperatures was followed by thermogravimetric analysis (TGA) in a TGA/SDTA 851 (Mettler-Toledo Inc., Schwerzenbach, Switzerland). Samples sizing 7–8 mg were placed in standard alumina crucibles and subjected to a heating program from 30 to 700 °C at a heating rate of 20 °C min^{-1} in nitrogen atmosphere (66 mL min^{-1}).

Infrared spectroscopy analysis of SCG

The treated and untreated SCG powder was analyzed by Fourier transform infrared spectroscopy (FTIR) using an infrared spectrometer Perkin-Elmer Spectrum BX (Perkin-Elmer Spain S.L., Madrid, Spain); each sample was subjected to 20 scans between 4000 and 600 cm^{-1}, with a resolution of 16 cm^{-1}. The samples were measured after being pressed in a KBr disc.

Water uptake of PP/SCG composites

Water uptake was determined with samples sizing 80×10×4 mm^3. Three different samples were tested to obtain average values. Prior to the water uptake test, PP/SCG composite samples were dried at 80 °C for 4 h to give constant weight. After this, samples were immersed in distilled water at room temperature for a period of 3 months and the weight change was measured every three days. The percentage water uptake was calculated by using the following expression:

$$\boldsymbol{Water\ Uptake}\ (\%) = \frac{(\boldsymbol{m_f - m_i})}{\boldsymbol{m_i}} \times \mathbf{100} \qquad \textbf{Equation II.1.2}$$

where m_f is the final weight after a certain immersion period and m_i is the initial weight of the sample before immersion.

Furthermore, the dynamic contact angle of treated and untreated spent coffee ground was obtained using an Easy drop Standard KRÜSS goniometer (KRÜSS GmbH, Hamburg, Germany), model FM140 (110/220 V, 50/60 Hz). In addition, the hydrophobicity of the treated and untreated spent coffee ground was measured using the capillary rise method used by Trong Dang-Vu for porous materials [24].

RESULTS AND DISCUSSION

Figure II.1.1 shows a SEM image corresponding to untreated SCG particles and hydrophobized SCG particles with palmitoyl chloride. As it can be detected, untreated SCG powder (Figure II.1.1a) is highly hydrophilic and this leads to formation of aggregates; although individual particle size is close to 15–20 μm, aggregates sizing 60–80 μm can be observed and this will have a negative effect on overall properties. On the other hand, Figure II.1.1b shows SCG particles subjected to hydrophobization treatment with palmitoyl chloride and individual particles do not tend to form aggregates and this will have a positive effect on particle dispersion and, subsequently, overall properties.

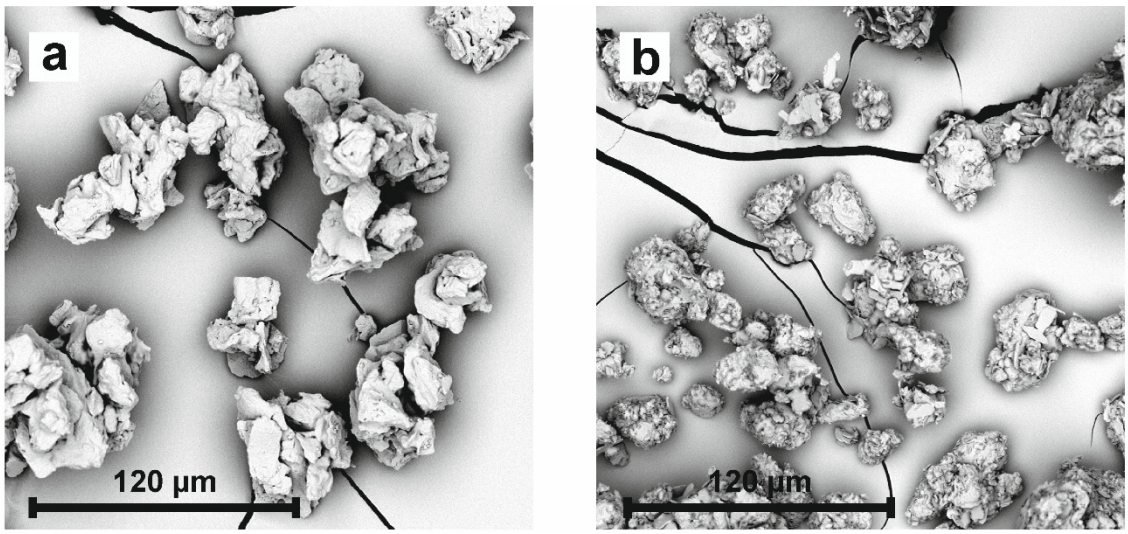

Figure II.1.1. SEM images (1000x) corresponding to (a) untreated SCG particles and (b) hydrophobized SCG particles with palmitoyl chloride.

Flexural properties of unfilled PP and PP/SCG composites can be observed in Figure II.1.2. As it can be observed in Figure II.1.2, strength suffers a slight decrease with addition of SCG, which is typical of composites due to stress concentration phenomena, since the SCG particle is not perfectly adhered with the PP matrix. It is important to remark that the real reinforcing effect is directly related to the aspect ratio of the filler as described by some authors [25]. A reinforcing effect can be obtained for aspect ratios higher than 6 which enable preferential direction and/or orientation which can have a positive effect on mechanical performance due to particle alignment. In this case SCG particles are very irregular in size with typical aspect ratios lower than 2 (see Figure II.1.1) and this leads to a slight decrease in flexural strength as no particle alignment can be obtained during

manufacturing [26-28]. Unfilled PP is characterized by a flexural strength of about 37 MPa and all four formulations with SCG show a flexural strength of about 33–34 MPa with no remarkable change in terms of the surface treatment and/or compatibilizer. The lowest percentage decrease of flexural strength is 9.7% and corresponds to untreated SCG but in the case of silane-treated SCG and hydrophobized-SCG, this reduction is 12.4 and 13.8% respectively. With regard to the flexural modulus, it is important to remark that it represents a ratio between the applied stress and the deflection. As we can see in Figure II.1.2, the flexural modulus of unfilled PP is close to 1034 MPa and this value is increased up to values of about 1222 MPa for PP composites with silanized-SCG. With regard to PP composites with hydrophobized-SCG (with palmitoyl chloride), the flexural modulus is similar to unfilled polypropylene and this could indicate better particle dispersion (see Figure II.1.1b). If SCG particles are well dispersed, the overall polymer-particle interaction increases and the stress concentration phenomena are not as intense. In general terms, addition of SCG leads to typical mechanical properties of particle-filled polymers with low aspect ratio fillers; a decrease in strength and a slight increase in elastic modulus. Decrease in flexural strength is related to poor adhesion between the lignocellulosic component (SCG) and the polypropylene matrix. If we take into account the relative small size of the SCG particles, a high surface area is provided by them so that particle-polymer interface phenomena achieve great relevance on final behavior of PP/SCG composites. This promotes formation of weak interface areas that do not transfer loads appropriately from the matrix to the particle filler thus leading to slightly lower strength values as observed in similar systems [29]. With regard to flexural modulus, it increases because it represents the ratio between the applied stress (flexural conditions) and flexural strain in the linear region. As in other polymer-filled systems, the decrease in strength is lower than that observed for the strain so that, it gives higher ratio values and, consequently, higher modulus values [30, 31]. In PP/SCG composites, the flexural modulus is slightly higher for all treatments except in the case of the hydrophobic treatment with palmitoyl chloride. This slight increase is directly related to low filler amounts. This behavior is typical of particle-filled polymer with other natural fillers such as kaolin, talc or $CaCO_3$ [32-34].

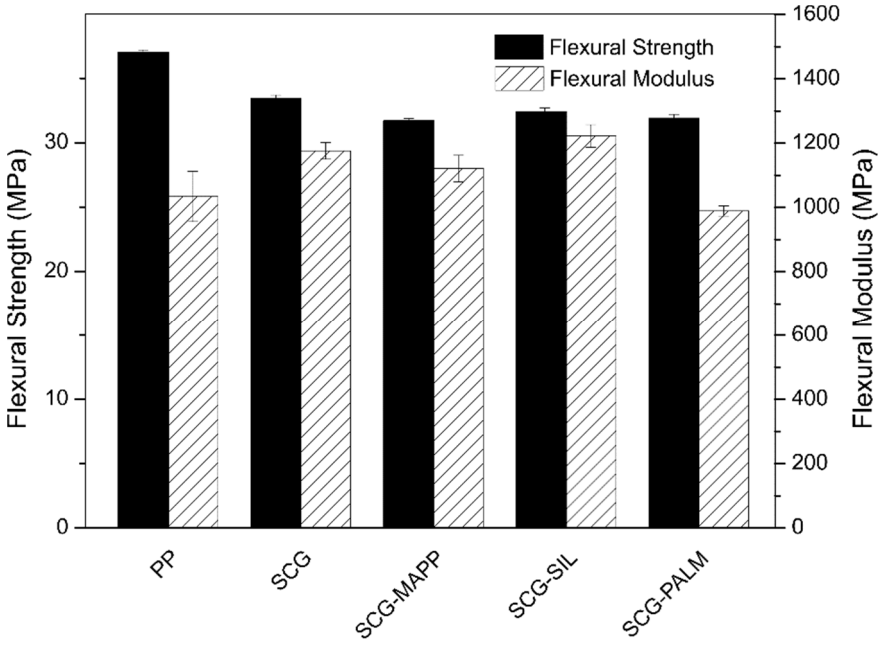

Figure II.1.2. Plot comparison of flexural properties (modulus and strength) for PP/SCG composites with different surface treatments or compatibilizers.

Figure II.1.3 shows the impact results (absorbed energy) for unfilled PP and PP/SCG composites. A clear reduction of the impact energy is detectable for all four PP/SCG composite formulations with regard to unfilled PP. As described by Yang *et al.* [35] the absence of interactions between PP and untreated SCG promotes formation of micro-cracks at the particle-polymer interface regions when impact conditions are applied. These micro-cracks can propagate since poor continuity in the matrix exists. This effect is still stronger as we are using notched samples so that we have two stress concentration phenomena: one provided by the particular notched geometry and one at a micro scale level promoted by the lack of interactions between SCG particles and the surrounding polymer matrix. If we compare only the four PP/SCG composite formulations, it is worth emphasizing that the maximum impact energy value is obtained for PP composites with hydrophobized-SCG with palmitoyl chloride with an impact energy of 1.7 kJ m^{-2} which represents more than 54% increase with regard to PP composite with untreated SCG (1.1 kJ m^{-2}). Both the use of PP-*g*-MA as compatibilizer and surface treatment with palmitoyl chloride leads to slightly higher impact energy values. This is directly related to stronger interactions among particle-polymer interface. Maleic anhydride groups in PP-*g*-MA can react with typical hydroxyl groups in SCG (lignocellulosic material) and, on the other hand, polypropylene segments in PP-*g*-MA rearrange towards surrounding PP chains. For this reason, PP-*g*-MA act as a bridge between highly hydrophilic SCG particles and the highly hydrophobic PP chains and this has

a positive effect on absorbed impact energy as micro-crack propagation is more difficult [23, 36]. On the other hand, hydrophobic treatment of SCG with palmitoyl chloride promotes high hydrophobicity on SCG particles which are, in turn, more compatible with the highly hydrophobic polypropylene matrix and this has a positive effect on interface phenomena thus restricting micro-crack propagation thus leading to higher absorbed energy values. Hydrophobic treatments of particle fillers have been used to enable good dispersion as well as mechanical performance of particle-filled polymers [37, 38].

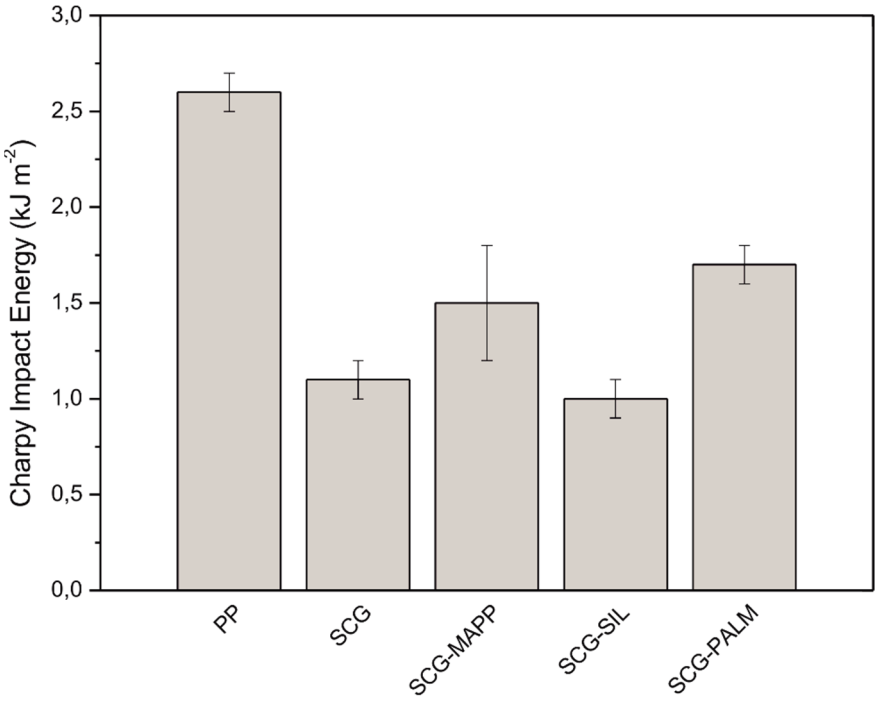

Figure II.1.3. Plot comparison of impact properties of PP/SCG composites with different surface treatments or compatibilizers.

The typical dark brown color of SCG is due to the Maillard reaction during roasting green coffee beans. Maillard reaction leads to formation of melanoidins which are responsible for the final color of the roasted coffee as well as antioxidant, antimicrobial, anticancer activity, etc. [39, 40]. The roasting process can be carried out at different temperatures; depending on the temperature, the final color will change from light to medium light, moderate dark, dark brown, very dark brown. So that, a very light roast level at about 195 °C gives a light brownish color while a very dark brown color is obtained at a roasting temperature of 245–250 °C. During the brewing process, coffee is subjected to hot water at 90–95 °C for optimum extraction. So that, SCG waste has been subjected to high

temperatures during the life cycle; high temperatures are responsible for some attracting reactions such as Maillard which increase its antioxidant capacity. So that, additional high temperatures of about 195–200 °C range for a short period do not promotes additional degradation during manufacturing. This can be observed by the study of the thermal stability at moderate temperatures (start of the oxidation processes). Table II.1.2 shows the main parameters corresponding to thermal transitions in PP and PP/SCG composites obtained by DSC analysis. With regard to the melt temperature the peak is located in the same temperature range (169–170 °C). It is in the onset degradation temperature where we observe significant differences. PP composites with untreated SCG show a clear increase in the onset degradation temperature (231.3 °C for unfilled PP) up to values 20 °C higher (251.3 °C) which represents a percentage increase of almost 9%. Such an increase in thermal stability at moderate temperatures (initial stages of the thermo-oxidative degradation) is directly related to presence of phenolic compounds in SCG (see Table II.1.1). In the case of untreated SCG, these phenolic compounds are directly in contact with polypropylene chains and can easily provide their antioxidant properties. On the other hand, we can observe that PP/SCG composites with silanized-SCG and hydrophobized-SCG are characterized by lower onset degradation temperatures (241.6 and 231.2 °C respectively) which can be attributed to formation of a thin covering layer that restricts migration of phenolic compounds from particles to the polymer matrix. For this reason, although the total content on SCG is constant (20 wt%), phenolic compounds are not easily available to stop thermo-oxidation and the overall stabilizing effect at moderate temperatures. With regard to crystallinity, Table II.1.2 shows the relative percentage crystallinity (X_c) for all PP/SCG composites as well as unfilled PP. We observe no significant change in crystallinity as both PP and PP/SCG composites are characterized by a percentage crystallinity in the 71–73% range. So that, no clear nucleating effect is observed which is typical of high filler content. Typical nucleating effect is found for low filler compositions (*i.e.*, 5–10 wt%) and crystallinity remains constant for high filler content [41, 42].

Table II.1.2. Thermal characterization of PP/SCG composites obtained by dynamic differential scanning calorimetry (DSC).

Sample reference	T_m (°C)	ΔH_m[a] (J g^{-1})	ΔH_m[b] (J g^{-1})	X_c (%)	Onset degradation (°C)
PP	169.5	−101.5	−101.5	73.6	231.3
SCG	170.1	−80.9	−101.1	73.3	251.3
SCG-MAPP	170.2	−80.4	−100.5	72.8	250.7
SCG-SIL	169.9	−81.6	−102.0	73.9	241.6
SCG-PALM	170.8	−79.3	−99.1	71.8	231.2

[a] Values obtained directly from DSC considering the diluting effect of 20 wt% SCG.

[b] Normalized values respect to the real PP mass weight.

Thermal degradation at high temperatures can be observed in Figure II.1.4. Degradation of spent coffee ground powder occurs in four different steps. The first one occurs between 50 and 170 °C and it is due to water removal and represents a percentage weight loss of 7%. The second stage is located in the 170–350 °C range and it is attributable to thermal depolymerisation of hemicelluloses with a typical weight loss of 43%. The third step occurs between 350 and 430 °C and it is directly related to cellulose degradation. Finally, the last stage starts at 430 °C and, due to the complex structure of lignin, this stage takes place slowly [43, 44]. Thermal degradation of PP proceeds in a single step between 250 to 550 °C with a weight loss higher than 95%. Degradation of PP/SCG composites proceeds in two clearly observable steps as the weight loss due to water removal is diluted due to the low content on SCG in PP/SCG composites. The first clear degradation step starts at about 170 °C and corresponds to degradation of hemicelluloses and celluloses in SCG with lower degradation temperature than PP chains so PP/SCG composites start the loss of weight at lower temperatures than unfilled PP. The second stage starts at about 430 °C and corresponds mainly to polypropylene chain degradation, as it can be observed the PP chains of PP/SCG composites end the thermal degradation at higher temperatures than unfilled PP. Although the stabilization effect at low moderate temperatures is lower for PP/SCG composites with silanized and hydrophobized-SCG due to the thin layer covering the particles it is important to note that this covering layer based on silane and palmitic acid respectively protects particle from degradation. This fact can be observed by a displacement of the typical degradation temperatures of the second stage compared to unfilled PP. With regard to untreated SCG, silane-treated SCG and the use of compatibilizer, the weight loss

corresponding to the first degradation step is similar; nevertheless, with regard to composites with hydrophobized-SCG with palmitoyl chloride, the weight loss in the first step is lower which indicates a clear stabilizing effect (protection) of the hydrophobic cover of SCG particles. At the end of the degradation process, residual weight (char) is similar in all four composites and slightly higher than unfilled PP [45-47].

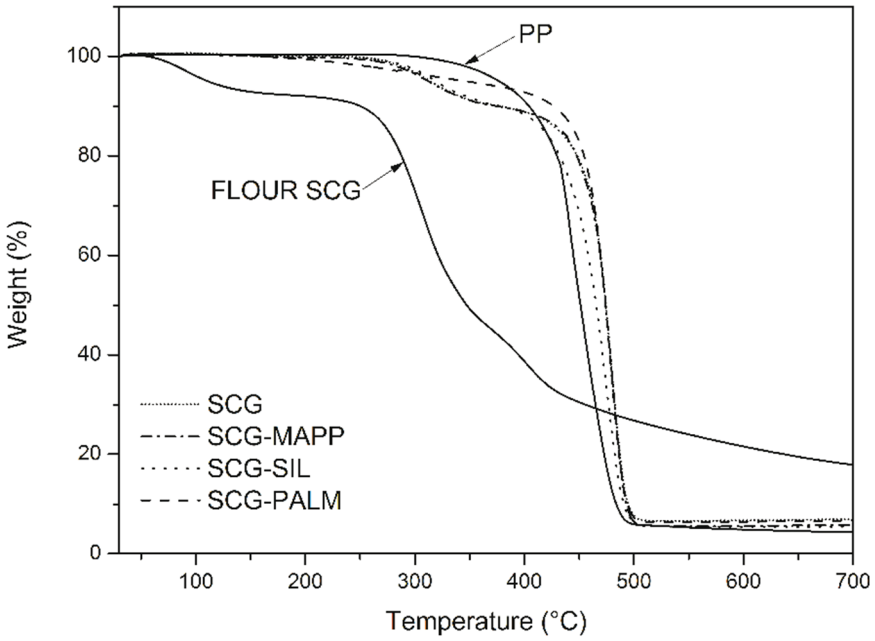

Figure II.1.4. Comparative plot of thermogravimetric curves (TGA) of PP and PP/SCG composites with different surface treatments or compatibilizers.

Figure II.1.5 shows SEM images of fractured surfaces from impact tests of PP/SCG composites. Addition of SCG fillers leads to lack of matrix continuity which is responsible for fragility as it has been described previously. Figure II.1.5a and b show SEM images of fractured surface from PP/SCG composites without any surface treatment nor compatibilizer. We observe a clear gap between the particle and the surrounding matrix and this is an evidence of the expected poor interaction between the SCG particles and polypropylene. We can also observe some micro-cracks that appear normal to the particle contour and this has a negative effect on energy absorption. On the other hand, PP/SCG composites with PP-*g*-MA compatibilizer (Figure II.1.5c and d) offer a smaller gap between the particle contour and the surrounding matrix. This is due to the bridge effect that PP-*g*-MA provides. PP-*g*-MA is characterized by dual functionality: on the one hand, highly hydrophilic maleic groups (MA) can interact with hydroxyl groups in the lignocellulosic component and, on the other hand, highly hydrophobic polypropylene segments in PP-*g*-

MA tend to interact with PP polymer chains. The final result is that PP-*g*-MA acts as a strong bridge (chemically linked) between the highly hydrophilic SCG particles and the highly hydrophobic PP chains [35]. The gap between SCG particles and the surrounding PP matrix is reduced by presence of PP-*g*-MA compatibilizer and this has a positive effect on overall properties as described previously. When PP-*g*-MA is absent, load transfer phenomena cannot occur in an appropriate way due to the large gap between SCG particles but when PP-*g*-MA is added it is placed at the particle-polymer interface due to its dual functionality and due to the strong links that it stablishes with both the particle and the surrounding polymer chains, it allows better load transfer from the polymer matrix to the stiffer SCG particles [23]. With regard to silane treatment, it also reduces the gap between the particle and the surrounding matrix (Figure II.1.5e and f) but the gap is higher than that observed for composites with PP-*g*-MA. Finally, PP/SCG composites with SCG subjected to a strong hydrophobizing treatment with palmitoyl chloride (Figure II.1.5g and h) show a gap between the particle and the surrounding matrix but small filaments can be observed (Figure II.1.5g) inside the gaps and these are representative for good compatibility.

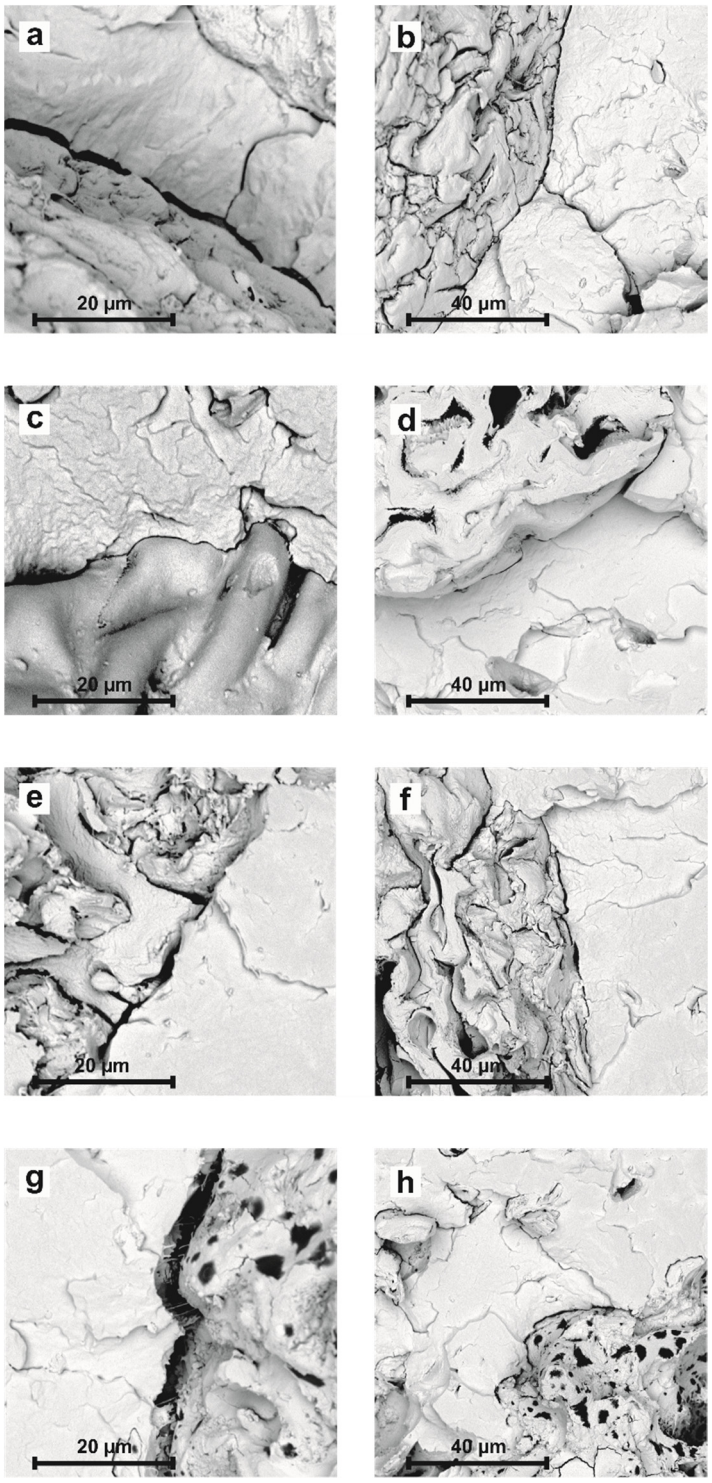

Figure II.1.5. SEM images of fractured surfaces from impact tests of PP/SCG composites with different surface treatments or compatibilizers: (a) untreated SCG (5000x); (b) untreated SCG (2500x); (c) PP/SCG compatibilized with PP-*g*-MA (5000x); (d) PP/SCG compatibilized with PP-*g*-MA (2500x); (e) silanized-SCG with (3-glycidyloxypropyl) trimethoxysilane (5000x); (f) silanized-SCG with (3-glycidyloxypropyl) trimethoxysilane (2500x); (g) hydrophobized-SCG with palmitoyl chloride (5000x) and (h) hydrophobized-SCG with palmitoyl chloride (2500x).

By analyzing the evolution of the storage modulus (*G*') in terms of temperature we can observe some interesting behavior. Figure II.1.6a shows a plot comparison of the storage modulus (*G*') as a function of temperature for unfilled PP and PP/SCG composites. Addition of SCG to polypropylene matrix leads to an increase in storage modulus mainly detectable at low temperatures. The improvement of stiffness of the PP/SCG composites is caused by the addition of a rigid filler into a semi rigid matrix. In the rubbery region the storage modulus of PP/SCG composites is still higher than unfilled PP because the particles promote a high degree of mechanical restraint, which reduces the mobility and deformability of the rubber PP matrix, however in this region the gap between storage modulus of PP and PP/SGC composites is lower than at high temperatures [48]. We can also observe that the best compatibilizing effect is achieved by using PP-*g*-MA as the *G*' values are higher if compared to the other treatments.

Figure II.1.6c shows the evolution of the tan δ as a function of the temperature. As it can be observed, unfilled PP exhibits a clear relaxation at around 9–11 °C. This peak is considered as the glass transition temperature (T_g) and shows the glass-rubber transition of the amorphous regions. With regard to the compatibilized PP/SCG systems, we observe a clear relaxation process at lower temperatures in the −2 to 5 °C range which indicates a clear restriction on chain mobility due to presence of highly dispersed rigid particles. In addition, as we have described previously the small particle size and high dispersion leads to high interface particle-matrix regions and, particularly, the chain mobility in these regions is slightly restricted [49]. This restriction can be observed in Figure II.1.6b by analyzing the evolution of the loss modulus (*G*") in the temperature range comprised between 50 and 60 °C as a small hump which is related to chain mobility in the particle-matrix interface regions as described by Sengupta *et al.* [49]. The first peak in *G*" values is directly related to the mobility of the polymer molecules in the bulk material. The higher damping factor is obtained for PP/SCG composites with PP-*g*-MA thus indicating the clear compatibilizing effect of the PP-*g*-MA which acts as a bridge between the SCG particles and polypropylene matrix thus allowing energy absorption.

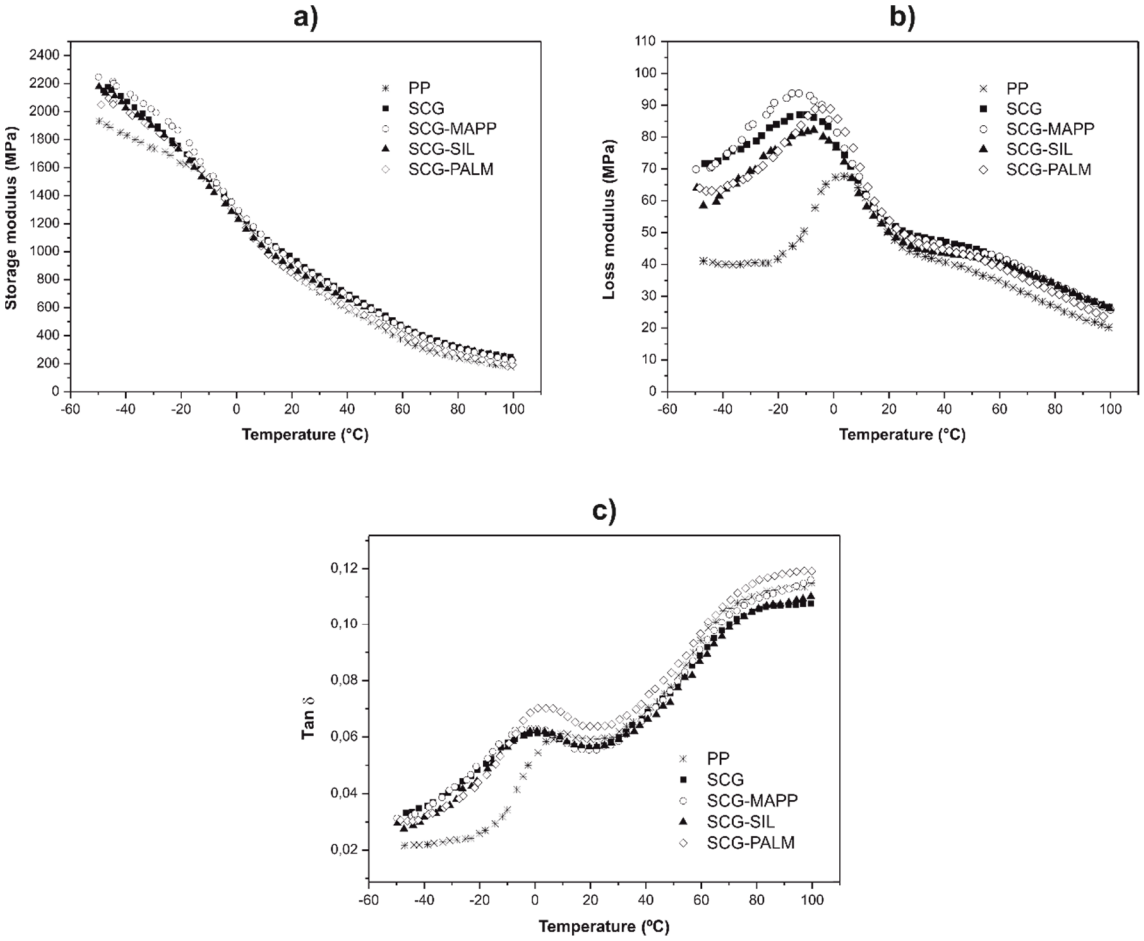

Figure II.1.6. Plot comparison of (a) storage modulus (*G*'), (b) loss modulus (*G*") and (c) tan δ, in terms of temperature for PP/SCG composites with different surface treatments or compatibilizers.

The effect of treatments performed at SCG was analyzed by FTIR spectroscopy. Figure II.1.7 shows the absorbance spectra of the SCG untreated, treated with silane and treated with palmitoyl chloride. As it can be observed, SCG subjected to a hydrophobization process with palmitoyl chloride shows a remarkable decrease in the intensity of the absorption band located between 3000 and 3600 cm^{-1} associated with typical hydroxyl groups in lignocellulosic materials. Reaction of palmitoyl chloride leads to an esterification reaction of hydroxyl groups in cellulose and hemicellulose thus leading to formation of a highly hydrophobic layer all around the surface of the SCG particles. In addition to a clear decrease in the intensity of the –OH band absorption, we observed an increase in the intensity of the absorption peak located between 1750 and 1700 cm^{-1} which is typical of the ester group (−COOR) from carboxylic acids. This reaction provides good link between the SCG particles and the thin hydrophobic layer which is more compatible with the highly

hydrophobic polypropylene matrix and this has a positive effect on the load transfer between filler and matrix and, subsequently, an improvement of mechanical properties [6, 50]. In the case of SCG treated with silane, slight changes can be observed; a slight increase in the peak at about 1108 and 1220 cm^{-1} as well as an increase in the intensity of the peak located at 809 cm^{-1} can be detected. These are associated with the stretching vibration of Si–O–Si/Si–O–C and Si–C bonds respectively thus indicating the formation of new chemical bonds after SCG treatment with silane, which promotes a better filler-matrix interaction [51, 52]. Nevertheless, the effectiveness of the silane treatment in terms of the decrease in the –OH band absorption, is lower than that observed with palmitoyl chloride.

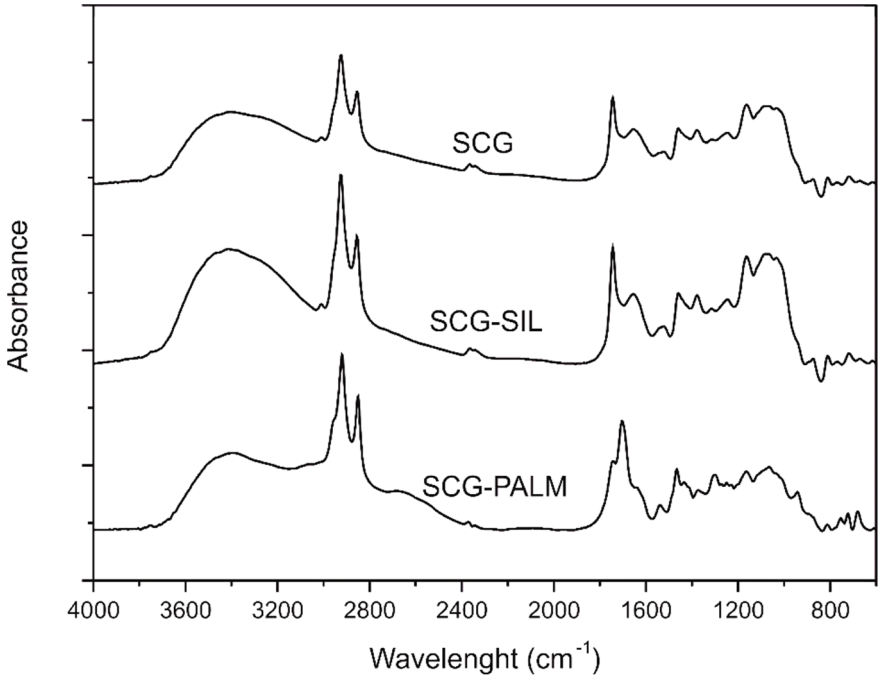

Figure II.1.7. Plot comparison of FTIR spectra for SCG with different surface treatments.

Figure II.1.8 shows the evolution of the water uptake of PP/SCG composites in terms of the immersion time. As can be seen the addition of SCG powder to composites significantly increases water absorption capacity thereof due to the highly hydrophilic lignocellulosic waste. The largest water absorption at an immersion time of three months is obtained for the PP/SCG composite with untreated SCG (1.6 wt%) and this is mainly due to hydrogen bond formation between water molecules and hydroxyl groups in cellulose and hemicelluloses [53]; absence of a previous surface treatment on SCG leads to high amount of accessible hydroxyl groups which can interact with water. PP/SCG composites with compatibilizer (PP-*g*-MA) and silanized-SCG offer lower water uptake values in the whole

considered range with values of 1.5 and 1.45 wt% respectively for an immersion time of three months. In the case of using PP-*g*-MA compatibilizer, maleic anhydride can react with hydroxyl groups in SCG and diminish the total amount of free OH groups that can interact with water. In the case of PP/SCG composite with silanized-SCG we observe a decrease in the water uptake process which is probably due to formation of a thin silane-based layer chemically bonded to the particle due to reaction of the hydrolyzed alkoxy groups in silane and subsequent drying; this fact also leads to a reduction in the total amount of free hydroxyl groups and this has a positive effect on overall water uptake [54]. It is in the case of PP/SCG composites with hydrophobized-SCG where we observe the positive effects of this particular surface treatment as the water uptake for an immersion time of three months is lower than 0.8 wt% and this clearly indicates the usefulness of the hydrophobizing treatment on SCG which allows a chemical anchorage of palmitic acid onto hydroxyl groups in cellulose and hemicelluloses through an esterification reaction to provide an hydrophobic cover (thin layer) onto SCG particles and this leads to a remarkable improvement of the water uptake response of these composites [6].

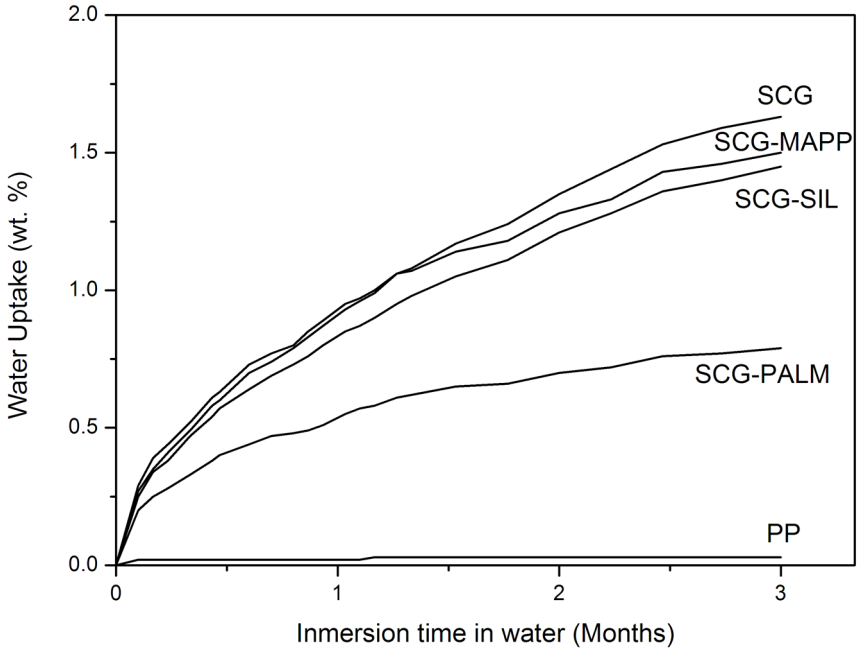

Figure II.1.8. Evolution of the water uptake in terms of the immersion time for PP/SCG composites with different surface treatments or compatibilizers.

The hydrophobization achieved by the treatment with palmitoyl chloride can also been followed by the capillary rise method as used by Trong Dang-Vu for porous materials [24]. Figure II.1.9 shows the evolution of the wetting process for a period of 125 min for

untreated SCG and surface-treated SCG. As it can be seen, untreated SCG absorbs more water with time and more quickly if compared to hydrophobized-SCG with palmitoyl chloride. These typical absorption curves could be characterized by two linear processes: one with a high slope at the start of the wetting process and another one with lower slope once absorption rate stabilizes at higher times. It is clear from observation of Figure II.1.9 that the typical slopes of the wetting process of hydrophobized-SCG are lower than the slopes corresponding to untreated SCG and silanized-SCG thus indicating the high efficiency of the surface treatment with palmitoyl chloride.

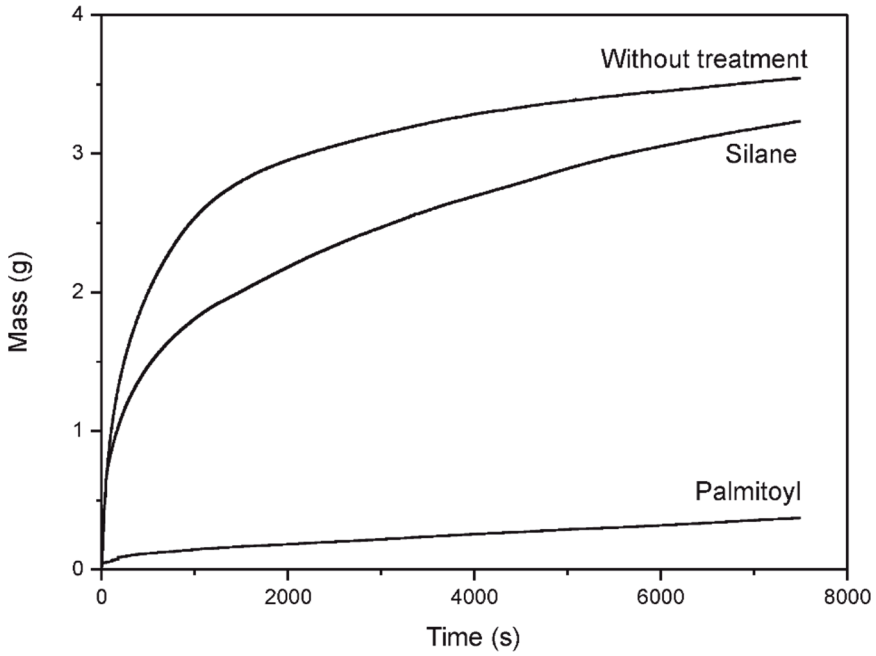

Figure II.1.9. Plot evolution of the absorbed water by capillary rise method of SCG without and with different surface treatments in terms of the time.

Figure II.1.10 shows the evolution of the dynamic contact angle with time, measured over a flat homogeneous surface with SCG with different surface treatments. This also provides a clear evidence of the high efficiency of the hydrophobizing process with palmitoyl chloride. With regard to the evolution of the dynamic contact angle for SCG subjected to surface treatment with palmitoyl chloride, we observe that the initial contact angle (around 140°) remains almost constant with time. This high value is representative for high hydrophobicity. On the other hand, untreated and silane-treated SCG are characterized by initial contact angle of about 120° and this value is rapidly decreased up to total wetting (very low contact angle values) for a time of 60 s.

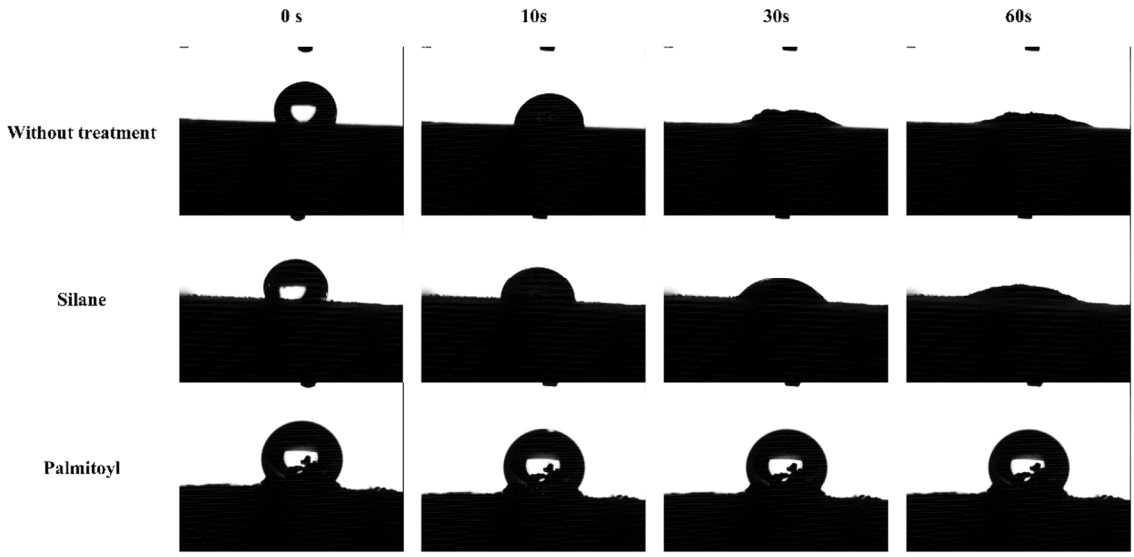

Figure II.1.10. Photographs of the evolution of dynamic contact angle measurements with water over a flat surface of SCG powder without and with surface treatments.

CONCLUSIONS

The obtained results show that addition of both treated and untreated SCG into a polypropylene matrix promotes a slight decrease in flexural strength and a restriction of the deformation due to stress concentration phenomena provided by dispersed particles in the PP matrix. The flexural modulus increases as a consequence of the remarkable decrease in deformation ability also evidenced by impact tests.

Use of conventional compatibilizers such as PP-*g*-MA on PP/SCG composites do not lead to a significant increase in mechanical and thermal performance and the water uptake remains one of the main drawbacks of these composites. Treatment of SCG with silanes provides some additional hydrophobicity but the water uptake behavior is similar to composites with untreated SCG. Surface treatment with palmitoyl chloride has evidenced an effective alternative to provide balanced mechanical and thermal properties together with highly improved water uptake behavior thus evidencing the high hydrophobicity provided by this treatment that also brings hydrophobicity closer to that of the polymer matrix which, in turn, provides good particle dispersion and matrix-particle interactions.

This research work offers an environmentally friendly alternative to upgrade the high waste volume generated by the coffee industry contributing to improve overall properties of composites in terms of mechanical, thermal and water uptake properties.

REFERENCES

[1] George J, Sreekala MS and Thomas S. *A review on interface modification and characterization of natural fiber reinforced plastic composites*. Polymer Engineering and Science, 2001. **41**(9):1471-1485.

[2] Sobczak L, Lang RW and Haider A. *Polypropylene composites with natural fibers and wood – General mechanical property profiles*. Composites Science and Technology, 2012. **72**(5):550-557.

[3] Tasdemir M, Biltekin H and Caneba GT. *Preparation and characterization of LDPE and PP-wood fiber composites*. Journal of Applied Polymer Science, 2009. **112**(5):3095-3102.

[4] Arbelaiz A, Fernández B, Ramos JA, Retegi A, Llano-Ponte R and Mondragon I. *Mechanical properties of short flax fibre bundle/polypropylene composites: Influence of matrix/fibre modification, fibre content, water uptake and recycling*. Composites Science and Technology, 2005. **65**(10):1582-1592.

[5] Joseph PV, Rabello MS, Mattoso LHC, Joseph K and Thomas S. *Environmental effects on the degradation behaviour of sisal fibre reinforced polypropylene composites*. Composites Science and Technology, 2002. **62**(10-11):1357-1372.

[6] Zhang Y, Xue Y, Toghiani H, Zhang J and Pittman CU. *Modification of wood flour surfaces by esterification with acid chlorides: Use in HDPE/wood flour composites*. Composite Interfaces, 2009. **16**(7-9):671-686.

[7] Corrales F, Vilaseca F, Llop M, Gironès J, Méndez JA and Mutjè P. *Chemical modification of jute fibers for the production of green-composites*. Journal of Hazardous Materials, 2007. **144**(3):730-735.

[8] Dányádi L, Móczó J and Pukánszky B. *Effect of various surface modifications of wood flour on the properties of PP/wood composites*. Composites Part A: Applied Science and Manufacturing, 2010. **41**(2):199-206.

[9] Kaewkuk S, Sutapun W and Jarukumjorn K. *Effects of interfacial modification and fiber content on physical properties of sisal fiber/polypropylene composites*. Composites Part B: Engineering, 2013. **45**(1):544-549.

[10] Baiardo M, Frisoni G, Scandola M and Licciardello A. *Surface chemical modification of natural cellulose fibers*. Journal of Applied Polymer Science, 2002. **83**(1):38-45.

[11] Mussatto SI, Machado EMS, Martins S and Teixeira JA. *Production, composition, and application of coffee and its industrial residues*. Food and Bioprocess Technology, 2011. **4**(5):661-672.

[12] Mussatto SI, Carneiro LM, Silva JPA, Roberto IC and Teixeira JA. *A study on chemical constituents and sugars extraction from spent coffee grounds*. Carbohydrate Polymers, 2011. **83**(2):368-374.

[13] Murthy PS and Naidu MM. *Sustainable management of coffee industry by-products and value addition – A review*. Resources, Conservation and Recycling, 2012. **66**:45-58.

[14] Givens DI and Barber WP. *In vivo evaluation of spent coffee grounds as a ruminant feed*. Agricultural Wastes, 1986. **18**(1):69-72.

[15] Adi AJ and Noor ZM. *Waste recycling: Utilization of coffee grounds and kitchen waste in vermicomposting*. Bioresource Technology, 2009. **100**(2):1027-1030.

[16] Kondamudi N, Mohapatra SK and Misra M. *Spent coffee grounds as a versatile source of green energy*. Journal of Agricultural and Food Chemistry, 2008. **56**(24):11757-11760.

[17] Kante K, Nieto-Delgado C, Rangel-Mendez JR and Bandosz TJ. *Spent coffee-based activated carbon: Specific surface features and their importance for H_2S separation process*. Journal of Hazardous Materials, 2012. **201**:141-147.

[18] Panusa A, Zuorro A, Lavecchia R, Marrosu G and Petrucci R. *Recovery of natural antioxidants from spent coffee grounds*. Journal of Agricultural and Food Chemistry, 2013. **61**(17):4162-4168.

[19] Kwon EE, Yi H and Jeon YJ. *Sequential co-production of biodiesel and bioethanol with spent coffee grounds*. Bioresource Technology, 2013. **136**:475-480.

[20] Caetano NS, Silva VFM, Melo AC, Martins AA and Mata TM. *Spent coffee grounds for biodiesel production and other applications*. Clean Technologies and Environmental Policy, 2014. **16**(7):1423-1430.

[21] Obruca S, Benesova P, Petrik S, Oborna J, Prikryl R and Marova I. *Production of polyhydroxyalkanoates using hydrolysate of spent coffee grounds*. Process Biochemistry, 2014. **49**(9):1409-1414.

[22] Zini E, Scandola M and Gatenholm P. *Heterogeneous acylation of flax fibers. Reaction kinetics and surface properties*. Biomacromolecules, 2003. **4**(3):821-827.

[23] Kim HS, Lee BH, Choi SW, Kim S and Kim HJ. *The effect of types of maleic anhydride-grafted polypropylene (MAPP) on the interfacial adhesion properties of bio-flour-filled polypropylene composites*. Composites Part A: Applied Science and Manufacturing, 2007. **38**(6):1473-1482.

[24] Dang-Vu T and Hupka J. *Characterization of porous materials by capillary rise method*. Physicochemical Problems of Mineral Processing, 2005. **39**:47-65.

[25] Kwon HJ, Sunthornvarabhas J, Park JW, Lee JH, Kim HJ, Piyachomkwan K, Sriroth K and Cho D. *Tensile properties of kenaf fiber and corn husk flour reinforced poly(lactic acid) hybrid bio-composites: Role of aspect ratio of natural fibers*. Composites Part B: Engineering, 2014. **56**:232-237.

[26] Yan W, Lin RJT and Bhattacharyya D. *Particulate reinforced rotationally moulded polyethylene composites – Mixing methods and mechanical properties*. Composites Science and Technology, 2006. **66**(13):2080-2088.

[27] Nourbakhsh A, Karegarfard A, Ashori A and Nourbakhsh A. *Effects of particle size and coupling agent concentration on mechanical properties of particulate-filled polymer composites*. Journal of Thermoplastic Composite Materials, 2010. **23**(2):169-174.

[28] Renner K, Kenyó C, Móczó J and Pukánszky B. *Micromechanical deformation processes in PP/wood composites: Particle characteristics, adhesion, mechanisms*. Composites Part A: Applied Science and Manufacturing, 2010. **41**(11):1653-1661.

[29] Kaymakci A, Ayrilmis N, Ozdemir F and Gulec T. *Utilization of sunflower stalk in manufacture of thermoplastic composite*. Journal of Polymers and the Environment, 2013. **21**(4):1135-1142.

[30] Kuciel S, Jakubowska P and Kuźniar P. *A study on the mechanical properties and the influence of water uptake and temperature on biocomposites based on polyethylene from renewable sources*. Composites Part B: Engineering, 2014. **64**:72-77.

[31] El Sayed AM, Shehata AB, Darwish NA, Abd El Megeed AA, Badawy NA, El-Bayaa AA and El-Mogy SA. *Effect of compatibilizing agents on the mechanical property of rice husk flour as nano-potential filler in polypropylene biocomposite*. Journal of Applied Polymer Science, 2012. **125**(2):1310-1317.

[32] Leong YW, Abu Bakar MB, Ishak ZAM, Ariffin A and Pukanszky B. *Comparison of the mechanical properties and interfacial interactions between talc, kaolin, and calcium carbonate filled polypropylene composites*. Journal of Applied Polymer Science, 2004. **91**(5):3315-3326.

[33] Premalal HGB, Ismail H and Baharin A. *Comparison of the mechanical properties of rice husk powder filled polypropylene composites with talc filled polypropylene composites*. Polymer Testing, 2002. **21**(7):833-839.

[34] Guerrica-Echevarria G, Eguiazábal JI and Nazábal J. *Influence of molding conditions and talc content on the properties of polypropylene composites*. European Polymer Journal, 1998. **34**(8):1213-1219.

[35] Yang HS, Kim HJ, Park HJ, Lee BJ and Hwang TS. *Effect of compatibilizing agents on rice-husk flour reinforced polypropylene composites*. Composite Structures, 2007. **77**(1):45-55.

[36] Yang HS, Kim HJ, Son J, Park HJ, Lee BJ and Hwang TS. *Rice-husk flour filled polypropylene composites; Mechanical and morphological study*. Composite Structures, 2004. **63**(3-4):305-312.

[37] Lee SH, Zhang Y, Kontopoulou M, Park CB, Wong A and Zhai W. *Optimization of dispersion of nanosilica particles in a PP matrix and their effect on foaming*. International Polymer Processing, 2011. **26**(4):388-398.

[38] Yao N, Zhang P, Song L, Kang M, Lu Z and Zheng R. *Stearic acid coating on circulating fluidized bed combustion fly ashes and its effect on the mechanical performance of polymer composites*. Applied Surface Science, 2013. **279**:109-115.

[39] Langner E and Rzeski W. *Biological properties of melanoidins: A review*. International Journal of Food Properties, 2014. **17**(2):344-353.

[40] Ludwig IA, Bravo J, De Peña MP and Cid C. *Effect of sugar addition (torrefacto) during roasting process on antioxidant capacity and phenolics of coffee*. LWT-Food Science and Technology, 2013. **51**(2):553-559.

[41] Bouza R, Pardo SG, Barral L and Abad MJ. *Design of new polypropylene-woodflour composites: Processing and physical characterization*. Polymer Composites, 2009. **30**(7):880-886.

[42] Li L, Wang Q and Guo C. *The influence of wood flour and compatibilizer (m-TMI-g-PP) on crystallization and melting behavior of polypropylene*. Journal of Thermal Analysis and Calorimetry, 2012. **107**(2):717-723.

[43] Essabir H, Nekhlaoui S, Malha M, Bensalah MO, Arrakhiz FZ, Qaiss A and Bouhfid R. *Bio-composites based on polypropylene reinforced with almond shells particles: Mechanical and thermal properties*. Materials & Design, 2013. **51**:225-230.

[44] Essabir H, Hilali E, Elgharad A, El Minor H, Imad A, Elamraoui A and Al Gaoudi O. *Mechanical and thermal properties of bio-composites based on polypropylene reinforced with nut-shells of argan particles*. Materials & Design, 2013. **49**:442-448.

[45] Joseph PV, Joseph K, Thomas S, Pillai CKS, Prasad VS, Groeninckx G and Sarkissova M. *The thermal and crystallisation studies of short sisal fibre reinforced polypropylene composites*. Composites Part A: Applied Science and Manufacturing, 2003. **34**(3):253-266.

[46] Sdrobiş A, Darie RN, Totolin M, Cazacu G and Vasile C. *Low density polyethylene composites containing cellulose pulp fibers*. Composites Part B: Engineering, 2012. **43**(4):1873-1880.

[47] Arrakhiz FZ, El Achaby M, Benmoussa K, Bouhfid R, Essassi EM and Qaiss A. *Evaluation of mechanical and thermal properties of pine cone fibers reinforced compatibilized polypropylene*. Materials & Design, 2012. **40**:528-535.

[48] Nuñez AJ, Kenny JM, Reboredo MM, Aranguren MI and Marcovich NE. *Thermal and dynamic mechanical characterization of polypropylene-woodflour composites*. Polymer Engineering and Science, 2002. **42**(4):733-742.

[49] Sengupta S, Maity P, Ray D and Mukhopadhyay A. *Stearic acid as coupling agent in fly ash reinforced recycled polypropylene matrix composites: Structural, mechanical, and thermal characterizations*. Journal of Applied Polymer Science, 2013. **130**(3):1996-2004.

[50] Prakash GK and Mahadevan KM. *Enhancing the properties of wood through chemical modification with palmitoyl chloride*. Applied Surface Science, 2008. **254**(6):1751-1756.

[51] Lu T, Liu S, Jiang M, Xu X, Wang Y, Wang Z, Gou J, Hui D and Zhou Z. *Effects of modifications of bamboo cellulose fibers on the improved mechanical properties of cellulose reinforced poly(lactic acid) composites*. Composites Part B: Engineering, 2014. **62**:191-197.

[52] Lu T, Jiang M, Jiang Z, Hui D, Wang Z and Zhou Z. *Effect of surface modification of bamboo cellulose fibers on mechanical properties of cellulose/epoxy composites*. Composites Part B: Engineering, 2013. **51**:28-34.

[53] Ichazo MN, Albano C, González J, Perera R and Candal MV. *Polypropylene/wood flour composites: Treatments and properties*. Composite Structures, 2001. **54**(2-3):207-214.

[54] Demir H, Atikler U, Balköse D and Tihminlioğlu F. *The effect of fiber surface treatments on the tensile and water sorption properties of polypropylene-luffa fiber composites*. Composites Part A: Applied Science and Manufacturing, 2006. **37**(3):447-456.

Composites Part B 78 (2015) 256–265

Contents lists available at ScienceDirect

Composites Part B

journal homepage: www.elsevier.com/locate/compositesb

Green composites based on polypropylene matrix and hydrophobized spend coffee ground (SCG) powder

D. García-García*, A. Carbonell, M.D. Samper, D. García-Sanoguera, R. Balart

Instituto de Tecnología de Materiales (ITM), Universitat Politècnica de València (UPV), Plaza Ferrandiz y Carbonell 1, 03801 Alcoy, Alicante, Spain

ARTICLE INFO

Article history:
Received 10 September 2014
Received in revised form
17 February 2015
Accepted 27 March 2015
Available online 4 April 2015

Keywords:
A. Polymer-matrix composites (PMCs)
B. Adhesion
B. Wettability
D. Thermal analysis
Spent coffee ground (SCG)

ABSTRACT

Green composites were prepared with polypropylene matrix and 20 wt.% spent coffee ground (SCG) powder for uses as a wood plastic composite (WPC). The effects of hydrophobic treatment with palmitoyl chloride on SCG powder is compared with conventional surface treatment based on silanization with (3-glycidyloxypropyl) trimethoxysilane and the use of a maleated copolymer compatibilizer (polypropylene-graft-maleic anhydride, PP-*g*-MA) in terms of mechanical properties, morphology, thermal properties and water uptake. Composites were previously mixed in a twin-screw co-rotating extruder and subsequently subjected to injection moulding. The comparative effect of the different surface treatments and or compatibilizers on mechanical performance was studied by flexural, impact tests and dynamic mechanical thermal analysis (DMTA-torsion); in addition, the stabilizing effect of SCG was revealed by differential scanning calorimetry (DSC) and thermogravymetric analysis (TGA). As one of the main drawbacks of wood plastic composites and natural fibre reinforced plastics is the moisture gain, water uptake tests were carried out in order to quantify the effectiveness of the hydrophobization process with palmitoyl chloride. Results show a slight increase in flexural modulus for composites with both untreated and treated/compatibilized SCG powder (20 wt.%). As expected, thermal stability is improved as indicated by an increase of more than 8% in the onset degradation temperature by DSC if compared to unfilled polypropylene. Fracture analysis by scanning electron microscopy (SEM) shows better particle dispersion for PP-SCG composites with hydrophobized SCG with palmitoyl chloride treatment; in addition a remarkable decrease in water uptake is observed for composites with hydrophobized SCG.

1. Introduction

Today, ecological concerns and issues such as recycling and environmental care are increasingly important. As a consequence of such environmental awareness we are witnessing a great interest in the research on more environmentally friendly materials as it is the case of polymer composites reinforced with natural fibres (natural fibre reinforced plastics-NFRP and wood plastic composites-WPC) [1–3]. Natural fillers are acquiring increasing importance as reinforcing materials in composites due to some advantages they provide such as low cost, low density, no toxicity, balanced mechanical properties and a clear lower environmental impact [3,4]. The main problem related to the use of natural fillers is their low compatibility with most polymer matrices. Most natural fillers are lignocellulosic-based materials and, consequently, highly hydrophilic, while most polymer matrices are intrinsically hydrophobic. This fact leads to low polymer-filler interactions which lead to poor mechanical properties thus making necessary the use of surface treatments on fillers (i.e. silanization) or addition of compatibilizer agents (maleated copolymers). In addition to the lack of compatibility between the two main components, moisture gain is another big drawback when using natural fibre reinforcements. Hydrophilicity in natural fibre reinforcements is provided by the high amount of cellulose and hemicelluloses with hydroxyl groups which are also responsible for high water absorption capacity. Moisture gain in NFRPs and WPCs is a critical issue as the water uptake leads to dimensional instability [4–6]. With the aim of improving polymer-filler interactions and reduce the water uptake, different physical or chemical modifications have been proposed (silanization, esterification, etherification, benzylation, etc.) as well as the use of compatibilizer agents (mainly maleated copolymers) [6–10].

* Corresponding author. Tel.: +34 96 652 84 33.
E-mail address: dagarga4@epsa.upv.es (D. García-García).

http://dx.doi.org/10.1016/j.compositesb.2015.03.080
1359-8368/

II.2

"Development and characterization of green composites from bio-based polyethylene and peanut shell"

Daniel García García[a], *Alfredo Carbonell Verdú*[a], *Amparo Jordá Vilaplana*[b], *Rafael Balart*[a], *David García Sanoguera*[a]

[a] Instituto de Tecnología de Materiales (ITM)
Universitat Politècnica de València (UPV)
Plaza Ferrándiz y Carbonell 1, 03801 Alcoy, Alicante, Spain.

[b] Departamento de Ingeniería Gráfica
Universitat Politècnica de València (UPV)
Plaza Ferrandiz y Carbonell 1, 03801 Alcoy, Alicante, Spain.

Journal of Applied Polymer Science

2016, 133:43940

Development and characterization of green composites from bio-based polyethylene and peanut shell

Abstract

In the present work, different compatibilizers, namely polyethylene-*graft*-maleic anhydride (PE-*g*-MA), polypropylene-*graft*-maleic anhydride (PP-*g*-MA) and polystyrene-*block*-poly(ethylene-*ran*-butylene)-*block*-polystyrene-*graft*-maleic anhydride (SEBS-*g*-MA) were used on green composites derived from biobased polyethylene and peanut shell (PNS) flour to improve particle-polymer interaction. Composites of high-density polyethylene/peanut shell powder (HDPE/PNS) with 10 wt% PNS flour were compatibilized with 3 wt% of the abovementioned compatibilizers. As per the results, PP-*g*-MA copolymer lead to best optimized properties as evidenced by mechanical characterization. In addition, best particle-matrix interface interactions with PP-*g*-MA were observed by scanning electron microscopy (SEM). Subsequently HDPE/PNS composites with varying PNS flour content in the 5–30 wt% range with PP-*g*-MA compatibilizer were obtained by melt extrusion and compounding followed by injection molding and were characterized by mechanical, thermal and morphological techniques. The results showed that PNS powder, leads to an increase in mechanical resistant properties (mainly, flexural modulus and strength) while a decrease in mechanical ductile properties, that is, elongation at break and impact absorbed energy is observed with increasing PNS flour content. Furthermore, PNS flour provides an increase in thermal stability due to the natural antioxidant properties of PNS. In particular, composites containing 30 wt% PNS powder present a flexural strength 24% and a flexural modulus 72% higher than the unfilled polyethylene and the thermo-oxidative onset degradation temperature is increased from 232 °C up to 254 °C thus indicating a marked thermal stabilization effect. Resultant composites can show a great deal of potential as base materials for wood plastic composites.

Keywords: Biopolymers and renewable polymers; compatibilization; composites; mechanical properties.

INTRODUCTION

In recent years, increased awareness on environmental issues has been detected. This fact, together with the problems related to petroleum depletion has led to a breakthrough in the field of environmentally friendly materials development; much of this progress has been observed in the field of polymer composites, mainly on natural fiber reinforced plastics (NFRPs) and wood plastic composites (WPCs) for everyday applications [1-4]. The use of natural fillers into a polymeric matrix provides attracting advantages such as reduced costs, lightness, excellent balanced mechanical properties, etc., together with a marked low environmental impact [5]. Moreover, due to their aesthetic appearance (wood or natural product like) and the advantageous position against wood (low maintenance, high dimensional stability in wet conditions and high resistance to biological attack), NFRPs and WPCs are increasingly used in sectors such as decoration, construction and automotive [3, 6-9].

The main disadvantages of using natural fillers in a polymeric matrix is the relatively poor dispersion of the filler in the matrix and the low polymer-particle compatibility which leads to poor interface phenomena thus giving poor final properties. The highly hydrophobic polymeric matrix is not compatible with the highly hydrophilic filler (lignocellulosic material) which gives poor adhesion among matrix-filler interface and this is responsible for a decrease in mechanical and thermal performance of composites [10-12]. One of the methods used to enhance filler dispersion and polymer-filler adhesion/interaction is the use of compatibilizer agents such as maleic anhydride-grafted polypropylene (PP-*g*-MA) or maleic anhydride-grafted polyethylene (PE-*g*-MA) [5, 10, 12-17]. These compatibilizers act as a bridge between the lignocellulosic particle and the polymeric chains because of their dual functionality. Firstly, polyethylene or polypropylene fraction in PE-*g*-MA and PP-*g*-MA, respectively, can interact with some polymer chains due to chemical affinity while maleic anhydride groups in the compatibilizer structure can react with hydroxyl groups in lignocellulosic particle by an esterification reaction to give increased matrix-filler interactions which have a positive effect on particle dispersion and stiffness [13, 18]. Despite this, ductile properties are not usually improved due to the brittleness that the filler provides because of presence of particle aggregates and matrix discontinuity, which promote stress concentration phenomena.

Peanut is one of the most important crops in the world. Its world production is estimated around 30 million tons per year and most of it, is sold without the shell, which contributes to a high waste generation coming from the shell. A small amount of these wastes is used as animal feeding or valued by incineration [19]. Nevertheless, the greater

part is disposed of in landfills with the subsequent high environmental impact. Peanut shell (PNS) is composed of natural polymers, mainly consisting in cellulose, lignin, hemicelluloses and tannins [20]. Its chemical composition is similar to that of hard wood but PNS possesses higher cellulose content [21]. This feature makes PNS an interesting candidate as lignocellulosic filler in polymeric matrices. Up to now there are not many works focused on the use of PNS as filler in polymer matrices. Sareena *et al.* [22] evaluated the mechanical properties of composite materials based on a natural rubber matrix with PNS fillers. The study was focused on the effect of the particle size and the previous alkaline treatment on final performance of composites. Wu [23], studied the effect of PNS reinforcements on mechanical and biodegradation properties of poly(butylene adipate-*co*-terephthalate) (PBAT) composites. This work also evidenced the synergistic effect of PBAT-based compatibilizers (PBAT-*g*-MA) on final performance of PBAT-based composites. Salasinska *et al.* [24] investigated the effect of PNS load on mechanical and thermal behavior of high density polyethylene (HDPE) films. Zaaba *et al.* [25] showed the positive effect of previous chemical modification of PNS with poly(vinyl alcohol) (PVA) to improve overall properties of recycled polypropylene (PP). Prabhakar *et al.* [26] analyzed the effect of PNS fillers (without and with a previous alkaline treatment) in epoxy thermosetting resins. In addition, the potential of PNS as base material for particle board manufacturing was studied [27, 28], but its use is not generalized. By taking into account the large amounts of PNS wastes and considering the increasing concern about environment and sustainable development, new materials are being demanded by our society to give an environmentally friendly solution to wastes. This has led to an increase in research about thermoplastic composites with natural fillers such as NFRPs and WPCs which use commodity, recycled or biodegradable plastics as matrices. Nevertheless, most of these studies are focused on the use of wastes coming from the wood industry [29-31].

One pioneer company in the development of biobased polyolefins is Braskem. This company produces at commercial scale a biobased polyethylene from bioethanol derived from sugarcane but with similar properties to those of conventional petroleum-based polyethylene; nevertheless, the environmental efficiency is considerably higher as 1 ton of the so called "green-PE" fixes 2.5 ton CO_2 thus having a positive overall effect on environment and the carbon footprint [32].

The main goal of this work is to obtain high environmentally friendly biobased composites by using biobased HDPE as matrix and PNS waste from the food industry. The effect of different compatibilizers and filler content is shown. In the first part of the study, the effect of 3 wt% of different maleic anhydride-based copolymers is evaluated. Several

studies in the literature suggest that this compatibilizer content can lead to optimum results in polymer composites with lignocellulosic fillers [33-35]. In particular, the effect of polyethylene-*graft*-maleic anhydride (PE-*g*-MA), polypropylene-*graft*-maleic anhydride (PP-*g*-MA) and polystyrene-*block*-poly(ethylene-*ran*-butylene)-*block*-polystyrene-*graft*-maleic anhydride (SEBS-*g*-MA) is evaluated in terms of mechanical properties and particle-polymer interaction. Once the best compatibilizer is selected, the PNS powder content is varied in the 5−30 wt% to investigate the effect of the filler loading on overall properties on compatibilized formulations. Mechanical properties are obtained by tensile, flexural, impact and hardness tests. Thermo-oxidative degradation is studied by differential scanning calorimetry (DSC). Thermo-mechanical behavior is assessed by following the evolution of the storage modulus (*G'*). Degradation at high temperatures is evaluated by thermogravimetric analysis (TGA) and finally, particle-polymer interaction is observed by scanning electron microscopy (SEM).

EXPERIMENTAL

Materials

The polymer matrix was a commercial biobased HDPE grade Green HDPE SHA7260 supplied by Braskem (BRASKEM, Sao Paulo, Brazil). This is obtained from bioethanol derived from sugarcane and its minimum biobased content is 94% according to ASTM D6866 as indicated in the technical datasheet. This polyethylene has a density of 0.955 g cm^{-3} and a melt flow index of 20 g $(10\ min)^{-1}$ measured at 190 °C.

The selected lignocellulosic filler was PNS from local food industry. Prior to composite manufacturing the PNS was subjected to a dry milling process in an ultra-centrifugal mill (Retsch GmbH, Hann, Germany) working at 8000 rpm, equipped with a 250 μm sieve; after the milling-sieving process, the obtained powder was subjected to a drying process at 80 °C for 4 h to remove residual moisture. The antioxidant capacity of PNS powder was determined by two different methods: DPPH and FRAP methods and the polyphenol and flavonoid total content was measured by the Folin-Ciocalteu method. Table II.2.1 summarizes the main properties of PNS powder.

Table II.2.1. Characterization of the antioxidant capacity and polyphenol and flavonoid total content of PNS powder.

Property	Value
Antioxidant capacity, DPPH (%RSA)	83 ± 2
Antioxidant capacity, FRAP (mg Trolox/g sample)	1.33 ± 0.05
Flavonoids (mg quercetin/g sample)	1.16 ± 0.06
Polyphenols FOLIN (mg quercetin/g sample)	6.16 ± 0.27

All three compatibilizer copolymers were supplied by Sigma Aldrich (Sigma Aldrich, Madrid, Spain) and were used to increase particle-polymer interactions and promote filler dispersion. These copolymers were polyethylene-*graft*-maleic anhydride (PE-*g*-MA), polypropylene-*graft*-maleic anhydride (PP-*g*-MA) and polystyrene-*block*-poly(ethylene-*ran*-butylene)-*block*-polystyrene-*graft*-maleic anhydride (SEBS-*g*-MA). Table II.2.2 shows the main characteristics of these compatibilizers.

Table II.2.2. Summary of the main characteristics of maleic anhydride-based compatibilizers: PP-*g*-MA, PE-*g*-MA and SEBS-*g*-MA.

Properties	PP-*g*-MA	PE-*g*-MA	SEBS-*g*-MA
Maleic anhydride content (wt%)	8–10	~0.5	~2
Density at 25°C (g mL^{-1})	0.934	0.92	0.91

HDPE/PNS composite manufacturing

In a first stage, four different composites were manufactured with HDPE and PNS powder. The PNS content was 10 wt% for all four composites and 3 wt% of different compatibilizers was added. Table II.2.3 summarizes the compositions used to evaluate the influence of the compatibilizer type.

Table II.2.3. Summary of compositions and codes of biobased HDPE/PNS powder formulations used to evaluate the influence of the compatibilizer type on overall properties of composites.

Code	Green-PE (wt%)	PNS powder (wt%)	Compatibilizer (wt%)
HDPE/PNS	90	10	-
HDPE/PNS/PE-*g*-MA	87	10	3 [PE-*g*-MA]
HDPE/PNS/PP-*g*-MA	87	10	3 [PP-*g*-MA]
HDPE/PNS/SEBS-*g*-MA	87	10	3 [SEBS-*g*-MA]

After selecting the most suitable compatibilizer for HDPE/PNS composites, new formulations containing 5, 10, 20 and 30 wt% PNS powder were manufactured.

All composites were obtained by following this procedure: polyethylene pellet, PNS powder and the corresponding amounts of compatibilizer were mechanically mixed in a zipper bag to homogenize and then fed into a twin screw co-rotating extruder with D = 25 mm and L/D = 24 from DUPRA S.L. (Alicante, Spain). The temperature profile was set to 160 °C, 160 °C, 165 °C and 170 °C (from hopper to die). After cooling at room temperature, the obtained compounds were pelletized in a mill and subsequently processed by injection molding in a Meteor 270/75 (Mateu & Solé, Barcelona, Spain) at an injection temperature profile of 160 °C (hopper), 160 °C, 165 °C, 170 °C and 170 °C (die). The filling time was 1 s and the cooling time was set to 10 s. After injection molding, standard samples for tensile tests (type 1B) as recommended by ISO 527 were obtained. Samples for tensile tests sized 150 mm in length, 4 mm thickness and 10 mm wide. In addition, rectangular samples sizing 80×10×4 mm^3 were obtained for further characterization.

Characterization techniques

Mechanical characterization of HDPE/PNS composites

Tensile and flexural properties of HDPE/PNS composites were tested in a universal test machine Ibertest ELIB 30 (S.A.E. Ibertest, Madrid, Spain) at room temperature, according to ISO 527-5 and ISO 178 respectively, with a load cell of 5 kN and a crosshead rate of 5 mm min^{-1}. A minimum of five different samples were tested and average values were calculated.

With regard to hardness, a Shore D durometer 673-D (J. Bot Instruments, Barcelona, Spain) was used according to the guidelines of the UNE-EN-ISO 868 standard.

Charpy impact tests were carried out in a 1 J Charpy pendulum (Metrotec S.A., San Sebastián, Spain) as indicated by the ISO 179:1993. Five different notched samples values were averaged. The notch was "V" type at 45° and notch radio of 0.25 mm.

In addition, dynamic mechanical thermal analysis (DMTA) was carried out in an oscillatory rheometer AR G2 (TA Instruments, New Castle, USA) equipped with a torsion clamp for solid samples. Rectangular samples sizing 40×10×4 mm^3 were subjected to a temperature sweep from −50 up to 100 °C at a heating rate of 2 °C min^{-1}. Samples were tested at a frequency of 1 Hz and a percentage deformation (γ) of 0.1%.

SEM characterization of fractured surfaces of HDPE/PNS composites

A SEM Phenom (FEI Company, Eindhoven, the Netherlands) operated at 5 kV and an emission current of 50 μA was used to analyze the fractured surfaces from impact tests. In a previous stage, samples were metallized with a gold-palladium alloy in vacuum conditions in a sputter coater EMITECH mod. SC7620 (Quorum Technologies Ltd., East Sussex, UK).

Thermal analysis of HDPE/PNS composites

Thermal properties of neat HDPE, PNS powder and different HDPE/PNS composites were evaluated by DSC and TGA. TGA tests were carried out in a TGA/SDTA 851 thermobalance (Mettler-Toledo Inc., Schwerzenbach, Switzerland) with a heating program from 30 up to 700 °C at a heating rate of 20 °C min^{-1} in nitrogen atmosphere (with a constant flow rate of 66 mL min^{-1}). Thermal transitions were studied by differential scanning calorimetry in a DSC Mettler-Toledo 821 (Mettler-Toledo Inc., Schwerzenbach, Switzerland). Samples with average weight of 10 mg were subjected to a heating program from 30 to 300 °C at a heating rate of 10 °C min^{-1} in air atmosphere to evaluate the effect of natural phenolic compounds and flavonoids on thermal stabilization.

Water uptake of HDPE/PNS composites

Water uptake was assessed by immersion of samples in distilled water at room temperature. Three different samples of each composite formulations (80×10×4 mm^3) were subjected to water uptake and average values were calculated. Before starting the tests, samples were dried at 80 °C for 4 h to remove residual moisture. Weight changes were

measured every 3 days for a total period of 7 months. The percentage water uptake was calculated by using Equation II.2.1:

$$\boldsymbol{Water\ Uptake}\ (\%) = \frac{(\boldsymbol{m_f} - \boldsymbol{m_i})}{\boldsymbol{m_i}} \times \mathbf{100} \qquad \textbf{Equation II.2.1}$$

where, m_f is the final weight of the sample at a particular time and m_i is the initial weight of the dry sample before immersion in water.

RESULTS AND DISCUSSION

Effect of different maleic anhydride-based copolymers as compatibilizers for HDPE/PNS composites

Figure II.2.1 gathers the information about mechanical properties of HDPE/PNS composites (tensile, flexural, impact and hardness) without and with different compatibilizers based on maleic anhydride modification. With regard to tensile properties (Figure II.2.1a), a slight decrease in tensile strength can be observed when PNS powder is added. Best results for tensile strength are obtained by using PP-*g*-MA (HDPE/PNS/PP-*g*-MA) that contributes to a tensile strength of 18.9 MPa which represents a percentage decrease of about 3% with regard to unfilled polyethylene (19.6 MPa). Tensile modulus is similar for all composites with values in the 400–500 MPa range, which is slightly higher in comparison to unfilled HDPE with a tensile modulus of about 373 MPa. In general, the tensile resistant properties are not remarkably influenced by the addition of 10 wt% PNS powder. Nevertheless, the elongation at break (ductile mechanical property) is reduced in a remarkable way as in most NFRP and WPC. The initial elongation at break of unfilled HDPE is around 520% and this value decreases dramatically up to values in the 2–4% range. This is due to presence of PNS particles dispersed in the polymeric matrix. The highly hydrophilic nature of PNS powder (lignocellulosic) is not compatible with the highly hydrophobic polyethylene matrix. This fact leads to a lack of particle-filler interactions which, in turn, has a key role in stress concentration phenomena [36]. Moreover, particle aggregates also contribute to stress concentration with a negative effect on cohesive properties such as elongation at break. Although slightly higher elongation at break is obtained for uncompatibilized HDPE/PNS composite, in general, the decrease in elongation at break is dramatic for all compositions with and without compatibilizer agents. It is evident that most of the elongation is lost with relatively low lignocellulosic filler content and this can restrict some final uses of HDPE/PNS composites (mainly in those that require high elongation

ability). The main advantage of these composites is related to aesthetics concerns as they emulate wood like materials. Some engineering applications require high stiffness materials while no high elongation levels are needed as it is the case of furniture, decking, flooring, etc. So that, alternative uses to HDPE can be derived with addition of PNS flour.

With regard to flexural properties (Figure II.2.1b), once again it is the HDPE/PNS/PP-*g*-MA composite the one that offers the highest flexural strength (26.6 MPa) which represents a percentage increase of about 16% with regard to unfilled HDPE (23 MPa) and 8% more than uncompatibilized HDPE/PNS composite. Identical tendency can be observed for the flexural modulus with values of 1017 MPa for composites compatibilized with PP-*g*-MA which represents a percentage increase of almost 26% with regard to the unfilled HDPE.

Impact energy (Figure II.2.1c) is another mechanical property highly sensitive to presence of stress concentrators. All composites show absorbed energy values close to 2 kJ m^{-2} which represents a percentage decrease of about 27% if compared to the unfilled material (2.75 kJ m^{-2}). Impact energy indicates the absorbed energy during deformation and fracture processes. This depends on several factors such as stress concentrators, crack formation and growth rate, filler particle size, etc. All these phenomena are involved in the overall deformation and, consequently, can affect the impact-absorbed energy. As we have seen before, the tensile strength is slightly lower and the flexural strength increases; nevertheless, the addition of PNS powder restricts in a remarkable way the ability of HDPE/PNS composites to deform so that, the overall effect is a small decrease in absorbed energy.

With regard to Shore D hardness (Figure II.2.1c), as it is a resistant mechanical property, a slight increase can be observed but no remarkable differences with the compatibilizer type can be distinguished.

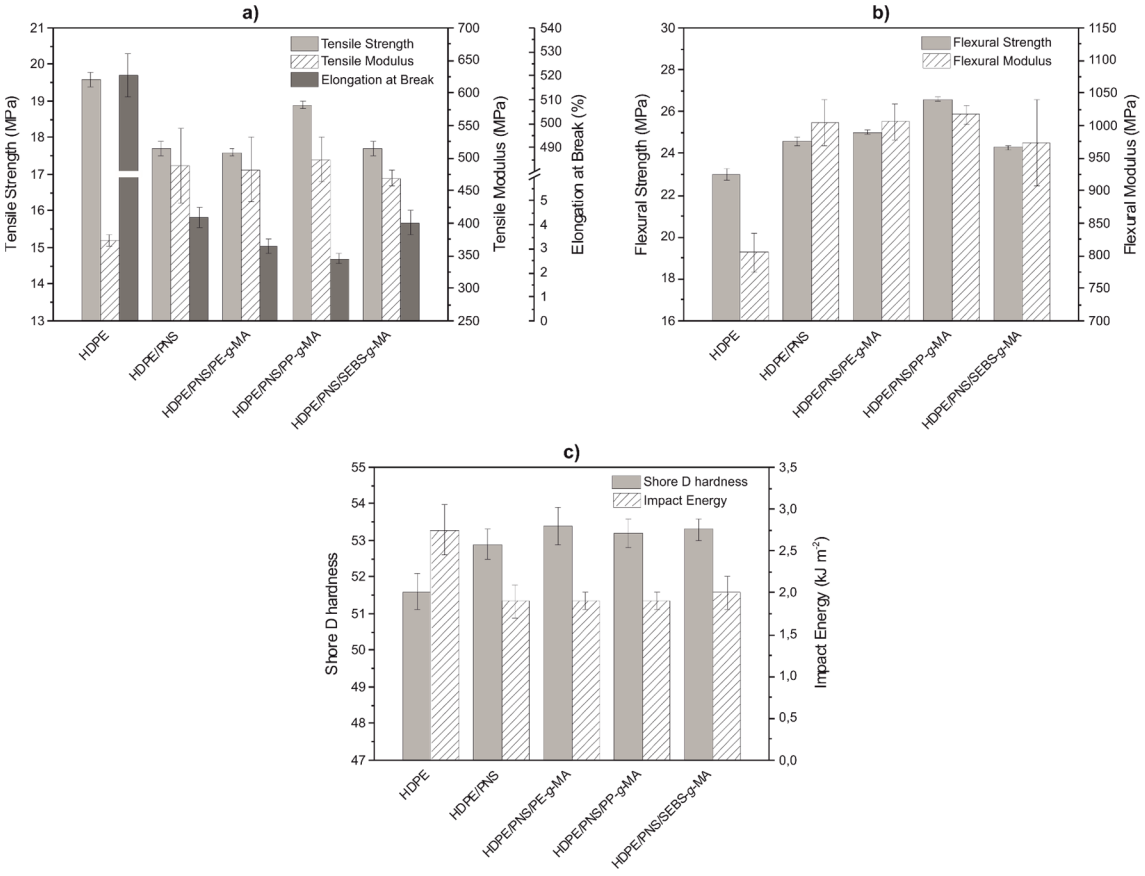

Figure II.2.1. Bar plot with the evolution of (a) tensile properties, (b) flexural properties and (c) Shore D hardness-impact energy of HDPE/PNS composites without and with different maleic anhydride based compatibilizers.

Thermal behavior of HDPE/PNS has been evaluated with DSC and TGA. Thermo-oxidative degradation at moderate temperatures in the processing window was studied by DSC whilst thermal degradation-decomposition at high temperatures was followed by TGA. Figure II.2.2 shows the melt temperature (peak) and the onset degradation (thermo-oxidative processes) temperature for unfilled and HDPE/PNS composites. Thermo-oxidative processes at moderate temperatures are related to free radical formation due to chain scission and subsequent reaction with oxygen moieties, but no detectable weight loss is observed at this stage. For this reason, thermo-oxidative processes are best detected by DSC. As we can see, the melt temperature for HDPE/PNS composites is slightly lower, probably due to nucleating effect of lignocellulosic particles but the overall effect is negligible. Nevertheless, it is important to remark a noticeable delay in the thermo-oxidative processes at moderate temperatures in the typical processing temperature range for all uncompatibilized and compatibilized HDPE/PNS composites. This delay leads to broaden the processing window of HDPE/PNS composites. The uncompatibilized

HDPE/PNS composite shows an onset thermo-oxidation temperature of 237.5 °C which is 5 °C higher than the unfilled HDPE (232.5 °C). All compatibilized HDPE/PNS composites offer slightly higher onset thermo-oxidation temperatures close to 240 °C but it is the use of PP-*g*-MA compatibilizer (HDPE/PNS/PP-*g*-MA) the one that gives the optimum results. This increase in the onset thermo-oxidation temperature is directly related to the presence of phenolic compounds and flavonoids with high free-radical scavenging activity as described previously.

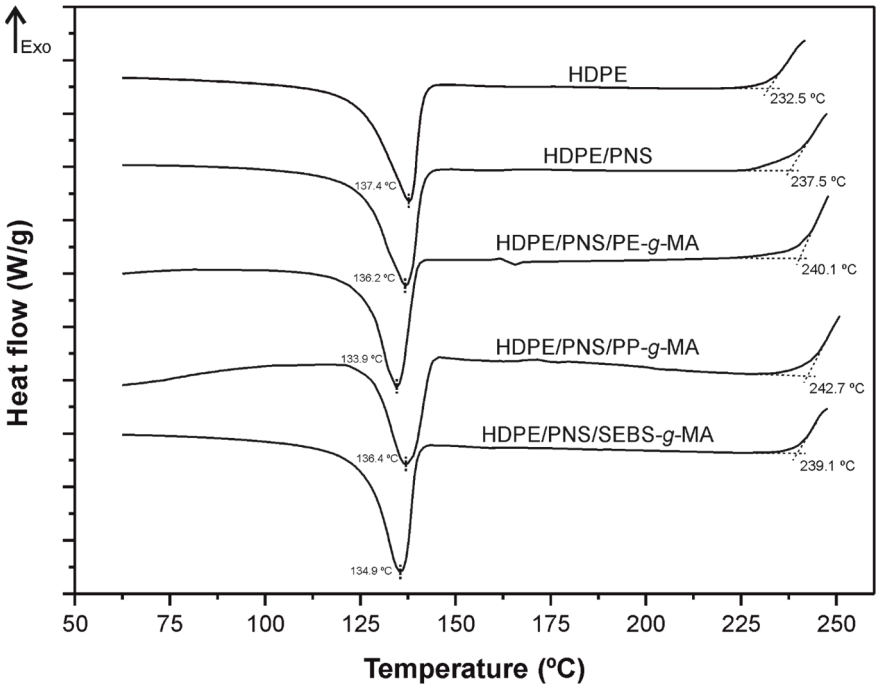

Figure II.2.2. Comparative plot of calorimetric (DSC) curves of neat HDPE and HDPE/PNS composites with different compatibilizer agents.

Degradation at high temperatures (beyond the thermo-oxidation temperature range) was studied by TGA. Figure II.2.3 shows TGA curves of HDPE/PNS composites together with TGA curves for raw materials. As it can be seen in the TGA curve for neat HDPE, no weight loss is detected in the temperature range of the thermo-oxidative process observed by DSC. For this reason, thermo-oxidative process was followed by DSC and degradation at high temperatures with the corresponding weight loss was studied by TGA. As it can be observed, degradation of PNS powder occurs in four different stages. The first one, with a weight loss of about 5%, is located between 50 and 150 °C and corresponds to residual moisture evaporation [27]. The second stage takes place in the 220–350 °C range with a weight loss of 40% which corresponds to decomposition of low molecular weight

components such as hemicelluloses and glycosidic bonds in cellulose. The third stage, characterized by a weight loss of 14%, occurs between 350 and 410 °C and is directly related to thermal decomposition of cellulose. Finally, above 410 °C lignin degradation occurs [5, 37]. It is worth to notice that lignin degradation starts prior to other components but the degradation rate is slower [38]. With regard to raw HDPE, degradation proceeds in a one step process that starts at about 350 °C and ends around 520 °C with a weight loss of almost 99% (very low char generation) [39]. To evaluate the degradation process of HDPE/PNS composites it is important to consider that some processes can be overlapped. HDPE is a highly hydrophobic polymer so that, no weight loss is observed in the temperature range comprised between 50 and 150 °C related to moisture removal and the typical degradation range for hemicelluloses (220–350 °C) is lower than the onset decomposition temperature for HDPE. As it can be observed, HDPE decomposition overlaps with the cellulose and lignin degradation in the 350–520 °C range. Decomposition of HDPE/PNS composites with and without compatibilizers show a combination of the two previously described behaviors. Presence of PNS powder in HDPE/PNS composites leads to a decrease in thermal stability at high temperatures and two different stages can be clearly identified. The first one occurs between 230 and 420 °C and corresponds to degradation of hemicelluloses, cellulose and lignin from PNS powder. Above 420 °C, degradation of HDPE chains occurs [10]. As we have previously observed, PNS powder degradation forms important amounts of char after combustion so that, residual char is also detectable for HDPE/PNS composites. It is also possible to observe that the overall effect of compatibilizers is positive as slightly better thermal stability is obtained compared with uncompatibilized HDPE/PNS. This fact is probably due to particle-matrix interactions as some hydroxyl groups in PNS powder particles (mainly from cellulose and hemicelluloses) are esterified with anhydride groups in the different compatibilizer agents [10].

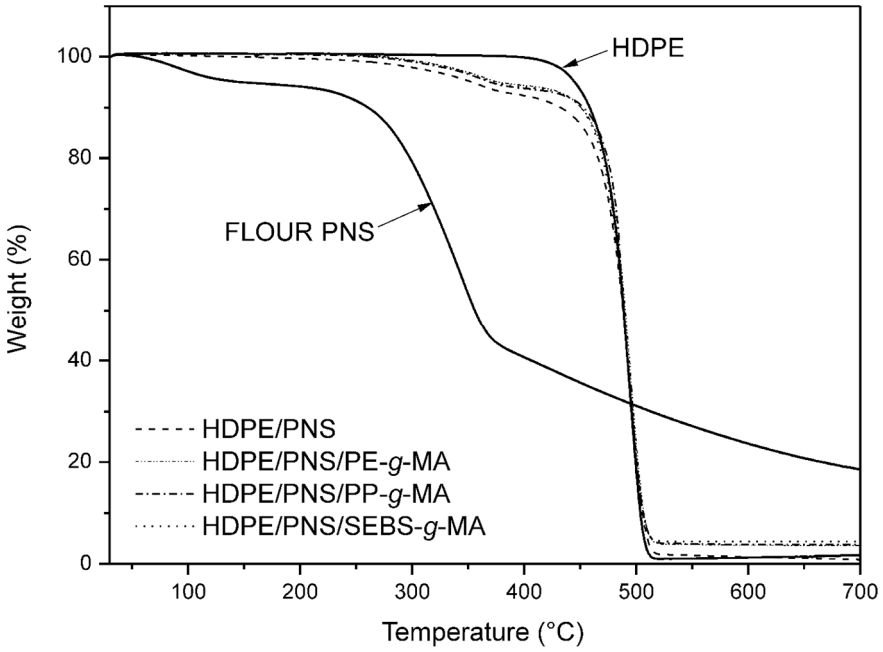

Figure II.2.3. Comparative plot of the thermogravimetric (TGA) curves of neat HDPE, PNS powder and HDPE/PNS composites with different compatibilizer agents.

With the aim of evaluating particle dispersion and particle-matrix interface phenomena, a SEM study on fractured surfaces from impact tests was carried out. Figure II.2.4a shows a rough surface corresponding to fractured surface of HDPE in impact conditions. Figure II.2.4b-e show fractured surfaces from impact tests corresponding to HDPE/PNS composites and quite good particle dispersion can be detected in a rough surface. Addition of highly hydrophilic PNS particles into a highly hydrophobic polyethylene matrix without compatibilizers leads to lack of continuity in HDPE/PNS composites and this is reflected by a remarkable decrease in elongation at break and impact energy. Particle-matrix interactions due to the action of the compatibilizer agents can be observed. In the case of uncompatibilized HDPE/PNS composite (Figure II.2.4b) a small gap between the particle and the surrounding matrix can be distinguished. In the case of HDPE/PNS composites compatibilized with PE-*g*-MA (Figure II.2.4c) and SEBS-*g*-MA (Figure II.2.4e) it is possible to observe persistence of a small gap between the continuous phase (polymer matrix) and the dispersed phase (PNS particles) thus indicating that although some interaction is achieved this is not enough and particle-matrix discontinuity still occurs. That is why cohesion properties such elongation at break and tensile strength are reduced. In these cases, presence of small gaps between particle and matrix confirm that particles act as stress concentrators and this fact leads to fracture with relative small elongation. Nevertheless, HDPE/PNS composites compatibilized with PP-*g*-MA (Figure II.2.4d) offer

better particle-matrix continuity and this has a positive effect on particle-matrix interactions and this is also reflected in better mechanical properties.

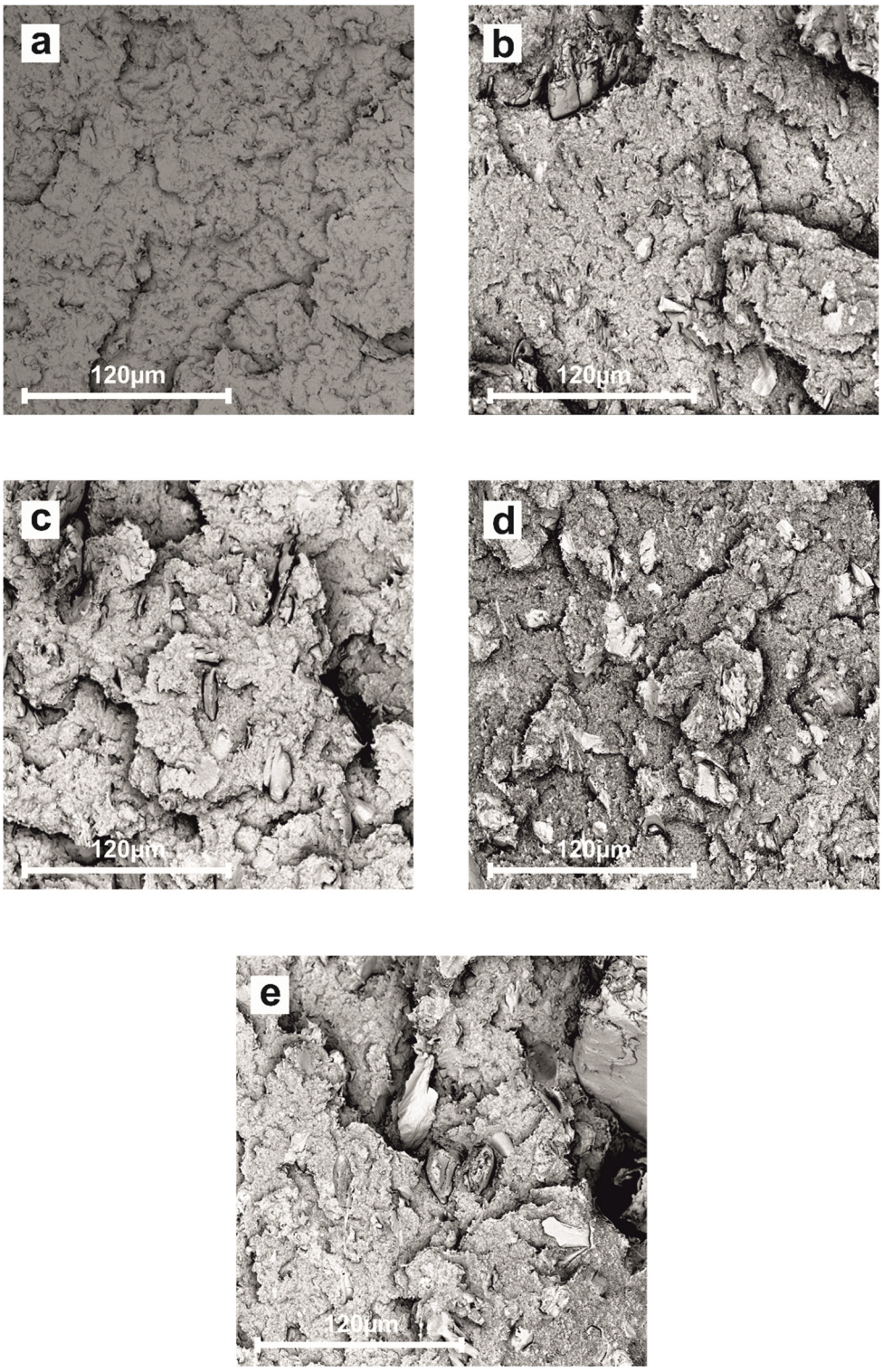

Figure II.2.4. SEM images from fractured surfaces (1000x) of neat HDPE and HDPE/PNS with different compatibilization systems: (a) HDPE; (b) HDPE/PNS; (c) HDPE/PNS/PE-*g*-MA; (d) HDPE/PNS/PP-*g*-MA and (e) HDPE/PNS/SEBS-*g*-MA.

Figure II.2.5 shows the plot evolution of the storage modulus (*G*') for HDPE and HDPE/PNS composites with different compatibilizing systems. As expected, *G*' decreases with temperature due to an increase in chain mobility as temperatures raises up to melt temperature and this is responsible for material softening. Addition of 10 wt% leads to an increase in storage modulus thus indicating a stiffer material; this is due to the fact that PNS particles are stiffer than HDPE polymer chains. In addition, the lack of total continuity leads to low cohesion, which promotes fracture with low deformation levels. If we take into account that a modulus relates the applied stress with the deformation in the elastic region, it is evident that a decrease in deformation leads to higher values for modulus. By comparing the behavior at room temperature as a reference temperature, the storage modulus of PP-*g*-MA compatibilized HDPE/PNS composite (HDPE/PNS/PP-*g*-MA) increases a percentage value of 37% with regard to unfilled HDPE and 26% more than HDPE/PNS composite without compatibilizer.

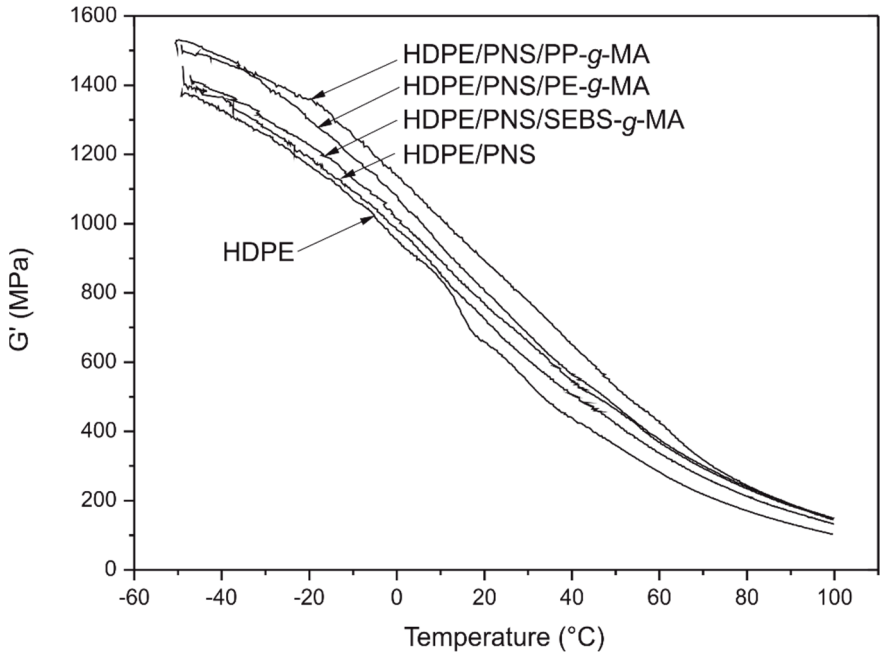

Figure II.2.5. Evolution of the storage modulus (*G*') of HDPE/PNS composites (10 wt% PNS) with and without different compatibilizer agents.

Figure II.2.6 shows the evolution of the water uptake (percentage increase) of HDPE/PNS composites compared with unfilled HDPE for a period of 7 months. As it can be seen, presence of PNS leads to increased water uptake values with regard to the unfilled HDPE with almost no water uptake due to its extremely high hydrophobicity. All HDPE/PNS composites show similar behavior in terms of the water uptake but PE-*g*-MA compatibilized

HDPE/PNS composite (HDPE/PNS/PE-*g*-MA) shows the maximum water uptake in the tested period. Unfilled HDPE shows a water uptake of about 0.04% after 7 months and PE-*g*-MA compatibilized offers a water uptake of about 0.56% for the same period and similar values are obtained for all other compatibilized composites. As described by Klyosov [40] typical values of water uptake for Wood Plastic Composites (WPCs) with 40–60 wt% wood component, are in the 18–22% range. The values obtained for HDPE composites with 10 wt% PNS are remarkably lower. This is due to the relative low content of lignocellulosic filler (only 10 wt%) but these values are interesting.

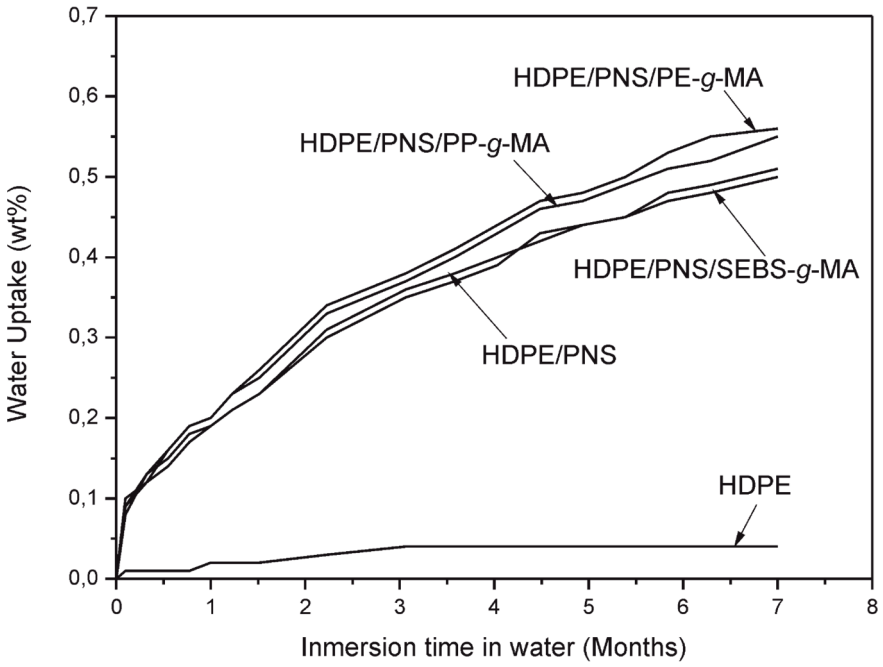

Figure II.2.6. Plot evolution of the water uptake of HDPE/PNS composites (10 wt% PNS) with different compatibilizer agents in terms of the immersion time.

By taking into consideration the overall properties obtained with the different maleic anhydride-based compatibilizers, it is possible to conclude that best compatibilizing properties are obtained with PP-*g*-MA (HDPE/PNS/PP-*g*-MA). Although all three compatibilizers offer similar chemical structure, it seems that the maleic anhydride grafting degree is the main parameter related to compatibilization and governs its effectiveness. As indicated in Table II.2.2, the PP-*g*-MA copolymer is characterized by a maleic anhydride content of 8–10 wt% which is remarkably higher than the values corresponding to PE-*g*-MA and SEBS-*g*-MA (0.5 and 2 wt% respectively).

The effect of PNS flour content of HDPE/PNS/PP-*g*-MA composites

In this section, the effect of the filler content on overall performance of HDPE/PNS/PP-*g*-MA composites is described. Figure II.2.7 shows the plot evolution of mechanical properties (tensile and flexural) of HDPE/PNS/ PP-*g*-MA composites with varying amounts of PNS powder. As we can see, addition of the lignocellulosic filler leads to a slight decrease in tensile strength regarding neat HDPE. The maximum is reached for the composite HDPE/PNS/PP-*g*-MA with 10 wt% PNS with values of about 18.9 MPa. In general, the variability of tensile strength occurs in a very narrow range so that indicating that tensile strength is not practically affected by the filler amount. Variability could be related to typical heterogeneity of polymer-filled materials, so that, maximum and minimum values are not indicative of a tendency. With regard to the Young's modulus it is possible to observe a clear increasing tendency with increasing PNS load. Thus, the modulus of neat HDPE, 373 MPa increases to 632 MPa for the HDPE/PNS/PP-*g*-MA composite containing 30 wt% PNS which represents a percentage increase close to 69%. Nevertheless, as expected, the elongation at break is dramatically reduced after filler addition. As the filler load increases, the elongation at break values change from 520% (unfilled HDPE) up to values of about 0.7% for HDPE/PNS/PP-*g*-MA composites with 30 wt% PNS. This behavior is typical of polymer-filled materials due to the stress concentration phenomena promoted by the presence of dispersed rigid, non-compatible lignocellulosic particles in a highly hydrophobic matrix.

With regard to the flexural properties, a clear increasing tendency in both flexural strength and modulus can be observed. The maximum is obtained for a PNS content of 30 wt%. Flexural strength changes from 23 MPa (unfilled HDPE) up to 28.5 MPa for composites containing 30 wt% PNS which represents a percentage increase of about 24%. In the case of the flexural modulus the initial value for unfilled HDPE, 805 MPa, is increased by 72% up to values of about 1387 MPa. Once again, the results give evidence of the negative effect of particle fillers on cohesive properties of polymer composites.

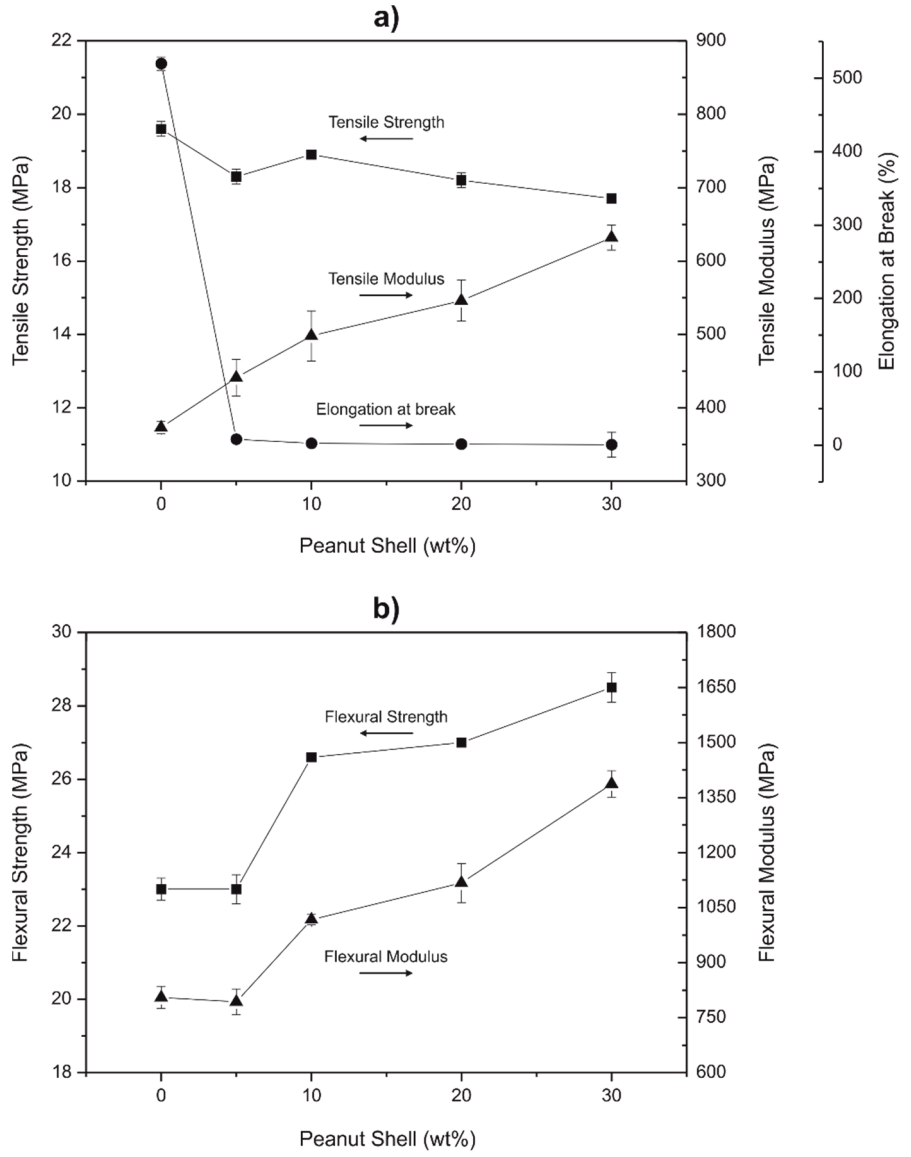

Figure II.2.7. Plot evolution of (a) tensile properties and (b) flexural properties of HDPE/PNS/PP-*g*-MA composites with different filler loads.

In addition to tensile and flexural properties, Shore D hardness and impact-absorbed energy (Charpy test) were determined for HDPE/PNS/PP-*g*-MA composites with different PNS powder content (Figure II.2.8). As expected, the impact-absorbed energy decreases with the filler content with a minimum value (1 kJ m^{-2}) for the composite with the highest filler content (30 wt%) which is remarkably lower to the value for unfilled HDPE (2.75 kJ m^{-2}). As previously indicated, impact energy is directly related to the ability of the material to absorb energy during deformation and fracture; nevertheless, as the deformation capacity of HDPE/PNS/PP-*g*-MA composites is dramatically restricted, then the impact energy is identically reduced. With regard to Shore D hardness, it follows similar tendency to that observed for other mechanical resistant properties. It increases up to 10%

higher values for HDPE/PNS/PP-*g*-MA composite with 30 wt% PNS with regard to the unfilled HDPE. In general, the evolution of these two parameters is in total accordance with previous tensile and flexural properties. As the impact-absorbed energy is related to the deformation ability, it follows similar tendency as observed for elongation at break and typical mechanical ductile properties. On the other hand, Shore D hardness is representative for a mechanical resistance property so that, it follows similar tendency as those observed for both tensile and flexural modulus.

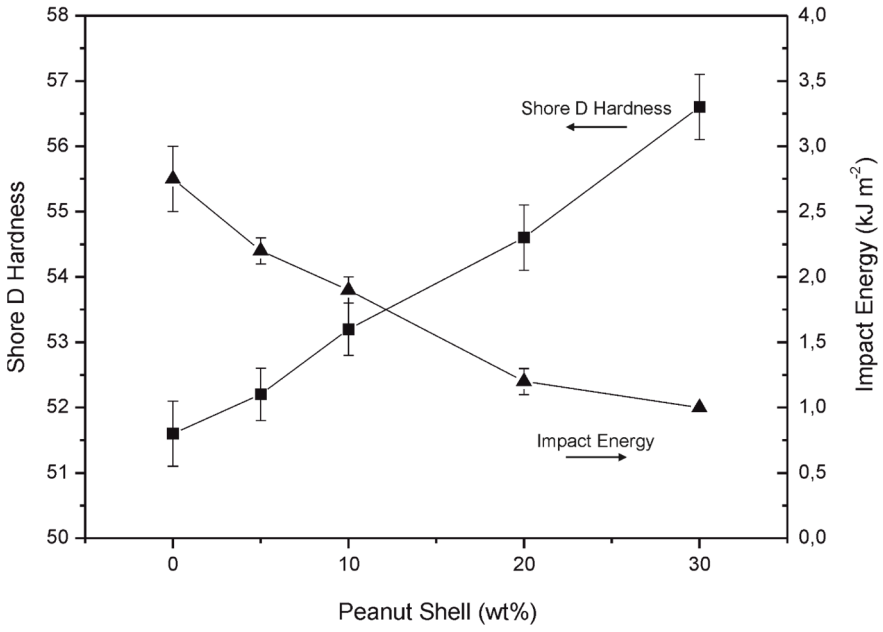

Figure II.2.8. Plot evolution of Shore D hardness and impact energy (Charpy test) for HDPE/PNS/PP-*g*-MA composites in terms of the PNS powder content.

The effect of the filler content on melting and thermo-oxidative degradation at moderate temperatures of HDPE/PNS/PP-*g*-MA composites was followed by DSC. Figure II.2.9 shows the plot evolution of melt peak temperatures and thermo-oxidative degradation onset values for HDPE/PNS/PP-*g*-MA composites containing different amounts of PNS powder, obtained by DSC. The melt temperature is slightly lower as the filler content increases changing from 137.4 °C (unfilled HDPE) up to 133.0 °C (HDPE/PNS/PP-*g*-MA composite with 30 wt% PNS). This slight change is related to a slight change in the peak shape but the overall variations in the main parameters related to the melt process are not significant. With regard to the degradation onset temperature at moderate temperatures (thermo-oxidative degradation) we observe a clear increase from 232.5 °C (unfilled HDPE) up to 256.6 °C (HDPE/PNS/PP-*g*-MA composite with 30 wt% PNS). This additional

functionality is related to the antioxidant capacity of some components in the lignocellulosic waste, which act as free-radical scavengers thus leading to improved thermal stability at moderate temperatures.

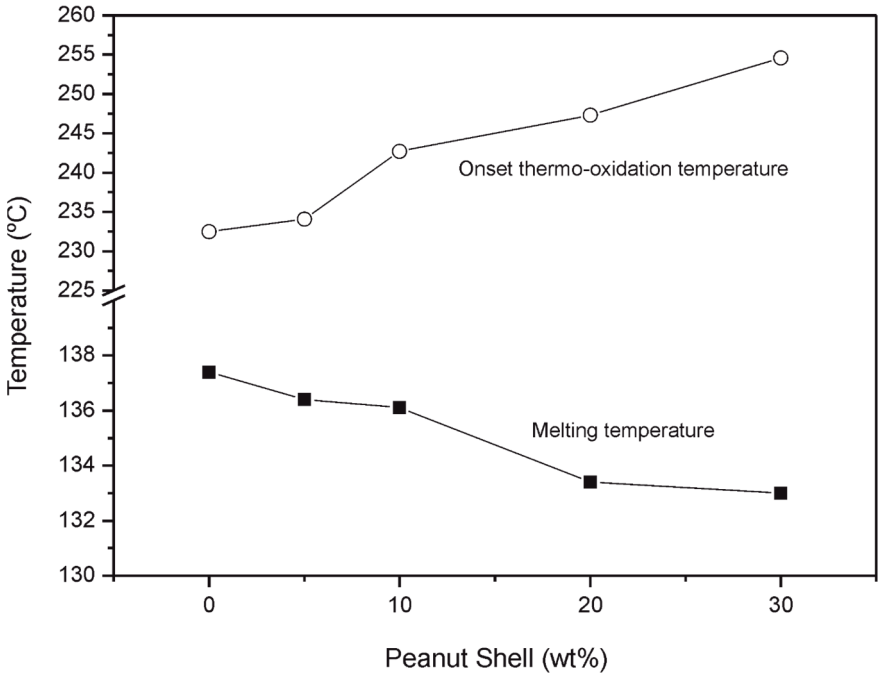

Figure II.2.9. Plot evolution of the thermal properties (melt peak and thermo-oxidation onset temperatures) for HDPE/PNS/PP-*g*-MA composites with different PNS powder content obtained by DSC.

Degradation/decomposition at high temperatures was followed by TGA by measuring the weight loss in function of increasing temperature. TGA curves, as well as the main parameters of the degradation/decomposition process of neat HDPE and HDPE/PNS/PP-*g*-MA composites, are gathered in Figure II.2.10 and Table II.2.4 respectively. Degradation at high temperatures occurs in two main stages as described previously for composites containing 10 wt% PNS. The addition of PNS powder leads to a decrease in thermal stability of HDPE. This decrease is much higher as the PNS content increases. As it can be seen in Table II.2.4, the onset degradation temperature (T_0) diminishes from 430 °C (neat HDPE) up to values of 287.3 °C for a HDPE/PNS/PP-*g*-MA composite with 30 wt% PNS which represents a percentage decrease of almost 33%. This decrease corresponds to the degradation start of the lignocellulosic component [41]. With regard to the temperature corresponding to the first degradation stage ($T_{\max\ 1st}$), it follows similar tendency so that, as the PNS content increases, a slight decrease in this characteristic

temperature can be distinguished. Regarding the characteristic degradation temperature of the second stage ($T_{max\ 2nd}$), it does not change in a remarkable way with values around 490 °C for all compositions. In Figure II.2.10 it is possible to observe that as the filler load increases, the step corresponding to PNS degradation increases proportionally and also the residual char increases with PNS content.

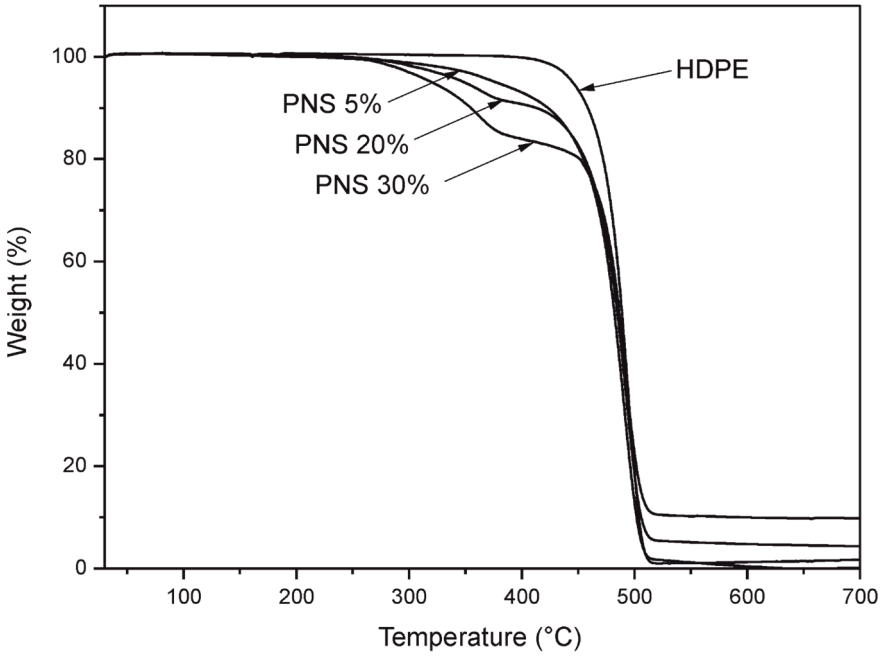

Figure II.2.10. Thermogravimetric curves (TGA) of HDPE/PNS/PP-*g*-MA composites with different PNS powder content.

Table II.2.4. Thermal degradation parameters of HDPE/PNS/PP-*g*-MA composites with different PNS powder content obtained by TGA.

wt% PNS	T_0[a] **(°C)**	$T_{max\ 1st}$ **(°C)**	$T_{max\ 2nd}$ **(°C)**
0 (HDPE)	430	-	495.3
5	327.3	-	490.3
10	325.3	364.3	490.3
20	305.0	363.0	491.0
30	287.3	360.6	490.6

[a] T_0, calculated at 5% mass loss.

The morphology of fractured surface from impact tests of HDPE/PNS/PP-*g*-MA composites with different PNS loading was studied by SEM analysis in order to evaluate the dispersion level and filler-matrix interactions (Figure II.2.11). Figure II.2.11a corresponds to fracture of unfilled HDPE and it is characterized by a rough surface. As the filler loading increases, a rough surface with dispersed particles embedded in the matrix (Figure II.2.11b-h) can be distinguished. In general, it can be observed quite good particle dispersion together with some particle-matrix interactions as the gaps between the particles and the surrounding matrix are small. Nevertheless, the increasing amount of filler leads to a remarkable decrease in ductile properties as evidenced by the evolution of elongation at break and impact energy.

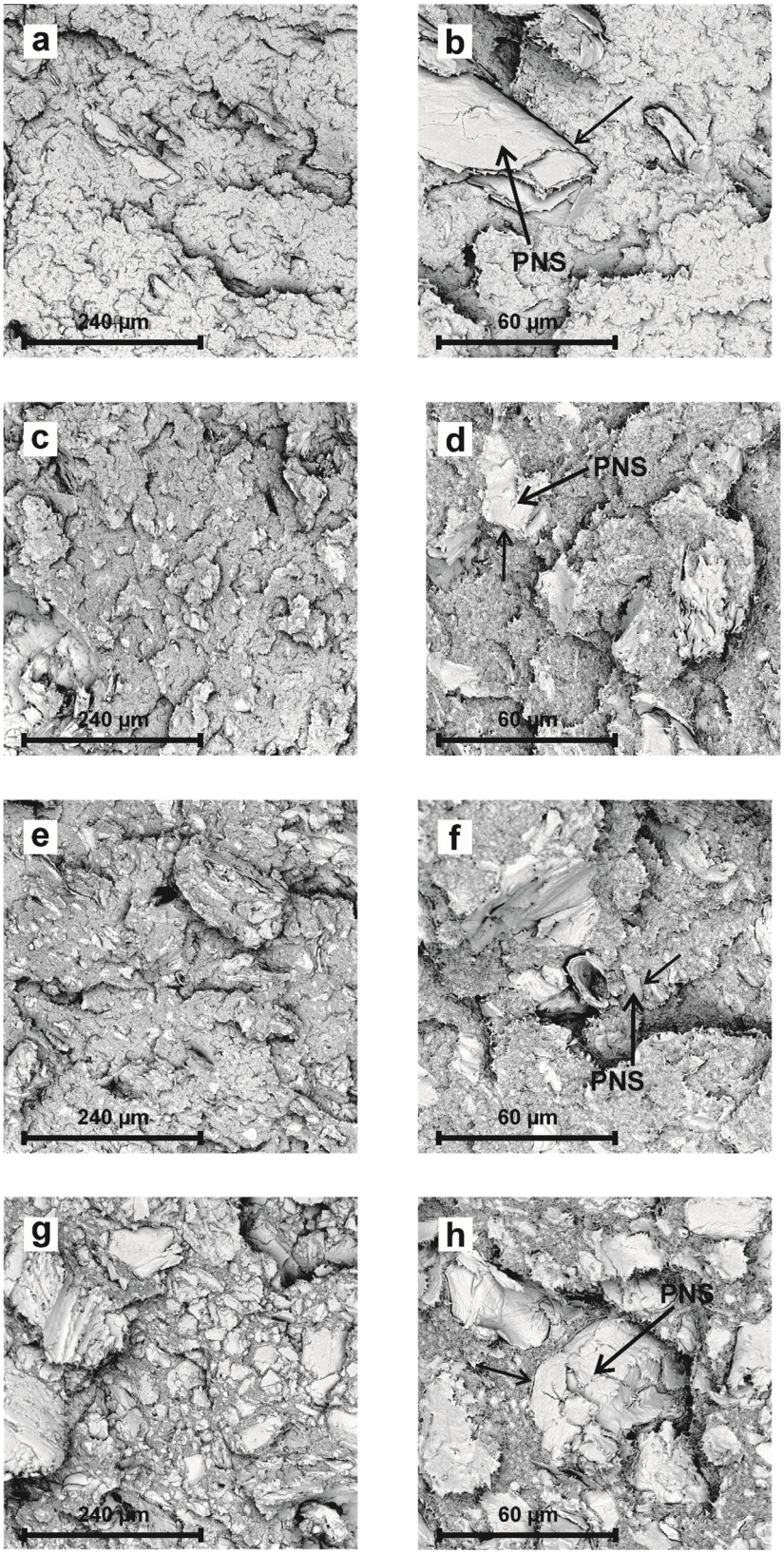

Figure II.2.11. SEM images of fractured surfaces of HDPE/PNS/PP-*g*-MA composites with different PNS powder: (a) 5 wt% (500x); (b) 5 wt% (2000x); (c) 10 wt% (500x); (d) 10 wt% (2000x); (e) 20 wt% (500x); (f) 20 wt% (2000x); (g) 30 wt% (500x) and (h) 30 wt% (2000x).

The effect of the filler content was also tested by DMTA in torsion mode. Figure II.2.12 shows a comparative plot of the storage modulus (*G*') of HDPE/PNS/PP-*g*-MA composites with varying filler content in terms of temperature. As we have described previously with regard to flexural and tensile properties a clear increase in the corresponding modulus occurs with increasing filler content. This fact is also observed with the evolution of the storage modulus with temperature for all HDPE/PNS/PP-*g*-MA composites. As the filler load increases, the ability to deform is restricted due to the stress concentration effect provided by the dispersed particles. If we compare the storage modulus values at room temperature, HDPE/PNS/PP-*g*-MA containing 30 wt% offers *G*' values 92% higher than unfilled HDPE. It is also important to remark that high differences in storage modulus are detected at room temperature but the difference gets lower as temperature increases.

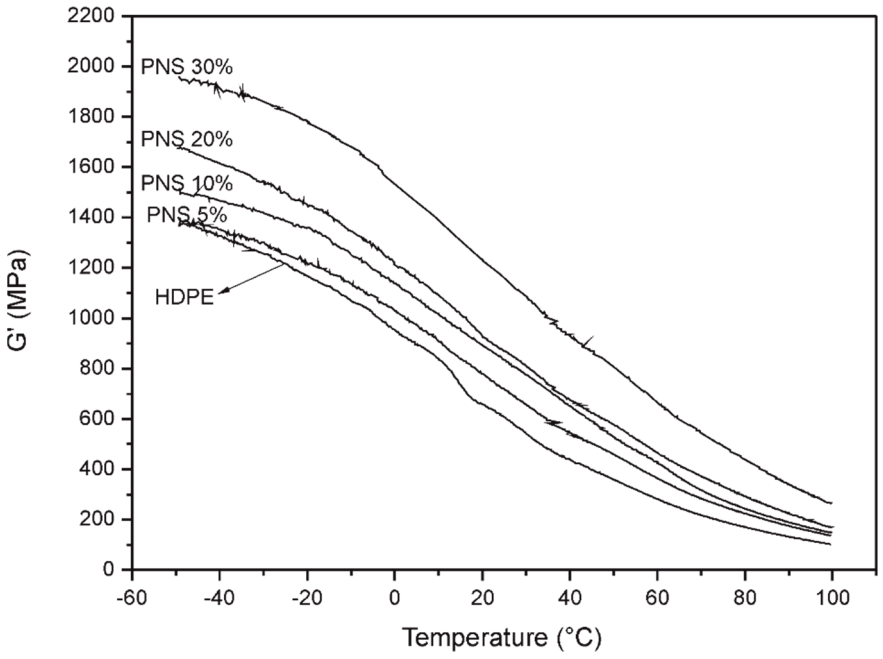

Figure II.2.12. Evolution of the storage modulus (*G*') of HDPE/PNS/PP-*g*-MA composites with different weight percentages of PNS powder.

CONCLUSIONS

The main aim of this work was to evaluate the influence of three different maleic anhydride copolymers as compatibilizers for HDPE/PNS composites, namely: polyethylene-*graft*-maleic anhydride (PE-*g*-MA), polypropylene-*graft*-maleic anhydride (PP-*g*-MA) and polystyrene-*block*-poly(ethylene-*ran*-butylene)-*block*-polystyrene-*graft*-maleic anhydride

(SEBS-*g*-MA). Although all three compatibilizers have maleic anhydride functionality, the best results were obtained with PP-*g*-MA with a percentage increase in tensile and flexural modulus of about 16 and 26% respectively with regard to unfilled HDPE. SEM analysis revealed absence of matrix-particle interaction in uncompatibilized HDPE/PNS composites. Despite this, all three compatibilizers offer some matrix-particle interactions as evidenced by a reduction of the gap size between the dispersed particles and the surrounding polymer matrix.

The addition of 30 wt% PNS led to composite materials with interesting properties from different points of view. In a first approach, flexural strength and modulus increased by 24 and 72% respectively, but the most interesting property was a remarkable increase in the thermo-oxidative degradation onset temperature which changed from 232 °C (unfilled HDPE) up to 256 °C in composites with 30 wt% PNS. This additional feature was due to the natural intrinsic antioxidant components in PNS (polyphenols and flavonoids) which act as free-radical scavengers thus delaying thermo-oxidative processes.

As a general conclusion it is possible to say that manufacturing of natural fiber reinforced plastics (NFRP) with biobased polyethylene and PNS powder, a by-product of the peanut industry, can be obtained by extrusion-compounding followed by injection molding. These composites offer a clearly positive environmental efficiency together with balanced overall properties.

ACKNOWLEDGEMENTS

This research was supported by the Ministry of Economy and Competitiveness (MINECO) [MAT2014-59242-C2-1-R]. The authors also thank the Conselleria d'Educació, Cultura i Esport – Generalitat Valenciana for financial support [GV/2014/008]. A. Carbonell-Verdu wants to thank Universitat Politècnica de València for financial support through an FPI grant. D. Garcia-Garcia wants to thanks the Spanish Ministry of Education, Culture and Sports for the financial support through an FPU grant [FPU13/06011].

REFERENCES

[1] Zini E and Scandola M. *Green Composites: An Overview*. Polymer Composites, 2011. **32**(12):1905-1915.

[2] Koutsomitopoulou AF, Bénézet JC, Bergeret A and Papanicolaou GC. *Preparation and characterization of olive pit powder as a filler to PLA-matrix bio-composites*. Powder Technology, 2014. **255**:10-16.

[3] Ashori A. *Wood-plastic composites as promising green-composites for automotive industries*!. Bioresource Technology, 2008. **99**(11):4661-4667.

[4] García-García D, Carbonell A, Samper MD, García-Sanoguera D and Balart R. *Green composites based on polypropylene matrix and hydrophobized spend coffee ground (SCG) powder*. Composites Part B: Engineering, 2015. **78**:256-265.

[5] Essabir H, Nekhlaoui S, Malha M, Bensalah MO, Arrakhiz FZ, Qaiss A and Bouhfid R. *Bio-composites based on polypropylene reinforced with almond shells particles: Mechanical and thermal properties*. Materials & Design, 2013. **51**:225-230.

[6] Mohanty AK, Misra M and Drzal LT. *Sustainable bio-composites from renewable resources: Opportunities and challenges in the green materials world*. Journal of Polymers and the Environment, 2002. **10**(1-2):19-26.

[7] Mohanty AK, Misra M and Hinrichsen G. *Biofibres, biodegradable polymers and biocomposites: An overview*. Macromolecular Materials and Engineering, 2000. **276**(1):1-24.

[8] Shah DU. *Developing plant fibre composites for structural applications by optimising composite parameters: A critical review*. Journal of Materials Science, 2013. **48**(18):6083-6107.

[9] Balart JF, Fombuena V, Fenollar O, Boronat T and Sánchez-Nacher L. *Processing and characterization of high environmental efficiency composites based on PLA and hazelnut shell flour (HSF) with biobased plasticizers derived from epoxidized linseed oil (ELO)*. Composites Part B: Engineering, 2016. **86**:168-177.

[10] Kim HS, Kim S, Kim HJ and Yang HS. *Thermal properties of bio-flour-filled polyolefin composites with different compatibilizing agent type and content*. Thermochimica Acta, 2006. **451**(1-2):181-188.

[11] Poletto M, Zattera AJ and Santana RMC. *Effect of natural oils on the thermal stability and degradation kinetics of recycled polypropylene wood flour composites*. Polymer Composites, 2014. **35**(10):1935-1942.

[12] Salleh FM, Hassan A, Yahya R, Lafia-Araga RA, Azzahari AD and Nazir MNZM. *Improvement in the mechanical performance and interfacial behavior of kenaf fiber reinforced high density polyethylene composites by the addition of maleic anhydride grafted high density polyethylene*. Journal of Polymer Research, 2014. **21**(5):439.

[13] Ayrilmis N and Kaymakci A. *Fast growing biomass as reinforcing filler in thermoplastic composites: Paulownia elongata wood*. Industrial Crops and Products, 2013. **43**:457-464.

[14] Sailaja RRN, Girija BG, Madras G and Balasubramanian N. *Effect of compatibilization on mechanical and thermal properties of polypropylene – Soy flour composites*. Journal of Materials Science, 2008. **43**(1):64-74.

[15] Etaati A, Pather S, Fang Z and Wang H. *The study of fibre/matrix bond strength in short hemp polypropylene composites from dynamic mechanical analysis*. Composites Part B: Engineering, 2014. **62**:19-28.

[16] Petchwattana N, Covavisaruch S and Chanakul S. *Mechanical properties, thermal degradation and natural weathering of high density polyethylene/rice hull composites compatibilized with maleic anhydride grafted polyethylene*. Journal of Polymer Research, 2012. **19**(7):9921.

[17] Hassanabadi HM, Alemdar A and Rodrigue D. *Polypropylene reinforced with nanocrystalline cellulose: Coupling agent optimization*. Journal of Applied Polymer Science, 2015. **132**(34):42438.

[18] Dányádi L, Móczó J and Pukánszky B. *Effect of various surface modifications of wood flour on the properties of PP/wood composites*. Composites Part A: Applied Science and Manufacturing, 2010. **41**(2):199-206.

[19] Wilson K, Yang H, Seo CW and Marshall WE. *Select metal adsorption by activated carbon made from peanut shells*. Bioresource Technology, 2006. **97**(18):2266-2270.

[20] Bilir MH, Sakalar N, Acemioglu B, Baran E and Alma MH. *Sorption of remazol brilliant blue R onto polyurethane-type foam prepared from peanut shell*. Journal of Applied Polymer Science, 2013. **127**(6):4340-4351.

[21] Rivilli PL, Alarcón R, Isasmendi GL and Pérez JD. *Stepwise isothermal fast pyrolysis (SIFP). Part II. SIFP of peanut shells – Antifungal properties of phenolic fractions*. BioResources, 2012. **7**(1):112-117.

[22] Sareena C, Ramesan MT and Purushothaman E. *Utilization of peanut shell powder as a novel filler in natural rubber*. Journal of Applied Polymer Science, 2012. **125**(3):2322-2334.

[23] Wu CS. *Utilization of peanut husks as a filler in aliphatic-aromatic polyesters: Preparation, characterization, and biodegradability*. Polymer Degradation and Stability, 2012. **97**(11):2388-2395.

[24] Salasinska K and Ryszkowska J. *Dimensional stability, physical, mechanical and thermal properties of high density polyethylene with peanut hulls composites*. Polimery, 2013. **58**(6):461-466.

[25] Zaaba NF, Ismail H and Jaafar M. *The effects of modifying peanut shell powder with polyvinyl alcohol on the properties of recycled polypropylene and peanut shell powder composites*. BioResources, 2014. **9**(2):2128-2142.

[26] Prabhakar MN, Shah AUR, Rao KC and Song JI. *Mechanical and thermal properties of epoxy composites reinforced with waste peanut shell powder as a bio-filler*. Fibers and Polymers, 2015. **16**(5):1119-1124.

[27] Batalla L, Nunez AJ and Marcovich NE. *Particleboards from peanut-shell flour*. Journal of Applied Polymer Science, 2005. **97**(3):916-923.

[28] Sareena C, Ramesan MT and Purushothaman E. *Transport studies of peanut shell powder reinforced natural rubber composites in aromatic solvents*. Polymer Composites, 2012. **33**(10):1678-1692.

[29] Adhikary KB, Pang S and Staiger MP. *Dimensional stability and mechanical behaviour of wood-plastic composites based on recycled and virgin high-density polyethylene (HDPE)*. Composites Part B: Engineering, 2008. **39**(5):807-815.

[30] Migneault S, Koubaa A, Perré P and Riedl B. *Effects of wood fiber surface chemistry on strength of wood-plastic composites*. Applied Surface Science, 2015. **343**:11-18.

[31] Chang FC, Kadla JF and Lam F. *The effects of wood flour content and coupling agent on the dynamic mechanical and relaxation properties of wood-plastic composites*. European Journal of Wood and Wood Products, 2016. **74**(1):23-30.

[32] Ferrero B, Fombuena V, Fenollar O, Boronat T and Balart R. *Development of natural fiber-reinforced plastics (NFRP) based on biobased polyethylene and waste fibers from Posidonia oceanica seaweed*. Polymer Composites, 2015. **36**(8):1378-1385.

[33] Sabetzadeh M, Bagheri R and Masoomi M. *Study on ternary low density polyethylene/linear low density polyethylene/thermoplastic starch blend films*. Carbohydrate Polymers, 2015. **119**:126-133.

[34] Liu H, Wu Q and Zhang Q. *Preparation and properties of banana fiber-reinforced composites based on high density polyethylene (HDPE)/Nylon-6 blends*. Bioresource Technology, 2009. **100**(23):6088-6097.

[35] Farsi M. *Some of the mechanical and thermal properties of wheat straw filled-PP composites*. Fibers and Polymers, 2012. **13**(4):515-521.

[36] Sewda K and Maiti SN. *Mechanical properties of teak wood flour-reinforced HDPE composites*. Journal of Applied Polymer Science, 2009. **112**(3):1826-1834.

[37] Lee SH and Wang S. *Biodegradable polymers/bamboo fiber biocomposite with bio-based coupling agent*. Composites Part A: Applied Science and Manufacturing, 2006. **37**(1):80-91.

[38] Bledzki AK, Mamun AA and Volk J. *Physical, chemical and surface properties of wheat husk, rye husk and soft wood and their polypropylene composites*. Composites Part A: Applied Science and Manufacturing, 2010. **41**(4):480-488.

[39] Ou R, Xie Y, Wang Q, Sui S and Wolcott MP. *Thermal, crystallization, and dynamic rheological behavior of wood particle/HDPE composites: Effect of removal of wood cell wall composition*. Journal of Applied Polymer Science, 2014. **131**(11):40331.

[40] Klyosov AA. *Wood-Plastic Composites*. 2007, New Jersey: John Wiley & Sons.

[41] Petinakis E, Liu X, Yu L, Way C, Sangwan P, Dean K, Bateman S and Edward G. *Biodegradation and thermal decomposition of poly(lactic acid)-based materials reinforced by hydrophilic fillers*. Polymer Degradation and Stability, 2010. **95**(9):1704-1707.

Journal of Applied Polymer Science

Development and characterization of green composites from bio-based polyethylene and peanut shell

Daniel Garcia-Garcia,[1] Alfredo Carbonell-Verdu,[1] Amparo Jordá-Vilaplana,[2] Rafael Balart,[1] David Garcia-Sanoguera[1]

[1]Instituto De Tecnología De Materiales (ITM), Universitat Politècnica De València (UPV), Plaza Ferrandiz Y Carbonell 1, 03801, Alcoy, Alicante, Spain

[2]Departamento De Ingeniería Gráfica, Universitat Politècnica De València (UPV), Plaza Ferrandiz Y Carbonell 1, 03801, Alcoy, Alicante, Spain

Correspondence to: D. Garcia-Garcia (E-mail: dagarga4@epsa.upv.es)

ABSTRACT: In the present work, different compatibilizers, namely polyethylene-*graft*-maleic anhydride (PE-*g*-MA), polypropylene-*graft*-maleic anhydride (PP-*g*-MA), and polystyrene-*block*-poly(ethylene-*ran*-butylene)-block-polystyrene-*graft*-maleic anhydride (SEBS-*g*-MA) were used on green composites derived from biobased polyethylene and peanut shell (PNS) flour to improve particle–polymer interaction. Composites of high-density polyethylene/peanut shell powder (HDPE/PNS) with 10 wt % PNS flour were compatibilized with 3 wt % of the abovementioned compatibilizers. As per the results, PP-*g*-MA copolymer lead to best optimized properties as evidenced by mechanical characterization. In addition, best particle–matrix interface interactions with PP-*g*-MA were observed by scanning electron microscopy (SEM). Subsequently HDPE/PNS composites with varying PNS flour content in the 5–30 wt % range with PP-*g*-MA compatibilizer were obtained by melt extrusion and compounding followed by injection molding and were characterized by mechanical, thermal, and morphological techniques. The results showed that PNS powder, leads to an increase in mechanical resistant properties (mainly, flexural modulus, and strength) while a decrease in mechanical ductile properties, that is, elongation at break and impact absorbed energy is observed with increasing PNS flour content. Furthermore, PNS flour provides an increase in thermal stability due to the natural antioxidant properties of PNS. In particular, composites containing 30 wt % PNS powder present a flexural strength 24% and a flexural modulus 72% higher than the unfilled polyethylene and the thermo-oxidative onset degradation temperature is increased from 232 °C up to 254 °C thus indicating a marked thermal stabilization effect. Resultant composites can show a great deal of potential as base materials for wood plastic composites. © 2016 Wiley Periodicals, Inc. J. Appl. Polym. Sci. **2016**, *133*, 43940.

KEYWORDS: biopolymers and renewable polymers; compatibilization; composites; mechanical properties

Received 10 December 2015; accepted 19 May 2016

DOI: 10.1002/app.43940

INTRODUCTION

In recent years, increased awareness on environmental issues has been detected. This fact, together with the problems related to petroleum depletion has led to a breakthrough in the field of environmentally friendly materials development; much of this progress has been observed in the field of polymer composites, mainly on natural fiber reinforced plastics (NFRP) and wood plastic composites (WPC) for everyday applications.[1–4] The use of natural fillers into a polymeric matrix provides attracting advantages such as reduced costs, lightness, excellent balanced mechanical properties, etc., together with a marked low environmental impact.[5] Moreover, due to their aesthetic appearance (wood or natural product like) and the advantageous position against wood (low maintenance, high dimensional stability in wet conditions, and high resistance to biological attack), NFRPs and WPCs are increasingly used in sectors such as decoration, construction, and automotive.[3,6–9]

The main disadvantages of using natural fillers in a polymeric matrix is the relatively poor dispersion of the filler in the matrix and the low polymer–particle compatibility which leads to poor interface phenomena thus giving poor final properties. The highly hydrophobic polymeric matrix is not compatible with the highly hydrophilic filler (ligno-cellulosic material) which gives poor adhesion among matrix–filler interface and this is responsible for a decrease in mechanical and thermal performance of composites.[10–12] One of the methods used to enhance filler dispersion and polymer–filler adhesion/interaction is the use of compatibilizer agents such as maleic anhydride-grafted polypropylene (PP-*g*-MA) or maleic anhydride-grafted polyethylene (PE-*g*-MA).[5,10,12–17] These compatibilizers act as a bridge

II.3

“Manufacturing and characterization of composite fiberboards with Posidonia oceanica wastes with an environmentally-friendly binder from epoxy resin”

Daniel García García[a], *Luis Quiles Carrillo*[a], *Néstor Montañés*[a], *Vicent Fombuena*[a], *Rafael Balart*[a]

[a] Instituto de Tecnología de Materiales (ITM)
Universitat Politècnica de València (UPV)
Plaza Ferrándiz y Carbonell 1, 03801 Alcoy, Alicante, Spain.

Materials

2017, 11:35

Manufacturing and characterization of composite fiberboards with Posidonia oceanica wastes with an environmentally-friendly binder from epoxy resin

Abstract

Highly environmentally-friendly fiberboards were manufactured by hot-press molding using *Posidonia oceanica* wastes and a partially biobased epoxy resin as binder. Fiberboards with a constant fiber content of 70 wt% were successfully manufactured by thermo-compression. The effects of a conventional alkali treatment were compared to the synergistic effects that additional silanization with two silanes (amino and glycidyl) can exert on the mechanical and thermo-mechanical properties of fiberboards. The results revealed a remarkable improvement of the mechanical properties with the combination of the alkali treatment followed by the silanization. Scanning electron microscopy also revealed increased resin-fiber interactions due to the synergistic effect of both amino- and glycidyl-silanes. These fiberboards represent a formaldehyde-free solution and can positively contribute to sustainable development as the lignocellulosic component is a waste and the binder resin is partially biobased.

Keywords: Biobased epoxy; fiberboards; waste management; Posidonia oceanica; hot-press manufacturing; coupling agents.

INTRODUCTION

Nowadays most developed countries are paying special attention to environmental issues. Some of the most important actions to protect the environment are focused on the optimum use of natural resources, the reduction of polluting gas emissions, upgrading industrial and/or agroforestry wastes, etc.; all this with the main aim of reducing the carbon footprint and positively contributing to sustainable development based on a circular economy concept. Fossil fuels are widely used as the main source for many applications, including the polymer and composites industries. Petroleum depletion is also acting as the leading force to the development of a new series of environmentally-friendly materials from renewable resources. This environmental sensitivity is particularly marked in the polymer and polymer-composite industries, which, traditionally, are highly dependent on petroleum-derived polymers and resins. With regard to thermosetting resins, petroleum-derived epoxies, unsaturated polyesters, vinyl esters, phenolics, acrylics, etc., still represent the main source of industrial resins for uses in the composites industry and for the manufacturing of fiber and particleboards.

Particle and fiberboards are widely used in the building industry as eco-friendly solutions to wood with increasing uses in thermal insulators, ceiling boards, wall partitions, etc., due to an excellent combination of mechanical, thermal and acoustic properties together with a competitive price. Particle and fiberboards consist of a major lignocellulosic component bonded with a resin, typically, phenol-formaldehyde (PF), urea-formaldehyde (UF), melamine-urea-formaldehyde (MUF) [1], by hot press molding [2]. Despite wood being one of the most relevant lignocellulosic components in particle/fiberboards [3], new lignocellulosic particles and fibers (mainly by-products from other industries) have been successfully introduced into these boards, *i.e.*, corncob, sawdust [2], date palm branches [4], sorghum stalk fibers [5], almond shell and rice husk [6], etc. As reported by Vaisanen *et al.* [7] natural fiber polymer composites (NFPCs) represent a technical and economical solution to upgrading agricultural and forest wastes.

With regard to the binder, some recycled thermoplastics have been proposed as binders in wood plastic composites and particleboards [8]. The current tendency is to avoid formaldehyde as it is considered a great pollutant [1], so that new formaldehyde-free binders are continuously being investigated. Most of them are derived from tannins [9, 10], lignin [11, 12], soy protein [13-15], etc. Although most of the commercial epoxies come from petroleum, in the last years, new environmentally-friendly epoxies from vegetable oils have been proposed as eco-friendly adhesives and composite matrices [16-18]. Obradovic *et al.* [19] reported the potential of acrylated epoxidized soybean oil (AESO) in producing

industrial foams with cellulose reinforcements. Even more, Arevalo *et al.* [20] have proposed the use of the self-binding capability of cellulose to obtain binderless fiberboards by hot-pressing. Kojima *et al.* [21] also explored the potential binding effects of lignocellulose nanofibers (LCNF) with wood flour to give composite boards with interesting properties.

Posidonia oceanica (PO) is an endemic seagrass of the Mediterranean Sea. It plays a key role in coast preservation, as it is present on seabeds and positively contributes to the delay or minimization of erosion effects. After strong storms, the whole plants or parts (stems, leaves) are torn off the seabed and move towards the shore. Consequently, huge amounts of this waste accumulates along many coastal beaches thus leading to an important visual impact together with intense odors due to decomposition. The coastal municipalities must periodically remove this waste to obtain the appropriate quality seals, such as the blue flag and others, which play a key role in attracting tourism. Over the last years, new uses for this waste has been proposed. Some authors have reported the potential of PO in the filtration and removal of different pollutants [22-27]. Due to its high cellulose content, some authors have focused their research on obtaining cellulose derivatives such as nanofibrillar cellulose, nanocrystals, cellulose acetate, glycidyl methacrylate grafted cellulose, etc., and their potential as reinforcements in different matrices [28-34]. It is worth mentioning the work of Cocozza *et al.* [35] which reports the alternative use of PO wastes as a compost material or for energy recovery. PO wastes have been used as a reinforcement into several polymer matrices such as polyethylene [36, 37], polyhydroxyalkanoates (PHAs) [38], processed by extrusion with PO contents up to 40 wt%. With regard to the use of PO in particleboards, Maciá *et al.* [39] have recently reported the partial substitution of pinewood by PO in particleboards with polyurethane binders with interesting applications in the building industry. Our previous work with PO showed the technical viability of fiberboards containing gluten as a biobased binder in the 10–40 wt% range, processed by hot press molding, but the impact toughness was poor [40].

This work is focused on the development of fiberboards with PO fibers using a partially biobased epoxy as the binder resin. With the aim of enhancing the impact toughness, different surface treatments on PO fibers are assessed.

EXPERIMENTAL

Materials

Posidonia oceanica (PO) balls (Figure II.3.1) were collected from the Mediterranean coast. These balls were ground to a fiber size comprised between 2 and 8 mm length. Sodium hydroxide (99%) was supplied in flake form by Cofarcas S.A. (Burgos, Spain). Two different coupling agents, namely (3-aminopropyl) trimethoxysilane (APTMS) and (3-glycidoxypropyl) trimethoxysilane (GLYMO) were used to improve fiber-matrix interactions. Both coupling agents were supplied by Sigma Aldrich Spain (Madrid, Spain) and were selected because of both amine and glycidyl functionalities can readily react with the epoxy resin and hardener during the crosslinking process. On the other hand, the hydrolyzed alkoxy groups can react with hydroxyl groups in cellulose fiber thus leading to a coupling phenomenon between the fiber and the epoxy matrix. Figure II.3.2 shows the chemical structure of both silanes. As binder, a partially biobased epoxy resin was supplied by Resineco under the tradename Greenpoxy 55 with its corresponding hardener GP 505. The recommended resin:hardener was 100:40 (by weight) or 2:1 (by volume). This partially biobased epoxy has a renewable content of at least 55 wt% (55 wt% of carbon comes from plant, vegetables and/or oils) and possesses a density of 1.15 g cm^{-3}, it is not soluble in water and its viscosity is 2000 cP at 25 °C.

Figure II.3.1. Image of "*Posidonia oceanica*" balls collected from the Mediterranean seashore.

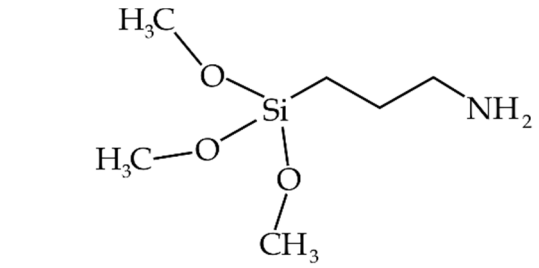

(3-aminopropyl)trimethoxysilane - APTMS

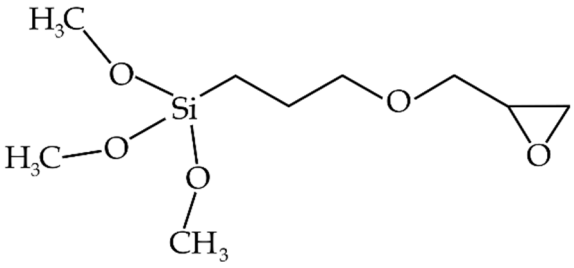

(3-glycidyloxypropyl)trimethoxysilane - GLYMO

Figure II.3.2. Schematic representation of the chemical structure of the silane-coupling agents.

Surface treatments on *Posidonia oceanica*

PO fibers with a length in the 2–8 mm range were washed in distilled water with the main aim of removing residual sand, soil, etc. This operation was repeated until the water was clean enough. Then, the fibers were dried at 60 °C for 24 h in an air-circulating oven Carbolite model PN (Hope Valley, UK). Some of these fibers did not receive any other treatment and were used as control. Some other dried fibers were subjected to an alkali treatment in an alkali water bath (5% NaOH) for 24 h with constant stirring. After this, the fibers were removed from the alkali bath, drained, washed with distilled water and subsequently dried at 60 °C for 24 h. An additional silanization treatment was carried out on alkali-treated PO fibers. Alkali treated fibers were placed in a water:acetone bath (50:50 v/v) containing 1% by weight of the corresponding silane and subjected to magnetic stirring for 2 h. After this treatment time, the silanized fires were removed from the bath, drained and dried at room temperature for 48 h.

Manufacturing of fiberboards

Four different fiberboards were manufactured by hot-press molding with untreated PO fibers (untreated), alkali treated fibers (NaOH) and alkali-treated fibers + silanization

(labeled as NaOH + APTMS and NaOH + GLYMO). All composites contained a constant binder amount of 30 wt%. Initially, the fibers and the binder (resin + hardener) were weighed and mechanically mixed to homogenization. Due to the low density and high porosity of the PO fibers, all the resin was absorbed by the fibers during the mixing. Then, the mixtures were dropped into an aluminum mold with a cavity of 5×7 cm^2 and placed in a hot plate press from DUPRA S.L. (Castalla, Spain). Then a pressure of 22–23 MPa was applied for 20 min to ensure full curing at 85 °C. Then, the temperature was switched off and a holding pressure of 22–23 MPa was maintained for an additional hour. After this, the molded fiberboards with an average thickness of 4–5 mm were obtained and cut for sample characterization.

Characterization techniques

Mechanical characterization

Flexural properties of the manufactured fiberboards were obtained in a universal test machine ELIB 30 from S.A.E. Ibertest (Madrid, Spain). Samples with an average size of 15×70×4.5 mm^3, were subjected to a three-point bending flexural test as indicated by ISO 178 with a crosshead speed of 2 mm min^{-1}. At least five different samples were tested and the average values of the flexural strength (σ_f) and modulus (E_f) were calculated following equations (Equation II.3.1 and Equation II.3.2 respectively):

$$\boldsymbol{\sigma_f = \frac{3FL}{2bh^2}} \qquad \textbf{Equation II.3.1}$$

where F stands for the maximum flexural force in N, L is the distance between supports in mm, b is the width of the sample in mm and h is the height expressed in mm.

$$\boldsymbol{E_f = \frac{\sigma_{f2}-\sigma_{f1}}{\varepsilon_{f2}-\varepsilon_{f1}}} \qquad \textbf{Equation II.3.2}$$

where σ_{fi} and ε_{fi} stand for the flexural stress and elongation at two different points in the linear region. The flexural stresses are calculated by following Equation II.3.1 and the corresponding elongations are calculated with Equation II.3.3.

$$\boldsymbol{s_i = \frac{\varepsilon_{fi}L^2}{6h}} \qquad \textbf{Equation II.3.3}$$

where s_i stands for the deflection and ε_{fi} is the corresponding elongation.

The impact-absorbed energy of the fiberboards was obtained by using a 1 J Charpy's pendulum from Metrotec following the guidelines of ISO 179:1993. Five different samples were tested in impact conditions and the average impact resistance was calculated from the absorbed-energy and the corresponding cross-section areas. In addition, the Shore D hardness of the manufactured fiberboards was obtained in a Shore D durometer from J. Bot Instruments (Barcelona, Spain). Each Shore D value corresponds to the average of, at least, five different measurements in different representative areas.

Dynamic mechanical thermal characterization (DMTA) was carried out in an oscillatory rheometer model AR-G2 from TA Instruments (New Castle, USA). This rheometer is equipped with a special clamp system for solid samples and it is possible to carry out dynamic tests in shear-torsion mode. The samples, with a size of 10×40×4 mm^3 were subjected to a temperature ramp from 35 °C up to 120 °C at 2 °C min^{-1}, under a maximum deformation (γ) of 0.1%. The frequency was set to 1 Hz. The most relevant dynamic properties, *i.e.*, storage modulus (G') and dynamic damping factor (tan δ) were collected.

Morphology of composite fiberboards

The fiberboards were morphologically characterized at two levels. Optical images of both the surface/appearance and fractures (from impact tests) were collected in a stereoscopic microscope Olympus model SZX7 (Barcelona, Spain) with a maximum magnification of 56x. Detailed images of fractured samples from impact tests were observed by scanning electron microscopy (SEM) in a Phenom microscope from FEI Company (Eindhoven, the Netherlands) at an acceleration voltage of 5 kV. Samples were subjected to a metallization process with gold in a sputter-coater EMITECH SC7620 from Quorum Technologies (East Sussex, UK).

RESULTS AND DISCUSSION

All composite boards show a wood-like finish appearance as can be seen in Figure II.3.3. This appearance is interesting as these composite fiberboards could find final applications in the building industry without any other surface finishing. As can be observed in Figure II.3.3, there is not a preferential orientation of the fibers. PO fibers are randomly dispersed in the biobased epoxy matrix, leading to quasi-isotropic behavior.

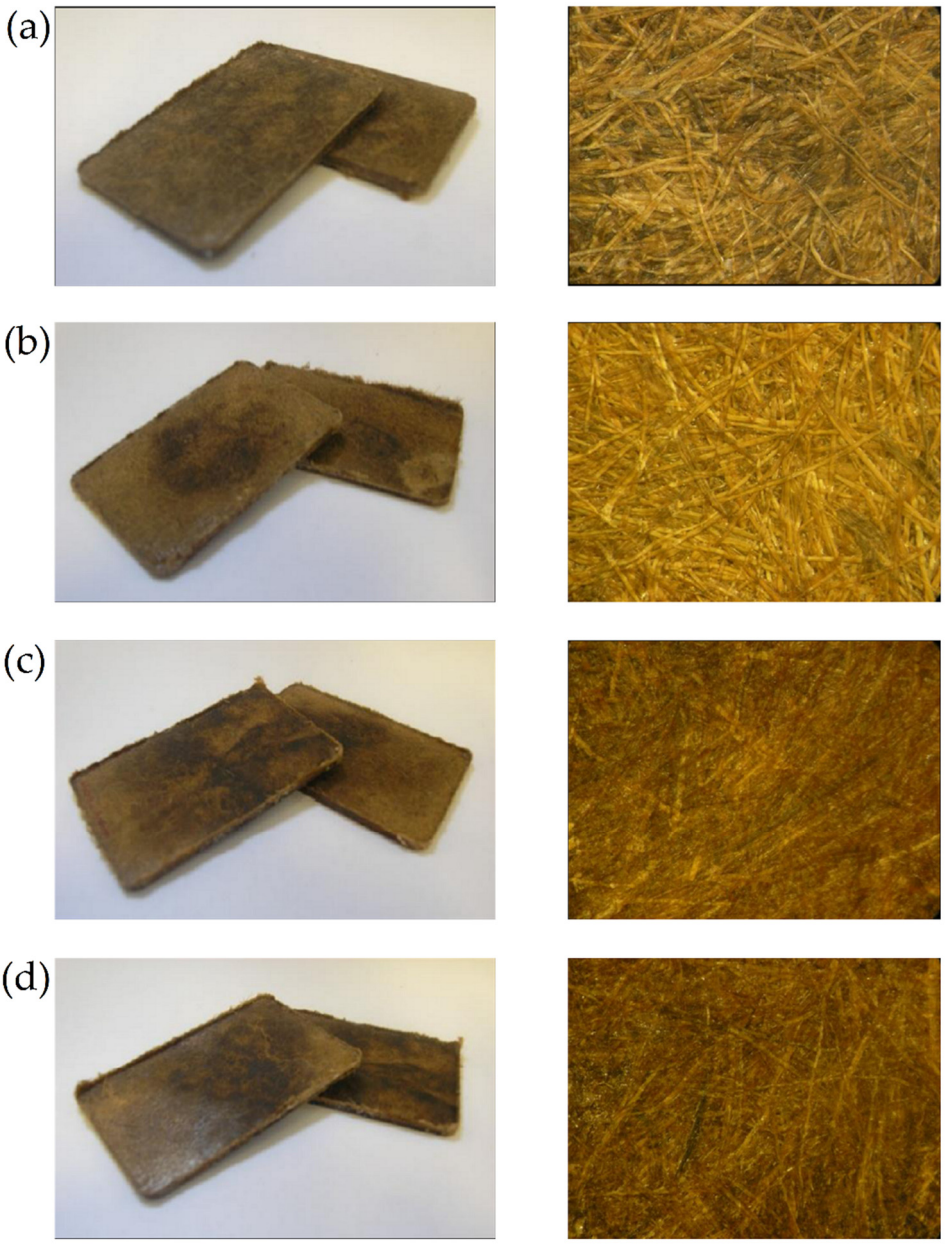

Figure II.3.3. Optical images of the fiberboards (left) and the surface appearance (right) with PO fibers subjected to different chemical treatments: (a) untreated; (b) NaOH; (c) NaOH + APTMS and (d) NaOH + GLYMO.

Regarding mechanical performance, Figure II.3.4 shows a plot representation of the flexural strength of the PO fiberboards with different surface treatments. Due to the non-preferential fiber orientation, these fiberboards show quasi-isotropic behavior, since the fibers are randomly oriented. The flexural strength of the neat resin is 73 MPa. As can be seen, the flexural strength of fiberboards with untreated PO fibers is close to 36.4 MPa, which is remarkably lower than the neat resin. This is due to the lack of (or very poor) interaction between the fiber and the epoxy resin. It is worth noting the remarkable

increase in flexural strength that a simple alkali treatment can provide. In fact, the flexural strength improves up to values around 70 MPa. The alkali treatment promotes a change in the morphology of PO fibers which leads to an increase in the surface roughness due to the removal of some fiber components such as lignin, hemicelluloses, impurities and other extractives [41]. With this, the α-cellulose content increases, as indicated by Jayaramudu *et al.* [42]. This has a positive effect on fiber/matrix interactions that allows better load transfer from the matrix to the fiber. Goud *et al.* [43] reported a remarkable increase in flexural and tensile strength on epoxy composites with royal palm fiber subjected to alkali treatment. After the alkali treatment, they reported an increase in the α-cellulose content from 58 to 65% with the subsequent increase in mechanical performance. In addition, the alkali treatment also promotes the breakage of the fiber bundles into smaller fibers, all this having a positive effect on fiber-matrix interactions due to increased wetting surface [44, 45]. As can be seen in Figure II.3.4, a silanization treatment after a previous alkali treatment also enhances the mechanical performance of PO fiberboards. Specifically, the flexural strength increases up to values of 76 MPa, which represents a percentage increase of almost 109% with regard to fiberboards with untreated PO fibers, thus showing the efficiency of the combined alkali + silanization surface treatment. These results are in total agreement with those reported by Zhu *et al.* [46] with flax-fiber-based composites, a different polymer matrix and different surface treatments, *i.e.*, mercerization, silanization, acylation and peroxide treatments to increase particle-polymer interaction. Nishitani *et al.* [47] also reported the positive effect of silane coupling agents in polyamide 1010/hemp fiber composites showing an improved tribological response due to increased polymer-reinforcement interaction.

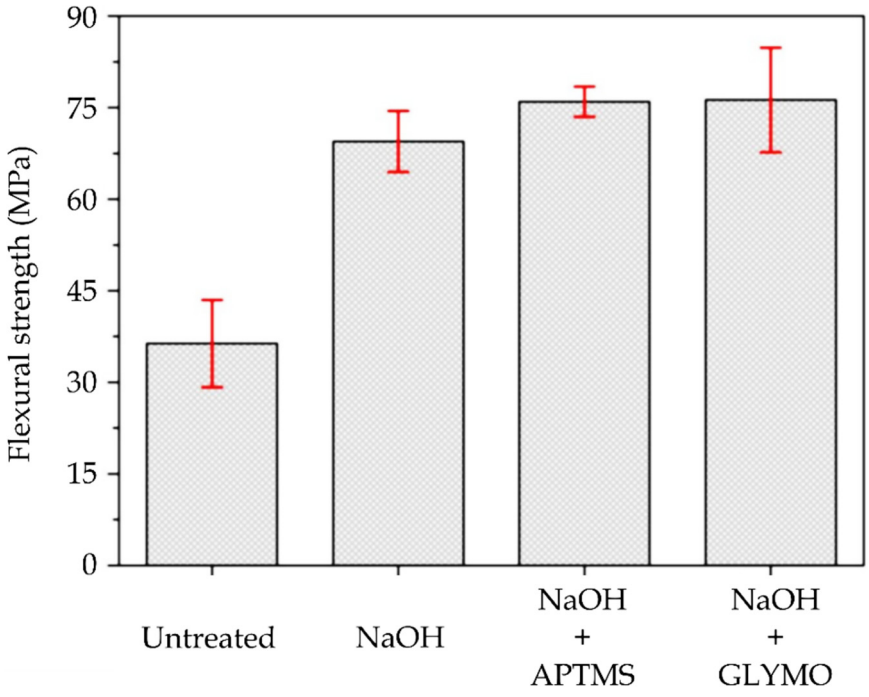

Figure II.3.4. Bar plot of the flexural strength of PO fiberboards with different surface treatments.

Similar effects can be observed for the flexural modulus (Figure II.3.5). If we take into account the flexural modulus of the neat epoxy resin, which is around 2.0 GPa, fiberboards with untreated PO fibers offer a lower flexural modulus of 1.4 GPa that can be ascribed to the above-mentioned poor fiber-matrix interaction. As it can be observed, the flexural modulus changes from 1.4 GPa (fiberboards with untreated PO fibers) up to 4.2–4.3 GPa for both silane-treated PO fiberboards. With regard to the alkali treatment, all the above-mentioned effects lead to a flexural modulus of about 3.2 GPa, thus showing the efficiency of the alkali treatment itself without additional treatments. Nevertheless, the obtained results suggest a synergistic effect with the additional silanization treatment, which leads to almost three times higher flexural modulus regarding the fiberboards with untreated PO fibers. In general, the flexural properties of the neat resin are improved, since the flexural strength remains at similar values of those of the neat resin, and the flexural modulus increases in a remarkable way.

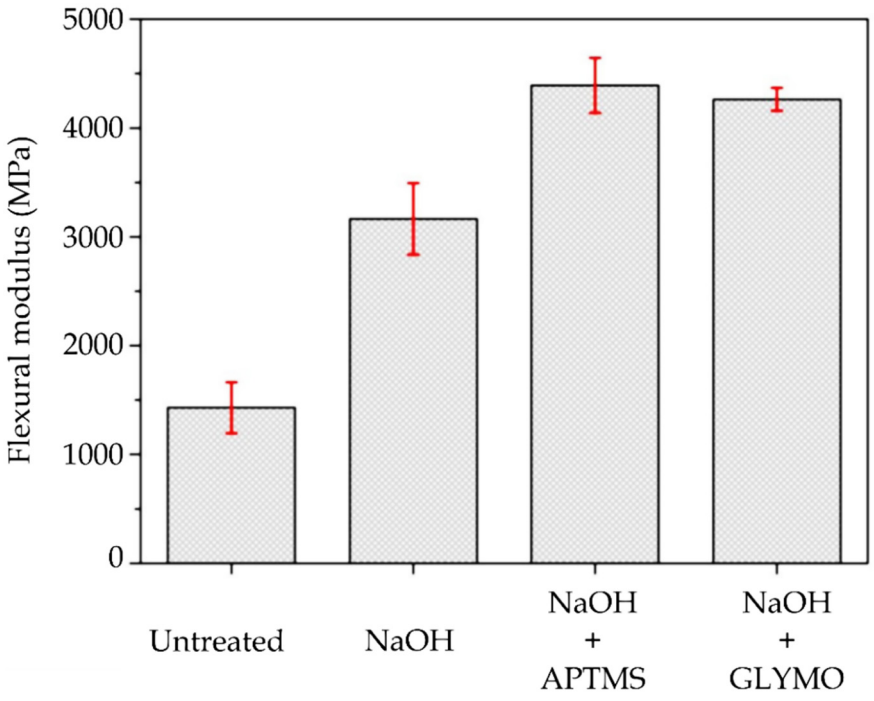

Figure II.3.5. Bar plot of the flexural modulus of PO fiberboards with different surface treatments.

These results are directly related to the surface treatment. Figure II.3.6 shows the morphology of PO fibers with different surface treatments. The alkali treatment promotes the removal of lignin, hemicelluloses and other compounds which leads to a slight change in roughness (Figure II.3.6b). With regard to the silanized PO fibers, the previous alkali treatment allows better interactions between the hydroxyl groups in cellulose and the hydrolyzed silane structure that could lead to a chemical bonding with the fiber surface as shown in Figure II.3.7. This bonding plays a key role in acting as a bridge between the PO fibers and the epoxy binder, with the subsequent improvement of mechanical performance. Figure II.3.6c and d show SEM images of silanized PO fibers after the above-mentioned alkali treatment. The most visible feature that silanes provide to the treated fibers is surface homogeneity, since an ultrathin homogeneous layer is chemically linked to the readily available hydroxyl groups in cellulose after the extraction of lignin and hemicellulose by the alkali treatment. Nevertheless, the changes in surface roughness are not remarkable, but silanized fibers allow better interactions with the partially biobased epoxy resin as mechanical properties suggest.

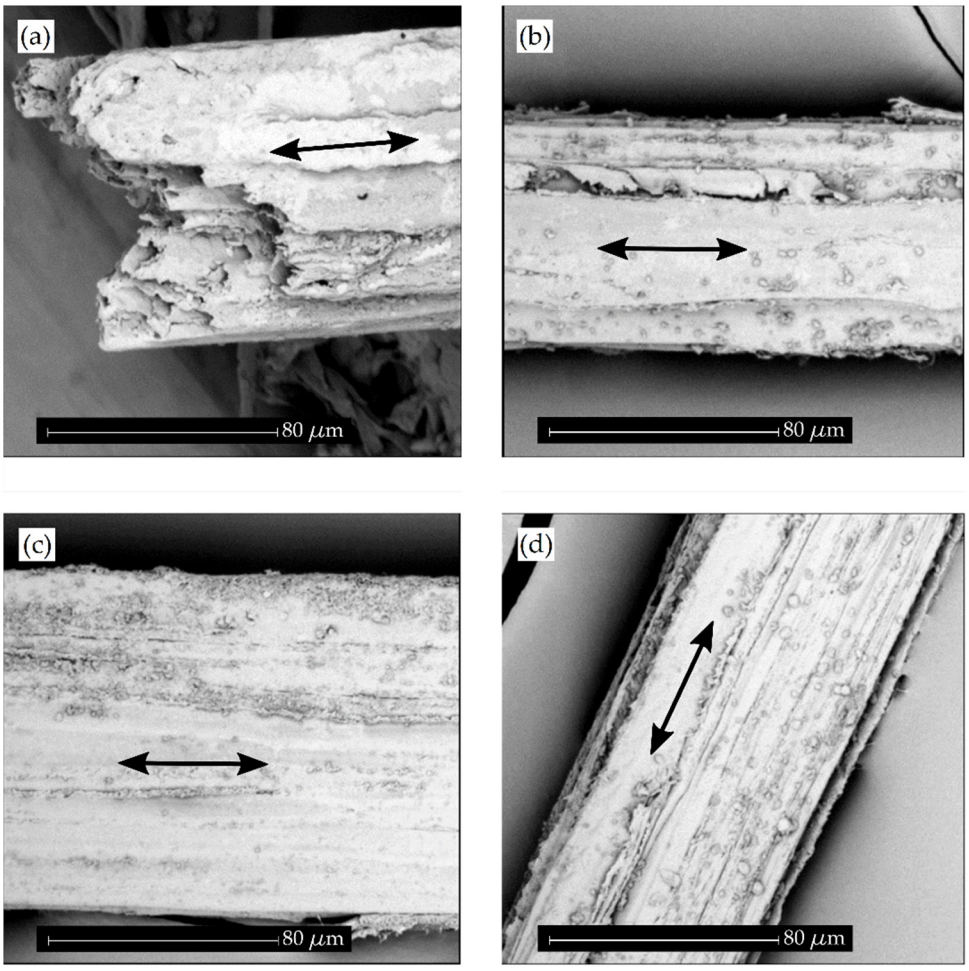

Figure II.3.6. SEM images at 1500x longitudinal PO fibers subjected to different chemical treatments: (a) untreated; (b) NaOH; (c) NaOH + APTMS and (d) NaOH + GLYMO (black arrows indicate the fiber axis).

As per the results, both the amino- and the glycidyl-silane seem to give a similar mechanical performance based on flexural behavior. This can be explained by assuming that both functional groups can react with the epoxy resin, thus leading to an additional coupling effect between PO fibers and the epoxy binder, as can be observed in Figure II.3.7. Although the alkali treatment is enough to give improved mechanical performance (mainly to increase roughness derived from lignin and hemicellulose extraction), hydrophilicity is high since after this treatment, the hydroxyl groups of cellulose are more readily available [48]. Silanes are characterized by dual functionality. On the one hand, silanes have one or several alkoxy groups and, in general, an additional organic functionality such as epoxy, amine, mercaptane, acrylic acid, vinyl, etc. When silanes are hydrolyzed, the alkoxy groups are converted into hydroxyl groups which can readily react with the hydroxyl groups in cellulose to form an ultrathin silane layer chemically bonded to the cellulose component.

The other functional group, *i.e.*, amine or glycidyl in this work, does not take part in this reaction with cellulose and remains free to react with the thermosetting resin (both the epoxy resin and the hardener). This allows a chemical link between the silane and the epoxy resin. The overall effect of the silane is a chemical attachment to both the cellulose fiber and the epoxy resin, thus acting as a bridge between them and, subsequently, improving fiber-matrix interactions.

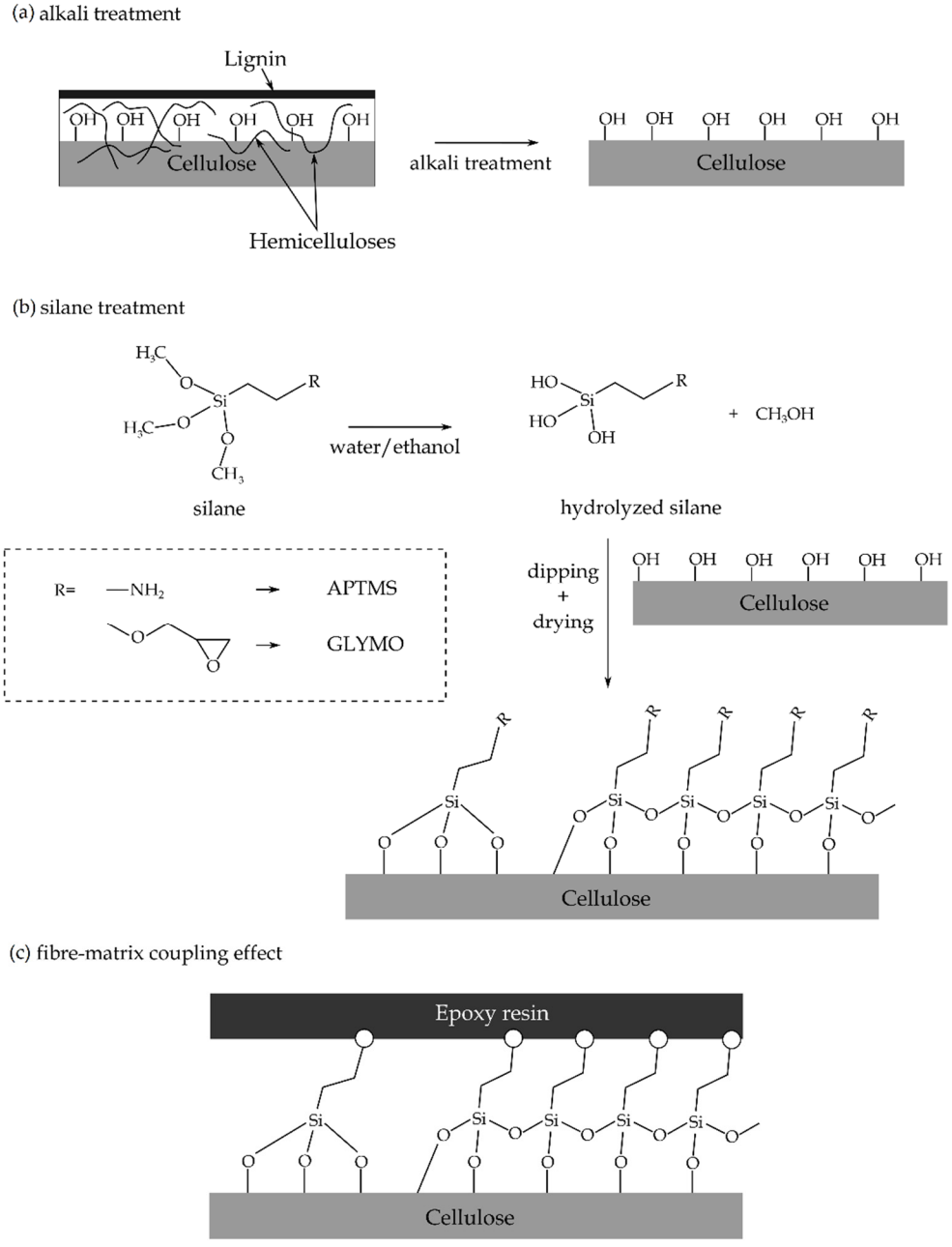

Figure II.3.7. Schematic representation of the effect of alkali and silane treatment on a natural fiber surface and a possible coupling mechanism between PO-treated fibers and epoxy resin.

With regard to the hardness, the Shore D values do not show significant changes, as can be seen in Figure II.3.8, despite the fact that slight variations can be detected. In fact, slightly lower values are obtained for the alkali-treated fiberboard and slightly higher values are observed for the silanized fiberboards. It is in the impact-absorbed energy that important differences can be detected, as observed in Figure II.3.9. The fiberboards with untreated PO fibers are characterized by a relatively low impact resistance due to low fiber/matrix interactions. This leads to an impact resistance of less than 5 kJ m^{-2}. The only alkali treatment leads to improved impact properties with values of about 8.3 kJ m^{-2}, but it is the glycidyl silane treatment which gives the best impact properties, with values of more than 9 kJ m^{-2}, thus showing its higher efficiency compared to the alkali and the alkali + amino silane treatment. The impact-absorbed energy is directly related to the silane chemical structure and its ability to react with different components. The amino silane offers a shorter carbon chain than the glycidyl silane. For this reason, the longer glycidyl silane chain can be stretched to a greater extent than the shorter amino silane chain, so that the glycidyl silane leads to increased toughness. On the other hand, the amine group in APTMS can directly react with epoxy groups in the resin with a similar effect to a typical amine hardener, and this leads to a short chain bridge between the cellulose and the epoxy. On the other hand, the glycidyl group in GLYMO can react with the hardener (an amine-type) which, in turn, can react with epoxy groups in the epoxy resin, thus leading to a longer bridging chain which contributes to improved toughness.

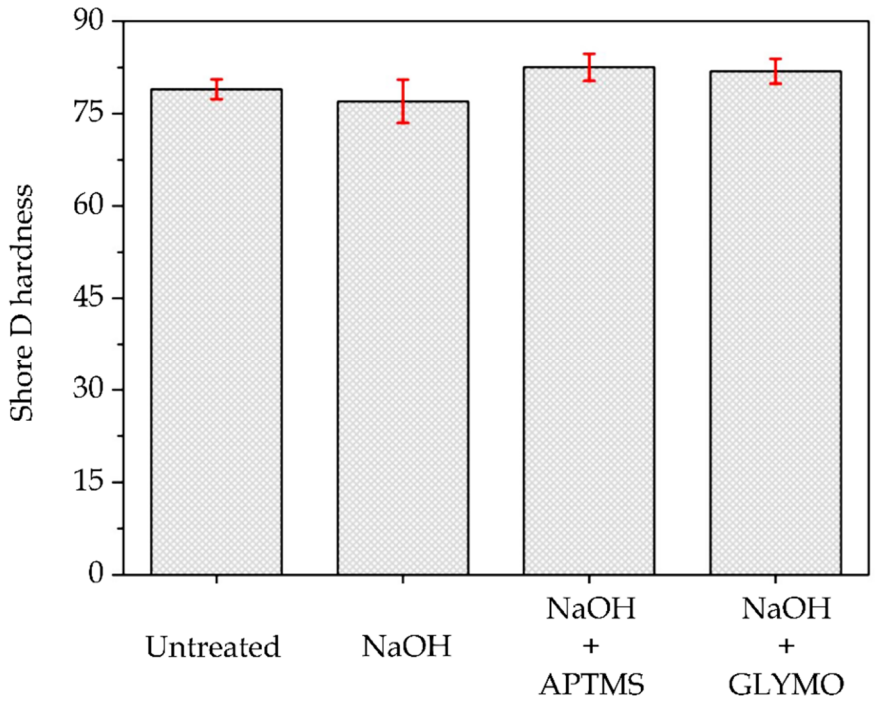

Figure II.3.8. Bar plot of the hardness (Shore D) of PO fiberboards with different surface treatments.

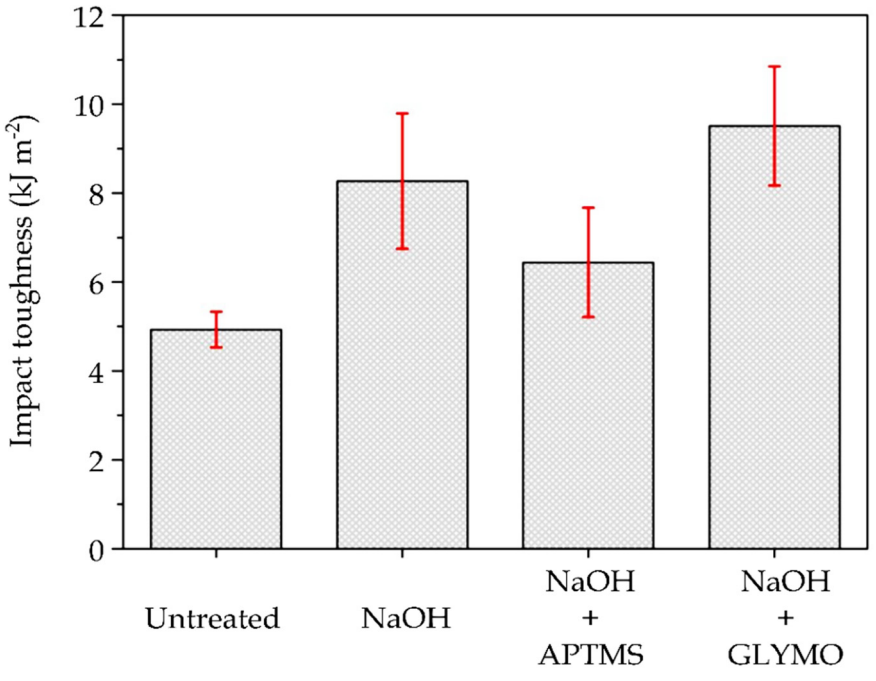

Figure II.3.9. Bar plot of the impact toughness (Charpy test) of PO fiberboards with different surface treatments.

Regarding the dynamic mechanical behavior of PO fiberboards, Figure II.3.10 gathers the evolution of the storage modulus (G') and the damping factor (tan δ) in terms of increasing temperature for the different treatments. The composite with untreated PO fibers shows the lowest G' value (344.7 MPa at 35 °C) (Figure II.3.10a). All three surface treatments promote an increase in the storage modulus in a similar way as previously described for the flexural modulus. It is worth noting that the maximum G' value was achieved for PO fiberboards with NaOH + APTMS silane treatment with values of about 1 GPa at 35 °C. These results are in total agreement with the above-mentioned results for flexural properties. By considering the glass transition temperature (T_g) at the peak value of the damping factor, it is possible to conclude that silanes exert a direct effect on T_g, as can be seen in Figure II.3.10b. The fiberboard with untreated PO fibers shows a T_g located around 74 °C. The alkali treatment with NaOH does not lead to a remarkable change in T_g. Nevertheless, both silanes (amino and glycidyl) produce a noticeable increase in the T_g, reaching values of 83.7 and 79.2 °C for the amino- and glycidyl-silane respectively. This indicates good coupling effects between the PO fibers and the binder epoxy resin. The glass transition temperature is increased, as can be seen in Table II.3.1. A direct relationship has been reported between the toughness and the damping factor. As the toughness increases the damping peak (and more specifically, the loss area) increases due to energy absorption. This situation can be seen in Figure II.3.10 as the loss area is higher for all treated fiberboards, thus indicating that the effect on toughness is positive [49].

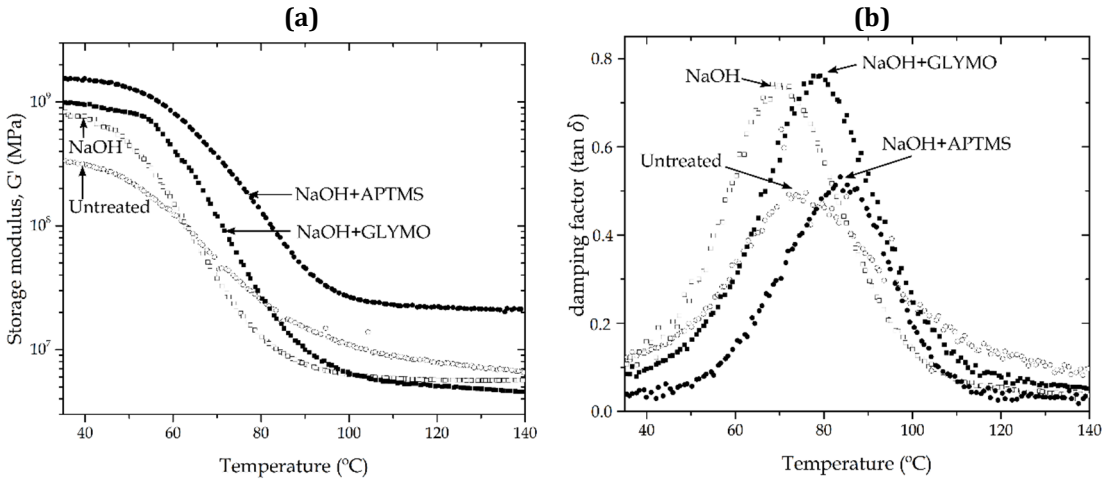

Figure II.3.10. Plot evolution of the (a) storage modulus (G') and (b) damping factor (tan δ) in function of temperature for fiberboards with PO subjected to different surface treatments.

Table II.3.1. Storage modulus (G') values at different temperatures and glass transition temperatures (T_g) for fiberboards with PO subjected to different surface treatments.

Surface Treatment	G' (MPa) at 35 °C	G' (MPa) at 100 °C	T_g (°C)
Untreated	344.7	11.0	73.7
NaOH	808.6	6.6	70.0
NaOH + APTMS	1551.0	26.4	83.7
NaOH + GLYMO	1014.0	6.3	79.2

The morphology of PO fiberboards has been analyzed by SEM to elucidate the potential fiber-matrix interactions. This partially biobased epoxy offers better wetting properties towards natural fibers than petroleum-derived epoxies, even without any surface treatment, as reported by Bertomeu *et al.* [50]. Figure II.3.11 gathers SEM images at different magnifications corresponding to fractured samples of PO fiberboards from impact tests. Figure II.3.11a and b correspond to composite fiberboards with untreated PO fibers. The lack of interaction between the PO fibers and the surrounding epoxy matrix is clearly observable. PO fibers do not interact with the epoxy resin and this leads to poor mechanical performance, as the loads cannot be transferred in an appropriate way. In addition, the SEM images suggest that the PO fibers are not wet by the epoxy resin. This situation is quite different in fiberboards with only an alkali treatment (Figure II.3.11c and d). As can be seen, fiberboards with alkali-treated PO fibers somewhat show fiber-matrix interactions that are responsible for the increase in mechanical performance, as has been previously described. The black arrows in Figure II.3.11d are representative of areas with increased wettability, as it seems that the PO fiber is covered by an epoxy layer. The superior effect of the silanized PO fibers can be observed in Figure II.3.11e and f (NaOH + APTMS) and Figure II.3.11g and h (NaOH + GLYMO). Both silanes produce similar morphologies, characterized by fully-embedded PO fibers in the epoxy matrix. Although some gaps can be detected, the overall effect of both silanes is a clear reduction of the gap between the PO fibers and the surrounding epoxy matrix, as emphasized by the black arrows in Figure II.3.11f and h, corresponding to fiberboards with PO fibers treated with NaOH + APTMS and NaOH + GLYMO, respectively.

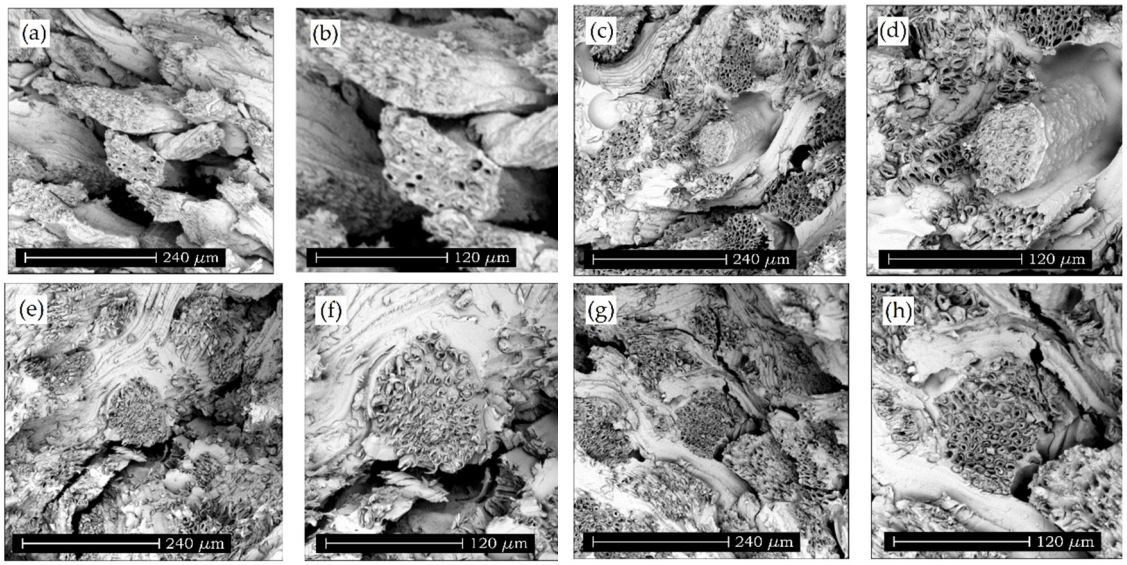

Figure II.3.11. SEM images at different magnifications (a, c, e, g taken at 500x; b, d, f, h taken at 1000x) of the fractured surface of fiberboards with PO fibers subjected to different chemical treatments: (a, b) untreated; (c, d) NaOH; (e, f) NaOH + APTMS and (g, h) NaOH + GLYMO. Black arrows show the improved wetting behavior between the PO fibers and the surrounding epoxy resin.

CONCLUSIONS

This work reports the development of highly environmentally-friendly composite fiberboards with *Posidonia oceanica* (PO) waste seagrass as the lignocellulosic component. Fiberboards with a constant fiber content of 70 wt% PO were manufactured by hot-press molding using a partially biobased epoxy binder resin, leading to fiberboards with more than 85 wt% biobased content. The obtained materials showed a wood-like appearance. The mechanical properties of untreated fiberboards were relatively poor due to the lack of interaction between the lignocellulosic component and the epoxy matrix. For this reason, several treatments were proposed, *i.e.*, alkali treatment with NaOH and alkali treatment followed by silanization with different silanes (amine silane, APTMS, and glycidyl silane, GLYMO). Although a simple alkali treatment improved the mechanical performance, the use of an alkali treatment followed by silanization led to a remarkable increase in the mechanical behavior of PO fiberboards. In particular, the flexural strength and modulus were remarkably improved and, interestingly, the impact toughness was noticeably increased due to the coupling effect that silanes can provide. The SEM study revealed increased fiber-matrix interaction, as the gap between them was remarkably reduced or even eliminated. In general, these fiberboards represent an interesting alternative to the

conventional natural fiber particle of fiberboards, as the used binder also offers high environmental efficiency.

ACKNOWLEDGEMENTS

This work was supported by the Ministry of Economy and Competitiveness (MINECO) [MAT2014-59242-C2-1-R]. D. Garcia-Garcia wants to thank the Spanish Ministry of Education, Culture and Sports for the financial support through a FPU grant [FPU13/06011]. L. Quiles-Carrillo acknowledges Generalitat Valenciana (GV) for financial support through a FPI grant [ACIF/2016/182] and the Spanish Ministry of Education, Culture and Sports for his FPU grant [FPU15/03812].

REFERENCES

[1] Moubarik A, Mansouri HR, Pizzi A, Charrier F, Allal A and Charrier B. *Corn flour-mimosa tannin-based adhesives without formaldehyde for interior particleboard production*. Wood Science and Technology, 2013. **47**(4):675-683.

[2] Akinyemi AB, Afolayan JO and Oluwatobi EO. *Some properties of composite corn cob and sawdust particle boards*. Construction and Building Materials, 2016. **127**:436-441.

[3] Sommerhuber PF, Welling J and Krause A. *Substitution potentials of recycled HDPE and wood particles from post-consumer packaging waste in wood-plastic composites*. Waste Management, 2015. **46**:76-85.

[4] Ghofrani M, Ashori A and Mehrabi R. *Mechanical and acoustical properties of particleboards made with date palm branches and vermiculite*. Polymer Testing, 2017. **60**:153-159.

[5] Khazaeian A, Ashori A and Dizaj MY. *Suitability of sorghum stalk fibers for production of particleboard*. Carbohydrate Polymers, 2015. **120**:15-21.

[6] Sabbatini A, Lanari S, Santulli C and Pettinari C. *Use of almond shells and rice husk as fillers of poly(methyl methacrylate) (PMMA) composites*. Materials, 2017. **10**(8):872.

[7] Väisänen T, Haapala A, Lappalainen R and Tomppo L. *Utilization of agricultural and forest industry waste and residues in natural fiber-polymer composites: A review*. Waste Management, 2016. **54**:62-73.

[8] Ashori A and Nourbakhsh A. *Characteristics of wood-fiber plastic composites made of recycled materials*. Waste Management, 2009. **29**(4):1291-1295.

[9] Elbadawi M, Osman Z, Paridah T, Nasroun T and Kantiner W. *Properties of particleboards made from acacia seyal var. Seyal using uf-tannin modified adhesives*. Cellulose Chemistry and Technology, 2015. **49**(3-4):369-374.

[10] Zhao Z and Umemura K. *Investigation of a new natural particleboard adhesive composed of tannin and sucrose. 2. Effect of pressing temperature and time on board properties, and characterization of adhesive*. BioResources, 2015. **10**(2):2444-2460.

[11] Koumba-Yoya G and Stevanovic T. *Study of organosolv lignins as adhesives in wood panel production*. Polymers, 2017. **9**(2):46.

[12] Santiago-Medina F, Foyer G, Pizzi A, Caillol S and Delmotte L. *Lignin-derived non-toxic aldehydes for ecofriendly tannin adhesives for wood panels*. International Journal of Adhesion and Adhesives, 2016. **70**:239-248.

[13] Ferguson RC, Mendon SK, Rawlins JW and Thames SF. *Formaldehyde-free wood composites from soybean protein adhesive*. Journal of Renewable Materials, 2014. **2**(3):166-172.

[14] Gu K, Huang J and Li KC. *Preparation and evaluation of particleboard bonded with a soy flour-based adhesive with a new curing agent*. Journal of Adhesion Science and Technology, 2013. **27**(18-19):2053-2064.

[15] Prasittisopin L and Li KC. *A new method of making particleboard with a formaldehyde-free soy-based adhesive*. Composites Part A: Applied Science and Manufacturing, 2010. **41**(10):1447-1453.

[16] Baroncini EA, Yadav SK, Palmese GR and Stanzione JF. *Recent advances in bio-based epoxy resins and bio-based epoxy curing agents*. Journal of Applied Polymer Science, 2016. **133**(45):44103.

[17] Saba N, Jawaid M, Alothman OY, Paridah MT and Hassan A. *Recent advances in epoxy resin, natural fiber-reinforced epoxy composites and their applications*. Journal of Reinforced Plastics and Composites, 2016. **35**(6):447-470.

[18] Kim N, Li Y and Sun XS. *Epoxidation of Camelina sativa oil and peel adhesion properties*. Industrial Crops and Products, 2015. **64**:1-8.

[19] Obradovic J, Voutilainen M, Virtanen P, Lassila L and Fardim P. *Cellulose fibre-reinforced biofoam for structural applications*. Materials, 2017. **10**(6):619.

[20] Arévalo R and Peijs T. *Binderless all-cellulose fibreboard from microfibrillated lignocellulosic natural fibres*. Composites Part A: Applied Science and Manufacturing, 2016. **83**:38-46.

[21] Kojima Y, Isa A, Kobori H, Suzuki S, Ito H, Makise R and Okamoto M. *Evaluation of binding effects in wood flour board containing ligno-cellulose nanofibers*. Materials, 2014. **7**(9):6853-6864.

[22] Krika F, Azzouz N and Ncibi MC. *Adsorptive removal of cadmium from aqueous media using Posidonia oceanica biomass: Equilibrium, dynamic and thermodynamic studies*. International Journal of Environmental Science and Technology, 2015. **12**(3):983-994.

[23] Krika F and Benlahbib OE. *Removal of methyl orange from aqueous solution via adsorption on cork as a natural and low-coast adsorbent: Equilibrium, kinetic and thermodynamic study of removal process*. Desalination and Water Treatment, 2015. **53**(13):3711-3723.

[24] Ncibi MC, Ranguin R, Pintor MJ, Jeanne-Rose V, Sillanpää M and Gaspard S. *Preparation and characterization of chemically activated carbons derived from mediterranean Posidonia oceanica (L.) fibres*. Journal of Analytical and Applied Pyrolysis, 2014. **109**:205-214.

[25] Douissa NB, Bergaoui L, Mansouri S, Khiari R and Mhenni MF. *Macroscopic and microscopic studies of methylene blue sorption onto extracted celluloses from Posidonia oceanica*. Industrial Crops and Product, 2013. **45**:106-113.

[26] Nakhli A, Bergaoui M, Aguir C, Khalfaoui M, M'Henni MF and Lamine AB. *Adsorption thermodynamics in the framework of the statistical physics formalism: Basic blue 41 adsorption onto Posidonia biomass*. Desalination and Water Treatment, 2016. **57**(27):12730-12742.

[27] Venault A, Ncibi MC, Pochat-Bohatier C, Vachoud L, Bouyer D and Faur C. *On the adsorption mechanisms of diethylamine by medically-certified activated carbons: Investigation of critical parameters controlling sorption properties*. Journal of the Taiwan Institute of Chemical Engineers, 2014. **45**(4):1937-1946.

[28] Bettaieb F, Khiari R, Dufresne A, Mhenni MF and Belgacem MN. *Mechanical and thermal properties of Posidonia oceanica cellulose nanocrystal reinforced polymer*. Carbohydrate Polymers, 2015. **123**:99-104.

[29] Bettaieb F, Khiari R, Dufresne A, Mhenni MF, Putaux JL and Boufi S. *Nanofibrillar cellulose from Posidonia oceanica: Properties and morphological features*. Industrial Crops and Products, 2015. **72**:97-106.

[30] Bettaieb F, Nechyporchuk O, Khiari R, Mhenni MF, Dufresne A and Belgacem MN. *Effect of the oxidation treatment on the production of cellulose nanofiber suspensions from Posidonia oceanica: The rheological aspect*. Carbohydrate Polymers, 2015. **134**:664-672.

[31] Khiari R, Marrakchi Z, Belgacem MN, Mauret E and Mhenni F. *New lignocellulosic fibres-reinforced composite materials: A stepforward in the valorisation of the Posidonia oceanica balls*. Composites Science and Technology, 2011. **71**(16):1867-1872.

[32] Fortunati E, Luzi F, Puglia D, Petrucci R, Kenny JM and Torre L. *Processing of PLA nanocomposites with cellulose nanocrystals extracted from Posidonia oceanica waste: Innovative reuse of coastal plant*. Industrial Crops and Products, 2015. **67**:439-447.

[33] Luzi F, Fortunati E, Puglia D, Petrucci R, Kenny JM and Torre L. *Modulation of acid hydrolysis reaction time for the extraction of cellulose nanocrystals from Posidonia oceanica leaves*. Journal of Renewable Materials, 2016. **4**(3):190-198.

[34] Coletti A, Valerio A and Vismara E. *Posidonia oceanica as a renewable lignocellulosic biomass for the synthesis of cellulose acetate and glycidyl methacrylate grafted cellulose*. Materials, 2013. **6**(5):2043-2058.

[35] Cocozza C, Parente A, Zaccone C, Mininni C, Santamaria P and Miano T. *Comparative management of offshore Posidonia residues: Composting vs. Energy recovery*. Waste Management, 2011. **31**(1):78-84.

[36] Puglia D, Petrucci R, Fortunati E, Luzi F, Kenny JM and Torre L. *Revalorisation of Posidonia oceanica as reinforcement in polyethylene/maleic anhydride grafted polyethylene composites*. Journal of Renewable Materials, 2014. **2**(1):66-76.

[37] Ferrero B, Fombuena V, Fenollar O, Boronat T and Balart R. *Development of natural fiber-reinforced plastics (NFRP) based on biobased polyethylene and waste fibers from Posidonia oceanica seaweed*. Polymer Composites, 2015. **36**(8):1378-1385.

[38] Seggiani M, Cinelli P, Mallegni N, Balestri E, Puccini M, Vitolo S, Lardicci C and Lazzeri A. *New bio-composites based on polyhydroxyalkanoates and Posidonia oceanica fibres for applications in a marine environment*. Materials, 2017. **10**(4):326.

[39] Maciá A, Baeza FJ, Saval JM and Ivorra S. *Mechanical properties of boards made in biocomposites reinforced with wood and Posidonia oceanica fibers*. Composites Part B: Engineering, 2016. **104**:1-8.

[40] Ferrero B, Boronat T, Moriana R, Fenollar O and Balart R. *Green composites based on wheat gluten matrix and Posidonia oceanica waste fibers as reinforcements*. Polymer Composites, 2013. **34**(10):1663-1669.

[41] Redy KO, Reddy KRN, Zhang J, Zhang J and Rajulu AV. *Effect of alkali treatment on the properties of century fibers*. Journal of Natural Fibers, 2013. **10**(3):282-296.

[42] Jayaramudu J, Guduri BR and Rajulu AV. *Characterization of natural fabric Sterculia urens*. International Journal of Polymer Analysis and Characterization, 2009. **14**(2):115-125.

[43] Goud G and Rao RN. *Effect of fibre content and alkali treatment on mechanical properties of Roystonea regia-reinforced epoxy partially biodegradable composites*. Bulletin of Materials Science, 2011. **34**(7):1575-1581.

[44] Mohanty AK, Khan MA and Hinrichsen G. *Surface modification of jute and its influence on performance of biodegradable jute-fabric/biopol composites*. Composites Science and Technology, 2000. **60**(7):1115-1124.

[45] Siregar JP, Sapuan SM, Rahman MZA and Zaman HMDK. *The effect of alkali treatment on the mechanical properties of short pineapple leaf fibre (PALF) reinforced high impact polystyrene (HIPS) composites*. Journal of Food, Agriculture & Environment, 2010. **8**(2):1103-1108.

[46] Zhu J, Zhu H, Njuguna J and Abhyankar H. *Recent development of flax fibres and their reinforced composites based on different polymeric matrices*. Materials, 2013. **6**(11):5171-5198.

[47] Nishitani Y, Kajiyama T and Yamanaka T. *Effect of silane coupling agent on tribological properties of hemp fiber-reinforced plant-derived polyamide 1010 biomass composites*. Materials, 2017. **10**(9):1040.

[48] Oushabi A, Sair S, Hassani FO, Abboud Y, Tanane O and El Bouari A. *The effect of alkali treatment on mechanical, morphological and thermal properties of date palm fibers (DPFs): Study of the interface of DPF-polyurethane composite*. South African Journal of Chemical Engineering, 2017. **23**:116-123.

[49] Roudsari GM, Mohanty AK and Misra M. *Exploring the effect of poly(propylene carbonate) polyol in a biobased epoxy interpenetrating network*. ACS Omega, 2017. **2**(2):611-617.

[50] Bertomeu D, García-Sanoguera D, Fenollar O, Boronat T and Balart R. *Use of eco-friendly epoxy resins from renewable resources as potential substitutes of petrochemical epoxy resins for ambient cured composites with flax reinforcements*. Polymer Composites, 2012. **33**(5):683-692.

materials

MDPI

Article

Manufacturing and Characterization of Composite Fibreboards with *Posidonia oceanica* Wastes with an Environmentally-Friendly Binder from Epoxy Resin

Daniel Garcia-Garcia, Luis Quiles-Carrillo, Nestor Montanes, Vicent Fombuena and Rafael Balart *

Instituto de Tecnología de Materiales-ITM, Universitat Politècnica de València-UPV, Plaza Ferrándiz y Carbonell 1, 03801 Alcoy, Spain; dagarga4@epsa.upv.es (D.G.-G.); luiquic1@epsa.upv.es (L.Q.-C.); nesmonmu@upvnet.upv.es (N.M.); vifombor@upvnet.upv.es (V.F.)
* Correspondence: rbalart@mcm.upv.es; Tel.: +34-966-528-400

Received: 29 October 2017; Accepted: 16 November 2017; Published: 26 December 2017

Abstract: Highly environmentally-friendly fibreboards were manufactured by hot-press moulding using *Posidonia ocaeanica* wastes and a partially biobased epoxy resin as binder. Fibreboards with a constant fibre content of 70 wt % were successfully manufactured by thermo-compression. The effects of a conventional alkali treatment were compared to the synergistic effects that additional silanization with two silanes (amino and glycidyl) can exert on the mechanical and thermo-mechanical properties of fibreboards. The results revealed a remarkable improvement of the mechanical properties with the combination of the alkali treatment followed by the silanization. Scanning electron microscopy also revealed increased resin-fibre interactions due to the synergistic effect of both amino- and glycidyl-silanes. These fibreboards represent a formaldehyde-free solution and can positively contribute to sustainable development as the lignocellulosic component is a waste and the binder resin is partially biobased.

Keywords: biobased epoxy; fiber boards; waste management; *Posidonia oceanica*; hot-press manufacturing; coupling agents

1. Introduction

Nowadays most developed countries are paying special attention to environmental issues. Some of the most important actions to protect the environment are focused on the optimum use of natural resources, the reduction of polluting gas emissions, upgrading industrial and/or agroforestry wastes, etc.; all this with the main aim of reducing the carbon footprint and positively contributing to sustainable development based on a circular economy concept. Fossil fuels are widely used as the main source for many applications, including the polymer and composites industries. Petroleum depletion is also acting as the leading force to the development of a new series of environmentally-friendly materials from renewable resources. This environmental sensitivity is particularly marked in the polymer and polymer-composite industries, which, traditionally, are highly dependent on petroleum-derived polymers and resins. With regard to thermosetting resins, petroleum-derived epoxies, unsaturated polyesters, vinyl esters, phenolics, acrylics, etc., still represent the main source of industrial resins for uses in the composites industry and for the manufacturing of fibre and particle boards.

Particle and fibreboards are widely used in the building industry as eco-friendly solutions to wood with increasing uses in thermal insulators, ceiling boards, wall partitions, etc. due to an excellent combination of mechanical, thermal and acoustic properties together with a competitive price. Particle and fibreboards consist of a major lignocellulosic component bonded with a resin, typically,

III. OBJETIVOS

III.1. OBJETIVO GENERAL

Esta tesis doctoral incorpora diversos estudios preliminares ligados al desarrollo de materiales de alto rendimiento medioambiental, centrados en el empleo de cargas lignocelulósicas derivadas de residuos industriales o agroforestales. A lo largo de esta etapa investigadora preliminar, se detectó la relevancia que podría adquirir el poli(3-hidroxibutirato) como material, tanto individual como para matrices en materiales compuestos. Es por ello, que el objetivo general del presente trabajo se centra en mejorar las propiedades del poli(3-hidroxibutirato) (PHB) mediante el desarrollo de formulaciones que permitan reducir sus principales inconvenientes, como son su elevada fragilidad, su estrecho rango de temperatura de procesado y su elevado coste, sin afectar a su biodegradabilidad. La finalidad última de la presente tesis doctoral es obtener formulaciones basadas en PHB que resulten más competitivas que el polímero puro y que permitan aumentar su aplicabilidad a nivel industrial.

III.2. OBJETIVOS ESPECÍFICOS

Para alcanzar el objetivo general se han planteado una serie de objetivos específicos, los cuales han sido desarrollados a lo largo de la presente tesis doctoral. Dichos objetivos específicos han sido clasificados en tres grupos dependiendo de la metodología a emplear para la mejora de las propiedades del poli(3-hidroxibutirato), entre las que se encuentran la plastificación, la mezcla física en fundido o "*blending*" y la incorporación de nanopartículas. Los objetivos específicos planteados en la presente tesis doctoral son:

Plastificación

- Estudio del efecto de la incorporación de diferentes cantidades de aceites vegetales epoxidados (aceite de soja epoxidado-ESBO y aceite de linaza epoxidado-ELO) en las propiedades mecánicas, térmicas y morfológicas del PHB.

- Estudio del efecto de la incorporación de diferentes cantidades de derivados de aceites vegetales (aceite de linaza maleinizado-MLO y ésteres de ácidos grasos epoxidados-EFAE) en las propiedades mecánicas, térmicas y morfológicas del PHB.

Mezcla física en fundido o "*Blending*"

- Evaluación de la miscibilidad y de las propiedades mecánicas, térmicas y morfológicas de mezclas de poli(3-hidroxibutirato)/poli(ε-caprolactona) (PHB/PCL) con diferentes composiciones.

- Estudio del efecto de la incorporación de diferentes cantidades de peróxido de dicumilo (DCP) en la compatibilidad y en las propiedades mecánicas, térmicas y morfológicas de las mezclas de PHB/PCL optimizadas, a través de la extrusión reactiva.

Incorporación de nanopartículas

- Estudio de la viabilidad del empleo de piñas de pino como materia prima para la obtención de nanocristales de celulosa (CNCs). Influencia del tiempo de hidrólisis ácida durante el proceso de síntesis en las propiedades físico-químicas y en el rendimiento de los nanocristales de celulosa obtenidos.

- Evaluación del efecto de la incorporación de diferentes cantidades de nanocristales de celulosa en las propiedades mecánicas, térmicas, morfológicas, ópticas y de humectabilidad de films de PHB/PCL optimizados. Estudio de la degradación de los films reforzados en condiciones de compostaje.

- Evaluación del efecto del tratamiento con diferentes ácidos (sulfúrico, acético y acrílico) en la morfología y la composición química de los nanotubos de haloisita (HNTs) como potenciales soportes para aditivos funcionales.

- Estudio del efecto de los tratamientos con silano y ácido cafeico en la hidrofobicidad de los nanotubos de haloisita. Evaluación del efecto de la incorporación de nanotubos de haloisita sin modificar y modificados en las propiedades mecánicas, térmicas y morfológicas de las mezclas de PHB/PCL compatibilizadas con peróxido de dicumilo.

En la Figura III.1 se observa la planificación realizada para cada uno de los objetivos específicos planteados.

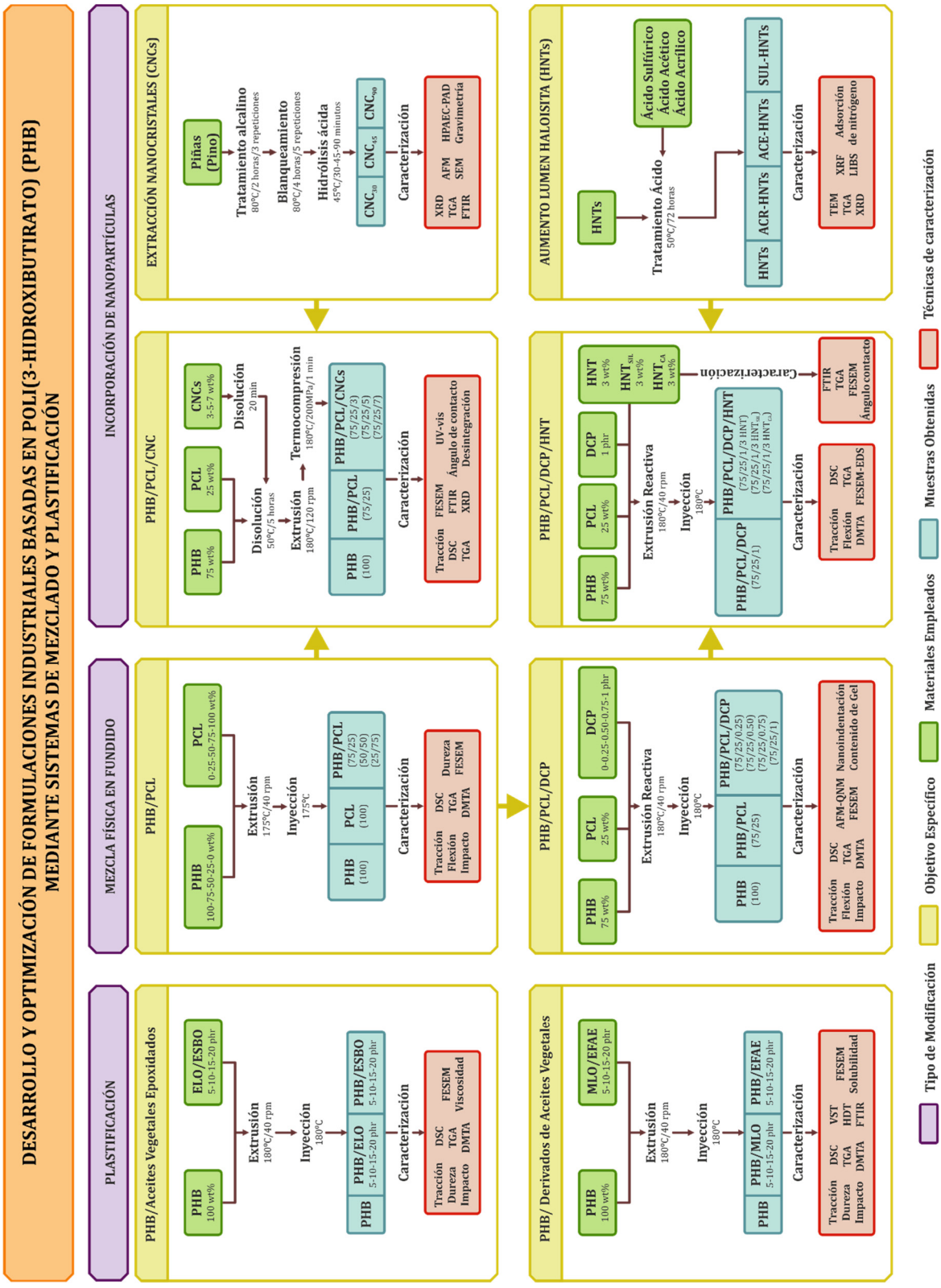

Figura III.1. Esquema del trabajo realizado en la presente tesis doctoral.

IV. RESULTS and DISCUSSION

The present research work is focused on the improvement of some of the main drawbacks that poly(3-hydroxybutyrate) (PHB) possesses, such as its high cost, high fragility and low thermal stability, which gives an extremely narrow processing window. With the aim of overcoming (or minimizing) these disadvantages several approaches have been used. All this with the main objective of improving PHB properties and, subsequently, leading to a wider use of this polymer at industrial level.

The following section covers the most relevant results with regard to PHB-improved formulations and is divided into eight chapters. All these chapters are structured into three different blocks depending on the main modification strategy used to improve the properties of PHB, *i.e.*, plasticization, physical blending with other biodegradable polymer and, finally, addition of small amounts of nanoparticles.

Plasticization

This block includes the main results obtained after PHB plasticization with different amounts of several biobased plasticizers: epoxidized linseed oil (ELO), epoxidized soybean oil (ESBO), maleinized linseed oil (MLO) and epoxidized fatty acid esters (EFAE). The effect of these four plasticizers on overall properties of PHB-based formulations is described in the following chapters:

Chapter IV.1

Plasticization effects of epoxidized vegetable oils on mechanical properties of poly(3-hydroxybutyrate).

Chapter IV.2

Improvement of mechanical ductile properties of poly(3-hydroxybutyrate) by using vegetable oil derivatives.

Physical blending

This block includes the main results obtained by blending PHB with different amounts of other biodegradable polyester, *i.e.*, poly(ε-caprolactone) (PCL). This block also covers the use of reactive extrusion with dicumyl peroxide (DCP) as a cost-effective pathway to increase miscibility on previously developed PHB/PCL blends. The most relevant results are described in the following chapters:

Chapter IV.3

Processing and characterization of binary poly(hydroxybutyrate) (PHB) and poly(caprolactone) (PCL) blends with improved impact properties.

Chapter IV.4

Improvement of the compatibility between poly(3-hydroxybutyrate) and poly(ε-caprolactone) by reactive extrusion with dicumyl peroxide.

Addition of nanoparticles

This block contains some novel results related to synthesis of cellulose nanocrystals (CNCs) from pine cones and the effect of the hydrolysis time. The synthesized CNCs were finally added to a PHB/PCL formulation to improve its properties and, subsequently, leading to a wider range of applications. This block also contains results regarding the use of selectively etched halloysite nanotubes (HNTs) as potential active filler in PHB/PCL industrial formulations. This study also covers the use of several treatments on HNTs such as silanization and caffeic acid loading to improve the properties of the reactively compatibilized PHB/PCL blend. These results are described in the following chapters:

Chapter IV.5

Optimizing the yield and physico-chemical properties of pine cone cellulose nanocrystals by different hydrolysis time.

Chapter IV.6

Reinforcing capability of cellulose nanocrystals obtained from pine cones in a biodegradable poly(3-hydroxybutyrate)/poly(ε-caprolactone) (PHB/PCL) thermoplastic blend.

Chapter IV.7

Characterization of selectively etched halloysite nanotubes by acid treatment.

Chapter IV.8

Improvement of mechanical and thermal properties of poly(3-hydroxybutyrate) (PHB) blends with surface-modified halloysite nanotubes (HNTs).

PLASTICIZATION

IV.1

“Plasticization effects of epoxidized vegetable oils on mechanical properties of poly(3-hydroxybutyrate)”

Daniel García García[a], *José M. Ferri*[a], *Néstor Montañés*[a], *Juan López Martínez*[a], *Rafael Balart*[a]

[a] Instituto de Tecnología de Materiales (ITM)
Universitat Politècnica de València (UPV)
Plaza Ferrándiz y Carbonell 1, 03801 Alcoy, Alicante, Spain.

Polymer International

2016, 65:1157-1164

Plasticization effects of epoxidized vegetable oils on mechanical properties of poly(3-hydroxybutyrate)

Abstract

The effect of various epoxidized vegetable oils as potential plasticizers for poly(3-hydroxybutyrate) (PHB) was evaluated in terms of changes in mechanical and thermal properties and morphology. PHB is a biodegradable aliphatic polyester obtained from bacterial fermentation. High stiffness and fragility are two of its main drawbacks. To overcome this behavior, PHB was plasticized with various amounts of two different epoxidized vegetable oils: epoxidized linseed oil (ELO) and epoxidized soybean oil (ESBO). The total ELO and ESBO content varied in the range 5 phr (per hundred resin) to 20 phr and plasticized PHB materials were obtained by melt extrusion and compounding followed by injection molding. The results show that the plasticizing effect provided by ELO is more efficient than that by ESBO with balanced properties at a concentration of 10 phr ELO. ELO addition leads to an improvement in mechanical ductile properties with a noticeable increase in elongation at break and impact absorbed energy. With regard to thermal properties, the addition of both ELO and ESBO leads to a marked increase in thermal stability of PHB. All these findings suggest that addition of 10 phr ELO leads to optimized PHB formulations with potential uses in technical applications.

Keywords: Poly(3-hydroxybutyrate) (PHB); epoxidized soybean oil (ESBO); epoxidized linseed oil (ELO); plasticization; biodegradable.

INTRODUCTION

Recent decades have witnessed a remarkable increase in the production and consumption of plastic materials, mainly from petroleum origin, such as polyethylene, polypropylene, poly(ethylene terephthalate), polystyrene, etc., that covers a wide range of properties that make them useful for diverse industrial sectors. Nevertheless, one important weakness of these petroleum-based polymers is that most of them are not biodegradable. Packing and packaging industries use large amounts of plastic materials and their products are characterized by a relatively short life cycle, and consequently a huge amount of non-biodegradable plastics is continuously generated with subsequent environmental impact. The increase in environmental concerns related to waste generation has led to an increased interest in the study and development of polymers that can undergo total degradation/decomposition under appropriate temperature and moisture conditions. This has a positive effect on the environment as it avoids generation of harmful and potentially toxic wastes [1]. These polymers, also known as biopolymers, can be classified into four different groups depending on the production process and the origin of the base material or monomer. One group includes all polymers obtained directly from biomass such as cellulose, starch, alginate, gluten, etc. Another group consists of all polymeric materials obtained by chemical synthesis from monomers derived from renewable resources as is the case for poly(lactic acid) (PLA). The third group is represented by those polymers that, although they are obtained from fossil and non-renewable resources, can undergo degradation/decomposition due to their particular chemical structure as is the case for some petroleum-derived polyesters, *e.g.*, poly(caprolactone) (PCL), poly(butylene succinate) (PBS), poly(butylene adipate-*co*-terephthalate) (PBAT), etc. Finally, some biodegradable polymers can be obtained from bacterial fermentation such as polyhydroxyalkanoates (PHAs) [2]. Therefore, the use of biodegradable polymers is one of the main alternatives for reducing the large amounts of wastes with a subsequent reduction of their environmental impact [3, 4].

Poly(3-hydroxybutyrate) (PHB) is one of the best known polyhydroxyalkanoates [5]. PHB is an aliphatic polyester obtained from controlled bacterial fermentation and is characterized by its intrinsic biodegradability and biocompatibility [6, 7]. PHB is readily biodegradable in such environments where the combination of nitrogen, phosphates, salts, moisture and temperature allows microorganism growth [8, 9]. These microorganisms use PHB polymer chains as nutrients. For this reason, PHB degradation can occur in various environments such as soil [10, 11], compost [12-14] and marine sediments [15, 16]. Otherwise, PHB can remain almost intact for long periods. PHB biodegradation depends on

several factors such as microbial activity of the environment, moisture, temperature, pH, initial molecular weight of polymer chains, crystallinity, etc. [17, 18]. In the case of PHB, biodegradation in compost at temperatures around 60 °C and a moisture content of 50–55% has been reported [19, 20].

The excellent combination of its properties makes PHB ideal for biodegradable packing products and resorbable medical devices [21]. Despite this, up to now there has not been a large production of PHB products because of its cost and some weaknesses in comparison with commodity and other technical plastics [22]. One of the main drawbacks of PHB is its intrinsic fragility due to its high crystallinity, which can be higher than 55%. This leads to low elongation at break and deformation ability which limit its field of applications [23, 24]. Another important drawback of PHB is its relatively low resistance to thermal degradation which leads to a markedly narrow processing window. The melt temperature of PHB is located at about 180 °C and it can be processed at about 190 °C as higher temperatures (or longer residence times) promote chain scission with subsequent decrease in molecular weight [25]. These problems can be overcome by using several techniques such as internal [26] or external plasticization [23, 25, 27] as well as physical blending with other polymers [28-30].

Among the various options for preparing industrial PHB formulations, external plasticization represents an interesting, simple and cost-effective route to improve the mechanical and thermal properties of raw PHB [31]. Generally, addition of plasticizers promotes a decrease in both the glass transition temperature (T_g) and the melt temperature (T_m), and this allows processing at lower temperatures thus reducing the risk of thermal degradation. Furthermore, plasticizers increase PHB ductility while its brittleness is noticeably reduced as a consequence of lower degree of crystallinity [32]. Petroleum-based plasticizers such as phthalates, trimellitates, dicarboxylates, adipates, etc., are widely used at the industrial level and some of them offer potential toxicity problems associated with plasticizer migration [33]. For this reason, new environmentally friendly plasticizers are continuously being investigated and tested. It has been shown that epoxidized vegetable oils are a viable alternative to petroleum-based conventional plasticizers. Epoxidized vegetable oils are obtained by epoxidation of vegetable oils sourced from various plants and seeds [34]. The chemical structure of vegetable oils is based on a triglyceride structure with various fatty acids [35, 36]. The presence of carbon–carbon unsaturations allows epoxidation by conventional processes. These unsaturations appear in conventional fatty acids such as oleic (C18:1), linoleic (C18:2) and linolenic (C18:3) acids with one, two and three carbon–carbon double bonds, respectively. Soybean oil is characterized by high

content of unsaturated fatty acids, mainly oleic (20–26%), linoleic (48–57%) and linolenic (6–10%), and linseed oil is highly rich in linolenic acid (51–46%) and other unsaturated fatty acids such as oleic (18–26%) and linoleic (14–20%). In addition, both soybean oil and linseed oil are commercially available as by-products of other industries and can be easily epoxidized with cost-effective processes; therefore, both these epoxidized vegetable oils are also commercially available [3]. Some research works report the successful use of epoxidized vegetable oils as plasticizers for thermoplastic matrices, both biodegradable and non-biodegradable [3, 4, 37-43]. The use of epoxidized soybean oil (ESBO) and epoxidized linseed oil (ELO) has been reported as plasticizers for poly(3-hydroxybutyrate-*co*-valerate) (PHBV). Seydibeyoğlu *et al.* [44] reported that addition of 10 wt% ELO and ESBO leads to a slight increase in elongation at break with a subsequent reduction of the tensile strength and Young's modulus. In addition, a slight decrease in the melt temperature was observed. Similar behavior was confirmed by Choi and Park [45] after the addition of 30 wt% ESBO to PHBV with a marked increase in both the impact resistance and the elongation at break. Plasticizer interaction is directly related to the chemical structure of both base polymer and plasticizer as well as other external processing parameters related to mixing and homogenization. It has been reported that PHBV and PHB possess similar solubility parameters due to similar chemical structure [46]. Nevertheless, it is possible that differences in chain length, crystallinity, amount of hydroxyvalerate co-monomer and other slight differences between PHB and PHBV polymers could have an important effect on plasticization. Plasticizer saturation promotes phase separation and this has a negative effect on overall properties of plasticized formulations. As indicated by Ren *et al.* [47], Xu and Qu [48] and Ferri *et al.* [49], plasticization of polyester-type polymers such as PLA occurs at relatively low plasticizer content. This behavior was also observed by Zhao *et al.* [38] for PBS plasticized with ESBO. As indicated by Choi and Park [45], plasticized PHBV formulations admit a relatively high plasticizer (ESBO) content. On the other hand, Seydibeyoğlu *et al.* [44] reported interesting results for intermediate plasticizer content with a different PHBV grade and different valerate content.

By taking into consideration the studies discussed above, the main aim of the work reported here was to assess the plasticization effect of both ELO and ESBO on PHB and determine the optimum plasticizer content before plasticizer saturation occurs. The effectiveness of the two cost-effective and commercially available epoxidized vegetable oils, ELO and ESBO, as potential plasticizers for PHB was evaluated. The effect of various plasticizer contents (in the range 0–20 phr) and type (ELO, ESBO) on the mechanical and thermal properties of PHB is described.

EXPERIMENTAL

Materials

PHB pellets, commercial grade P226, were supplied by Biomer (Krailling, Germany). This PHB grade has an average molecular weight of 426,000 g mol^{-1}, a density at 23 °C of 1.25 g cm^{-3} and a melt flow index of 10 g $(10\ min)^{-1}$ tested at 180 °C and 5 kg loading. ESBO and ELO were used as PHB plasticizers. ELO has a density at 20 °C between 1.05 and 1.06 g cm^{-3}, an epoxide equivalent weight of 178 g $equiv^{-1}$ and an acid value below 1 mg KOH g^{-1}. ESBO has a density at 20 °C between 0.990 and 0.997 g cm^{-3}, an epoxide equivalent weight of 238 g $equiv^{-1}$ and an acid value below 0.75 mg KOH g^{-1}. Both of them were supplied by Traquisa S.L. (Barcelona, Spain) and were used as received without any other treatment. The hydroxyl and peroxide values of both epoxidized vegetable oils are almost negligible as indicated by the supplier.

Sample preparation

PHB pellets were vacuum dried at 70 °C for 24 h before blending to remove moisture. After this, PHB and the corresponding amounts of ELO or ESBO were mechanically mixed in a zipper bag. The total plasticizer content varied in the range 0–20 phr. All PHB plasticized formulations were processed in a twin-screw co-rotating extruder with D = 25 mm and L/D ratio = 24. The temperature profile was accurately selected to avoid thermal degradation and was set to 170 °C (hopper), 170 °C, 175 °C and 180 °C (die). All materials were obtained at a screw speed of 40 rpm. After extrusion, the material was cooled and pelletized in a mill. After this, standard samples for tensile tests and rectangular samples of size 80×10×4 mm^3 were obtained by injection molding in a Meteor 270/75 injection molding machine (Mateu & Solé, Barcelona, Spain) at a temperature of 180 °C. PHB processing led to a decrease in molecular weight due to its high sensitivity to thermal degradation [50]. The percentage decrease in molecular weight of unplasticized PHB after the extrusion process was around 11.6%, whilst this reduction was still more accentuated after the injection molding process with a percentage decrease of about 34.2% with regard to unprocessed PHB pellets. This noticeable decrease in the PHB average molecular weight is directly related to thermal degradation and affects in a marked way the overall mechanical and thermal features of PHB-derived materials [51]. Nevertheless, this work is focused on the effect of the two plasticizers (type and amount) on final properties of plasticized PHB and all formulations were subjected to the same processing conditions to give comparable results.

Characterization techniques

Viscosity molecular weight

Intrinsic viscosity (η) of PHB before processing and after extrusion and extrusion+injection molding was obtained using an Ubbelohde viscometer type 1C at room temperature following the guidelines of ISO 1628. All samples were dissolved in chloroform with three different concentrations for each sample. The viscosity molecular weight (M_v) for each sample was obtained using the Mark–Houwink equation with K and a values of 1.18×10^{-2} and 0.780, respectively, for PHB as reported elsewhere [52]:

$$[\eta] = K \times M_V^a \qquad \textbf{Equation IV.1.1}$$

Mechanical properties

Tensile tests of neat PHB and ELO/ESBO-plasticized PHB formulations were carried out at a rate of 5 mm min^{-1} using an electromechanical universal test machine (Ibertest ELIB 30, S.A.E. Ibertest, Madrid, Spain) with a 5 kN load cell at room temperature, following ISO 527. A set of five different samples was tested and average values were calculated. In addition, an axial extensometer was used to obtain the Young's modulus in a more accurate way.

Impact testing was done using a 1 J Charpy impact pendulum (Metrotec S.A., San Sebastián, Spain) according to ISO 179 standard. At least five different notched samples ("V" type at 45° with a radius of 0.25 mm) were tested and the average value of the absorbed energy was calculated.

Shore D hardness values of ELO/ESBO-plasticized PHB were obtained with a Shore D hardness durometer model 676-D (J. Bot Instruments, Barcelona, Spain) following ISO 868. At least five different measurements were taken and average values were calculated.

Thermal properties

The melting and crystallization behavior of neat PHB and ELO/ESBO-plasticized PHB was studied using DSC (model 821, Mettler-Toledo Inc., Schwerzenbach, Switzerland). The sample weight was approximately 7–9 mg range. All samples were subjected to a four-step thermal programme to remove thermal history. First step: dynamic heating from –50 to 180 °C at a heating rate of 10 °C min^{-1}; second step: isothermal programme at 180 °C for 2 min; third step: dynamic cooling from 180 to –50 °C at a cooling rate of 10 °C min^{-1}; fourth

step: dynamic heating from –50 to 300 °C at 10 °C min^{-1}. All the tests were conducted in nitrogen atmosphere at a constant flow rate of 66 mL min^{-1}. Both melt temperature (T_m) and melt enthalpy (ΔH_m) were obtained from the second heating programme to eliminate the influence of material processing. The percentage crystallinity of PHB ($X_{c\ PHB}$) was calculated using the following equation:

$$\boldsymbol{X_c}\ (\%) = \left[\frac{\boldsymbol{\Delta H_m}}{\boldsymbol{\Delta H_0 \cdot w}}\right] \times \mathbf{100} \qquad \textbf{Equation IV.1.2}$$

where ΔH_m is the melt enthalpy, ΔH_0 is the melt enthalpy for a theoretical 100% crystalline PHB, assumed to be 146 J g^{-1} [20], and w is the weight fraction of PHB in all tested formulations.

The thermal stability of the samples was studied using TGA with a TGA/SDTA 851 thermobalance (Mettler-Toledo Inc., Schwerzenbach, Switzerland). Samples with an average weight of 8 mg were heated from 25 to 600 °C at a heating rate of 10 °C min^{-1}. All tests were carried out in nitrogen atmosphere with a constant nitrogen flow rate of 66 mL min^{-1}. The onset degradation temperature (T_0) was taken as the temperature for a mass loss of 5% and the maximum degradation rate (T_{max}) for each degradation stage was determined through the peaks in the first derivative from TGA curves.

Field emission scanning electron microscopy (FESEM)

Morphology of fractured surfaces from impact tests of neat PHB and ELO/ESBO-plasticized PHB was observed using FESEM (ZEISS ULTRA55, Oxford instruments), with an acceleration voltage of 2 kV. Prior to FESEM observation, all surfaces were sputter coated with a thin layer of platinum in a high-vacuum sputterer (EM MED020, Leica Microsystems) in order to make the samples electrically conductive.

Dynamic mechanical thermal analysis (DMTA)

DMTA in torsion mode of neat PHB and plasticized PHB was conducted between –50 to 80 °C at a heating rate of 2 °C min^{-1} using an oscillatory rheometer (AR G2, TA Instruments, New Castle, USA). Samples of size 40×10×4 mm^3 were subjected to the abovementioned thermal programme at a frequency of 1 Hz and a maximum deformation (γ) of 0.1%. The storage modulus (G') and the damping factor (tan δ) were measured in

terms of increasing temperature and the glass transition temperature (T_g) was taken at the point at which the tan δ peak reaches its maximum value.

RESULTS AND DISCUSSION

Mechanical properties of ELO/ESBO-plasticized PHB

The effect of the plasticizer type (ELO or ESBO) and content (0–20 phr) can be observed in Figure IV.1.1. The evolution of tensile mechanical properties is one of the most used indicators to assess plasticization. As can be seen, as the plasticizer content (both ELO and ESBO) increases, both tensile strength and Young's modulus decrease. Some authors have reported a similar tendency with regard to the tensile strength and Young's modulus in several polymers plasticized with ELO and ESBO [38, 44, 48]. On the other hand, we observe a slight increase in elongation at break when PHB is plasticized with ELO. As seen in Figure IV.1.1, the maximum decrease in tensile strength is obtained for the PHB/ESBO system; in particular, the tensile strength of unplasticized PHB changes from 24.1 to 15.4 MPa for an ESBO increase of 16.6 wt% (from 0 to 20 phr) which represents a decrease of about 36% in tensile strength. Regarding the PHB/ELO system, the tensile strength reduces to 16.2 MPa for an ELO content of 20 phr (representing a decrease of 33%). With regard to elongation at break, it can be observed that the plasticized PHB has different behavior depending on the plasticizer type and content. In the case of ELO-plasticized PHB a slight increase from 9.7% (unplasticized PHB) to 13.6% for an ELO content of 10 phr can be observed which represents an increase of about 40%. Higher ELO content leads to lower elongation at break, thus indicating that maximum plasticization effect can be achieved for an ELO content of around 10 phr as observed in Figure IV.1.1c. This could be related to plasticizer saturation at this composition, so that higher plasticizer load leads to phase separation with a marked effect on ductile properties. Seydibeyoğlu *et al.* [44] also demonstrated that the optimum epoxy soyate (the esterified form of ESBO) concentration in a PHBV matrix was located at around 10 wt%. The PHB/ESBO system follows different behavior and, although some plasticization effect can be observed through the evolution of tensile strength (Figure IV.1.1a), the elongation at break is not improved; in fact, a very slight decrease in elongation at break is detected with a change from 9.7% for unplasticized PHB to about 8.5–9.0%. This behavior is different from that observed in previous works in which an increase in flexibility was achieved with ESBO addition and, subsequently, elongation at break was improved in different polymers such as PHBV, PLA or PBS. Choi and Park [45] reported a slight increase in elongation at break in PHBV on addition of 30 wt% ESBO plasticizer. Similar trend was observed by Xu and Qu [48] achieving 63% higher

elongation at break values on addition of 9 wt% ESBO, while Zhao *et al.* [38] achieved markedly high values of elongation at break of 1400% on the addition of 5 wt% ESBO to PBS. With regard to Young's modulus, it is important to note that it follows the same tendency as tensile strength for both systems: as the plasticizer content increases (ELO and ESBO), Young's modulus decreases. It is worth noting that Young's modulus represents the ratio between the stress and the elongation in the linear region. As indicated, the tensile strength decreases in a marked way with plasticizer content while the elongation at break follows different behavior: slight increase for the PHB/ELO system for 10 phr ELO and a very slight decrease for the PHB/ESBO system. As Young's modulus represents the stress to elongation ratio, its value is lower due to lower stress values and slightly higher (or equal) elongation values. Young's modulus of unplasticized PHB is located at about 1872 MPa and the addition of both ELO and ESBO leads to lower values located at 1400 and 1550 MPa, respectively. Increasing ELO and ESBO load up to 20 phr leads to values of around 1350 MPa for both systems. By observing mechanical properties, we can conclude that ESBO is not as good as ELO for PHB plasticization as, even with a decrease in tensile strength and Young's modulus, the elongation at break is not improved. With regard to ELO, it also provides a decrease in tensile strength and modulus with increasing load but the most important parameter is the 40% increase in elongation at break for 10 phr ELO. The greater effectiveness of ELO versus ESBO as plasticizer for PHBV was reported by Seydibeyoğlu *et al.* [44].

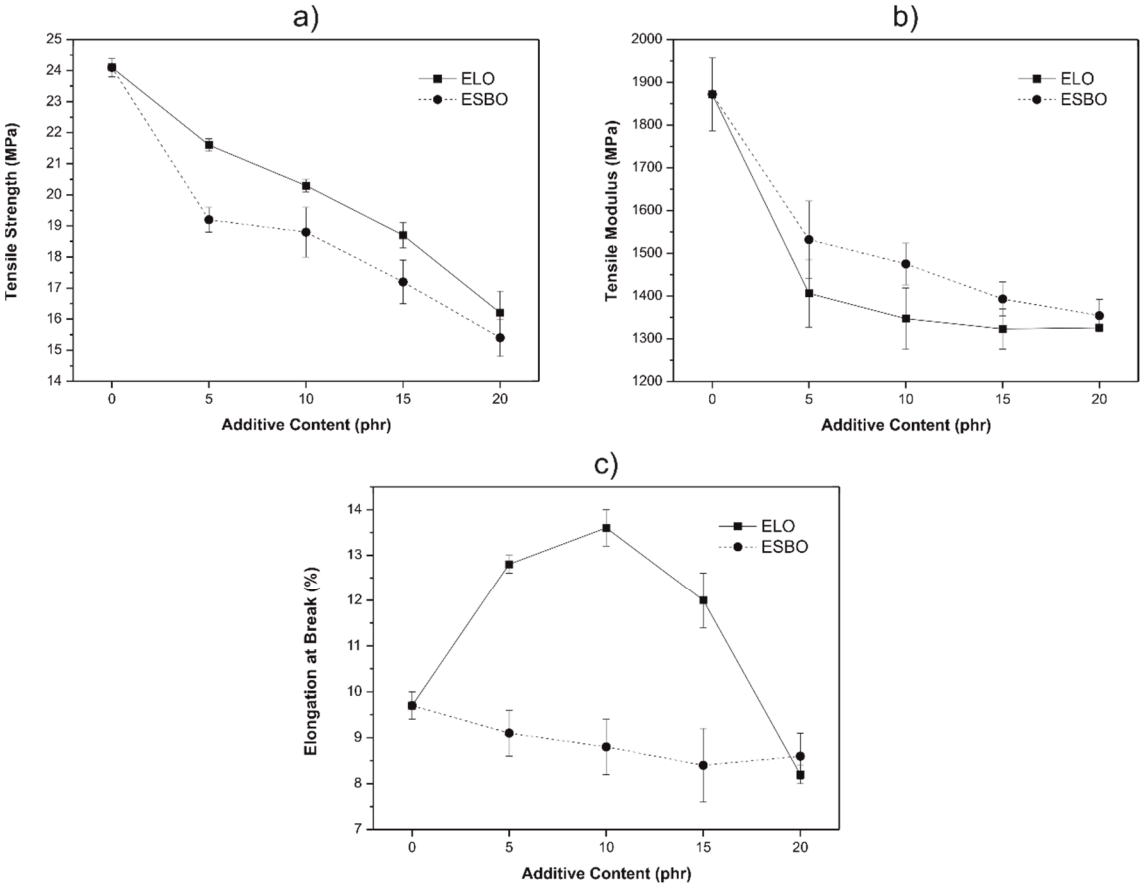

Figure IV.1.1. Effect of biobased plasticizers ELO and ESBO and their content on mechanical properties of PHB: (a) tensile strength; (b) tensile modulus; (c) elongation at break.

Figure IV.1.2 shows the evolution of the impact absorbed energy (Charpy) and Shore D hardness values for both PHB/ESBO and PHB/ELO systems. Impact results (Figure IV.1.2a) confirm the efficiency of ELO as plasticizer for PHB with a slight increase in the absorbed energy for 5–10 phr ELO from 2.1 to around 3 kJ m^{-2} (increase of about 40%). Once again, over 10 phr ELO, the impact energy decreases, thus indicating that plasticizer saturation occurs. Nevertheless, Seydibeyoğlu *et al.* [44] showed that addition of 10 wt% ELO to PHBV matrix did not affect the impact absorbed energy that remained almost constant. With regard to the PHB/ESBO system, the impact energy remains almost constant as observed in Figure IV.1.2a. Low plasticizer content up to 5 phr ESBO provides a very slight increase in impact energy but, in general terms, ESBO addition leads to invariable impact energy values. Choi and Park [45] reported that the highest impact absorbed energy for PHBV was reached after addition of 30 wt% ESBO. Similar findings were reported by Seydibeyoğlu *et al.* [44] by using 20 wt% epoxy soyate to achieve maximum impact absorbed energy values on PHBV. Regarding Shore D hardness values, Figure IV.1.2b shows

the evolution in terms of the plasticizer type (ELO and ESBO) and content. As can be seen, the addition of both ELO and ESBO leads to softer materials with decreasing hardness as the plasticizer content increases. Nevertheless, the best efficiency can be observed for ELO as the Shore D hardness values are less than those obtained with ESBO for each composition. These results are in total agreement with previous mechanical characterization, thus indicating the high efficiency of ELO versus ESBO for PHB plasticization.

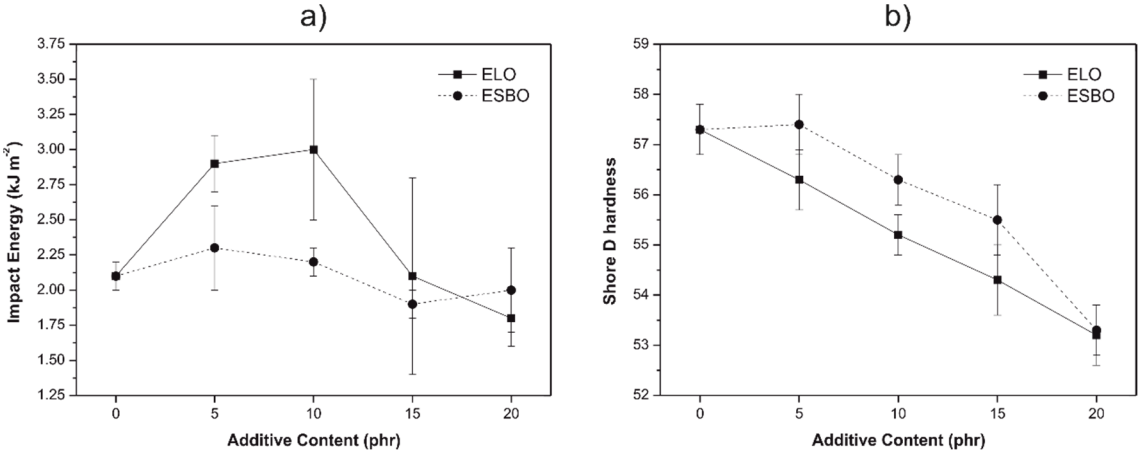

Figure IV.1.2. Effect of biobased plasticizers ELO and ESBO and their content on (a) impact energy and (b) Shore D hardness of PHB.

Thermal properties of ELO/ESBO-plasticized PHB

The influence of both biobased plasticizers, ELO and ESBO, on the thermal properties of PHB was investigated using DSC. Table IV.1.1 summarizes results for melt enthalpy (ΔH_m) and percentage crystallinity (X_c) for different plasticizer formulations. The melt peak of unplasticized PHB is located at 174.8 °C; a very small peak can also be detected at 52.3 °C which can be attributed to a low-molecular-weight additive in the commercial PHB formulation [53]. On the other hand, T_g of PHB is located at *ca* –2.2 °C and it could not be detected in a clear way using DSC, so that it was determined using DMTA. With regard to DSC behavior of ELO/ESBO-plasticized PHB formulations we observe the same melt peaks described before for neat PHB, but it is worth noting a slight decrease in the corresponding values with a change from 174.8 °C (neat PHB) to 171.2 °C (PHB with 10 phr ELO) and 172.2 °C (PHB with 10 phr ESBO). This is related to an increase in chain mobility with added plasticizer. This same behavior has been reported by other authors that employed epoxidized vegetable oils as plasticizers for biodegradable polymers. Seydibeyoğlu *et al.* [44] observed that 10 wt% of ELO or ESBO led to a decrease in the melt temperature of

about 5 °C with regard to neat PHBV, the decrease being slightly greater using ELO. Ali *et al.* [54] also observed a decrease in the melt temperature of neat PLA from 166.8 to 161.8 °C on addition of 30 phr ESBO. The normalized ΔH_m values of the various plasticized PHB formulations were used to calculate the percentage crystallinity of each formulation as the crystallinity plays an important role in mechanical properties. As can be seen from Table IV.1.1, addition of both ELO and ESBO leads to a slight decrease in crystallinity from 51.9% (unplasticized PHB) to about 46–47% for ELO-plasticized PHB and 47–48% for ESBO-plasticized PHB. The decrease in crystallinity is directly linked to a decrease in mechanical resistant properties as observed previously with tensile strength, Young's modulus and Shore D hardness. Once again, it is evident that the best performance is shown by ELO versus ESBO as plasticizer for PHB as the melt peak and the crystallinity provided by ELO are slightly lower than those provided by ESBO.

Table IV.1.1. Thermal parameters of ELO/ESBO-plasticized PHB obtained using DSC.

Sample (PHB/Plasticizer type/phr)	**DSC Parameters**			
	$T_{m\ PHB}$ **(°C)**	$\Delta H_{m\ PHB}$[a] **(J g^{-1})**	$\Delta H_{m\ PHB}$[b] **(J g^{-1})**	$X_{c\ PHB}$ **(%)**
PHB	174.8	–75.8	–75.8	51.9
PHB/ELO/5	172.5	–65.3	–68.6	47.0
PHB/ELO/10	171.2	–61.4	–67.5	46.3
PHB/ESBO/5	172.7	–66.1	–69.4	47.5
PHB/ESBO/10	172.2	–63.3	–69.6	47.7

[a] Values obtained directly from DSC.

[b] Normalized values with respect to the real polymer mass weight.

Thermal degradation of unplasticized PHB and ELO/ESBO-plasticized PHB was studied using TGA. Figure IV.1.3 shows a comparative plot of the TGA curves and derivative curves (DTG) for ELO- and ESBO-plasticized PHB with 5 and 10 phr, as these values are those that can provide attractive plasticized properties as observed in the previous characterization. The main thermal degradation parameters such as onset degradation temperature (T_0), first-stage maximum degradation rate temperature (T_{max1}) and second-stage maximum degradation rate temperature (T_{max2}) are summarized in Table IV.1.2. As can be observed in Figure IV.1.3a, PHB thermal degradation occurs in two main steps which can be clearly identified in the DTG curves by the presence of two different peaks. This is

due to the fact that commercial PHB contains a complex formulation to make it useful at an industrial level so that it contains small amounts of plasticizers, nucleating agents, fillers and stabilizers [53]. The addition of both ELO and ESBO plasticizers leads to a noticeable improvement in the thermal stability. This improvement is achieved by the interaction of the epoxidized vegetable oil molecules and the polymer chains thus leading to the formation of a thin physical barrier on the surface which obstructs permeability of volatile products towards the exterior and this has a positive effect on thermal degradation delay [55]. In addition, it is important to remark that epoxidized vegetable oils confer improved thermal stability as they are able to scavenge acid groups by catalytic degradation during degradation thus leading to improved thermal stability as well as light and heat stability [4, 37, 56].

In the case of ELO-plasticized PHB we observe that the onset degradation temperature (T_0) of neat PHB increases in a marked way with plasticizer content, changing from 246.7 °C (unplasticized PHB) to 272.3 and 274.7 °C for an ELO content of 5 and 10 phr, respectively. With regard to the ESBO-plasticized system the maximum thermal stabilization is observed for an ESBO content of 5 phr with a degradation onset temperature of 277 °C. In accordance with this, the maximum degradation rate temperatures are also moved to higher values for both degradation stages. Using ELO/ESBO plasticizers the maximum degradation rate temperatures (T_{max1} and T_{max2}) are moved from 272.3 and 382 °C to values of 293 and 410 °C, respectively, for both ELO and ESBO with very slight changes with total plasticizer content.

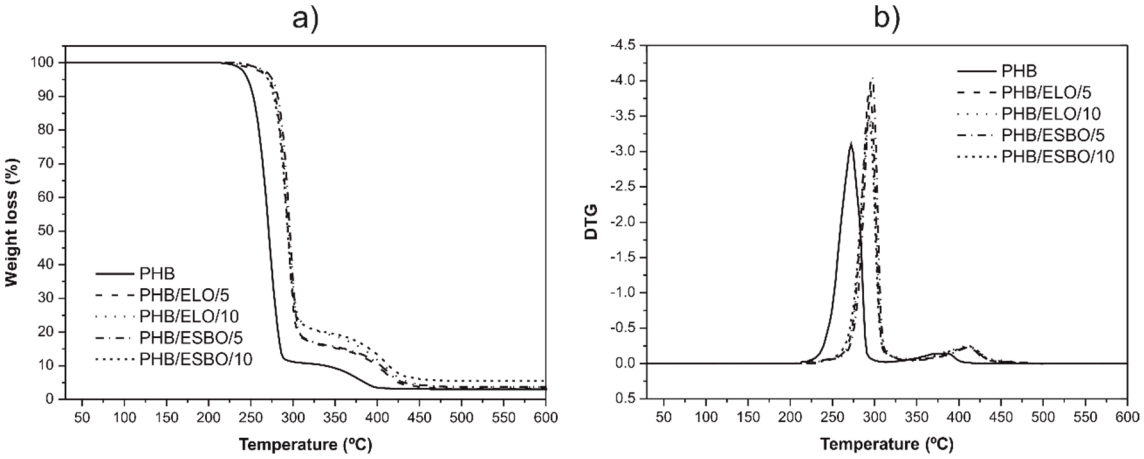

Figure IV.1.3. (a) TGA curves and (b) DTG curves of PHB formulations plasticized with biobased plasticizers ELO and ESBO.

Table IV.1.2. Characterization of thermal degradation process of ELO/ESBO-plasticized PHB obtained using TGA.

Sample (PHB/Plasticizer type/phr)	TGA Parameters		
	T_0[a] (°C)	T_{max1} (°C)	T_{max2} (°C)
PHB	246.7	272.3	382.0
PHB/ELO/5	272.3	293.3	410.0
PHB/ELO/10	274.7	293.3	410.0
PHB/ESBO/5	277.0	295.7	412.3
PHB/ESBO/10	272.3	293.3	410.0

[a] T_0, calculated at 5% mass loss.

Morphology of ELO/ESBO-plasticized formulations

FESEM was employed to characterize the morphology of PHB formulations plasticized with biobased ELO and ESBO. As can be seen in Figure IV.1.4a, PHB shows an irregular fracture surface with high roughness areas typical of a brittle behavior in addition to a porous morphology with many voids. In addition it is possible to observe different immiscible formations due to the chemical formulation of industrial PHB as observed in the thermal degradation [53]. Addition of 10 phr of both ELO and ESBO plasticizers promotes a slight change in surface morphology. FESEM images corresponding to PHB with 10 phr ELO (Figure IV.1.4b) and PHB with 10 phr ESBO (Figure IV.1.4c) show a softer topography with less pronounced fracture edges. Furthermore, all the voids seem to have disappeared and the plasticized structures have filled them leading to a more homogeneous fracture surface. Phase separation is not detectable as these compositions (mainly in the case of ELO plasticizer) give optimum results in terms of mechanical and thermal properties. Epoxidized vegetable oils containing epoxy groups are able to react with terminal hydroxyl groups (OH) of PHB through hydrogen bonds [3, 56]. The good ductile properties that can be achieved using ELO versus ESBO can be related to the stronger interactions that ELO can exert with PHB chains and end groups.

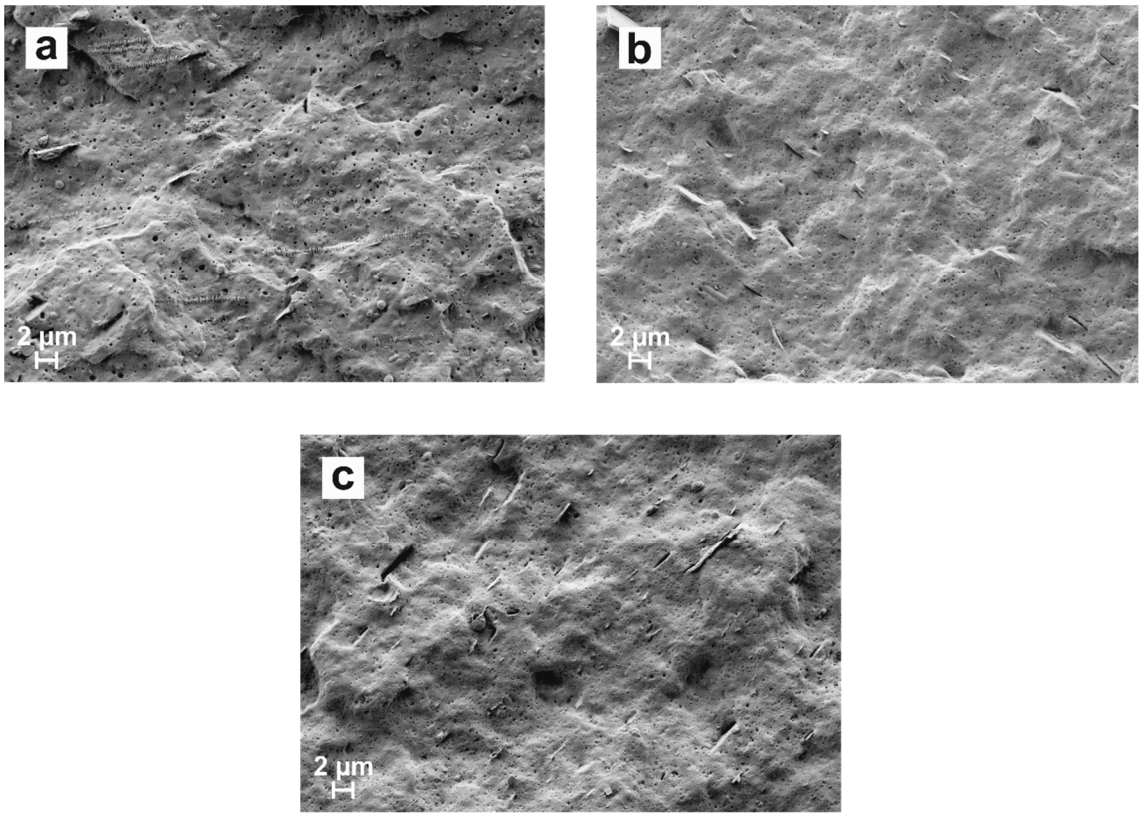

Figure IV.1.4. FESEM images (2000x) of fractured surface of ELO/ESBO-plasticized PHB formulations: (a) unplasticized PHB; (b) PHB with 10 phr ELO; (c) PHB with 10 phr ESBO.

Dynamic mechanical behavior of ELO/ESBO-plasticized PHB formulations

As the best plasticization system is obtained with ELO, dynamic mechanical properties of ELO-plasticized PHB formulations were determined. Figure IV.1.5 shows the evolution of the storage modulus (G') and the damping factor (tan δ) of unplasticized PHB and ELO-plasticized PHB with 5 and 10 phr ELO. As can be seen, G' decreases on addition of ELO plasticizer thus indicating the clear plasticization effect that ELO provides to the PHB matrix. The plasticizer promotes chain mobility and this has a positive effect on ductility and flexibility. In addition, the evolution of G' shows a small step in the range –5 to 0 °C which is attributed to T_g of PHB. The glass transition value can be more accurately determined through the peak of the damping factor (tan δ) as can be seen in Figure IV.1.5b. Clear evidence of the plasticization effect of a particular plasticizer is the reduction of T_g to lower values. The plasticizer increases the free volume and this makes polymer chain interactions of less intensity and promotes chain mobility with the subsequent reduction in T_g. As we can see, T_g of unplasticized PHB is close to –2.2 °C and it is reduced to almost –7 °C for an ELO content of 10 phr, thus indicating good miscibility with PHB in this composition range [55]. This decrease in T_g was previously observed by various authors

using epoxidized vegetable oils as biobased plasticizers for biodegradable polymers [38, 44, 45, 54].

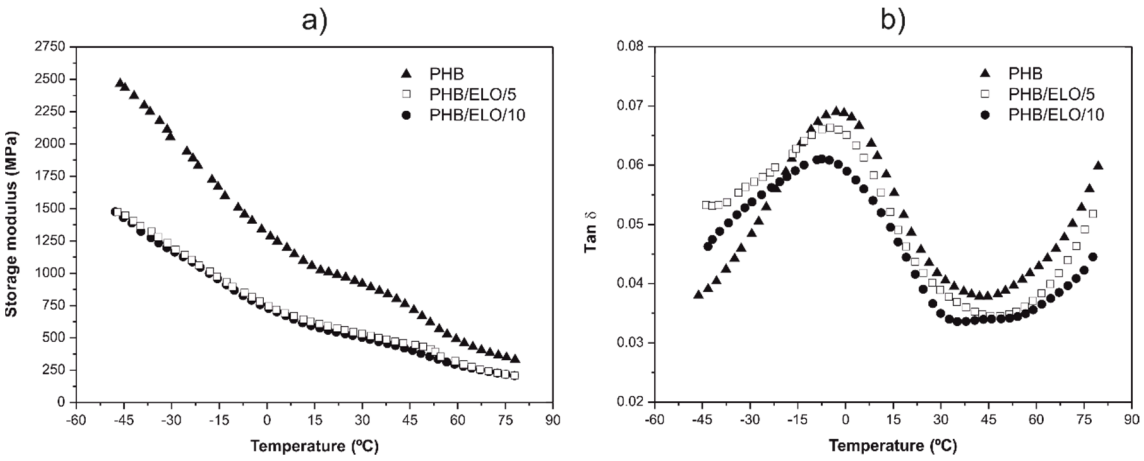

Figure IV.1.5. DMTA of ELO-plasticized PHB formulations with various plasticizer contents: (a) storage modulus (G') and (b) damping factor (tan δ) as a function of temperature.

CONCLUSIONS

In this work, new PHB industrial formulations were developed by the addition of biobased plasticizers from vegetable oils. ELO and ESBO were added at different loads in the range 0–20 phr to PHB to improve its low intrinsic ductility. Fragility and brittleness are two of the main weaknesses of PHB, but this work has found that addition of 10 phr ELO leads to a marked increase in elongation at break (increase of about 40%) with regard to neat/as-supplied PHB and this can widen industrial applications of PHB. Although ESBO plasticizer leads to a marked decrease in stiffness and tensile strength, it does not provide improved elongation at break so that it is not as efficient as ELO for PHB plasticization. DMTA also reveals that ELO addition promotes a decrease of T_g from –2 to –7 °C for an ELO content of 10 phr. Even though ESBO does not provide clear and evident plasticization properties, both ELO and ESBO provide a strong thermal stabilization effect with a marked increase in the onset degradation temperature from 246 to over 270 °C for ELO- and ESBO-plasticized PHB formulations, and this has a positive effect on processing/manufacturing as PHB is highly sensitive to thermal degradation even at moderate temperatures. Hence, we can conclude that addition up to 10 phr of ELO is an environmentally friendly, cost-effective and technical solution to overcome the high intrinsic fragility of PHB and widen its industrial applications.

ACKNOWLEDGEMENTS

This research was supported by the Ministry of Economy and Competitiveness (MINECO) [MAT2014-59242-C2-1-R]. The authors also thank the Conselleria d'Educació, Cultura i Esport – Generalitat Valenciana for financial support [GV/2014/008]. D. Garcia-Garcia thanks the Spanish Ministry of Education, Culture and Sports for financial support through an FPU grant [FPU13/06011].

REFERENCES

[1] Rhim JW, Park HM and Ha CS. *Bio-nanocomposites for food packaging applications*. Progress in Polymer Science, 2013. **38**(10-11):1629-1652.

[2] Bordes P, Pollet E and Avérous L. *Nano-biocomposites: Biodegradable polyester/nanoclay systems*. Progress in Polymer Science, 2009. **34**(2):125-155.

[3] Chieng BW, Ibrahim NA, Then YY and Loo YY. *Epoxidized vegetable oils plasticized poly(lactic acid) biocomposites: Mechanical, thermal and morphology properties*. Molecules, 2014. **19**(10):16024-16038.

[4] Silverajah VSG, Ibrahim NA, Yunus WMZW, Hassan HA and Woei CB. *A comparative study on the mechanical, thermal and morphological characterization of poly(lactic acid)/epoxidized palm oil blend*. International Journal of Molecular Sciences, 2012. **13**(5):5878-5898.

[5] Garcia-Garcia D, Ferri JM, Boronat T, Lopez-Martinez J and Balart R. *Processing and characterization of binary poly(hydroxybutyrate) (PHB) and poly(caprolactone) (PCL) blends with improved impact properties*. Polymer Bulletin, 2016. **73**(12):3333-3350.

[6] Arrieta MP, Samper MD, López J and Jiménez A. *Combined effect of poly(hydroxybutyrate) and plasticizers on polylactic acid properties for film intended for food packaging*. Journal of Polymers and the Environment, 2014. **22**(4):460-470.

[7] Safari S and van de Ven TGM. *Effect of crystallization conditions on the physical properties of a two-layer glassine paper/polyhydroxybutyrate structure*. Journal of Materials Science, 2015. **50**(10):3686-3696.

[8] Rousk J and Bååth E. *Growth of saprotrophic fungi and bacteria in soil*. FEMS Microbiology Ecology, 2011. **78**(1):17-30.

[9] Rath KM and Rousk J. *Salt effects on the soil microbial decomposer community and their role in organic carbon cycling: A review*. Soil Biology and Biochemistry, 2015. **81**:108-123.

[10] Mergaert J, Webb A, Anderson C, Wouters A and Swings J. *Microbial degradation of poly(3-hydroxybutyrate) and poly(3-hydroxybutyrate-co-3-hydroxyvalerate) in soils*. Applied and Environmental Microbiology, 1993. **59**(10):3233-3238.

[11] Boyandin AN, Prudnikova SV, Karpov VA, Ivonin VN, Đỗ NL, Nguyễn TH, Lê TMH, Filichev NL, Levin AL, Filipenko ML, Volova TG and Gitelson II. *Microbial degradation of polyhydroxyalkanoates in tropical soils*. International Biodeterioration & Biodegradation, 2013. **83:**77-84.

[12] Mergaert J, Anderson C, Wouters A and Swings J. *Microbial degradation of poly(3-hydroxybutyrate) and poly(3-hydroxybutyrate-co-3-hydroxyvalerate) in compost*. Journal of Environmental Polymer Degradation, 1994. **2**(3):177-183.

[13] Takaku H, Kimoto A, Kodaira S, Nashimoto M and Takagi M. *Isolation of a Gram-positive poly(3-hydroxybutyrate) (PHB)-degrading bacterium from compost, and cloning and characterization of a gene encoding PHB depolymerase of Bacillus megaterium N-18-25-9*. FEMS Microbiology Letters, 2006. **264**(2):152-159.

[14] Romen F, Reinhardt S and Jendrossek D. *Thermotolerant poly(3-hydroxybutyrate)-degrading bacteria from hot compost and characterization of the PHB depolymerase of Schlegelella sp. KB1a*. Archives of Microbiology, 2004. **182**(2-3):157-164.

[15] Mabrouk MM and Sabry SA. *Degradation of poly(3-hydroxybutyrate) and its copolymer poly(3-hydroxybutyrate-co-3-hydroxyvalerate) by a marine Streptomyces sp. SNG9*. Microbiological Research, 2001. **156**(4):323-335.

[16] Kasuya K, Mitomo H, Nakahara M, Akiba A, Kudo T and Doi Y. *Identification of a marine benthic P(3HB)-degrading bacterium isolate and characterization of its P(3HB) depolymerase*. Biomacromolecules, 2000. **1**(2):194-201.

[17] Reddy CSK, Ghai R, Rashmi and Kalia VC. *Polyhydroxyalkanoates: An overview*. Bioresource Technology, 2003. **87**(2):137-146.

[18] Philip S, Keshavarz T and Roy I. *Polyhydroxyalkanoates: Biodegradable polymers with a range of applications*. Journal of Chemical Technology and Biotechnology, 2007. **82**(3):233-247.

[19] Ruka DR, Sangwan P, Garvey CJ, Simon GP and Dean KM. *Biodegradability of poly-3-hydroxybutyrate/bacterial cellulose composites under aerobic conditions, measured via evolution of carbon dioxide and spectroscopic and diffraction methods*. Environmental Science & Technology, 2015. **49**(16):9979-9986.

[20] Arrieta MP, López J, Hernández A and Rayón E. *Ternary PLA-PHB-Limonene blends intended for biodegradable food packaging applications*. European Polymer Journal, 2014. **50**:255-270.

[21] Holmes PA. *Applications of PHB – A microbially produced biodegradable thermoplastic*. Physics in Technology, 1985. **16**(1):32-36.

[22] Wei L, Liang S and McDonald AG. *Thermophysical properties and biodegradation behaviour of green composites made from polyhydroxybutyrate and potato peel waste fermentation residue*. Industrial Crops and Products, 2015. **69**:91-103.

[23] Wang L, Zhu W, Wang X, Chen X, Chen GQ and Xu K. *Processability modifications of poly(3-hydroxybutyrate) by plasticizing, blending, and stabilizing*. Journal of Applied Polymer Science, 2008. **107**(1):166-173.

[24] Kurusu RS, Demarquette NR, Gauthier C and Chenal JM. *Effect of ageing and annealing on the mechanical behaviour and biodegradability of a poly(3-hydroxybutyrate) and poly(ethylene-co-methyl-acrylate-co-glycidyl-methacrylate) blend*. Polymer International, 2014. **63**(6):1085-1093.

[25] Janigová I, Lacík I and Chodák I. *Thermal degradation of plasticized poly(3-hydroxybutyrate) investigated by DSC*. Polymer Degradation and Stability, 2002. **77**(1):35-41.

[26] Doi Y, Kunioka M, Nakamura Y and Soga K. *Nuclear magnetic resonance studies on unusual bacterial copolyesters of 3-hydroxybutyrate and 4-hydroxybutyrate*. Macromolecules, 1988. **21**(9):2722-2727.

[27] Erceg M, Kovačić T and Klarić I. *Thermal degradation of poly(3-hydroxybutyrate) plasticized with acetyl tributyl citrate*. Polymer Degradation and Stability, 2005. **90**(2):313-318.

[28] Antunes MCM and Felisberti MI. *Blends of poly(hydroxybutyrate) and poly(ε-caprolactone) obtained from melting mixture*. Polímeros, 2005. **15**(2):134-138.

[29] Ma P, Hristova-Bogaerds DG, Lemstra PJ, Zhang Y and Wang S. *Toughening of PHBV/PBS and PHB/PBS blends via in situ compatibilization using dicumyl peroxide as a free-radical grafting initiator*. Macromolecular Materials and Engineering, 2012. **297**(5):402-410.

[30] Ma P, Xu P, Chen M, Dong W, Cai X, Schmit P, Spoelstra AB and Lemstra PJ. *Structure-property relationships of reactively compatibilized PHB/EVA/starch blends*. Carbohydrate Polymers, 2014. **108**:299-306.

[31] Choi JS and Park WH. *Effect of biodegradable plasticizers on thermal and mechanical properties of poly(3-hydroxybutyrate)*. Polymer Testing, 2004. **23**(4):455-460.

[32] Baltieri RC, Mei LHI and Bartoli J. *Study of the influence of plasticizers on the thermal and mechanical properties of poly(3-hydroxybutyrate) compounds*. Macromolecular Symposia, 2003. **197**(1):33-44.

[33] Fenollar O, Garcia-Sanoguera D, Sanchez-Nacher L, Lopez J and Balart R. *Effect of the epoxidized linseed oil concentration as natural plasticizer in vinyl plastisols*. Journal of Materials Science, 2010. **45**(16):4406-4413.

[34] Carbonell-Verdu A, Bernardi L, Garcia-Garcia D, Sanchez-Nacher L and Balart R. *Development of environmentally friendly composite matrices from epoxidized cottonseed oil*. European Polymer Journal, 2015. **63:**1-10.

[35] Tan CP and Man YBC. *Comparative differential scanning calorimetric analysis of vegetable oils: I. Effects of heating rate variation*. Phytochemical Analysis, 2002. **13**(3):129-141.

[36] Tan SG and Chow WS. *Biobased epoxidized vegetable oils and its greener epoxy blends: A review*. Polymer-Plastics Technology and Engineering, 2010. **49**(15):1581-1590.

[37] Prempeh N, Li J, Liu D, Das K, Maiti S and Zhang Y. *Plasticizing effects of epoxidized sun flower oil on biodegradable polylactide films: A comparative study*. Polymer Science Series A, 2014. **56**(6):856-863.

[38] Zhao Y, Qu J, Feng Y, Wu Z, Chen F and Tang H. *Mechanical and thermal properties of epoxidized soybean oil plasticized polybutylene succinate blends*. Polymers for Advanced Technologies, 2012. **23**(3):632-638.

[39] Bouchoul B, Benaniba MT and Massardier V. *Effect of biobased plasticizers on thermal, mechanical, and permanence properties of poly(vinyl chloride)*. Journal of Vinyl and Additive Technology, 2014. **20**(4):260-267.

[40] Sun B, Chaudhary BI, Shen CY, Mao D, Yuan DM, Dai GC, Li B and Cogen JM. *Thermal stability of epoxidized soybean oil and its absorption and migration in poly(vinylchloride)*. Polymer Engineering & Science, 2013. **53**(8):1645-1656.

[41] Wadhi MM and Weliam R. *Effect of epoxidized sunflower oil on polylactic acid properties*. Research on Chemical Intermediates, 2014. **40**(1):399-406.

[42] Bueno-Ferrer C, Garrigós MC and Jiménez A. *Characterization and thermal stability of poly(vinyl chloride) plasticized with epoxidized soybean oil for food packaging*. Polymer Degradation and Stability, 2010. **95**(11):2207-2212.

[43] Audic JL, Lemiègre L and Corre YM. *Thermal and mechanical properties of a polyhydroxyalkanoate plasticized with biobased epoxidized broccoli oil*. Journal of Applied Polymer Science, 2014. **131**(6):39983.

[44] Seydibeyoğlu MÖ, Misra M and Mohanty A. *Synergistic improvements in the impact strength and % elongation of polyhydroxybutyrate-co-valerate copolymers with functionalized soybean oils and POSS*. International Journal of Plastics Technology, 2010. **14**(1):1-16.

[45] Choi JS and Park WH. *Thermal and mechanical properties of poly(3-hydroxybutyrate-co-3-hydroxyvalerate) plasticized by biodegradable soybean oils*. Macromolecular Symposia, 2003. **197**(1):65-76.

[46] Jost V and Kopitzky R. *Blending of polyhydroxybutyrate-co-valerate with polylactic acid for packaging applications – Reflections on miscibility and effects on the mechanical and barrier properties*. Chemical and Biochemical Engineering Quarterly, 2015. **29**(2):221-246.

[47] Ren Z, Dong L and Yang Y. *Dynamic mechanical and thermal properties of plasticized poly(lactic acid)*. Journal of Applied Polymer Science, 2006. **101**(3):1583-1590.

[48] Xu YQ and Qu JP. *Mechanical and rheological properties of epoxidized soybean oil plasticized poly(lactic acid)*. Journal of Applied Polymer Science, 2009. **112**(6):3185-3191.

[49] Ferri JM, Samper MD, García-Sanoguera D, Reig MJ, Fenollar O and Balart R. *Plasticizing effect of biobased epoxidized fatty acid esters on mechanical and thermal properties of poly(lactic acid)*. Journal of Materials Science, 2016. **51**(11):5356-5366.

[50] Pachekoski WM, Dalmolin C and Agnelli JAM. *The influence of the industrial processing on the degradation of poly(hidroxybutyrate)-PHB*. Materials Research, 2013. **16**(2):327-332.

[51] Luo S, Grubb DT and Netravali AN. *The effect of molecular weight on the lamellar structure, thermal and mechanical properties of poly(hydroxybutyrate-co-hydroxyvalerates)*. Polymer, 2002. **43**(15):4159-4166.

[52] Špitalský Z, Lacík I, Lathová E, Janigová I and Chodák I. *Controlled degradation of polyhydroxybutyrate via alcoholysis with ethylene glycol or glycerol*. Polymer Degradation and Stability, 2006. **91**(4):856-861.

[53] Prakalathan K, Mohanty S and Nayak SK. *Reinforcing effect and isothermal crystallization kinetics of poly(3-hydroxybutyrate) nanocomposites blended with organically modified montmorillonite*. Polymer Composites, 2014. **35**(5):999-1012.

[54] Ali F, Chang YW, Kang SC and Yoon JY. *Thermal, mechanical and rheological properties of poly(lactic acid)/epoxidized soybean oil blends*. Polymer Bulletin, 2009. **62**(1):91-98.

[55] Silverajah VSG, Ibrahim NA, Zainuddin N, Yunus WMZW and Hassan HA. *Mechanical, thermal and morphological properties of poly(lactic acid)/epoxidized palm olein blend*. Molecules, 2012. **17**(10):11729-11747.

[56] Al-Mulla EAJ, Yunus WMZW, Ibrahim NAB and Rahman MZA. *Properties of epoxidized palm oil plasticized polytlactic acid*. Journal of Materials Science, 2010. **45**(7):1942-1946.

Research Article

Received: 2 February 2016 Revised: 5 May 2016 Accepted article published: 28 May 2016 Published online in Wiley Online Library: 15 June 2016

(wileyonlinelibrary.com) DOI 10.1002/pi.5164

Plasticization effects of epoxidized vegetable oils on mechanical properties of poly(3-hydroxybutyrate)

Daniel Garcia-Garcia,* Jose M Ferri, Nestor Montanes, Juan Lopez-Martinez and Rafael Balart

Abstract

The effect of various epoxidized vegetable oils as potential plasticizers for poly(3-hydroxybutyrate) (PHB) was evaluated in terms of changes in mechanical and thermal properties and morphology. PHB is a biodegradable aliphatic polyester obtained from bacterial fermentation. High stiffness and fragility are two of its main drawbacks. To overcome this behaviour, PHB was plasticized with various amounts of two different epoxidized vegetable oils: epoxidized linseed oil (ELO) and epoxidized soybean oil (ESBO). The total ELO and ESBO content varied in the range 5 phr (per hundred resin) to 20 phr and plasticized PHB materials were obtained by melt extrusion and compounding followed by injection moulding. The results show that the plasticizing effect provided by ELO is more efficient than that by ESBO with balanced properties at a concentration of 10 phr ELO. ELO addition leads to an improvement in mechanical ductile properties with a noticeable increase in elongation at break and impact absorbed energy. With regard to thermal properties, the addition of both ELO and ESBO leads to a marked increase in thermal stability of PHB. All these findings suggest that addition of 10 phr ELO leads to optimized PHB formulations with potential uses in technical applications.

Keywords: poly(3-hydroxybutyrate) (PHB); epoxidized soybean oil (ESBO); epoxidized linseed oil (ELO); plasticization; biodegradable

INTRODUCTION

Recent decades have witnessed a remarkable increase in the production and consumption of plastic materials, mainly from petroleum origin, such as polyethylene, polypropylene, poly(ethylene terephthalate), polystyrene, etc., that covers a wide range of properties that make them useful for diverse industrial sectors. Nevertheless, one important weakness of these petroleum-based polymers is that most of them are not biodegradable. Packing and packaging industries use large amounts of plastic materials and their products are characterized by a relatively short life cycle, and consequently a huge amount of non-biodegradable plastics is continuously generated with subsequent environmental impact. The increase in environmental concerns related to waste generation has led to an increased interest in the study and development of polymers that can undergo total degradation/decomposition under appropriate temperature and moisture conditions. This has a positive effect on the environment as it avoids generation of harmful and potentially toxic wastes.[1] These polymers, also known as biopolymers, can be classified into four different groups depending on the production process and the origin of the base material or monomer. One group includes all polymers obtained directly from biomass such as cellulose, starch, alginate, gluten, etc. Another group consists of all polymeric materials obtained by chemical synthesis from monomers derived from renewable resources as is the case for poly(lactic acid) (PLA). The third group is represented by those polymers that, although they are obtained from fossil and non-renewable resources, can undergo degradation/decomposition due to their particular chemical structure as is the case for some petroleum-derived polyesters, e.g. polycaprolactone, poly(butylene succinate) (PBS), poly[(butylene adipate)-*co*-terephthalate], etc. Finally, some biodegradable polymers can be obtained from bacterial fermentation such as polyhydroxyalkanoates.[2] Therefore, the use of biodegradable polymers is one of the main alternatives for reducing the large amounts of wastes with a subsequent reduction of their environmental impact.[3,4]

Poly(3-hydroxybutyrate) (PHB) is one of the best known polyhydroxyalkanoates.[5] PHB is an aliphatic polyester obtained from controlled bacterial fermentation and is characterized by its intrinsic biodegradability and biocompatibility.[6,7] PHB is readily biodegradable in such environments where the combination of nitrogen, phosphates, salts, moisture and temperature allows microorganism growth.[8,9] These microorganisms use PHB polymer chains as nutrients. For this reason, PHB degradation can occur in various environments such as soil,[10,11] compost[12–14] and marine sediments.[15,16] Otherwise, PHB can remain almost intact for long periods. PHB biodegradation depends on several factors such as microbial activity of the environment, moisture,

* *Correspondence to: D Garcia-Garcia, Instituto de Tecnología de Materiales (ITM), Universitat Politècnica de València (UPV), Plaza Ferrándiz y Carbonell 1, 03801 Alcoy, Alicante, Spain. E-mail: dagarga4@epsa.upv.es*

Instituto de Tecnología de Materiales (ITM), Universitat Politècnica de València (UPV), Plaza Ferrándiz y Carbonell 1, 03801 Alcoy, Alicante, Spain

IV.2

"Improvement of mechanical ductile properties of poly(3-hydroxybutyrate) by using vegetable oil derivatives"

Daniel García García[a], *Octavio Fenollar*[a], *Vicent Fombuena*[a], *Juan López Martínez*[a], *Rafael Balart*[a]

[a] Instituto de Tecnología de Materiales (ITM)
Universitat Politècnica de València (UPV)
Plaza Ferrándiz y Carbonell 1, 03801 Alcoy, Alicante, Spain.

Macromolecular Materials and Engineering

2017, 302:1600330

Improvement of mechanical ductile properties of poly(3-hydroxybutyrate) by using vegetable oil derivatives

Abstract

Poly(3-hydroxybutyrate) (PHB) is a thermoplastic polyester synthesized from bacterial fermentation with potential uses in packaging due to its biodegradability. Nevertheless, PHB is a fragile material and its processing temperature window is very narrow which restricts its use. This study explores the potential of vegetable oil-derived plasticizers, *i.e.*, maleinized linseed oil (MLO) and an epoxidized fatty acid ester (EFAE) in the 5–20 phr range as environmentally friendly solutions for PHB industrial formulations with improved toughness. The results show that optimum balance between ductile properties is achieved with low plasticizer content (5 phr) for both plasticizer types. Elongation at break and the impact resistance are increased by 28 and 71% respectively after addition of 5 phr MLO. With regard to EFAE, the elongation at break is improved by 40% and the impact resistance is increased to twice the value of PHB. Another effect that both plasticizers provide is the thermal stabilization with a delay in the onset degradation temperature.

Keywords: Biodegradable; compatibility; mechanical properties; plasticizer; poly(3-hydroxybutyrate).

INTRODUCTION

Polymer materials have become an essential part of our lifestyle due to a wide range of advantages they can offer. A wide range of commodity, engineering and high performance plastics are currently used. Moreover, new polymers are continuously being synthesized thus widening the potential of these materials. With the recent development of nanotechnologies, *in situ* polymerization with nanomaterials, widens new and useful applications of polymers in different sectors [1, 2]. Advances in polymer colloids has also gained increasing interest due to their potential in combination with nanotechnologies [3-5]. For these reasons, the use of both conventional and new ad hoc synthesized polymers is continuously increasing. Subsequently, million tons of plastic wastes are generated every year with a remarkable negative effect on environment contamination [6]. This fact, together with the petroleum depletion has led to a growing interest in research on environmentally friendly polymers with the main aim of obtaining low environmental impact materials with similar physical and chemical properties to those of conventional petroleum-based polymer such as polyethylene, polypropylene or others [7-9]. These environmentally friendly polymers include those obtained from renewable resources as it is the case of poly(lactic acid) (PLA), lignin, thermoplastic starch, cellulose, chitosan, proteins (gluten, casein, ovalbumin, etc.), bacterial polymers, etc., with an evident positive effect on the carbon footprint. Some other polymers obtained from petroleum resources such as poly(caprolactone), poly(butylene succinate), poly(vinyl alcohol), poly(glycolic acid), etc., can also be considered as environmentally friendly as they can undergo disintegration in compost soil thus giving solution to waste accumulation [10]. Among the wide variety of environmentally friendly polymers, poly(3-hydroxybutyrate) (PHB) is one of the most promising ones because of its excellent balanced properties such as disintegration in compost soil, biocompatibility, UV light resistance, mechanical features similar to polypropylene, etc. [11, 12]. All these features make PHB an excellent candidate for biomedicine applications [13, 14] or disposable products from the packaging industry [15, 16]. PHB is one of the best well-known polymers pertaining to polyhydroxyalkanoates [17]. It is a crystalline thermoplastic aliphatic polyester that can be synthesized from different bacteria species as energy reserves [18, 19]. PHB offers a high melt temperature in the 175–180 °C range and a high crystallinity that can be higher than 55% [20, 21]. Additionally, it degrades to carbon dioxide and water by natural microbial mineralization [6]. However, its extensive use at industrial scale is restricted because of some drawbacks. One of these is its relatively narrow processing window as its thermal degradation occurs at temperatures slightly higher to the melt temperature. Temperatures over 190 °C as well as high residence time give rise to a quick thermal degradation on PHB [22]. Thermal

degradation of PHB results in chain scission which leads to a rapid decrease in the molecular weight and this has a negative effect on its overall properties [20]. On the other hand, one important drawback of PHB is its high stiffness which results in a high fragile polymer due to its high crystallinity [23]. Moreover, PHB undergoes physical aging due to post-crystallization processes at room temperature during the storage, which lead to irregular pores formation on the surface [24, 25]. Therefore, flexibility of polymer chains in amorphous domains is restricted and this has a negative effect on elongation at break [26-29]. Finally, at present, the production costs of PHB are still higher compared to other environmentally friendly polymers and most commodity petroleum-based plastics [30].

One of the main routes to overcome the abovementioned drawbacks is external plasticization that is a relatively simple and cost-effective way to improve some mechanical and thermal properties of raw PHB [31]. Wang *et al.* [27] observed a remarkable increase in ductility by addition of commercial plasticizers such as acetyl tributyl citrate (ATBC). Both the glass transition temperature (T_g) and the melt peak temperature (T_m) were moved to lower temperatures and the optimum plasticizer content was obtained for 30 wt%. They also reported an increase in the degradation onset temperature (T_0). Similar tendency was observed by Baltieri *et al.* [32] with several commercial plasticizers, *i.e.*, dioctyl phthalate (DOP), dioctyl adipate (DOA), triacetyl glycerol (TAG) and polyadipate (PA). They reported the best results for formulations containing 30 wt% TAG and PA with a noticeable decrease in both T_g and T_m and a remarkable improvement in elongation at break by 123 and 51% for TAG and PA formulations respectively. Fernandes *et al.* [33] proved the effectiveness of poly(ethylene glycol) (PEG) and tri(ethylene glycol) bis(2-ethylhexanoate) (TEGB) as plasticizers for poly(3-hydroxybutyrate) (PHB) formulations with a noticeable decrease in T_g from 1 °C of neat PHB to –23 °C for plasticized formulations with PEG and TEGB. Similar tendency was observed for the melt process. With regard to the thermal stability, they reported a slight decrease in the onset degradation temperature for PEG while thermal stability did not change with TEGB.

Use of plasticizers from natural sources is of great interest from an environmental point of view and could represent a feasible alternative to petroleum-based plasticizers [34]. These natural-origin plasticizers are still more interesting for environmentally friendly polymers as they allow to obtain fully compostable formulations. In the last years it has been reported the effectiveness of some vegetable oil-derived plasticizers (epoxidized vegetable oils, maleinized vegetable oils) as plasticizers for some compostable polymers with a remarkable increase in toughness and thermal stability [31, 35-41]. Moreover, these plasticizers show some additional advantages that make them still more interesting for

industrial formulations for different reasons: they are obtained from renewable resources, they have been reported to be disintegrable in compost soil, they are more respectful with environment than conventional petroleum-based plasticizers, they are readily available at large-scale and finally, they can be obtained in huge amounts at cost-effective prices [35]. Currently, these epoxidized vegetable oils are widely used as secondary plasticizers and stabilizers for industrial polyvinyl chloride (PVC) formulations [42-44]. Other uses in engineering applications include biodegradable lubricants, polyol production and manufacturing of environmentally friendly polyurethane foams [45-50].

The aim of this work is to improve the low intrinsic toughness of PHB to widen its industrial applications by melt extrusion plasticization with two different vegetable oil-derived plasticizers, *i.e.*, maleinized linseed oil (MLO) and an epoxidized fatty acid ester (EFAE). The effect of these two biobased plasticizers and their content on PHB formulations is evaluated in terms of mechanical and thermal properties as well as blends morphology.

EXPERIMENTAL

Materials

The PHB polymer used in this study was a commercial grade P226 supplied by Biomer (Krailling, Germany). This grade possesses a molecular weight (M_w) of 460,000 g mol^{-1}, a density of 1.25 g cm^{-3} and a melt flow index of 10 g $(10\ min)^{-1}$ measured at a temperature of 180 °C and a load of 5 kg. Two biobased plasticizers derived from vegetable oils were used: an MLO Veomer LIN supplied by Vandeputte (Mouscron, Belgium) with a viscosity of 1000 cP at 20 °C and an acid value between 105 and 130 mg KOH g^{-1} and an EFAE (octyl epoxy stearate), tradename "Plasticizer 201" supplied by Traquisa S.L. (Barcelona, Spain) with a viscosity of 20–30 cP at 20 °C, a molecular weight of 408 g mol^{-1}, an epoxy equivalent weigh of 484.8 g $equiv^{-1}$ and an oxirane number comprised in the 3.1–3.3% range (ASTM D1652).

Sample preparation

Initially, PHB pellets were dried at 70 °C for 24 h in an air-circulating oven with the aim of removing the residual moisture contained because polyesters are highly sensitive to hydrolysis. After this initial stage, different plasticized PHB formulations were prepared with MLO and EFAE as summarized in Table IV.2.1. PHB pellets were mechanically mixed with the plasticizers used in different amounts in a zipper bag and subsequently

compounded in a twin screw co-rotating extruder with *D* = 25 mm and *L/D* ratio of 24 at a rotating speed of 40 rpm. The temperature profile was set to 165 °C (hopper), 170 °C, 175 °C and 180 °C (die) and after cooling to room temperature, the extruded materials were pelletized. Standard samples for tensile tests according to ISO 527 and impact tests as recommended in ISO 179 were molded using an injection molding machine Meteor 270/75 from Mateu & Solé S.A. (Barcelona, Spain). The temperature profile was set to 160 °C, 165 °C, 170 °C, 175 °C and 180 °C from the hopper to the injection nozzle and the cooling time was set to 10 s.

Table IV.2.1. Composition and coding of plasticized PHB formulations with MLO and EFAE.

Code	PHB content (parts by weight/wt%)	MLO content (parts by weight/wt%)	EFAE content (parts by weight/wt%)
PHB	100/100	-	-
PHB/MLO/5	100/95.2	5/4.8	-
PHB/MLO/10	100/90.9	10/9.1	-
PHB/MLO/15	100/87.0	15/13.0	-
PHB/MLO/20	100/83.3	20/16.7	-
PHB/EFAE/5	100/95.2	-	5/4.8
PHB/EFAE/10	100/90.9	-	10/9.1
PHB/EFAE/15	100/87.0	-	15/13.0
PHB/EFAE/20	100/83.3	-	20/16.7

Characterization techniques

Mechanical properties

Tensile properties of neat PHB and plasticized PHB formulations were determined at room temperature using an electromechanical universal test machine Ibertest ELIB 30 from S.A.E. Ibertest (Madrid, Spain), following ISO 527. A 5 kN load cell and a crosshead speed of 5 mm min^{-1} were used. In addition, an axial extensometer from S.A.E. Ibertest (Madrid, Spain) was coupled to accurately measure the tensile modulus. At least five different samples were tested for each material and average values of tensile strength and tensile modulus were calculated.

The fracture toughness was evaluated using the Charpy's test in a 1 J pendulum from Metrotec S.A. (San Sebastián, Spain) according to ISO 179 standard. Five different notched samples ("V" notch type at 45°; notch radius = 0.25 mm) for each plasticized PHB formulation were tested and average values of impact resistance were calculated.

Shore D hardness values were measured with a Shore D hardness durometer model 676-D from Instruments J. Bot S.A. (Barcelona, Spain) as recommended by the ISO 868. At least five different measurements were obtained at room temperature and average values were calculated.

Thermal properties

Thermal properties of neat PHB and plasticized PHB formulations with MLO and EFAE were characterized by thermogravimetry (TGA) and differential scanning calorimetry (DSC). DSC analysis was conducted in a DSC 821 calorimeter by Mettler-Toledo Inc. (Schwerzenbach, Switzerland) under nitrogen atmosphere at a flow rate of 66 mL min^{-1}. Samples (7–9 mg) were first heated from −50 to 180 °C and held isothermally at 180 °C during 2 min in order to remove any prior thermal history resulting from previous processing by extrusion and injection molding (1st heating). Subsequently, samples were cooled down to −50 °C and then, finally reheated to 300 °C (2nd heating). The heating rate for all steps was 10 °C min^{-1}. Melting parameters, *i.e.*, melt temperature (T_m) and melt enthalpy (ΔH_m) were determined as the peak temperature and the area of the melting endotherm from the second heating respectively. The degree of crystallinity of PHB ($X_{c\ PHB}$) in all formulations was calculated using the following equation:

$$\boldsymbol{X_c}\ (\%) = \left[\frac{\Delta \boldsymbol{H_m}}{\Delta \boldsymbol{H_0} \cdot \boldsymbol{w}}\right] \times \mathbf{100} \qquad \textbf{Equation IV.2.1}$$

were ΔH_m is the melt enthalpy taken from the 2nd heating in DSC runs, ΔH_0 is the melt enthalpy of 100% crystalline PHB (theoretical value of 146 J g^{-1} [51]) and w is the weight fraction of PHB in each formulation.

Thermal stability of plasticized PHB formulations at high temperatures was assessed using a TGA/SDTA 851 thermobalance by Mettler-Toledo Inc. (Schwerzenbach, Switzerland) with a temperature program from 25 to 600 °C at a constant heating rate of 10 °C min^{-1} and continuous nitrogen flow rate of 66 mL min^{-1}. The degradation onset temperature (T_0) was determined as the temperature corresponding to a weight loss of 5%.

All DSC and TGA tests were run in triplicate to obtain reliable thermal properties. Average values and statistical errors of the main thermal parameters were calculated.

Field emission scanning electron microscopy (FESEM)

Fractured surfaces from impact tests of neat PHB and plasticized PHB formulations were studied using FESEM in a ZEISS ULTRA55 microscope from Oxford instruments (Oxfordshire, United Kingdom) with an acceleration voltage of 2 kV. In order to observe the samples, it was necessary to coat them with a thin layer of platinum in a high vacuum sputter coatter EM MED020 from Leica Microsystems (Milton Keynes, United Kingdom).

Thermo-mechanical properties

The effect of temperature on mechanical properties of neat PHB and plasticized PHB formulations with different plasticizer type and amount was assessed by dynamic mechanical thermal analysis (DMTA), Vicat softening temperature (VST) and heat deflection temperature (HDT). DMTA was studied in the temperature range comprised between −50 and 80 °C using an oscillatory rheometer AR G2 by TA Instruments (New Castle, USA) equipped with a special clamp system for solid samples working in torsion mode. Rectangular samples sizing 40×10×4 mm^3 were subjected to a temperature sweep at a constant heating rate of 2 °C min^{-1}. The frequency of the dynamic force was set to 1 Hz and a maximum shear strain (γ) of 0.1% was used in all tests. The evolution of the storage modulus (G') and the damping factor (tan δ) was analyzed in terms of increasing temperature. As the damping factor (tan δ) represents the ratio between the loss modulus (G'') and the storage modulus (G'), its evolution with temperature contains both viscous (lost energy) and elastic (stored energy) responses; so that, the glass transition temperature (T_g) can be taken at tan δ peak maximum as the ratio between the lost energy and the stored energy reaches its maximum value.

The VST and the HDT were determined in a VICAT/HDT station DEFLEX 687-A2 by Metrotec S.A. (San Sebastián, Spain). Vicat test was carried with a load of 50 N and a heating rate of 50 °C h^{-1} as recommended by the ISO 306. With regard to HDT, it was obtained according to ISO 75, which recommends a load of 1.8 MPa and a heating rate of 120 °C h^{-1}. All VST and HDT tests were run in triplicate and the average values were calculated.

Fourier transformed infrared spectroscopy (FTIR)

FTIR spectra of neat PHB and PHB plasticized formulations were obtained in total attenuated reflectance in a FTIR spectrometer Spectrum BX from Perkin-Elmer (Madrid, Spain). All the spectra were recorded in the wavenumber range comprised between 4000 and 600 cm^{-1}. Twenty different scans were collected and averaged at room temperature with a resolution of 4 cm^{-1}.

RESULTS AND DISCUSSION

Mechanical properties of PHB plasticized with vegetable oil-derived plasticizers

One of the main aims of this work is to assess the effectiveness of the two vegetable oil-derived plasticizers through their influence on mechanical performance. Figure IV.2.1 shows the evolution of mechanical properties, *i.e.*, tensile strength and elastic modulus for both plasticized PHB systems with MLO and EFAE. As it can be clearly observed, both plasticizers promote a remarkable decrease in tensile strength and elastic modulus with regard to neat PHB. Neat PHB possesses a tensile strength of 24.1 MPa and an elastic modulus of 1872 MPa. For low plasticizer content (5 phr), mechanical resistant properties do not decrease in a great extent, reaching tensile strength values of 18.7 and 19.0 MPa for MLO and EFAE plasticized PHB formulations respectively. Ferri *et al.* [52] described a similar tendency by adding EFAE to poly(lactic acid) with a decrease in tensile strength with increasing plasticizer content. Regarding the elastic modulus, it decreases to values of 1600 MPa for both plasticized systems. Over this plasticizer content, tensile strength decreases down to values of 17 MPa for both plasticizers except the plasticized formulations with 20 phr MLO with a tensile strength of 13.8 MPa (which represents a percentage decrease of 26% with regard to neat PHB). Similar tendency can be observed for the elastic modulus, which tends to stabilize to values around 1600 and 1450 MPa for plasticized PHB formulations with MLO and EFAE respectively. Garcia-Garcia *et al.* [53] also observed a decrease in tensile strength and tensile modulus of neat PHB with increasing content of different plasticizers from epoxidized linseed oil (ELO) and epoxidized soybean oil (ESBO).

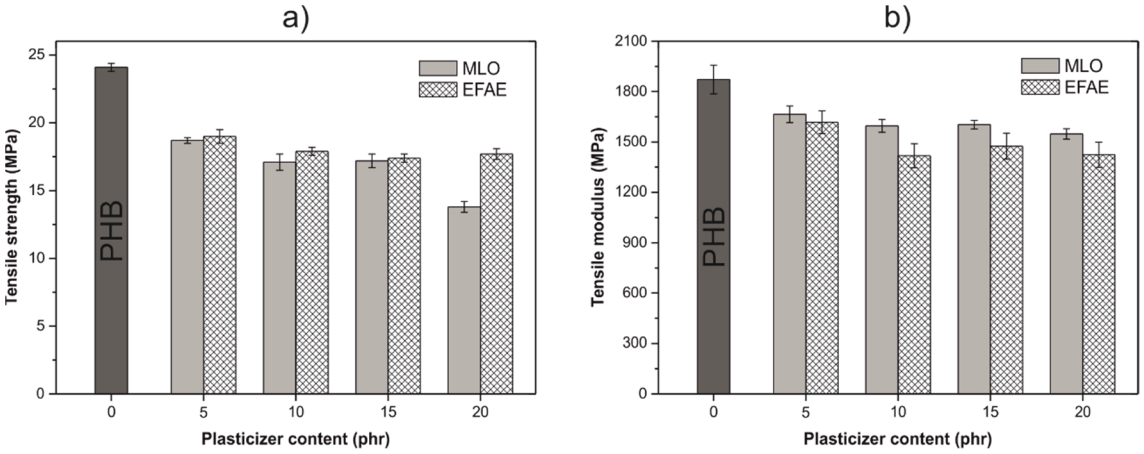

Figure IV.2.1. Bar plot with the evolution of (a) tensile strength and (b) tensile modulus for neat PHB and plasticized PHB formulations with different content of MLO and EFAE.

Regarding the ductile properties, Figure IV.2.2 shows a plot evolution of the elongation at break values and the impact resistance as a function of the type and amount of plasticizer. As it can be seen, addition of a low plasticizer concentration (5 phr) leads to an increase in elongation at break and a subsequent increase in PHB toughness. Regarding MLO-plasticized formulations, the elongation at break changes from 9.7% (neat PHB) up to values of 12.4% for formulations containing 5 phr MLO. By using the same plasticizer amount (5 phr) of EFAE the elongation at break is improved to 13.6%, which represents a percentage increase of almost 40% regarding neat PHB. Over 5 phr of plasticizer the elongation at break undergoes a slight decrease and tends to stabilize at values of 10 and 12% for the MLO and EFAE plasticized systems respectively. With regard to the impact resistance, neat PHB is characterized by very low toughness with values of 2.1 kJ m^{-2}. In a similar way to elongation at break, a low plasticizer content of 5 phr leads to an increase in the impact resistance to values of 3.6 and 4.4 kJ m^{-2} for plasticized PHB formulations with MLO and EFAE respectively, which represents a percentage increase of 71% (with MLO) and 109% (with EFAE) compared to neat PHB. Higher plasticizer content (>5 phr) leads to a slight decrease in the maximum value reached at 5 phr for both plasticizers. This behavior is similar to that reported by Ferri *et al.* [52] in which the elongation at break and the impact resistance of PLA was remarkably improved by 370 and 75% respectively with the addition of 5 phr EFAE plasticizer. Over this plasticizer content, a decrease in mechanical ductile properties occurs due to plasticizer saturation. This fact suggests that plasticizer saturation occurs at about 5 phr. Above this composition, phase separation occurs with the subsequent negative effect on mechanical ductile properties as reported by other authors Chieng *et al.* [35], Xu and Qu [54] and Zhao *et al.* [55]. By taking into account both mechanical resistant

and ductile properties, the results show higher effectiveness of the plasticized PHB system with EFAE in comparison to MLO. The chemical nature of the base polymer (PHB) and the employed plasticizers determine their miscibility and, obviously, the plasticizer efficiency. A simple way to evaluate the miscibility between two different components in a mixture is by comparing their solubility parameters (δ). Two substances with similar solubility parameters must be mutually soluble [56]. The solubility parameters (δ) of PHB and both plasticizers were calculated by using Equation IV.2.2.

$$\boldsymbol{\delta = \frac{\rho \sum G}{M}} \qquad \textbf{Equation IV.2.2}$$

where δ represents the solubility parameter, ρ is the density of each substance, G is the sum of the molar attraction constants for each chemical group calculated from the Small's molar attraction constants [57] and M is the average molecular weight per repetitive unit.

The solubility parameter of PHB (δ_{PHB}) is close to 9.1 $MPa^{1/2}$. With regard to the proposed plasticizers, the MLO and the EFAE possess a solubility parameter of 7.9 and 8.1 $MPa^{1/2}$ respectively. As per their solubility parameters, both plasticizers seem to be compatible with PHB as their corresponding differences in solubility parameters is not so high. Nevertheless, slightly better results are expectable from the solubility parameter of EFAE which is closer to that of the PHB.

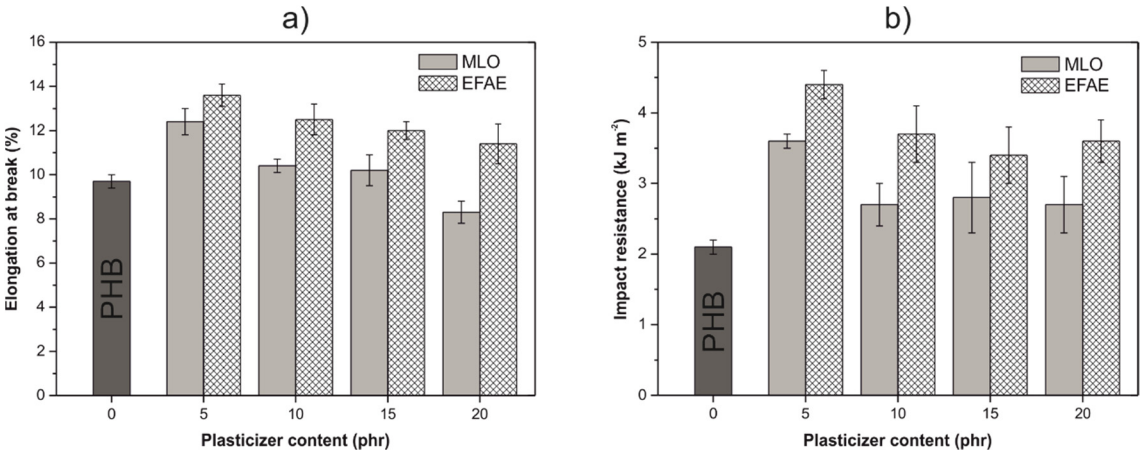

Figure IV.2.2. Bar plot with the evolution of (a) elongation at break and (b) impact resistance for neat PHB and plasticized PHB formulations with different content of MLO and EFAE.

Figure IV.2.3 shows a bar plot with Shore D hardness values of plasticized PHB formulations. Shore D hardness follows similar evolution as that observed for other mechanical resistant properties such as elastic modulus or tensile strength. Neat PHB possesses a Shore D hardness of 57. By the addition of 5 phr of both MLO and EFAE, the Shore D hardness does not change and remains at about 57. Higher plasticizer content leads to slight decrease in hardness, which is more pronounced for 20 phr MLO.

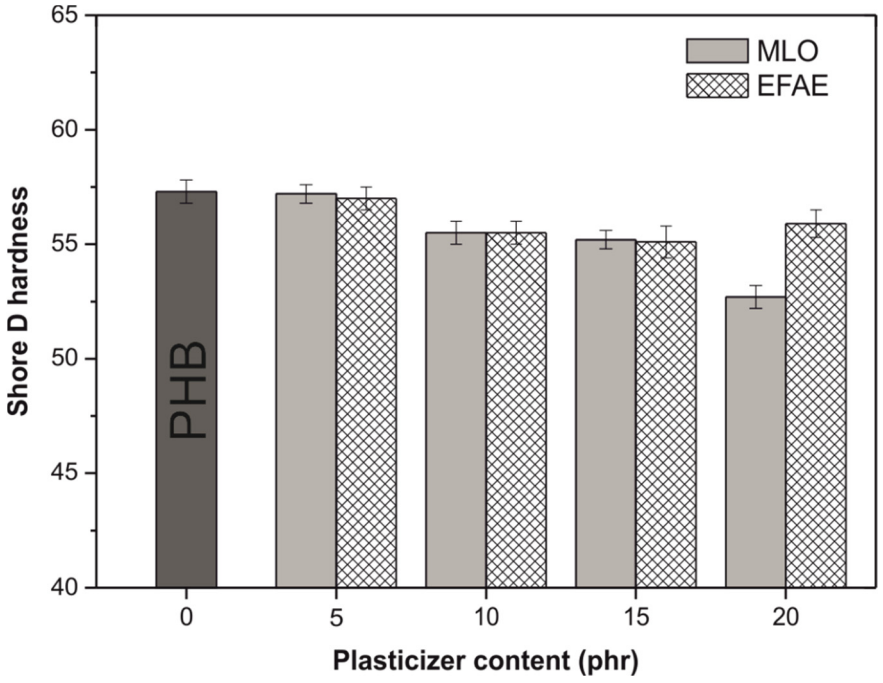

Figure IV.2.3. Bar plot with the evolution of Shore D hardness for neat PHB and plasticized PHB formulations with different content of MLO and EFAE.

Thermal properties of PHB plasticized with vegetable oil-derived plasticizers

Thermal characterization was carried out to assess the effects of the type and amount of plasticizer on thermal parameters of PHB-based formulations. Table IV.2.2 shows a summary of the main thermal parameters obtained by DSC for neat PHB and its plasticized formulations with MLO and EFAE. It was not possible to detect the glass transition temperature (T_g) by DSC so that, T_g values in Table IV.2.2 correspond to the glass transition temperature obtained by DMTA. As shown in Figure IV.2.4, neat PHB shows an endothermic melt peak at 174.8 °C ($T_{m2\ PHB}$). An addition slow melt peak can be detected for all compositions. This small peak is located at 52.3 °C ($T_{m1\ PHB}$) and it is related to the melting process of low molecular weight commercial additives contained in the industrial PHB formulation as reported by Prakalathan *et al.* [58]. After plasticizer addition, the melt

temperature decreases to 171 °C for almost all compositions independent of the plasticizer type. During melt mixing, plasticizer molecules move toward PHB polymer chains and are placed between them. As both plasticizers possess similar solubility parameter to that of the neat PHB, somewhat PHB-plasticizer interactions are allowed. These plasticizer molecules placed between PHB chains restrict formation of packed structures, thus leading to a decrease in crystallinity. On the other hand, due to the lubrication effect that plasticizers provide, some PHB chains are more likely to move thus leading to a decrease in the melt peak temperature. This decrease in the melt peak and in the degree of crystallinity was also observed by Wang *et al.* [27] after addition of ATBC plasticizer on PHB formulations. Baltieri *et al.* [32] and Fernandes *et al*. [33] also reported the same tendency after the addition of several commercial plasticizer to PHB formulations. The normalized melt enthalpy (ΔH_m) of the different formulations was used to determine the degree of crystallinity of PHB in each formulation as crystallinity plays a key role in overall properties and, specifically on mechanical response. As it can be deduced from Table IV.2.2, the degree of crystallinity (X_c) decreases with addition of both plasticizers. This decrease is more pronounced for MLO-plasticized formulations. Previous section revealed that best mechanical properties for MLO-plasticized PHB formulations were obtained with 5 phr. Regarding changes in crystallinity, neat PHB possesses a degree of crystallinity of 51.9% and this is reduced up to 44.7% for the abovementioned formulation. With regard to the EFAE-plasticized PHB materials, addition of 5 phr leads to a crystallinity decrease from 51.9 to 42.3%. It is worth to note that plasticizer content over 5 phr does not provide additional significant decrease in the degree of crystallinity. Plasticizer molecules diffuse inside the PHB matrix and are placed between PHB polymeric chains. Polymer-plasticizer interactions allow the plasticizer to remain mixed between PHB chains and this restricts formation of packed structures with the subsequent decrease in crystallinity. Crystallinity is directly related to mechanical resistant properties leading to stiff and rigid materials. The decrease in the degree of crystallinity leads to improved toughness, therefore mechanical resistant properties are reduced and, subsequently, ductile properties such as elongation at break are improved.

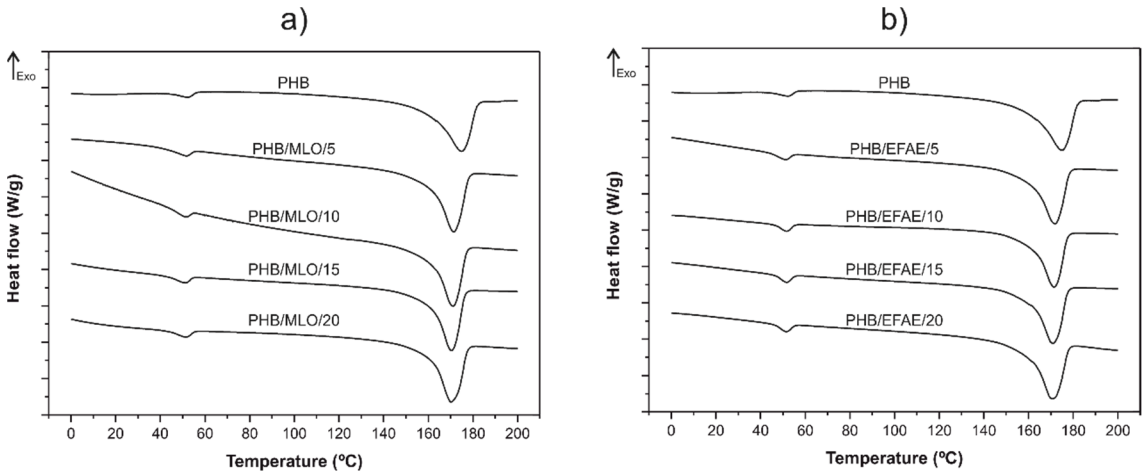

Figure IV.2.4. Comparative DSC curves during second heating scan of neat PHB and plasticized PHB with different contents of (a) MLO and (b) EFAE.

Concerning thermal stability, Table IV.2.2 also shows some thermal parameters obtained by TGA. In particular, the onset degradation temperature (T_0) was defined as the temperature at which a weight loss of 5% occurs. As it has been reported by Prakalathan *et al*. [58] commercial PHB grades, contain somewhat plasticizers, nucleating agents, fillers and stabilizers. For this reason, the thermal degradation occurs in two stages, as shown in Figure IV.2.5. The first stage is related to PHB decomposition and it has been followed through the evolution of the maximum peak temperature in the corresponding DTG plot (T_{max1}). The second degradation stage, at higher temperatures, is probably related to degradation of others components such as processing aids, nucleating agents and stabilizers, and its corresponding peak in the derivative thermogravimetric (DTG) curves (T_{max2}) has been used to characterize it [58]. Both plasticizers provide improved thermal stability to PHB as the onset degradation temperature (T_0) increases in a remarkable way. The onset degradation temperature for neat PHB is 246.7 °C and it is noticeably increased by more than 30 °C up to values near 280 °C which represents a percentage increase in the thermal stability of about 13.5% compared to neat PHB. Same tendency can be observed for EFAE-based PHB formulations but in this case, the increase in the thermal stabilization is slightly lower that observed with MLO. In particular, EFAE-based formulations delay the degradation onset up to 273 °C which represents a percentage increase of almost 10.6% regarding neat PHB. This remarkable increase in the thermal stability is directly related to intense polymer-plasticizer interactions that act as a physical barrier that obstruct removal of volatile products resulting from decomposition and this has a positive effect on delaying degradation as reported by Silverajah *et al.* [59]. It has been reported that the onset degradation temperature for some plasticized PHB formulations with poly(ethylene glycol)

(PEG) and acetyl tributyl citrate (ATBC) decreases [27, 33, 60]. As it has been described previously the vegetable oil-derived plasticizers positively contribute to the overall thermal stabilization of PHB formulations, which is an interesting feature if we consider the relatively narrow processing window of this polymer. The increase in the onset degradation temperature for different polymers after plasticization with vegetable oil derivatives has been previously reported by Garcia-Garcia *et al.* [53]. They reported an increase in the onset degradation temperature of neat PHB of 25 and 30 °C after plasticization with 5 phr ELO and 5 phr ESBO respectively. Chieng *et al.* [35] also obtained a remarkable increase in the onset degradation by 40 °C of neat PLA by the addition of 5 wt% epoxidized palm oil (EPO). With regard to the maximum degradation rates, measured with the two peak temperatures (T_{max1} and T_{max2}), similar tendency can be detected with higher values for plasticized formulations with both MLO and EFAE plasticizers regarding neat PHB. With regard to the MLO-plasticized PHB formulations, T_{max1} changes from 272.3 °C (neat PHB) up to values close to 300 °C while EFAE-plasticized formulations give T_{max1} values close to 295 °C. The tendency is similar to that observed for the onset degradation temperature (T_0). The temperature at which maximum degradation rate of the second stage occurs (T_{max2}) also follows the same behavior with a slightly higher stabilization effect of MLO versus EFAE. In Table IV.2.2, it is possible to observe how the char residue at 550 °C increases as the total plasticizer content increases for both plasticizers.

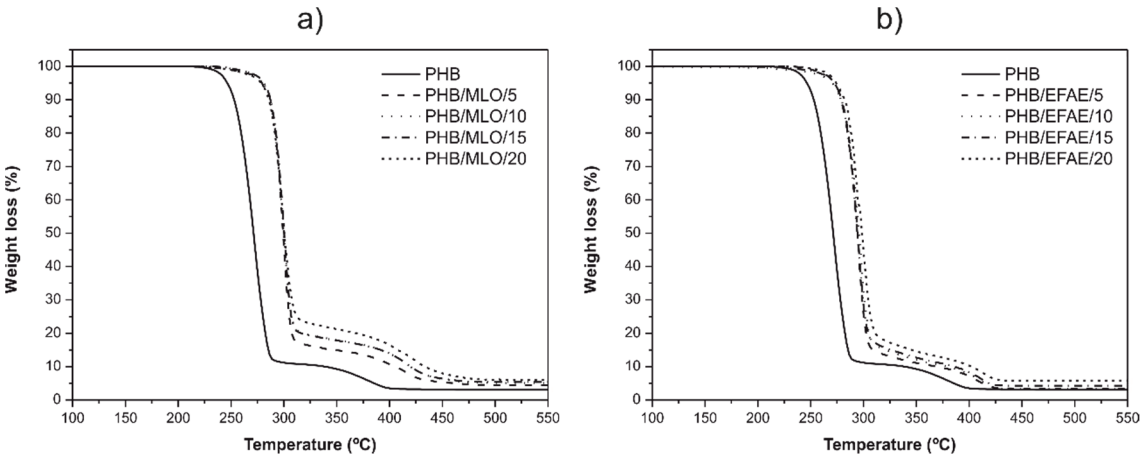

Figure IV.2.5. Comparative thermogravimetric curves of neat PHB and plasticized PHB with different contents of (a) MLO and (b) EFAE.

Table IV.2.2. Thermal properties of neat PHB and plasticized PHB formulations with MLO and EFAE.

Samples	DSC parameters					TGA parameters			
	T_g[a] (°C)	T_{m1} (°C)	T_{m2} (°C)	ΔH_m (J g^{-1})	X_c (%)	T_0[b] (°C)	T_{max1} (°C)	T_{max2} (°C)	Char residue[c] (%)
PHB	–2.2	52.3 ± 0.2	174.8 ± 0.2	–75.8 ± 0.4	51.9	246.7 ± 0.3	272.3 ± 0.3	382.0± 0.3	3.0 ± 0.6
PHB/MLO/5	–3.9	51.4 ± 0.2	171.4 ± 0.2	–65.2 ± 0.6	44.7	279.3 ± 0.6	298.0 ± 0.7	410.0 ± 0.2	4.4 ± 0.4
PHB/MLO/10	–3.6	51.1 ± 0.1	171.0 ± 0.2	–58.6 ± 0.7	40.1	280.0 ± 0.5	300.3 ± 0.4	417.0 ± 0.1	5.1 ± 0.5
PHB/MLO/15	–3.5	51.3 ± 0.4	170.5 ± 0.4	–54.9 ± 0.5	37.6	280.3 ± 0.3	300.3 ± 0.5	417.0 ± 0.1	5.4 ± 0.3
PHB/MLO/20	–3.4	51.3 ± 0.2	170.2 ± 0.2	–52.5 ± 0.5	36.0	279.0 ± 0.4	298.0 ± 0.5	417.0 ± 0.2	6.0 ± 0.1
PHB/EFAE/5	–3.3	51.5 ± 0.3	171.9 ± 0.3	–61.7 ± 0.4	42.3	273.0 ± 0.7	295.6 ± 1.2	412.3 ± 0.1	3.3 ± 0.3
PHB/EFAE/10	–1.7	51.6 ± 0.5	171.4 ± 0.2	–52.8 ± 0.2	36.2	270.3 ± 0.2	298.0 ± 0.3	412.3 ± 0.3	3.3 ± 0.5
PHB/EFAE/15	–1.6	51.6 ± 0.4	171.0 ± 0.4	–56.2 ± 0.8	38.5	272.0 ± 0.5	296.3 ± 0.7	412.3 ± 0.3	4.2 ± 0.1
PHB/EFAE/20	–1.7	51.5 ± 0.1	170.9 ± 0.4	–55.6 ± 0.6	38.1	274.6 ± 0.8	298.0 ± 0.3	414.6 ± 0.4	5.8 ± 0.3

[a] T_g is the glass transition temperature. The values correspond to the maximum peak of the damping factor by DMTA analysis as it was not possible to detect it by DSC.

[b] T_0 is the degradation onset temperature calculated at 5% mass loss.

[c] Char content at 550 °C.

Thermo-mechanical properties of PHB plasticized with vegetable oil-derived plasticizers

Figure IV.2.6 shows the evolution of the storage modulus (*G*') and the damping factor (tan δ) as a function of increasing temperature for both neat PHB and plasticized PHB formulations with different MLO (Figure IV.2.6a and b) and EFAE (Figure IV.2.6c and d) content. As it can be seen, the storage modulus for neat PHB decreases from 2.5 GPa at –50 °C up to values of 0.3 GPa measured at 80 °C. Similar tendency can be observed for plasticized PHB formulations with both MLO and EFAE. Nevertheless, the storage modulus curve for all plasticized formulations are located below the curve of neat PHB thus indicating the plasticizer effect that both MLO and EFAE can provide with the subsequent increase in chain mobility. This has a positive effect on ductile properties and a decrease in mechanical resistant properties. Regarding the EFAE-plasticized PHB formulations, all *G*' curves for different EFAE content appear overlapped and this could be related to plasticizer saturation which occurs at relatively low plasticizer content of about 5 phr EFAE. All EFAE-based formulations show a *G*' of 1.6 GPa at –50 °C and it is progressively reduced up to values of 0.2 GPa at 80 °C. With regard to the MLO-plasticized system, the plasticized formulation with 5 phr MLO is characterized by a lower storage modulus at –50 °C (1.9 GPa) while formulations with higher MLO content in the 10–20 phr MLO range are defined by a slightly lower storage modulus of 1.8 GPa at the same temperature thus evidencing the slightly better plasticizing effect of EFAE against MLO.

The glass transition temperature (T_g) was calculated at the peak maximum from the damping factor curve. As it can be seen in Figure IV.2.6b and d (see also Table IV.2.2) the glass transition temperature changes from –2.2 °C for neat PHB to –3.9 and –3.3 °C for plasticized formulations (5 phr) of MLO and EFAE respectively. This decrease in T_g is a clear evidence of the plasticization effectiveness of both plasticizers. The plasticizer molecules are placed between PHB polymer chains thus reducing the intensity of the secondary forces between polymer chains. In addition, plasticizers provide a lubricity effect and the overall free volume is increased. All these phenomena lead to improved chain mobility thus allowing PHB polymer chains to move at lower temperatures. This effect is clearly evident for low plasticizer contents of 5 phr for both MLO and EFAE plasticizers whilst the T_g suffers a slight increase over this plasticizer content thus suggesting, as indicated previously, that plasticizer saturation occurs at relatively low plasticizer content. Wang *et al.* [27], Baltieri *et al.* [32] and Garcia-Garcia *et al*. [53] also observed the same decrease in the glass transition temperature of neat PHB after plasticization with different plasticizers.

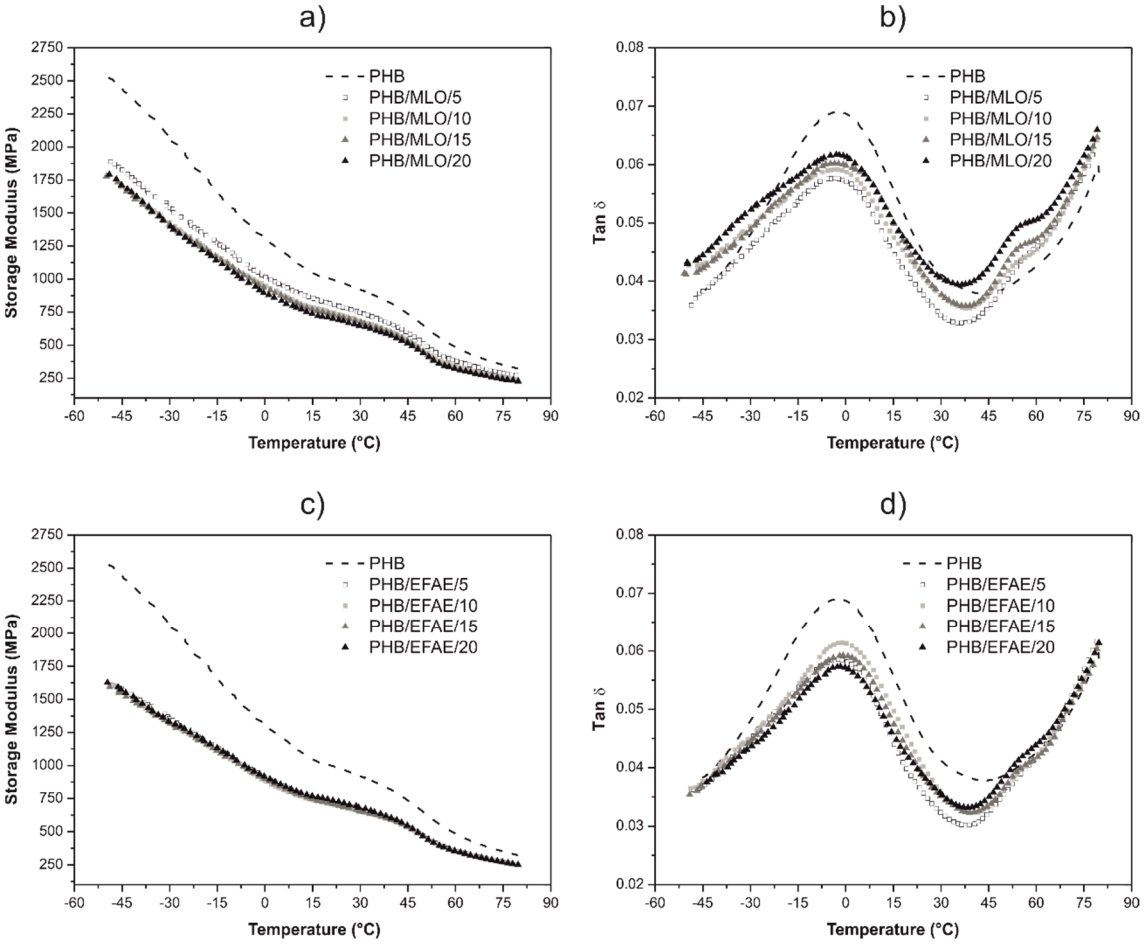

Figure IV.2.6. DMTA (torsion mode) curves of neat PHB and plasticized PHB formulations with MLO and EFAE as a function of increasing temperature. The storage modulus (*G*') is represented in Figure IV.2.6a and c, the damping factor (tan *δ*) is shown in Figure IV.2.6b and d for MLO and EFAE-plasticized systems respectively.

The effect of both plasticizers is also evident by following the evolution of two different thermo-mechanical properties, *i.e.*, VST and HDT as shown in Table IV.2.3. Neat PHB possesses a VST value of 93.4 °C and an HDT of 55.4 °C. Regarding HDT, plasticizer addition leads to lower values. This decrease is progressive for the MLO-plasticized PHB system up to values of 53 °C, whilst this decrease up to 53 °C occurs even for very low EFAE-plasticizer content. The evolution of the Vicat softening temperature follows similar tendency. The VST of neat PHB (93.4 °C) highly decreases down to values of 78.4 and 87.4 °C for 5 phr MLO and EFAE respectively. Further plasticizer addition leads to progressive lower VST values up to 66.8 and 78 °C for MLO and EFAE plasticized formulations respectively. This behavior is in total agreement with previous mechanical properties thus giving clear evidences of the plasticization effectiveness of both MLO and EFAE.

Table IV.2.3. VST and HDT of neat PHB and plasticized PHB formulations with MLO and EFAE.

Samples	Vicat softening temperature VST (°C)	Heat deflection temperature HDT (°C)
PHB	93.4 ± 1.5	55.4 ± 0.3
PHB/MLO/5	78.4 ± 1.9	55.2 ± 0.6
PHB/MLO/10	72.4 ± 0.9	52.6 ± 0.4
PHB/MLO/15	69.8 ± 1.2	53.0 ± 0.4
PHB/MLO/20	66.8 ± 1.5	53.0 ± 0.8
PHB/EFAE/5	87.4 ± 1.3	53.6 ± 0.3
PHB/EFAE/10	81.6 ± 1.7	53.2 ± 0.3
PHB/EFAE/15	81.0 ± 0.5	53.0 ± 0.5
PHB/EFAE/20	78.0 ± 0.9	53.2 ± 0.5

Morphology of PHB plasticized with vegetable oil-derived plasticizers

Figure IV.2.7 shows FESEM images corresponding to fractured surfaces from impact tests of neat PHB and plasticized PHB formulations with 5 phr MLO and EFAE. Figure IV.2.7a and b shows the morphology of fractured samples of neat PHB. The surface appears to be very rough with presence of many voids that give evidences of high porosity. In general, the fracture of PHB is fragile. Also it is possible to observe presence of particle fillers which are typical in commercial PHB formulations [58]. After addition of 5 phr plasticizer the surface topography appears to be less rough (Figure IV.2.7c-f). In both cases surface appears to be smoother and homogeneous. It is not detectable the phase separation using this low plasticizer concentration thus giving evidences of good plasticizer-polymer compatibility. Both plasticizers also have a positive effect on reducing the overall porosity and, subsequently, mechanical properties are remarkably improved as previously described. Figure IV.2.7e and f show fractured surface of EFAE-plasticized PHB with 5 phr. As it can be seen, presence of porosity is much lower than neat PHB and MLO-plasticized PHB formulations. This provides excellent compatibility and good matrix continuity which has a positive effect on load transfer and, subsequently, on mechanical properties.

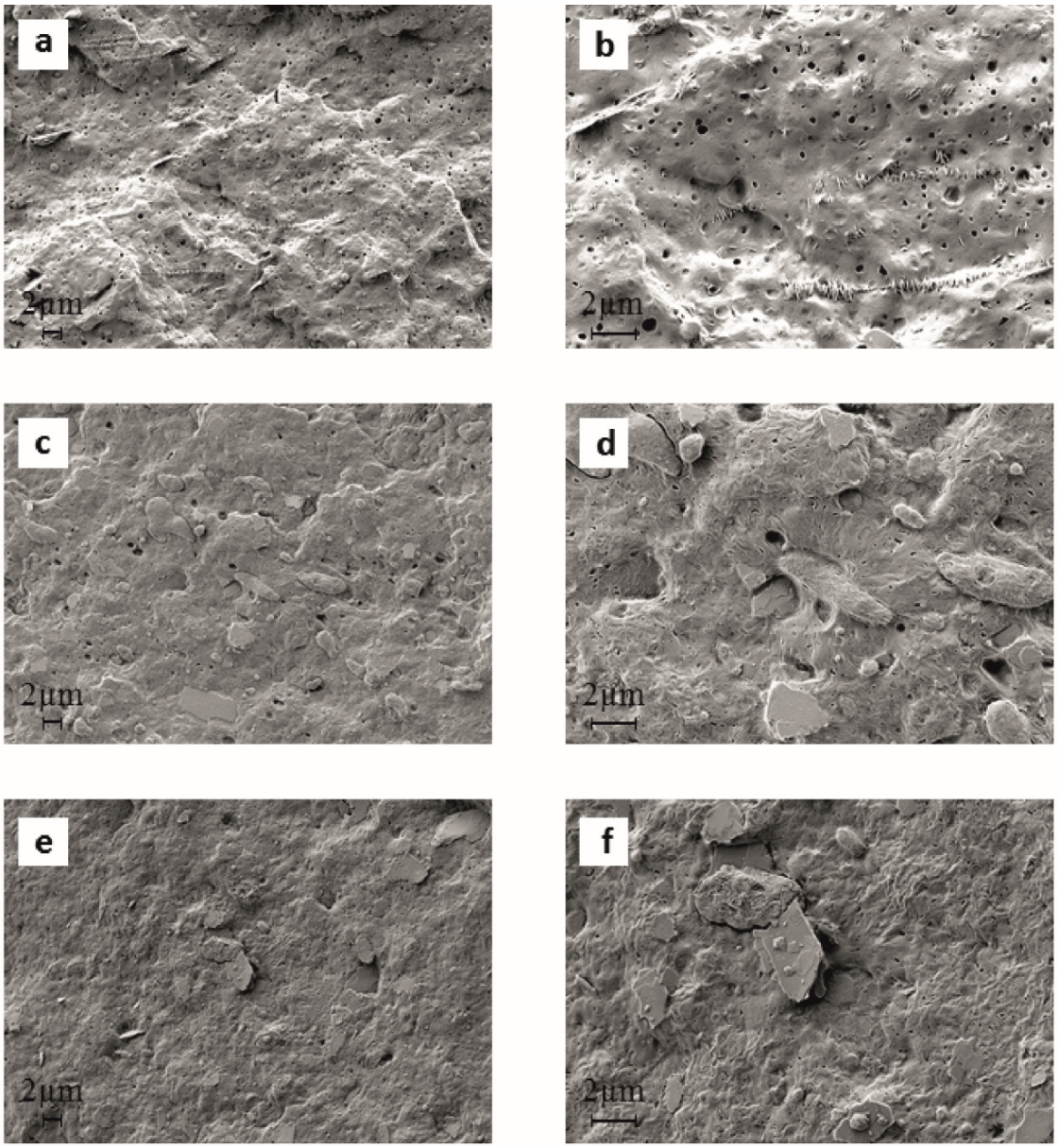

Figure IV.2.7. FESEM photographs of fracture surface of (a) PHB (2000x), (b) PHB (5000x), (c) PHB/MLO/5 (2000x), (d) PHB/MLO/5 (5000x), (e) PHB/EFAE/5 (2000x) and (f) PHB/EFAE/5 (5000x).

FTIR of PHB plasticized with vegetable oil-derived plasticizers

With the aim of analyzing the effect of the different plasticizers on the chemical structure of the plasticized PHB formulations, FTIR spectra were recorded. Figure IV.2.8 shows the FTIR spectra of neat PHB and PHB plasticized with 5 phr of MLO and EFAE in the 3200–600 cm^{-1} range. As it can be seen, the typical IR stretching bands of PHB can be observed in all the studied formulations, as it is the main component in the plasticized formulations. The main IR absorbing bands of PHB are located in the 3000–2900 cm^{-1} range,

which corresponds to the C–H stretching vibrations [14]. A typical characteristic peak at 1720 cm^{-1}, attributed to the stretching vibrations of crystalline carbonyl groups C=O can also be seen. At the same time, the amorphous carbonyl vibration of PHB at 1740 cm^{-1} is very weak and cannot be clearly detected in the corresponding spectra [61]. Some peaks located in the 1500–1000 cm^{-1} range are related to CH_3, CH_2, CH bending vibration, C–O–C and C–C stretching vibration [62]. It is worthy to note the peak located at 1226 cm^{-1}, which is attributed to the stretching of C–O–C in the crystalline regions while the peaks located at 1268 and 1180 cm^{-1} correspond to the stretching of C–O–C in the amorphous regions [62, 63]. Addition of 5 phr MLO and EFAE does not produce remarkable changes in the corresponding IR spectra with regard to neat PHB. Nevertheless, some small differences related to plasticizer-polymer interactions can be observed. As it can be seen in Figure IV.2.8, the typical wavenumber of the carbonyl group changes from 1720 cm^{-1} down to 1718 cm^{-1} after addition of 5 phr of both MLO and EFAE. This small shift is related to some miscibility and is representative for somewhat polymer-plasticizer interactions. This shift could be related to interactions between the hydroxyl groups in PHB and the epoxy groups in EFAE and maleic anhydride in MLO as other authors have reported for similar plasticized systems [40, 59]. This decrease in the wavenumber was also observed by Râpă *et al.* [64] after the addition of different plasticizers, *i.e.*, ATBC, TEC and TBC in PHB formulations. Silverajah *et al.* [59] also observed a decrease in the position of the peak corresponding to the stretching vibrations of crystalline carbonyl groups in PLA plasticized with 1 and 5 wt% EPO. Moreover, the peak intensity comprised in the 3000–2900 cm^{-1} (C–H) increases in a remarkable way after addition of both plasticizers, which gives evidences of the presence of plasticizers in PHB formulations [59].

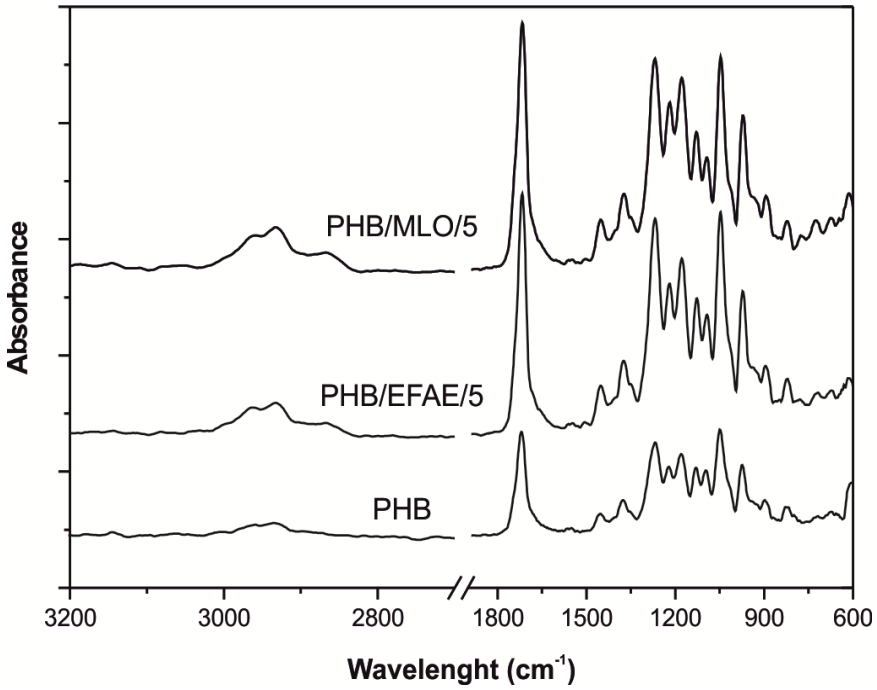

Figure IV.2.8. Infrared spectra of neat PHB and plasticized PHB formulations with 5 phr of MLO and EFAE.

CONCLUSIONS

The present work explores the potential of two plant-derived plasticizers for PHB formulations with improved toughness. The effect of MLO and an EFAE on mechanical, thermal and thermo-mechanical properties is evaluated. The results show that a small addition of both plasticizers (5 phr) provides increased elongation at break values together with a remarkable increase in the impact resistance and, subsequently, toughness improvement. Although both plasticizers offer high plasticization efficiency due to similar solubility parameters, slightly better properties are obtained with the EFAE. Compositions above 5 phr lead to plasticizer saturation as evidenced by worse mechanical properties and potential antiplasticization properties. Morphology of fractured samples from impact tests revealed good compatibility between the PHB matrix and both plasticizers with a remarkable decrease in porosity thus leading to homogeneous materials with high matrix continuity. Dynamic mechanical thermal analysis revealed a decrease in the glass transition temperature due to increased chain mobility. One important feature that both MLO and EFAE plasticizers provide to PHB formulations is a widening of the processing window due to different phenomena: on one hand, the melt peak temperature is decreased and on the other hand, the onset degradation temperature increases in a remarkable way. The combination of these two phenomena leads to widening the processing window of neat PHB

which is typically a very narrow range. In general, MLO and EFAE offer high plasticization efficiency to PHB formulations to overcome some of its main drawbacks by improving toughness, processing window and increasing the biobased content in PHB formulations.

ACKNOWLEDGEMENTS

The authors thank the Ministry of Economy and Competitiveness (MINECO) for financial support [MAT2014-59242-C2-1-R]. The authors also thank the Conselleria d'Educació, Cultura i Esport – Generalitat Valenciana for financial support [GV/2014/008]. D. Garcia-Garcia thanks the Spanish Ministry of Education, Culture and Sports for the financial support through an FPU grant [FPU13/06011].

REFERENCES

[1] Hassan M, Reddy KR, Haque E, Minett AI and Gomes VG. *High-yield aqueous phase exfoliation of graphene for facile nanocomposite synthesis via emulsion polymerization*. Journal of Colloid and Interface Science, 2013. **410**:43-51.

[2] Hassan M, Reddy KR, Haque E, Faisal SN, Ghasemi S, Minett AI and Gomes VG. *Hierarchical assembly of graphene/polyaniline nanostructures to synthesize free-standing supercapacitor electrode*. Composites Science and Technology, 2014. **98**:1-8.

[3] Choi SH, Kim DH, Raghu AV, Reddy KR, Lee HI, Yoon KS, Jeong HM and Kim BK. *Properties of graphene/waterborne polyurethane nanocomposites cast from colloidal dispersion mixtures*. Journal of Macromolecular Science, Part B, 2012. **51**(1):197-207.

[4] Reddy KR, Lee KP and Gopalan AI. *Self-assembly directed synthesis of poly(ortho-toluidine)-metal (gold and palladium) composite nanospheres*. Journal of Nanoscience and Nanotechnology, 2007. **7**(9):3117-3125.

[5] Zhang YP, Lee SH, Reddy KR, Gopalan AI and Lee KP. *Synthesis and characterization of core-shell SiO_2 nanoparticles/poly(3-aminophenylboronic acid) composites*. Journal of Applied Polymer Science, 2007. **104**(4):2743-2750.

[6] Bhagowati P, Pradhan S, Dash HR and Das S. *Production, optimization and characterization of polyhydroxybutyrate, a biodegradable plastic by Bacillus spp*. Bioscience, Biotechnology, and Biochemistry, 2015. **79**(9):1454-1463.

[7] D'Amico DA, Montes MLI, Manfredi LB and Cyras VP. *Fully bio-based and biodegradable polylactic acid/poly(3-hydroxybutirate) blends: Use of a common plasticizer as performance improvement strategy*. Polymer Testing, 2016. **49**:22-28.

[8] Lai SM, Sun WW and Don TM. *Preparation and characterization of biodegradable polymer blends from poly(3-hydroxybutyrate)/poly(vinyl acetate)-modified corn starch*. Polymer Engineering & Science, 2015. **55**(6):1321-1329.

[9] Mittal V, Akhtar T and Matsko N. *Mechanical, thermal, rheological and morphological properties of binary and ternary blends of PLA, TPS and PCL*. Macromolecular Materials and Engineering, 2015. **300**(4):423-435.

[10] Bordes P, Pollet E and Avérous L. *Nano-biocomposites: Biodegradable polyester/nanoclay systems*. Progress in Polymer Science, 2009. **34**(2):125-155.

[11] Fan X, Jiang Q, Sun Z, Li G, Ren X, Liang J and Huang TS. *Preparation and characterization of electrospun antimicrobial fibrous membranes based on polyhydroxybutyrate (PHB)*. Fibers and Polymers, 2015. **16**(8):1751-1758.

[12] Garcia-Garcia D, Ferri JM, Boronat T, Lopez-Martinez J and Balart R. *Processing and characterization of binary poly(hydroxybutyrate) (PHB) and poly(caprolactone) (PCL) blends with improved impact properties*. Polymer Bulletin, 2016. **73**(12):3333-3350.

[13] Karahaliloglu Z, Ercan B, Taylor EN, Chung S, Denkbaş EB and Webster TJ. *Antibacterial nanostructured polyhydroxybutyrate membranes for guided bone regeneration*. Journal of Biomedical Nanotechnology, 2015. **11**(12):2253-2263.

[14] Romero AI, Bermudez JM, Villegas M, Ashur MFD, Parentis ML and Gonzo EE. *Modeling of progesterone release from poly(3-hydroxybutyrate) (PHB) membranes*. AAPS PharmSciTech, 2016. **17**(4):898-906.

[15] Bucci DZ, Tavares LBB and Sell I. *Biodegradation and physical evaluation of PHB packaging*. Polymer Testing, 2007. **26**(7):908-915.

[16] Bucci DZ, Tavares LBB and Sell I. *PHB packaging for the storage of food products*. Polymer Testing, 2005. **24**(5):564-571.

[17] Meszynska A, Pollet E, Odelius K, Hakkarainen M and Avérous L. *Effect of oligo-hydroxyalkanoates on poly(3-hydroxybutyrate-co-4-hydroxybutyrate)-based systems*. Macromolecular Materials and Engineering, 2015. **300**(6):661-666.

[18] Zhijiang C, Yi X, Haizheng Y, Jia J and Liu Y. *Poly(hydroxybutyrate)/cellulose acetate blend nanofiber scaffolds: Preparation, characterization and cytocompatibility*. Materials Science and Engineering: C, 2016. **58**:757-767.

[19] Safari S and van de Ven TGM. *Effect of crystallization conditions on the physical properties of a two-layer glassine paper/polyhydroxybutyrate structure*. Journal of Materials Science, 2015. **50**(10):3686-3696.

[20] Arza CR, Jannasch P, Johansson P, Magnusson P, Werker A and Maurer FHJ. *Effect of additives on the melt rheology and thermal degradation of poly[(R)-3-hydroxybutyric acid]*. Journal of Applied Polymer Science, 2015. **132**(15):41836.

[21] Sharhan O, Yahaya AH and Nasef MM. *Preparation and characterization of poly(3-hydroxybutyric acid)/poly(vinyl acetate) blend films*. Asian Journal of Chemistry, 2015. **27**(3):979-983.

[22] Janigová I, Lacík I and Chodák I. *Thermal degradation of plasticized poly(3-hydroxybutyrate) investigated by DSC*. Polymer Degradation and Stability, 2002. **77**(1):35-41.

[23] Ke Y, Zhang XY, Ramakrishna S, He LM and Wu G. *Synthetic routes to degradable copolymers deriving from the biosynthesized polyhydroxyalkanoates: A mini review*. Express Polymer Letters, 2016. **10**(1):36-53.

[24] Hong SG, Gau TK and Huang SC. *Enhancement of the crystallization and thermal stability of polyhydroxybutyrate by polymeric additives*. Journal of Thermal Analysis and Calorimetry, 2011. **103**(3):967-975.

[25] Wen X, Lu X, Peng Q, Zhu F and Zheng N. *Crystallization behaviors and morphology of biodegradable poly(3-hydroxybutyrate-co-4-hydroxybutyrate)*. Journal of Thermal Analysis and Calorimetry, 2012. **109**(2):959-966.

[26] Hong SG, Hsu HW and Ye MT. *Thermal properties and applications of low molecular weight polyhydroxybutyrate*. Journal of Thermal Analysis and Calorimetry, 2013. **111**(2):1243-1250.

[27] Wang L, Zhu W, Wang X, Chen X, Chen GQ and Xu K. *Processability modifications of poly(3-hydroxybutyrate) by plasticizing, blending, and stabilizing.* Journal of Applied Polymer Science, 2008. **107**(1):166-173.

[28] Auriemma M, Piscitelli A, Pasquino R, Cerruti P, Malinconico M and Grizzuti N. *Blending poly(3-hydroxybutyrate) with tannic acid: Influence of a polyphenolic natural additive on the rheological and thermal behavior*. European Polymer Journal, 2015. **63:**123-131.

[29] Khasanah, Reddy KR, Sato H, Takahashi I and Ozaki Y. *Intermolecular hydrogen bondings in the poly(3-hydroxybutyrate) and chitin blends: Their effects on the crystallization behavior and crystal structure of poly(3-hydroxybutyrate)*. Polymer, 2015. **75**:141-150.

[30] Puglia D, Fortunati E, D'Amico DA, Miri V, Stoclet G, Manfredi LB, Cyras VP and Kenny JM. *Influence of processing conditions on morphological, thermal and degradative behavior of nanocomposites based on plasticized poly(3-hydroxybutyrate) and organo-modified clay*. Journal of Polymers and the Environment, 2016. **24**(1):12-22.

[31] Choi JS and Park WH. *Effect of biodegradable plasticizers on thermal and mechanical properties of poly(3-hydroxybutyrate)*. Polymer Testing, 2004. **23**(4):455-460.

[32] Baltieri RC, Mei LHI, and Bartoli J. *Study of the influence of plasticizers on the thermal and mechanical properties of poly(3-hydroxybutyrate) compounds*. Macromolecular Symposia, 2003. **197**(1):33-44.

[33] Fernandes EG, Pietrini M and Chiellini E. *Thermo-mechanical and morphological characterization of plasticized poly[(R)-3-hydroxybutyric acid]*. Macromolecular Symposia, 2004. **218**(1):157-164.

[34] Bocqué M, Voirin C, Lapinte V, Caillol S and Robin JJ. *Petro-based and bio-based plasticizers: Chemical structures to plasticizing properties*. Journal of Polymer Science Part A: Polymer Chemistry, 2016. **54**(1):11-33.

[35] Chieng BW, Ibrahim NA, Then YY and Loo YY. *Epoxidized vegetable oils plasticized poly(lactic acid) biocomposites: Mechanical, thermal and morphology properties*. Molecules, 2014. **19**(10):16024-16038.

[36] Silverajah VSG, Ibrahim NA, Yunus WMZW, Hassan HA and Woei CB. *A comparative study on the mechanical, thermal and morphological characterization of poly(lactic acid)/epoxidized palm oil blend*. International Journal of Molecular Sciences, 2012. **13**(5):5878-5898.

[37] Wadhi MM and Weliam R. *Effect of epoxidized sunflower oil on polylactic acid properties*. Research on Chemical Intermediates, 2014. **40**(1):399-406.

[38] Prempeh N, Li J, Liu D, Das K, Maiti S and Zhang Y. *Plasticizing effects of epoxidized sun flower oil on biodegradable polylactide films: A comparative study*. Polymer Science Series A, 2014. **56**(6):856-863.

[39] Santos EF, Oliveira RVB, Reiznautt QB, Samios D and Nachtigall SMB. *Sunflower-oil biodiesel-oligoesters/polylactide blends: Plasticizing effect and ageing*. Polymer Testing, 2014. **39:**23-29.

[40] Ferri JM, Garcia-Garcia D, Sánchez-Nacher L, Fenollar O and Balart R. *The effect of maleinized linseed oil (MLO) on mechanical performance of poly(lactic acid)-thermoplastic starch (PLA-TPS) blends*. Carbohydrate Polymers, 2016. **147:**60-68.

[41] Ruellan A, Guinault A, Sollogoub C, Chollet G, Ait-Mada A, Ducruet V and Domenek S. *Industrial vegetable oil by-products increase the ductility of polylactide*. Express Polymer Letters, 2015. **9**:1087-1103.

[42] Fenollar O, Garcia-Sanoguera D, Sánchez-Nácher L, López J and Balart R. *Characterization of the curing process of vinyl plastisols with epoxidized linseed oil as a natural-based plasticizer*. Journal of Applied Polymer Science, 2012. **124**(3):2550-2557.

[43] Nihul PG, Mhaske ST and Shertukde VV. *Epoxidized rice bran oil (ERBO) as a plasticizer for poly(vinyl chloride) (PVC)*. Iranian Polymer Journal, 2014. **23**(8):599-608.

[44] Fenollar O, Garcia-Sanoguera D, Sanchez-Nacher L, Lopez J and Balart R. *Effect of the epoxidized linseed oil concentration as natural plasticizer in vinyl plastisols*. Journal of Materials Science, 2010. **45**(16):4406-4413.

[45] Sharma BK, Adhvaryu A, Liu Z and Erhan SZ. *Chemical modification of vegetable oils for lubricant applications*. Journal of the American Oil Chemists' Society, 2006. **83**(2):129-136.

[46] Tan SG and Chow WS. *Biobased epoxidized vegetable oils and its greener epoxy blends: A review*. Polymer-Plastics Technology and Engineering, 2010. **49**:1581-1590.

[47] Campanella A, Rustoy E, Baldessari A and Baltanás MA. *Lubricants from chemically modified vegetable oils*. Bioresource Technology, 2010. **101**(1):245-254.

[48] Zhang C, Ding R and Kessler MR. *Reduction of epoxidized vegetable oils: A novel method to prepare bio-based polyols for polyurethanes*. Macromolecular Rapid Communications, 2014. **35**(11):1068-1074.

[49] Lee A and Deng Y. *Green polyurethane from lignin and soybean oil through non-isocyanate reactions*. European Polymer Journal, 2015. **63:**67-73.

[50] Zhang C, Wu H and Kessler MR. *High bio-content polyurethane composites with urethane modified lignin as filler*. Polymer, 2015. **69**:52-57.

[51] Domínguez-Díaz M, Meneses-Acosta A, Romo-Uribe A, Peña C, Segura D and Espin G. *Thermo-mechanical properties, microstructure and biocompatibility in poly-β-hydroxybutyrates (PHB) produced by OP and OPN strains of Azotobacter vinelandii*. European Polymer Journal, 2015. **63:**101-112.

[52] Ferri JM, Samper MD, García-Sanoguera D, Reig MJ, Fenollar O and Balart R. *Plasticizing effect of biobased epoxidized fatty acid esters on mechanical and thermal properties of poly(lactic acid)*. Journal of Materials Science, 2016. **51**(11):5356-5366.

[53] Garcia-Garcia D, Ferri JM, Montanes N, Lopez-Martinez J and Balart R. *Plasticization effects of epoxidized vegetable oils on mechanical properties of poly(3-hydroxybutyrate)*. Polymer International, 2016. **65**(10):1157-1164.

[54] Xu YQ and Qu JP. *Mechanical and rheological properties of epoxidized soybean oil plasticized poly(lactic acid)*. Journal of Applied Polymer Science, 2009. **112**(6):3185-3191.

[55] Zhao Y, Qu J, Feng Y, Wu Z, Chen F and Tang H. *Mechanical and thermal properties of epoxidized soybean oil plasticized polybutylene succinate blends*. Polymers for Advanced Technologies, 2012. **23**(3):632-638.

[56] Arrieta MP, Samper MD, López J and Jiménez A. *Combined effect of poly(hydroxybutyrate) and plasticizers on polylactic acid properties for film intended for food packaging*. Journal of Polymers and the Environment, 2014. **22**(4):460-470.

[57] Small PA. *Some factors affecting the solubility of polymers*. Journal of Chemical Technology and Biotechnology, 1953. **3**(2):71-80.

[58] Prakalathan K, Mohanty S and Nayak SK. *Reinforcing effect and isothermal crystallization kinetics of poly(3-hydroxybutyrate) nanocomposites blended with organically modified montmorillonite*. Polymer Composites, 2014. **35**(5):999-1012.

[59] Silverajah VSG, Ibrahim NA, Zainuddin N, Yunus WMZW and Hassan HA. *Mechanical, thermal and morphological properties of poly(lactic acid)/epoxidized palm olein blend*. Molecules, 2012. **17**(10):11729-11747.

[60] Erceg M, Kovačić T and Klarić I. *Thermal degradation of poly(3-hydroxybutyrate) plasticized with acetyl tributyl citrate*. Polymer Degradation and Stability, 2005. **90**(2):313-318.

[61] Zhang M and Thomas NL. *Blending polylactic acid with polyhydroxybutyrate: The effect on thermal, mechanical, and biodegradation properties*. Advances in Polymer Technology, 2011. **30**(2):67-79.

[62] Furukawa T, Sato H, Murakami R, Zhang J, Duan YX, Noda I, Ochiai S and Ozaki Y. *Structure, dispersibility, and crystallinity of poly(hydroxybutyrate)/poly(L-lactic acid) blends studied by FT-IR microspectroscopy and differential scanning calorimetry*. Macromolecules, 2005. **38**(15):6445-6454.

[63] Patrício PSO, Pereira FV, Dos Santos MC, De Souza PP, Roa JPB and Orefice RL. *Increasing the elongation at break of polyhydroxybutyrate biopolymer: Effect of cellulose nanowhiskers on mechanical and thermal properties*. Journal of Applied Polymer Science, 2013. **127**(5):3613-3621.

[64] Râpă M, Darie-Niţă RN, Grosu E, Tănase EE, Trifoi AR, Pap T and Vasile C. *Effect of plasticizers on melt processability and properties of PHB*. Journal of Optoelectronics and Advanced Materials, 2015. **17**(11-12):1778-1784.

Macromolecular
Materials and Engineering

Macromolecular Journals

Full Paper

Improvement of Mechanical Ductile Properties of Poly(3-hydroxybutyrate) by Using Vegetable Oil Derivatives

Daniel Garcia-Garcia,* Octavio Fenollar, Vicent Fombuena, Juan Lopez-Martinez, Rafael Balart

Poly(3-hydroxybutyrate), P3HB is a thermoplastic polyester synthesized from bacterial fermentation with potential uses in packaging due to its biodegradability. Nevertheless, P3HB is a fragile material and its processing temperature window is very narrow which restricts its use. This study explores the potential of vegetable oil-derived plasticizers, i.e., maleinized linseed oil (MLO) and an epoxidized fatty acid ester (EFAE) in the 5–20 phr range as environmentally friendly solutions for P3HB industrial formulations with improved toughness. The results show that optimum balance between ductile properties is achieved with low plasticizer content (5 phr) for both plasticizer types. Elongation at break and the impact resistance are increased by 28 and 71% respectively after addition of 5 phr MLO. With regard to EFAE, the elongation at break is improved by 40% and the impact resistance is increased to twice the value of P3HB. Another effect that both plasticizers provide is the thermal stabilization with a delay in the onset degradation temperature.

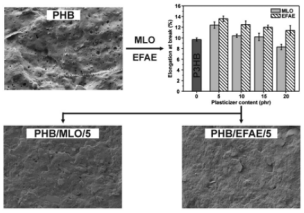

1. Introduction

Polymer materials have become an essential part of our lifestyle due to a wide range of advantages they can offer. A wide range of commodity, engineering, and high performance plastics are currently used. Moreover, new polymers are continuously being synthesized thus widening the potential of these materials. With the recent development of nanotechnologies, in situ polymerization with nanomaterials, widens new and useful applications of polymers in different sectors.[1,2] Advances in polymer colloids has also gained increasing interest due to their potential in combination with nanotechnologies.[3–5] For these reasons, the use of both conventional and new ad hoc synthesized polymers is continuously increasing. Subsequently, million tons of plastic wastes are generated every year with a remarkable negative effect on environment contamination.[6] This fact, together with the petroleum depletion has led to a growing interest in research on environmentally friendly polymers with the main aim of obtaining low environmental impact materials with similar physical and chemical properties to those of conventional petroleum-based polymer such as polyethylene, polypropylene, or others.[7–9] These environmentally friendly polymers include those obtained from renewable resources as it is the case of poly(lactic acid) (PLA), lignin, thermoplastic starch, cellulose, chitosan, proteins (gluten, casein, ovalbumin, etc.), bacterial polymers, etc. with an evident positive effect on the carbon footprint. Some other polymers obtained from petroleum resources such as poly(caprolactone), poly(butylene succinate), poly(vinyl-alcohol), poly(glycolic acid), etc. can also be considered as

D. Garcia-Garcia, Dr. O. Fenollar, Dr. V. Fombuena, Prof. J. Lopez-Martinez, Prof. R. Balart
Instituto de Tecnología de Materiales (ITM)
Universitat Politècnica de València (UPV)
Plaza Ferrándiz y Carbonell s/n
03801 Alcoy, Alicante, Spain
E-mail: dagarga4@epsa.upv.es

Macromol. Mater. Eng. **2017**, *302*, 1600330

DOI: 10.1002/mame.201600330

PHYSICAL BLENDING

IV.3

"Processing and characterization of binary poly(hydroxybutyrate) (PHB) and poly(caprolactone) (PCL) blends with improved impact properties"

Daniel García García[a], José M. Ferri[a], Teodomiro Borornat[a], Juan López Martínez[a], Rafael Balart[a]

[a] Instituto de Tecnología de Materiales (ITM)
Universitat Politècnica de València (UPV)
Plaza Ferrándiz y Carbonell 1, 03801 Alcoy, Alicante, Spain.

Polymer Bulletin

2016, 73:3333-3350

Processing and characterization of binary poly(hydroxybutyrate) (PHB) and poly(caprolactone) (PCL) blends with improved impact properties

Abstract

The present work is focused on the development of binary blends from poly(hydroxybutyrate) (PHB) and poly(caprolactone) (PCL). Miscibility, mechanical and thermal properties as well as blends morphology are evaluated in terms of the blend composition. Binary PHB/PCL blends were manufactured by melt compounding in a twin screw co-rotating extruder and injection molded. The composition of PHB/PCL covered the full range between individual polymers at 25 wt% increments. The obtained results show that PCL acts as an impact modifier, thus leading to an increase in flexibility and ductility as the PCL content in the PHB/PCL blends increases with a noticeable increase in elongation at break and on the energy absorption in impact conditions. The tensile strength and the elastic modulus decrease with increasing PCL content in the PHB/PCL blends; nevertheless, the flexural strength and the flexural modulus reach the highest values for PHB/PCL blends containing 25 wt% PCL, with a remarkable decrease over this composition. The analysis of fractured surfaces by field emission scanning electron microscopy and thermal properties obtained by differential scanning calorimetry (DSC) and thermogravimetric analysis (TGA) give clear evidences of the immiscibility of these two biodegradable polymers. Additionally, DSC results showed an increase in crystallinity of both PHB and PCL with regard to individual polymers for PHB/PCL blends containing 25 wt% PCL. Furthermore, an increase in the degradation onset (T_0) of about 30 °C higher was detected for the same blends. Dynamic mechanical thermal analysis (DMTA) showed slightly shifted glass transition temperatures of each individual polymer, thus indicating that although both PHB and PCL are not fully miscible, some interactions between them occur.

Keywords: Poly(hydroxybutyrate) (PHB); poly(caprolactone) (PCL); biodegradable; blends; miscibility.

INTRODUCTION

In the last decades, a remarkable increase in the use and consumption of polymeric materials has been detected; this increase has been particularly noticeable in the packaging industry. This fact has led to large waste generation around the world. An important fraction of these wastes are incinerated or poured into controlled landfills because of technical or economical reasons, thus leading to important environmental problems such as waste removal from the environment, soil contamination or toxic gas emissions from incineration processes. This acts as a leading force to the study, development and use of bio-based and/or biodegradable polymers characterized by low environmental impact [1-3].

Poly(hydroxybutyrate) (PHB) is one of the most studied biopolymer from the family of polyhydroxyalkanoates (PHAs) due to its biodegradability and biocompatibility [4]. It is an aliphatic polyester synthesized by controlled bacterial fermentation [5, 6]. It is characterized by a high crystallinity degree and a relatively high melt temperature, near 170 °C [2, 6]. Despite this, its high production cost in comparison to commercial plastics, high fragility due to high crystallinity, relatively low melt viscosity as well as thermal instability at moderate temperatures restrict its use [2, 7]. With the aim of improving some of its properties, PHB has been blended with several biodegradable polymers such as poly(lactic acid) (PLA) [2, 8], poly(p-dioxanone) (PPD) [5], poly(butylene succinate) (PBS) [9, 10], poly(ethylene succinate) (PES) [11] or poly(caprolactone) (PCL) [12-14].

The present work is focused on the use of PCL as co-component in binary PHB/PCL blends. PCL is a readily biodegradable, semicrystalline thermoplastic polyester which is produced by the ring opening polymerization of caprolactone monomer by using a catalyst [15]. PCL is characterized by a low melting point at around 60 °C and a very low glass transition temperature (T_g) at about –60 °C; nevertheless, the thermal decomposition temperature is relatively high, with values around 350 °C [16, 17]. With regard to its mechanical properties, PCL is extremely ductile with a high elongation at break value and low modulus [18, 19].

Physical blending of polymers by melt compounding is a good and cost-effective method to obtain materials with tailored properties [20]. Due to its high ductility, PCL offers attractive properties to PHB as it can reduce its low intrinsic fragility. PCL shows good miscibility behavior with a wide variety of polymers [21]; nevertheless, immiscibility with PHB has been reported in the literature together with different studies to increase the compatibility between them [12, 13, 22, 23].

The main aim of this work is to study the PHB/PCL system in terms of miscibility as well as mechanical, thermal and morphological properties of PHB/PCL blends obtained by melt compounding in a twin screw co-rotating extruder. The mechanical properties of PHB/PCL blends are evaluated by tensile, flexural, impact and hardness tests as well as by dynamic mechanical thermal analysis (DMTA) using an oscillatory rheometer with accessory for solid samples in a torsion-shear mode. The effect of the blend composition on thermal properties was evaluated by differential scanning calorimetry (DSC) and thermogravimetric analysis (TGA). Miscibility was assessed by thermal analysis together with morphological characterization by field emission scanning electron microscopy (FESEM).

EXPERIMENTAL

Materials

PHB under the trade name P226E (M_w = 426,000 g mol^{-1}) was supplied by Biomer (Krailling, Germany). PCL of commercial grade CAPA 6500 (M_w = 50,000 g mol^{-1}) was supplied by Perstorp Holdings AB (Malmö, Sweden).

Sample preparation

PHB and PCL pellets were dried in an air-circulating oven for 24 h at 70 and 40 °C, respectively, before further processing to remove moisture. The appropriate amounts of each polymer in the blends was weighed and mechanically mixed in a zip bag. After this, the pellet mixtures were compounded in a twin screw co-rotating extruder with a temperature profile ranging from 160 °C (hopper) to 175 °C (die) and a screw speed of 40 rpm. The extruded material was cooled in air and subsequently pelletized in a plastic mill. The compounding was further processed by injection molding in a Mateu & Solé mod. Meteor 270/75 (Barcelona, Spain) at 175 °C to obtain standard samples for testing. The blend composition ranges from individual PHB and PCL polymers to different compositions with 25 wt% increment. Table IV.3.1 summarizes the compositions for all the PHB/PCL blends manufactured.

Table IV.3.1. Composition of PHB/PCL blends and labeling of each composition.

Designation	PHB (wt%)	PCL (wt%)
PHB100/PCL0	100	0
PHB75/PCL25	75	25
PHB50/PCL50	50	50
PHB25/PCL75	25	75
PHB0/PCL100	0	100

Characterization techniques

Mechanical properties

The tensile and flexural properties of PHB/PCL biodegradable blends were obtained using an electromechanical universal test machine Ibertest ELIB 30 from S.A.E. Ibertest (Madrid, Spain) with a 5 kN load cell at room temperature, following the guidelines of ISO 527 and ISO 178 standards, respectively. The crosshead speed was set to 5 mm min^{-1}.

The impact-absorbed energy was measured in accordance with ISO 179 standard; impact tests were carried out on "V" notched samples ("V" at 45° and a notch radius of 0.25 mm) in a 1 J Charpy impact pendulum from Metrotec S.A. (San Sebastián, Spain).

The hardness of PHB/PCL blends was determined in a Shore D hardness durometer model 676-D from J. Bot Instruments (Barcelona, Spain) according to ISO 868.

The values reported for all mechanical parameters were obtained for at least five different samples and averaged.

Thermal properties

Thermal characterization of PHB/PCL blends was carried out by differential scanning calorimetry (DSC) and thermogravimetric analysis (TGA). Thermal transitions were obtained by DSC in a Mettler Toledo 821 from Mettler-Toledo Inc. (Schwerzenbach, Switzerland). A sample size of 7–9 mg was placed in standard 40 μL Al crucibles and subjected to an initial temperature program from –50 up to 180 °C at a constant heating rate of 10 °C min^{-1}. After this, the temperature was maintained at 180 °C for 2 min and subsequently cooled to –50 °C at a cooling rate of –10 °C min^{-1} to remove the previous thermal history. Then, samples were subjected to a second thermal program from –50 to

300 °C at 10 °C min^{-1}. DSC tests were carried out in a nitrogen atmosphere (66 mL min^{-1}). The melt temperature of PHB and PCL was determined by considering the information provided by the second heating ramp. The crystallinity degree of both PHB ($X_{c\,PHB}$) and PCL ($X_{c\,PCL}$) in the blends was calculated by following equation:

$$\boldsymbol{X_c}\,(\%) = \left[\frac{\Delta \boldsymbol{H_m}}{\Delta \boldsymbol{H_0} \cdot \boldsymbol{w}}\right] \times \mathbf{100} \qquad \textbf{Equation IV.3.1}$$

where ΔH_m is the fusion enthalpy and ΔH_0 is the enthalpy related to the corresponding 100% crystallinity (theoretical value) polymer; these values were assumed to be 146 J g^{-1} [1] for PHB and 156.8 J g^{-1} [3] for PCL. Finally, *w* represents the weight fraction of PHB and PCL in each PHB/PCL blend.

Thermogravimetric analysis was carried in a TGA/SDTA 851 horizontal thermobalance from Mettler-Toledo Inc. (Schwerzenbach, Switzerland). Samples of size 7–9 mg were placed in standard alumina crucibles and subjected to a heating program from 30 to 600 °C at a heating rate of 10 °C min^{-1} in nitrogen atmosphere (constant flow rate of 66 mL min^{-1}). The onset degradation temperature (T_0) was determined at 2 wt% mass loss and the maximum rate degradation temperature (T_{max}) was obtained by analyzing the DTG curves (first derivative of the TGA curve).

Field emission scanning electron microscopy (FESEM)

A field emission scanning electron microscope (FESEM) ZEISS ULTRA55 (Oxford instruments) at an acceleration voltage of 2 kV was used to observe the fractured surfaces of samples subjected to a cryofracture process. Cryofractured samples of each blend were subjected to a selective extraction of PCL with acetone. Firstly, all samples were dried in an air-circulating oven at 40 °C for 24 h and subsequently immersed in acetone for an additional 24 h at room temperature to selectively remove the PCL portion which allows to better distinguish the phase distribution in the blend [24]. Prior to sample observation of the samples before and after selective extraction, the surfaces were covered with a thin layer of platinum in vacuum conditions with a sputter coater.

Dynamic mechanical thermal analysis (DMTA)

Dynamic mechanical thermal analysis (DMTA) in torsion mode was carried out in an oscillatory rheometer AR G2 from TA Instruments (New Castle, USA). Rectangular samples of size 40×10×4 mm^3 were subjected to a dynamic temperature program from

–100 to 150 °C at a constant heating rate of 2 °C min^{-1} at a frequency of 1 Hz and constant deformation (γ) of 0.1%. The evolutions of the storage modulus (G'), loss modulus (G'') and damping factor (tan δ) were followed in terms of increasing temperature.

RESULTS AND DISCUSSION

Mechanical properties of PHB/PCL blend system

The mechanical properties (tensile and flexural) of PHB/PCL blend system are summarized in Table IV.3.2. With regard to tensile properties, we can see that individual PHB is characterized by a remarkably higher tensile strength and elastic modulus compared to raw PCL, but, obviously, lower deformation ability as can be derived by the relatively low elongation at break value of 8.1%. PHB is a rigid polymer. As we have indicated, the soft and flexible nature of PCL allows its use as an impact modifier for rigid polymers such as PHB. As the PCL content in PHB/PCL blends increases, we observe a decrease in both tensile strength and elastic modulus values; but, in contrast, the elongation at break (ductile properties) is remarkably improved. In fact, raw PCL and PHB/PCL blends with high PCL content (PHB25/PCL75) did not break; the samples showed the maximum displacement of the machine with elongation values over 1000% [25]. As can be observed, for PHB/PCL blends with less than 50 wt% PCL, the elongation at break is relatively low and the presence of PCL leads to a slight increase in elongation at break from values of 8.1% (raw PHB) up to 17.6% for PHB/PCL blends with 50 wt% PCL. It is expectable that PHB is the matrix in these blend compositions as the blend properties are mainly defined by PHB. Nevertheless, for compositions with high PCL content, the elongation at break increases up to values over 1000% and it is expected that PCL acts as matrix. Therefore, matrix inversion occurs for PCL contents higher than 50 wt%, as the properties of the blend are clearly defined by PCL for these composition ranges. PCL acts as an impact modifier with a remarkable increase in flexibility and ductility as PCL content increases and, specifically, for compositions with more than 50 wt% PCL.

The evolution of flexural properties is similar to those observed in the tensile mode. Individual PHB offers higher flexural strength and modulus values than individual PCL; nevertheless, we can see slight differences as the only addition of 25 wt% PCL leads to a slight increase in both flexural strength (from 36.7 to 38.5 MPa) and modulus (from 1515 to 1605 MPa) which represent a percentage increase of almost 5 and 6% respectively. Higher PCL contents in blends than 25 wt% lead to the expected behavior with decreasing

mechanical resistant properties such as flexural strength and modulus and an improvement in the deformation properties.

Table IV.3.2. Tensile and flexural properties of PHB/PCL blend system.

Samples	Tensile properties			Flexural properties	
	TS (MPa)	*E* (MPa)	ε_b (%)	FS (MPa)	*E* (MPa)
PHB100/PCL0	22.2 ± 0.6	1939 ± 11	8.1 ± 0.7	36.7 ± 0.6	1515 ± 64
PHB75/PCL25	21.4 ± 0.3	1643 ± 59	11.2 ± 0.5	38.5 ± 0.6	1605 ± 62
PHB50/PCL50	19.8 ± 0.2	1387 ± 57	17.6 ± 1.2	34.9 ± 0.4	1265 ± 65
PHB25/PCL75	17.3 ± 0.4	690 ± 26	>1000[a]	27.0 ± 0.7	716 ± 31
PHB0/PCL100	17.3 ± 0.3	341 ± 10	>1000[a]	22.8 ± 0.8	405 ± 29

[a] Does not fail.

Figure IV.3.1 shows the evolution of the impact-absorbed energy (Charpy pendulum) and Shore D hardness for the PHB/PCL blend system. The absorbed energy is directly related to the ability of the material to absorb energy during the fracture in impact conditions, mainly due to deformation before fracture, so that this property is representative of ductility, while Shore D hardness is representative of resistance. The evolution of the absorbed energy follows a similar tendency to that observed for elongation at break. We detected a slight increase from 2 kJ m^{-2} (individual PHB) up to values around 3.5 kJ m^{-2} for PHB/PCL blend with 50 wt% PCL and a remarkable increase for higher PCL content (values around 10.6 kJ m^{-2} for PHB/PCL blend with 75 wt% PCL) up to the maximum value achieved by individual PCL (15.1 kJ m^{-2}). In general terms, we can conclude that the addition of PCL leads to an improvement in the ductile behavior of PHB/PCL blends which is more evident for compositions with more than 50 wt% PCL. As expected, Shore D hardness offers opposite behavior as it is a mechanically resistant property. PHB is characterized by a Shore D of 57.3, while PCL is much softer with a Shore D value of 46.5. As the PCL content of PHB/PCL blends increases, we observe a decrease in Shore D values which is more evident for composition with more than 25–50 wt%.

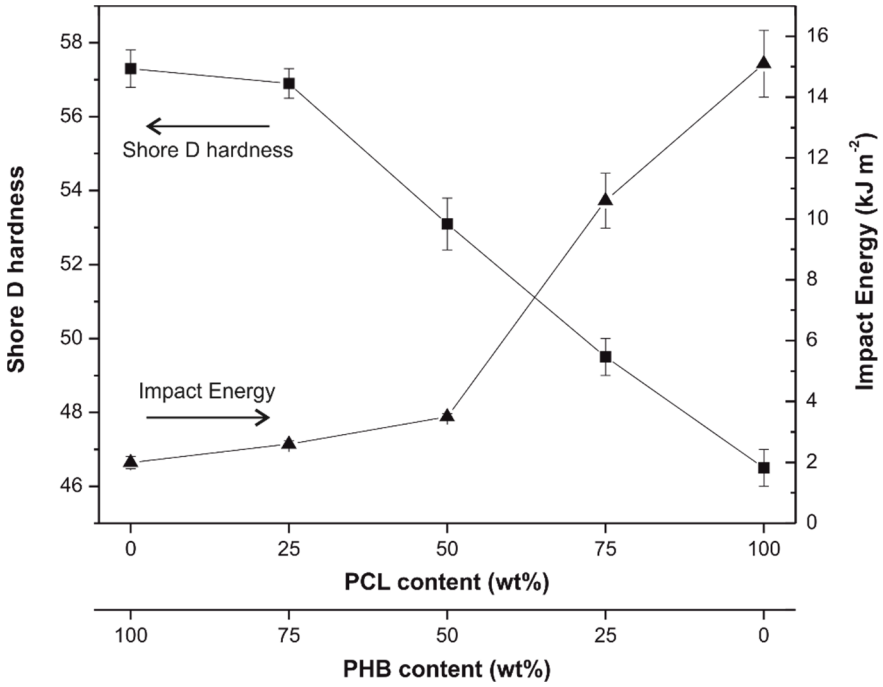

Figure IV.3.1. Impact energy and Shore D hardness values for the PHB/PCL blend system in terms of the PCL content.

Thermal properties of PHB/PCL blend system

Figure IV.3.2 shows a comparative plot of the DSC curves of PHB/PCL blend system with varying composition. Figure IV.3.2a shows the cooling curves after removal of thermal history and Figure IV.3.2b shows the DSC curves corresponding to the second heating cycle and the base curve for determining the values of ΔH_m for PHB, PCL and their blends (unnormalized values and normalized values with respect to the sample weight), the melt temperatures (T_m) as well as the crystallinity degree (X_c); all these values are shown in Table IV.3.3. As seen in Figure IV.3.2b, individual PHB shows two melt peaks: one located at 168.3 °C which is related to the melting of PHB and a small peak at 52.3 °C which can be attributable to some low molecular weight additive in the formulation [26, 27]. With regard to the glass transition temperature, typical values of T_g for PHB are located at the 2–7 °C range. We can see a slight change in the baseline in a wide temperature range covering –10 to 10 °C, but no clear evidence of T_g is detected. With regard to individual PCL, we observe a unique peak located at 60 °C and the T_g cannot be detected as it is below –50 °C [16]; for this reason, the T_g study was conducted using DMTA. DSC of PHB/PCL blend system shows a clear evidence of the immiscibility of these two biodegradable polymers, as two individual peaks located at the typical temperature values of each melting point can be detected: one at about 170 °C attributable to PHB and the other melt peak located at about 60 °C which is

related to the melting of PCL. Table IV.3.3 shows that as the PCL content on PHB/PCL blends increases, a slight increase in both melt peak temperatures of PHB ($T_{m\ PHB}$) and PCL can be detected ($T_{m\ PCL}$).

The normalized melt enthalpy (ΔH_m) for both polymers, obtained in the second heating cycle, was used to calculate the crystallinity degree of each material in the blend. Crystallinity plays an important role in the mechanical performance of PHB, PCL and their blends. The percentage crystallinity of individual PHB ($X_{c\ PHB}$) is higher than 55%, while the percentage crystallinity of raw PCL ($X_{c\ PCL}$) is about 46%. The percentage crystallinity of each polymer in the blends is slightly higher for PHB/PCL blends: with 25 wt% PCL, the percentage crystallinity of PHB ($X_{c\ PHB}$) changes from 55.1 up to 58.2% and the value of ($X_{c\ PCL}$) changes from 46.4 to 51.3%. The percentage crystallinity of each polymer for the remaining blend compositions is slower as observed in Table IV.3.3. That is why we have previously observed a slight increase in flexural strength and modulus in PHB/PCL blends with 25 wt% PCL.

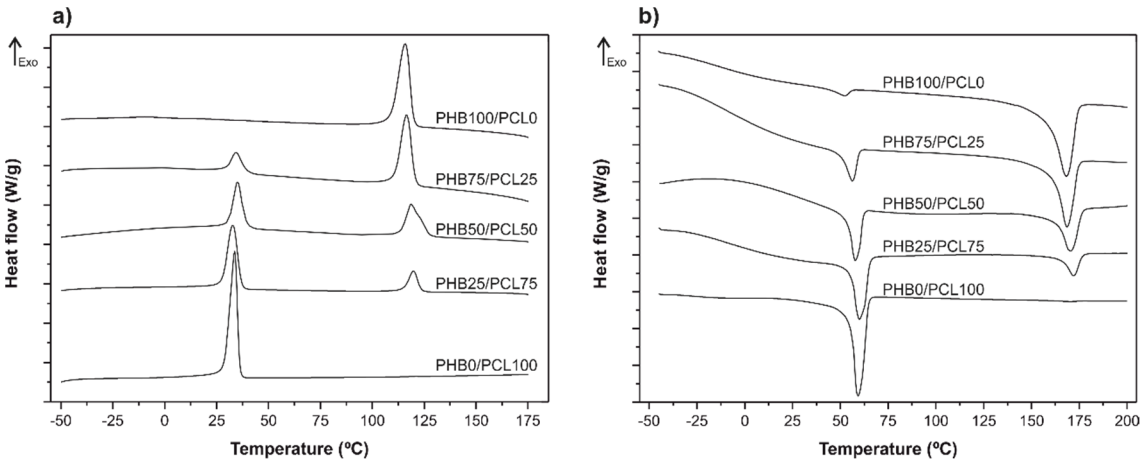

Figure IV.3.2. DSC thermograms during the (a) cooling scan and (b) second heating scan of PHB/PCL blend system.

Table IV.3.3. Thermal parameters of PHB/PCL blend system obtained by differential scanning calorimetry (DSC).

Samples	DSC Parameters							
	$T_{m\ PCL}$ (°C)	$\Delta H_{m\ PCL}$ (J g^{-1})[a]	$\Delta H_{m\ PCL}$ (J g^{-1})[b]	$X_{c\ PCL}$ (%)	$T_{m\ PHB}$ (°C)	$\Delta H_{m\ PHB}$ (J g^{-1})[a]	$\Delta H_{m\ PHB}$ (J g^{-1})[b]	$X_{c\ PHB}$ (%)
PHB100/PCL0	-	-	-	-	168.3	–80.5	–80.5	55.1
PHB75/PCL25	56.2	–20.1	–80.5	51.3	168.6	–63.7	–85.0	58.2
PHB50/PCL50	57.9	–34.1	–68.2	43.5	170.6	–39.9	–79.9	54.7
PHB25/PCL75	59.3	–41.4	–55.2	35.2	172.2	–15.3	–61.4	42.0
PHB0/PCL100	60.0	–72.8	–72.8	46.4	-	-	-	-

[a] Values obtained directly from DSC.

[b] Normalized values respect to the real polymer mass weight.

Thermogravimetric curves (TGA) of both individual PHB and PCL as well as the PHB/PCL blends are shown in Figure IV.3.3a and the main thermal parameters regarding degradation are summarized in Table IV.3.4. As can be observed, PCL degrades in a single-step process with an onset degradation temperature ($T_{0\ PCL}$) of 359.5 °C and a maximum degradation rate temperature ($T_{max\ PCL}$) of 415.5 °C [28]. On the other hand, PHB degradation proceeds in several stages due to the formulation of the commercial polymer which contains plasticizers, nucleating agents and stabilizers [26]. The onset degradation temperature for PHB ($T_{0\ PHB}$) is 231.3 °C and the maximum rate ($T_{max\ PHB}$) is achieved at 290 °C. These values are remarkably lower than those obtained for individual PCL, thus giving clear evidence of the lower thermal stability of PHB compared to PCL. The TGA curves for PHB/PCL blends occur in two different stages, attributable to PHB and PCL. The first degradation stage is related to PHB degradation and the second stage, located at higher temperatures is related to PCL degradation with slight changes in the characteristic degradation temperatures corresponding to each polymer. This is also a clear evidence of the lack of strong interactions between the two biodegradable polymers, thus giving evidence of immiscibility (or very low miscibility). In general terms, we can see that the presence of PCL leads to a slight increase in the thermal stability of PHB. Although PHB and PCL show very restricted miscibility as revealed by the DSC analysis, PCL is characterized by a remarkably high thermal stability compared to PHB and all blends with PCL show a slight increase in the thermal onset degradation temperature which could be somewhat related to interactions between the two components. Thus, it is possible to expect phase separation with a PCL-

rich phase with very low content on PHB chains and, in the same way, a PHB-rich phase with very low amounts of dissolved PCL chains. This fact could be responsible for the slight increase in the thermal stability of the PHB-rich phase and, conversely, a slight decrease in the onset degradation temperature of the PCL-rich phase. We can see in Table IV.3.4 how the onset degradation temperature (T_0) is increased from 231.3 °C (individual PHB) up to values in the 260–270 °C for PHB/PCL blends with PCL content in the 25–75 wt% range. A similar tendency (but less intense) can be observed for the maximum thermal degradation rate (T_{max}) for both PHB and PCL. With regard to the maximum degradation rate temperature of PHB ($T_{max\ PHB}$) changes from 290.0 °C (individual PHB) up to values of 296.8 °C for PHB/PCL blends with 75 wt% PCL. The maximum degradation rate temperature for PCL ($T_{max\ PCL}$) changes in a very narrow range from 413.8 to 415.5 °C for blend composition containing 75 wt% PCL.

Derivative thermogravimetric curves (DTG) are shown in Figure IV.3.3b and we can observe the peak temperatures corresponding to the maximum weight loss rate. DTG curves of PHB/PCL blends are characterized by two main peaks attributable to PHB degradation (low temperature) and PCL degradation (high temperature). As previously discussed, the maximum degradation rate temperature for PHB ($T_{max\ PHB}$) slightly increases, while the maximum degradation rate temperature for PCL ($T_{max\ PCL}$) remains in a very narrow temperature range (413–415 °C).

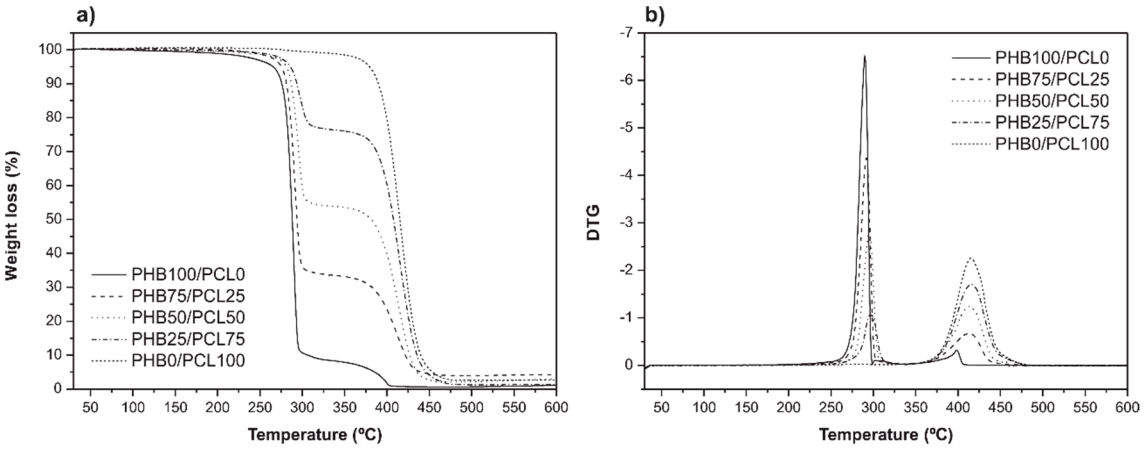

Figure IV.3.3. (a) TGA and (b) DTG curves of PHB/PCL blend system.

Table IV.3.4. Thermal degradation parameters of PHB/PCL blend system obtained by thermogravimetric analysis (TGA).

Samples	TGA Parameters		
	T_0[a] (°C)	$T_{max\ PHB}$ (°C)	$T_{max\ PCL}$ (°C)
PHB100/PCL0	231.3	290.0	-
PHB75/PCL25	260.8	291.7	413.8
PHB50/PCL50	264.7	295.3	412.5
PHB25/PCL75	270.6	296.8	415.5
PHB0/PCL100	359.5	-	415.8

[a] T_0, calculated at 2% mass loss.

Morphological characterization of PHB/PCL blend system

Figure IV.3.4 shows the FESEM images of cryofractured surfaces of PHB, PCL and their blends in terms of the PCL content. We can observe a clear fragile fracture surface due to cryofracture conditions. The fracture surface of individual PHB can be seen in Figure IV.3.4a and it is characterized by different immiscible components in the commercial formulation. As we have indicated, this commercial PHB grade is composed of plasticizers and other components which are not fully miscible in PHB [26], thus resulting in very small spherical formations (lower than 500 nm). With regard to PHB/PCL blends morphology, we can clearly see phase separation between PHB and PCL, thus giving clear evidence of the immiscibility (or very low miscibility) of these two biodegradable polymers. For all intermediate compositions, we observe a matrix phase and dispersed circular shapes of size between 2 and 10 μm (we did not observe the typical spherical droplets and holes of immiscible polymers, due to the cryofracture process which also breaks dispersed spherical droplets) corresponding to the dispersed phase. In the PHB/PCL blend with 25 wt% PCL, Figure IV.3.4b, the spherical droplets are higher than those observed in PHB/PCL blends in which PCL is the main component and acts as matrix. In addition, for the PHB/PCL blend with 25 wt% PCL, we can see the lack of interaction between PCL droplets and the surrounding PHB matrix (Figure IV.3.4b). The largest droplets can be observed in Figure IV.3.4c which corresponds to the PHB/PCL blend with 50 wt% PCL. As can be seen in Figure IV.3.5, we observe a small ring around the dispersed phase which can be representative for some miscibility between the two polymers. In Figure IV.3.5, the generalized lack of interactions between the two polymers is clearly detectable.

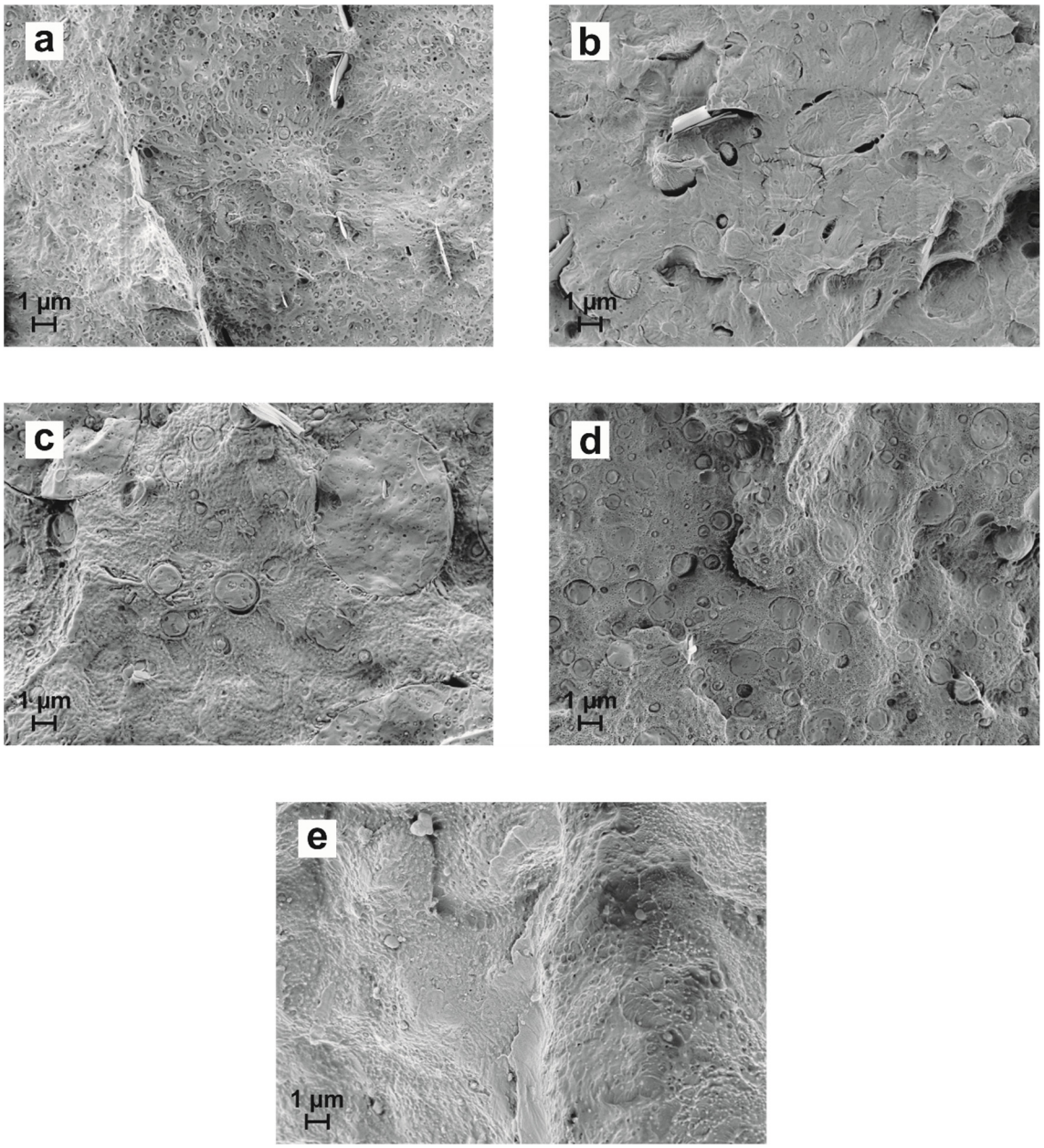

Figure IV.3.4. FESEM images at 5000x of cryofractured surfaces of PHB/PCL blends: (a) PHB100/PCL0; (b) PHB75/PCL25; (c) PHB50/PCL50; (d) PHB25/PCL75; (e) PHB0/PCL100.

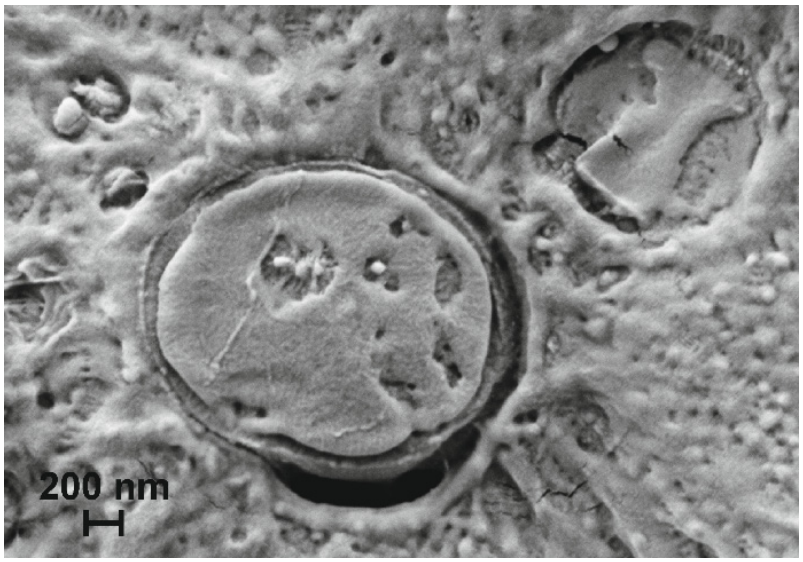

Figure IV.3.5. FESEM image of cryofractured surface of PHB50/PCL50 at 25,000x.

With the aim of analyzing the surface morphology, a selective extraction process was performed with acetone for a period of 24 h to selectively dissolve PCL [24]. In Figure IV.3.6a and b, we can see how the small PCL droplets have been fully dissolved, leading to the formation of small voids on the fractured surface, while larger PCL droplets have not been fully attacked leading to a flake-like structure. The blend composition with 25 wt% PCL (PHB75/PCL25) shows that PCL is highly dispersed in the PHB matrix that was not clearly detectable by conventional FESEM without previous selective attack of the PCL-rich phase. With regard to the blend compositions with 50 wt% PCL (PHB50/PCL50), we see that PCL acts as the matrix in the blend with the typical flake morphology described before. Such morphology is also observed for PCL-rich blend with 75 wt% PCL. In both cases, the selective extraction with acetone leads to the appearance of small PHB spherical droplets immersed in the PCL matrix.

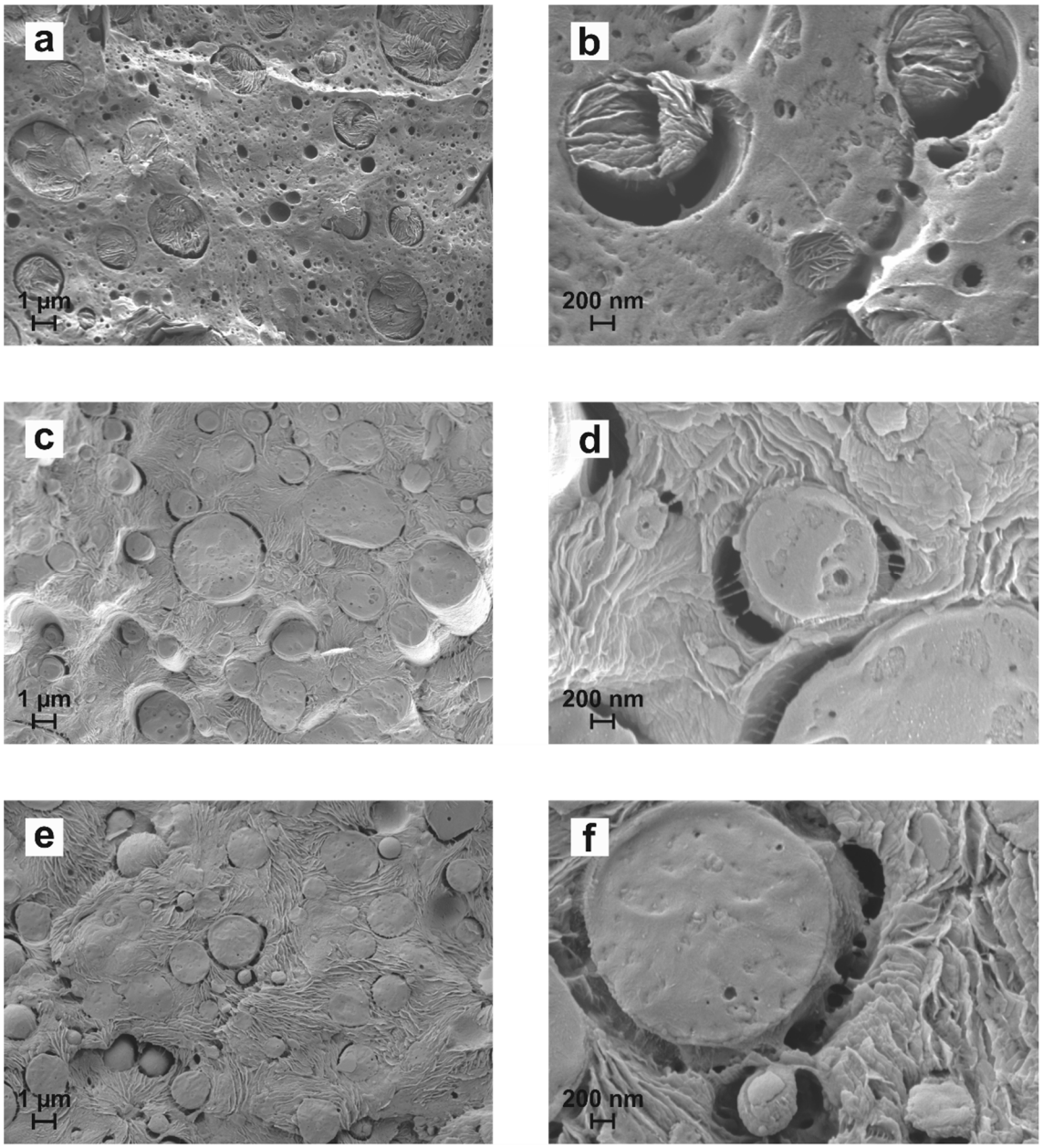

Figure IV.3.6. FESEM images of cryofractured surfaces of PHB/PCL blends subjected to a selective extraction with acetone: (a) PHB75/PCL25 (5000x); (b) PHB75/PCL25 (25,000x); (c) PHB50/PCL50 (5000x); (d) PHB50/PCL50 (25,000x); (e) PHB25/PCL75 (5000x); (f) PHB25/PCL75 (25,000x).

Dynamic mechanical thermal analysis (DMTA) of PHB/PCL blend system

Figure IV.3.7 shows the evolution of the storage modulus (G'), the loss modulus (G'') and the damping factor (tan δ) for individual PHB and PCL as well as their blends in terms of increasing temperature. As seen in Figure IV.3.7a, the storage modulus decreases with temperature. PHB is stiffer than PCL and that is why the G' curve corresponding to PHB is

shifted to high values. The storage modulus for PHB shows two main steps: one located at around –7 °C which is related to its glass transition temperature ($T_{g\,PHB}$) and another in the temperature range between 55 and 60 °C which can be attributable to some commercial additive in PHB [26]. With regard to the storage modulus evolution for PCL, a remarkable decrease can be detected once its glass transition temperature ($T_{g\,PCL}$) is surpassed at around –53 °C. This dramatic drop in *G'* values for PCL can also be observed in the PHB/PCL blends with high PCL content (50 and 75 wt%), while a not so remarkable peak is observable for blends with 25 wt% PCL. The storage modulus for blends with high PCL contents reaches values near 0 MPa once the melt temperature of PCL ($T_{m\,PCL}$) has been surpassed (around 60 °C), which also gives evidences that PCL acts as the matrix for a polymer blend composition of 50 wt% PCL. The blend composition with 25 wt% PCL (PHB75/PCL25) shows, at room temperature, a similar storage modulus to that obtained for individual PHB, but a remarkable decrease is detected at temperatures higher than 60 °C, in which PCL melt occurs. As seen, as the PCL content increases, the *G'* curves are moved to lower values, thus indicating that PCL provides an impact modifier effect on PHB.

With regard to the loss modulus (*G''*) and damping factor (tan δ), Figure IV.3.7b and c shows their corresponding evolutions with temperature. PHB/PCL blends show two peaks that are attributable to PHB and PCL, which in turn gives evidences of immiscibility or poor miscibility of both polymers in the amorphous regions. The first peak, located at –53 °C is representative for the glass transition temperature of PCL ($T_{g\,PCL}$) and the other main peak is located at around –7 °C and corresponds to the glass transition temperature of PHB ($T_{g\,PHB}$). Nevertheless, it can be observed that the glass transition temperature of each polymer in the blend is slightly different compared to the individual material, which could be attributable to some interactions between both polymers.

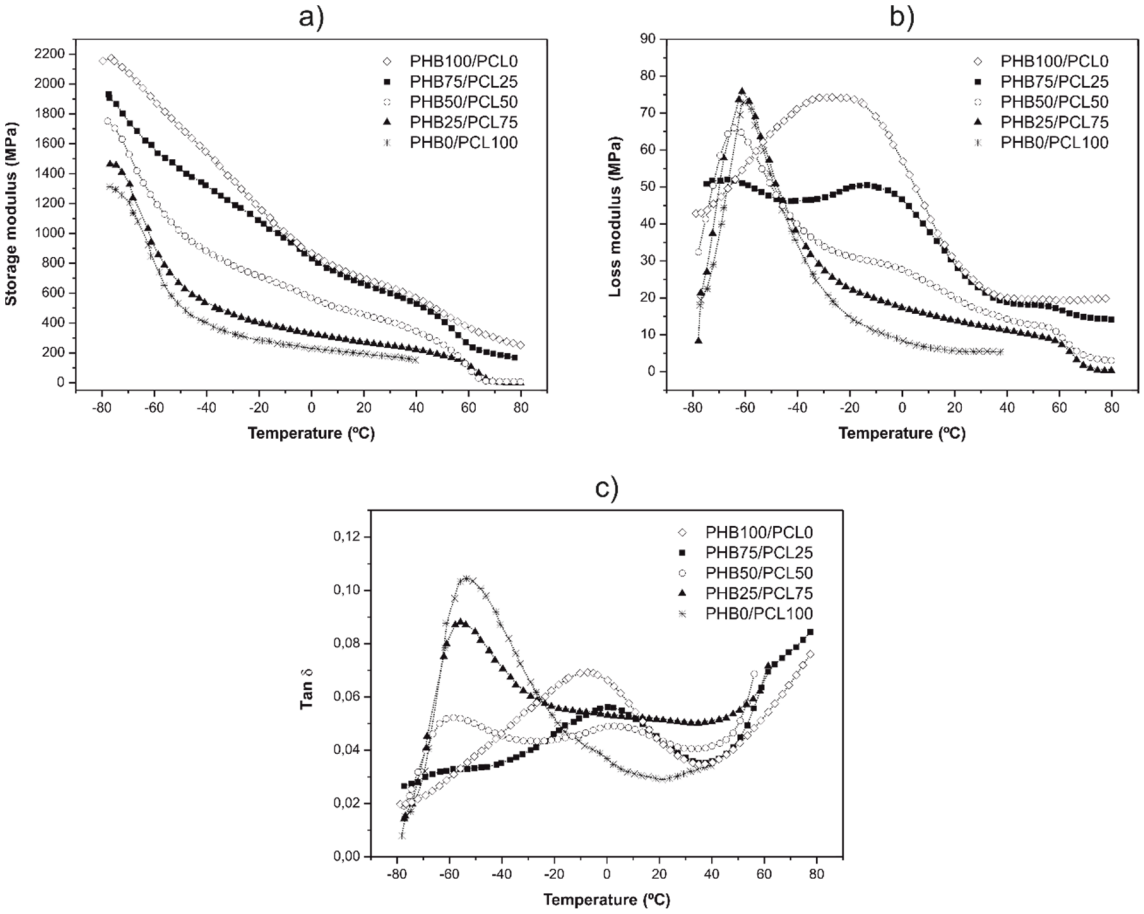

Figure IV.3.7. DMTA (torsion mode) curves of PHB/PCL blend system: (a) storage modulus (G'); (b) loss modulus (G'') and (c) damping factor (tan δ).

CONCLUSIONS

The main aim of this research work was the development of PHB blends with PCL to improve the high intrinsic fragility of PHB. The obtained results show that PCL acts as an impact modifier, thus providing higher flexibility and ductility and, obviously, a decrease in mechanical resistant properties such as strength and modulus. As the PCL content in PHB/PCL blends increases, we observe an increase in the impact-absorbed energy as well as the elongation at break in tensile tests. This increase is particularly remarkable for PHB/PCL blends with more than 50 wt% PCL. The elongation at break changes from 11.2% up to values over 1000% for a blend composition of 75 wt% PCL. With regard to flexural strength and modulus, we observe a slight increase for the blend containing 25 wt% PCL. This is related to the crystallization phenomena and the DSC study revealed a noticeable increase in the crystallinity degree (X_c) of both PHB and PCL for this particular blend composition. PHB and PCL have been proved to be immiscible as revealed by the FESEM of cryofractured samples. Such immiscibility is also evident by DSC and TGA analysis. The DSC

study does not show significant changes in the melt peak temperature for PHB and PCL, and TGA analysis of PHB/PCL blends shows a slight improvement in the typical degradation temperatures, but it is not significant. The TGA study also reveals the relatively low thermal stability of individual PHB compared to PCL, but the addition of PCL to PHB promotes slight improvement on the typical degradation temperatures of PHB. Dynamic mechanical thermal analysis (DMTA) confirmed the very low miscibility between these polymers with two glass transition temperatures located at around –53 and –7 °C for the PCL-rich phase and PHB-rich phase respectively. Nevertheless, some slight changes in the T_g values are observed which could be representative for some PHB/PCL interactions.

ACKNOWLEDGEMENTS

This research was supported by the Ministry of Economy and Competitiveness (MINECO) [MAT2014-59242-C2-1-R]. The authors also thank the Conselleria d'Educació, Cultura i Esport – Generalitat Valenciana for financial support [GV/2014/008]. D. Garcia-Garcia thanks the Spanish Ministry of Education, Culture and Sports for their financial support through an FPU grant [FPU13/06011].

REFERENCES

[1] Arrieta MP, Samper MD, López J and Jiménez A. *Combined effect of poly(hydroxybutyrate) and plasticizers on polylactic acid properties for film intended for food packaging*. Journal of Polymers and the Environment, 2014. **22**(4):460-470.

[2] Zhang M and Thomas NL. *Blending polylactic acid with polyhydroxybutyrate: The effect on thermal, mechanical, and biodegradation properties*. Advances in Polymer Technology, 2011. **30**(2):67-79.

[3] Simões CL, Viana JC and Cunha AM. *Mechanical properties of poly(ε-caprolactone) and poly(lactic acid) blends*. Journal of Applied Polymer Science, 2009. **112**(1):345-352.

[4] Wei L, Liang S and McDonald AG. *Thermophysical properties and biodegradation behavior of green composites made from polyhydroxybutyrate and potato peel waste fermentation residue*. Industrial Crops and Products, 2015. **69**:91-103.

[5] Dias M, Antunes MCM, Santos AR and Felisberti MI. *Blends of poly(3-hydroxybutyrate) and poly(p-dioxanone): Miscibility, thermal stability and biocompatibility*. Journal of Materials Science: Materials in Medicine, 2008. **19**(12):3535-3544.

[6] Çatiker E and Sancaktar E. *Blends of poly(3-hydroxybutyrate) with poly(β-alanine) and its derivatives*. Journal of Applied Polymer Science, 2014. **131**(13):40484.

[7] Janigová I, Lacík I and Chodák I. *Thermal degradation of plasticized poly(3-hydroxybutyrate) investigated by DSC*. Polymer Degradation and Stability, 2002. **77**(1):35-41.

[8] Abdelwahab MA, Flynn A, Chiou BS, Imam S, Orts W and Chiellini E. *Thermal, mechanical and morphological characterization of plasticized PLA-PHB blends*. Polymer Degradation and Stability, 2012. **97**(9):1822-1828.

[9] Ma P, Cai X, Wang W, Duan F, Shi D and Lemstra PJ. *Crystallization behavior of partially crosslinked poly(β-hydroxyalkonates)/poly(butylene succinate) blends*. Journal of Applied Polymer Science, 2014. **131**(21):41020.

[10] Ma P, Hristova-Bogaerds DG, Zhang Y and Lemstra PJ. *Enhancement in crystallization kinetics of the bacterially synthesized poly(β-hydroxybutyrate) by poly(butylene succinate)*. Polymer Bulletin, 2014. **71**(4):907-923.

[11] Al-Salah HA. *Crystallization and morphology of poly(ethylene succinate) and poly(β-hydroxybutyrate) blends*. Polymer Bulletin, 1998. **41**(5):593-600.

[12] Gassner F and Owen AJ. *Physical properties of poly(β-hydroxybutyrate)-poly(ε-caprolactone) blends*. Polymer, 1994. **35**(10):2233-2236.

[13] Lovera D, Márquez L, Balsamo V, Taddei A, Castelli C and Muller AJ. *Crystallization, morphology, and enzymatic degradation of polyhydroxybutyrate/polycaprolactone (PHB/PCL) blends*. Macromolecular Chemistry and Physics, 2007. **208**(9):924-937.

[14] Kim BO and Woo SI. *Compatibilizing capability of poly(β-hydroxybutyrate-co-ε-caprolactone) in the blend of poly(β-hydroxybutyrate) and poly(ε-caprolactone)*. Polymer Bulletin, 1998. **41**(6):707-712.

[15] García AV, Santonja MR, Sanahuja AB and Selva MCG. *Characterization and degradation characteristics of poly(ε-caprolactone)-based composites reinforced with almond skin residues*. Polymer Degradation and Stability, 2014. **108**:269-279.

[16] Patrício T and Bártolo P. *Thermal stability of PCL/PLA blends produced by physical blending process*. Procedia Engineering, 2013. **59**:292-297.

[17] Harrison KL and Jenkins MJ. *The effect of crystallinity and water absorption on the dynamic mechanical relaxation behaviour of polycaprolactone*. Polymer International, 2004. **53**(9):1298-1304.

[18] Fukushima K, Feijoo JL and Yang MC. *Comparison of abiotic and biotic degradation of PDLLA, PCL and partially miscible PDLLA/PCL blend*. European Polymer Journal, 2013. **49**(3):706-717.

[19] Li Y, Dong Q, Han C, Bian Y, Zhang X and Dong L. *Toward environment-friendly composites of poly(ε-caprolactone) reinforced with stereocomplex-type poly(L-lactide)/poly(D-lactide)*. Journal of Applied Polymer Science, 2014. **131**(9):40208.

[20] Imre B and Pukánszky B. *Compatibilization in bio-based and biodegradable polymer blends*. European Polymer Journal, 2013. **49**(6):1215-1233.

[21] Hinüber C, Häussler L, Vogel R, Brünig H, Heinrich G and Werner C. *Hollow fibers made from a poly(3-hydroxybutyrate)/poly-ε-caprolactone blend*. Express Polymer Letters, 2011. **5**(7):643-652.

[22] Kumagai Y and Doi Y. *Enzymatic degradation and morphologies of binary blends of microbial poly(3-hydroxy butyrate) with poly(ε-caprolactone), poly(1,4-butylene adipate and poly(vinyl acetate)*. Polymer Degradation and Stability, 1992. **36**(3):241-248.

[23] Avella M, Martuscelli E and Raimo M. *Review: Properties of blends and composites based on poly(3-hydroxy)butyrate (PHB) and poly(3-hydroxybutyrate-hydroxyvalerate) (PHBV) copolymers*. Journal of Materials Science, 2000. **35**(3):523-545.

[24] Katsumata K, Saito T, Yu F, Nakamura N and Inoue Y. *The toughening effect of a small amount of poly(ε-caprolactone) on the mechanical properties of the poly(3-hydroxybutyrate-co-3-hydroxyhexanoate)/PCL blend*. Polymer Journal, 2011. **43**(5):484-492.

[25] Monticelli O, Calabrese M, Gardella L, Fina A and Gioffredi E. *Silsesquioxanes: Novel compatibilizing agents for tuning the microstructure and properties of PLA/PCL immiscible blends*. European Polymer Journal, 2014. **58**:69-78.

[26] Prakalathan K, Mohanty S and Nayak SK. *Reinforcing effect and isothermal crystallization kinetics of poly(3-hydroxybutyrate) nanocomposites blended with organically modified montmorillonite*. Polymer Composites, 2014. **35**(5):999-1012.

[27] Wang L, Zhu W, Wang X, Chen X, Chen GQ and Xu K. *Processability modifications of poly(3-hydroxybutyrate) by plasticizing, blending, and stabilizing*. Journal of Applied Polymer Science, 2008. **107**(1):166-173.

[28] Mofokeng JP and Luyt AS. *Morphology and thermal degradation studies of melt-mixed poly(hydroxybutyrate-co-valerate) (PHBV)/poly(ε-caprolactone) (PCL) biodegradable polymer blend nanocomposites with TiO_2 as filler*. Journal of Materials Science, 2015. **50**(10):3812-3824.

Polym. Bull. (2016) 73:3333–3350
DOI 10.1007/s00289-016-1659-6

ORIGINAL PAPER

Processing and characterization of binary poly(hydroxybutyrate) (PHB) and poly(caprolactone) (PCL) blends with improved impact properties

D. Garcia-Garcia[1] · J. M. Ferri[1] · T. Boronat[1] · J. Lopez-Martinez[1] · R. Balart[1]

Received: 8 October 2015 / Revised: 17 March 2016 / Accepted: 2 April 2016 /
Published online: 7 April 2016

Abstract The present work is focused on the development of binary blends from poly(hydroxybutyrate) (PHB) and poly(caprolactone) (PCL). Miscibility, mechanical and thermal properties as well as blends morphology are evaluated in terms of the blend composition. Binary PHB–PCL blends were manufactured by melt compounding in a twin screw co-rotating extruder and injection molded. The composition of PHB–PCL covered the full range between individual polymers at 25 wt% increments. The obtained results show that PCL acts as an impact modifier, thus leading to an increase in flexibility and ductility as the PCL content in the PHB–PCL blends increases with a noticeable increase in elongation at break and on the energy absorption in impact conditions. The tensile strength and the elastic modulus decrease with increasing PCL content in the PHB–PCL blends; nevertheless, the flexural strength and the flexural modulus reach the highest values for the PHB–PCL blends containing 25 wt% PCL, with a remarkable decrease over this composition. The analysis of fractured surfaces by field emission scanning electron microscopy and thermal properties obtained by differential scanning calorimetry (DSC) and TGA give clear evidences of the immiscibility of these two biodegradable polymers. Additionally, DSC results showed an increase in crystallinity of both PHB and PCL with regard to individual polymers for PHB–PCL blends containing 25 wt% PCL. Furthermore, an increase in the degradation onset (T_0) of about 30 °C higher was detected for the same blends. Dynamic mechanical thermal analysis showed slightly shifted glass transition temperatures of each individual polymer, thus indicating that although both PHB and PCL are not fully miscible, some interactions between them occur.

✉ D. Garcia-Garcia
dagarga4@epsa.upv.es

[1] Instituto de Tecnología de Materiales (ITM), Universitat Politècnica de València (UPV), Plaza Ferrandiz y Carbonell 1, 03801 Alcoy, Alicante, Spain

IV.4

"Improvement of the compatibility between poly(3-hydroxybutyrate) and poly(ε-caprolactone) by reactive extrusion with dicumyl peroxide"

Daniel García García[a], *Emilio Rayón*[a], *Alfredo Carbonell Verdú*[a], *Juan López Martínez*[a], *Rafael Balart*[a]

[a] Instituto de Tecnología de Materiales (ITM)
Universitat Politècnica de València (UPV)
Plaza Ferrándiz y Carbonell 1, 03801 Alcoy, Alicante, Spain.

European Polymer Journal

2017, 86:41-57

Improvement of the compatibility between poly(3-hydroxybutyrate) and poly(ε-caprolactone) by reactive extrusion with dicumyl peroxide

Abstract

Poly(3-hydroxybutyrate) is a biodegradable aliphatic polyester obtained through bacterial fermentation that has gained attention in the last few years; nevertheless, its industrial applications are restricted because of some drawbacks related to its high stiffness and fragility which is associated to its high crystallinity. In this work, poly(3-hydroxybutyrate) (PHB) was melt blended with poly(ε-caprolactone) (PCL) at a constant weight ratio of 75/25 (PHB/PCL) by reactive extrusion with different contents of dicumyl peroxide (DCP) in the 0–1 wt% range. The effects of the DCP load on mechanical, thermal and morphology of the PHB/PCL blend were studied. Results showed a positive increase in the elongation at break and the impact-absorbed energy of 91 and 231% respectively with regard the uncompatibilized PHB/PCL blend by the addition of 1 wt% DCP, being this a clear evidenced of the improved compatibility between these polymers. Moreover, morphology of DCP-compatibilized PHB/PCL blend obtained by field emission electron microscopy (FESEM) and atomic force microscopy (AFM) showed a remarkable decrease in the particle size of poly(ε-caprolactone)-rich domains randomly dispersed in the poly(3-hydroxybutyrate). In addition, both FESEM and AFM also revealed improved interfacial adhesion between PHB- and PCL-rich phases with a noticeable decrease in the gap between them. Addition of 1 wt% DCP also contributes to lowering the degree of crystallinity of PHB by 14% in the blend and other thermal properties are not highly affected by the reactive extrusion with DCP.

Keywords: Poly(3-hydroxybutyrate); poly(ε-caprolactone); dicumyl peroxide; reactive compatibilization; blends.

INTRODUCTION

During the last years, a global marked driven by consumerism along with the relatively low price of plastic materials has led to a remarkable growth in the plastic production and consumption. Only in Europe the plastic production in 2014 was estimated to 59 million tons whilst the global plastic production was of about 299 million tons. The packaging industry is the biggest consumer which accounts for 39.5% with a wide variety of products characterized by a very short life cycle [1]. One of the main problems related to the massive use of plastics is the huge amounts of wastes that are generated after the end of their life cycled as only a small amount is recycled, upgraded or incinerated for energy production. The most common situation is that huge amounts of plastic wastes are continuously deposited into controlled landfills with a marked negative effect on environment. It has been estimated that in 2014 the total amount of plastic wastes poured into European's landfills accounts to 8 million tons [1]. The use of biodegradable plastics is an environmentally friendly solution to the abovementioned problems. There is a wide variety of biodegradable plastics that are compostable in certain conditions. Among this, it is possible to find biodegradable polymers from both petroleum and renewable resources. Nevertheless, most of them are currently expensive and this restricts their use at industrial scale. On the other hand, biodegradable plastics have to face an important technical challenge as currently, most of them offer inferior properties to conventional commodity and engineering plastics from petroleum origin [2]. During the last years, a remarkable increase in the research and development of industrial formulations based on biodegradable plastics has been detected with the main aim of obtaining a set of environmentally friendly materials that are capable to compete with conventional petroleum-derived plastics in terms of technical features and costs [3].

Poly(3-hydroxybutyrate) (PHB) is one of the most promising biopolymers. It is an aliphatic polyester that is synthesized through bacterial fermentation and it is characterized by its biocompatibility and biodegradability [4]. Despite these interesting features, PHB polymer chains are highly stereoregular and this gives highly crystalline polymers (with a degree of crystallinity over 55%). On the other hand, as its glass transition temperature (T_g) is located below the room temperature (typically around 0–2 °C), PHB undergoes physical aging related to secondary crystallization [5, 6]. For this reason, PHB is a highly fragile polymer with very low plastic deformation [7]. Another important drawback is its relatively narrow processing window in terms of temperature as it degradation occurs close to its melting [8]. All these technical drawbacks, together with its high price compared to conventional commodity plastics, restrict its use at industrial scale [9].

There have been many attempts to overcome the intrinsic fragility of PHB polymers by different approaches: internal copolymerization with other flexible monomers [10-12], external plasticization [13-15] or melt blending with different polymers and/or copolymers [16-19]. External mixing of PHB with several polymers is an effective method, from both technical and economical points of view, to overcome all the above mentioned drawbacks. In a previous work [20], PHB was melt blended with poly(ε-caprolactone) (PCL) and as per the results, PHB/PCL blends with 25 wt% PCL led to materials with improved toughness with a slight increase in both elongation at break and impact-absorbed energy by 38 and 30% respectively. Nevertheless, PHB and PCL polymers are immiscible (or very low miscible) polymers and phase separation occurs when melt-blended leading to a typical droplet structure with a PHB-rich matrix phase in which PCL-rich domains are embedded [21]. For this reason, compatibilization of PHB/PCL blends is a critical issue to be addressed as the overall mechanical properties of a multiphase system are directly related to the ability of its components to transfer stresses [22]. One interesting method to improve compatibility is by reactive extrusion during compounding; this method is technologically preferable to addition of tailored copolymers [23]. Reactive extrusion is a simple and cost effective technique for polymer processing. In this, the extruder plays the role of a continuous chemical reactor in which, two different operations occur simultaneously. Melt extrusion and chemical reaction (polymer synthesis and/or modification or *in situ* compatibilization of polymer blends) are carried out in just one stage [24, 25]. Reactive extrusion offers some advantages such as it is not necessary to use solvents, allows a full control of the residence times, it is an online process and the technical equipment and accessories are relatively cheap [25, 26]. Dicumyl peroxide (DCP) is a free radical initiator widely used in polymerization processes, natural rubber vulcanization and as crosslinker [23]. It has been used to promote compatibilization of immiscible polymers in different binary blends. Dong *et al*. [27] observed an increase in tensile strength of 5 MPa and a remarkable improvement of the energy absorption of about 30% by the only addition of 0.5 wt% DCP to binary blends of PHB and PDLLA (70/30). They also reported a noticeable decrease in the PDLLA domain size dispersed in the PHB matrix which is representative for somewhat partial reticulation between these two polymers. Ma *et al.* [21] also observed an increase in the elongation at break and the impact-absorbed energy after addition of 0.5 wt% DCP in a PHB/PBS (70/30) blend with regard to the same uncompatibilized system. In fact, the elongation at break changed from 2 to 11% and the impact-absorbed energy increased from 9 to 54 kJ m^{-2}.

The present work is focused on the evaluation of the effects of DCP on final performance of binary blends from poly(3-hydroxybutyrate) (PHB) and poly(ε-

caprolactone) (PCL) processed by *in situ* reactive compatibilization extrusion. The effects of different DCP loads (0, 0.25, 0.50, 0.75 and 1 wt%) is evaluated in terms of mechanical and thermal properties of the PHB/PCL (75/25) blend as well as its morphology.

EXPERIMENTAL

Materials

Poly(3-hydroxybutyrate) (PHB) pellets (P226, M_w = 426,000 g mol^{-1}) were supplied by Biomer (Krailling, Germany). Poly(ε-caprolactone) (PCL) (CAPA 6500, M_w = 50,000 g mol^{-1}) was provided by Perstorp Holding AB (Malmö, Sweden). Dicumyl peroxide (DCP) (98% purity) was supplied from Sigma Aldrich (Madrid, Spain).

Sample preparation

PHB and PCL were dried in an air-circulating oven at 70 and 40 °C for 24 h respectively to remove residual moisture. PHB/PCL (75/25) blends with different DCP (0, 0.25, 0.50, 0.75 and 1 wt%) were melt-blended in a twin-screw co-rotating extruder (L/D = 24, D = 25 mm) from DUPRA S.L. (Castalla, Spain) at a rotating speed of 40 rpm. Under these conditions, the residence time for the *in situ* compatibilization of PHB/PCL blends by reactive extrusion process was about 55 s. The temperature profile of the extrusion barrel was set to 165 °C (hopper), 170 °C, 175 °C and 180 °C (die). Before the *in situ* compatibilization extrusion process, all three components (PHB, PCL and DCP) were mechanically mixed in a zipper bag to obtain homogeneous pre-mixing. After extrusion, the material was cooled to room temperature and subsequently, it was pelletized. Standard samples for tensile, flexural and impact tests were obtained by injection molding in a Meteor 270/75 from Mateu & Solé (Barcelona, Spain) with a temperature profile of 165 °C, 165 °C, 170 °C, 175 °C and 180 °C from the hopper to the injection nozzle. Table IV.4.1 summarizes the compositions and labeling of the different formulations.

Table IV.4.1. Composition and labeling of binary poly(3-hydroxybutyrate) (PHB) and poly(ε-caprolactone) (PCL) blends *in situ* compatibilized by reactive extrusion with different amounts of dicumyl peroxide (DCP).

Coding	PHB (wt%)	PCL (wt%)	DCP (wt%)
PHB	100	0	0
PHB/PCL	75	25	0
PHB/PCL/DCP/25	75	25	0.25
PHB/PCL/DCP/50	75	25	0.50
PHB/PCL/DCP/75	75	25	0.75
PHB/PCL/DCP/100	75	25	1

Characterization techniques

Gel fraction

The gel fraction of the PHB/PCL blends *in situ* compatibilized with different DCP amount was determined by soxhlet extraction in boiling chloroform for 72 h. The extracted samples were dried in an air-circulating oven at 40 °C until a constant weight was obtained. The gel fraction was calculated using the following equation:

$$\boldsymbol{Gel\ fraction}\ (\mathbf{wt}\%) = \frac{\boldsymbol{m_1}}{\boldsymbol{m_0}} \times \mathbf{100} \qquad \textbf{Equation IV.4.1}$$

where m_0 and m_1 represent the weight of the dry samples before and after the extraction process respectively.

Mechanical properties

The glass transition temperature of PHB is located below room temperature, typically in the 0–2 °C range. When PHB is stored at room temperature, secondary crystallization occurs which has a marked effect on physical aging as it has been reported [28]. This process causes a remarkable decrease in the elongation at break while the elastic modulus and tensile strength are not highly affected. The most important changes take place in the first two weeks and tend to stabilize at an aging time of 21 days. For this reason, mechanical properties of the PHB/PCL blend compatibilized with different DCP loads were obtained by standard tensile, flexural an impact tests after 22 days of the injection molding.

Tensile and flexural properties were obtained according to ISO 527 and ISO 178 standards respectively, using a universal test machine Ibertest ELIB 30 from S.A.E. Ibertest (Madrid, Spain) at room temperature. Both tests were carried out with a 5 kN load cell and a crosshead speed of 5 mm min^{-1}. At least five different specimens were tested and average values of the main mechanical parameters were calculated. In addition, the elastic modulus was accurately determined using an axial extensometer IB/MFQ-R2 from Ibertest (Madrid, Spain) coupled to the universal test machine.

A 1 J Charpy impact pendulum from Metrotec S.A. (San Sebastián, Spain) was used to obtain the impact-absorbed energy of the PHB/PCL blend compatibilized with different DCP loads. Standard notched samples ("V" notch type at 45° with a notch radius of 0.25 mm) were tested following the guidelines of the ISO 179 international standard. The values of the impact-absorbed energy were calculated as the average of the energies obtained for five different samples.

Thermal properties

Thermal degradation at elevated temperatures of PHB/PCL blend compatibilized with different DCP loads was analyzed by thermogravimetry (TGA) in a TGA/SDTA 851 thermobalance from Mettler-Toledo Inc. (Schwerzenbach, Switzerland). Samples with an average size ranging from 7 to 9 mg were placed in standard alumina pans and were subjected to a heating program from 30 up to 600 °C at a constant heating rate of 10 °C min^{-1} under nitrogen atmosphere with a flow rate of 66 mL min^{-1}. The onset degradation temperature (T_0) was determined as the temperature corresponding to a weight loss of 5% and the maximum degradation rate temperature for each stage was obtained as the corresponding peak in the derivative TGA curve (DTG).

Differential scanning calorimetry (DSC) experiments were carried out in a DSC Mettler-Toledo 821 calorimeter from Mettler-Toledo Inc. (Schwerzenbach, Switzerland). The heating and cooling rates for the all scans were set to 10 °C min^{-1} under nitrogen atmosphere (flow rate 66 mL min^{-1}). 7–10 mg of the corresponding material were placed in standard 40 μL aluminum pans. The thermal program consisted on a first heating cycle from –50 to 180 °C, a second stage consisting on an isothermal cycle at 180 °C for 2 min. Then a cooling process down to –50 °C was applied and, finally, a heating cycle up to 300 °C was applied. The melting temperature (T_m) was obtained from the second heating cycle and the degree of crystallinity of PHB ($X_{c\ PHB}$) and PCL ($X_{c\ PCL}$) was calculated by the following equation:

$$\boldsymbol{X_c}\,(\%) = \left[\frac{\Delta \boldsymbol{H_m}}{\Delta \boldsymbol{H_0} \cdot \boldsymbol{w}}\right] \times \mathbf{100} \qquad \textbf{Equation IV.4.2}$$

where ΔH_m is the thermodynamic melt enthalpy per gram, ΔH_0 is the theoretical melt enthalpy associated to the corresponding 100% crystalline polymer (these values were assumed to be 146 J g^{-1} [29] for PHB and 156.8 J g^{-1} [30] for PCL), and w is the weight fraction of the corresponding polymer (PHB or PCL) in the blend.

Dynamic mechanical thermal analysis (DMTA)

The evolution of the storage modulus (G') and the damping factor (tan δ) of PHB/PCL blend compatibilized with different DCP loads as a function of temperature was obtained by an oscillatory rheometer AR G2 from TA Instruments (New Castle, USA) equipped with a special clamp system for solid samples. Samples with a size of 40×10×4 mm^3 were subjected to a temperature program from –100 up to 100 °C at a constant heating rate of 2 °C min^{-1}, a frequency of 1 Hz and a maximum shear strain (γ) of 0.1%. The glass transition temperature (T_g) was assumed as the peak maximum of the damping factor curve.

Field emission scanning electron microscopy (FESEM)

Fractured surfaces from impact tests were coated with a thin layer of platinum in a high vacuum sputter coater EM MED20 from Leica Microsystem (Milton Keynes, United Kingdom) prior to be observed the phase morphology in a field emission scanning electron microscopy (FESEM) ZEISS ULTRA55 (Oxford instruments) operated at a voltage of 2 kV. Micrographs were registered at 2500x and 10,000x magnification.

Atomic force microscopy (AFM) and PeakForce QNM

Young´s modulus of each individual phase in the PHB/PCL and PHB/PCL compatibilized with 1 wt% DCP blends was obtained using an atomic force microscope (AFM) model Nanoscop II from Veeco National Instrument (Santa Barbara, California, USA) working in peak force tapping mode by the quantitative nanomechanical measurement, QNM method [31, 32]. With this analysis the height map, deformation and adhesion of each area was obtained. By using this method it is possible the acquisition of force-penetration curves by indenting the material, at a high speed (2 kHz) under very low penetration depths [33, 34]. By using these indentation curves, the software generates different image maps

with z-heights, elastic modulus (E), adhesion and elastic deformation. The Derjaguin-Muller-Toporov (DMT) model was selected to calculate the elastic modulus as it has given good results for soft materials, nanocomposites, fibrils, live cells and very thin layers from the data provided by instrumented indentation techniques [35-39]. The DMT model alloys calculation of the elastic modulus by analyzing the unload stage using the following expression [40].

$$\boldsymbol{F_{tip} = F - F_{adh} = \frac{4}{3} E_r \sqrt{R(d - d_0)^3}} \qquad \textbf{Equation IV.4.3}$$

where $F–F_{adh}$ is the force on the cantilever relative to the adhesion force, R is the tip radius, and $d–d_0$ is the deformation of the sample. In this study, the region comprised between 10% and 70% of the unload curve was fitted by DMT model calculations. The contact radius (R) was determined for a fixed working z-displacement of 5–10 nm. Calibration was carried out by the relative calibration method which uses a sample of known modulus to obtain the ratio of the spring constant to the square root of the tip end radius. In this study a polystyrene (PS) pattern with a nominal elastic modulus (E) of 2.7 GPa was used as the reference material and the obtained $R_{5–10\ nm}$ value was 9 nm. Calibration of the tip radius was done before and after finishing the study to guarantee negligible changes due to wear. The spring constant was calibrated, reporting a stiffness of 5 N m^{-1}. The applied force during the scanning was the required to keep a contact depth in the 5–10 nm range. The scan frequency was 0.75, 0.5 and 0.3 Hz on squared areas sizing 3×3, 10×10 and 20×20 μm^2. All tests were conducted on 500 μm thick films obtained by environmental ultramicrotomy.

Nanomechanical properties

Nanoindentation tests were carried out in a Nanoindenter G-200 from Agilent Nanotechnology (Santa Clara, California, USA). A Berkovich tip was calibrated with Pyrex as reference material. An array of 75 indentations with a depth of 150 nm with a separation of 3 μm between them was programmed. Calculation of the stiffness was done by using the Continuous Stiffness Measurement method [41] with an oscillation of 2 nm at a frequency of 70 Hz. Calculation of hardness (H) and the elastic modulus (E) was done using the Oliver & Pharr method [42] by averaging the values in a depth range between 100 and 150 nm. All the depth values were corrected by taking into account the adjustment proposed by Loubet [43, 44] for polymeric materials with adhesive contact and assuming a Poisson ratio (υ) of 0.3 to calculate the elastic modulus (E).

RESULTS AND DISCUSSION

Gel fraction of PHB/PCL blends compatibilized by reactive extrusion with DCP

Figure IV.4.1 shows the plot evolution of the gel fraction with increasing DCP content during the *in situ* compatibilization by reactive extrusion of PHB and PCL blends. As it can be seen, the gel content increases with the DCP content with a maximum of 18.8% for a DCP content of 1 wt%. DCP decomposes and acts as a free radical initiator. These free radicals promote the formation of PHB and PCL macroradicals by hydrogen abstraction. Then, the combination of these macroradicals leads to formation of PHB-*co*-PCL copolymers that positively contribute to compatibilization and formation of partially crosslinked networks in the blends. Nevertheless, not only PHB and PCL reactions occur but also PCL-rich domains can establish stronger interactions with the PHB polymer matrix. Hence, the use of DCP during the reactive extrusion process gives a series of products such as grafted/branched/crosslinked PHB and PCL chains, PHB-*co*-PCL copolymers and partially crosslinked PHB/PCL networks [21, 45]. Furthermore, the melting process also promotes chain scission due to the high thermal instability of PHB together with the high thermal stability of the free radicals, thus leading to formation of more complex products. These reactions can be observed in Figure IV.4.2 [46, 47].

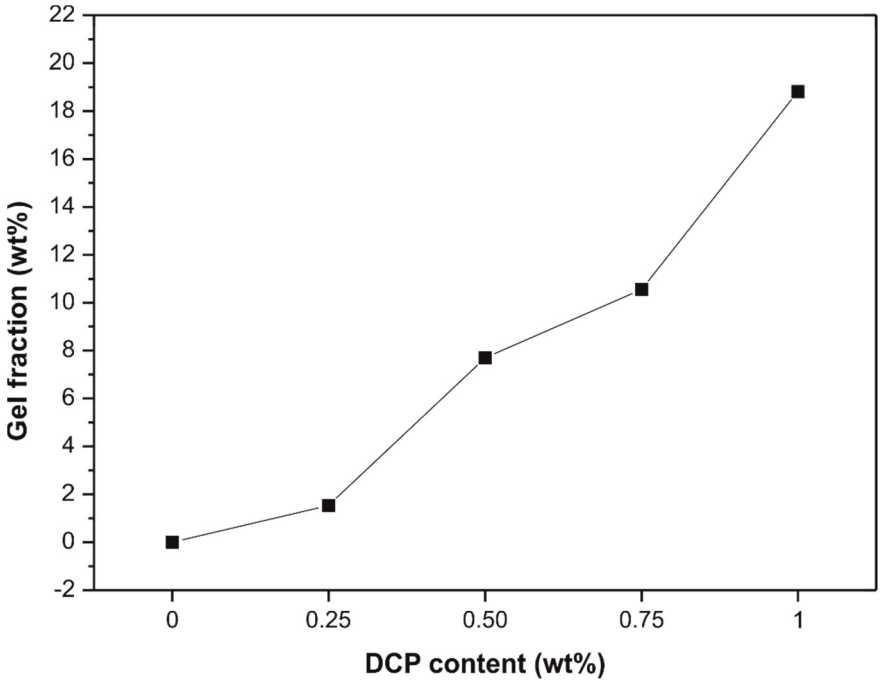

Figure IV.4.1. Plot evolution of the gel fraction obtained by soxhlet extraction of the PHB/PCL (75/25) blend as a function of DCP content used for reactive extrusion.

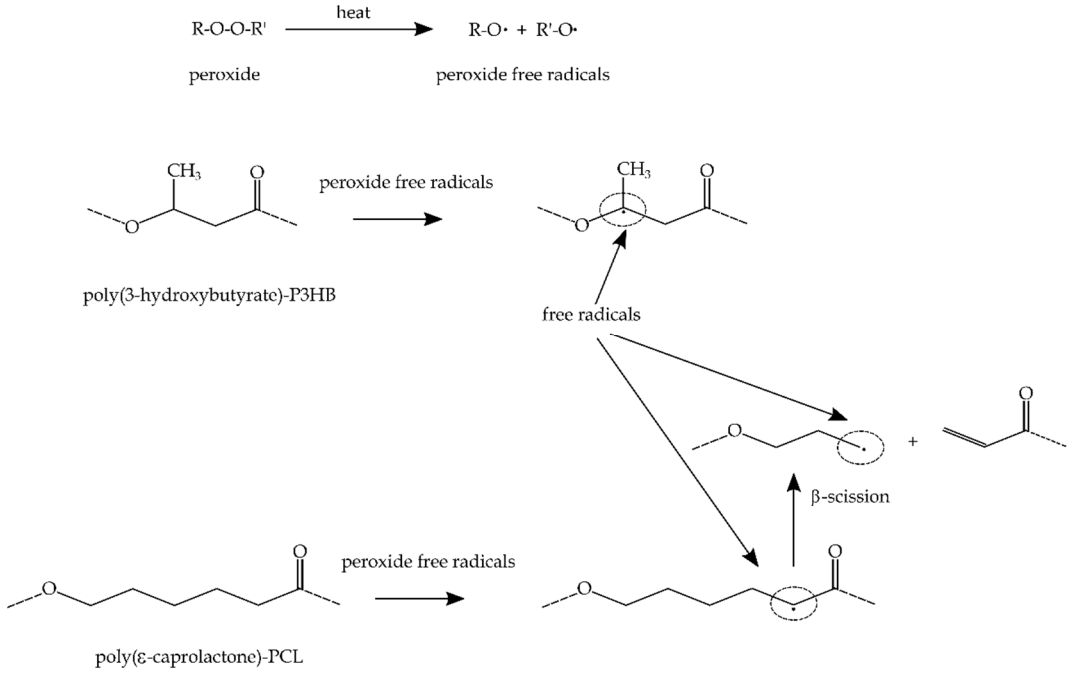

Figure IV.4.2. Schematic representation of free radical formation on poly(3-hydroxybutyrate) and poly(ε-caprolactone) polymer chains by reaction with peroxide free radicals.

Mechanical properties of PHB/PCL blends compatibilized by reactive extrusion with DCP

The only addition of 25 wt% PCL to PHB leads improved toughness. These uncompatibilized blends, are characterized by a droplet structure in which, PCL-rich domains are finely dispersed into the PHB matrix. Although a slight increase in ductile properties are achieved, this improvement is not so high as we report in a previous work [20]. Figure IV.4.3 gathers the main results corresponding to mechanical characterization of PHB/PCL (75/25) blends with different DCP used for the reactive extrusion process. With regard to tensile properties, it is clear to see that the only addition of 0.25 wt% DCP during the reactive extrusion leads to increased compatibility. In fact, the tensile strength is slightly increased from 23.1 MPa (uncompatibilized PHB/PCL) up to 24 MPa. DCP content over 0.25 wt% leads to slightly lower tensile strength values of 22.5 MPa for the compatibilized blend with 1 wt% DCP. So that, it is worthy to note that reactive extrusion with different DCP loads does not affect in a noticeable way to tensile strength. On the other hand, the elongation at break is remarkably improved as the DCP load for reactive extrusion increases. As it can be seen in Figure IV.4.3a, uncompatibilized PHB/PCL (75/25) blend is characterized by a relatively low elongation at break value of 11.1%. In fact, the elongation at break for compatibilized PHB/PCL blend with 0.75 and 1.0 wt% DCP changes up to values close to

21.3% which represents a percentage increase of almost 91%, thus giving clear evidences of improved ductile properties after the reactive extrusion. This could be related to improved interactions between the PHB-rich phase and the PCL-rich phase. Regarding the tensile modulus, as it is defined as the ratio of stress to elongation in the linear region, it is expectable a decrease. As it has been stated previously, the tensile strength does not change in a noticeable way whilst the elongation at break increases in a remarkable way. For this reason, the ratio stress to elongation decreases. In fact, the tensile modulus changes from 1649 MPa (uncompatibilized PHB/PCL blend) down to 1104 MPa for the blend compatibilized with 1 wt% DCP during the reactive extrusion process which represents a percentage decrease of about 33%.

Similar tendency can be observed for flexural properties. The flexural strength remains almost constant at values of 37 MPa for DCP content in the 0–0.25 wt% range while a slight decrease is detected over 0.25 wt% DCP with minimum values of 33.2 MPa for the PHB/PCL blend compatibilized with 1 wt% DCP during the reactive extrusion. The flexural modulus offers identical tendency as that observed for the tensile modulus with a decrease from 1606 MPa for the uncompatibilized blend down to 1170 MPa for the blend compatibilized by reactive extrusion with 1 wt% DCP.

The impact-absorbed energy is, as other ductile properties in a polymer blend such as the elongation at break, highly sensitive to compatibility between components as it is related to material cohesion and the typical droplet structure of an immiscible blend negatively contributes to cohesion. Figure IV.4.3c shows the evolution of the impact-absorbed energy with increasing DCP content during the reactive extrusion. It is worthy to note the remarkable increase in the impact-absorbed energy from values of about 2 kJ m^{-2} (uncompatibilized blend) up to values of 6.3 kJ m^{-2} that represents a percentage increase of 231%. This noticeable increase indicates a clear improvement of the cohesion and this indicates that interactions between PHB-rich phase and PCL-rich phase have improved as a consequence of the use of the peroxide as *in situ* compatibilizer by reactive extrusion. In the case of the uncompatibilized PHB/PCL (75/25) blend, the lack of interactions between both polymers promotes phase separation and this leads to interface failure when an external stress is applied; then, microcrack formation and subsequent growth is very fast and this has a negative effect on the total impact-absorbed energy with a pronounced fragile behavior. Reactive extrusion with DCP increases interactions between the PHB-rich phase and the PCL-rich phase and this has a positive effect on load transfer due to improved phase-continuity. Hence, it is possible to conclude that reactive extrusion with DCP has a positive effect on compatibilizing PHB and PCL in their blends with a remarkable improvement of

ductile properties such as elongation at break and impact-absorbed energy due to increased material cohesion.

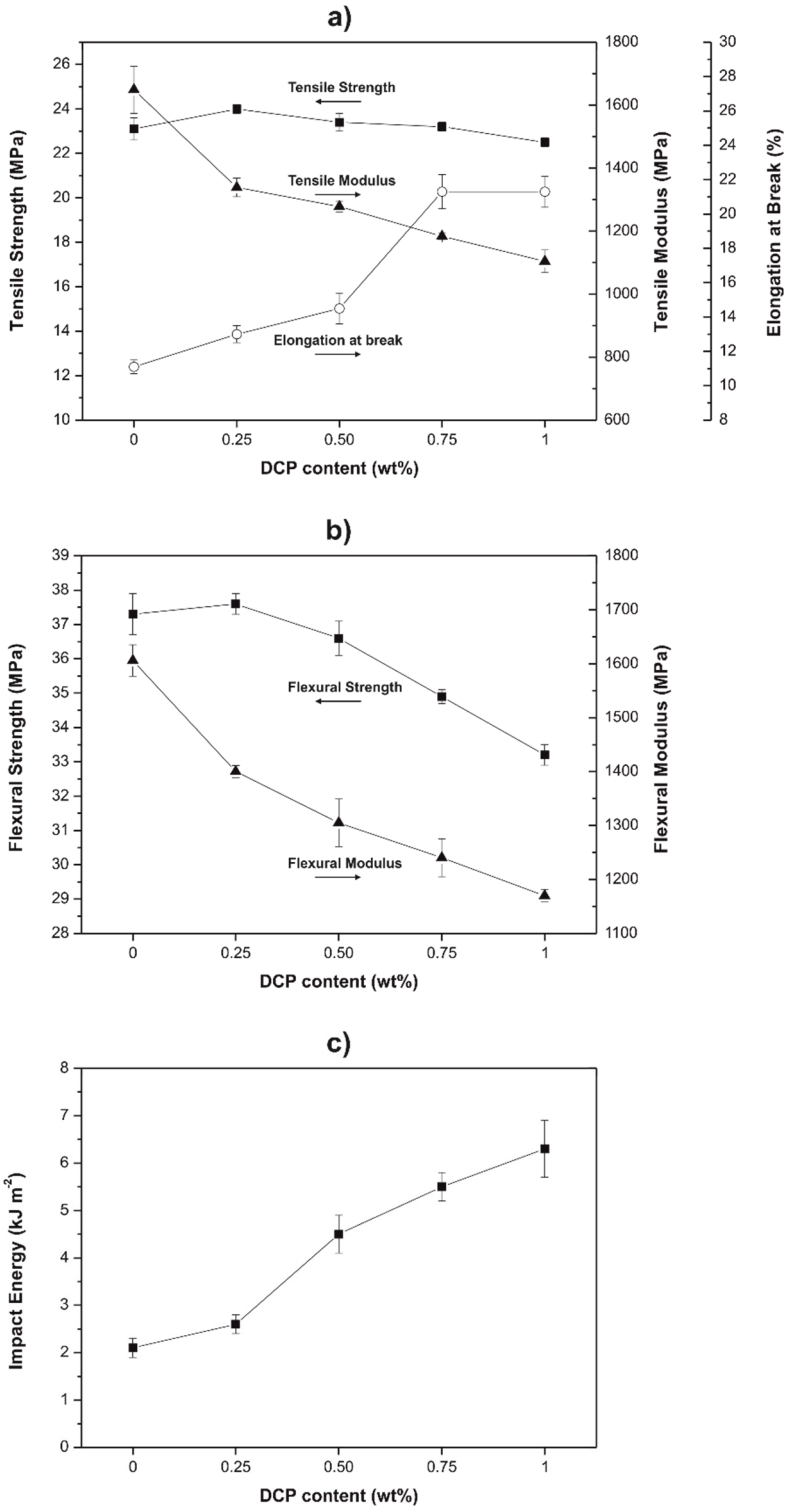

Figure IV.4.3. Mechanical properties of the PHB/PCL (75/25) blend as a function of DCP content used for reactive extrusion: (a) tensile properties; (b) flexural properties and (c) impact properties.

Thermal properties of PHB/PCL blends compatibilized by reactive extrusion with DCP

DSC curves of the second heating cycle of PHB/PCL (75/25) blend are shown in Figure IV.4.4 and the main thermal parameters obtained from DSC analysis are summarized in Table IV.4.2. As it can be seen, the DSC thermogram of neat PHB shows a main melting peak at 174.8 °C and a small melt peak located at 52.3 °C which could be related to the melting of some low molecular weight additive contained in the commercial formulation [48]. As expected, uncompatibilized PHB/PCL (75/25) blend offers two clear melt processes located at 172.9 and 56.3 °C that correspond to the melting of PHB and PCL individual polymers respectively. Compatibilization by reactive extrusion with DCP leads to some changes in the thermal behavior of the blend. As it can be seen, the peak size of PCL is smaller as the DCP content in the reactive extrusion process increases. This fact suggests a conversion of the PCL-rich domains into amorphous as the DCP content increases. On the other hand, DCP does not affect the melting temperature of PCL but it is worthy to note a slight decrease in the PHB melting temperature by almost 4 °C with regard to the uncompatibilized blend. Regarding the degree of crystallinity of both PHB and PCL in the PHB/PCL (75/25) blend, values of 39.8 and 45.7%, respectively, are obtained. The use of 0.25 and 0.50 wt% DCP during the reactive extrusion process does not affect in a noticeable way to the crystallinity of both PHB- and PCL-rich domains. Over 0.50 wt% DCP it is possible to observe a slight decrease in the overall crystallinity of both polymers in the blend. This fact also explains why both tensile and flexural moduli are lower with increasing DCP content during the reactive extrusion.

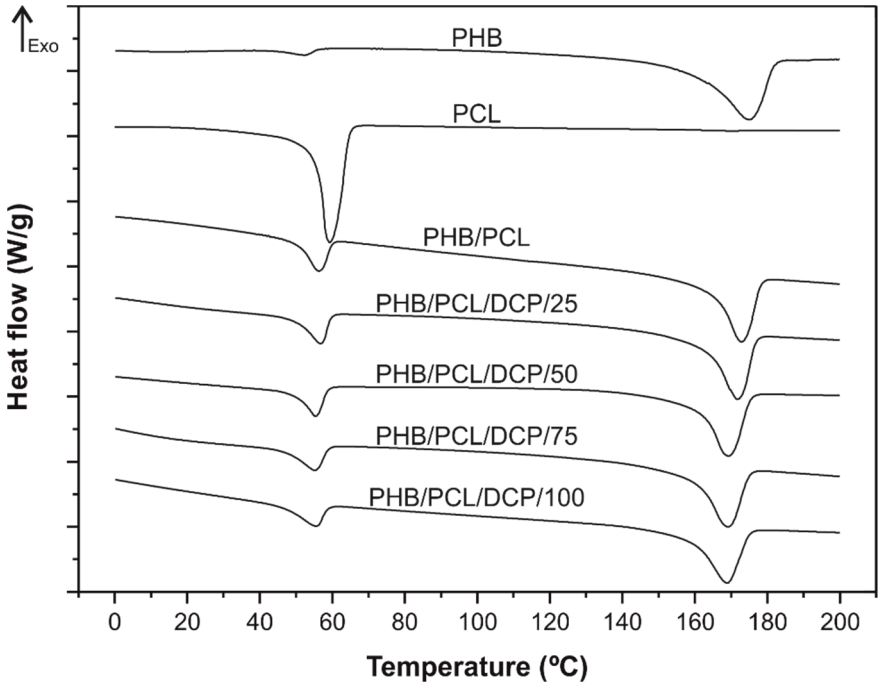

Figure IV.4.4. DSC curves of the second heating cycle of neat PHB, neat PCL, uncompatibilized PHB/PCL (75/25) blend and compatibilized blend by reactive extrusion with different DCP content.

The main thermal parameters corresponding to the thermal degradation of PHB/PCL (75/25) blend are summarized in Table IV.4.2. Thermal degradation of neat PHB occurs in two separated stages which is directly related to the complex chemical composition of the commercial formulation with plasticizers, nucleating agents, fillers and stabilizers [48]. Uncompatibilized PHB/PCL (75/25) blend also shows two degradation stages. The first one is characterized by a maximum degradation rate temperature of 302.3 °C and is assigned to PHB whilst the second one, at higher temperatures of 422.3 °C corresponds to the maximum degradation rate temperature of PCL as this is more stable than PHB to thermal degradation. Regarding the onset degradation temperature (T_0) it is possible to observe that, in general, PCL has a positive effect on thermal stabilization with an increase from 246.7 °C for neat PHB up to 282.7 °C for its blend with 25 wt% PCL (uncompatibilized). The obtained data indicate that no significant change in the onset degradation temperature is obtained by reactive extrusion with different DCP loads as T_0 ranges from 280 to 285 °C for all DCP contents used in the reactive extrusion process.

Table IV.4.2. Thermal parameters of neat PHB, neat PCL, uncompatibilized PHB/PCL (75/25) blend and PHB/PCL (75/25) blends compatibilized by reactive extrusion with different DCP contents.

Samples	DSC Parameters						TGA Parameters		
	$T_{m\ PCL}$ (°C)	$\Delta H_{m\ PCL}$ (J g^{-1})	$X_{c\ PCL}$ (%)	$T_{m\ PHB}$ (°C)	$\Delta H_{m\ PHB}$ (J g^{-1})	$X_{c\ PHB}$ (%)	T_0[a] (°C)	$T_{max\ PHB}$ (°C)	$T_{max\ PCL}$ (°C)
PHB	-	-	-	174.8	–75.8	51.9	246.7	272.3	382.0
PCL	60.0	–72.8	46.4	-	-	-	379.5	-	415.8
PHB/PCL	56.3	–62.5	39.8	172.9	–66.8	45.7	282.7	302.3	422.3
PHB/PCL/DCP/25	56.7	–61.2	39.0	171.7	–66.8	45.7	283.6	302.3	422.3
PHB/PCL/DCP/50	55.5	–58.4	37.4	169.2	–66.3	45.4	285.4	302.3	422.3
PHB/PCL/DCP/75	55.2	–54.8	35.0	169.1	–60.5	41.4	282.6	302.3	422.3
PHB/PCL/DCP/100	55.5	–49.0	31.3	168.8	–57.3	39.3	279.0	302.3	422.3

[a] T_0, calculated at 5% mass loss.

Dynamic mechanical thermal analysis (DMTA) of PHB/PCL blends compatibilized by reactive extrusion with DCP

Figure IV.4.5 shows the plot evolution of the damping factor (tan δ) and the storage modulus (G') of uncompatibilized PHB/PCL (75/25) blend and the same blend composition compatibilized with different DCP content by reactive extrusion. The glass transition temperature (T_g) was obtained through the peak maximum in the damping factor curves. As one can see, two different relaxation processes are present which are attributed to immiscibility between PHB and PCL. Reactive extrusion with DCP leads to partially compatibilized blends with a slight increase in the T_g of the PCL-rich domains from –68.3 °C (uncompatibilized blend) up to –65 °C for the blend compatibilized by reactive extrusion with 0.75 and 1 wt% DCP. This slight increase can be attributed to a restriction of the PCL segments movement along the interphase with increased miscibility [21]. On the other hand, the glass transition temperature of the PHB-rich domains does not change in a significant way and remains at values around 1 °C. By observing the evolution of the storage modulus (G') in Figure IV.4.5b it can be clearly seen a decrease of G' for all blends compatibilized with different DCP contents. At low temperatures (below the $T_{g\ PCL}$), all blends show high storage modulus values (more than 2000 MPa) due to high rigidity of the polymeric chains. After reactive extrusion with DCP, a slight decrease in G' can be observed as the DCP content increases. In fact, the lowest G' values are obtained for the blend compatibilized by reactive extrusion with 1 wt% DCP. The effects of this *in situ* compatibilization by reactive extrusion are more evident in the rubbery state comprised between the glass transition of both neat polymers, –53 °C for PCL and 1 °C for PHB [20]; this is due to the fact that *in situ* compatibilization affects the overall movement of the molecular chain segments instead of the localized macromolecule movements [45]. This decrease is due to increased compatibility which is achieved by anchoring poly(ε-caprolactone) macroradicals (promoted by DCP at elevated temperatures) to poly(3-hydroxybutyrate) macroradicals. In addition, PHB-PHB, PCL-PCL and PHB-PCL crosslinking can also occur as a consequence of the radicals formed by DCP.

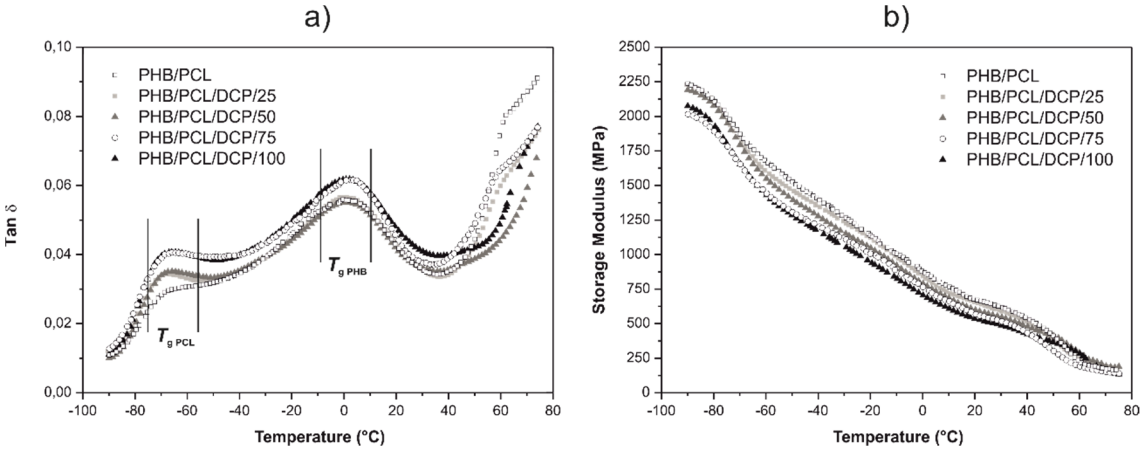

Figure IV.4.5. Dynamic mechanical thermal analysis (DMTA) of uncompatibilized PHB/PCL (75/25) blend and compatibilized blends by reactive extrusion with different DCP contents as a function of temperature: (a) damping factor (tan δ) and (b) storage modulus (G').

Morphology study of PHB/PCL blends compatibilized by reactive extrusion with DCP

Figure IV.4.6 shows the morphology of fractured surfaces from impact tests without compatibilization and with compatibilization by reactive extrusion with different DCP content. As it can be observed, uncompatibilized PHB/PCL (75/25) blend (Figure IV.4.6a and b) shows a clear phase separation with a typical droplet structure indicating immiscibility. The PCL-rich domains appear as randomly dispersed droplets with a particle size comprised in a wide range into the PHB polymer matrix. In addition, small gaps can be detected along PCL-rich and PHB-rich domains thus evidencing poor interfacial adhesion between these two polymers as stated by Garcia-Garcia *et al.* [20]. It is also detectable some plastic deformation of PCL-rich domains during the impact test. The reactive extrusion with DCP has a remarkable effect on the morphology of the PHB/PCL (75/25) blend as it can be seen in Figure IV.4.6c-f. As it can be seen, the gaps between the PCL- and PHB-rich domains have almost disappeared and the interface between them is not detectable. The use of DCP as reactive compatibilizer leads to a decrease in size on PCL-rich domains leading to a high homogeneous fracture surface without the typical filament formation on PCL-rich domains. All these features are indicating that the reactive extrusion with DCP has a positive effect on improving the miscibility of PHB and PCL polymers with the subsequent improvement on mechanical ductile properties as described before.

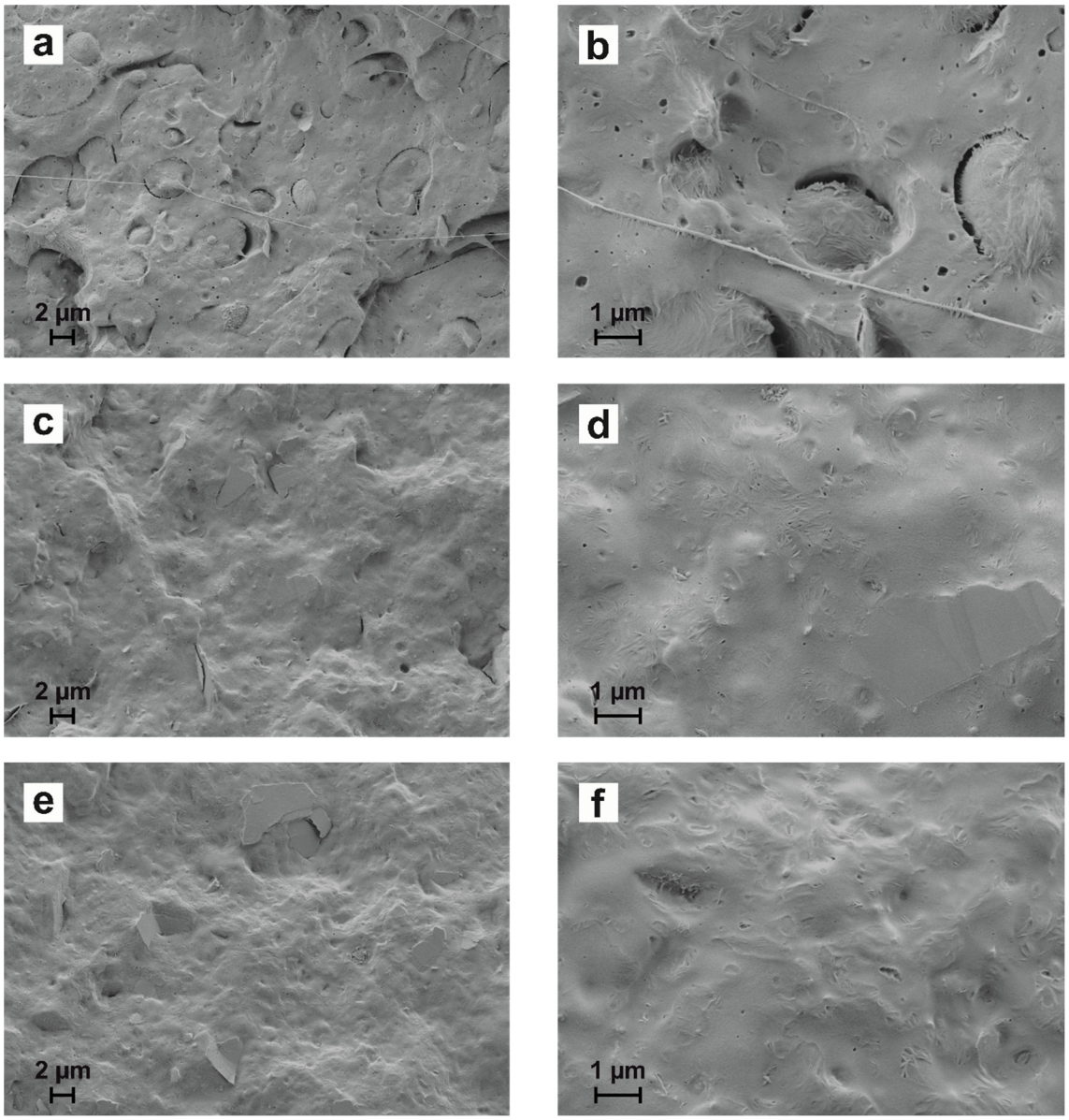

Figure IV.4.6. FESEM images of impact-fractured surfaces of: (a) uncompatibilized PHB/PCL (75/25) at 2500x; (b) uncompatibilized PHB/PCL at 5000x; (c) PHB/PCL (75/25) compatibilized by reactive extrusion with 0.50 wt% DCP at 2500x; (d) PHB/PCL (75/25) compatibilized by reactive extrusion with 0.50 wt% DCP at 5000x; (e) PHB/PCL (75/25) compatibilized by reactive extrusion with 1 wt% DCP at 2500x and (f) PHB/PCL (75/25) compatibilized by reactive extrusion with 1 wt% DCP at 5000x.

Atomic force microscopy (AFM) and PeakForce QNM of PHB/PCL blends compatibilized by reactive extrusion with DCP

An in-depth study of the effect of DCP on the microstructure of PHB/PCL blends was carried using atomic force microscopy (AFM) working in the Quantitative Nanomechanical

PeakForce, QNM mode. This method allows obtaining an image map not only of deformations and z-displacements but also of the elastic and adhesive properties of the analyzed surface. Ultramicrotome samples of PHB/PCL and PHB/PCL compatibilized with 1 wt% DCP were analyzed by the AFM technique. Some attempts did not give useful image maps due to the high roughness of fractured samples as reported by other authors [49].

Figure IV.4.7 shows the image maps of the abovementioned PHB/PCL systems (uncompatibilized and compatibilized system by reactive extrusion with 1 wt% DCP) under different AFM channels. Figure IV.4.7a shows the topographic AFM image (height channel) of the uncompatibilized PHB/PCL system. This topography is similar to that observed by FESEM, *i.e.*, immiscible PCL-rich domains can be clearly distinguished dispersed in the PHB matrix. However, the topographic AFM image corresponding to the PHB/PCL system compatibilized with 1 wt% DCP (Figure IV.4.7b) is remarkably different. In fact, no clear evidence of dispersed PCL-rich domains can be seen due to the compatibilization effect provided by reactive extrusion with DCP. This compatibilization leads to lower PCL-rich domain size as well as a more homogeneous PCL-rich domain dispersion. Plot of the elastic modulus image map obtained by the Derjaguin-Muller-Toporov model (Figure IV.4.7c and d) the microstructure is clearly revealed. A logarithmic plot of the elastic modulus image map reveals some interesting features: (i) the uncompatibilized PHB/PCL system shows a typical phase-separation morphology in which, spherical PCL-rich domains are uniformly dispersed in the PHB-rich matrix. Some evidences of interface failure (marked with arrows in Figure IV.4.7c) can be observed. Failure occurs because of the lack of cohesion among the interface between the PCL-rich phase and the PHB-rich phase. This could be related to a pull effect of the ultramicrotome thus supporting the lack (or very low) compatibility between these two polymers. PCL-rich domains possess an average size comprised between 1 and 5 μm. (ii) On the other hand, the morphology of the compatibilized PHB/PCL system by reactive extrusion with DCP shows a PCL-rich phase finely dispersed in the PHB-rich phase matrix. PCL-rich phase appears in the form of small filaments with a thickness of less than 1 μm. Although PHB and PCL are not fully miscible, the effect of the reactive extrusion with DCP is highly positive to achieve somewhat interactions between them. (iii) The typical failure at the PCL-PHB interface of the uncompatibilized system does not appear in a clear way in the compatibilized blend which confirms improved interactions among PCL-PHB interface with the subsequent improvement of mechanical properties at a macro scale. (iv) Both elastic modulus image maps are shown under the same scale depth with logarithmic values to show that the contrast between PCL-rich and PHB-rich phases is remarkably lower (the differences in the elastic moduli between phases is much lower) in the compatibilized PHB/PCL system than the uncompatibilized one. (v) The PHB-rich phase in the

compatibilized blend is darker which is representative for lower elastic modulus values. This effect can be related to a decrease in the overall PHB crystallinity and/or the formation of PHB-PCL grafted oligomers and polymer chains. Figure IV.4.7e and f shows the elastic modulus histograms of the uncompatibilized and compatibilized PHB/PCL systems respectively. Finely dispersed PCL domains possess a narrow distribution centered at 1 GPa for the uncompatibilized PHB/PCL system, whilst the compatibilized systems offers a distribution centered at ~0.75 GPa. However, the average elastic modulus of the PHB-rich phase changes from 3.5 GPa (uncompatibilized blend) to 2.7 GPa (DCP compatibilized blend). These results are in total agreement with the previously reported tensile and flexural moduli and similar to previously reported values for this material [50-52]. It is worth to note that the elastic modulus of the PHB-rich phase was not constant along the whole section, with values varying from 2.5 to 4 GPa. This phenomenon can be explained by taking into account the cooling profile. The highest *E* value was obtained far from the surface which is related to the higher crystalline character of the PHB due to lower cooling rates typical of this zone. However, *E* values of about 2.5 GPa were recorded close to the topmost surface of the sample, probably due to higher amorphous degree of PHB achieved by higher cooling rates expected in this zone.

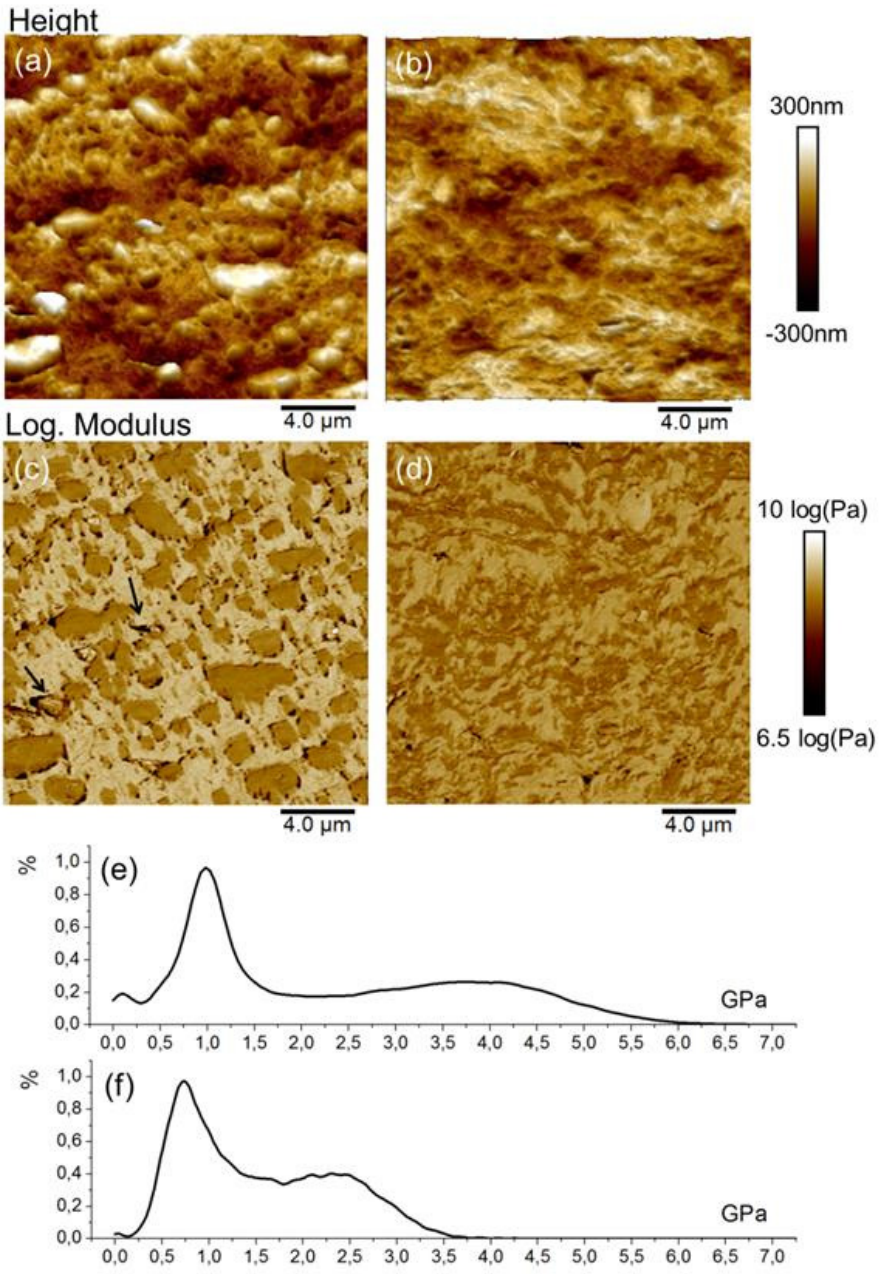

Figure IV.4.7. Results obtained by AFM-QNM (20×20 µm^2) showing the topographic AFM image (height channel), the elastic modulus image map (logarithmic scale) and the frequency histogram of the elastic modulus for uncompatibilized PHB/PCL blend (a, c and e) and DCP compatibilized PHB/PCL blend (b, d and f).

An in-depth analysis of the elastic modulus image map at higher magnification allowed determining the elastic modulus of each individual phase as observed in Figure IV.4.8. The uncompatibilized PHB/PCL blend (Figure IV.4.8a and c) shows a stiffness profile characterized by abrupt changes in the elastic modulus value from 2.5–3.0 GPa (PHB-rich

phase) down to 0.75 GPa (PCL-rich phase). On the other hand, the stiffness profile for the DCP compatibilized PHB/PCL blend is more homogenous as it can be seen in Figure IV.4.8b and d. The interface width was measured for both uncompatibilized and DCP compatibilized PHB/PCL blends. Similar values of about 350 nm were observed for both systems thus indicating that compatibilization by reactive extrusion with DCP does not change the mechanical properties profile between the phases but their cohesion. These findings corroborate the hypothesis that reactive extrusion with DCP contributes to improve the interfacial interaction between PHB-rich and PCL-rich phases, thus leading to a decrease of the elastic modulus of the PHB-rich phase which seems to be chemically bonded to a PCL-rich phase. All this has a positive effect on mechanical ductile properties with a remarkable increase in the impact-absorbed energy and elongation at break.

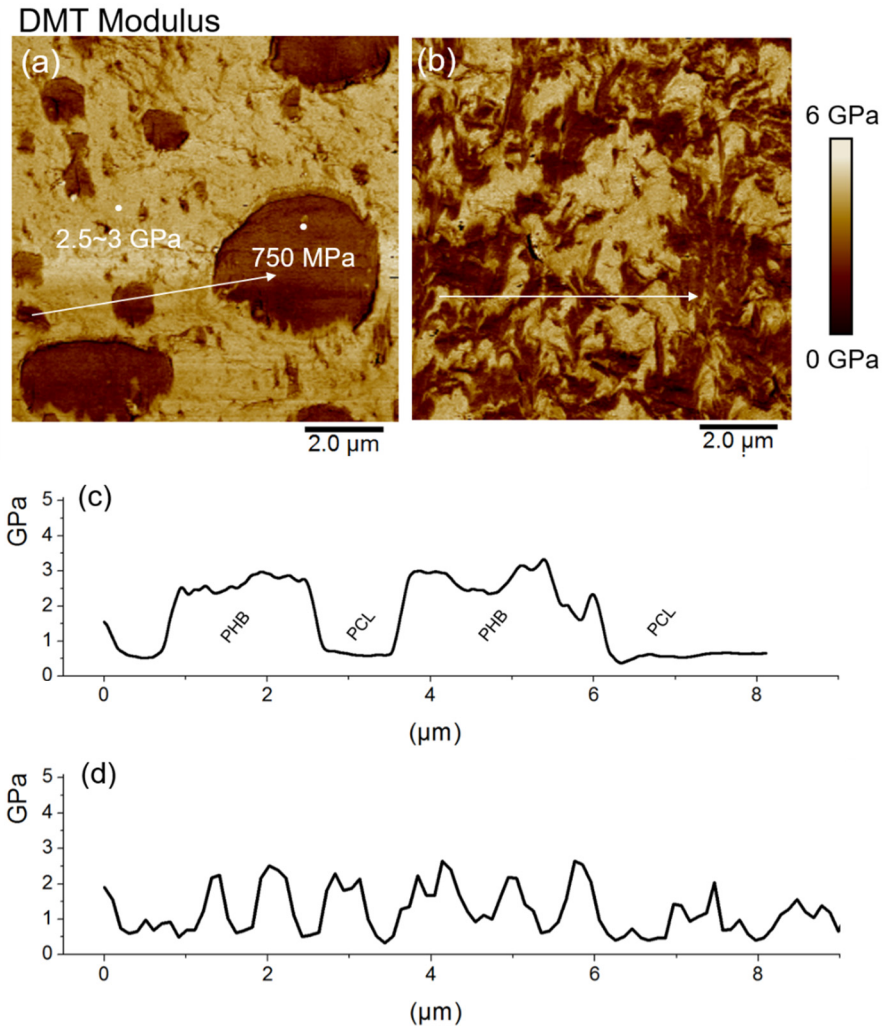

Figure IV.4.8. Results obtained by AFM-QNM (10×10 µm²) the elastic modulus image map and the elastic modulus profile for uncompatibilized PHB/PCL blend (a and c) and DCP compatibilized PHB/PCL blend (b and d).

If we take into account the rule of mixtures, the elastic modulus values obtained through the tensile and flexural tests seem to agree to the weighted average values calculated by using the individual elastic modulus values for each phase as obtained by AFM-QNM analysis. As it has been previously stated, the Derjagin-Muller-Toropov (DMT) method was selected to calculation of the elastic modulus versus other proposed models such as Herts, JKR, Oliver & Pharr or Sneddon [53]. The DMT model was selected after an in-depth observation of the force-distance curves taken at different regions which suggested that the adhesion DMT model was more appropriate than the other ones. Figure IV.4.9 shows the force-displacement curve corresponding to two different AFM indentations on PHB and PCL. The cantilever translation under a sinusoidal movement of 500 μm amplitude (Figure IV.4.9a) generated a clear interaction between the tip and the surface sample in a particular point previously programmed as the Peak Force SetPoint. In this moment, the force-time curve (heart-beat curve) was registered and it is shown in Figure IV.4.9b and c for the PHB and PCL phase respectively. Then, the registered signals revealed the typical approximation stage (A) until the electrostatic attraction effect and contact with sample (B) or SetPoint. In this moment, the indentation (B→C stage) occurs, followed by the withdrawal process (C→D). Due to short-range forces and the adhesion effect by capillarity between the sample and the tip, a subsequent stage was revealed. This stage (jump-off-contact) was characterized by a negative force to allow the tip detachment (C→D). The curves obtained for each individual phase show that the necessary force to allow the tip detachment is higher for PCL as it can be seen in the corresponding force-tip sample separation curves (Figure IV.4.9d and e). The blue represents the trace direction while the red corresponds to the retrace direction. It is clearly deduced that PCL possesses an important adhesive component thus indicating the usefulness of the Derjaguin-Muller-Toporov (DMT) model. On the other hand, this fact reveals that PCL is chemically more active than PHB. The same picture shows the length used for the DMT adjustment (70% of the unload stage).

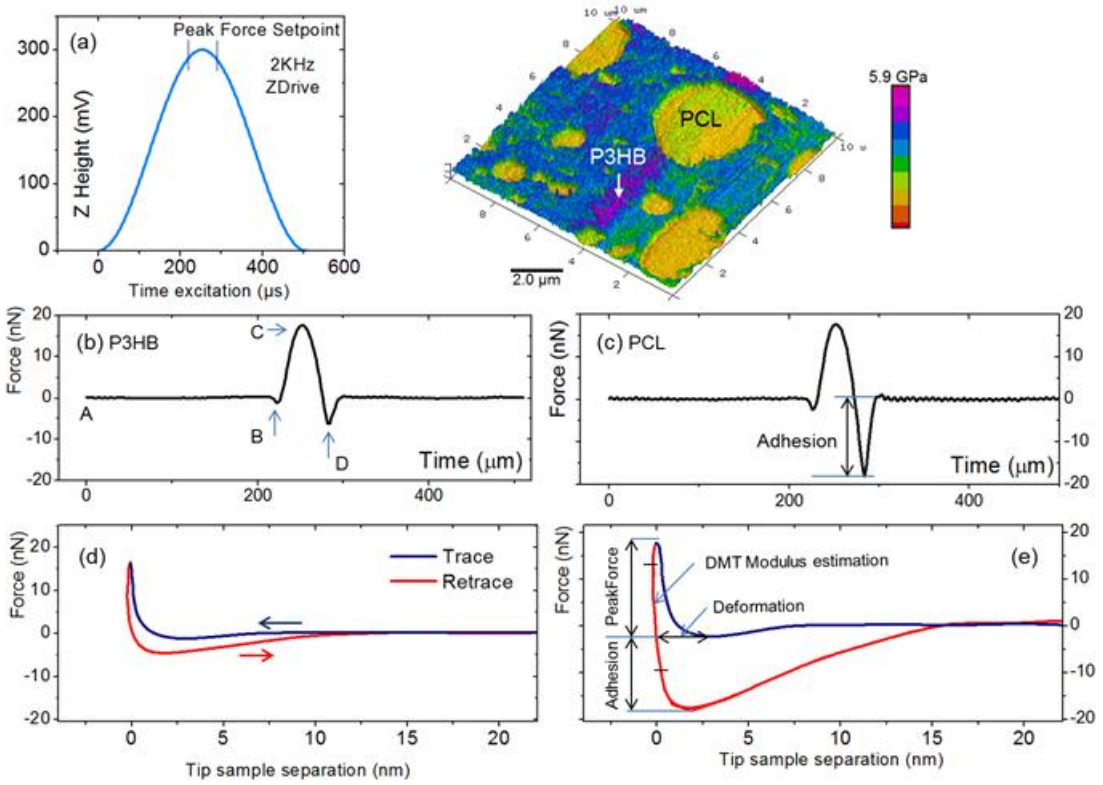

Figure IV.4.9. PeakForce curves obtained on PHB and PCL individual phases, (a) cantilever deflection, (b and c) approach (trace) and withdrawal (retrace) curves, (d and e) force-tip sample separation curves.

Figure IV.4.10 shows the deformation and adhesion image maps that are in total agreement with those shown in Figure IV.4.9. The adhesion image maps confirm that PCL offers a higher adhesion component. Furthermore, the DCP compatibilized PHB/PCL blend shifts the adhesion to higher values as it can be seen in the corresponding adhesion profiles (Figure IV.4.10d and e). The higher adhesion value observed for the DCP compatibilized PHB/PCL blend could be related to presence of oxidized moieties resulting from reaction of free radicals achieved during the reactive extrusion with air which leads to a chemically more active surface [49, 54].

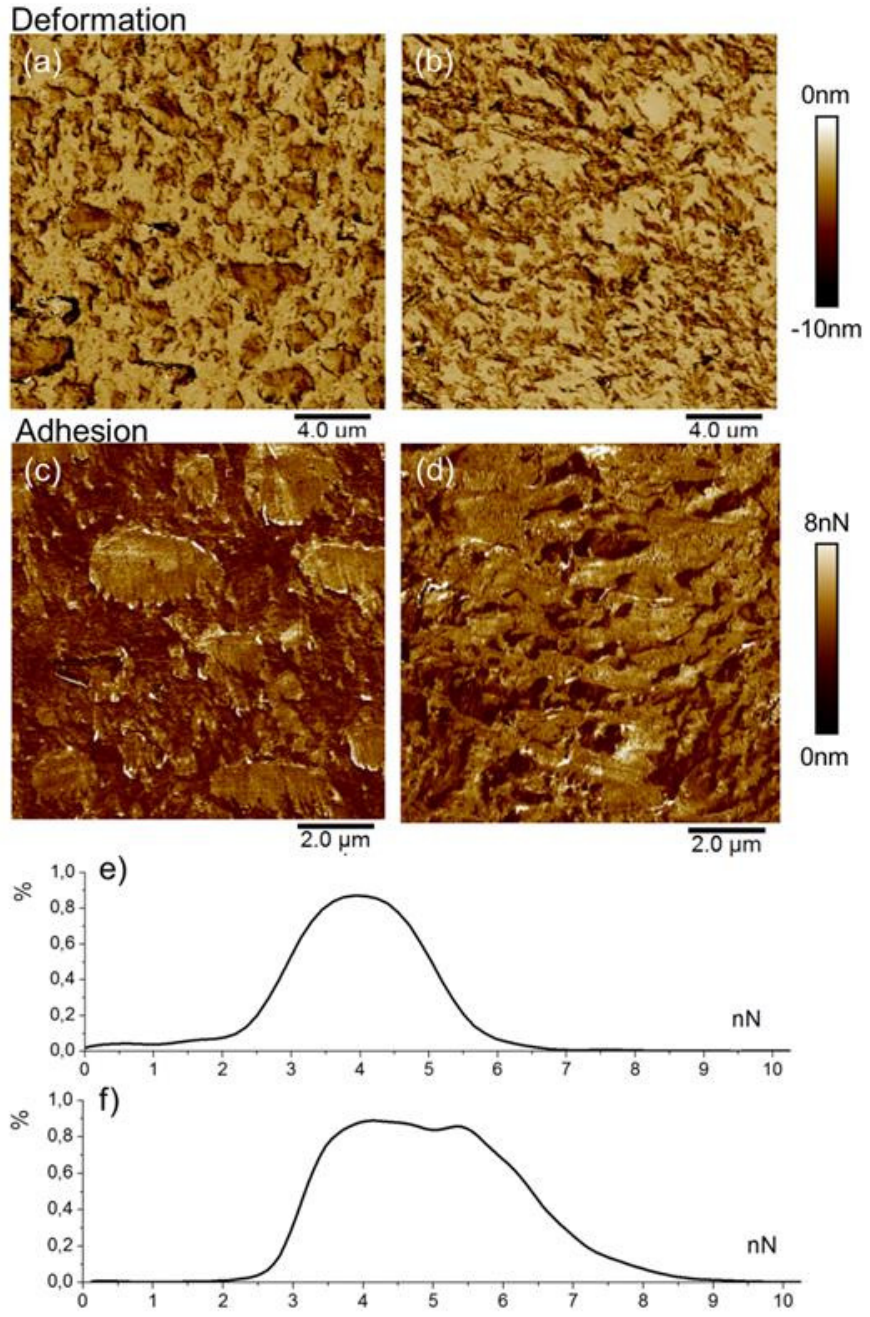

Figure IV.4.10. Results obtained by AFM-QNM (10×10 μm^2). Deformation image map (tip penetration), adhesion image map and adhesion profile for uncompatibilized PHB/PCL blend (a, c and e) and DCP compatibilized PHB/PCL blend (b, d and f).

Nanomechanical properties of PHB/PCL blends compatibilized by reactive extrusion with DCP

With the aim of obtaining the hardness of the two samples analyzed by AFM a 75 indentation array (100 nm depth) was programmed on ultramicrotome samples. The elastic

modulus (*E*) and the hardness values (*H*) were determined by the well stablished Oliver & Pharr method with some corrections using the Loubet model to correct the adhesion component [44]. It is worth to note that the results obtained by nanoindentation are not comparable to those obtained by AFM as the mathematical models are different and the test depths are also different (100 nm for nanoindentation and 5–10 nm for AFM). Figure IV.4.11a and b shows the elastic modulus distributions are rather similar to those obtained by AFM analysis. The elastic modulus of the uncompatibilized PHB/PCL blend shows two different distributions centered at ~4 and at ~2 GPa which correspond to the PHB-rich phase and the PCL-rich phase respectively (Figure IV.4.11a). The average value of the elastic modulus for the uncompatibilized PHB/PCL blend is 2.5 GPa. With regard to the DCP compatibilized PHB/PCL blend, it is worth to note that it is difficult to observe the two distributions and the average elastic modulus is around 1 GPa (Figure IV.4.11b). These results are in total agreement with those obtained by the AFM technique. Regarding the hardness, it was difficult to observe the different phases but the overall hardness of the uncompatibilized PHB/PCL blend was remarkably higher (83 MPa) than the DCP compatibilized system with a hardness value of 47 MPa which is in accordance with the previously reported improvement of mechanical ductile properties.

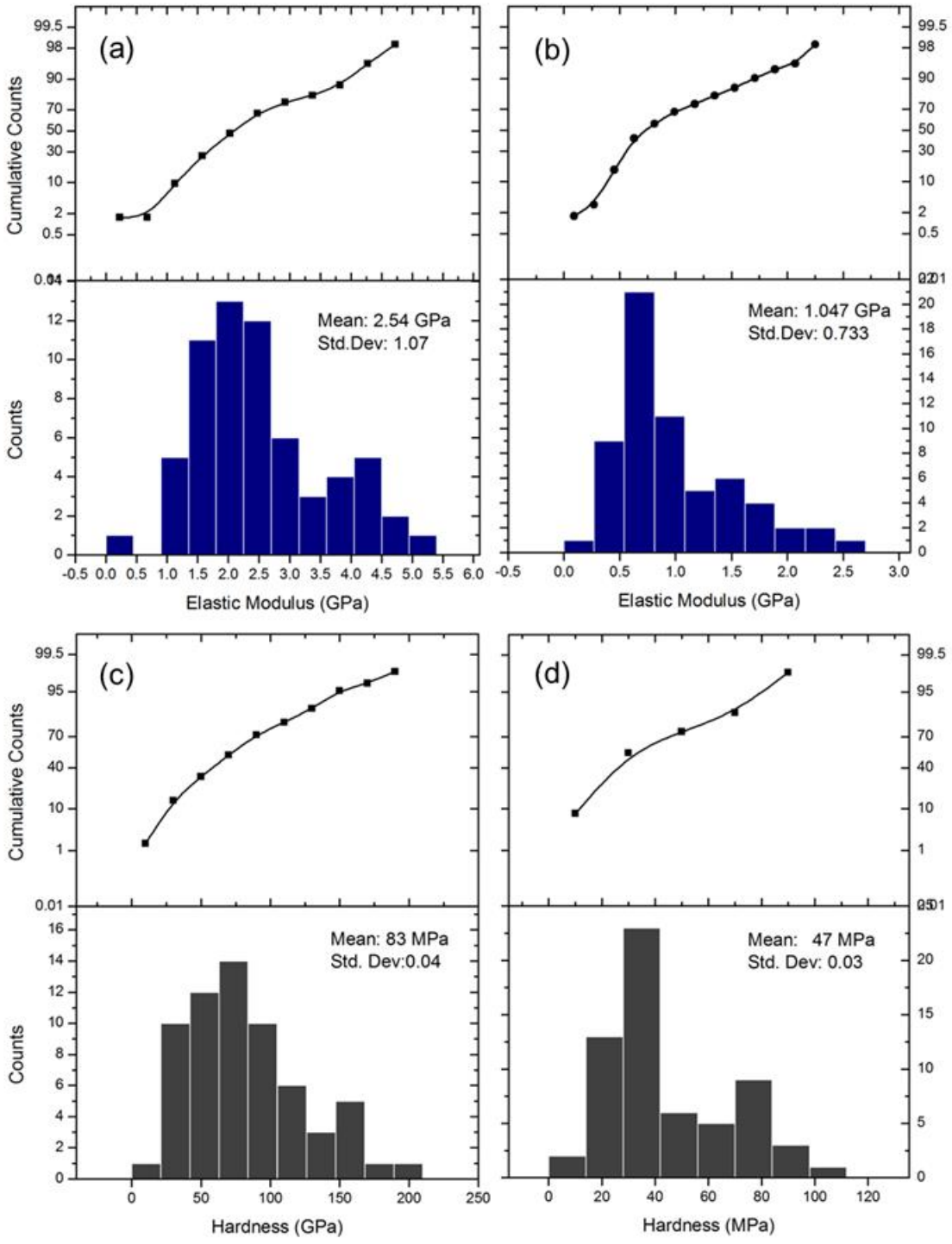

Figure IV.4.11. Probability and histogram results of elastic modulus and hardness of uncompatibilized (a, c) and DCP compatibilized PHB/PCL blend (b, d), obtained by nanoindentation.

CONCLUSIONS

The compatibility of binary poly(3-hydroxybutyrate) (PHB) and poly(ε-caprolactone) (PCL) with a constant composition (75/25 wt/wt) was remarkably improved by reactive extrusion with different dicumyl peroxide (DCP) contents. The use of 1 wt% DCP during *in situ* compatibilization process by reactive extrusion led to a remarkable increase in ductile properties such as elongation at break and impact-absorbed energy with percentage increase of 91 and 231% respectively while the tensile strength remains almost at constant values. FESEM study revealed a clear change in the morphology for *in situ* compatibilized PHB/PCL (75/25) blend. While the uncompatibilized blend shows a clear phase separation with PCL-rich domains randomly embedded in the PHB-rich domains, compatibilized blends by reactive extrusion do not show a clear phase separation and the gap between PCL- and PHB-rich phases has almost disappeared. Results obtained by AFM confirm an increase of compatibility/miscibility between PHB and PCL by using reactive extrusion with 1 wt% DCP. Although full miscibility is not achieved with DCP compatibilization, the size of PCL-rich domains is remarkably reduced. AFM also revealed a noticeable decrease in the elastic modulus of the PHB-rich phase thus indicating that some PCL oligomers have been attached to its structure with the subsequent decrease in crystallinity and the corresponding decrease on mechanical resistant properties.

ACKNOWLEDGEMENTS

This research was supported by the Ministry of Economy and Competitiveness (MINECO) [MAT2014-59242-C2-1-R]. D. Garcia-Garcia wants to thank the Spanish Ministry of Education, Culture and Sports for the financial support through an FPU grant [FPU13/06011]. A. Carbonell-Verdu acknowledges Universitat Politècnica de València for financial support through an FPI grant.

REFERENCES

[1] *An analysis of European plastics production, demand and waste data*. PlasticsEurope (Association of Plastics Manufacturers), 2015.

[2] Imre B and Pukánszky B. *Compatibilization in bio-based and biodegradable polymer blends*. European Polymer Journal, 2013. **49**(6):1215-1233.

[3] Mittal V, Akhtar T and Matsko N. *Mechanical, thermal, rheological and morphological properties of binary and ternary blends of PLA, TPS and PCL*. Macromolecular Materials and Engineering, 2015. **300**(4):423-435.

[4] Arrieta MP, López J, López D, Kenny JM and Peponi L. *Biodegradable electrospun bionanocomposite fibers based on plasticized PLA-PHB blends reinforced with cellulose nanocrystals*. Industrial Crops and Products, 2016. **93**:290-301.

[5] Hong SG, Hsu HW and Ye MT. *Thermal properties and applications of low molecular weight polyhydroxybutyrate*. Journal of Thermal Analysis and Calorimetry, 2013. **111**(2):1243-1250.

[6] Arza CR, Jannasch P, Johansson P, Magnusson P, Werker A and Maurer FHJ. *Effect of additives on the melt rheology and thermal degradation of poly [(R)-3-hydroxybutyric acid]*. Journal of Applied Polymer Science, 2015. **132**(15):41836.

[7] Auriemma M, Piscitelli A, Pasquino R, Cerruti P, Malinconico M and Grizzuti N. *Blending poly(3-hydroxybutyrate) with tannic acid: Influence of a polyphenolic natural additive on the rheological and thermal behavior*. European Polymer Journal, 2015. **63**:123-131.

[8] Mousavioun P, Doherty WOS and George G. *Thermal stability and miscibility of poly(hydroxybutyrate) and soda lignin blends*. Industrial Crops and Products, 2010. **32**(3):656-661.

[9] Godbole S, Gote S, Latkar M and Chakrabarti T. *Preparation and characterization of biodegradable poly-3-hydroxybutyrate-starch blend films*. Bioresource Technology, 2003. **86**(1):33-37.

[10] Kulkarni SO, Kanekar PP, Nilegaonkar SS, Sarnaik SS and Jog JP. *Production and characterization of a biodegradable poly(hydroxybutyrate-co-hydroxyvalerate) (PHB-co-PHV) copolymer by moderately haloalkalitolerant Halomonas campisalis MCM B-1027 isolated from Lonar Lake, India*. Bioresource Technology, 2010. **101**(24):9765-9771.

[11] Nakamura S, Kunioka M and Doi Y. *Biosynthesis and characterization of bacterial poly(3-hydroxybutyrate-co-3-hydroxypropionate)*. Macromolecular Reports, 1991. **28**(1):15-24.

[12] Ganzeveld KJ, Van Hagen A, Van Agteren MH, De Koning W and Uiterkamp AJMS. *Upgrading of organic waste: Production of the copolymer poly-3-hydroxybutyrate-co-valerate by Ralstonia eutrophus with organic waste as sole carbon source*. Journal of Cleaner Production, 1999. **7**(6):413-419.

[13] Wang L, Zhu W, Wang X, Chen X, Chen GQ and Xu K. *Processability modifications of poly(3-hydroxybutyrate) by plasticizing, blending, and stabilizing*. Journal of Applied Polymer Science, 2008. **107**(1):166-173.

[14] Bibers I, Tupureina V, Dzene A and Kalnins M. *Improvement of the deformative characteristics of poly-β-hydroxybutyrate by plasticization*. Mechanics of Composite Materials, 1999. **35**(4):357-364.

[15] Garcia-Garcia D, Ferri JM, Montanes N, Lopez-Martinez J and Balart R. *Plasticization effects of epoxidized vegetable oils on mechanical properties of poly(hydroxybutyrate)*. Polymer International, 2016. **65**(10):1157-1164.

[16] Hinüber C, Häussler L, Vogel R, Brünig H, Heinrich G and Werner C. *Hollow fibers made from a poly(3-hydroxybutyrate)/poly-ε-caprolactone blend*. Express Polymer Letters, 2011. **5**(7):643-652.

[17] Gunaratne LMWK and Shanks RA. *Miscibility, melting, and crystallization behavior of poly(hydroxybutyrate) and poly(D,L-lactic acid) blends*. Polymer Engineering & Science, 2008. **48**(9):1683-1692.

[18] Lovera D, Márquez L, Balsamo V, Taddei A, Castelli C and Müller AJ. *Crystallization, morphology, and enzymatic degradation of polyhydroxybutyrate/polycaprolactone (PHB/PCL) blends*. Macromolecular Chemistry and Physics, 2007. **208**(9):924-937.

[19] Dacko P, Kowalczuk M, Janeczek H and Sobota M. *Physical properties of the biodegradable polymer compositions containing natural polyesters and their synthetic analogues*. Macromolecular Symposia, 2006. **239**(1):209-216.

[20] Garcia-Garcia D, Ferri JM, Boronat T, Lopez-Martinez J and Balart R. *Processing and characterization of binary poly(hydroxybutyrate) (PHB) and poly(caprolactone) (PCL) blends with improved impact properties*. Polymer Bulletin, 2016. **73**(12):3333-3350.

[21] Ma P, Hristova-Bogaerds DG, Lemstra PJ, Zhang Y and Wang S. *Toughening of PHBV/PBS and PHB/PBS blends via in situ compatibilization using dicumyl peroxide as a free-radical grafting initiator*. Macromolecular Materials and Engineering, 2012. **297**(5):402-410.

[22] Díaz MF, Barbosa SE and Capiati NJ. *Reactive compatibilization of PE/PS blends. Effect of copolymer chain length on interfacial adhesion and mechanical behavior*. Polymer, 2007. **48**(4):1058-1065.

[23] Yang L, Huang J, Lu X, Jia S, Zhang H, Jin G and Qu J. *Influences of dicumyl peroxide on morphology and mechanical properties of polypropylene/poly (styrene-b-butadiene-b-styrene) blends via vane-extruder*. Journal of Applied Polymer Science, 2015. **132**(9):41543.

[24] Michaeli W, Greefenstein A and Berghaus U. *Twin-screw extruders for reactive extrusion*. Polymer Engineering & Science, 1995. **35**(19):1485-1504.

[25] Raquez JM, Narayan R and Dubois P. *Recent advances in reactive extrusion processing of biodegradable polymer-based compositions*. Macromolecular Materials and Engineering, 2008. **293**(6):447-470.

[26] Moad G. *The synthesis of polyolefin graft copolymers by reactive extrusion*. Progress in Polymer Science, 1999. **24**(1):81-142.

[27] Dong W, Ma P, Wang S, Chen M, Cai X and Zhang Y. *Effect of partial crosslinking on morphology and properties of the poly(β-hydroxybutyrate)/poly(D,L-lactic acid) blends.* Polymer Degradation and Stability, 2013. **98**(9):1549-1555.

[28] Kurusu RS, Demarquette NR, Gauthier C and Chenal JM. *Effect of ageing and annealing on the mechanical behaviour and biodegradability of a poly (3-hydroxybutyrate) and poly(ethylene-co-methyl-acrylate-co-glycidyl-methacrylate) blend*. Polymer International, 2014. **63**(6):1085-1093.

[29] Arrieta MP, Samper MD, López J and Jiménez A. *Combined effect of poly(hydroxybutyrate) and plasticizers on polylactic acid properties for film intended for food packaging*. Journal of Polymers and the Environment, 2014. **22**(4):460-470.

[30] Simões CL, Viana JC and Cunha AM. *Mechanical properties of poly(ε-caprolactone) and poly(lactic acid) blends*. Journal of Applied Polymer Science, 2009. **112**(1):345-352.

[31] Butt HJ, Cappella B and Kappl M. *Force measurements with the atomic force microscope: Technique, interpretation and applications*. Surface Science Reports, 2005. **59**(1):1-152.

[32] Frybort S, Obersriebnig M, Müller U, Gindl-Altmutter W and Konnerth J. *Variability in surface polarity of wood by means of AFM adhesion force mapping*. Colloids and Surfaces A: Physicochemical and Engineering Aspects, 2014. **457**:82-87.

[33] Smolyakov G, Formosa-Dague C, Severac C, Duval RE and Dague E. *High speed indentation measures by FV, QI and QNM introduce a new understanding of bionanomechanical experiments*. Micron, 2016. **85**:8-14.

[34] Smolyakov G, Pruvost S, Cardoso L, Alonso B, Belamie E and Duchet-Rumeau J. *AFM PeakForce QNM mode: Evidencing nanometre-scale mechanical properties of chitin-silica hybrid nanocomposites*. Carbohydrate Polymers, 2016. **151**:373-380.

[35] Roa JJ, Oncins G, Díaz J, Capdevila XG, Sanz F and Segarra M. *Study of the friction, adhesion and mechanical properties of single crystals, ceramics and ceramic coatings by AFM*. Journal of the European Ceramic Society, 2011. **31**(4):429-449.

[36] Dokukin ME and Sokolov I. *Quantitative mapping of the elastic modulus of soft materials with HarmoniX and PeakForce QNM AFM modes*. Langmuir, 2012. **28**(46):16060-16071.

[37] Adamcik J, Lara C, Usov I, Jeong JS, Ruggeri FS, Dietler G, Lashuel HA, Hamley IW and Mezzenga R. *Measurement of intrinsic properties of amyloid fibrils by the peak force QNM method*. Nanoscale, 2012. **4**(15):4426-4429.

[38] Sweers K, Van der Werf K, Bennink M and Subramaniam V. *Nanomechanical properties of α-synuclein amyloid fibrils: A comparative study by nanoindentation, harmonic force microscopy, and Peakforce QNM*. Nanoscale Research Letters, 2011. **6**:270-279.

[39] Pletikapić G, Berquand A, Radić TM and Svetličić V. *Quantitative nanomechanical mapping of marine diatom in seawater using peak force tapping atomic force microscopy*. Journal of Phycology, 2012. **48**(1):174-185.

[40] Derjaguin BV, Muller VM and Toporov YP. *Effect of contact deformations on the adhesion of particles*. Journal of Colloid and Interface Science, 1975. **53**(2):314-326.

[41] Oliver WC and Pharr GM. *Measurement of hardness and elastic modulus by instrumented indentation: Advances in understanding and refinements to methodology*. Journal of Materials Research, 2004. **19**(1):3-20.

[42] Oliver WC and Pharr GM. *An improved technique for determining hardness and elastic modulus using load and displacement sensing indentation experiments*. Journal of Materials Research, 1992. **7**(6):1564-1583.

[43] Hochstetter G, Jimenez A and Loubet JL. *Strain-rate effects on hardness of glassy polymers in the nanoscale range. Comparison between quasi-static and continuous stiffness measurements*. Journal of Macromolecular Science, Part B: Physics, 1999. **38**(5):681-692.

[44] Giró-Paloma J, Roa JJ, Díez-Pascual AM, Rayón E, Flores A, Martínez M, Chimenos JM and Fernández AI. *Depth-sensing indentation applied to polymers: A comparison between standard methods of analysis in relation to the nature of the materials*. European Polymer Journal, 2013. **49**(12):4047-4053.

[45] Ma P, Cai X, Zhang Y, Wang S, Dong W, Chen M and Lemstra PJ. *In-situ compatibilization of poly(lactic acid) and poly(butylene adipate-co-terephthalate) blends by using dicumyl peroxide as a free-radical initiator*. Polymer Degradation and Stability, 2014. **102**:145-151.

[46] Semba T, Kitagawa K, Ishiaku US and Hamada H. *The effect of crosslinking on the mechanical properties of polylactic acid/polycaprolactone blends*. Journal of Applied Polymer Science, 2006. **101**(3):1816-1825.

[47] Wei L, McDonald AG and Stark NM. *Grafting of bacterial polyhydroxybutyrate (PHB) onto cellulose via in situ reactive extrusion with dicumyl peroxide*. Biomacromolecules, 2015. **16**(3):1040-1049.

[48] Prakalathan K, Mohanty S and Nayak SK. *Reinforcing effect and isothermal crystallization kinetics of poly(3-hydroxybutyrate) nanocomposites blended with organically modified montmorillonite*. Polymer Composites, 2014. **35**(5):999-1012.

[49] Martínez-Tong DE, Najar AS, Soccio M, Nogales A, Bitinis N, López-Manchado MA and Ezquerra TA. *Quantitative mapping of mechanical properties in polylactic acid/natural rubber/organoclay bionanocomposites as revealed by nanoindentation with atomic force microscopy*. Composites Science and Technology, 2014. **104**:34-39.

[50] Arrieta MP, López J, López D, Kenny JM and Peponi L. *Development of flexible materials based on plasticized electrospun PLA-PHB blends: Structural, thermal, mechanical and disintegration properties*. European Polymer Journal, 2015. **73**:433-446.

[51] Armentano I, Fortunati E, Burgos N, Dominici F, Luzi F, Fiori S, Jiménez A, Yoon K, Ahn J, Kang S and Kenny JM. *Processing and characterization of plasticized PLA/PHB blends for biodegradable multiphase systems*. Express Polymer Letters, 2015. **9**(7):583-596.

[52] Arrieta MP, Castro-López MM, Rayón E, Barral-Losada LF, López-Vilariño JM, López J and González-Rodríguez MV. *Plasticized poly(lactic acid)-poly(hydroxybutyrate) (PLA-PHB) blends incorporated with catechin intended for active food-packaging applications*. Journal of Agricultural and Food Chemistry, 2014. **62**(41):10170-10180.

[53] Roa JJ, Rayon E, Morales M and Segarra M. *Contact mechanics at nanometric scale using nanoindentation technique for brittle and ductile materials*. Recent Patents on Engineering, 2012. **6**(2):116-126.

[54] Lyne ÅL, Wallqvist V and Birgisson B. *Adhesive surface characteristics of bitumen binders investigated by atomic force microscopy*. Fuel, 2013. **113**:248-256.

European Polymer Journal 86 (2017) 41–57

Contents lists available at ScienceDirect

European Polymer Journal

journal homepage: www.elsevier.com/locate/europolj

Improvement of the compatibility between poly(3-hydroxybutyrate) and poly(ε-caprolactone) by reactive extrusion with dicumyl peroxide

D. Garcia-Garcia *, E. Rayón, A. Carbonell-Verdu, J. Lopez-Martinez, R. Balart

Instituto de Tecnología de Materiales-ITM, Universitat Politècnica de València, Plaza Ferrandiz y Carbonell 1, 03801 Alcoy, Alicante, Spain

ARTICLE INFO

Article history:
Received 13 September 2016
Received in revised form 10 November 2016
Accepted 17 November 2016
Available online 18 November 2016

Keywords:
Poly(3-hydroxybutyrate)
Poly(ε-caprolactone)
Dicumyl peroxide
Reactive compatibilization
Blends

ABSTRACT

Poly(3-hydroxybutyrate) is a biodegradable aliphatic polyester obtained through bacterial fermentation that has gained attention in the last few years; nevertheless, its industrial applications are restricted because of some drawbacks related to its high stiffness and fragility which is associated to its high crystallinity. In this work, poly(3-hydroxybutyrate) (P3HB) was melt blended with poly(ε-caprolactone) (PCL) at a constant weight ratio of 75/25 (P3HB/PCL) by reactive extrusion with different contents of dicumyl peroxide (DCP) in the 0–1 wt% range. The effects of the DCP load on mechanical, thermal and morphology of the P3HB/PCL blend were studied. Results showed a positive increase in the elongation at break and the impact-absorbed energy of 91% and 231% respectively with regard the uncompatibilized P3HB/PCL blend by the addition of 1 wt% DCP, being this a clear evidenced of the improved compatibility between these polymers. Moreover, morphology of DCP-compatibilized P3HB/PCL blend obtained by field emission electron microscopy (FESEM) and atomic force microscopy (AFM) showed a remarkable decrease in the particle size of poly(ε-caprolactone)-rich domains randomly dispersed in the poly(3-hydroxybutyrate). In addition, both FESEM and AFM also revealed improved interfacial adhesion between P3HB- and PCL-rich phases with a noticeable decrease in the gap between them. Addition of 1 wt% DCP also contributes to lowering the degree of crystallinity of PHB by 14% in the blend and other thermal properties are not highly affected by the reactive extrusion with DCP.

1. Introduction

During the last years, a global marked driven by consumerism along with the relatively low price of plastic materials has led to a remarkable growth in the plastic production and consumption. Only in Europe the plastic production in 2014 was estimated to 59 million tons whilst the global plastic production was of about 299 million tons. The packaging industry is the biggest consumer which accounts for 39.5% with a wide variety of products characterized by a very short life cycle [1]. One of the main problems related to the massive use of plastics is the huge amounts of wastes that are generated after the end of their life cycled as only a small amount is recycled, upgraded or incinerated for energy production. The most common situation is that huge amounts of plastic wastes are continuously deposited into controlled landfills with a marked negative

* Corresponding author.
E-mail address: dagarga4@epsa.upv.es (D. Garcia-Garcia).

http://dx.doi.org/10.1016/j.eurpolymj.2016.11.018
0014-3057/

ADDITION OF NANOPARTICLES

IV.5

"Optimizing the yield and physico-chemical properties of pine cone cellulose nanocrystals by different hydrolysis time"

Daniel García García[a], *Rafael Balart*[a], *Juan López Martínez*[a], *Monica Ek*[b], *Rosana Moriana*[b,c]

[a] Instituto de Tecnología de Materiales (ITM)
Universitat Politècnica de València (UPV)
Plaza Ferrándiz y Carbonell 1, 03801 Alcoy, Alicante, Spain.

[b] School of Engineering Science in Chemistry, Biotechnology and Health
Department of Fibre and Polymer Technology
Royal Institute of Technology (KTH)
100 44 Stockholm, Sweden.

[c] School of Engineering Science
University of Skövde (HIS)
Högskolevägen, 541 28 Skövde, Sweden.

Cellulose

2018

Optimizing the yield and physico-chemical properties of pine cone cellulose nanocrystals by different hydrolysis time

Abstract

Cellulose nanocrystals (CNCs) were isolated for the first time from pine cones (PC) by alkali and bleaching treatments and subsequent sulfuric acid hydrolysis (64 %) at 45 °C. The influence of the hydrolytic reaction time (30, 45 and 90 min) on the yield, chemical composition and structure, and thermal stability of CNCs was evaluated. The removal of non-cellulosic constituents during the alkaline and bleaching treatment resulted in high pure cellulosic fibers. The isolation of CNCs from these cellulosic fibers at different reaction times was verified by the nano-dimensions of the individual crystals (< 3 and <335 nm of average diameter and length, respectively). The highest yield (15%) and the optimum CNCs properties in terms of aspect ratio, thermal stability and crystallinity were obtained for an extraction time of 45 min. PC appeared to be a new promising source of cellulose fibers and CNCs with potential to be applied as reinforcement in composites and for food-packaging.

Keywords: Pine cones; cellulose nanocrystals; sulfuric hydrolysis conditions; physico-chemical properties; yield-recovery.

INTRODUCTION

During the last years, concerns about sustainable development have increased significantly leading to a major interest for the research and development of environmentally friendly materials as an alternative to petroleum-based materials. Cellulose is the most abundant biopolymer on earth and is characterized by being renewable, biodegradable and non-toxic [1, 2]. Cellulose consists of linear homopolysaccharide chains of β-D-glucopyranose units linked together by β-1,4-glycosidic bonds [3]. Intramolecular and intermolecular hydrogen bonds are established between the cellulosic chains resulting in ordered/packed crystalline structures which are intercalated with amorphous regions in the fibril structure [4-7]. These crystalline domains can be separated from each other by overcoming the extensive and strong inter-fibrillar hydrogen bonds with acid treatment [8-10], specific enzymes [11] and/or intense mechanical forces [12, 13]. Among these extractive methods, the use of sulfuric acid to provoke the cleavage of the glycosidic bonds, achieving the disintegration of the cellulose amorphous region, has been the most widely used [4, 14, 15]. Cellulose nanocrystals (CNCs) obtained from sulfuric acid hydrolysis have been of great scientific interest due to their high crystallinity, low density, rod-like shape, high aspect ratio (diameter/length), high specific surface area, good mechanical properties (high stiffness and elastic modulus), low coefficient of thermal expansion, stability in aggressive media, gas permeability and optical transparency [2, 7, 16, 17]. Most of these CNCs properties (such as aspect ratio, morphology, thermal stability and degree of crystallinity) are highly dependent on the hydrolysis conditions as well as on the raw cellulosic material they are extracted from [18]. The reaction time has been identified as one of the most important parameters to consider during the CNCs extraction. Kargarzadeh *et al.* [19] obtained CNCs from kenaf with different hydrolysis reaction times (20, 30, 40, 60, 90 and 120 min) and specific thermal and crystallinity properties were achieved for each time. Silvéiro *et al.* [20] also studied the effect of the acid hydrolysis time (30, 60 and 90 min) on the chemical, physical and thermal properties of CNCs from corncob and the highest crystallinity and thermal stability were obtained with a hydrolytic time of 60 min. The origin of the cellulose raw materials on the particular performance of CNCs has been also evaluated through different comparative studies, where the hydrolysis conditions were fixed. CNCs were obtained from a variety of sources; however, most research efforts have been focused on partially purified versions of woods (such as microcrystalline cellulose and bleached pulp). Beck-Candanedo *et al.* [21] investigated the suspension properties of CNCs obtained by hydrolysis of a softwood (spruce) and a hardwood (eucalyptus) pulp. These two suspensions had similar CNCs dimensions and surface charge, implying that the basic unit of wood cellulose organization is the same for the two species.

During the last decade, the use of residual lignocellulosic biomass from agriculture, food and forest to produce CNCs has become impellent due to the increasing demand of finding cheaper sources and higher extraction yields alternatives to produce nanocelluloses as reinforcing agents for composites [22]. Deepa *et al.* [23] obtained CNCs from various biomass residues (sisal, kapok, banana rachis, pineapple leaf and coir) and differences in their size, crystallinity and thermal stability were detected depending on the used raw material. In previous studies, bark, pine needles, branches and woody chips were proposed as new cost-effective forest raw materials to isolate CNCs. The feasibility of obtaining CNCs with specific performances depending on the physico-chemical properties of the cellulose fibers in the forest residues was proved [18, 24]. A comparative study of the aspect ratio, crystallinity and thermal stability of the extracted CNCs was proposed to assess their performance as reinforcing agent in composites [24].

In this paper, we investigate for the first time the feasibility of using pine cones from *Pinus Pinea* (Stone pine) as a raw material to produce CNCs. *Pinus Pinea* (Stone pine) is one of the most important species in the Mediterranean region due mainly to the production of pine nuts, a culinary ingredient with an increasing demand [25]. Nowadays, Spain, Portugal and Italy are the countries with the largest population of this tree species with 490,000; 175,000 and 46,000 ha respectively [26]. After collecting the pine nuts the cones are discarded, leading to a high amount of residue, which has no industrial or economic value. Currently, small amounts of pine cones are being used as home fuel, however most of this waste ends up being incinerated or thrown into the field creating a risk of fire [27]. The study and research of alternatives for the recovery of this food-waste by obtaining value-added products will contribute to move towards a circular biobased economy and to develop a biorefinery concept with environmental, social and economic benefits [28]. The goals of this study are: to evaluate the feasibility of isolating CNCs from pine cones using different hydrolytic times (30, 45 and 90 min); to determine the overall recovery yield, the physico-chemical properties and thermal behavior of the produced CNCs; and, to estimate the optimal processing conditions to obtain CNCs suitable for being used as reinforcements in polymeric-based composites.

EXPERIMENTAL

Materials

Pine cones (PC) were collected from a Pine forest (*Pinus Pinea*) in Alicante area (Spain). These forest residues were conditioned at 40 °C during one week. The raw PC were

ground in a Wiley mill (Thomas Scientific, New Jersey, USA) to pass through a 20 μm mesh screen. Analytical grade chemicals used for the experimental procedure were: sodium hydroxide (NaOH 99%), sulfuric acid (H_2SO_4 98%), sodium chlorite ($NaClO_2$ 80%), sodium acetate ($C_2H_3NaO_2$ > 99%) and glacial acetic acid (CH_3COOH 99.7%). All of them were purchased from Sigma-Aldrich (Sigma-Aldrich, Germany). All water used was purified by Milli-Q water (Millipore Corporate, USA). Polysaccharide standards (cellulose, starch, galactomannan, glucomannan, arabinoxylan, arabinogalactan, arabinan) for the chemical analysis were purchased from Sigma-Aldrich or Megazyme (Megazyme, Ireland).

Isolation of cellulose nanocrystals (CNCs)

The isolation of the CNCs was achieved by subjecting milled PC samples to different chemical treatments. First, an alkaline and bleaching treatment was proposed to remove the extractives, lignin and hemicelluloses and to produce the subsequent isolation of the cellulose fibers from the raw material. Second, a hydrolytic treatment with sulfuric acid was performed to remove the amorphous regions to obtain the CNCs.

Alkaline and bleaching treatment

Milled PC samples were subjected to an alkaline and bleaching treatment following the same methodology previously described by Moriana *et al.* [24]. Three different batches of PC (4% w/v) were treated with sodium hydroxide solution (4.5% w/v NaOH) for 2 h at 80 °C under vigorous mechanical stirring. This alkaline treatment was repeated three times and after each treatment, the resulting material was washed with water until the removal of the chemicals and subsequently dried at room temperature overnight. After alkali treatment, three different batches (4% w/v) of alkaline pine cones (APC) were bleached with a solution made up of equal parts (1:1:1) of 1.7 wt% aqueous sodium chlorite, acetate buffer (0.2 M, pH 4.8) and water. The bleaching procedure was performed at 80 °C for 4 h and repeated five times. After each bleaching treatment the bleached pine cones (BPC) were filtered and washed with Milli-Q water and dried at room temperature for 24 h.

Acid hydrolysis treatment

The acid hydrolysis treatment was performed on the BPC. BPC were dried at 40 °C for 24 h in an air-circulating oven and subsequently grinded in a Wiley Mill (Thomas Scientific, New Jersey, USA) using a 20 μm mesh screen. The milled BPC were hydrolyzed in

sulfuric acid solution (65 wt%) at 45 °C for 30, 45 and 90 min under mechanical stirring. At least three different batches at 4% w/v of BPC were prepared for each hydrolyzed time. The suspensions were diluted with ice cubes to stop the hydrolysis reaction. Afterwards, they were washed with Milli-Q water by successive centrifugations in an Avanti J-E centrifuge (Beckman Coulter, California, USA) at 13,000 rpm for 10 min at 4 °C until the supernatant reached a constant pH of 5. After, the suspensions were dialyzed with purified water during one week until the neutral pH. Finally, the suspensions were sonicated for 5 min at an amplitude of 27% using an ultrasonic homogenizer Vibra-cell Mod. VCX 750 (Sonics and Materials Inc., Connecticut, USA) in an ice bath to avoid overheating. To remove the largest particles, the suspensions were centrifuged and the sediments were discharged. The CNC suspensions were stored at 4 °C for further characterization. The obtained CNC suspensions were labeled depending on the extraction time as follows: CNC_{30}, CNC_{45} and CNC_{90}, for the CNC suspensions extracted at 30, 45 and 90 min respectively.

Characterization techniques

Gravimetric analysis

The gravimetric yield of each experimental treatment (alkaline, bleaching and hydrolysis) was determined by weighing the dried samples before and after of each experimental procedure. At least three different replications of each sample and batch were considered to calculate the average and the standard deviations.

Chemical composition analysis

The chemical composition of all the studied samples (PC, APC, BPC, CNC_{30}, CNC_{45} and CNC_{90}) was evaluated following the methodology previously described by Moriana *et al.* [29]. The dry matter of samples was determined in a Mettler Toledo HB43 moisture analyzer (Mettler Toledo S.A.E., USA). The ash content was determined gravimetrically after heating the dry samples in a furnace at 525 °C for 6 h, following the TAPPI standard method T211 om-02. The determination of acid insoluble (Klason) lignin in the samples was carried out according to the TAPPI T222. The total amount of soluble extractives in the PC was determined by sequential extraction with ethanol, toluene and hot water [30]. The carbohydrates composition was assessed by conventional two-step Saeman hydrolysis [31], followed by quantification of the released monosaccharides using high-pH anion-exchange chromatography with pulsed amperometric detection (HPAEC-PAD). In short, 1 mg of dry sample was initially pre-hydrolyzed with 250 µL 72% H_2SO_4 at room temperature for 3 h,

diluted until a final concentration of 1 M H_2SO_4, and then subjected to a second hydrolysis step at 100 °C for 3 h. The hydrolysates were centrifuged at 4 °C and subjected to analysis directly without any other purification or neutralization. The released monosaccharides were separated on a Dionex ICS3000 system (Dionex Corporation, California, USA) by 10 µL injection of the filtered hydrolysates on a Dionex Carbopac PA1 column at 30 °C at a flow rate of 1 mL min^{-1}. Neutral sugars (glucose, mannose, xylose, arabinose, galactose and rhamnose) and uronic acids (galacturonic and glucuronic acid) were analyzed separately using different elution profiles [32]. The samples were analyzed in triplicate.

Scanning electron microscopy (SEM)

The morphologies of PC, APC and BPC were evaluated using a scanning electron microscopy Phenom (FEI Company, Eindhoven, the Netherlands) operated at 5 kV acceleration voltage. Prior the analysis the samples were coated with a thin layer of gold/palladium alloy in a sputter coater EMITECH model SC7620 (Quorum Technologies Ltd., East Sussex, UK).

Atomic force microscopy (AFM)

AFM imaging of CNCs with different hydrolysis times was performed in a Nanoscope IIIa Multimode scanning probe microscope (Digital Instruments Inc., New York, USA). A few drops of diluted nanocrystals suspension were deposited onto a freshly cleaved mica surface and air-dried. All images were obtained using the tapping-mode in air at room temperature with RTESP silica cantilevers (Bruker) having a tip with a radius of 8 nm and a spring constant of 20–80 N m^{-1} and resonance frequencies between 306 and 366 kHz. Lengths and diameters were obtained from printouts of several height mode AFM images, using the section analysis tool of the NanoScope Analysis software Version 1.40. AFM samples from each type of CNCs were prepared from the three different batches to evaluate the reproducibility of the experimental procedure. No significant differences in the CNC dimensions were detected from batch to batch. Therefore, more than a hundred CNCs of each material were randomly selected and measured to determine their average length and diameter.

Thermogravimetric analysis (TGA)

The thermal behavior of PC, APC, BPC and the different CNCs was evaluated by thermogravimetric analysis (TGA) [18]. The samples, with an average mass of 4.5 mg, were placed in an alumina crucible (70 μL) and heated from 25 to 750 °C at a constant heating rate of 10 °C min^{-1} on a Mettler-Toledo TGA/DSC 1 thermobalance (Schwerzenbach, Switzerland) under nitrogen atmosphere (50 mL min^{-1}). The onset temperature, maximum decomposition temperature and mass loss percentages, for each thermal decomposition process were obtained using the STAR^e Evaluation Software. At least three replicates of each sample were performed and evaluated.

X-ray diffraction spectroscopy (XRD)

X-ray diffraction of all the studied samples was obtained using a Bruker CCD-Apex apparatus equipped with an X-ray generator (Ni filtered Cu-Kα radiation) operated at 40 kV and 40 mA with 2θ varying from 10° to 60° at a scan rate of 2° min^{-1}. The measurements were repeated at least twice for each sample. The crystalline index (CrI) of the PC before and after the different treatments and the CNCs with different hydrolysis times was determined by referring to diffraction intensity of crystalline and amorphous regions using the empirical method proposed by Segal *et al.* [33]:

$$\boldsymbol{CrI = \frac{I_{200} - I_{am}}{I_{200}} \times 100} \qquad \textbf{Equation IV.5.1}$$

where I_{200} is the maximum intensity at plane 200 located at a diffraction angle around 2θ = 22°, and I_{am} stands for the minimum intensity from the amorphous part of the sample, measured approximately at a diffraction angle of around 2θ = 18°.

Fourier transform infrared spectrometry (FTIR)

FTIR spectra of all the samples were collected at room temperature on a Spectrum 2000 FTIR spectrometer from Perkin-Elmer (Perkin-Elmer Inc., Massachusetts, USA) equipped with a golden single-reflection accessory for ATR measurements. Each spectrum was obtained as 24 individual scans at 4 cm^{-1} resolution in the wavenumber range comprised between 4000 to 600 cm^{-1}. The measurements were repeated three times for each sample. The spectra were automatically baseline-corrected and smoothened using Omnic 7 Software.

RESULTS AND DISCUSSION

Visual description and gravimetric yield of the isolation procedure

The visual appearance of the PC samples during the entire isolation process together with the gravimetric yields obtained after each chemical treatment are shown in Figure IV.5.1. The removal of 35% of the initial PC sample mass during the alkaline treatment, resulted in a sample with a lighter brown appearance, indicating the partially removal of lignin, pectins and hemicelluloses [15]. During the bleaching treatment, 26% of mass was lost and the obtained white fibrous sample indicated most of the lignin was removed and the cellulose fibers were isolated [34]. The acid hydrolysis of the bleached samples resulted in a blurry suspension with a gel-like behavior. Similar yields were obtained for the CNC_{30} and CNC_{45} samples, whereas the CNC_{90} had the lowest yield. During the second centrifugation step, different amounts of cellulosic solid residues (CSR) were precipitated for each hydrolytic time (7.5, 1 and 2% for CNC_{30}, CNC_{45} and CNC_{90} respectively). The higher CSR obtained for the CNC_{30} indicates higher agglomerates and less homogenous hydrolysis was produced due to an insufficient hydrolytic time to uniformly remove the amorphous domains of the bleached samples. On the other hand, the similar content of CSR obtained at 45 and 90 min and the lowest yield value for the CNC_{90} suggests a partial degradation of the crystalline domains. The higher overall yield was therefore for the CNC_{45} with a value of 14.7%. Similar yields were published for CNCs extracted from branches, pine-needles, rachis of date palms tree and capim dourado under similar isolation conditions [6, 24, 35].

The effect of the specific hydrolysis times on the chemical composition, morphology, crystallinity and thermal stability of the resulting CNCs was evaluated to assess the most suitable conditions to produce CNCs to be used as reinforcing agents for polymer matrices in composites.

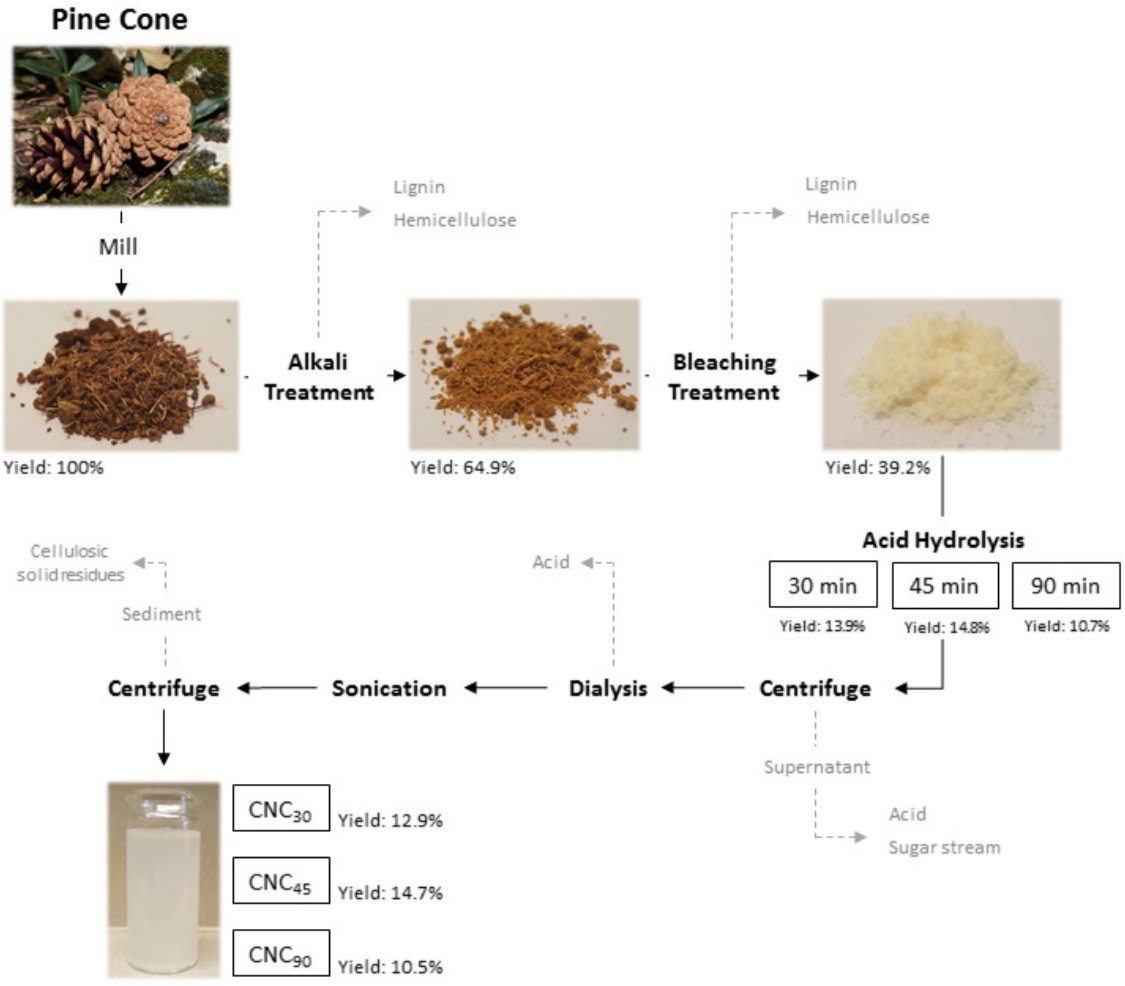

Figure IV.5.1. Schematic representation of the pine cone CNC isolation procedure with different hydrolysis times.

Chemical composition

The identification of the relative amount of each component present in each stage of the isolation process was performed by the combined results from the carbohydrate composition, the ash content, extractives estimation and lignin Klason determination (Table IV.5.1). The carbohydrate composition was determined from the quantification of the area peaks from chromatographic curves corresponding to the glucose, mannose, xylose, arabinose, galactose, rhamnose, galacturonic and glucuronic acid of each sample. The amount of cellulose results from the percentage of glucose, whereas the amount of hemicellulose/pectin (such as mannans, xylans, arabinogalactans, galacturonan) corresponds to the percentage of the remaining sugars. Some hemicelluloses may contain as well glucose monomers in their structure (*e.g.*, glucomannans) but their contribution is

somewhat minor compared to cellulose, as it can be observed in the low mannose percentage shown in the . The PC samples show a high amount of glucose (45.3%) and lignin in their composition (39.6%). The hemicellulose/pectin content can be primarily assigned to galactoglucomannan, (with a 2.9% of mannose and 1.3% of galactose) which is the main hemicellulose present in softwoods [36]. The chemical composition of PC showed a higher cellulose content compared to other forest residues that were previously proposed as raw materials to obtain CNCs such as woody chips, pine needles, branches or bark spruce [18, 29]. During the alkali treatment the lignin and hemicellulose/pectin content was reduced. However, the most significant reduction of lignin took place during the bleaching step reaching a content of 4.1%. On the other hand, the hemicellulose/pectin content did not decrease due to the bleaching process (4.4%), but the reached value was still lower than those from other forest residues at this stage (21% for the branches and pine-needles) [18, 29]. These low values of both lignin and hemicellulose/pectin resulted in BPC samples with an extraordinary high cellulose content (89%), showing their potential to be used as raw materials to isolate CNCs.

During the hydrolytic treatment is expected hemicelluloses and pectins hydrolyzed together with the amorphous part of the cellulose and became soluble [29]. However, it was observed that the mannose content in CNC_{30} and CNC_{45} was similar to that present in the BPC sample. This is because the mannose is more resistant to hydrolysis and dissolution during the preparation of the CNCs than other amorphous cell wall components [37, 38]. However, in the CNC_{90} the mannose content significantly decreases, thus indicating greater removal of the hemicellulose content and, maybe, the degradation of the cellulose. This fact can also be pointed out due to the small gravimetric yield (Table IV.5.1) of the CNC_{90} in comparison to CNC_{45}. The CNC yields for CNC_{30} and CNC_{90} (32.7 and 26.8% respectively) are similar to those reported by Le Normand *et al.* [18] for spruce bark and by Brito *et al.* [39] for bamboo fibers. However, the CNC_{45} yields are higher and more similar to those reported by Moriana *et al.* [24] for woody chips.

Table IV.5.1. Yield obtained after each chemical treatment and chemical composition of PC, APC, BPC and CNCs with different hydrolysis times.

Treatment	PC	APC	BPC	CNC_{30}	CNC_{45}	CNC_{90}
Yield[a]	100	64.9 ± 3.5	60.3 ± 1.5	32.7 ± 0.4	37.1 ± 0.4	26.8 ± 0.3
Arabinose	0.23 ± 0.01	0.20 ± 0.00	0.11 ± 0.01	<0.1	<0.1	<0.1
Rhamnose	<0.1	<0.1	<0.1	<0.1	<0.1	<0.1
Galactose	1.31 ± 0.03	1.10 ± 0.00	0.88 ± 0.07	<0.1	<0.1	<0.1
Glucose	45.33 ± 0.04	62.62 ± 0.02	88.99 ± 0.14	95.99 ± 0.07	95.65 ± 0.01	97.85 ± 0.05
Xylose	0.23 ± 0.01	0.14 ± 0.02	0.11 ± 0.00	0.16 ± 0.03	0.23 ± 0.01	<0.1
Mannose	2.91 ± 0.05	2.34 ± 0.03	2.76± 0.22	2.40 ± 0.04	2.50 ± 0.00	0.50 ± 0.02
Galacturonic Acid	0.39 ± 0.08	0.13 ± 0.04	0.21 ± 0.07	<0.1	<0.1	<0.1
Glucuronic Acid	0.30 ± 0.07	0.18 ± 0.03	0.30 ± 0.09	0.18 ± 0.02	0.17 ± 0.01	<0.1
Total Carbohydrates	50.71 ± 0.30	66.70 ± 0.13	93.36 ± 0.61	98.86 ± 0.17	98.66 ± 0.03	98.47 ± 0.10
Cellulose	45.33 ± 0.04	62.62 ± 0.02	88.99 ± 0.14	95.99 ± 0.07	95.65 ± 0.01	97.85 ± 0.05
Hemicellulose	5.38 ± 0.25	4.08 ± 0.12	4.37 ± 0.47	2.87 ± 0.09	3.01 ± 0.02	0.62 ± 0.02
Extractives	6.51 ± 0.31	-	-	-	-	-
Klason lignin	39.66 ± 0.01	29.76 ± 0.02	4.10 ± 0.06	N/A	N/A	N/A
Ash	3.12 ± 0.25	3.54 ± 0.23	2.54 ± 0.32	1.14 ± 0.04	1.34 ± 0.04	1.53 ± 0.05

[a] The gravimetric yields for each treatment were calculated based on the total dry weight (100%) of the previous treatment.

Morphological surface

SEM and AFM images were used to follow the morphological surface changes in materials during the entire CNC isolation process. Figure IV.5.2 shows the SEM micrographs of the raw PC (Figure IV.5.2a), after alkali (Figure IV.5.2b) and bleaching treatment (Figure IV.5.2c). PC is composed of oriented fiber bundles that are bonded together by a large amount of amorphous material, many irregularities and impurities are also seen on the surface. After the alkaline treatment, a greater definition of the cellulosic fibers was observed (Figure IV.5.2b). The non-cellulosic components of the PC that act as binders of the cellulosic fibers, such as hemicellulose, lignin, pectin and other impurities were partially removed, achieving an opening of the matrix that will enhance the penetration of the bleaching agents during the subsequent treatment [40]. After bleaching, most of lignin present in the PC was removed; chlorine is able to oxidize lignin, giving rise to the formation of hydroxyl, carbonyl and carboxylic groups, which allow lignin solubilization [41]. Removal of most lignin and hemicellulose increased the defibrillation, resulting in a large amount of individual cellulosic fibers, with an average diameter of 24.2 ± 4.5 μm (Figure IV.5.2c). These values are similar to the average width observed for other forest residues, such as woody chips (around 23.5 μm) and branches (around 19.6 μm) [24].

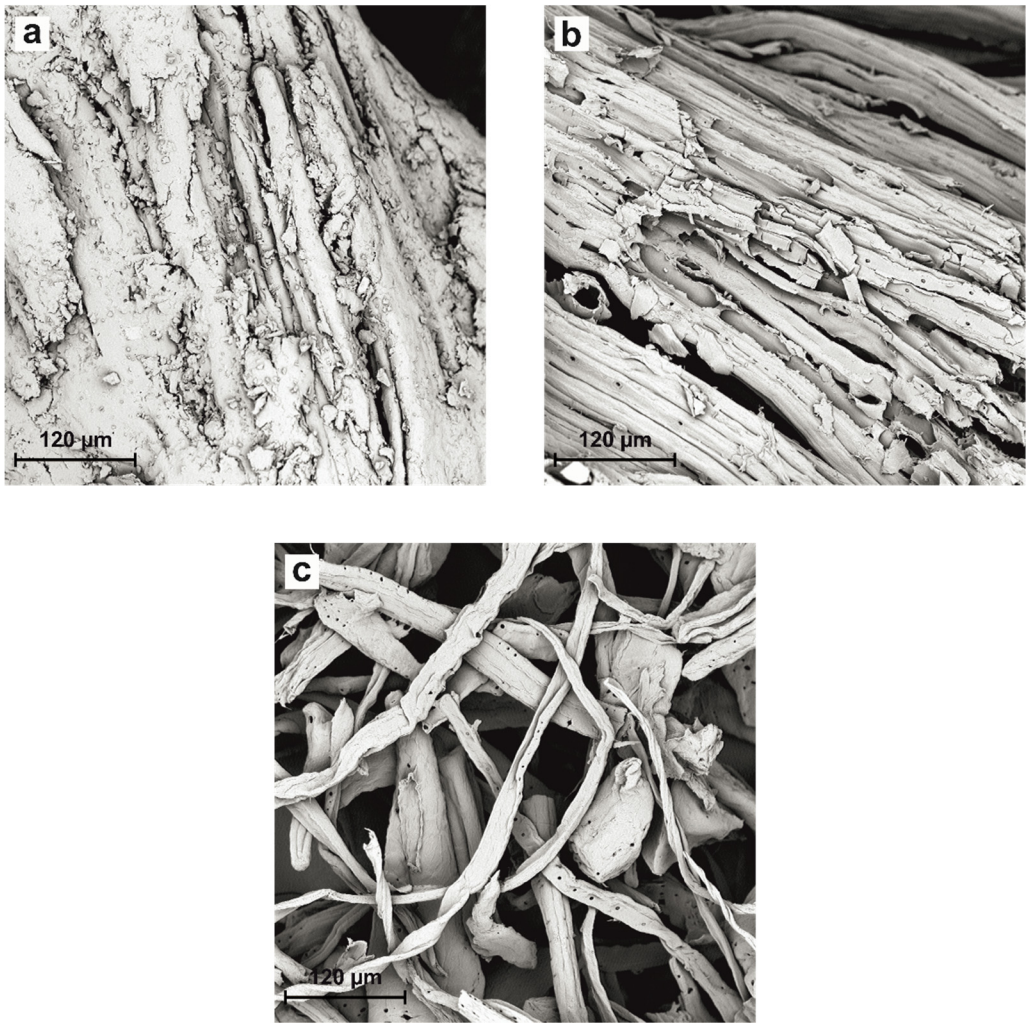

Figure IV.5.2. SEM micrographs of (a) raw pine cone (PC), (b) alkaline (APC) and (c) bleached (BPC) samples.

The morphology and size distribution of CNCs with different hydrolysis times were studied by AFM. Figure IV.5.3 shows an example of AFM images of the isolated CNC_{45}, as well as the histograms of each CNCs, with the corresponding length (*L*) and width (*D*) distribution. The obtained PC nanocrystals had a rod-like aspect. Nevertheless, some aggregates between them can be observed. This is mainly due to the strong hydrogen bonds established between crystals [18]. The lowest diameter dispersion was for the CNC_{45} with a diameter ranging from 1.8 to 5.7 nm. These dimensions are typical values for CNC widths from wood [21]. On the other hand, the CNC_{90} showed the lowest length dispersion (from 106.7 to 410 nm). These dimensions are similar to typical length values for wood CNCs (100 to 400 nm) [21, 42]. The obtained nanoparticles were characterized by their average length and width and their limit values (maximum and minimum) together with their aspect ratio (*L/D*) (Table IV.5.2). The average dimensions of the CNC_{30} and CNC_{45} were very similar

between them (330 nm of length and 3 nm of width), which is very similar in diameter to other forest residues (branches and bark) [18, 24], but much higher in length. For longer hydrolysis times (90 min), a considerable decrease in CNC size, (206.5 nm of length and 2.4 nm of width) was detected. This might be due to the partial destruction of the crystalline domain due to the long hydrolysis time [15]. The CNC aspect ratio is one of the most important parameters in determining their reinforcing capacity for nanocomposite applications. Nanocrystals with a high aspect ratio can provide higher reinforcement effect, leading to an increase in mechanical and thermal properties at low loadings [43]. In this case, CNC_{30} and CNC_{45} offer a greater reinforcement potential than the CNC_{90} in nanocomposite applications. PC nanocrystals have a higher aspect ratio than those CNCs obtained from other agro-forestry residues under similar conditions, such as woody chips, branches, pine needles [24], spruce bark [18], black spruce [21], *Pandanus tectorius* [5], rice straw [8], rice husk [40] and soy hull [15].

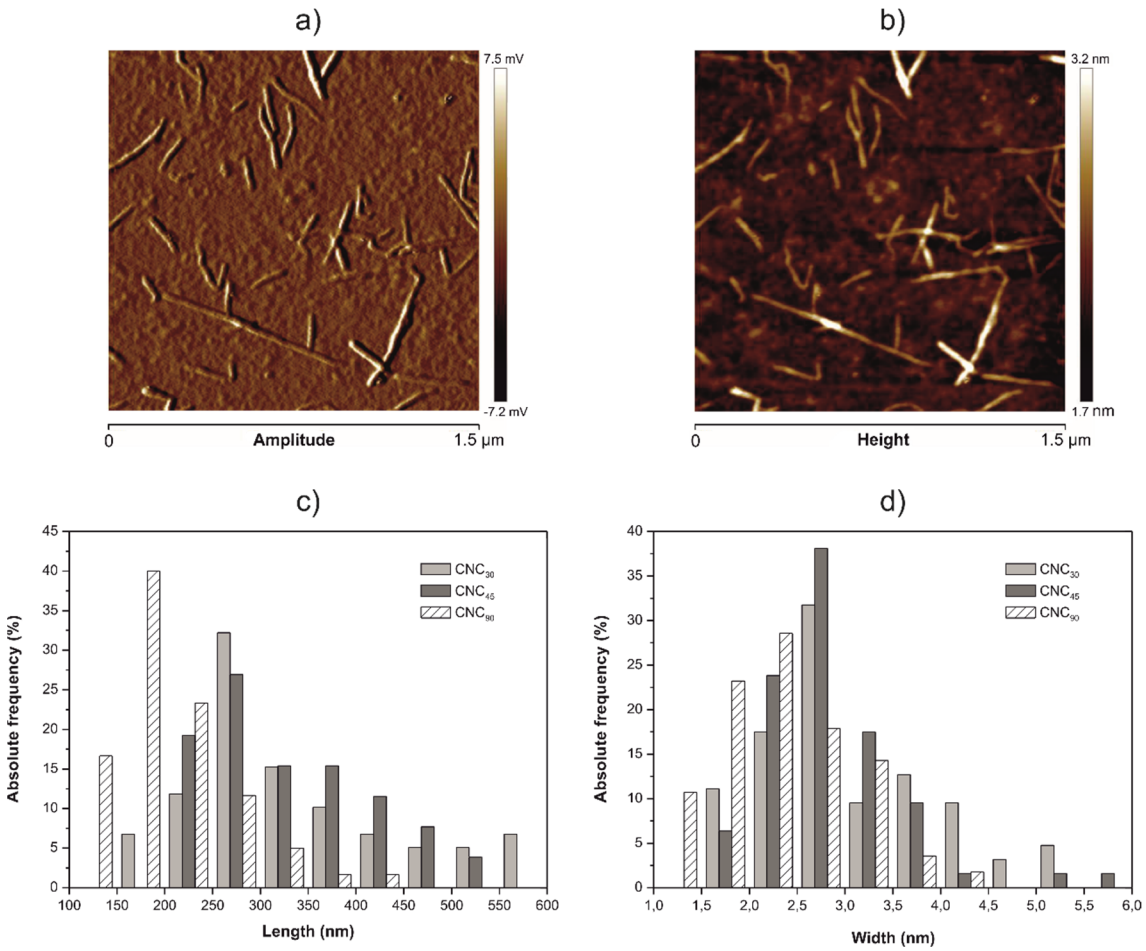

Figure IV.5.3. AFM images of CNC_{45} in (a) amplitude and (b) height mode (scale bar 1.5 µm). Size distribution histograms of the CNCs at different hydrolysis time: (c) length and (d) width.

Table IV.5.2. Length, width and aspect ratio of CNCs with different hydrolysis times obtained by AFM analysis.

Sample	Length *L* (nm)			Width *D* (nm)			Average aspect ratio (*L*/*D*)
	Max	Min	Average	Max	Min	Average	
CNC_{30}	572.3	165.6	334.9 ± 112.3	5.5	1.6	3.0 ± 0.9	111.6
CNC_{45}	501.2	223.4	328.9 ± 82.2	5.7	1.8	2.9 ± 0.7	113.4
CNC_{90}	410.0	106.7	206.5 ± 64.5	4.4	1.2	2.4 ± 0.7	86.0

Crystallinity and crystal size

The X-ray method was used to characterize the crystalline structure changes in the samples during the entire isolation process and to assess the differences due to the hydrolysis time. Figure IV.5.4 shows the X-ray patterns of PC at different stages of treatment. As it can be seen, all the patterns are characterized by two peaks around 2θ = 16.3° and 22.5°, typical of the crystalline structure of cellulose I, and an amorphous broad hump (2θ = 18°−19°). After the chemical treatments the peak around 22.5° increased and became more defined. This indicates a higher crystallinity degree due to the partial removal of the amorphous regions [5].

During the alkaline and bleaching treatments, an increment in the CrI was observed (from 42.6 to 65.1%) due to the reduction and removal of amorphous non-cellulosic compounds such as lignin and hemicellulose [12, 44]. During the hydrolysis treatment, an increase in the CrI with respect to the BPC due to the hydrolytic scission of the glycosidic bonds occurred. This phenomenon allowed releasing individual crystals and removing the amorphous domains [9, 45]. Comparing the CrI of the CNCs with different hydrolysis times, the same behavior as that observed for the gravimetric yield was observed; samples showed an increase in their crystallinity from 30 to 45 min and then, decreased at 90 min. Therefore, the highest crystallinity is achieved for a hydrolysis time of 45 min (88.5%) whereas the CNC_{90} showed the lowest CrI (80.8%). This may be due to the fact that crystalline regions can be partially destroyed with high acid hydrolysis times [15, 46]. The CNC crystallinity indexes obtained from PC are similar to those obtained in other agro-industrial and forest residues such as rice straw [8], spruce bark [18] or Swedish forest residues (Scots pines and Norway spruce) [24], being higher to those obtained in other lignocellulosic residues such as soy hulls [15] or kenaf fibers [19].

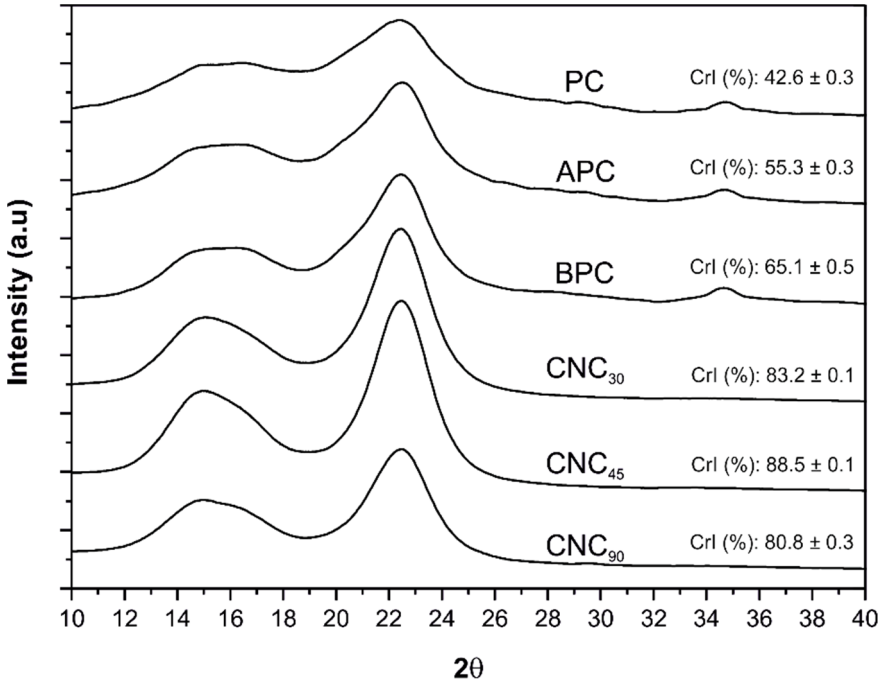

Figure IV.5.4. X-ray diffraction patterns and crystallinity index (CrI) of PC, APC, BPC and CNCs with different hydrolysis times.

Chemical structure

The infrared spectra of the PC, APC, BPC and the CNCs with different hydrolysis times are gathered in Figure IV.5.5. Significant changes in the spectra were detected after the different treatments performed, thus demonstrating the effectiveness of each one of them. The peak located around 3330 cm^{-1}, which corresponds to stretching vibrations of OH groups of cellulose and lignin [47], became narrower after the different treatments due to the removal of part of the amorphous components [18]. The peak around 2900 cm^{-1}, which corresponds to the C–H stretching of methyl and methylene groups in cellulose [9], decreased after the alkaline and bleaching treatment. The peak located at 1730 cm^{-1} attributed to the acetyl and uronic ester groups of the hemicellulose or the ester linkage of carboxylic group of ferulic and p-coumaric acids of lignin and/or hemicelluloses, was also reduced and practically disappeared after bleaching. [12, 15]. The same was observed for the peak at 1509 cm^{-1} that corresponds to the C–H deformation in methyl, methylene and methoxyl groups of lignin and aromatic C=C ring stretching. Similar behavior was observed for the peak located at 1260 cm^{-1} that corresponds to the C–O–C vibration of acetyl groups in hemicellulose. The absence of these peaks in the BPC and CNCs spectra indicates that most of the hemicellulose and lignin was removed, thus leading to a material with high cellulose content as it was shown by chemical analysis.

In CNCs spectra for the different hydrolysis times, it is worthy to note the appearance of a new small peak at 1205 cm^{-1} related to S=O vibration. This can be explained by considering the esterification reaction during the hydrolysis process [20]. This peak had a higher intensity as the hydrolysis time increased.

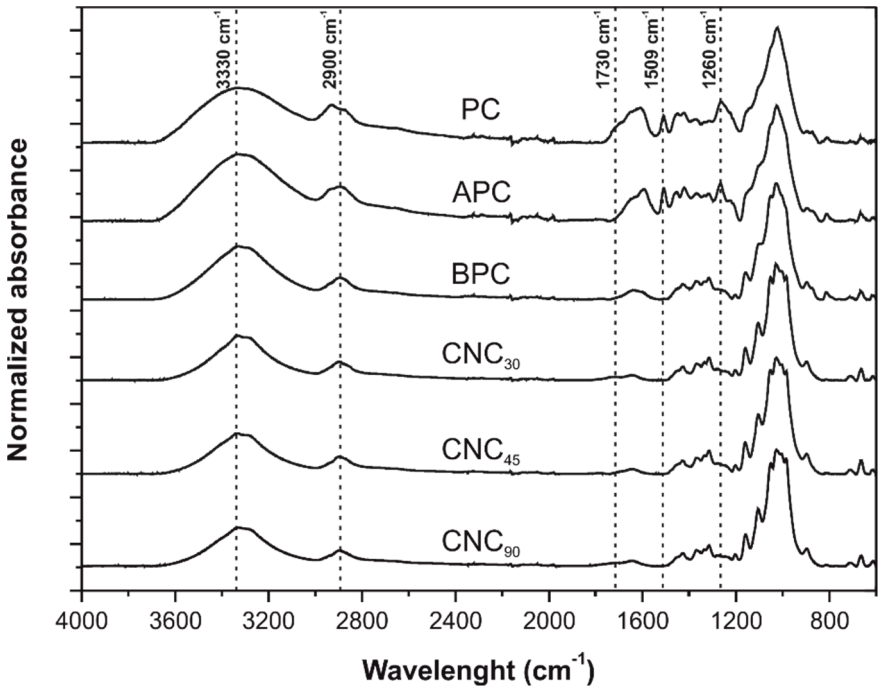

Figure IV.5.5. FTIR spectra of PC, APC, BPC and CNCs with different hydrolysis times.

Thermal stability and behavior

Thermogravimetric (TG) and first derivative thermogravimetric (DTG) curves for all the studied samples are shown in Figure IV.5.6. Two main mass-loss regions were identified during the thermal decomposition of each sample: a first mass loss (<6.5%) between 25 and 150 °C related to the moisture evaporation and a second region between 150 and 650 °C, where the mass loss was due to thermal degradation of the cellulose, hemicellulose and lignin components. Figure IV.5.6a and c show that the thermal degradation of PC occurs in three overlapped process between 150 and 650 °C: the first process was related to the thermal degradation of hemicellulose and pectins and appeared between 200 and 340 °C; the second one was associated with the cellulose degradation (between 340 and 400 °C) and showed a well-defined peak at 364 °C [48, 49]; and the third process related with most of the lignin degradation that appeared as a small shoulder at higher temperatures, between 415 and 525 °C [18, 23]. After the alkaline and bleaching treatment the peak located around 330 °C and the shoulder at the highest temperatures disappeared due to the removal of

hemicellulose and lignin after both chemical treatments [5]. Furthermore, an improvement in thermal stability was observed due to the removal of hemicellulose, which decomposes before lignin and cellulose as a result of the presence of acetyl groups in hemicellulose molecules [19].

Figure IV.5.6b shows the thermal degradation behavior of CNCs at different acid hydrolysis times. The acid hydrolysis of the bleached fibers led to a decrease in thermal stability due to the substitution of hydroxyl groups by sulfate groups. First, evaporation of water absorbed by the CNCs occurred, being lower than in the previous steps due to the dehydration of cellulose fibers occurred during the acid hydrolysis [48]. Three overlapping processes took place at higher temperatures (>145 °C): the first one centered at approximately 175 °C was related to the sulfate groups that catalyze cellulose dehydration; the second peak centered at 220–234 °C was associated with the breakdown of the more accessible region in the crystal interior; and the last one, with a temperature around 364 °C, was associated with the less accessible crystal interior of the CNCs [20]. The thermal degradation behavior of CNC_{30} was similar to CNC_{45}, however CNC_{90} displayed a slightly lower thermal stability and a higher second peak due to the higher sulfate content and the degradation of the most labile region in the crystal interior. The residual mass in the CNCs was larger than in the bleached samples and could be explained by the presence of sulfuric acid that promoted the dehydration reactions and acted as a flame retardant [48, 50].

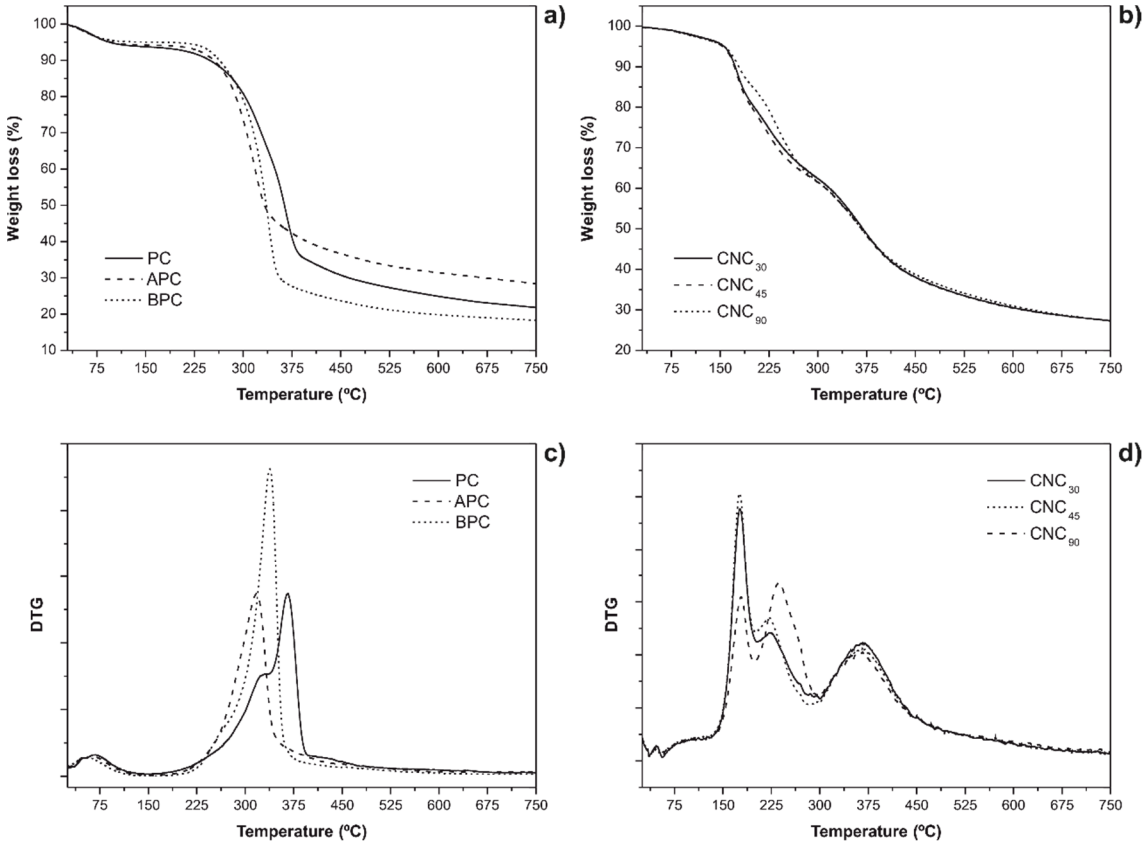

Figure IV.5.6. TGA and DTG curves of (a, c) PC, APC, BPC and (b, d) CNCs with different hydrolysis times.

CONCLUSIONS

Cellulose nanocrystals (CNCs) were successfully isolated from pine cones (PC), an abundant and cheap biomass residue. In this work the changes in the chemical composition, morphology, crystallinity and thermal properties of the biomass during the alkaline and bleaching treatment and the influence of the acid hydrolysis time (30, 45 and 90 min) on the overall yield and on performance of the resulting CNCs have been studied. The progressive removal of lignin and hemicelluloses resulted in extraordinary high cellulosic fiber samples suitable for the subsequent CNC isolation. The CNC_{45} showed similar chemical composition, aspect ratio, crystalline size and thermal behavior to those for the CNC_{30} however, the yield and crystallinity were higher for the CNC_{45}. The CNC_{90} exhibited the lowest yield, crystal size, crystallinity index, aspect ratio and thermal stability, indicating that partial destruction of crystalline domains could occur. Therefore, these results show that PC is an effective renewable source for the production of CNCs with an optimal extraction time of around 45 min during hydrolysis at 45 °C with 65% sulfuric acid. The high aspect ratio, the high crystallinity and the good thermal stability of the obtained CNCs show

great potential for their use as reinforcement in polymeric composites for different applications.

ACKNOWLEDGEMENTS

This work was supported by the Ministry of Economy and Competitiveness (MINECO) [MAT2014-59242-C2-1-R]. D. Garcia-Garcia wants to thanks the Spanish Ministry of Education, Culture and Sports for their financial support through an FPU grant [FPU13/06011].

REFERENCES

[1] Haafiz MKM, Eichhorn SJ, Hassan A and Jawaid M. *Isolation and characterization of microcrystalline cellulose from oil palm biomass residue*. Carbohydrate Polymers, 2013. **93**(2):628-634.

[2] Peng BL, Dhar N, Liu HL and Tam KC. *Chemistry and applications of nanocrystalline cellulose and its derivatives: A nanotechnology perspective*. The Canadian Journal of Chemical Engineering, 2011. **89**(5):1191-1206.

[3] Luzi F, Fortunati E, Puglia D, Petrucci R, Kenny JM and Torre L. *Modulation of acid hydrolysis reaction time for the extraction of cellulose nanocrystals from posidonia oceanica leaves*. Journal of Renewable Materials, 2016. **4**(3):190-198.

[4] Mariano M, El Kissi N and Dufresne A. *Cellulose nanocrystals and related nanocomposites: Review of some properties and challenges*. Journal of Polymer Science Part B: Polymer Physics, 2014. **52**(12):791-806.

[5] Sheltami RM, Abdullah I, Ahmad I, Dufresne A and Kargarzadeh H. *Extraction of cellulose nanocrystals from mengkuang leaves (Pandanus tectorius)*. Carbohydrate Polymers, 2012. **88**(2):772-779.

[6] Siqueira G, Bras J and Dufresne A. *Cellulosic bionanocomposites: A review of preparation, properties and applications*. Polymers, 2010. **2**(4):728-765.

[7] Jiang F and Hsieh YL. *Chemically and mechanically isolated nanocellulose and their self-assembled structures*. Carbohydrate Polymers, 2013. **95**(1):32-40.

[8] Lu P and Hsieh YL. *Preparation and characterization of cellulose nanocrystals from rice straw*. Carbohydrate Polymers, 2012. **87**(1):564-573.

[9] Lamaming J, Hashim R, Sulaiman O, Leh CP, Sugimoto T and Nordin NA. *Cellulose nanocrystals isolated from oil palm trunk*. Carbohydrate Polymers, 2015. **127**:202-208.

[10] Espinosa SC, Kuhnt T, Foster EJ and Weder C. *Isolation of thermally stable cellulose nanocrystals by phosphoric acid hydrolysis*. Biomacromolecules, 2013. **14**(4):1223-1230.

[11] Satyamurthy P, Jain P, Balasubramanya RH and Vigneshwaran N. *Preparation and characterization of cellulose nanowhiskers from cotton fibres by controlled microbial hydrolysis*. Carbohydrate Polymers, 2011. **83**(1):122-129.

[12] Chen W, Yu H, Liu Y, Chen P, Zhang M and Hai Y. *Individualization of cellulose nanofibers from wood using high-intensity ultrasonication combined with chemical pretreatments*. Carbohydrate Polymers, 2011. **83**(4):1804-1811.

[13] Deepa B, Abraham E, Cherian BM, Bismarck A, Blaker JJ, Pothan LA, Leao AL, de Souza SF and Kottaisamy M. *Structure, morphology and thermal characteristics of banana nano fibers obtained by steam explosion*. Bioresource Technology, 2011. **102**(2):1988-1997.

[14] Lu H, Gui Y, Zheng L and Liu X. *Morphological, crystalline, thermal and physicochemical properties of cellulose nanocrystals obtained from sweet potato residue*. Food Research International, 2013. **50**(1):121-128.

[15] Neto WPF, Silvério HA, Dantas NO and Pasquini D. *Extraction and characterization of cellulose nanocrystals from agro-industrial residue – Soy hulls*. Industrial Crops and Products, 2013. **42**:480-488.

[16] Mueller S, Weder C and Foster EJ. *Isolation of cellulose nanocrystals from pseudostems of banana plants*. RSC Advances, 2014. **4**(2):907-915.

[17] Ioelovich M. *Optimal conditions for isolation of nanocrystalline cellulose particles*. Nanoscience and Nanotechnology, 2012. **2**(2):9-13.

[18] Le Normand M, Moriana R and Ek M. *Isolation and characterization of cellulose nanocrystals from spruce bark in a biorefinery perspective*. Carbohydrate Polymers, 2014. **111**:979-987.

[19] Kargarzadeh H, Ahmad I, Abdullah I, Dufresne A, Zainudin SY and Sheltami RM. *Effects of hydrolysis conditions on the morphology, crystallinity, and thermal stability of cellulose nanocrystals extracted from kenaf bast fibers*. Cellulose, 2012. **19**(3):855-866.

[20] Silvério HA, Neto WPF, Dantas NO and Pasquini D. *Extraction and characterization of cellulose nanocrystals from corncob for application as reinforcing agent in nanocomposites*. Industrial Crops and Products, 2013. **44**:427-436.

[21] Beck-Candanedo S, Roman M and Gray DG. *Effect of reaction conditions on the properties and behavior of wood cellulose nanocrystal suspensions*. Biomacromolecules, 2005. **6**(2):1048-1054.

[22] Maiti S, Jayaramudu J, Das K, Reddy SM, Sadiku R, Ray SS and Liu D. *Preparation and characterization of nano-cellulose with new shape from different precursor*. Carbohydrate Polymers, 2013. **98**(1):562-567.

[23] Deepa B, Abraham E, Cordeiro N, Mozetic M, Mathew AP, Oksman K, Faria M, Thomas S and Pothan LA. *Utilization of various lignocellulosic biomass for the production of nanocellulose: A comparative study*. Cellulose, 2015. **22**(2):1075-1090.

[24] Moriana R, Vilaplana F and Ek M. *Cellulose nanocrystals from forest residues as reinforcing agents for composites: A study from macro- to nano-dimensions*. Carbohydrate Polymers, 2016. **139**:139-149.

[25] Özgüven F and Vursavuş K. *Some physical, mechanical and aerodynamic properties of pine (Pinus pinea) nuts*. Journal of Food Engineering, 2005. **68**(2):191-196.

[26] Loewe V, Navarro-Cerrillo RM, García-Olmo J, Riccioli C and Sánchez-Cuesta R. *Discriminant analysis of mediterranean pine nuts (Pinus pinea L.) from chilean plantations by near infrared spectroscopy (NIRS)*. Food Control, 2017. **73**:634-643.

[27] Almendros AI, Martín-Lara MA, Ronda A, Pérez A, Blázquez G and Calero M. *Physico-chemical characterization of pine cone shell and its use as biosorbent and fuel*. Bioresource Technology, 2015. **196**:406-412.

[28] Li D, Moriana R and Ek M. *From forest residues to hydrophobic nanocomposites with high oxygen-barrier properties*. Nordic Pulp & Paper Research Journal, 2016. **31**(2):261-269.

[29] Moriana R, Vilaplana F and Ek M. *Forest residues as renewable resources for bio-based polymeric materials and bioenergy: Chemical composition, structure and thermal properties*. Cellulose, 2015. **22**(5):3409-3423.

[30] de Carvalho DM, Sevastyanova O, Penna LS, da Silva BP, Lindström ME and Colodette JL. *Assessment of chemical transformations in eucalyptus, sugarcane bagasse and straw during hydrothermal, dilute acid, and alkaline pretreatments*. Industrial Crops and Products, 2015. **73**:118-126.

[31] Saeman JF, Moore WE, Mitchell RL and Millett MA. *Techniques for the determination of pulp constituents by quantitiative paper chromatography*. Tappi Journal, 1954. **37**(8):336-343.

[32] Wright PJ and Wallis AFA. *Rapid determination of carbohydrates in hardwoods by high performance anion exchange chromatography*. Holzforschung-International Journal of the Biology, Chemistry, Physics and Technology of Wood, 1996**. 50**(6):518-524.

[33] Segal L, Creely JJ, Martin Jr AE and Conrad CM. *An empirical method for estimating the degree of crystallinity of native cellulose using the X-ray diffractometer*. Textile Research Journal, 1959. **29**(10):786-794.

[34] dos Santos RM, Neto WPF, Silvério HA, Martins DF, Dantas NO and Pasquini D. *Cellulose nanocrystals from pineapple leaf, a new approach for the reuse of this agro-waste*. Industrial Crops and Products, 2013. **50**:707-714.

[35] Bendahou A, Habibi Y, Kaddami H and Dufresne A. *Physico-chemical characterization of palm from phoenix dactylifera-L, preparation of cellulose whiskers and natural rubber-based nanocomposites*. Journal of Biobased Materials and Bioenergy, 2009. **3**(1):81-90.

[36] Willför S, Sundberg A, Hemming J and Holmbom B. *Polysaccharides in some industrially important softwood species*. Wood Science and Technology, 2005. **39**(4):245-257.

[37] Hannuksela T, Tenkanen M and Holmbom B. *Sorption of dissolved galactoglucomannans and galactomannans to bleached kraft pulp*. Cellulose, 2002. **9**(3-4):251-261.

[38] Iwata T, Indrarti L and Azuma JI. *Affinity of hemicellulose for cellulose produced by Acetobacter xylinum*. Cellulose, 1998. **5**(3):215-228.

[39] Brito BSL, Pereira FV, Putaux JL and Jean B. *Preparation, morphology and structure of cellulose nanocrystals from bamboo fibers*. Cellulose, 2012. **19**(5):1527-1536.

[40] Johar N, Ahmad I and Dufresne A. *Extraction, preparation and characterization of cellulose fibres and nanocrystals from rice husk*. Industrial Crops and Products, 2012. **37**(1):93-99.

[41] Cherian BM, Leão AL, de Souza SF, Thomas S, Pothan LA and Kottaisamy M. *Isolation of nanocellulose from pineapple leaf fibres by steam explosion*. Carbohydrate Polymers, 2010. **81**(3):720-725.

[42] Bondeson D, Mathew A and Oksman K. *Optimization of the isolation of nanocrystals from microcrystalline cellulose by acid hydrolysis*. Cellulose, 2006. **13**(2):171-180.

[43] Eichhorn SJ, Dufresne A, Aranguren M, Marcovich NE, Capadona JR, Rowan SJ, Weder C, Thielemans W, Roman M, Renneckar S, Gindl W, Veigel S, Keckes J, Yano H, Abe K, Nogi M, Nakagaito AN, Mangalam A, Simonsen J, Benight AS, Bismarck A, Berglund LA and Peijs T. *Review: Current international research into cellulose nanofibres and nanocomposites*. Journal of Materials Science, 2010. **45**(1):1-33.

[44] Rosli NA, Ahmad I and Abdullah I. *Isolation and characterization of cellulose nanocrystals from Agave angustifolia fibre*. BioResources, 2013. **8**(2):1893-1908.

[45] Lu QL, Tang LR, Wang S, Huang B, Chen YD and Chen XR. *An investigation on the characteristics of cellulose nanocrystals from Pennisetum sinese*. Biomass and Bioenergy, 2014. **70**:267-272.

[46] Chen Y, Liu C, Chang PR, Cao X and Anderson DP. *Bionanocomposites based on pea starch and cellulose nanowhiskers hydrolyzed from pea hull fibre: Effect of hydrolysis time*. Carbohydrate Polymers, 2009. **76**(4):607-615.

[47] Reddy JP and Rhim JW. *Isolation and characterization of cellulose nanocrystals from garlic skin*. Materials Letters, 2014. **129**:20-23.

[48] Roman M and Winter WT. *Effect of sulfate groups from sulfuric acid hydrolysis on the thermal degradation behavior of bacterial cellulose*. Biomacromolecules, 2004. **5**(5):1671-1677.

[49] García-García D, Carbonell A, Samper MD, García-Sanoguera D and Balart R. *Green composites based on polypropylene matrix and hydrophobized spend coffee ground (SCG) powder*. Composites Part B: Engineering, 2015. **78**:256-265.

[50] Kim DY, Nishiyama Y, Wada M and Kuga S. *High-yield carbonization of cellulose by sulfuric acid impregnation*. Cellulose, 2001. **8**(1):29-33.

Cellulose
https://doi.org/10.1007/s10570-018-1760-0

ORIGINAL PAPER

Optimizing the yield and physico-chemical properties of pine cone cellulose nanocrystals by different hydrolysis time

Daniel García-García · Rafael Balart · Juan Lopez-Martinez · Monica Ek · Rosana Moriana

Received: 15 December 2017 / Accepted: 15 March 2018

Abstract Cellulose nanocrystals (CNCs) were isolated for the first time from pine cones (PC) by alkali and bleaching treatments and subsequent sulfuric acid hydrolysis (64%) at 45 °C. The influence of the hydrolytic reaction time (30, 45, and 90 min) on the yield, chemical composition and structure, and thermal stability of CNCs was evaluated. The removal of non-cellulosic constituents during the alkaline and bleaching treatment resulted in high pure cellulosic fibres. The isolation of CNCs from these cellulosic fibres at different reaction times was verified by the nano-dimensions of the individual crystals (< 3 and < 335 nm of average diameter and length, respectively). The highest yield (15%) and the optimum CNCs properties in terms of aspect ratio, thermal stability and crystallinity were obtained for an extraction time of 45 min. PC appeared to be a new promising source of cellulose fibres and CNCs with potential to be applied as reinforcement in composites and for food-packaging.

Keywords Pine cones · Cellulose nanocrystals · Sulfuric hydrolysis conditions · Physico-chemical properties · Yield-recovery

D. García-García · R. Balart · J. Lopez-Martinez
Instituto de Tecnología de Materiales (ITM), Universitat Politècnica de València (UPV), Plaza Ferrándiz y Carbonell 1, 03801 Alcoy, Alicante, Spain

M. Ek · R. Moriana (✉)
School of Engineering Sciences in Chemistry, Biotechnology and Health, Department of Fibre and Polymer Technology, KTH-Royal Institute of Technology, 100 44 Stockholm, Sweden
e-mail: rosana@kth.se;
rosana.moriana.torro@his.se

R. Moriana
School of Engineering Science, HIS-University of Skövde, Skövde, Högskolevägen, 541 28 Skövde, Sweden

Published online: 23 March 2018

Introduction

During the last years, concerns about sustainable development have increased significantly leading to a major interest for the research and development of environmentally friendly materials as an alternative to petroleum-based materials. Cellulose is the most abundant biopolymer on earth and is characterized by being renewable, biodegradable and non-toxic (Haafiz et al. 2013; Peng et al. 2011). Cellulose consists of linear homopolysaccharide chains of β-D-glucopyranose units linked together by β-1,4-glycosidic bonds (Luzi et al. 2016). Intramolecular and intermolecular hydrogen bonds are established between the cellulosic chains resulting in ordered/-packed crystalline structures which are intercalated with amorphous regions in the fibril structure (Jiang and Hsieh 2013; Mariano et al. 2014; Sheltami et al. 2012; Siqueira et al. 2010). These crystalline domains can be separated from each other by overcoming the

IV.6

"Reinforcing capability of cellulose nanocrystals obtained from pine cones in a biodegradable poly(3-hydroxybutyrate)/poly(ε-caprolactone) (PHB/PCL) thermoplastic blend"

Daniel García García[a], *Juan López Martínez*[a], *Rafael Balart*[a], *Emma Strömberg*[b], *Rosana Moriana*[b,c]

[a] Instituto de Tecnología de Materiales (ITM)
Universitat Politècnica de València (UPV)
Plaza Ferrándiz y Carbonell 1, 03801 Alcoy, Alicante, Spain.

[b] School of Engineering Science in Chemistry, Biotechnology and Health
Department of Fibre and Polymer Technology
Royal Institute of Technology (KTH)
100 44 Stockholm, Sweden.

[c] School of Engineering Science
University of Skövde (HIS)
Högskolevägen, 541 28 Skövde, Sweden.

European Polymer Journal

2018, 104:10-18

Reinforcing capability of cellulose nanocrystals obtained from pine cones in a biodegradable poly(3-hydroxybutyrate)/poly(ε-caprolactone) (PHB/PCL) thermoplastic blend

Abstract

In this work, different loads (3, 5 and 7 wt%) of pine cone cellulose nanocrystals (CNCs) were added to films of poly(3-hydroxybutyrate)/poly(ε-caprolactone) (PHB/PCL) blends with a composition of 75 wt% PHB and 25 wt% PCL (PHB_{75}/PCL_{25}). The films were obtained after solvent casting followed by melt compounding in an extruder and finally subjected to a thermocompression process. The influence of different CNCs loadings on the mechanical, thermal, optical, wettability and disintegration in controlled compost properties of the PHB_{75}/PCL_{25} blend was discussed. Field emission scanning electron microscopy (FESEM) revealed the best dispersion of CNCs on the polymeric matrix was at a load of 3 wt%. Over this loading, CNCs aggregates were formed enhancing the films embrittlement due to stress concentration phenomena. However, the addition of CNCs improved the optical properties of the PHB_{75}/PCL_{25} films by increasing their transparency and accelerated the film disintegration in controlled soil conditions. In general, the blend with 3 wt% CNCs offers the best balanced properties in terms of mechanical, thermal, optical and wettability.

Keywords: Poly(3-hydroxybutyrate); poly(ε-caprolactone); biodegradability; cellulose nanocrystals (CNCs); thermoplastic blends.

INTRODUCTION

The recent increase in the social concern about environmental issues together with the increasing price of fossil fuels due to petroleum depletion [1], has given a rise in the development of new environmentally friendly materials as it is the case of biodegradable polymers. Biodegradable polymers challenges are related to their relatively poor mechanical and thermal properties compared to petroleum-based commodities and engineering plastics, restricting their wide use in industrial application [2]. The reinforcement of biodegradable polymers with nanoparticles has recently been proposed as a strategy to overcome some of the above-mentioned drawbacks. Specifically, bio-based nanoscale particles have been used to reinforce thermoplastic biodegradable polymers, such as poly(lactic acid) (PLA) [3-5], poly(3-hydroxybutyrate) (PHB) [6], poly(ε-caprolactone) (PCL) [7, 8] and poly(butylene adipate-*co*-terephthalate) (PBAT) [9]. The improved thermo-mechanical performance of these nanoscale-reinforced polymer composites, together with their potential biodegradation, could lead these new materials to compete with many traditional petroleum-based polymers, such as polypropylene (PP), polyethylene (PE) or polyethylene terephthalate (PET) [10, 11].

Cellulose nanocrystals (CNCs) from residual biomass (food, agriculture and forest) may be defined as one of the most promising reinforcing agents in terms of biodegradability, renewability, abundance in nature, variety and price [12, 13]. These highly crystalline cellulose particles are obtained from lignocellulosic fibers generally through two main steps: first, an alkaline and bleaching treatment to isolate the cellulose fibers from the raw material and second, a hydrolytic treatment with acid which allows the selective removal of the amorphous cellulosic phase remaining the crystalline phase almost unaltered [14-16]. The physico-chemical properties of CNCs can vary widely, depending on the source of the cellulosic raw material and the conditions selected to perform the hydrolysis [17, 18]. In previous studies, pine cones fibers were selected as raw materials to produce CNCs and the influence of the hydrolytic time on their properties and the processing yield was evaluated [19]. Furthermore, the potential of using the pine cone CNCs as reinforcement in composites was discussed in terms of aspect ratio, crystallinity and thermal stability. It is known that the influence of the matrix-reinforcement interface and compatibility is of foremost importance for the resulting performance of the composite materials. Therefore, in this study, we propose to evaluate the reinforcing capability of the pine cone CNCs in a biodegradable thermoplastic blend composed of 75% poly(3-hydroxybutyrate) and 25% poly(ε-caprolactone) (PHB_{75}/PCL_{25}). The overall effect of CNCs as reinforcement in thermoplastic composites highly depends on the percentage of loading nanoparticles and

the particle dispersion in the polymer matrix [20]. The main challenge to overcome to design CNCs based composites is related to the poor dispersion of these nanoparticles in hydrophobic polymers due to their high hydrophilic nature [21, 22]. Chemical modification of the CNCs or the use of surfactants during the compounding step are the most used approaches to enhance the dispersion of CNCs on the polymeric matrix, avoiding the formation of aggregates [23, 24]. However, Wang *et al.* [25] shown how the chemical modification of CNCs could disrupt their crystalline structure with the subsequent decrease in rigidity. Another important challenge in using CNCs in thermoplastic composites is their low thermal stability which could potentially be compromised during polymer processing, thus leading to partial CNCs degradation [26].

PHB_{75}/PCL_{25} is a promising biodegradable blend of different thermoplastic polyesters that offers better thermal, impact resistance and elongation properties than the neat PHB, due to the high ductility (high elongation at break values together with low modulus which leads to a rubber-like behavior) that PCL can provide to this blend. However, PHB_{75}/PCL_{25} shows low miscibility resulting in a phase separation when melt-blended occurs [27], where finely dispersed PCL droplets positively contribute to improve toughness in a similar way as polybutadiene rubber has on toughened styrene-derived polymers such as poly(styrene-*co*-acrylonitrile) + polybutadiene rubber (ABS) [28]. Despite this, the lack of compatibility between the polymers affects the mechanical properties of the blend, because they are directly related to the ability of its components to transfer stresses [29]. In addition, it is expected that the higher difficulty of degradation of the PCL decreases the biodegradation rate of the blend with respect to the neat PHB [30]. Several studies have corroborated that cellulose nanoparticles could potentially act as compatibilizers between immiscible polymers through their preferential location among the polymeric interfaces, reducing interface tension which prevents from coalescence of the dispersed phase [31], all this, having a positive effect on the overall properties of composite blends. In this sense, Arrieta *et al.* [32, 33] observed an improvement on interface adhesion between PLA and PHB extruded blends (75/25 wt%) by the addition of 5 wt% of CNCs. The incorporation of CNCs on this PLA/PHB blends enhanced the biodegradation rate, with respect to the unreinforced PLA/PHB blend.

The present work aims to study the reinforcing capability of different pine cone CNCs loads (3, 5 and 7 wt%) on the performance and disintegration rate of the biodegradable thermoplastic PHB_{75}/PCL_{25} blend. The influence of different CNCs loadings on the mechanical, thermal, morphological, optical and wettability of the PHB_{75}/PCL_{25} blend were studied. The effect of the CNCs on the disintegration rate of the PHB_{75}/PCL_{25} blend has

also been compared with the disintegration of the neat PHB. The dispersion of the CNCs in the matrix have been performed by a combination of solvent casting procedure and subsequent manufacturing by extrusion and thermocompression.

EXPERIMENTAL

Materials

Poly(3-hydroxybutyrate) (PHB) pellets (commercial grade P226) with an average molecular weight of 426,000 g mol^{-1}, a density of 1.25 g cm^{-3} and a melt flow index of 10 g $(10\ min)^{-1}$ (measured at 180 °C with a load of 5 kg) were supplied by Biomer (Krailling, Germany). Poly(ε-caprolactone) (PCL) in pellet form (commercial grade CAPA 6500) with an average molecular weight of 50,000 g mol^{-1} was provided by Perstorp Holding AB (Malmö, Sweden). Chloroform ($CHCl_3$ ≥ 99%) was purchased from Sigma Aldrich (Sigma-Aldrich, Germany). Pine cones (*Pinus Pinea*) were collected from a local pine forest in Alicante (Spain).

Preparation and characteristics of pine cone cellulose nanocrystals

Pine cones were conditioned at 40 °C for 1 week and then were grinded in a Wiley mill from Thomas Scientific (New Jersey, USA) and subsequently sieved with a 20 μm mesh screen. Cellulose nanocrystals (CNCs) were isolated from pine cone following the procedure described by García-García *et al.* [19]. In summary, grinded pine cone particles were subjected to an alkaline and bleaching treatment to remove the amorphous components, such as lignin and hemicellulose. Then, the bleached pine cones were hydrolyzed with sulfuric acid (65 wt%) at 45 °C for 45 min. The obtained suspension was washed with Milli-Q water by using repetitive centrifugations with the following conditions: 10 min at 13.000 rpms and at a temperature of 4 °C. After this stage, the solution was dialyzed during 7 days with Milli-Q water with the aim of removing the free acid until the wash water reached a constant pH. The resulting CNCs shown a crystallinity index of 88.5%, an onset degradation temperature (T_0) of 150.3 °C, an average aspect ratio (L/D) of 113.4, an average diameter of 2.9 nm and a percentage cellulose of 95.7% [19]. Moreover, an ion exchange resin Dowex Marathon MR-3 (hydrogen and hydroxide form) was added to the cellulose suspension for additional 48 h and the removed by filtration with the main aim of ensuring that all ionic moieties were removed except the H^+ counter ions associated with the sulfate groups attached to the CNCs surfaces [11]. The resulting suspension was then sonicated using a

Sonics Vibra-Cell VCX 750 sonicator from Sonics and Materials Inc. (Connecticut, USA) to promote CNCs dispersion and remove the remaining unhydrolyzed fibers by centrifugation. The final suspension containing CNCs was neutralized by adding NaOH (0.25 mol L^{-1}) until pH of 9 was reached. Finally, a freeze-drying process was carried out to obtain dry CNCs.

Processing of PHB_{75}/PCL_{25} films with pine cone CNCs

Films of PHB_{75}/PCL_{25} with different CNCs loading (3, 5 and 7 wt%) were prepared by combined melting processing technologies. Table IV.6.1 summarized the composition of all the developed materials. The films were obtained by solvent casting, granulated/pelletized and subsequently subjected to extrusion and thermocompression process. The solvent casting procedure was as follows: the specific amounts of both PHB and PCL were weighed and dissolved in $CHCl_3$ (1 g 25 mL^{-1}) by stirring at 50 °C for 5 h until full dissolution was achieved; then, the corresponding CNCs loads were dispersed in $CHCl_3$ by using a Sonics Vibra-Cell VCX 750 sonicator for 20 min (5×4 min) in an ice bath; after that, the dispersed CNCs were mixed together with the PHB_{75}/PCL_{25} solution in $CHCl_3$ and the mixtures were vigorously stirred for 1 h; and, finally, the mixture was maintained at room temperature until $CHCl_3$ was completely evaporated, followed by oven vacuum drying at 40 °C overnight.

Table IV.6.1. Composition and codes for poly(3-hydroxybutyrate)/poly(ε-caprolactone) (PHB/PCL) blend films with pine cone cellulose nanocrystals (CNCs).

Coding	PHB (wt%)	PCL (wt%)	CNC (wt%)
PHB	100	0	0
PHB_{75}/PCL_{25}	75	25	0
3% CNC	72.75	24.25	3
5% CNC	71.25	23.75	5
7% CNC	69.75	23.25	7

To increase the CNCs dispersion in the PHB_{75}/PCL_{25}, the solvent casting films were reduced until reaching pieces of about 3 mm and subjected to a compounding process in a DSM Xplore Micro 5cc twin screw microextruder from Xplore Instruments BV (Sittard, the Netherlands) at 180 °C. The screw speed was set to 120 rpm and the mixing time did not

exceed 3 min to avoid thermal degradation of PHB and CNCs. Then, the material was discharged and cooled at room temperature, pelletized and vacuum dried at 40 °C overnight. Finally, the dry compounded material was compression molded to 100 μm films using a hot press Fontijne model TP400 (Barendrecht, the Netherlands). The material was preheated up to 180 °C for 1 min and then, subjected to a pressure of 200 MPa for 1 additional min. After this, the obtained materials were cooled down to room temperature by maintaining the compaction pressure.

Characterization techniques

UV–vis spectrometry

The light transmission properties of the PHB_{75}/PCL_{25} films with the different CNCs loads, were measured in the 250−700 nm wavelength range with a Shimadzu UV-2550 UV-Vis spectrophotometer from Shimadzu Scientific Instruments (Columbia, USA). The software UVProbe 2.0 was used to obtain and analyze the data. The measurements were done in triplicate and the average of the three spectra was obtained.

Static contact angle measurements

The static contact angle of neat PHB and PHB_{75}/PCL_{25} films with different CNCs loadings was obtained using a CAM 200 goniometer from KSV Instruments (Helsinki, Finland) equipped with a Basler A602f camera. The liquid for the contact angle measurement was Milli-Q water and the volume of the droplets was 5 μL. Prior to contact angle measurements, all samples were conditioned at 23 °C and 50% RH for 48 h. The static water contact angle was obtained using the CAM200 software applying the Young-Laplace fitting method. All contact angles were taken 5 s after the droplet was dropped into the film surface. At least, five different measurements for each film were obtained and averaged.

Field emission scanning electron microscopy (FESEM)

Cross section of nitrogen cryofractured films was investigated in a field emission scanning electron microscope (FESEM) ZEISS ULTRA55 (Oberkochen, Germany) working at an acceleration voltage of 2 kV. With the aim of providing electrical conductivity to the polymeric samples, the fracture surfaces were coated with a thin layer of platinum in a high vacuum sputter coater EM MED20 from Leica Microsystems (Wetzlar, Germany).

Mechanical properties

Tensile tests on films were carried out with an Instron 5944 machine from Instron Ltd. (Norwood, USA) using a 500 N load cell. Film samples with dimensions of 50×5 mm^2 were subjected to an initial gauge length of 25 mm and then, a crosshead speed was 2 mm min^{-1} was applied to obtain the main tensile parameters: tensile modulus, tensile strength and elongation at break. The thickness of the films was accurately measured with a Mitutoyo micrometer by taking the average thickness of five different areas of each film. All the films were subjected to a conditioning stage at 23 ± 1 °C and 50% RH for 48 h prior to testing. Five different replicates of each sample were tested and the average values of the above-mentioned tensile properties were calculated.

Thermal properties

Thermal properties of the films were obtained by means of thermogravimetric analysis (TGA) and differential scanning calorimetry (DSC). TGA was conducted in a Mettler-Toledo TGA/DSC 1 thermobalance (Schwerzenbach, Switzerland) under nitrogen atmosphere (the flow rate was set to 50 mL min^{-1}). The films were cut into small pieces (5–6 mg) and were taken and placed into standard alumina crucibles. A dynamic heating program from 30 to 750 °C at a heating rate of 10 °C min^{-1} was applied. The onset degradation temperature (T_0) was assumed as the temperature at which, a weight loss of 5% with regard the initial mass, occurs. The maximum degradation rate temperature (T_{max}) for each degradation stage was located at the corresponding peak in the first derivative curve (DTG).

DSC measurements were obtained in a Mettler-Toledo DSC 822e calorimeter (Schwerzenbach, Switzerland). The tests were run under nitrogen atmosphere with a flow rate of 50 mL min^{-1}. In a similar way to sample preparation for TGA, the films were cut into small pieces and, approximately 4 mg were placed in standard aluminum crucibles (40 μL). The thermal program was as follows: a first heating stage from −50 to 180 °C was applied to remove the thermal history; then, an isothermal stage at 180 °C for 1 min was scheduled. After this, a cooling process down to −50 °C was programmed and, finally, a second heating stage from −50 up to 300 °C was applied. The heating/cooling rate for all stages was set to 10 °C min^{-1}. All DSC tests were run in triplicate to obtain reliable results. The melt peak temperature (T_m) was taken from the second heating stage and the degree of crystallinity (X_c) of both PHB and PCL was calculated by following this equation:

$$\boldsymbol{X_c}\,(\%) = \left[\frac{\Delta \boldsymbol{H_m}}{\Delta \boldsymbol{H_0} \cdot \boldsymbol{w}}\right] \times \mathbf{100} \qquad \textbf{Equation IV.6.1}$$

where ΔH_m stands for the thermodynamic melt enthalpy per gram, ΔH_0 represents the theoretical melt enthalpy associated to the corresponding 100% crystalline polymer (these values were assumed to be 146 J g^{-1} [34] for PHB and 156.8 J g^{-1} [35] for PCL), and *w* is the weight fraction of the corresponding polymer (PHB or PCL) in the blend.

Fourier transformed infrared spectroscopy (FTIR)

FTIR spectra of PHB and PHB_{75}/PCL_{25} films with different CNCs content were obtained at room temperature on a Perkin-Elmer Spectrum 2000 FTIR instrument (Waltham, USA) equipped with a single reflection attenuated total reflectance (ATR) accessory unit, with a diamond ATR crystal Golden Gate from Specac Ltd. (Kent, England). Each spectrum was acquired in the wavelength range of 600−4000 cm^{-1} from 16 scans with a resolution of 4 cm^{-1}. All spectra were fitted to an automatic base line correction and normalized using the Perkin-Elmer software Spectrum.

X-ray diffraction spectroscopy (XRD)

X-ray diffraction (XRD) characterization of PHB and PHB_{75}/PCL_{25} of films was carried out using an X-ray diffraction on a Bruker CCD-Appex apparatus equipped with an X-ray generator (Ni filtered Cu-Kα radiation) operated at 40 kV and 40 mA. The samples were scanned from 5° to 40° (2θ) at a scanning rate of 2° min^{-1}.

Disintegration under composting conditions

The degradation rate under controlled compost soil of PHB and PHB_{75}/PCL_{25} blend with different CNCs content was carried out as indicated by ISO 20200. Films were cut into squared shapes (25×25 mm^2) with an average thickness of 100 μm. Initially, samples were dried overnight at 40 °C, weighed and subsequently, were buried at a depth of 4−6 cm in a plastic reactor containing a solid synthetic wet soil prepared with 40 wt% sawdust, 30 wt% rabbit-feed, 10 wt% corn starch, 10 wt% compost, 5 wt% sugar, 4 wt% corn oil and 1 wt% urea. Finally, distilled water was added to the synthetic solid waste to a 45:55 ratio. Samples were subjected to an aerobic degradation (disintegration) at a constant temperature of 50 °C in an air-circulating oven for a total time of 70 days. Periodically, as recommended by the standard, samples were extracted from the reactor, washed with distilled water, dried at 40

± 2 °C for 24 h and, finally, weighed at different testing times to follow the weight evolution during the disintegration process.

RESULTS AND DISCUSSION

Optical properties

Figure IV.6.1a shows the visual appearance of the obtained films over a picture to see their transparency. All the developed films show high transparency as the lower logo can be clearly seen. Visually, there are not significant differences between the loaded or unloaded films; only, a slight change to dark tones can be detected in films as the CNCs content increases. UV-vis characterization was carried out to evaluate the light transmission of the films in the wavelength range comprised between 250–700 nm. Figure IV.6.1b shows the light transmission spectra corresponding to films of PHB_{75}/PCL_{25} blend with varying CNCs content. As can be seen, the blend PHB_{75}/PCL_{25} shows the lowest transmittance value at 700 nm (2.8%) which is directly relate to lower transparency. Nevertheless, after the addition of CNCs to the PHB_{75}/PCL_{25} blend, the transmittance is noticeably improved, being the films with 3 wt% CNCs the ones that show the highest transmittance (17.8%). This noticeable increment in the transmittance could be related to a good CNCs dispersion and a good CNC/matrix interaction in the 3% CNC films. Seoane *et al.* [36] and Chen *et al.* [37] confirmed how these two phenomena contribute to lower light dispersion and, consequently, enhancing the light transmission through the film. On the other hand, the lower transmittance of the 5% CNC and 7% CNC films may be due to formation of CNCs aggregates which contributes to poor dispersion and, subsequently, the optical properties get worse [38]. However, the transmittance values in the UV region for all the films are lower than 5%, giving evidence of the good UV barrier properties in comparison to other biobased polyesters such as PLA [39]. The UV protection that the herein developed formulations offer, together with the high transparency after addition of 3 wt% CNC, could represent interesting features for the food-packaging industry which requires both properties: on one hand, food protection against light and, on the other hand, good transparency to see the packaging content [40].

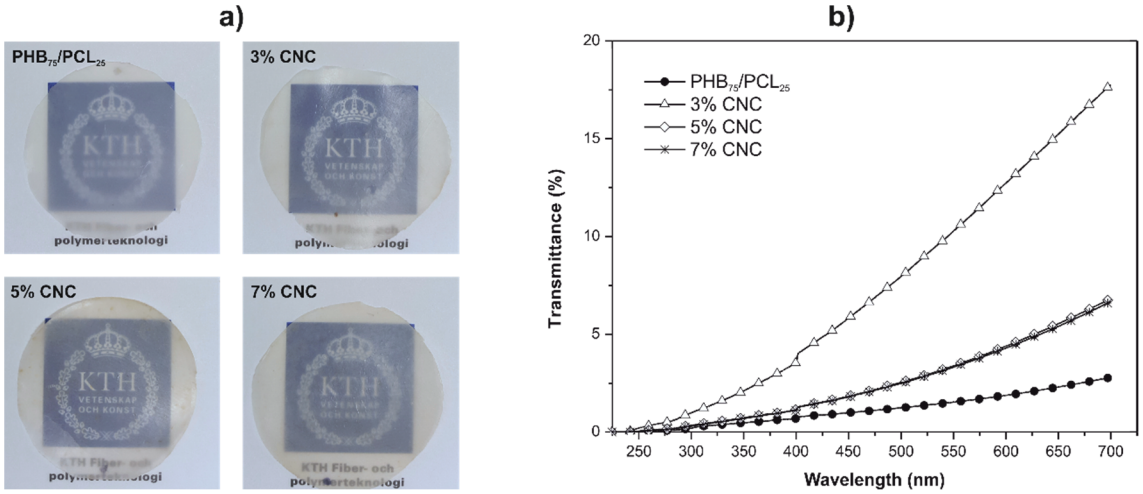

Figure IV.6.1. (a) Visual appearance and (b) UV-vis spectra of PHB_{75}/PCL_{25} films with different CNCs content.

Wettability

The water contact angle values of films were obtained to assess the wetting behavior of the different developed films. Figure IV.6.2 shows a bar plot of the static water contact angle (θ_w) for all the developed films. As suggested by Vogler [41] θ_w values lower than 65° are representative for a hydrophilic behavior while θ_w values over 65 °C stand for hydrophobic surfaces. PHB_{75}/PCL_{25}, shows higher values of θ_w (80°) due to the high hydrophobic nature of PCL [42]. The addition of CNCs in the PHB_{75}/PCL_{25} films provides a progressive decrease in its surface hydrophobicity as a function of the CNCs increment. This is evidenced by a decrease in θ_w down to values of 72.3° for 7% CNC films, and it is directly related to an increase in the hydroxyl groups that CNCs provide to films [43]. As it can be outlined, addition of CNCs to the PHB_{75}/PCL_{25} film does not affect in a remarkable way to its hydrophobic nature. This is an important feature for food-packaging industry where food protection against moisture is needed during transportation and storage [33].

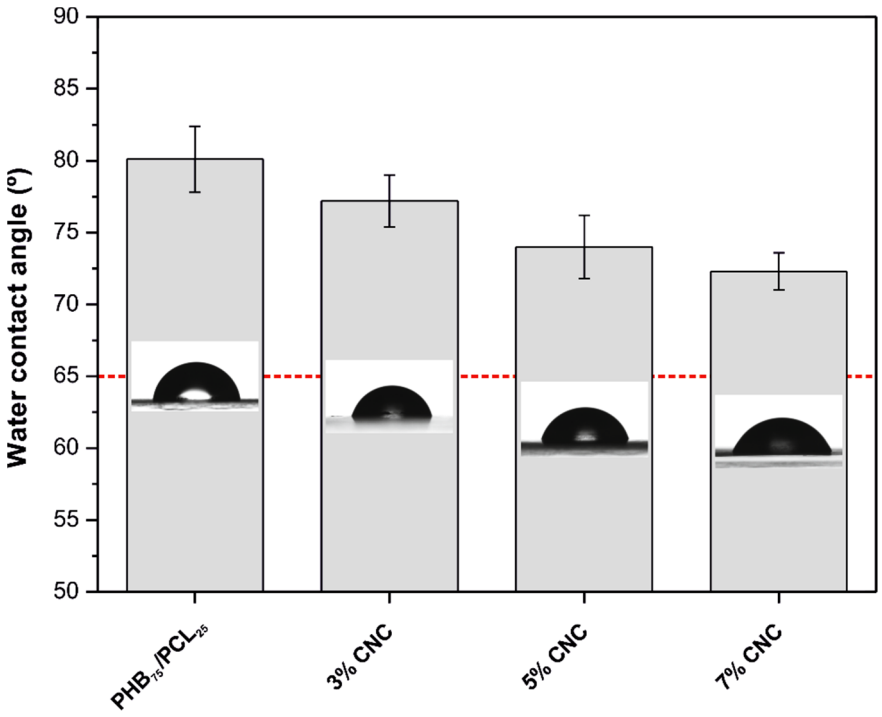

Figure IV.6.2. Contact angle measurement of PHB_{75}/PCL_{25} films with different CNCs content.

Morphological properties

Field emission scanning electron microscopy (FESEM) of PHB_{75}/PCL_{25} films with different CNCs loadings was carried out on the cross-section of films to evaluate the morphology and analyze CNCs dispersion in the polymer matrix (Figure IV.6.3). The fracture of the PHB_{75}/PCL_{25} blend (Figure IV.6.3a) shows a typical droplet structure, specifically, spherical PCL-rich particles can be clearly distinguishable as a randomly dispersed droplet-like phase, indicating both polymers are immiscible [27]. On the other hand, 3% CNC film show a homogeneous dispersion without aggregates indicating the presence of CNCs enhances the compatibility between the immiscible polymers, reducing the phase separation which may contribute to improved mechanical properties. The films with higher CNCs loading (5 and 7 wt%) display an increase in surface roughness with irregular protrusions and holes, which are typical of CNCs aggregate formation. These aggregates can be observed in the fracture surface in the Figure IV.6.3c and d. This may corroborate that higher CNCs amounts in the PHB_{75}/PCL_{25} blend leads to aggregate CNCs formation, thus leading to a poor particle dispersion. These aggregates contribute to a lack of continuity into the matrix, which may have a negative effect on stress transfer.

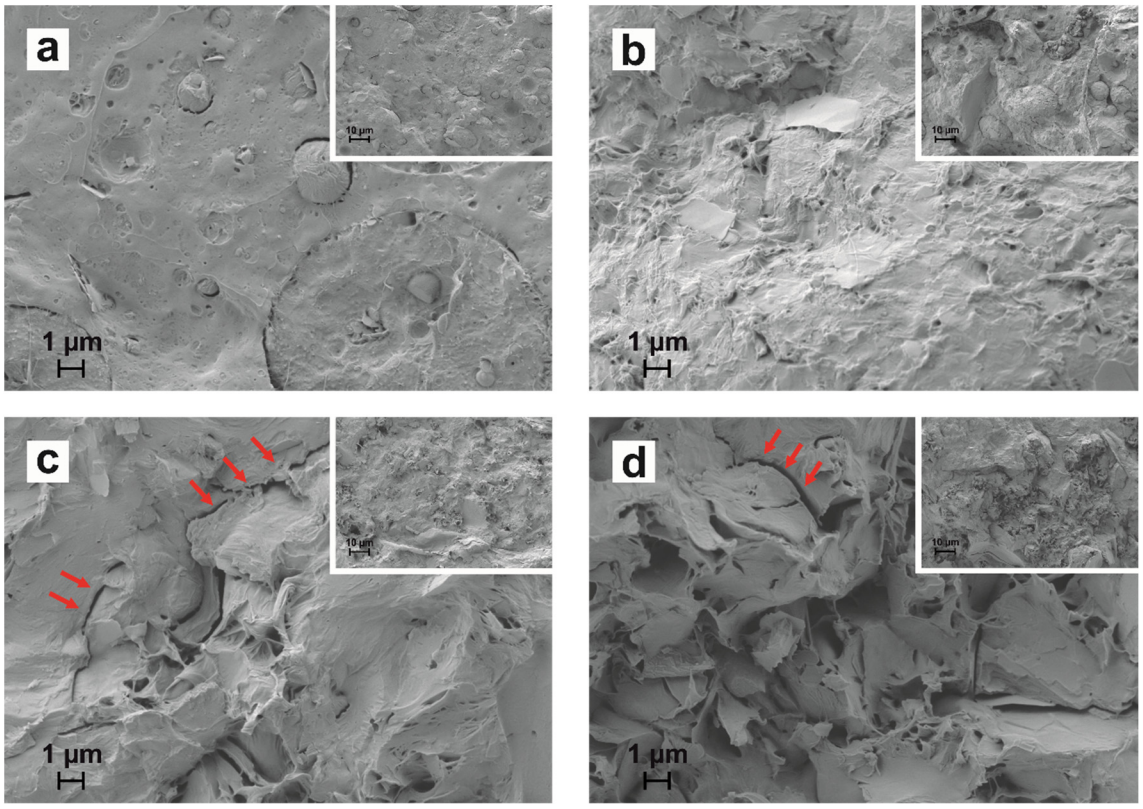

Figure IV.6.3. Field emission scanning electron microscopy (FESEM) images of fracture surface of (a) PHB_{75}/PCL_{25}; (b) 3% CNC; (c) 5% CNC and (d) 7% CNC.

Mechanical properties

The mechanical properties of the developed films with different CNCs loading are compared with those obtained for the PHB_{75}/PCL_{25} blend (Table IV.6.2). The PHB_{75}/PCL_{25} blend has a tensile strength of 14.7 MPa, an elastic modulus of 949 MPa and an elongation at break close to 4%. These mechanical properties remain similar with the addition of 3 wt% CNCs. However, a significant reduction in the standard deviation of all parameters can be observed, which could be related to a good CNCs dispersion which gives increased interface adhesion and, subsequently, leads to more homogenous interactions between PHB and PCL. Over this load percentage, both the tensile strength and elongation at break significantly decreases, whereas the elastic modulus increases with regard to the PHB_{75}/PCL_{25} blend. Therefore, the addition of 5 and 7% CNCs in the PHB_{75}/PCL_{25} resulted in a more fragile and stiffer film due to the presence of CNCs aggregates. This poor dispersion of the CNCs on the blend leads to a lack of continuity in the matrix with the subsequent embrittlement and stress concentration phenomena [44].

Table IV.6.2. Tensile properties of PHB_{75}/PCL_{25} blends with different CNCs content.

Sample	Tensile Strength (MPa)	Tensile Modulus (MPa)	Elongation at break (%)
PHB_{75}/PCL_{25}	14.7 ± 1.3	949 ± 90	3.9 ± 0.7
3% CNC	14.5 ± 0.7	902 ± 56	4.1 ± 0.4
5% CNC	9.3 ± 1.4	1066 ± 65	1.8 ± 0.9
7% CNC	6.5 ± 1.7	972 ± 96	0.4 ± 1.1

Thermal properties

The effect of CNCs addition on the thermal stability PHB_{75}/PCL_{25} blends were studied by thermogravimetric analysis. Figure IV.6.4 shows the thermogravimetric and first derivative (DTG) curves for all the studied materials. PHB_{75}/PCL_{25} blend is characterized by an onset degradation temperature (T_0) of 249.5 °C and displays two degradation stages: the first weight loss is directly related to PHB with a maximum degradation rate ($T_{\text{max PHB}}$) of 277.5 °C; and the second stage is mainly attributable to PCL degradation which a maximum degradation rate ($T_{\text{max PCL}}$) of 409.5 °C [29]. Addition of CNCs to the PHB_{75}/PCL_{25} blend leads to a decrease in the thermal stability (Table IV.6.3). Specifically, the onset degradation for the films moves to lower values (229.5, 224.0 and 221.0 °C for the blends containing 3, 5 and 7 wt% CNCs) that are more similar to the PHB onset [27]. Moreover, a decrease in the maximum degradation rate (T_{max}) related to the PHB and PCL in the PHB_{75}/PCL_{25} blend also occurs as a function of the CNCs content. This phenomenon is related to the lower thermal stability of CNCs with a maximum degradation rate located around 308 °C. Despite this low thermal stability of CNCs, all reinforced blends showed enough thermal stability during the different manufacturing stages.

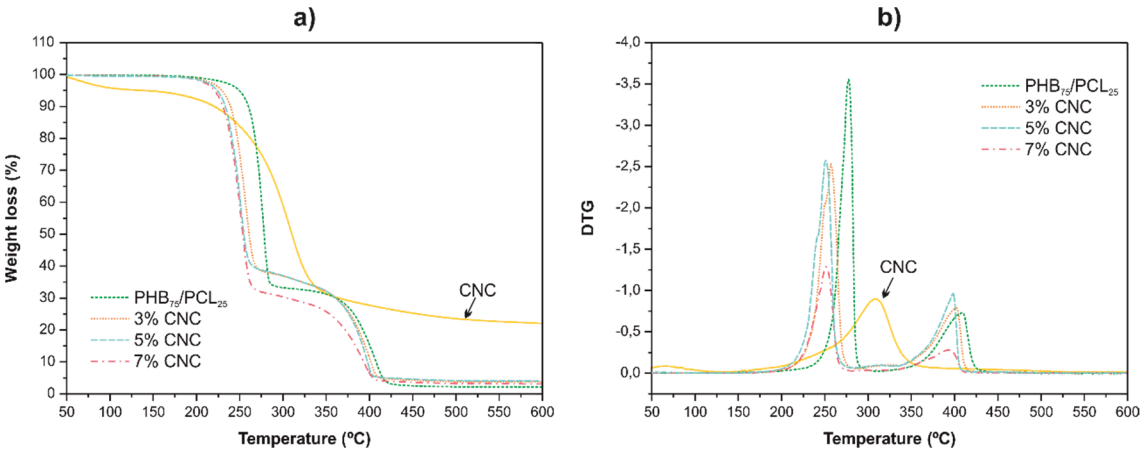

Figure IV.6.4. Thermal degradation of PHB_{75}/PCL_{25} films with different CNCs content: (a) weight loss and (b) first derivative DTG curves.

The effects of CNCs on the crystalline phase (melting and crystallization) of the thermoplastic blends (PHB_{75}/PCL_{25}) was followed by differential scanning calorimetry (DSC). DSC curves corresponding to the second heating cycle (after removing thermal history) of all the developed materials are gathered in Figure IV.6.5. The main thermal parameters obtained by DSC are summarized in Table IV.6.3. Due to the high immiscibility between PHB and PCL, the melting processes of both polymers can be clearly seen in Figure IV.6.5. The melt peak temperature for PCL is located at 54.7 °C while the melt peak temperature for PHB is around 169.5 °C [27]. After addition of CNCs to the PHB_{75}/PCL_{25} blend, important changes in the thermal transitions can be observed. The peak related to the melting of PHB splits, leading to the formation of two peaks. This effect could be due to the heterogeneous nucleating effect of CNCs on PHB which, give rise to the development of PHB small crystals with different morphology compared to typical PHB crystals [45, 46]. Therefore, the presence of multiple PHB melting peaks may be related to the formation of a different crystal structures [47]. The melt peak temperature and crystallinity decreases with increasing CNCs content in the films, indicating imperfect crystals leads an easier and faster melting of the PHB as the content of CNCs increases [48]. According to Yu *et al.* [46] CNCs may modify chain diffusion and folding during polyester spherulitic growth due to hydrogen bonding interactions between CNCs and polyester matrix, resulting in a decrease of crystallinity. Therefore, the larger CNCs content in the films could provoke larger number of hydrogen bonding interactions and lower crystallinity. On the other hand, CNCs do not affect in a remarkable way to the PCL crystallinity as previously reported by Mi *et al.* [8].

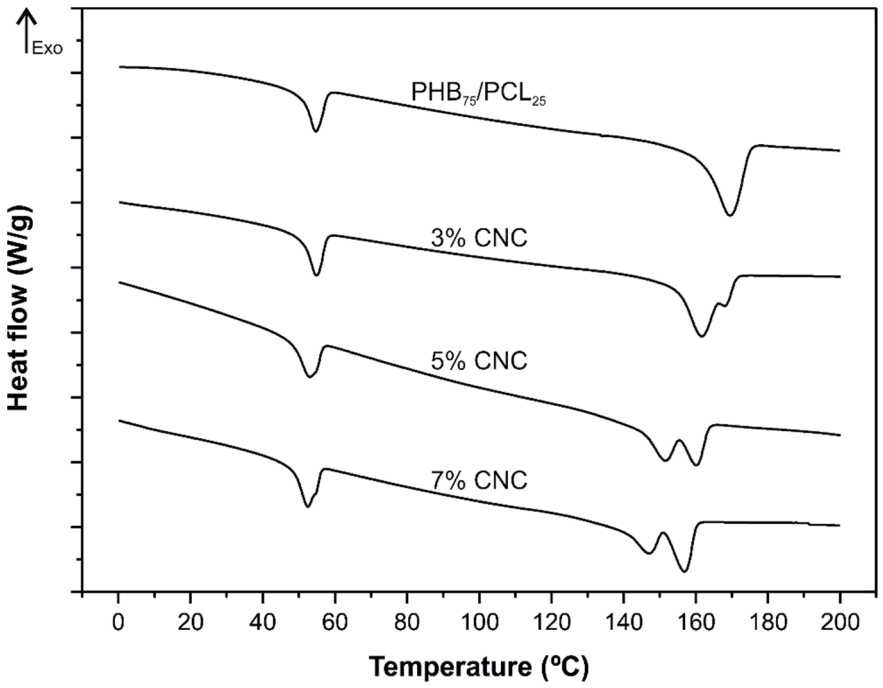

Figure IV.6.5. DSC thermograms of the second heating cycle of PHB_{75}/PCL_{25} blend with different CNCs content.

Table IV.6.3. Main thermal parameters of neat PHB and PHB_{75}/PCL_{25} blend with different CNCs content.

Samples	DSC Parameters						TGA Parameters		
	$T_{m\ PCL}$ (°C)	$\Delta H_{m\ PCL}$ (J g^{-1})	$X_{c\ PCL}$ (%)	$T_{m\ PHB}$ (°C)	$\Delta H_{m\ PHB}$ (J g^{-1})	$X_{c\ PHB}$ (%)	T_0[a] (°C)	$T_{max\ PHB}$ (°C)	$T_{max\ PCL}$ (°C)
PHB	-	-	-	167.4	−74.8	51.3	233.5	267.0	-
PHB_{75}/PCL_{25}	54.7	−67.8	43.2	169.5	−67.3	46.1	249.5	277.5	409.5
3% CNC	54.8	−65.2	41.6	161.7/168.0	−66.8	45.7	229.5	257.0	401.5
5% CNC	53.0	−66.3	42.3	151.7/160.1	−59.9	41.0	224.0	251.0	398.0
7% CNC	52.4	−68.0	43.4	147.1/156.8	−55.7	38.2	221.0	251.0	393.0

[a] T_0, calculated at 5% mass loss.

Chemical structural properties

The infrared spectra of PHB_{75}/PCL_{25} blend and its films with different CNCs loads are gathered in Figure IV.6.6. The PHB_{75}/PCL_{25} spectrum shows the characteristic bands of both PHB and PCL: the broad band at 3000–2900 cm^{-1} which is assigned to $-CH_3$, asymmetric $-CH_2$, and $-CH_2$ symmetric stretching vibrations [6]; the peak located at 1720 cm^{-1} which is directly related to the ester carbonyl C=O [49]; the peak located at 1280 cm^{-1} which is attributed to C–O stretching [50]; the peak around 1165 cm^{-1} which is attributed to C–O–C stretching [42]. After CNCs addition to the PHB_{75}/PCL_{25} blend, an increase in the intensity of the hydroxyl absorption band (3400–3200 cm^{-1}), specifically is clearly detected as a function of the CNCs loading [33]. It is also possible to observe an increase in the peak intensity at 2940 cm^{-1} which is related to the –CH vibration contribution of CNCs [51]. Two additional peaks at 1420 and 1370 cm^{-1} can be clearly identified in the FTIR spectra of PHB_{75}/PCL_{25} blends with the different CNCs load. The first one, located at 1420 cm^{-1} is related with the bending vibration mode of hydroxyl group [51], while the other one, around 1370 cm^{-1} stands for the –C–H bending from the crystalline region of cellulose [49].

The effect of CNCs on the decrease in the PHB crystallinity can be detected by FTIR as the typical peaks/bands of the crystalline PHB regions (980, 1228, 1276 and 1720 cm^{-1}) are less intense [49, 52]. On the other hand, the intensity of the peak located at 1740 cm^{-1}, related to carbonyl groups in PHB amorphous regions, is more intense and therefore the carbonyl region become broader with the addition of CNCs (Figure IV.6.6b). These results proved the formation of hydrogen bonding interactions between OH groups of CNCs and C=O groups of PHB_{75}/PCL_{25} blends [53]. These hydrogen bonding interactions may hinder the diffusion rate and folding of crystalline polyester chains, resulting in a slight decrease of crystallinity [46]. Therefore, the CNCs addition on the PHB_{75}/PCL_{25} decreases the PHB crystallinity values as shown in DSC analysis.

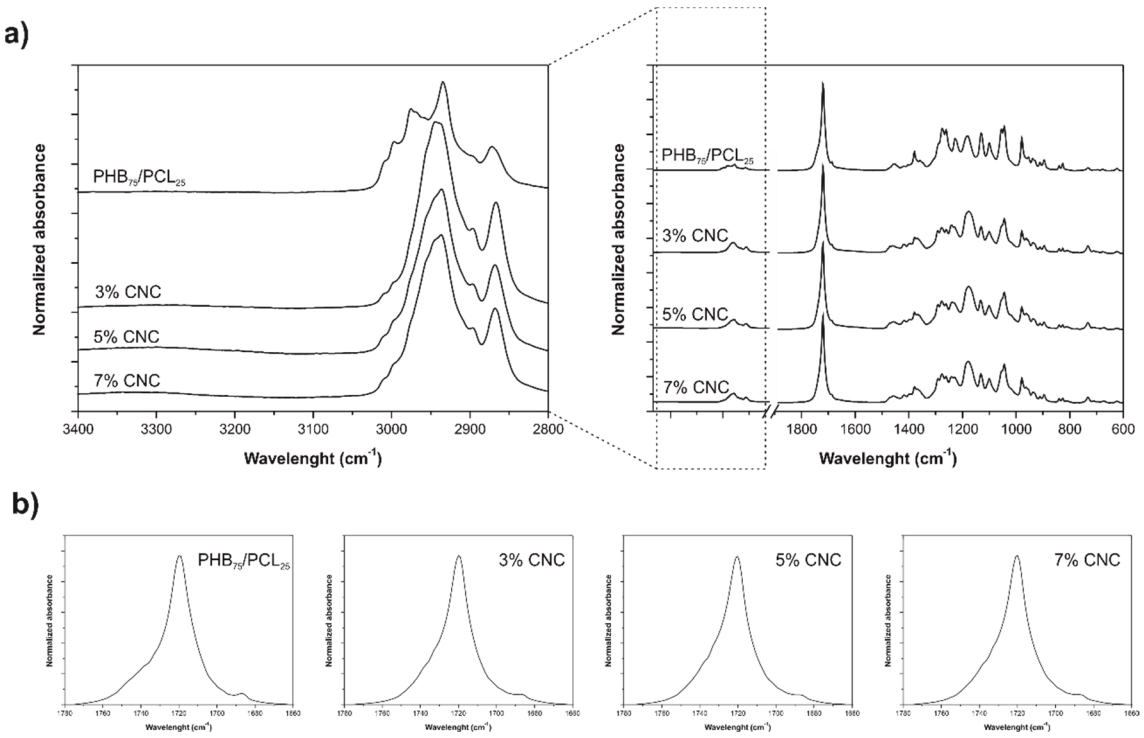

Figure IV.6.6. (a) FTIR spectra diffraction patterns of PHB_{75}/PCL_{25} blend with different CNCs content. (b) FTIR spectra magnification in the wavelength between 1660 and 1780 cm^{-1}.

Figure IV.6.7 shows the XRD diffractograms of PHB_{75}/PCL_{25} blends with different CNCs loads and compared them with the unreinforced PHB_{75}/PCL_{25} blend. The PHB_{75}/PCL_{25} blend shows the characteristic peaks of both polymers. A typical XRD diffractogram of PHB shows a series of characteristic crystallinity peaks at 2θ = 13.5°, 16.9°, 20.1°, 21.4° 22.5°, 25.1° and 28.6° which correspond to the reflection planes (020), (110), (021), (101), (121), (040) and (002) characteristics of the orthorhombic unit cell of PHB [53-55]. On the other hand, the typical XRD peaks of PCL are located at 2θ = 21.4° and 2θ = 23.7°. These two peaks are directly related to the main reflection planes of PCL, namely the plane (110) and (200), typical of the orthorhombic unit cell of PCL [54, 56]. In general, after the addition of CNCs, no significant changes can be detected, being all the XRD spectra similar to those of the PHB_{75}/PCL_{25} blend. Despite this, a slight decrease in the intensity of the typical diffraction peaks corresponding to planes (020), (110) and (002) of PHB crystals can be detected which is representative for the slight decrease in crystallinity suggested by both DSC analysis and FTIR characterization. CNCs also affect the crystal structure of the base polymers in the blend. It is possible to detect an increase in the intensity of the peak located at 2θ = 22.5° (clearly distinguishable for composites with 7 wt% CNCs) as this peak is characteristic of the diffraction pattern of cellulose [57].

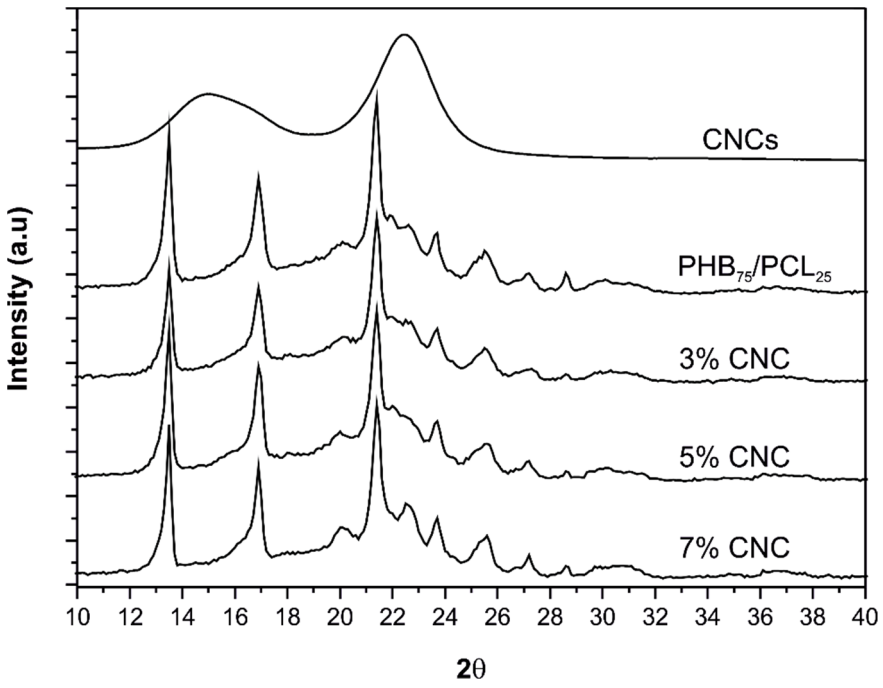

Figure IV.6.7. X-ray diffraction patterns of PHB_{75}/PCL_{25} blend with different CNCs content.

Disintegration under composting

The visual appearance of neat PHB and the PHB_{75}/PCL_{25} blend with different CNCs loads during the disintegration test in controlled compost soil can be seen in Figure IV.6.8a. Figure IV.6.8b shows in a quantitative way the weight loss evolution during the disintegration test in terms of incubation/disintegration time. The line at 90% weight loss, stands for the goal of disintegrability as indicated in the corresponding standard [33]. It is possible to conclude that all the developed materials, start losing mass after the first day. The disintegration rate of neat PHB has been also studied with the aim of evaluating the influence of the PCL on the biodegradability of the PHB. As can be seen, neat PHB offers the highest weight loss during the first 10 incubation days; nevertheless, it becomes highly brittle after 28 days incubation time and reaching 90% weight loss at 53 days. PCL is more resistant to disintegration than PHB. For this reason, PHB_{75}/PCL_{25} blend show increased degradation time. Specifically, this blend becomes highly brittle for an incubation time of 49 days while a 90% weight loss is reached after 67 days which represents a degradation time two weeks later than neat PHB. This is attributable to the lower disintegration rate of PCL compared to PHB [30]. CNCs have a positive effect on enhancing disintegration. In fact, all the films with CNCs become highly brittle (see Figure IV.6.8a) at about 14 days and a disintegration level of 90% is reached after 47, 41 and 40 days for blends containing 3, 5

and 7 wt% CNCs respectively. This increment in the degradation rate could be related to the hydrophilicity of the PHB_{75}/PCL_{25} blend after the addition of CNCs as it was previously observed by contact angle measurements (Figure IV.6.2). This hydrophilicity provided by CNCs favor disintegration of PHB by a hydrolysis process in which, high molecular PHB chains hydrolyze to form low molecular weight chains [58]. On the other hand, the decrease in the disintegration time in all blends with CNCs is also affected by the crystallinity degree, since crystalline regions are more resistant to hydrolysis [40]. In accordance with the change in crystallinity observed by DSC, FTIR and XRD, presence of CNCs contributes to reduce the crystalline regions in the thermoplastic blend and this has a positive effect on enhancing the disintegration rate.

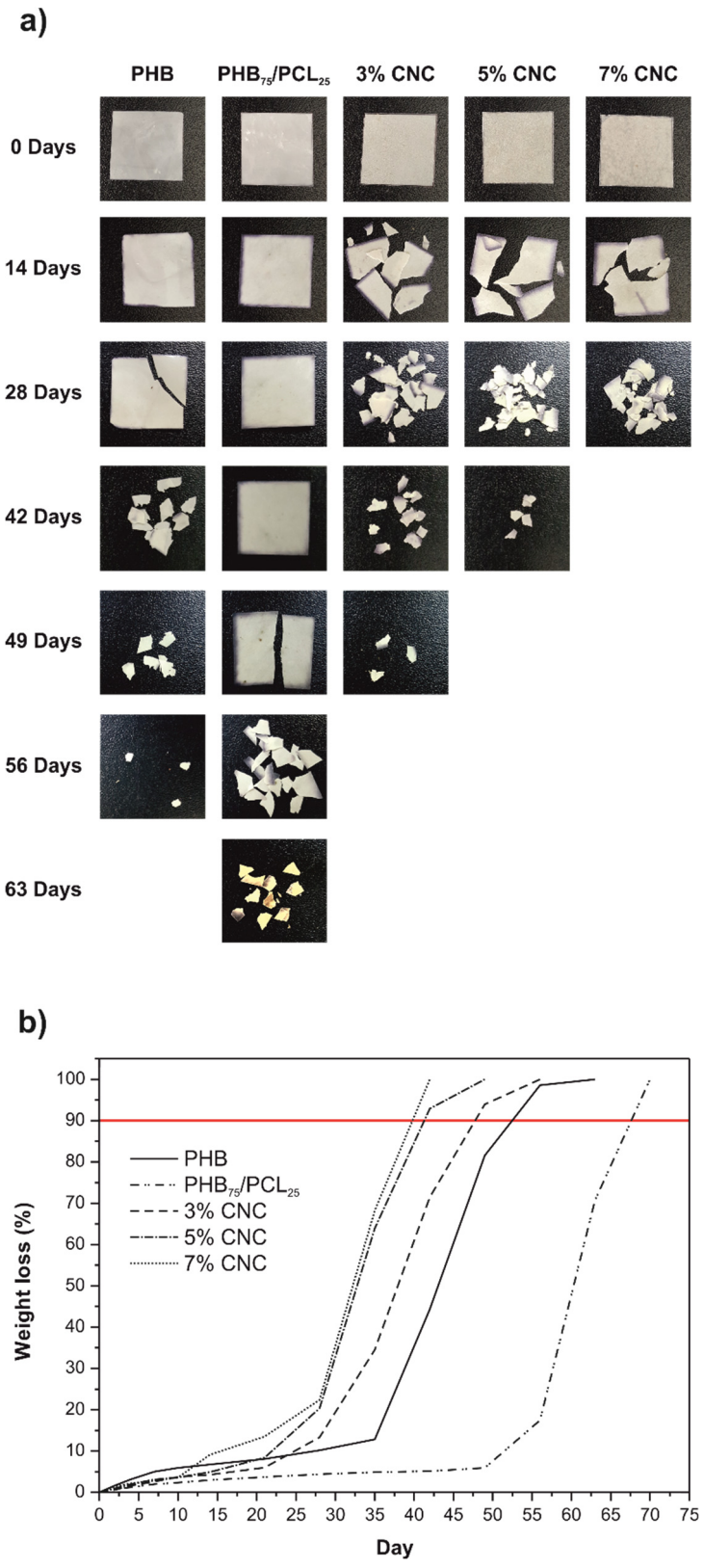

Figure IV.6.8. Evolution of the disintegration in controlled compost soil in terms of the incubation time of neat PHB and PHB_{75}/PCL_{25} blends with different CNCs load: (a) qualitative visual appearance of the aged films and (b) weight loss during the disintegration process on aged films.

CONCLUSIONS

Different amounts of cellulose nanocrystals (3, 5 and 7 wt%) obtained from pine cone by acid hydrolysis were successfully incorporated into PHB / PCL blends (75/25) by solvent casting followed by extrusion and thermocompression. In the present work the reinforcing capability of different amounts of CNCs on the mechanical, thermal, chemical, morphological, optical and wettability properties of PHB_{75}/PCL_{25} blends has been studied. The incorporation of low quantities of CNCs (3 wt%) to the blend of PHB_{75}/PCL_{25} gives a good dispersion and improves the interfacial adhesion between both polymers, considerably improving the transparency of the film without affecting the mechanical properties. Higher amounts of CNCs (5 and 7 wt%) tend to form aggregates, resulting in a loss of transparency and poorer mechanical properties that the unreinforced PHB_{75}/PCL_{25} blend. The incorporation of CNCs in the blend also causes an increase in wettability, due to the hydrophilic character. The disintegration test demonstrated that the incorporation of CNCs to PHB_{75}/PCL_{25} blend accelerates considerably the disintegration process with respect to the unreinforced blend, obtaining a faster disintegration as the content of CNC increases. The results obtained show how the best balance between mechanical, thermal, optical and disintegration rate properties is obtained after the incorporation of a 3 wt% CNCs.

Some of the results obtained in the present work, such as the high transparency level and the high degradation rate of PHB_{75}/PCL_{25} films after addition of 3 wt% CNCs, together with a high hydrophobicity, good UV barrier properties and balanced mechanical properties, give interesting applications to these materials in the food-packaging industry.

ACKNOWLEDGEMENTS

This research was supported by the Ministry of Economy and Competitiveness (MINECO) [MAT2014-59242-C2-1-R]. D. Garcia-Garcia wants to thank the Spanish Ministry of Education, Culture and Sports for the financial support through a FPU grant [FPU13/06011].

REFERENCES

[1] Haafiz MKM, Hassan A, Zakaria Z, Inuwa IM, Islam MS and Jawaid M. *Properties of polylactic acid composites reinforced with oil palm biomass microcrystalline cellulose*. Carbohydrate Polymers, 2013. **98**(1):139-145.

[2] Yu HY, Qin ZY, Yan CF and Yao JM. *Green nanocomposites based on functionalized cellulose nanocrystals: A study on the relationship between interfacial interaction and property enhancement*. ACS Sustainable Chemistry & Engineering, 2014. **2**(4):875-886.

[3] Fortunati E, Peltzer M, Armentano I, Torre L, Jiménez A and Kenny JM. *Effects of modified cellulose nanocrystals on the barrier and migration properties of PLA nano-biocomposites*. Carbohydrate Polymers, 2012. **90**(2):948-956.

[4] Zhou C, Shi Q, Guo W, Terrell L, Qureshi AT, Hayes DJ and Wu Q. *Electrospun bio-nanocomposite scaffolds for bone tissue engineering by cellulose nanocrystals reinforcing maleic anhydride grafted PLA*. ACS Applied Materials & Interfaces, 2013. **5**(9):3847-3854.

[5] Fortunati E, Luzi F, Puglia D, Dominici F, Santulli C, Kenny JM and Torre L. *Investigation of thermo-mechanical, chemical and degradative properties of PLA-limonene films reinforced with cellulose nanocrystals extracted from Phormium tenax leaves*. European Polymer Journal, 2014. **56**:77-91.

[6] Patrício PSO, Pereira FV, dos Santos MC, de Souza PP, Roa JPB and Orefice RL. *Increasing the elongation at break of polyhydroxybutyrate biopolymer: Effect of cellulose nanowhiskers on mechanical and thermal properties*. Journal of Applied Polymer Science, 2013. **127**(5):3613-3621.

[7] Goffin AL, Raquez JM, Duquesne E, Siqueira G, Habibi Y, Dufresne A and Dubois P. *Poly(ε-caprolactone) based nanocomposites reinforced by surface-grafted cellulose nanowhiskers via extrusion processing: Morphology, rheology, and thermo-mechanical properties*. Polymer, 2011. **52**(7):1532-1538.

[8] Mi HY, Jing X, Peng J, Salick MR, Peng XF and Turng LS. *Poly(ε-caprolactone) (PCL)/cellulose nano-crystal (CNC) nanocomposites and foams*. Cellulose, 2014. **21**(4):2727-2741.

[9] Pinheiro IF, Ferreira FV, Souza DHS, Gouveia RF, Lona LMF, Morales AR and Mei LHI. *Mechanical, rheological and degradation properties of PBAT nanocomposites reinforced by functionalized cellulose nanocrystals*. European Polymer Journal, 2017. **97**:356-365.

[10] Bitinis N, Verdejo R, Bras J, Fortunati E, Kenny JM, Torre L and López-Manchado MA. *Poly(lactic acid)/natural rubber/cellulose nanocrystal bionanocomposites Part I. Processing and morphology*. Carbohydrate Polymers, 2013. **96**(2):611-620.

[11] Fortunati E, Armentano I, Zhou Q, Iannoni A, Saino E, Visai L, Berglund LA and Kenny JM. *Multifunctional bionanocomposite films of poly(lactic acid), cellulose nanocrystals and silver nanoparticles*. Carbohydrate Polymers, 2012. **87**(2):1596-1605.

[12] Soykeabkaew N, Tawichai N, Thanomsilp C and Suwantong O. *Nanocellulose-reinforced "green" composite materials*. Walailak Journal of Science and Technology, 2017. 14(5):353-368.

[13] Ng HM, Sin LT, Tee TT, Bee ST, Hui D, Low CY and Rahmat AR. *Extraction of cellulose nanocrystals from plant sources for application as reinforcing agent in polymers*. Composites Part B: Engineering, 2015. **75**:176-200.

[14] Habibi Y, Lucia LA and Rojas OJ. *Cellulose nanocrystals: Chemistry, self-assembly, and applications*. Chemical Reviews, 2010. **110**(6):3479-3500.

[15] Pei A, Zhou Q and Berglund LA. *Functionalized cellulose nanocrystals as biobased nucleation agents in poly (l-lactide)(PLLA) – Crystallization and mechanical property effects*. Composites Science and Technology, 2010. **70**(5):815-821.

[16] Moriana R, Vilaplana F and Ek M. *Cellulose nanocrystals from forest residues as reinforcing agents for composites: A study from macro- to nano-dimensions*. Carbohydrate Polymers, 2016. **139**:139-149.

[17] Le Normand M, Moriana R and Ek M. *Isolation and characterization of cellulose nanocrystals from spruce bark in a biorefinery perspective*. Carbohydrate Polymers, 2014. **111**:979-987.

[18] Kargarzadeh H, Ahmad I, Abdullah I, Dufresne A, Zainudin SY and Sheltami RM. *Effects of hydrolysis conditions on the morphology, crystallinity, and thermal stability of cellulose nanocrystals extracted from kenaf bast fibers*. Cellulose, 2012. **19**(3):855-866.

[19] García-García D, Balart R, Lopez-Martinez J, Ek M and Moriana R. *Optimizing the yield and physico-chemical properties of pine cone cellulose nanocrystals by different hydrolysis time*. Cellulose, 2018. 1-14.

[20] Yu HY, Qin ZY, Liu YN, Chen L, Liu N and Zhou Z. *Simultaneous improvement of mechanical properties and thermal stability of bacterial polyester by cellulose nanocrystals*. Carbohydrate Polymers, 2012. **89**(3):971-978.

[21] Arias A, Heuzey MC, Huneault MA, Ausias G and Bendahou A. *Enhanced dispersion of cellulose nanocrystals in melt-processed polylactide-based nanocomposites*. Cellulose, 2015. **22**(1):483-498.

[22] Pracella M, Haque MMU and Puglia D. *Morphology and properties tuning of PLA/cellulose nanocrystals bio-nanocomposites by means of reactive functionalization and blending with PVAc*. Polymer, 2014. **55**(16):3720-3728.

[23] Espino-Pérez E, Bras J, Ducruet V, Guinault A, Dufresne A and Domenek S. *Influence of chemical surface modification of cellulose nanowhiskers on thermal, mechanical, and barrier properties of poly (lactide) based bionanocomposites*. European Polymer Journal, 2013. **49**(10):3144-3154.

[24] Yu H, Yan C and Yao J. *Fully biodegradable food packaging materials based on functionalized cellulose nanocrystals/poly(3-hydroxybutyrate-co-3-hydroxyvalerate) nanocomposites*. RSC Advances, 2014. **4**(104):59792-59802.

[25] Wang D, Yu J, Zhang J, He J and Zhang J. *Transparent bionanocomposites with improved properties from poly(propylene carbonate) (PPC) and cellulose nanowhiskers (CNWs)*. Composites Science and Technology, 2013. **85**:83-89.

[26] Siqueira G, Bras J and Dufresne A. *Cellulose whiskers versus microfibrils: Influence of the nature of the nanoparticle and its surface functionalization on the thermal and mechanical properties of nanocomposites*. Biomacromolecules, 2009. **10**(2):425-432.

[27] Garcia-Garcia D, Ferri JM, Boronat T, Lopez-Martinez J and Balart R. *Processing and characterization of binary poly(hydroxybutyrate) (PHB) and poly(caprolactone) (PCL) blends with improved impact properties*. Polymer Bulletin, 2016. **73**(12):3333-3350.

[28] Donald AM and Kramer EJ. *Plastic deformation mechanisms in poly (acrylonitrile-butadiene styrene) [ABS]*. Journal of Materials Science, 1982. **17**(6):1765-1772.

[29] Garcia-Garcia D, Rayón E, Carbonell-Verdu A, Lopez-Martinez J and Balart R. *Improvement of the compatibility between poly(3-hydroxybutyrate) and poly(ε-caprolactone) by reactive extrusion with dicumyl peroxide*. European Polymer Journal, 2017. **86**:41-57.

[30] Rosa DS, Calil MR, Guedes CGF and Rodrigues TC. *Biodegradability of thermally aged PHB, PHB-V, and PCL in soil compostage*. Journal of Polymers and the Environment, 2004. **12**(4):239-245.

[31] Fenouillot F, Cassagnau P and Majesté JC. *Uneven distribution of nanoparticles in immiscible fluids: Morphology development in polymer blends*. Polymer, 2009. **50**(6):1333-1350.

[32] Arrieta MP, Fortunati E, Dominici F, Rayón E, López J and Kenny JM. *Multifunctional PLA-PHB/cellulose nanocrystal films: Processing, structural and thermal properties*. Carbohydrate Polymers, 2014. **107**:16-24.

[33] Arrieta MP, Fortunati E, Dominici F, Rayón E, López J and Kenny JM. *PLA-PHB/cellulose based films: Mechanical, barrier and disintegration properties*. Polymer Degradation and Stability, 2014. **107**:139-149.

[34] Arrieta MP, Samper MD, López J and Jiménez A. *Combined effect of poly(hydroxybutyrate) and plasticizers on polylactic acid properties for film intended for food packaging*. Journal of Polymers and the Environment, 2014. **22**(4):460-470.

[35] Simões CL, Viana JC and Cunha AM. *Mechanical properties of poly(ε-caprolactone) and poly(lactic acid) blends*. Journal of Applied Polymer Science, 2009. **112**(1):345-352.

[36] Seoane IT, Fortunati E, Puglia D, Cyras VP and Manfredi LB. *Development and characterization of bionanocomposites based on poly(3-hydroxybutyrate) and cellulose nanocrystals for packaging applications*. Polymer International, 2016. **65**(9):1046-1053.

[37] Chen Y, Liu C, Chang PR, Cao X and Anderson DP. *Bionanocomposites based on pea starch and cellulose nanowhiskers hydrolyzed from pea hull fibre: Effect of hydrolysis time*. Carbohydrate Polymers, 2009. **76**(4):607-615.

[38] Atef M, Rezaei M and Behrooz R. *Preparation and characterization agar-based nanocomposite film reinforced by nanocrystalline cellulose*. International Journal of Biological Macromolecules, 2014. **70**:537-544.

[39] Yang W, Dominici F, Fortunati E, Kenny JM and Puglia D. *Effect of lignin nanoparticles and masterbatch procedures on the final properties of glycidyl methacrylate-g-poly(lactic acid) films before and after accelerated UV weathering*. Industrial Crops and Products, 2015. **77**:833-844.

[40] Arrieta MP, Fortunati E, Dominici F, López J and Kenny JM. *Bionanocomposite films based on plasticized PLA-PHB/cellulose nanocrystal blends*. Carbohydrate Polymers, 2015. **121**:265-275.

[41] Vogler EA. *Structure and reactivity of water at biomaterial surfaces*. Advances in Colloid and Interface Science, 1998. **74**(1):69-117.

[42] de Campos A, Tonoli GHD, Marconcini JM, Mattoso LHC, Klamczynski A, Gregorski KS, Wood D, Williams T, Chiou BS and Imam SH. *TPS/PCL composite reinforced with treated sisal fibers: Property, biodegradation and water-absorption*. Journal of Polymers and the Environment, 2013. **21**(1):1-7.

[43] Mo Y, Guo R, Liu J, Lan Y, Zhang Y, Xue W and Zhang Y. *Preparation and properties of PLGA nanofiber membranes reinforced with cellulose nanocrystals*. Colloids and Surfaces B: Biointerfaces, 2015. **132**:177-184.

[44] García-García D, Carbonell A, Samper MD, García-Sanoguera D and Balart R. *Green composites based on polypropylene matrix and hydrophobized spend coffee ground (SCG) powder*. Composites Part B: Engineering, 2015. **78**:256-265.

[45] Martínez-Sanz M, Villano M, Oliveira C, Albuquerque MGE, Majone M, Reis M, Lopez-Rubio A and Lagaron JM. *Characterization of polyhydroxyalkanoates synthesized from microbial mixed cultures and of their nanobiocomposites with bacterial cellulose nanowhiskers*. New Biotechnology, 2014. **31**(4):364-376.

[46] Yu HY and Yao JM. *Reinforcing properties of bacterial polyester with different cellulose nanocrystals via modulating hydrogen bonds*. Composites Science and Technology, 2016. **136**:53-60.

[47] Yu HY, Zhang H, Song ML, Zhou Y, Yao J and Ni QQ. *from cellulose nanospheres, nanorods to nanofibers: Various aspect ratio induced nucleation/reinforcing effects on polylactic acid for robust-barrier food packaging*. ACS Applied Materials & Interfaces, 2017. **9**(50):43920-43938.

[48] Yu HY, Wang C and Abdalkarim SYH. *Cellulose nanocrystals/polyethylene glycol as bifunctional reinforcing/compatibilizing agents in poly(lactic acid) nanofibers for controlling long-term in vitro drug release*. Cellulose, 2017. **24**(10):4461-4477.

[49] Wei L, Stark NM and McDonald AG. *Interfacial improvements in biocomposites based on poly(3-hydroxybutyrate) and poly(3-hydroxybutyrate-co-3-hydroxyvalerate) bioplastics reinforced and grafted with α-cellulose fibers*. Green Chemistry, 2015. **17**(10):4800-4814.

[50] Barud HS, Souza JL, Santos DB, Crespi MS, Ribeiro CA, Messaddeq Y and Ribeiro SJL. *Bacterial cellulose/poly(3-hydroxybutyrate) composite membranes*. Carbohydrate Polymers, 2011. **83**(3):1279-1284.

[51] Cano A, Fortunati E, Cháfer M, González-Martínez C, Chiralt A and Kenny JM. *Effect of cellulose nanocrystals on the properties of pea starch-poly (vinyl alcohol) blend films*. Journal of Materials Science, 2015. **50**(21):6979-6992.

[52] Xu J, Guo BH, Yang R, Wu Q, Chen GQ and Zhang ZM. *In situ FTIR study on melting and crystallization of polyhydroxyalkanoates*. Polymer, 2002. **43**(25):6893-6899.

[53] Wei L, McDonald AG and Stark NM. *Grafting of bacterial polyhydroxybutyrate (PHB) onto cellulose via in situ reactive extrusion with dicumyl peroxide*. Biomacromolecules, 2015. **16**(3):1040-1049.

[54] Vergara-Porras B, Gracida-Rodríguez JN and Pérez-Guevara F. *Thermal processing influence on mechanical, thermal, and biodegradation behavior in poly(β-hydroxybutyrate)/poly(ε-caprolactone) blends: A descriptive model*. Journal of Applied Polymer Science, 2016. **133**(27): 43569.

[55] Del Gaudio C, Ercolani E, Nanni F and Bianco A. *Assessment of poly(ε-caprolactone)/poly(3-hydroxybutyrate-co-3-hydroxyvalerate) blends processed by solvent casting and electrospinning*. Materials Science and Engineering: A, 2011. **528**(3):1764-1772.

[56] Cavalcante MP, Toledo ALMM, Rodrigues EJR, Neto RPC and Tavares MIB. *Correlation between traditional techniques and TD-NMR to determine the morphology of PHB/PCL blends*. Polymer Testing, 2017. **58**:159-165.

[57] Dasan YK, Bhat AH and Ahmad F. *Polymer blend of PLA/PHBV based bionanocomposites reinforced with nanocrystalline cellulose for potential application as packaging material*. Carbohydrate Polymers, 2017. **157**:1323-1332.

[58] Puglia D, Fortunati E, D'amico DA, Manfredi LB, Cyras VP and Kenny JM. *Influence of organically modified clays on the properties and disintegrability in compost of solution cast poly(3-hydroxybutyrate) films*. Polymer Degradation and Stability, 2014. **99**:127-135.

European Polymer Journal 104 (2018) 10–18

Contents lists available at ScienceDirect

European Polymer Journal

journal homepage: www.elsevier.com/locate/europolj

Reinforcing capability of cellulose nanocrystals obtained from pine cones in a biodegradable poly(3-hydroxybutyrate)/poly(ε-caprolactone) (PHB/PCL) thermoplastic blend

Daniel Garcia-Garcia[a,*], Juan Lopez-Martinez[a], Rafael Balart[a], Emma Strömberg[c], Rosana Moriana[b,c,*]

[a] Instituto de Tecnología de Materiales-ITM, Universitat Politècnica de València, Plaza Ferrandiz y Carbonell 1, 03801 Alcoy, Alicante, Spain
[b] School of Engineering Science, HIS-University of Skövde, Skövde, Högskolevägen, 541 28 Skövde, Sweden
[c] School of Engineering Science in Chemistry, Biotechnology and Health, Department of Fibre and Polymer Technology, KTH-Royal Institute of Technology, SE-100 44 Stockholm, Sweden

ARTICLE INFO

Keywords:
Poly(3-hydroxybutyrate)
Poly(ε-caprolactone)
Biodegradability
Cellulose nanocrystals (CNCs)
Thermoplastic blends

ABSTRACT

In this work, different loads (3, 5 and 7 wt%) of pine cone cellulose nanocrystals (CNCs) were added to films of poly(3-hydroxybutyrate)/poly(ε-caprolactone) (PHB/PCL) blends with a composition of 75 wt% PHB and 25 wt % PCL (PHB_{75}/PCL_{25}). The films were obtained after solvent casting followed by melt compounding in an extruder and finally subjected to a thermocompression process. The influence of different CNCs loadings on the mechanical, thermal, optical, wettability and disintegration in controlled compost properties of the PHB_{75}/PCL_{25} blend was discussed. Field emission scanning electron microscopy (FESEM) revealed the best dispersion of CNCs on the polymeric matrix was at a load of 3 wt%. Over this loading, CNCs aggregates were formed enhancing the films fragilization due to stress concentration phenomena. However, the addition of CNCs improved the optical properties of the PHB_{75}/PCL_{25} films by increasing their transparency and accelerated the film disintegration in controlled soil conditions. In general, the blend with 3 wt% CNCs offers the best balanced properties in terms of mechanical, thermal, optical and wettability.

1. Introduction

The recent increase in the social concern about environmental issues together with the increasing price of fossil fuels due to petroleum depletion [1], has given a rise in the development of new environmentally friendly materials as it is the case of biodegradable polymers. Biodegradable polymers challenges are related to their relatively poor mechanical and thermal properties compared to petroleum-based commodities and engineering plastics, restricting their wide use in industrial application [2]. The reinforcement of biodegradable polymers with nanoparticles has recently been proposed as a strategy to overcome some of the above-mentioned drawbacks. Specifically, bio-based nanoscale particles have been used to reinforce thermoplastic biodegradable polymers, such as poly(lactic acid) (PLA) [3–5], poly (hydroxybutyrate) (PHB) [6], poly(ε-caprolactone) (PCL) [7,8] and poly(butylene adipate-*co*-terephthalate) (PBAT) [9]. The improved thermo-mechanical performance of these nanoscale-reinforced polymer composites, together with their potential biodegradation, could lead these new materials to compete with many traditional petroleum-based polymers, such as polypropylene (PP), polyethylene or polyethylene terephthalate (PET) [10,11].

Cellulose nanocrystals (CNCs) from residual biomass (food, agriculture and forest) may be defined as one of the most promising reinforcing agents in terms of biodegradability, renewability, abundance in nature, variety and price [12,13]. These highly crystalline cellulose particles are obtained from lignocellulosic fibres generally through two main steps: first, an alkaline and bleaching treatment to isolate the cellulose fibres from the raw material and second, a hydrolytic treatment with acid which allows the selective removal of the amorphous cellulosic phase remaining the crystalline phase almost unaltered [14–16]. The physico-chemical properties of CNCs can vary widely, depending on the source of the cellulosic raw material and the conditions selected to perform the hydrolysis [17,18]. In previous studies, pine cones fibres were selected as raw materials to produce CNCs and

* Corresponding authors at: School of Engineering Science in Chemistry, Biotechnology and Health, Department of Fibre and Polymer Technology, KTH-Royal Institute of Technology, SE-100 44 Stockholm, Sweden (R. Moriana). Instituto de Tecnología de Materiales-ITM, Universitat Politècnica de València, Plaza Ferrandiz y Carbonell 1, 03801 Alcoy, Alicante, Spain (D. Garcia-Garcia).
E-mail addresses: dagarga4@epsa.upv.es (D. Garcia-Garcia), rosana@kth.se (R. Moriana).

https://doi.org/10.1016/j.eurpolymj.2018.04.036
Received 2 January 2018; Received in revised form 12 March 2018; Accepted 25 April 2018
Available online 26 April 2018

IV.7

"Characterization of selectively etched halloysite nanotubes by acid treatment"

Daniel García García[a], José M. Ferri[a], Laura Ripoll[b], Montserrat Hidalgo[b], Juan López Martínez[a], Rafael Balart[a]

[a] Instituto de Tecnología de Materiales (ITM)
Universitat Politècnica de València (UPV)
Plaza Ferrándiz y Carbonell 1, 03801 Alcoy, Alicante, Spain.

[b] Departamento de Química Analítica, Nutrición y Bromatología
Instituto Universitario de Materiales (IUMA)
Universidad de Alicante (UA)
Apdo. 99, 03080, Alicante, Spain.

Applied Surface Science

2017, 422:616-625

Characterization of selectively etched halloysite nanotubes by acid treatment

Abstract

Halloysite nanotubes (HNTs) are a type of naturally occurring inorganic nanotubes that are characterized by a different composition between their external and internal walls. The internal walls are mainly composed of alumina whilst external walls are composed of silica. This particular structure offers a dual surface chemistry that allows different selective surface treatments which can be focused on increasing the lumen, increasing porosity, etc. In this work, HNTs were chemically treated with different acids (sulfuric, acetic and acrylic acid), for 72 h at a constant temperature of 50 °C. As per the obtained results, the treatment with sulfuric acid is highly aggressive and the particular shape of HNTs is almost lost, with a remarkable increase in porosity. The BET surface area increases from 52.9 (untreated HNTs) up to 132.4 $m^2 g^{-1}$ with sulfuric acid treatment, thus showing an interesting potential in the field of catalysis. On the other hand, the treatment with acetic acid led to milder effects with a noticeable increase in the lumen diameter that changed from 13.8 nm (untreated HNTs) up to 18.4 nm which the subsequent increase in the loading capacity by 77.8%. The aluminum content was measured by X-ray fluorescence (XRF) and laser induced breakdown spectroscopy (LIBS). The final results using two systems, suggest a good correlation between the acid strength and the aluminum reduction. Consequently, is possible to conclude that new applications for HNTs can be derived from selective etching with acids. Sulfuric acid widens the potential of HNTs in the field of catalysis while weak acids such as acetic and acrylic acids give a controlled and homogeneous lumen increase with the corresponding increase in the loading capacity.

Keywords: Halloysite nanotubes; lumen enlargement; acid treatment; catalysis; LIBS.

INTRODUCTION

One of the main features of nanomaterials is their high surface to volume ratio which gives an exponential increase in the reactivity of the molecules thus leading to a remarkable change in their electronic, optical, chemical or mechanical properties with regard to their bulk counterpart materials. For this reason, nanomaterials offer a great potential in a wide range of research areas such as biomedicine, cosmetics, food and food packaging, coatings, electronics, catalysis or materials sciences [1]. A wide variety of metal oxides, nanoclays, carbon nanomaterials, organometallic nanocomposites (MOFs) have been successfully introduced in new materials [2], with the particular feature that nanoparticles offer a strong different behavior than their counterpart micro/macro particles. Nanoclays have been widely studied as support for different catalysts [3]. In particular, the petroleum industry is leading the introduction of nanoparticles as supports for catalysts in several reactions. It has been reported the potential of activated carbon and carbon nanotubes (CNTs) as support for ethanol oxidation [4], aluminosilicates, cordierites [5], zeolites [6], other feldspars, kaolinite derivate such sepiolites [7], HNTs, etc., which allow the conversion of crude oil in a wide range of products. Nanomaterials are continuously acquiring new features in the catalysis industry. Abbasov *et al.* [8] reported the positive effects of a previous acid treatment on HNTs with HCl to improve the efficiency as support for NiO and CoO for fuel production from heavy crude oil. Zhang *et al.* [9] used a silane treatment with aminopropyltriethoxysilane as a previous treatment to increase Pd adsorption on HNTs as catalytic system for the conversion of styrene to ethylbenzene. In a parallel way, CNTs are also being investigated as support for different catalysts [10]. Nevertheless, the use of CNTs is restricted in the medicine field due to their potential health risks. On the other hand, their high cost is a key disadvantage for a wide use in the field of composites.

Other important application of nanoparticles is hydrogen storage on micro/nanoporous materials [11]. Many of the abovementioned materials are intrinsically porous of can be modified to increase the overall porosity and surface area. Another feature of porous nanoparticles is related to their potential use as container for controlled drug release [12]. Despite it is true that a wide variety of encapsulated structures for controlled delivery are currently used, aluminosilicates own a privileged position due to their low cost and health safety. Aluminosilicates are currently being used for controlled delivery of antimicrobials in the cosmetic industry [13], non-foaming oxygen nanocontainer [14], support of compatibilizer agents in immiscible polymer blends [15], flame retardant containers [16, 17], heavy metal nanoadsorbers [18], with a remarkable effect on the prolonged effect with time [19]. In addition, aluminosilicates can be loaded with active

additives such as thermal stabilizers, antioxidants, UV light stabilizers, etc., to protect polymers for prolonged exposure to environment. The use of aluminosilicates HNTs has been widely reported in polymer formulations to improve mechanical properties [20, 21]; also, their use in the food-contact products is increasing as HNTs can provide controlled delivery of preservatives, antibacterials and others [22]. HNTs have been also used in pharmacology, prosthesis [23], bone repairing and therapy against cancer [24]. HNTs are characterized by extremely high biocompatibility [25]. They are good drug carriers for controlled drug release [26, 27]. Qi *et al.* [28] manufactured nanofiber mats with poly(lactide-*co*-glycolide) with HNTs previously loaded with tetracycline hydrochloride antibiotic. Other aluminosilicates nanotubes, *i.e.*, imogolite nanotubes, were successfully used as scaffolds for cell growth [29].

The particular aluminosilicate structure of HNTs with an internal alumina layer and an external silicate layer allows a wide variety of chemical modifications such as acid [30-32], alkali [33] and other [34] to selectively change porosity, lumen size, surface activity, etc. Acid treatments promote the removal of Al_2O_3 while an alkaline treatment preferably attacks the silica layer. Both the acid and the alkali treatments lead to electrically charged structures which play a key role in substance absorption. Different research works have been done in the last years, focused on HNTs modification. Abdullayev *et al.* [35] used sulfuric acid at different concentrations and treatment-times with the main aim of increasing the average diameter of the HNTs lumen. They reported an increase in the load capacity by 2–3 times higher regarding the initial capacity. Wang *et al.* [36] studied the effect of several concentration of hydrochloric acid (HCl) on the morphology, the crystalline structure and the porous texture of HNTs. They concluded that very slight changes in the crystalline structure and the hollow shape were obtained with this treatment. Nevertheless, to our knowledge, an in depth comparative study of the effects of different acids (including sulfuric acid which is the most used for this treatments) on chemical and morphological changes of HNTs has not been carried out.

The present work explores the effect of the strength of different acids (sulfuric, acrylic and acetic acids) on the morphology of chemically modified HNTs to define their possibilities in the field of catalysis and/or container for controlled delivery. The novelty of the present work is focused on the use of weak acids, *i.e.*, acetic and acrylic acids, to treat HNTs and study their effect on the chemical changes and morphology, compared to the effects of a widely used acid for this type of treatments, sulfuric acid. The work covers the use of different techniques: transmission electron microscopy (TEM), X-ray fluorescence (XRF), X-ray diffraction spectroscopy (XRD), laser induced breakdown spectroscopy (LIBS),

thermogravimetric analysis (TGA) and specific surface area (BET) to give new insights on the chemical changes produced by acid treatment on HNTs.

EXPERIMENTAL

Materials

Halloysite nanotubes were supplied by Sigma Aldrich (Madrid, Spain). Sulfuric acid (95% H_2SO_4) and acetic acid (99.7% CH_3COOH) were supplied by PanReac Applichem (Barcelona, Spain) and acrylic acid (99% CH_2=CHCOOH) was obtained from Sigma Aldrich (Madrid, Spain). All reagents were used without any other purification.

Selective etching of HNTs by acid treatment

An acid treatment was carried out on HNTs which allows a selective etching of the alumina located in the interior parts of HNTs with a similar procedure as that described by Abdullayev *et al.* [35]. In summary, HNTs were previously dried overnight at 100 °C. Then, 5 g of HNTs were poured into 500 mL of the corresponding acid solutions with a constant concentration of 1 mol L^{-1}. The obtained suspension was maintained with magnetic stirring for 72 h on a hot plate at 50 °C. After this stage, chemically modified HNTs were collected by centrifugation and washed with distilled water until the obtained pH was in the 6–7 range. Finally, HNTs were dried at 50 °C for 24 h prior to further characterizations.

Characterization techniques

Transmission electron microscopy (TEM)

The morphology and size distribution of raw HNTs and the etched-HNTs were studied by transmission electron microscopy (TEM) in a Philips mod. CM10 (Eindhoven, the Netherlands) using an acceleration voltage of 100 kV. Prior to TEM observation, a small amount of the corresponding HNTs samples was dispersed in acetone immersed in an ultrasound bath; subsequently, a drop of this dispersion was poured onto a carbon grid and subjected to solvent evaporation at room temperature. The lumen size of HNTs was obtained from the collected TEM images and a minimum of 50 measurements were done to obtain the size distribution.

X-ray fluorescence spectroscopy (XRF)

The chemical composition of HNTs before and after the corresponding acid treatments was obtained by X-ray fluorescence spectroscopy in a sequential X-ray spectrometer PHILIPS MAGIX PRO PW2400 (Panalytical B.V., the Netherlands) equipped with a rhodium tube and a beryllium window. Results of the chemical compositions were analyzed by using the SuperQ analytical software. Each treated-sample was subjected to three different analyzes and the average values were calculated.

Laser induced breakdown spectroscopy (LIBS)

LIBS analysis of raw and chemically etched HNTs was performed by a μ-LIBS system based on a MODI' LIBS equipment (Mobile Dual-Pulse Instrument) [37]. The system is equipped with a double-pulse Nd:YAG laser, emitting at 1064 nm with pulse energy up to 60 mJ (20 ns FWHM pulse width). Laser radiation was focused through an optical microscope model Axio Scope A1 (Zeiss, Germany) on the sample to analyze. The microscope is equipped with a 10x objective having a focal distance of 10 mm. For LIBS analysis, the sample was placed on a motorized stage which develops a 2D scanning of the sample surface. The optical signal from the laser-induced plasmas was collected by an optical fiber, placed at an angle of about 45° and at a distance of 10 mm from the laser spot, and then sent to a broadband spectrometer model AvaSpec-2048-2 from Avantes (Eerbeek, the Netherlands) covering the spectral range comprised between 180 and 900 nm. The synchronization between the laser firing, data acquisition and x-y movement of the motorized stage was obtained using Labview® software. Data processing was performed by the spectroscopic software of the MODI' instrument (LIBS++®, v 5.0, ALS LAB). In this study, the Nd:YAG laser was operated at a pulse energy of 40 mJ. Double pulse LIBS analysis was performed in collinear mode, with 1 μs delay between both laser pulses. LIBS spectra were acquired 1.3 μs after the second laser pulse, with 2.5 ms acquisition time.

The HNTs samples were pressed into pellets for LIBS analysis, in order to avoid the powdered material to be ejected out due to the laser-induced shock wave. Circular pellets of about 25 mm diameter and 3 mm thickness were obtained by pressing the powder with an automatic mounting press machine Buehler SimpliMet 1000 (Illinois, USA) at a pressure of 200 bar during 10 min, after a previous mixing with KBr as the binder component. For quantitative LIBS analysis using standard addition calibration, a series of standards were prepared by mixing a fixed amount of halloysite (1.5 g) with increasing amounts of alumina.

The standards were finally adjusted to the same final weight (2.5 g) by addition of KBr binder.

The analysis of the samples was carried out by programing a matrix of 10×3 laser shots separated 200 μm in the central part. The resulting LIBS spectra were collected, averaged and processed by the spectroscopic LIBS++ software. All the data shown correspond to the mean value of three replicate measurements.

Porous texture

The porous texture characterization of untreated and selectively etched HNTs was carried out by nitrogen adsorption-desorption at 77 K with a Autosorb-6 volumetric equipment from Quantachrome Instruments (Odelzhausen, Germany). All the samples were outgassed at 250 °C under vacuum for 8 h prior to adsorption experiments. The specific surface area was determined by the Brunauer-Emmett-Teller (BET) procedure [38]. The pore volume was determined by the nitrogen adsorption volume at a relative pressure (P/P_0) of around 0.96. The mesopore size distribution was obtained by the Barret-Joyner-Halenda (BJH) method from the data collected from the corresponding nitrogen adsorption isotherm [39]. The measurements of each sample were repeated three times for each sample to ensure their accuracy.

Thermogravimetric analysis (TGA)

Thermogravimetric analysis of all HNTs samples was carried out using the experimental methodology previously proposed for Zhang *et al.* [40] to characterize raw HNTs and HNTs treated with sulfuric acid. The analysis was conducted in duplicate for each sample in a TGA/SDTA 851e thermobalance from Mettler-Toledo (Schwerzenbach, Switzerland) under nitrogen atmosphere at a constant flow rate of 50 mL min^{-1}. Samples with an average weight of 3–5 mg were placed into standard alumina crucibles (70 μL) subjected to a dynamic heating program from 25 to 700 °C at a constant heating rate of 10 °C min^{-1}.

X-ray diffraction spectroscopy (XRD)

The crystal structure of raw HNTs and chemically etched HNTs was determined by X-ray diffraction on a Bruker CCD-Appex apparatus equipped with an X-ray generator (Ni filtered Cu-Kα radiation) operated at 40 kV and 40 mA. Samples in powder form were

scanned from 5° to 90° (2θ) at a step of 2° min^{-1}, following the experimental methodology proposed by Bordeepong *et al.* [41].

RESULTS AND DISCUSSION

Effect of selective acid treatment on the morphology of HNTs

Figure IV.7.1 shows the TEM images and the size distribution of the lumen diameter of raw HNTs and the selectively etched HNTs by acid treatment. The morphology of the unmodified HNTs can be observed in Figure IV.7.1a with the typical tube shape. Unmodified HNTs possess an average lumen diameter of 13.8 ± 1.4 nm with an external diameter ranging from 30 to 70 nm (average external diameter of 50 nm) [42]. With regard to their length, it is comprised between 1 and 3 μm as measured and in total agreement with the information provided by the supplier. After the selective etching by acid treatment, remarkable changes can be observed. With regard to the acid treatments with acetic and acrylic acids (Figure IV.7.1c and d respectively) an interesting increase in the average lumen diameter is obtained. In particular, the lumen diameter increases up to 18.4 ± 2.9 and 17.1 ± 2.1 nm with the acetic and acrylic acid treatments, which represents a percentage increase of 33.3% and 23.9% respectively compared to untreated HNTs. This increase also leads to a remarkable increase in the lumen volume, which increases by 77.8% for the acetic acid-etched HNTs and up to 53.5% for HNTs chemically etched with acrylic acid with regard to the initial lumen volume of untreated HNTs. This involves a noticeable increase in the potential of HNTs as carriers for different loads. It is worthy to note that both acid treatments with acetic and acrylic acid do not change the morphology in a great extent without any evidence of pore formation and breakage. Nevertheless, the morphology of HNTs chemically etched by sulfuric acid (Figure IV.7.1b) is noticeably different to previous acid treatments. The lumen diameter (average size) is increased up to values of about 31.6 ± 6.7 nm but as the TEM image suggests, the treatment with sulfuric acid is so aggressive and, as it can be seen, a highly porous structure, partially decomposed morphology can be detected. While the average lumen size for HNTs treated with acetic and acrylic acids follows a relatively narrow distribution, in the case of HNTs treated with sulfuric acid, the average diameter offers a wider distribution which gives evidences of partial decomposition due to aggressive etching. This is due to the fact that sulfuric acid is able to react with both the internal and external HNTs layers with a clear peeling effect on the external layer which contributes to the complete destruction of the internal hollow tube morphology as Zhang *et al.* concluded [40].

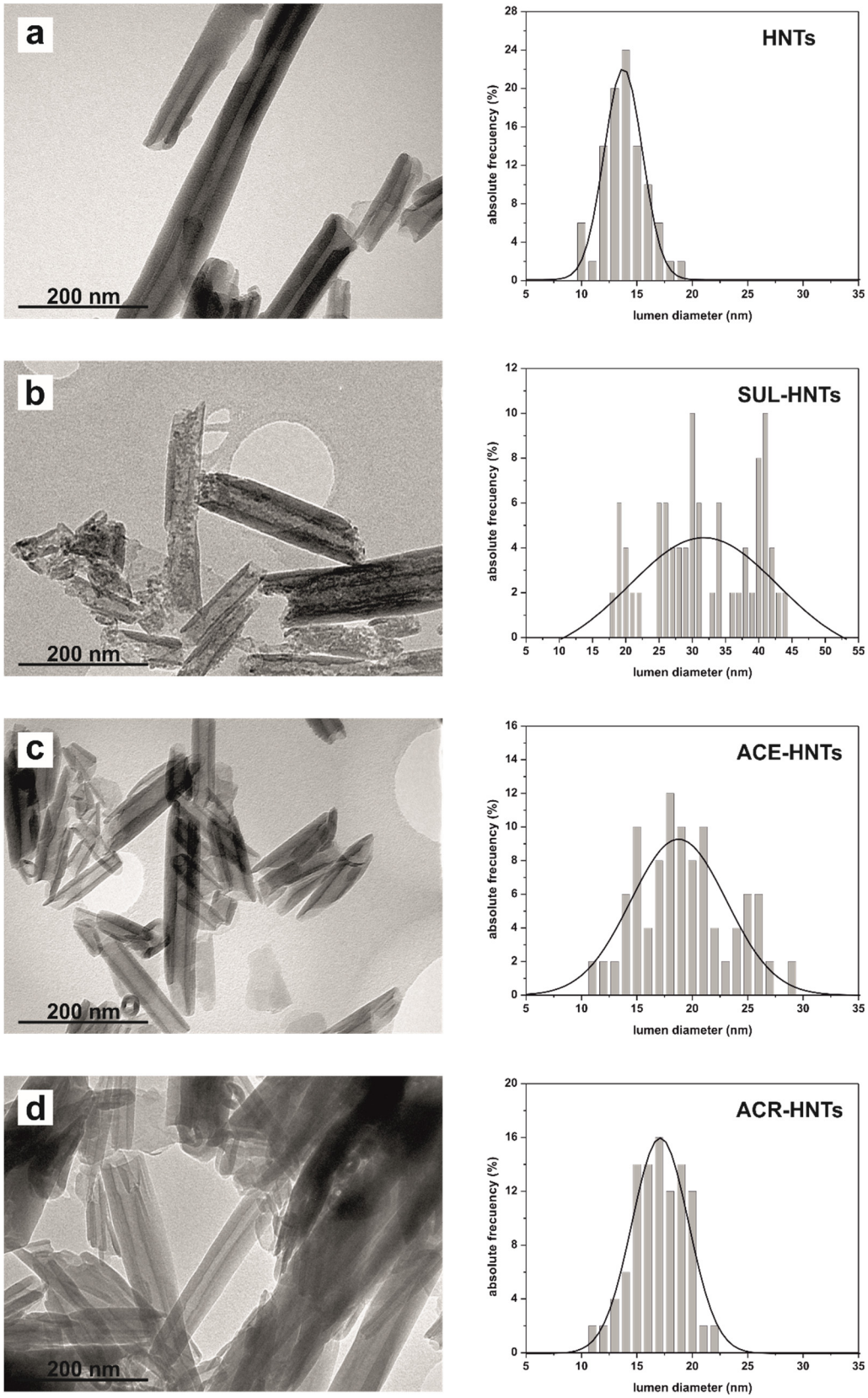

Figure IV.7.1. TEM images and plot representation of the lumen diameter distribution of HNTs subjected to chemical etching with different acids: (a) untreated, (b) sulfuric acid, (c) acetic acid and (d) acrylic acid.

Effect of selective acid treatment on the chemical composition of HNTs

The effects of the etching by acid treatment on the chemical composition of HNTs were studied by X-ray fluorescence spectroscopy. In a typical HNTs the silicon atom is combined with four adjacent oxygen atoms whilst each aluminum atom is coordinated with two hydroxyl groups and an additional oxygen atom as indicated by Yah *et al.* [32]. Table IV.7.1 summarizes the compositions for neat HNTs and acid-treated HNTs. As it can be seen, presence of both silica (SiO_2) and alumina (Al_2O_3) is in total agreement with the chemical structure of a typical aluminosilicate. In fact, both silica and alumina represent more than 98% of the total composition while the remaining (P_2O_5, Fe_2O_3, SO_3, CaO, TiO_2 and MgO) only represents a very small proportion (less than 2%). As it can be seen in Table IV.7.1, the alumina content decreases with both weak acid treatments, while this decrease is remarkable for the strong sulfuric acid treatment. This decrease in the alumina content could be related to the lixiviation of Al^{3+} cations from the octahedral layer due to the hydrolysis in acid conditions as reported by Panda *et al.* [43].

Table IV.7.1. Chemical composition of untreated and chemically etched HNTs with different acids as obtained by XRF analysis.

Compound	Sample			
	HNTs	**ACR-HNTs**	**ACE-HNTs**	**SUL-HNTs**
SiO_2	53.75 ± 0.64	53.96 ± 0.09	54.45 ± 0.27	61.64 ± 0.18
Al_2O_3	44.57 ± 0.67	44.26 ± 0.09	43.92 ± 0.07	36.71 ± 0.17
P_2O_5	0.64 ± 0.04	0.77 ± 0.03	0.65 ± 0.02	0.47 ± 0.02
SO_3	0.29 ± 0.03	0.20 ± 0.05	0.21 ± 0.03	0.24 ± 0.02
CaO	0.12 ± 0.02	0.18 ± 0.03	0.15 ± 0.02	0.25 ± 0.01
TiO_2	0.02 ± 0.01	0.04 ± 0.01	0.03 ± 0.01	0.04 ± 0.00
Fe_2O_3	0.38 ± 0.02	0.38 ± 0.01	0.35 ± 0.05	0.31 ± 0.03
MgO	0.07 ± 0.06	0.06 ± 0.10	0.05 ± 0.09	0.20 ± 0.01
Sum	99.84	99.85	99.86	99.86
LOI	0.16	0.15	0.14	0.14

Table IV.7.2 shows the atomic percentage of the main chemical elements (oxygen, silicon and aluminum) present in HNTs obtained by XRF. As it can be seen, the Si/Al ratio in

unmodified HNTs is close to 1.1. Nevertheless, after the acid treatment with sulfuric acid, the Si/Al ratio increases up to values around 1.5 due to the selective etching of the interior alumina layers. Sulfuric acid preferentially dissolves the interior AlO_6 layers leading to the collapse of the external tetrahedral SiO_6 layers thus leading to a highly porous morphology mainly consisting on amorphous silicon as reported by Zhang *et al.* [40]. Regarding the Si/Al ratio for HNTs treated with weak acids such as acetic and acrylic, it remains with typical values of untreated HNTs with values close to 1.1. This is also in accordance with the mild effects of these acid treatments compared to the strong effects that sulfuric acid provides. As it can be seen in Table IV.7.2, the overall amount of aluminum decreases with the acid treatments. This decrease is much higher with the etching action of strong acids such as sulfuric.

Table IV.7.2. The atomic equivalent of the major elements in untreated and chemically etched HNTs with different acids measured by XRF analysis.

Sample	Element content (atm%)			
	O	Si	Al	Si/Al
HNTs	50.34 ± 0.03	25.13 ± 0.30	23.59 ± 0.35	1.07 ± 0.03
ACR-HNTs	50.36 ± 0.02	25.22 ± 0.04	23.42 ± 0.05	1.08 ± 0.01
ACE-HNTs	50.38 ± 0.02	25.45 ± 0.13	23.24 ± 0.04	1.09 ± 0.01
SUL-HNTs	50.80 ± 0.07	28.81 ± 0.08	19.43 ± 0.10	1.49 ± 0.01

In addition to XRF, a new approach to the characterization of the effects of different acid etching on chemical composition of HNTs has been studied using LIBS. This technique is based on focusing a laser beam on a small area of the sample to analyze, resulting in the generation of a highly energetic plasma in with the sample is atomized, ionized and excited. Spectral resolution of plasma emission provides qualitative and quantitative information on the sample content. A preliminary qualitative analysis was performed in order to identify the elements presents in untreated HNTs. Figure IV.7.2 shows a LIBS spectrum corresponding to untreated HNTs. As it can be seen, most of the emission lines appearing in the LIBS spectrum of untreated HNTs correspond to the more abundant elements: aluminum, silicon and oxygen. Moreover, LIBS spectrum also shows some emission lines that could be related to presence of impurities such as titanium. In addition, LIBS reveals the presence of other elements such as calcium, sodium, etc., which could appear as they are

present in the environment. In a similar way, the environmental oxygen, nitrogen or hydrogen are mainly responsible for the signal observe for these elements although in the case of oxygen, an important contribution comes from the alumina and silica.

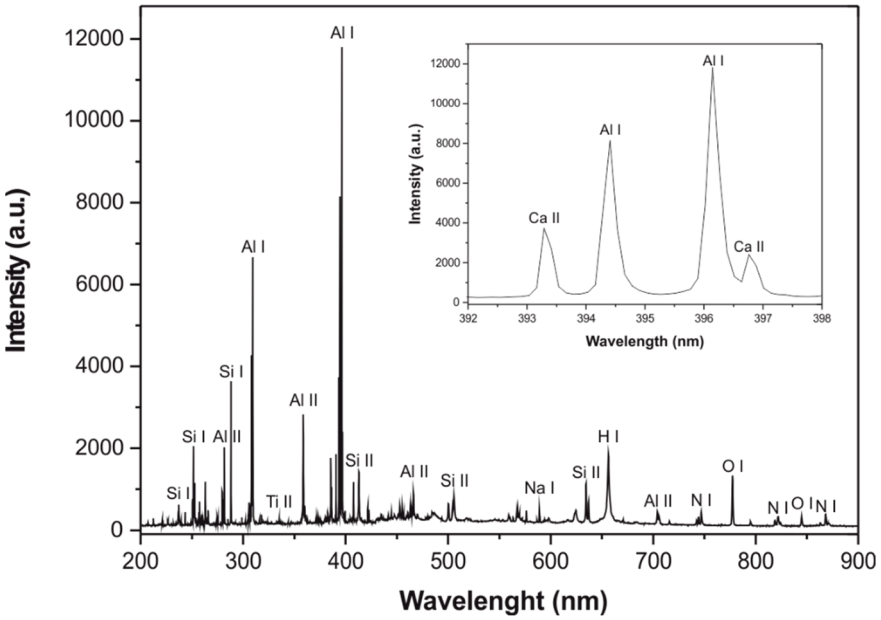

Figure IV.7.2. LIBS spectrum of untreated HNTs showing the main emission lines.

Figure IV.7.3 shows a detailed plot of the emission lines corresponding to Al I (265.4 nm) and Al I (266.1 nm) of untreated HNTs and chemically etched HNTs with different acids. As it can be seen, after the acid treatment, a decrease in the signal of both spectral lines is detected but this decrease is more pronounced for HNTs chemically etched with sulfuric acid. Regarding the etching treatments with acetic and acrylic acids, the intensity of the Al I lines is slightly reduced thus giving evidences of the mildest conditions compared to sulfuric acid. These results are in total agreement with the previous exposed XRF and TEM results.

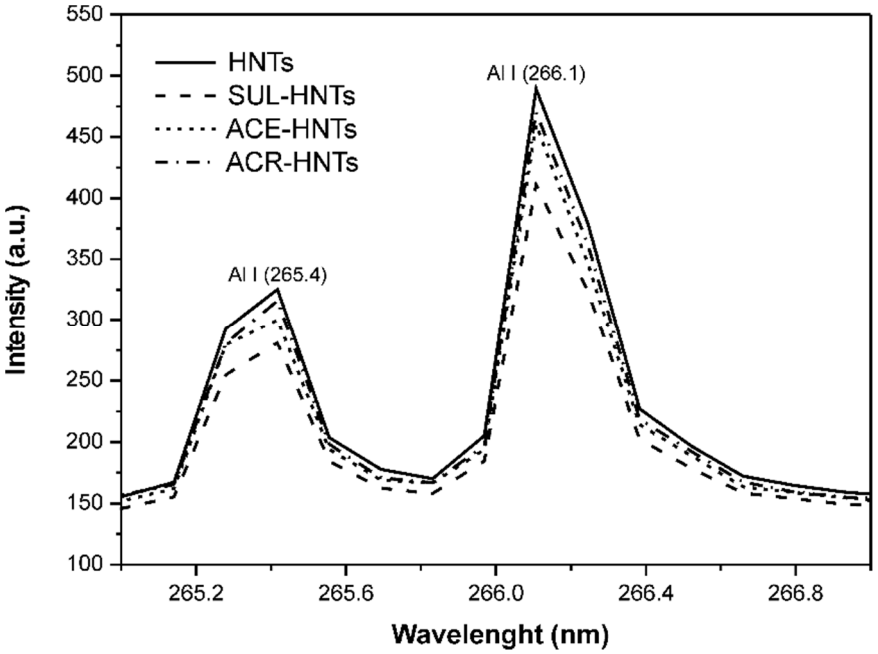

Figure IV.7.3. Aluminum emission lines obtained in LIBS analysis of untreated and chemically etched HNTs with different acid treatments.

LIBS technique allows also quantitative analysis, so that it is possible to use LIBS to characterize the effects of the different acid etching treatments on the chemical composition of HNTs, as well as the presence of impurities due to the high sensitiveness. With the aim of revealing the amount of aluminum in HNTs and the effects of the selective etching on the alumina interior layer, aluminum was analyzed in a quantitative way from LIBS results. The Al I (265.4 nm) was selected for quantitative determination as it does not overlap with other nearest emission lines and it offers an acceptable emission intensity for quantitative analysis. In addition, an emission line of a second element was used as internal pattern, to correct potential oscillations in the LIBS signal during measurements due to some factors such as small shot-to-shot pulse energy variations. The selected emission line was Si I (243.5 nm) as it does not show any interference and this line is placed near to the analytic line Al I (265.4 nm). An initial calibration was carried out by the standard addition method, leading to good linear correlation with $r^2 = 0.992$, with repeatability values for the calibration points in the line between 1.19% and 5.316% RSD (n = 3). Once the aluminum concentration in untreated HNTs was assessed and the relationship between the emission intensity of LIBS and the actual aluminum concentration was established, chemically etched HNTs with different acid treatments were quantitatively analyzed. The obtained results are summarized in Table IV.7.3 which shows the average values obtained from three independent replicates. As it can be seen, the aluminum content in untreated HNTs is 25.5%.

After the acid treatments, the aluminum content decreases for all three acid treatments but once again, it is the sulfuric acid which gives the minimum aluminum content of 18.9% due to the aggressive etching phenomena on the interior alumina layers. With regard to the aluminum content for HNTs chemically etched with acetic and acrylic acid, it reaches values of 24.1 and 22.6% respectively thus giving evidence of the milder effects of these two organic acids compared to sulfuric acid. Table IV.7.3 also shows the ratio between the Si I (243.5 nm) and the Al I (265.4 nm). As it can be seen, as the aluminum content decreases, the Si/Al ratio increases as previously observed by XRF. The obtained results by using the LIBS technique are in total agreement with those obtained by XRF analysis. Both techniques indicate the strong effects that sulfuric acid etching has on HNTs, compared to acetic and acrylic acid.

Table IV.7.3. Aluminum content of untreated and chemically etched HNTs with different acids as obtained by quantitative analysis using LIBS.

Sample	Al (%)	Si I (243.5nm)/Al I (265.4 nm)
HNTs	25.5 ± 0.1	1.04 ± 0.18
ACR-HNTs	24.1 ± 0.4	1.10 ± 0.05
ACE-HNTs	22.6 ± 0.5	1.17 ± 0.06
SUL-HNTs	18.9 ± 0.4	1.43 ± 0.15

Although a slight difference regarding the aluminum content between XRF and LIBS can be observed, it is important to remark that both techniques show similar compositions for untreated and chemically etched HNTs. In particular, XRF results offer similar Si/Al ratios for untreated HNTs and HNTs subjected to mild treatment with weak acids (acetic and acrylic). On the other hand, LIBS has revealed an increase in the Si/Al ratio for all acid-treated HNTs which could indicate that LIBS is more sensitive than XRF for this analysis.

Effect of selective acid treatment on the porous texture of HNTs

Figure IV.7.4 shows the corresponding nitrogen adsorption-desorption isotherms of untreated and selectively etched HNTs. As it can be seen, all four samples show a type IV isotherm according to IUPAC classification [44], which is typical of a mesoporous structure. The hysteresis loop of these samples is similar to type H3, which is typical of agglomerates of plate-like particles containing slit-shaped pores [43]. The hysteresis loops can be

observed in the P/P_0 range comprised between 0.4–1, which is associated with the capillary condensation in mesopores (pore width: 2–30 nm). Table IV.7.4 summarized the BET values and the pore volume of untreated and chemically etched HNTs. As it can be seen, untreated HNTs show a BET surface area of 52.9 $m^2 g^{-1}$ and a pore volume of 0.146 $cm^3 g^{-1}$. After the acid treatment, a remarkable increase in the BET surface area and the pore volume is detected, being the sulfuric acid treatment which leads to the highest values. Specifically, the BET surface area increases up to values of 132.4 $m^2 g^{-1}$ and a pore volume of 0.308 $cm^3 g^{-1}$. This increase in both the surface and the pore volume is directly related to the selective dissolution of the octahedral AlO_6 layers with the subsequent increase in the average diameter of the lumen. Several authors such as Wang *et al.* [36], Zhang *et al.* [40] or Belkassa *et al.* [45] have reported that an increase in the acid concentration or the treatment time also gives an increase in the surface area and the pore volume for HNTs. For these reasons, selective etching of HNTs with acids is very interesting for new applications such as drug supporters, enzyme carriers and selective adsorbents.

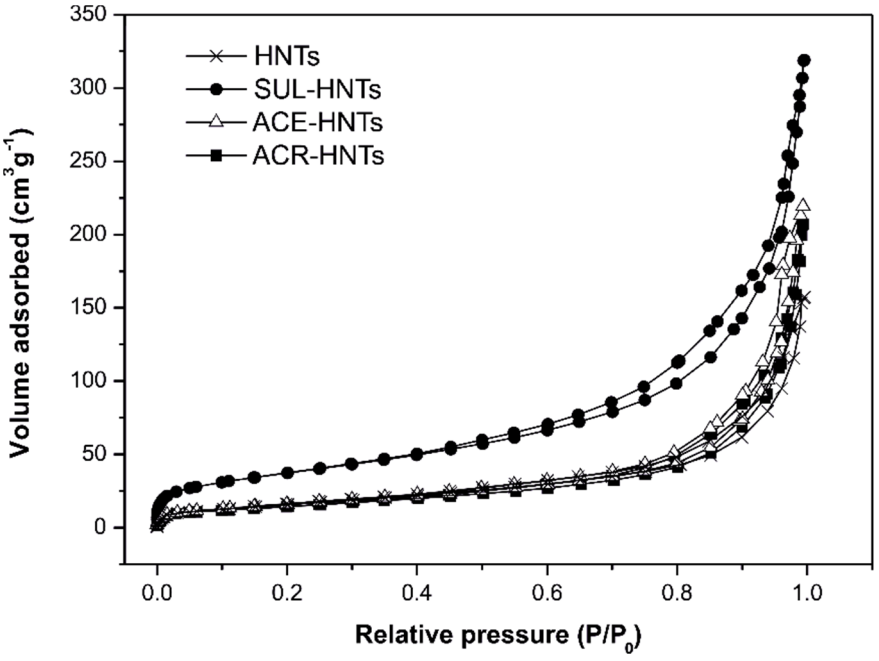

Figure IV.7.4. Nitrogen adsorption isotherms of untreated and chemically etched HNTs with different acids.

Table IV.7.4. BET surface area and total pore volume of untreated and chemically etched HNTs with different acid treatments.

Sample	BET surface area ($m^2\ g^{-1}$)	Total pore volume ($cm^3\ g^{-1}$)
HNTs	52.9 ± 0.8	0.146 ± 0.004
ACR-HNTs	58.5 ± 0.7	0.176 ± 0.005
ACE-HNTs	60.1 ± 0.9	0.195 ± 0.004
SUL-HNTs	132.4 ± 10.5	0.308 ± 0.018

Figure IV.7.5 shows the BJH pore size distribution obtained from the data collected from the desorption isotherm of the different HNTs. As it can be seen, untreated HNTs show two pore sizes distributions. One with an average pore size of 2 nm which is attributed to the small internal and external pores [46]. The second distribution is centered at about 6–9 nm and is mainly related to the lumen [47]. Such pore size distribution corroborates the mesoporous structure of HNTs. After the different acid treatments, some changes in the pore size distribution can be observed. Specifically, the peak centered at 2 nm is moved to 4 nm which suggests an increase in the average pore size. With regard to the peak centered at 6–9 nm it is also detectable a displacement towards higher values of 12 nm due to the selective removal of Al^{3+} cations from octahedral layers contained in HNTs [48]. It is worthy to note that HNTs treated with sulfuric acid show additional peaks through a wide range this giving evidences of a heterogeneous porosity inside HNTs which is directly related to the aggressiveness of this acid treatment. Another interesting finding is macropore formation by acid treatment with sulfuric and acetic acid. This is mainly due to the penetration of protons into the clay mineral layers and attack to the structural hydroxyl groups resulted in the dehydroxylation and a successive leaching of the Al^{3+} ions from the octahedral layers, this produces a selective destruction of some layers and/or fragments which are responsible for the formation of holes inside de halloysitic matrix with the subsequent formation of macropores [43, 45].

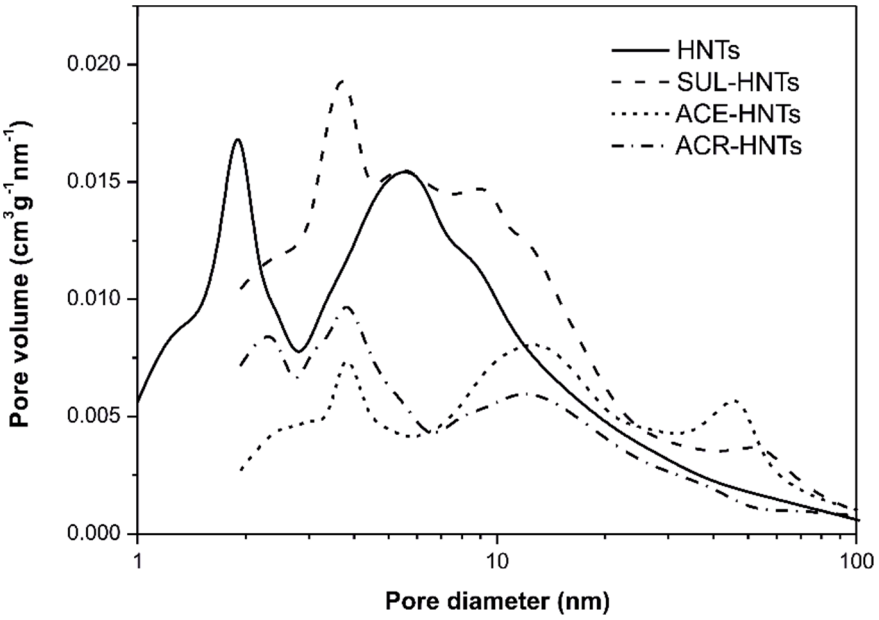

Figure IV.7.5. BJH pore size distribution of untreated and chemically etched HNTs with different acids.

Effect of selective acid treatment on the thermal stability of HNTs

Figure IV.7.6 shows the TGA curves (Figure IV.7.6a) and their corresponding derivative curves (DTG) (Figure IV.7.6b) for untreated and chemically etched HNTs with different acid treatments. Two main weight loss stages can be identified for all samples. The first weight loss is comprised between 30 and 100 °C, and this is related to desorption of the water that is physically adsorbed onto HNTs surface as well as desorption of the interlayer water [49]. These water molecules are weakly linked to HNTs and can be removed easily at relatively low temperatures. It is possible to observe that the weight loss in this stage is higher for HNTs treated with sulfuric acid, which suggests that these HNTs contain more adsorbed water due to the porous structure that sulfuric acid provides [43] as well as the highly hygroscopic nature of the sulfuric acid residues in comparison with other acids. The second and highest weight loss can be observed in the 400–600 °C (with a DTG peak at about 500 °C) and is directly related to the dehydroxylation of the structural Al-OH groups of halloysite [49-51]. As it can be seen, the weight loss in this stages highly depends on the acid treatment. HNTs subjected to etching with sulfuric acid show less weight loss compared to HNTs subjected to acetic or acrylic acid treatments. This could be related to the fact that hydroxyl groups present in the octahedral layer of AlO_6 are removed together with the Al^{3+} solution [40]. This lower weight loss gives evidences of the aggressiveness of the sulfuric acid treatment which is responsible for a higher removal of Al-OH groups in comparison to the other acid treatments. The weight loss in this second

stage is similar for untreated HNTs and HNTs subjected to a mild etching process with acetic and acrylic treatments.

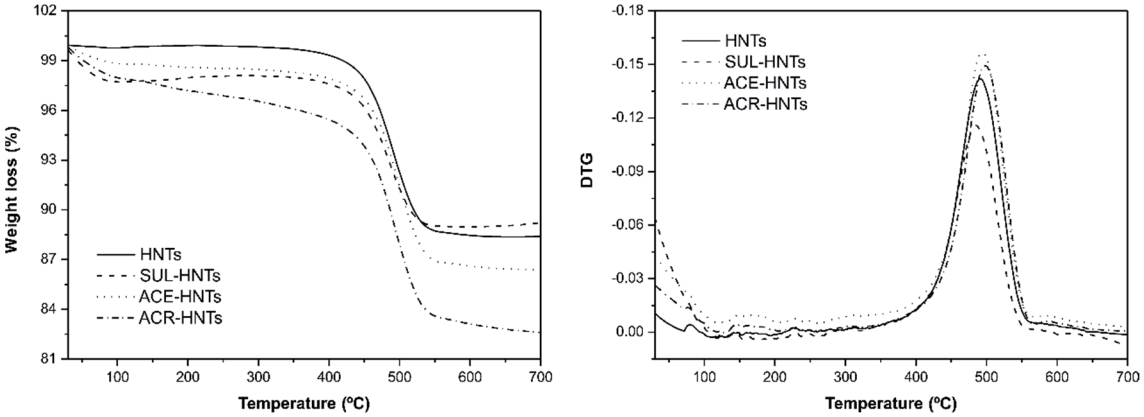

Figure IV.7.6. TGA (a) and DTG (b) curves for untreated and chemically etched HNTs with different acid treatments.

Effect of selective acid treatment on the crystal structure of HNTs

The effect of the acid treatment was also observed on the crystal structure of untreated and chemically etched HNTs. Figure IV.7.7 shows the XRD patterns of untreated HNTs and chemically etched HNTs with different acid treatments. XRD patterns of untreated HNTs are in total agreement with previously reported results [50, 52, 53]. As it can be seen, a diffraction peak appears at 2θ = 11.8° which corresponds to d_{001} diffraction planes with a basal spacing of 0.754 nm. An additional peak is observed at 2θ = 24.8° which can be attributed to the d_{002} diffraction plane with a basal spacing of 0.358 nm. These two main diffraction peaks in untreated HNTs indicate that these HNTs correspond to a dehydrated halloysite structure (halloysite-7Å) [54]. The intense diffraction observed at 2θ = 20.0°, which is attributed to the d_{020} plane with a basal spacing of 0.444 nm, confirms the tubular structure of halloysite [55]. The diffraction peak at 2θ = 26.6°, corresponds to quartz (SiO_2) d_{020} plane in halloysite [56]. As it can be seen, all chemically-etched HNTs show similar XRD patterns to untreated HNTs which indicates that the crystal structure is maintained after the acid treatments. Wang *et al.* [36] and Saklar *et al.* [57] also observed as the crystalline structure of HNTs was not affected after the acid treatment with HCl and $(COOH)_2$. Despite this, some authors reported the disruption of the crystalline structure after acid treatment with more aggressive conditions as Zhang *et al.* [40] or Belkassa *et al.* [45] concluded. The diffraction peak at d_{001} is not shifted to lower angles which indicates that the acid molecules are not inserted between different layers. This fact corroborates that the chemical attack

proceeds from the lumen (internal alumina layers) to the external walls [35]. It is worthy to note that the acid treatments give a decrease in the intensity of the 2θ = 11.8° peak as a consequence of the dealumination process. This decrease is directly related to the increase in intensity of the silica d_{011} peak [35, 40, 58]. These phenomena are more pronounced for HNTs treated with sulfuric acid thus giving clear evidences of the high aggressiveness of sulfuric acid compared to acetic or acrylic acids.

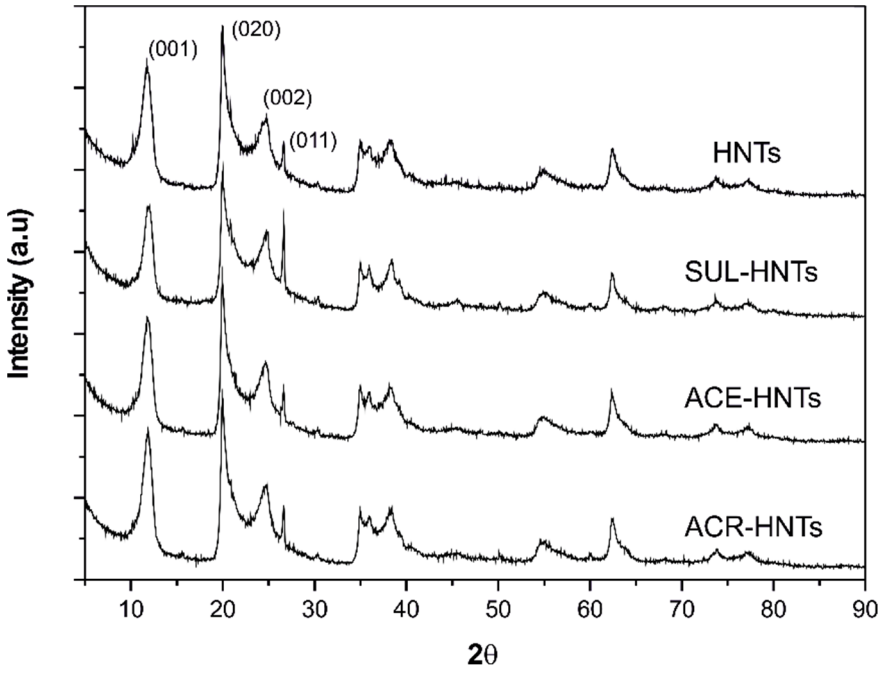

Figure IV.7.7. XRD diffraction patterns of untreated and chemically etched HNTs with different acid treatments.

CONCLUSIONS

The present work assesses the effects of different acid treatments on the morphology and chemical composition of HNTs. Acid treatment is an effective way to selectively modify HNTs for different purposes. Chemical treatment with strong acids such as sulfuric acid leads to a highly aggressive etching on HNTs characterized by a highly porous structure and partial nanotube decomposition. The specific surface area of HNTs modified with sulfuric acid is of about 132.4 $m^2 g^{-1}$ which indicates the potential of HNTs in catalysis applications. On the other hand, the selective etching by using weak acids such as acetic and acrylic acid, leads to a noticeable increase in the lumen (inner hollow diameter) in HNTs which has a positive effect on the overall potential of HNTs as carrier for different loads. As per the results, the lumen diameter changes from 13.8 nm up to 18.4 and 17.1 nm

for acetic and acrylic acid treatments respectively which lead to an increase in the carrying volume of 77.8 and 53.5% respectively. The results obtained in this work, widens new and interesting applications for natural nanotubes from halloysite by selective etching with different acids to obtain tailored morphologies and properties.

ACKNOWLEDGEMENTS

This work was supported by the Ministry of Economy and Competitiveness (MINECO) [MAT2014-59242-C2-1-R]. D. Garcia-Garcia wants to thanks the Spanish Ministry of Education, Culture and Sports for their financial support through an FPU grant [FPU13/06011].

REFERENCES

[1] López-Serrano A, Olivas RM, Landaluze JS and Cámara C. *Nanoparticles: A global vision. Characterization, separation, and quantification methods. Potential environmental and health impact*. Analytical Methods, 2014. **6**:38-56.

[2] Haroosh HJ, Dong Y, Chaudhary DS, Ingram GD and Yusa SI. *Electrospun PLA: PCL composites embedded with unmodified and 3-aminopropyltriethoxysilane (ASP) modified halloysite nanotubes (HNT)*. Applied Physics A, 2013. **110**(2):433-442.

[3] Fu X, Ding Z, Zhang X, Weng W, Xu Y, Liao J and Xie Z. *Preparation of halloysite nanotube-supported gold nanocomposite for solvent-free oxidation of benzyl alcohol*. Nanoscale Research Letters, 2014. **9**:282-285.

[4] López-Suárez FE, Carvalho-Filho CT, Bueno-López A, Arboleda J, Echavarría A, Eguiluz KIB and Salazar-Banda GR. *Platinum–tin/carbon catalysts for ethanol oxidation: Influence of Sn content on the electroactivity and structural characteristics*. International Journal of Hydrogen Energy, 2015. **40**(37):12674-12686.

[5] Zhu Y, Yu L, Wang X, Zhou Y and Ye H. *A novel monolithic Pd catalyst supported on cordierite with graphene coating*. Catalysis Communications, 2013. **40**:98-102.

[6] Moteki T, Murakami Y, Noda S, Maruyama S and Okubo T. *Zeolite surface as a catalyst support material for synthesis of single-walled carbon nanotubes*. The Journal of Physical Chemistry C, 2011. **115**(49):24231-24237.

[7] Akkari M, Aranda P, Rhaiem HB, Amara ABH and Ruiz-Hitzky E. *ZnO/clay nanoarchitectures: Synthesis, characterization and evaluation as photocatalysts*. Applied Clay Science, 2016. **131**:131-139.

[8] Abbasov VM, Ibrahimov HC, Mukhtarova GS and Abdullayev E. *Acid treated halloysite clay nanotubes as catalyst supports for fuel production by catalytic hydrocracking of heavy crude oil*. Fuel, 2016. **184**:555-558.

[9] Zhang Y, He X, Ouyang J and Yang H. *Palladium nanoparticles deposited on silanized halloysite nanotubes: Synthesis, characterization and enhanced catalytic property*. Scientific Reports, 2013. **3**:2948-2953.

[10] Xiong H, Motchelaho MA, Moyo M, Jewell LL and Coville NJ. *Effect of Group I alkali metal promoters on Fe/CNT catalysts in Fischer–Tropsch synthesis*. Fuel, 2015. **150**:687-696.

[11] Jin J, Zhang Y, Ouyang J and Yang H. *Halloysite nanotubes as hydrogen storage materials*. Physics and Chemistry of Minerals, 2014. **41**(5):323-331.

[12] Berger D, Nastase S, Mitran RA, Petrescu M, Vasile E, Matei C and Negreanu-Pirjol T. *Mesostructured silica and aluminosilicate carriers for oxytetracycline delivery systems*. International Journal of Pharmaceutics, 2016. **510**(2):524-531.

[13] Yu L, Zhang Y, Zhang B and Liu J. *Enhanced antibacterial activity of silver nanoparticles/halloysite nanotubes/graphene nanocomposites with sandwich-like structure*. Scientific Reports, 2014. **4**:4551-4555.

[14] Cavallaro G, Lazzara G, Milioto S, Palmisano G and Parisi F. *Halloysite nanotube with fluorinated lumen: Non-foaming nanocontainer for storage and controlled release of oxygen in aqueous media*. Journal of Colloid and Interface Science, 2014. **417**:66-71.

[15] Pal P, Kundu MK, Malas A and Das CK. *Compatibilizing effect of halloysite nanotubes in polar-nonpolar hybrid system*. Journal of Applied Polymer Science, 2014. **131**(1):39587.

[16] Attia NF, Hassan MA, Nour MA and Geckeler KE. *Flame-retardant materials: Synergistic effect of halloysite nanotubes on the flammability properties of acrylonitrile-butadiene-styrene composites*. Polymer International, 2014. **63**(7):1168-1173.

[17] Zhao J, Deng CL, Du SL, Chen L, Deng C and Wang YZ. *Synergistic flame-retardant effect of halloysite nanotubes on intumescent flame retardant in LDPE*. Journal of Applied Polymer Science, 2014. **131**(7):40065.

[18] Kiani G. *High removal capacity of silver ions from aqueous solution onto halloysite nanotubes*. Applied Clay Science, 2014. **90**:159-164.

[19] Rawtani D and Agrawal YK. *Multifarious applications of halloysite nanotubes: A review*. Reviews on Advanced Materials Science, 2012. **30**:282-295.

[20] Lee K, Chang YW and Kim SW. *Ethylene-propylene-diene terpolymer/halloysite nanocomposites: Thermal, mechanical properties, and foam processing*. Journal of Applied Polymer Science, 2014. **131**(11):40307.

[21] Albdiry MT and Yousif BF. *Role of silanized halloysite nanotubes on structural, mechanical properties and fracture toughness of thermoset nanocomposites*. Materials & Design, 2014. **57**:279-288.

[22] Lvov YM, Shchukin DG, Möhwald H and Price RR. *Halloysite clay nanotubes for controlled release of protective agents*. ACS Nano, 2008. **2**(5):814-820.

[23] Deen I and Zhitomirsky I. *Electrophoretic deposition of composite halloysite nanotube-hydroxyapatite-hyaluronic acid films*. Journal of Alloys and Compounds, 2014. **586**:S531-S534.

[24] Shi YF, Tian Z, Zhang Y, Shen HB and Jia NQ. *Functionalized halloysite nanotube-based carrier for intracellular delivery of antisense oligonucleotides*. Nanoscale Research Letters, 2011. **6**:608-614.

[25] Abdullayev E and Lvov Y. *Halloysite clay nanotubes as a ceramic "skeleton" for functional biopolymer composites with sustained drug release*. Journal of Materials Chemistry B, 2013. **1**:2894-2903.

[26] Lin X, Ju X, Xie R, Jiang M, Wei J and Chu L. *Halloysite nanotube composited thermo-responsive hydrogel system for controlled-release*. Chinese Journal of Chemical Engineering, 2013. **21**(9):991-998.

[27] Tan D, Yuan P, Annabi-Bergaya F, Yu H, Liu D, Liu H and He H. *Natural halloysite nanotubes as mesoporous carriers for the loading of ibuprofen*. Microporous and Mesoporous Materials, 2013. **179**:89-98.

[28] Qi R, Guo R, Shen M, Cao X, Zhang L, Xu J, Yu J and Shi X. *Electrospun poly(lactic-co-glycolic acid)/halloysite nanotube composite nanofibers for drug encapsulation and sustained release*. Journal of Materials Chemistry, 2010. **20**:10622-10629.

[29] Ishikawa K, Akasaka T, Abe S, Yawaka Y, Suzuki M and Watari F. *Application of imogolite, almino-silicate nanotube, as scaffold for the mineralization of osteoblasts*. Bioceramics Development and Applications, 2009. **22**:303-306.

[30] Banaś D, Kubala-Kukuś A, Braziewicz J, Majewska U, Pajek M, Wudarczyk-Moćko J, Czech K, Garnuszek M, Słomkiewicz P and Szczepanik B. *Study of properties of chemically modified samples of halloysite mineral with X-ray fluorescence and X-ray powder diffraction methods*. Radiation Physics and Chemistry, 2013. **93**:129-134.

[31] Duce C, Ciprioti SV, Ghezzi L, Ierardi V and Tinè MR. *Thermal behavior study of pristine and modified halloysite nanotubes*. Journal of Thermal Analysis and Calorimetry, 2015. **121**(3):1011-1019.

[32] Yah WO, Takahara A and Lvov YM. *Selective modification of halloysite lumen with octadecylphosphonic acid: New inorganic tubular micelle*. Journal of the American Chemical Society, 2012. **134**(3):1853-1859.

[33] Pal P, Kundu MK, Kalra S and Das CK. *Mechanical and crystalline behavior of polymeric nanocomposites in presence of natural clay*. Open Journal of Applied Sciences, 2012. **2**:277-282.

[34] Zhong S, Zhou C, Zhang X, Zhou H, Li H, Zhu X and Wang Y. *A novel molecularly imprinted material based on magnetic halloysite nanotubes for rapid enrichment of 2,4-dichlorophenoxyacetic acid in water*. Journal of Hazardous Materials, 2014. **276**:58-65.

[35] Abdullayev E, Joshi A, Wei W, Zhao Y and Lvov Y. *Enlargement of halloysite clay nanotube lumen by selective etching of aluminum oxide*. ACS Nano, 2012. **6**(8):7216-7226.

[36] Wang Q, Zhang J, Zheng Y and Wang A. *Adsorption and release of ofloxacin from acid- and heat-treated halloysite*. Colloids and Surfaces B: Biointerfaces, 2014. **113**:51-58.

[37] Bertolini A, Carelli G, Francesconi F, Francesconi M, Marchesini L, Marsili P, Sorrentino F, Cristoforetti G, Legnaioli S, Palleschi V, Pardini L and Salvetti A. *Modì: A new mobile instrument for in situ double-pulse LIBS analysis*. Analytical and Bioanalytical Chemistry, 2006. **385**(2):240-247.

[38] Brunauer S, Emmett PH and Teller E. *Adsorption of gases in multimolecular layers*. Journal of the American Chemical Society, 1938. **60**:309-319.

[39] Barrett EP, Joyner LG and Halenda PP. *The determination of pore volume and area distributions in porous substances. I. Computations from nitrogen isotherms*. Journal of the American Chemical Society, 1951. **73**:373-380.

[40] Zhang AB, Pan L, Zhang HY, Liu ST, Ye Y, Xia MS and Chen XG. *Effects of acid treatment on the physico-chemical and pore characteristics of halloysite*. Colloids and Surfaces A: Physicochemical and Engineering Aspects, 2012. **396**:182-188.

[41] Bordeepong S, Bhongsuwan D, Pungrassami T and Bhongsuwan T. *Characterization of halloysite from Thung Yai District, Nakhon Si Thammarat Province, in Southern Thailand*. Sonklanakarin Journal of Science and Technology, 2011. **33**(5):599-607.

[42] Zhong B, Jia Z, Hu D, Luo Y, Guo B and Jia D. *Surface modification of halloysite nanotubes by vulcanization accelerator and properties of styrene-butadiene rubber nanocomposites with modified halloysite nanotubes*. Applied Surface Science, 2016. **366**:193-201.

[43] Panda AK, Mishra BG, Mishra DK and Singh RK. *Effect of sulphuric acid treatment on the physico-chemical characteristics of kaolin clay*. Colloids and Surfaces A: Physicochemical and Engineering Aspects, 2010. **363**(1):98-104.

[44] Sangwichien C, Aranovich GL and Donohue MD. *Density functional theory predictions of adsorption isotherms with hysteresis loops*. Colloids and Surfaces A: Physicochemical and Engineering Aspects, 2002. **206**(1):313-320.

[45] Belkassa K, Bessaha F, Marouf-Khelifa K, Batonneau-Gener I, Comparot J and Khelifa A. *Physicochemical and adsorptive properties of a heat-treated and acid-leached Algerian halloysite*. Colloids and Surfaces A: Physicochemical and Engineering Aspects, 2013. **421**:26-33.

[46] Pasbakhsh P, Churchman GJ and Keeling JL. *Characterisation of properties of various halloysites relevant to their use as nanotubes and microfibre fillers*. Applied Clay Science, 2013. **74**:47-57.

[47] Guo B, Chen F, Lei Y, Liu X, Wan J and Jia D. *Styrene-butadiene rubber/halloysite nanotubes nanocomposites modified by sorbic acid*. Applied Surface Science, 2009. **255**(16):7329-7336.

[48] White RD, Bavykin DV and Walsh FC. *The stability of halloysite nanotubes in acidic and alkaline aqueous suspensions*. Nanotechnology, 2012. **23**(6):065705.

[49] Ismail AF, Hashemifard SA and Matsuura T. *Facilitated transport effect of Ag^{+} ion exchanged halloysite nanotubes on the performance of polyetherimide mixed matrix membrane for gas separation*. Journal of Membrane Science, 2011. **379**(1):378-385.

[50] Sun P, Liu G, Lv D, Dong X, Wu J and Wang D. *Effective activation of halloysite nanotubes by piranha solution for amine modification via silane coupling chemistry*. RSC Advances, 2015. **5**:52916-52925.

[51] Liu C, Yu L, Zhang Y, Zhang B, Liu J and Zhang H. *Preparation of poly(sodium acrylate-acrylamide) superabsorbent nanocomposites incorporating graphene oxide and halloysite nanotubes*. RSC Advances, 2013. **3**:13756-13763.

[52] Zhai R, Zhang B, Liu L, Xie Y, Zhang H and Liu J. *Immobilization of enzyme biocatalyst on natural halloysite nanotubes*. Catalysis Communications, 2010. **12**(4):259-263.

[53] Mellouk S, Cherifi S, Sassi M, Marouf-Khelifa K, Bengueddach A, Schott J and Khelifa A. *Intercalation of halloysite from Djebel Debagh (Algeria) and adsorption of copper ions*. Applied Clay Science, 2009. **44**(3):230-236.

[54] Chen H, Yan H, Pei Z, Wu J, Li R, Jin Y and Zhao J. *Trapping characteristic of halloysite lumen for methyl orange*. Applied Surface Science, 2015. **347**:769-776.

[55] Sahnoun S, Boutahala M, Zaghouane-Boudiaf H and Zerroual L. *Trichlorophenol removal from aqueous solutions by modified halloysite: Kinetic and equilibrium studies*. Desalination and Water Treatment, 2016. **57**(34):15941-15951.

[56] Wu X, Liu C, Qi H, Zhang X, Dai J, Zhang Q, Zhang L, Wu Y and Peng X. *Synthesis and adsorption properties of halloysite/carbon nanocomposites and halloysite-derived carbon nanotubes*. Applied Clay Science, 2016. **119**:284-293.

[57] Saklar S and Yorukoglu A. *Effects of acid leaching on halloysite*. Physicochemical Problems of Mineral Processing, 2015. **51**(1):83-94.

[58] Falcón JM, Sawczen T and Aoki IV. *Dodecylamine-loaded halloysite nanocontainers for active anticorrosion coatings*. Frontiers in Materials, 2015. **2**:69-81.

Applied Surface Science 422 (2017) 616–625

Contents lists available at ScienceDirect

Applied Surface Science

journal homepage: www.elsevier.com/locate/apsusc

Full Length Article

Characterization of selectively etched halloysite nanotubes by acid treatment

Daniel Garcia-Garcia[a,*], Jose M. Ferri[a], Laura Ripoll[b], Montserrat Hidalgo[b], Juan Lopez-Martinez[a], Rafael Balart[a]

[a] Instituto de Tecnología de Materiales (ITM), Universitat Politècnica de València (UPV), Plaza Ferrándiz y Carbonell 1, 03801, Alcoy, Alicante, Spain
[b] Departamento de Química Analítica, Nutrición y Bromatología, Instituto Universitario de Materiales (IUMA), Universidad de Alicante (UA), Apdo. 99, 03080, Alicante, Spain

ARTICLE INFO

Article history:
Received 27 March 2017
Received in revised form 5 June 2017
Accepted 8 June 2017

Keywords:
Halloysite nanotubes
Lumen enlargement
Acid treatment
Catalysis
LIBS

ABSTRACT

Halloysite nanotubes (HNTs) are a type of naturally occurring inorganic nanotubes that are characterized by a different composition between their external and internal walls. The internal walls are mainly composed of alumina whilst external walls are composed of silica. This particular structure offers a dual surface chemistry that allows different selective surface treatments which can be focused on increasing the lumen, increasing porosity, etc. In this work, HNTs were chemically treated with different acids (sulphuric, acetic and acrylic acid), for 72 h at a constant temperature of 50 °C. As per the obtained results, the treatment with sulphuric acid is highly aggressive and the particular shape of HNTs is almost lost, with a remarkable increase in porosity. The BET surface area increases from 52.9 (untreated HNTs) up to 132.4 $m^2 g^{-1}$ with sulphuric acid treatment, thus showing an interesting potential in the field of catalysis. On the other hand, the treatment with acetic acid led to milder effects with a noticeable increase in the lumen diameter that changed from 13.8 nm (untreated HNTs) up to 18.4 nm which the subsequent increase in the loading capacity by 77.8%. The aluminium content was measured by X-ray fluorescence (XRF) and laser induced breakdown spectroscopy (LIBS). The final results using two systems, suggest a good correlation between the acid strength and the aluminium reduction. Consequently, is possible to conclude that new applications for HNTs can be derived from selective etching with acids. Sulphuric acid widens the potential of HNTs in the field of catalysis while weak acids such as acetic and acrylic acids give a controlled and homogeneous lumen increase with the corresponding increase in the loading capacity.

1. Introduction

One of the main features of nanomaterials is their high surface to volume ratio which gives an exponential increase in the reactivity of the molecules thus leading to a remarkable change in their electronic, optical, chemical or mechanical properties with regard to their bulk counterpart materials. For this reason, nanomaterials offer a great potential in a wide range of research areas such as biomedicine, cosmetics, food and food packaging, coatings, electronics, catalysis or materials sciences [1]. A wide variety of metal oxides, nanoclays, carbon nanomaterials, organometallic nanocomposites (MOFs) have been successfully introduced in new materials [2], with the particular feature that nanoparticles offer a strong different behavior than their counterpart micro/macro particles. Nanoclays have been widely studied as support for different catalysts [3]. In particular, the petroleum industry is leading the introduction of nanoparticles as supports for catalysts in several reactions. It has been reported the potential of activated carbon and carbon nanotubes (CNTs) as support for ethanol oxidation [4], aluminosilicates, cordierites [5], zeolites [6], other feldspars, kaolinite derivate such sespiolites [7], HNTs, etc., which allow the conversion of crude oil in a wide range of products. Nanomaterials are continuously acquiring new features in the catalysis industry. Abbasov et al. [8] reported the positive effects of a previous acid treatment on HNTs with HCl to improve the efficiency as support for NiO and CoO for fuel production from heavy crude oil. Zhang et al. [9] used a silane treatment with aminopropyltriethoxysilane as a previous treatment to increase Pd adsorption on HNTs as catalytic system for the conversion of styrene to ethylbenzene. In a parallel way, CNTs are also being investigated as support for different catalysts [10]. Nevertheless, the use of CNTs is restricted in the medicine field due to their potential health risks. On the other hand, their high cost is a key disadvantage for a wide use in the field of composites.

* Corresponding author.
E-mail address: dagarga4@epsa.upv.es (D. Garcia-Garcia).

http://dx.doi.org/10.1016/j.apsusc.2017.06.104
0169-4332/

IV.8

"Improvement of mechanical and thermal properties of poly(3-hydroxybutyrate) (PHB) blends with surface-modified halloysite nanotubes (HNTs)"

Daniel García García[a], *David García Sanoguera*[a], *Vicent Fombuena*[a], *Juan López Martínez*[a], *Rafael Balart*[a]

[a] Instituto de Tecnología de Materiales (ITM)
Universitat Politècnica de València (UPV)
Plaza Ferrándiz y Carbonell 1, 03801 Alcoy, Alicante, Spain.

Applied Clay Science

2018, (under review)

Improvement of mechanical and thermal properties of poly(3-hydroxybutyrate) (PHB) blends with surface-modified halloysite nanotubes (HNTs)

Abstract

The effect of two hydrophobic treatments on the hydrophilic nature of halloysite nanotubes (HNTs) has been studied in this research work: a silanization with (3-glycidyloxypropyl) trimethoxysilane (GLYMO) and a surface treatment with a natural aromatic compound, *i.e.*, caffeic acid (CA). In addition, the effect of 3 wt% of unmodified HNTs, silanized HNTs (HNT_{SIL}) and caffeic acid-modified HNTs (HNT_{CA}) on mechanical, thermal and morphological properties of a binary blend of poly(3-hydroxybutyrate) (PHB) and poly(ε-caprolactone) (PCL) with a weight ratio of 75/25, respectively, was evaluated. These blends and their corresponding composites with HNTs were partially compatibilized by reactive extrusion with dicumyl peroxide (DCP) and further processed by injection molding. The effectiveness of the surface treatments on HNTs was followed by Fourier transformed infrared spectroscopy (FTIR), thermogravimetric analysis (TGA), field emission scanning electron microscopy (FESEM) and contact angle measurements. The obtained results suggested a clear hydrophobizing effect of both surface treatments on HNTs but the hydrophobic nature the caffeic acid treatment can provide to HNTs is greater than silanization. FESEM study on HNTs-loaded PHB/PCL blends showed increased compatibility between modified-HNTs and the polymeric matrix, as well as a better particle dispersion. In particular, 3 wt% HNT_{CA} lead to an increase in tensile strength and elongation at break of 11.4% and 74%, respectively, with regard to composites with unmodified HNTs. In addition, thermal analysis, evaluated by differential scanning calorimetry (DSC) and thermogravimetric analysis (TGA), revealed a decrease in the melt peak temperature of 6.5 °C for composites with 3 wt% HNT_{CA} as well a delay in the onset degradation temperature, thus leading to a broader processing window which enhances PHB processing by conventional techniques.

Keywords: Poly(3-hydroxybutyrate); poly(ε-caprolactone); dicumyl peroxide; halloysite nanotubes; silane; caffeic acid.

INTRODUCTION

In the last years, important advances in the field of biodegradable polymers have been observed. Nevertheless, some of these polymers still show important drawbacks that restrict their wide use in industry. Poly(3-hydroxybutyrate) (PHB) is one of the most promising biopolyesters obtained from bacterial fermentation but it has to face an important challenge related to its fragility (due to its high crystallinity) and its extremely narrow processing window, since its thermal degradation is slightly higher than its melt process [1]. These drawbacks, together with a still high price compared to commodity plastics are responsible for a very restricted industrial use [2]. To overcome or minimize these drawbacks, several approaches have been addressed in the last years with the main aim of increasing its thermo-mechanical performance. It is worthy to note the interesting results obtained by using natural-derived plasticizers such as epoxidized linseed oil [3], epoxidized soybean oil [4] or maleinized linseed oil [5], among others. Another approach has been physical blending with a wide variety of biodegradable polymers such as poly(lactic acid) (PLA) [6], poly(butylene succinate) (PBS) [7], poly(ε-caprolactone) (PCL) [8, 9] or poly(vinyl alcohol) (PVA) [10, 11]. Finally, the use of nanoparticles has been revealed as an interesting alternative to plasticizing and/or blending. It has been reported the positive effect of TiO_2 nanoparticles [12], ZnO nanoparticles [13] or cellulose nanowiskers [14] on mechanical, thermal and barrier properties of PHB-based composites.

In our previous works, it was reported the positive effect of a binary blend of PHB and PCL with a weight ratio of 75/25 respectively, on overall thermal and mechanical ductile properties. Nevertheless, it was concluded that these two polyesters showed a highly restricted miscibility, leading to phase separation due to the poor interactions among PHB-PCL interface and this restricts the improvements PCL can provide [15]. To overcome this, 1 phr dicumyl peroxide (DCP) was successfully used to promote reactive extrusion during blending, thus leading to a remarkable increase in ductile properties. In particular, the obtained elongation at break was increased by 231% with regard to the uncompatibilized PHB/PCL blend. Regarding the impact properties, the impact-absorbed energy (Charpy test) was improved by 91% thus giving clear evidences of the compatibilizing effect DCP provides, without compromising other mechanical resistant properties [16].

The interest on ternary blends containing two polymers and one nanofiller is increasing due to the positive effect of nanoparticles on overall properties of blends. These nanoparticles provide a structural reinforcing role together with potential compatibilization. When two immiscible polymers are mixed together, there are not any interactions between the molecular segments of both polymers, which gives high surface

tension between these polymers. This phenomenon is responsible for a poor dispersion of each polymer on the other, thus leading to phase separation with the typical drop-like structure [17]. Several authors have reported that the addition of small amounts of different nanofillers gives reduced surface tension between the two polymers thus lading to coalescence inhibition and a remarkable decrease in the particle size of the dispersed phase. This contributes to improved interface adhesion and gives improved compatibility to blends [18-23].

One of the most promising nanofillers in the last decade are halloysite nanotubes (HNTs). These nanotubes are natural aluminosilicates with the molecular formula of $Al_2Si_2O_5(OH)_4 \cdot nH_2O$ [24]. HNTs offer a hollow tubular structure composed of multiple layers of hollow cylinders with an elevated aspect ratio. An interesting feature of HNTs is the different chemical structure of the outer surfaces with regard to the inner areas. The external (outer) surface is composed of siloxane (Si–O–Si) while the inner layers are composed of aluminol groups (Al–OH) [25, 26]. Furthermore, typical HNTs show an inner diameter of 15 nm which allows using HNTs as carriers for selective loads, thus allowing their use for controlled delivery systems [27, 28]. All these features, together with a relatively low price make HNTs high attractive as a functional additive in polymeric systems. Pal *et al.* [29], studied the effect of the addition of 1 wt% unmodified halloysite and silanized halloysite with N-(*β*-aminoethyl)-*γ*-aminopropyltrimethoxysilane on overall properties of an immiscible blend between poly(oxymethylene) (POM) and polypropylene (PP). They reported an improvement on compatibilization and a slight increase in the thermal degradation onset. Nevertheless, one of the main drawbacks of a widespread use of HNTs is their high hydrophilicity, due to the presence of a huge number of hydroxyl groups which contributes to aggregate formation. This hydrophilicity contributes to poor dispersion with the subsequent negative effect on overall properties [30]. To minimize these effects, during the last years, several research works have been focused on reducing the hydrophilicity of HNTs, mainly by silanization surface treatments [31-33].

This work focuses on the use of a novel surface treatment with caffeic acid (CA). Caffeic acid is plant-derived aromatic compound which shows interesting properties such as antioxidant, anticancer, anti-inflammatory, antiviral activity, among others [34]. CA is used in this work with two main purposes. On one hand, its potential as surfactant material is studied with the aim of reducing hydrophilic properties of HNTs and, on the other hand, its antioxidant potential to delay thermal degradation is addressed. A common silanization process with (3-glycidyloxypropyl) trimethoxysilane (GLYMO) is also carried out to compare the effects on the hydrophilic properties of HNTs. Moreover, the effect of 3 wt%

unmodified and modified (silanized and caffeic acid-modified) HNTs on overall properties of a binary blend composed of PHB and PCL with a weight ratio of 75/25, respectively, partially compatibilized by reactive extrusion with dicumyl peroxide (DCP), is studied.

EXPERIMENTAL

Materials

Poly(3-hydroxybutyrate) (PHB) pellets commercial grade P304 were supplied by Biomer (Krailling, Germany). Poly(ε-caprolactone) (PCL) pellets commercial grade CAPA 6500 were provided by Perstorp Holding AB (Malmö, Sweden). Dicumyl peroxide (DCP) (98% purity), halloysite nanotubes (HNTs), caffeic acid and the silane used for surface treatment of HNTs ((3-glycidyloxypropyl) trimethoxysilane) were supplied from Sigma Aldrich (Madrid, Spain) and used without further purification. Acetic acid (99.7% CH_3COOH) was used as a mild acid to increase the lumen size in HNTs. This was supplied by PanReac Applichem (Barcelona, Spain).

Silanization treatment of HNTs

Functionalization of HNTs with silane was carried out following the procedure described by Krishnaiah *et al.* [30]. Approx. 6 g silane (GLYMO) was dissolved in 250 mL ethanol (96%) and the solution was mechanically stirred for 15 min at 60 °C to hydrolyze alkoxy groups. Subsequently, acetic acid was added drop by drop until reaching a pH value around 5 and then, 25 g HNTs were added while maintaining mechanical stirring at 60 °C for two additional hours. HNTs were obtained by filtration and were washed with ethanol. Finally, silanized HNTs were dried at 70 °C for 8 h with the aim of removing the residual moisture.

Acid treatment of HNTs and caffeic acid loading

Prior to load caffeic acid into HNTs, the lumen diameter was selectively etched with acetic acid following the procedure described by Garcia-Garcia *et al.* [35]. To this, HNTs were previously dried at 100 °C for 8 h. Then, 5 g dried HNTs were poured into a 500 mL flask with an acetic acid solution in distilled water with a concentration of 1 mol L^{-1}. The solution was maintained with mechanical stirring for 72 h at 50 °C. After this treatment, chemically modified HNTs were collected by centrifugation and washed with distilled water until a neutral pH was obtained. Finally, acid-treated HNTs were dried at 50 °C for 24 h.

After this surface treatment to increase the loading capacity, HNTs were loaded with caffeic acid following the procedure described by Hendessi *et al.* [36]. A summary of this procedure is as follows: caffeic acid was dissolved in ethanol (96%) until saturation. Then, 5 g of HNTs were poured to the solution. The suspension was sonicated for 5 min using an amplitude of 33% in an ultrasonic homogenizer Sonoplus HD 2200 from Bandelin (Berlin, Germany). After this, the mixture was subjected to vacuum (1 mbar) for 30 min to remove the trapped air inside HNTs; then the vacuum was broken and the suspension remained at atmospheric pressure for 10 min to allow caffeic acid molecules to enter into the HNTs lumen. The cycle was repeated 3 times to improve the loading efficiency. Finally, caffeic acid loaded HNTs was separated by centrifugation at 4000 rpm for 5 min and washed with ethanol to remove the caffeic acid excess. Caffeic acid-loaded HNTs were dried at 40 °C for 24 h.

Manufacturing of PHB/PCL blends with HNTs

PHB and HNTs were dried in an air-circulating oven at 70 °C for 8 hours while PCL was dried at 40 °C overnight to remove residual moisture before use. The appropriate amounts of PHB, PCL, DCP and 3 wt% unmodified HNTs, silanized HNTs (HNT_{SIL}) and caffeic acid-treated HNTs (HNT_{CA}) were pre-mixed mechanically in a zipper bag prior to compounding. The composition of PHB/PCL/DCP/HNT blends are listed in Table IV.8.1. All the samples were melt-blended in a co-rotating twin-screw extruder from DUPRA S.L. (Alicante, Spain) with a screw diameter of 25 mm and a length (*L*) to diameter (*D*) ratio, *i.e.*, *L/D*, of 24. The screw speed was set to 40 rpm to allow reactive extrusion and the temperature profile of the extrusion barrel was set to 165 °C (hopper), 170 °C, 175 °C and 180 °C (extrusion die). The obtained compounds were cooled down to room temperature, pelletized and subsequently processed by injection molding in a Meteor 270/75 from Mateu & Solé (Barcelona, Spain) to obtain standard samples for further characterization. The temperature profile for the injection process was set to 165 °C, 165 °C, 170 °C, 175 °C and 180 °C from feeding zone to the injection nozzle. The cavity filling and cooling times were set to 1 and 30 s respectively. Prior to characterization, standard samples were stored at room conditions (23 ± 1 °C and 50% HR) for 21 days with the main aim of stabilizing mechanical properties of the obtained blends since PHB undergoes physical aging due to crystallization with time. Previous results have reported that mechanical properties tend to stabilize after the above-mentioned aging time [37].

Table IV.8.1. Composition and labeling of binary PHB/PCL compatibilized by reactive extrusion with DCP and reinforced with unmodified and modified HNTs.

Coding	PHB (wt%)	PCL (wt%)	HNT (wt%)	DCP (phr)
PHB/PCL/DCP	75	25	0	1
3-HNT	72.75	24.25	3	1
3-HNT_{SIL}	72.75	24.25	3	1
3-HNT_{CA}	72.75	24.25	3	1

Characterization techniques

Fourier transformed infrared spectroscopy (FTIR)

The effect of the different treatments on the chemical structure of HNTs was studied by Fourier transformed infrared spectroscopy in a FTIR spectrometer Spectrum BX from Perkin-Elmer (Madrid, Spain). HNTs were subjected to 20 scans between 4000 and 400 cm^{-1} with a resolution of 16 cm^{-1}. Prior to sample characterization, all HNTs were pressed into a KBr disc.

Field emission scanning electron microscopy and energy dispersive X-ray analysis (FESEM-EDS)

The effect of the different surface treatments on HNTs, as well as the morphology of fractured blends from impact tests was studied in a field emission scanning electron microscope (FESEM) ZEISS model ULTRA 55 (Oberkochen, Germany), equipped with an energy dispersive spectrometer (EDS). Image acquisition was carried out at an accelerating voltage of 5 kV. Prior to be observed fractured surfaces of samples were coated with a thin layer of platinum in a high vacuum sputter coater EM MED20 from Leica Microsystem (Milton Keynes, United Kingdom).

Dynamic contact angle measurements

The effect of the surface treatments of HNTs on their wetting properties was analyzed by optical goniometry in an Easy Drop Standard KRÜSS goniometer (KRÜSS GmbH, Hamburg, Germany), model FM140 (110/220 V, 50/60 Hz).

Mechanical properties

Tensile and flexural properties of PHB/PCL blends loaded with HNTs were obtained using a universal test machine Ibertest ELIB 30 from S.A.E. Ibertest (Madrid, Spain) according to ISO 527 and ISO 178 respectively. Both tests were carried out with a 5 kN load cell and a crosshead speed of 5 mm min^{-1}. Moreover, for a more accurate determination of the Young's modulus, an axial extensometer IB/MFQ-R2 from Ibertest (Madrid, Spain) coupled to the universal test machine was used. All specimens were tested at room temperature (23 ± 1 °C) and at least five samples for each material were analyzed for each mechanical test and averaged values of the main mechanical parameters were calculated.

Thermal properties

The effect of loading HNTs on thermal properties of the partially compatibilized PHB/PCL blend was studied by differential scanning calorimetry (DSC) in a DSC 821 calorimeter from Mettler-Toledo (Schwerzenbach, Switzerland). Approximately, 6 mg of each material were placed into standard 40 mL aluminum crucibles and were subjected to a dynamic program under nitrogen atmosphere (flow rat 66 mL min^{-1}) divided in three steps: a first heating cycle from −50 up to 180 °C. This was followed by an isothermal stage at 180 °C for 2 min. Then, a cooling stage down to −50 °C was applied and, finally, a second heating stage up to 300 °C was scheduled. The heating and cooling rates for all the scans were set to 10 °C min^{-1}. The melting temperature peak (T_m) and the degree of crystallinity (X_c) were obtained from the second heating cycle. The degree of crystallinity of PHB ($X_{c\,PHB}$) and PCL ($X_{c\,PCL}$) in each sample was determined using the following equation:

$$\boldsymbol{X_c}\,(\%) = \left[\frac{\Delta \boldsymbol{H_m}}{\Delta \boldsymbol{H_0} \cdot \boldsymbol{w}}\right] \times \mathbf{100} \qquad \textbf{Equation IV.8.1}$$

where ΔH_m stands for the thermodynamic melt enthalpy per gram of each polymer obtained from the second heating cycle, ΔH_0 is the theoretical enthalpy corresponding to the melting of a 100% crystalline PHB (146 J g^{-1} [38]) or PCL (156.8 J g^{-1} [39]), and w is the weight fraction of the corresponding polymer (PHB or PCL) in the blend.

The thermal stability of unmodified and chemically modified HNTs, as well as the PHB/PCL blends with HNTs was studied by thermogravimetric analysis (TGA) in a TGA PT1000 from Linseis Inc. (Selb, Germany). Approximately 12 mg of each sample were subjected to a dynamic heating program from 30 up to 700 °C at a heating rate of 10 °C min^{-1} under nitrogen atmosphere with a constant flow rate of 66 mL min^{-1}. The onset degradation

temperature (T_0) was defined as the temperature at which a 5% weight loss occurs. In addition, the maximum degradation temperature (T_{max}) for each stage was obtained as the corresponding peak of the first derivative (DTG).

Dynamic mechanical thermal analysis (DMTA)

Dynamic mechanical thermal analysis (DMTA) was performed in an oscillatory rheometer AR G2 by TA Instruments (New Castle, USA) working in shear/torsion mode. This rheometer is equipped with a special clamp system for solid samples thus allowing evaluation of dynamical-mechanical properties as a function of temperature. Samples with a size of 40×10×4 mm^3 were subjected to a temperature sweep from −100 up to 100 °C at a constant heating rate of 2 °C min^{-1}, a frequency of 1 Hz and a maximum shear strain (γ) of 0.1%. The values of storage modulus (G') and tan δ versus temperature were recorded for each sample. The glass transition temperature (T_g) was assumed as the peak maximum of the tan δ curve.

RESULTS AND DISCUSSION

Effect of chemical modification of HNTs

Figure IV.8.1 shows a comparative plot of the FTIR spectra of unmodified HNTs, silanized HNTs with GLYMO (HNT_{SIL}) and HNTs treated with caffeic acid (HNT_{CA}). As it can be seen, the spectrum of unmodified HNTs shows characteristic peaks located at 3695, 3624 and 912 cm^{-1} which are attributable to stretching of inner-surface Al−OH, the stretching of inner Al−OH and bending vibration of the inner Al−OH respectively. The peaks located at 3450 and 1650 cm^{-1} are directly related to O–H stretching and bending vibration of the adsorbed water respectively. Peaks centered at 1118, 1036 and 538 cm^{-1} are ascribed to the apical Si–O stretching vibration, in-plane Si–O stretching vibrations and Si–O bending vibration respectively. It can also be detected, the presence of two peaks at 792 and 754 cm^{-1} which can be assigned to the symmetric stretching of Si–O–Si and the perpendicular stretching of Si–O–Al respectively [40-43]. The spectrum of the silanized HNTs (HNT_{SIL}) (Figure IV.8.1a) show a clear decrease in the absorbance of hydroxyl groups (–OH) in both internal and external layers related to peaks located at 3695, 3624 and 912 cm^{-1}. This can be explained by taking into account that silanol (Si–OH) groups obtained after the hydrolysis of the alkoxy groups in GLYMO, can react with hydroxyl groups of aluminol (Al–OH) in the inner layers of HNTs as well as with the edges of the HNTs and external surface defects on HNTs. This decrease in the intensity of these peaks confirm the interaction of

silane with HNTs thus leading to formation of Al–O–Si bonds [44]. New absorption bands can be detected for the silanized HNTs (HNT_{SIL}). It is worthy to note the peaks located at 2930 and 2860 cm^{-1} which can be assigned to the asymmetric and symmetric stretching vibration of aliphatic $–CH_2$; the peak located at 1480 cm^{-1} is related to the deformation vibration of $–CH_2$ and corroborate the effectiveness of the silane treatment [31, 45]. Finally, the absorbance of the peaks related to the adsorbed water on HNTs, located at 3450 and 1650 cm^{-1} decreases after the silane treatment. This could be due to two overlapping phenomena: on one hand, this could be related to an increase in hydrophobicity after silanization, which restricts water adsorption. On the other hand, condensation reaction of silanol groups with aluminol groups leads to water generation that is removed after the drying process, thus contributing to a decrease on the overall amount of the adsorbed water between layers [46]. With regard to caffeic acid modified HNTs (HNT_{CA}) Figure IV.8.1b shows the typical peaks ascribed to unmodified HNTs but new peaks can identified. These peaks are located at 1646, 1622, 1452 and 1280 cm^{-1} and are related to C=C stretching, (–C=O) stretching of the –COOH group, the ring stretching and phenol (C–O) stretching from caffeic acid respectively [47]. Furthermore, the peak related to the adsorbed water at 3450 cm^{-1} also decreases with regard to unmodified HNTs, thus giving evidence of the hydrophobizing effect that caffeic acid can give on HNTs.

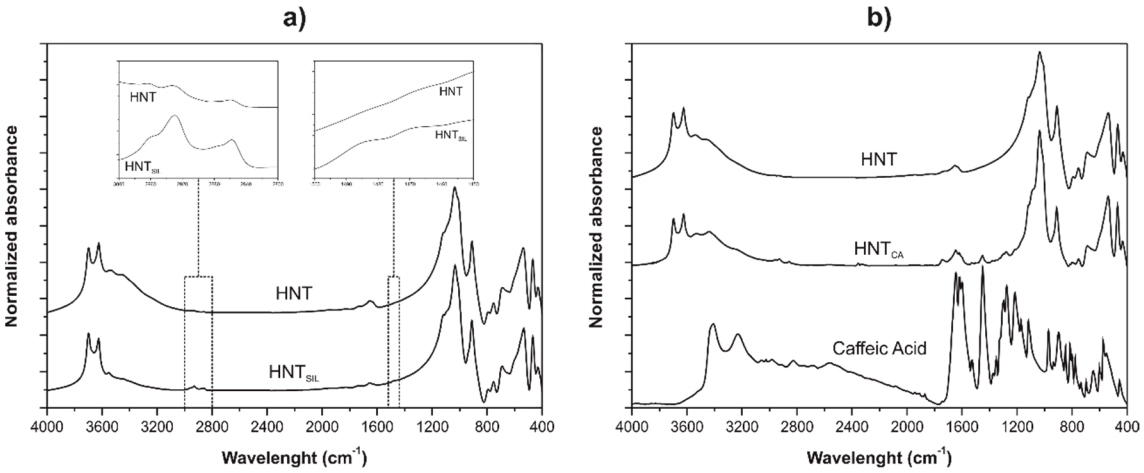

Figure IV.8.1. FTIR spectra of (a, b) unmodified HNT, (a) silanized HNTs with GLYMO (HNT_{SIL}) and (b) caffeic acid-loaded HNTs (HNT_{CA}).

The effect of the different surface treatments on HNTs was also followed by thermogravimetry (TGA). Figure IV.8.2 shows TGA curves corresponding to unmodified HNTs, silanized HNTs (HNT_{SIL}) and caffeic acid-loaded HNTs (HNT_{CA}). As it can be seen,

unmodified HNTs show two main weight loss steps. The first one is located in the temperature range comprised between 30 and 150 °C and is directly related to desorption of the water that is physically adsorbed onto HNTs interlayers and surface, and a second weight loss step located between 400–550 °C which is related to structural dehydroxylation of Al–OH groups of HNTs [35]. After the silanization process, it is clearly distinguishable that the first weight loss step is smaller with regard to unmodified HNTs. This is representative for the hydrophobizing properties the silane provides to HNTs. Therefore, the amount of adsorbed water in the interlayer and surface is lower compared to unmodified HNTs [31]. In addition, the overall weight loss on silanized HNTs is slightly higher than unmodified HNTs. This is due to thermal decomposition of organic compounds in GLYMO grafted to HNTs [30, 48], thus giving evidence of the efficiency of the silanization process. With regard to the caffeic acid-loaded HNTs, it can be also detected a decrease in the first weight loss step, thus indicating an increase in hydrophilic properties of HNTs. The weight loss located in the 200–400 °C range is directly related to caffeic acid degradation. Caffeic acid decomposes in two main stages as reported in literature [34]. Regarding the weight loss at about 600 °C, which represents a weight percentage of 28%, can be ascribed to removal of caffeic acid molecules chemically bonded to HNTs or located into the lumen. Therefore, TGA analysis confirms the effectiveness of both silanized and caffeic acid-modified HNTs.

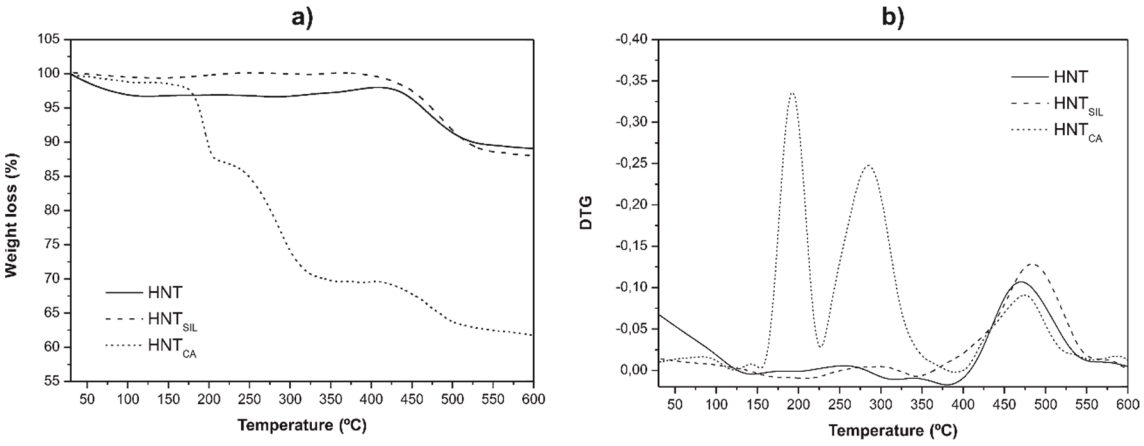

Figure IV.8.2. (a) TGA and (b) DTG of unmodified HNT, silanized HNTs with GLYMO (HNT_{SIL}) and caffeic acid-loaded HNTs (HNT_{CA}).

Figure IV.8.3 gathers FESEM images of unmodified and chemically modified HNTs. As it can be seen, HNTs tend to form aggregates due to their intrinsic hydrophilic nature due to hydroxyl groups. These aggregates can reach a size of 50 μm, and this can negatively affect the overall performance of the PHB/PCL blend. After both silane and caffeic acid

treatments, the hydrophobicity of HNTs increases in a remarkable way due to the reaction of hydroxyl groups in HNTs with GLYMO or caffeic acid which leads to formation of a thin hydrophobic layer that covers the external surface. One of the effects of hydrophobization is a remarkable decrease in the aggregate size, which is more evident in HNTs loaded with caffeic acid, Figure IV.8.3c. Table IV.8.2 contains the chemical composition of unmodified and chemically modified HNTs obtained by EDS. As it can be outlined, silane treatment gives an increase in Si content with regard to unmodified HNTs. After loading caffeic acid, the carbon content increases while both Al and Si content decrease which confirms the formation of a thin hydrophobic layer. So that, FESEM reveals the usefulness of both silane and caffeic acid treatments as the aggregate size is remarkable reduced and this has a positive effect on particle dispersion, which, in turn, will be able to improve the overall performance of the PHB/PCL blend.

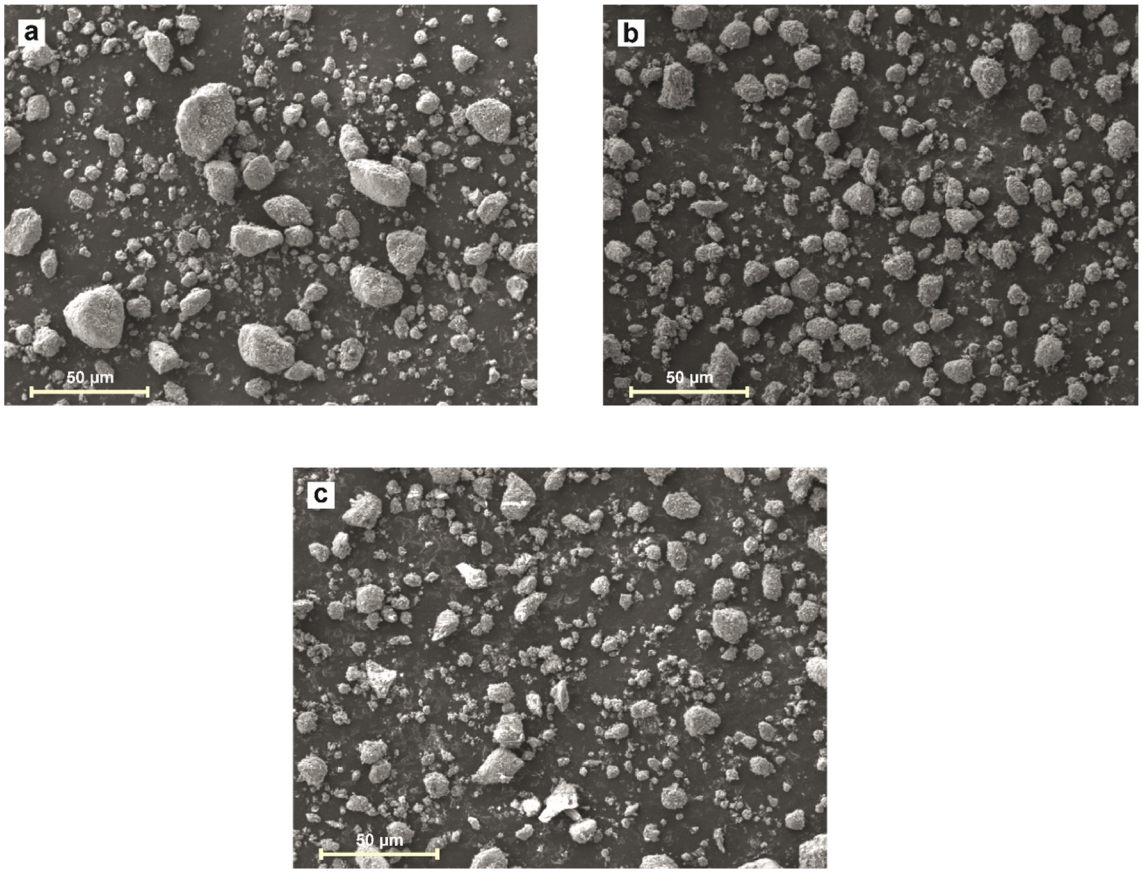

Figure IV.8.3. FESEM images of (a) unmodified HNTs, (b) HNTs modified with GLYMO silane (HNT_{SIL}) and (c) HNTs modified/loaded with caffeic acid (HNT_{CA}).

Table IV.8.2. Chemical composition of unmodified HNTs, HNTs modified with GLYMO silane (HNT_{SIL}) and HNTs modified/loaded with caffeic acid (HNT_{CA}) obtained by EDS.

Samples	Element content (wt%)			
	C	O	Al	Si
HNT	2.5 ± 0.8	50.9 ± 4.2	23.7 ± 2.1	22.9 ± 1.8
HNT_{SIL}	2.1 ± 0.2	50.9 ± 0.9	23.1 ± 0.8	23.9 ± 0.9
HNT_{CA}	6.4 ± 1.4	50.6 ± 1.3	21.6 ± 1.0	21.3 ± 1.2

The increase in hydrophobicity was also studied by dynamic contact angle measurements, which is extremely sensitive to chemical changes in the surface. Figure IV.8.4 gathers the evolution of the dynamic contact angle (distilled water) on a homogeneous HNTs base (unmodified and chemically modified). The initial contact angle value (θ_0) for unmodified HNTs is 120° but it quickly drops down to values around 0° (maximum hydrophilicity) after 15 s. This is a clear evidence of the hydrophilic nature of unmodified HNTs. After both silane and caffeic acid treatments, hydrophobicity is remarkable improved. In both cases, the water drop remains with the same contact angle with very slight changes with time. Specifically, silanized HNTs show an initial contact angle (θ_0) of 120° and drops down to a constant value of 100° that does not change with time. With regard to caffeic acid loaded HNTs the hydrophobic behavior is still more accentuated. In fact, the initial contact angle at 0 s (θ_0) is 140° and decreases to a constant value of 120°, almost invariable with time.

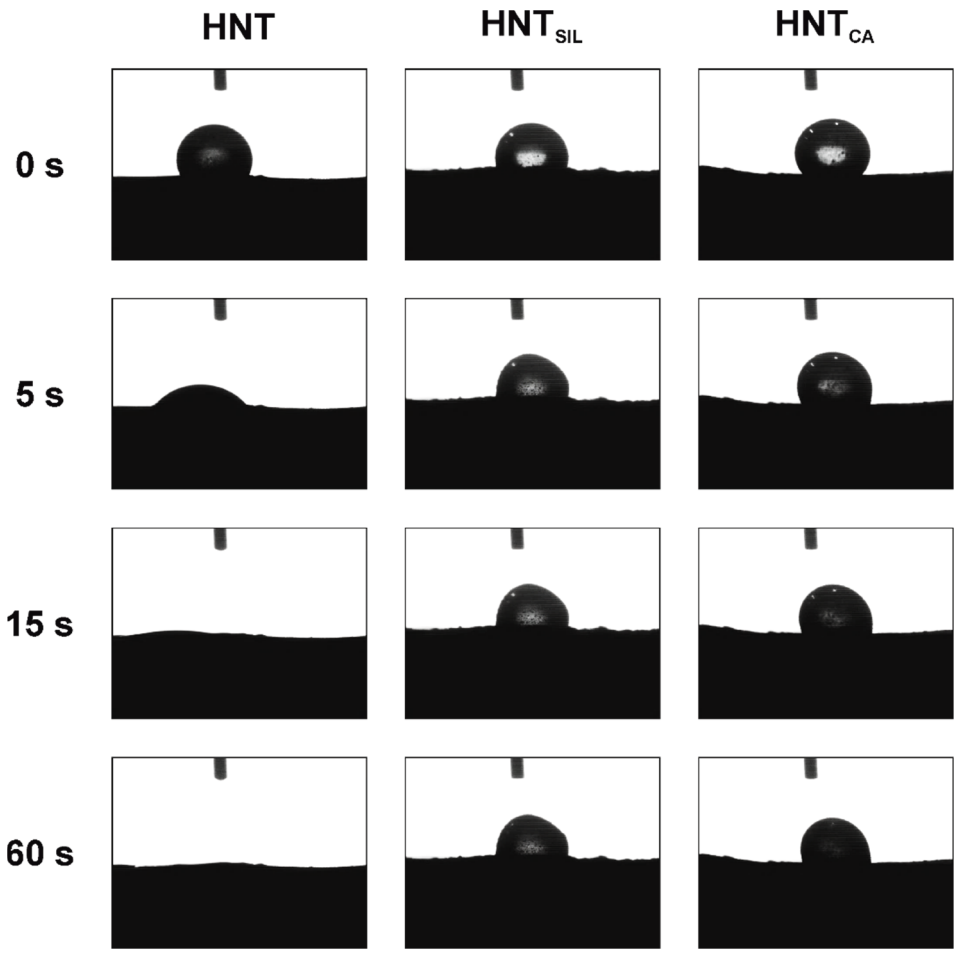

Figure IV.8.4. Dynamic contact angle of water on a homogeneous layer of unmodified HNTs, HNTs modified with GLYMO silane (HNT_{SIL}) and caffeic acid modified/loaded HNTs (HNT_{CA}).

Characterization of PHB/PCL nanocomposites with HNTs

Mechanical properties

Mechanical properties (tensile and flexural) of the PHB/PCL blend reinforced with unmodified HNTs and chemically modified HNTs can be observed in Figure IV.8.5. Unloaded blend, shows a tensile strength of 22 MPa and an elastic modulus of 1324 MPa. Regarding ductile properties, the use of reactive extrusion with 1 phr dicumyl peroxide (DCP) allows a remarkable improvement on elongation at break up to values of 21.8% which are similar to other previous results [16]. After the addition of 3 wt% HNTs the blend becomes more brittle and a decrease in tensile strength down to 17.5 MPa and a remarkable decrease in elongation at break down to 11.2%. The elastic modulus, in contrast, remains almost constant with values of about 1315 MPa. This increase in brittleness is due to the presence of HNTs aggregates in the matrix and the poor dispersion, which leads to a lack of continuity.

HNTs aggregates contribute to stress concentration with the subsequent embrittlement effect. Moreover, the highly hydrophilic nature of HNTs is not compatible with the highly hydrophobic PHB/PCL blend, which also contributes to poor particle dispersion and stress concentration phenomena. Both silane and caffeic acid treatments increase hydrophobicity with a positive effect on particle dispersion as the aggregate size decreases in a remarkable way. This also allows an increase in compatibility between PHB and PCL which, in turn, will give improved mechanical performance regarding unmodified HNTs [3]. As it can be elucidated from the observation of Figure IV.8.5a, PHB/PCL blend reinforced with 3 wt% of silanized and caffeic acid-loaded HNTs show slightly increased tensile strength values of 19.8 and 19.9 MPa respectively. In addition to an increase in mechanical resistant properties, the elongation at break is remarkably improved up to values of 15.8 and 19.5% for blends treated with silane and caffeic acid respectively. It is worthy to note the percentage increase in elongation at break that both silane and caffeic acid give to the base PHB/PCL blend which are 41 and 74% respectively. In a parallel way, the rigidity is reduced. In particular, the elastic modulus of the silanized and caffeic acid-loaded blend is 1282 and 1224 MPa respectively. In general, it is possible to say that caffeic acid gives better properties to the base PHB/PCL blend with elongation at break values near the unreinforced blend values. This is mainly due to the hydrophobicity that caffeic acid provides to HNTs which lead to smaller size aggregates and a better dispersion, all these having a positive effect on load transfer due to increased compatibility.

With regard to flexural properties, similar tendency can be observed (Figure IV.8.5b). Addition of 3 wt% unmodified HNTs leads to a decrease in the flexural strength of the PHB/PCL blend which changes from 39.3 MPa (unreinforced PHB/PCL blend) down to 32.4 MPa (PHB/PCL blend with 3 wt% unmodified HNTs). The modulus is increased from 1151 up to 1323 MPa (reinforced blend with unmodified HNTs). Silanized HNTs give better properties to the base PHB/PCL blend with an increase in both the flexural strength and modulus up to 34.8 MPa and 1338 MPa respectively. Flexural properties of PHB/PCL blends containing 3 wt% caffeic acid-loaded HNTs show similar flexural to composites with unmodified HNTs but the flexural modulus is slightly lower, around 1196 MPa which indicates less rigidity.

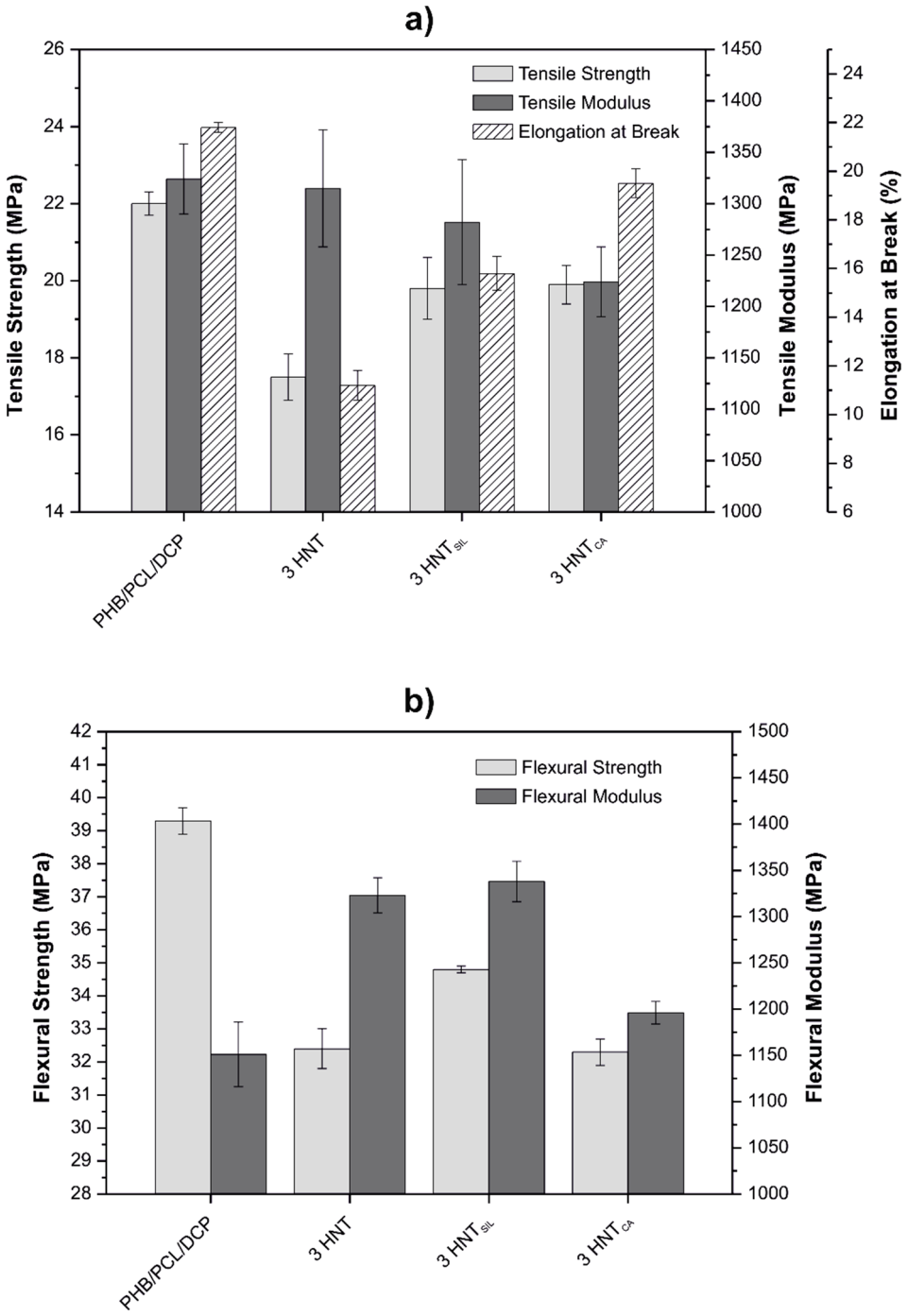

Figure IV.8.5. (a) Tensile properties and (b) flexural properties of unreinforced PHB/PCL/DCP blend and PHB/PCL/DCP blend reinforced with 3 wt% of unmodified HNTs, silanized HNTs (HNT_{SIL}) and caffeic acid-loaded HNTs (HNT_{CA}).

Thermal properties

The main thermal parameters obtained by DSC and TGA of the base PHB/PCL blend and their composites with HNTs are summarized in Table IV.8.3. As PHB and PCL are immiscible, two melt points are identified. The partially compatibilized PHB/PCL blend with

reactive extrusion with DCP, shows two clear melt peak: one located at 54.4 °C which is attributed to the PCL rich phase and another one at 170.9 °C which is assigned to the PHB-rich phase. The effect of DCP is a slight decrease in both melt peak temperatures as reported in previous work, due to a slight increase in compatibility [16]. As it can be seen in Table IV.8.3, addition of both unmodified and chemically-modified HNTs does not affect in a remarkable way to the melt peak of the PCL-rich phase; nevertheless, the melt peak temperature corresponding to the PHB-rich phase decreases in a noticeable way. Regarding unmodified HNTs, they provide a decrease in the characteristic melt peak of the PHB-rich phase of about 3 °C. This decrease is more evident for composites containing both silanized and caffeic acid-loaded HNTs with characteristic peak values of 166.2 and 164.5 °C respectively. This decrease could be related with a better particle dispersion after the above mentioned treatments. Well dispersed HNTs positively contribute to increase compatibility at the PHB/PCL interface which leads to a decrease in the peak temperature of neat PHB, and consequently, the PHB/PCL blend can be processed at lower temperatures. This feature is especially important for PHB-based blends as PHB shows poor thermal stability over its melt point. Caffeic acid-loaded HNTs lead to a decrease in the melt peak of about 6.5 °C which expands the processing window of the blends, avoiding thermal degradation of PHB. The degree of crystallinity is also influenced by the presence of HNTs as it can be observed in Table IV.8.3. The neat crystallinity of PCL is not highly affected after the addition of unmodified HNTs and is maintained at levels of 26–28% for all blends with unmodified and chemically-modified HNTs. Nevertheless, the effects of HNTs on the overall crystallinity of the PHB-rich phase are more pronounced. As it can be outlined from Table IV.8.3, the PHB/PCL blend containing 3 wt% unmodified HNTs slightly increase up to values around 50.7%. This could be due to the nucleating effect of HNTs, despite this effect is restricted [49]. Regarding PHB/PCL blends with chemically-modified HNTs, it is worthy to note a remarkable decrease in the overall crystallinity down to values of 41.0 and 42.8% for silanized and caffeic acid-loaded HNTs respectively, due to a better particle dispersion over the matrix.

The thermal stability of PHB/PCL blends at high temperatures was studied by TGA and the main thermal parameters are summarized in Table IV.8.3. These properties are the onset degradation temperature (T_0), the maximum degradation rate temperature for PCL ($T_{\max PCL}$) and the maximum degradation rate temperature for the PHB-rich phase ($T_{\max PHB}$), and were obtained from the corresponding TGA and DTG curves. All the developed materials show two main degradation steps related to PHB and PCL degradation respectively, which is also representative for poor miscibility. The unreinforced PHB/PCL blend shows a T_0 of 271.2 °C, a $T_{\max PHB}$ of 288.4 °C and a $T_{\max PCL}$ of 402.0 °C thus showing the

exceptional thermal stability of PCL compared to PHB. Incorporation of HNTs to the PHB/PCL blend does not affect in a remarkable extent to the thermal stability. Nevertheless, a slight increase (4 °C) in the onset degradation peak (T_0) can be detected after the addition of 3 wt% unmodified HNTs. This thermal stabilization effect is more pronounced by using chemically-modified HNTs reaching T_0 values of 277.8 and 276.4 °C for silanized and caffeic acid-loaded HNTs, respectively. This slight increase can be due, as suggested by Du *et al.* [50], to the fact that some volatile compounds generated in the initial degradation stages can be trapped inside the HNTs lumen thus leading to a delay in the mass transfer with the subsequent increase in the thermal stability. Moreover, the better dispersion achieved with chemically-modified HNTs results in higher randomness of lumen ends, thus leading to an increased effectiveness to trap some volatile degradation products. For this reason, PHB/PCL blend with chemically-modified HNTs show improved thermal stability, measured through the T_0 value. It is also worthy top note that caffeic acid-loaded HNTs offer a slightly lower T_0 compared to the silanized HNTs. This could be due to the fact that the lumen in caffeic acid-loaded HNTs is occupied by some caffeic acid molecules. With regard to the maximum degradation rate temperature of the PHB-rich phase ($T_{\max \mathrm{PHB}}$), changes are negligible after addition of HNTs, whatever their treatment. Nevertheless, a slight decrease in the thermal stability of the PCL-rich phase ($T_{\max \mathrm{PCL}}$) from 402 °C down to 395.3 and 395.8 °C for PHB/PCL blend with silanized and caffeic acid-loaded HNTs, respectively, can be seen. This behavior has been previously reported by Çakman *et al.* [51] and Terzopoulou *et al.* [52].

Table IV.8.3. Thermal parameters of unreinforced PHB/PCL/DCP blend and PHB/PCL/DCP blend reinforced with 3 wt% of unmodified HNTs, silanized HNTs (HNT_{SIL}) and caffeic acid-loaded HNTs (HNT_{CA}), obtained by differential scanning calorimetry (DSC) and thermogravimetric analysis (TGA).

Samples	DSC Parameters						TGA Parameters		
	$T_{m\ PCL}$ (°C)	$\Delta H_{m\ PCL}$ (J g^{-1})	$X_{c\ PCL}$ (%)	$T_{m\ PHB}$ (°C)	$\Delta H_{m\ PHB}$ (J g^{-1})	$X_{c\ PHB}$ (%)	T_0[a] (°C)	$T_{max\ PHB}$ (°C)	$T_{max\ PCL}$ (°C)
PHB/PCL/DCP	54.4	−44.7	28.5	170.9	−70.8	48.5	271.2	288.4	402.0
3-HNT	53.7	−43.6	27.8	168.1	−74.0	50.7	275.0	288.3	401.6
3-HNT_{SIL}	53.4	−40.6	25.9	166.2	−59.9	41.0	277.8	288.1	395.3
3-HNT_{CA}	53.6	−41.4	26.4	164.5	−62.5	42.8	276.4	288.4	395.8

[a] T_0, calculated at 5% mass loss.

Dynamic mechanical thermal analysis (DMTA)

The evolution of the storage modulus (G') and the damping factor (tan δ) of the PHB/PCL without and with HNTs can be seen in Figure IV.8.6. As it can be deduced, G' decreases with increasing temperature due to an increase in chain mobility with temperature. In addition, two relaxation processes can be clearly identified, which is also representative for low miscibility between PHB and PCL. As it can be seen in Figure IV.8.6a, G' increases after addition of HNTs to the PHB/PCL base blend. This difference is much pronounced in the rubbery state which is located between the glass transition temperature of both polymers (−52.6 and 9.8 °C) [15]. This increase in G' is due to HNTs since these nanoparticles provide a high level of mechanical restriction thus, reducing chain mobility and overall deformation ability, with the subsequent embrittlement. Unmodified and silanized HNTs give the highest G' values which is representative for poor interactions between HNTs and the surrounding matrix. This lack of compatibility gives poor material cohesion and leads to fracture with low deformation. With regard to caffeic acid-loaded HNTs, they contribute to lower the G' values which is a clear evidence of somewhat interactions between HNTs and the PHB/PCL blend.

The glass transition temperature (T_g) was obtained and analyzed through the peak values of the damping factor (tan δ). As it can be seen in Figure IV.8.6b, two clear peaks are observed for all samples which give evidence of immiscibility. After that addition of HNTs the T_g of the PHB-rich phase is not highly affected and is maintained at values of 9–10 °C for all samples independently of the surface treatment on HNTs. Nevertheless, the T_g of the PCL-rich phase is more affected by the presence of HNTs, especially chemically-modified HNTs. In fact, the initial T_g of the PCL-rich phase in unfilled PHB/PCL blend is −52.6 °C and it still decreased down to values of −63.0 and −62.2 °C in blends with silanized and caffeic acid-loaded HNTs respectively. This is not the expected behavior since HNTs contribute to restricted chain mobility with the subsequent increase in T_g [53]. This unexpected behavior could be related to the plasticization effect of the surfactants in HNTs [54] together with an increase in the amorphous volume fraction due to the addition of the HNTs [41].

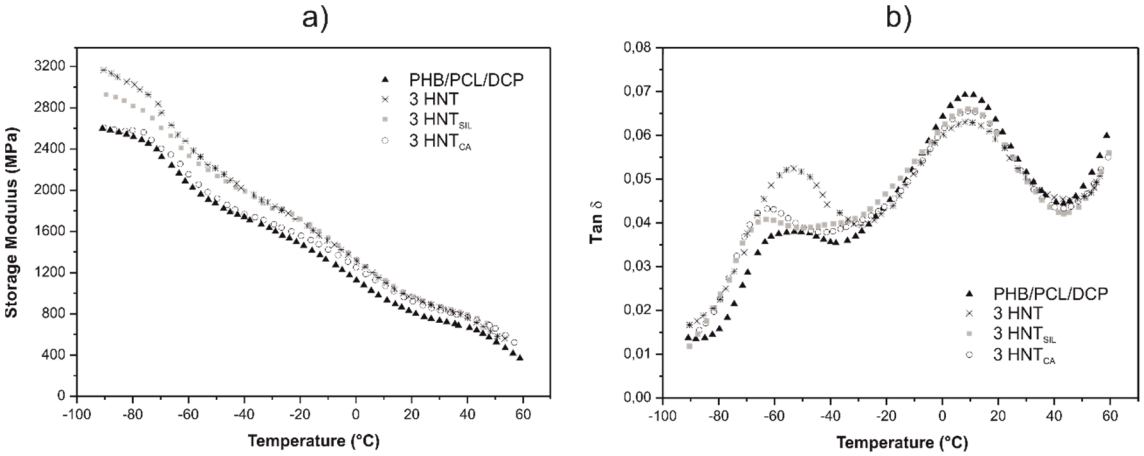

Figure IV.8.6. DMTA curves: (a) storage modulus (G') and (b) damping factor (tan δ) of unreinforced PHB/PCL/DCP blend and PHB/PCL/DCP blend reinforced with 3 wt% of unmodified HNTs, silanized HNTs (HNT_{SIL}) and caffeic acid-loaded HNTs (HNT_{CA}).

Surface morphology study

FESEM images of the fractured surfaces from impact tests of PHB/PCL blend without and with HNTs with different surface treatments are gathered in Figure IV.8.7. As it can be observed, all samples show a homogeneous fracture surface without the typical phase separation (drop-like) structure in immiscible polymer blends. It is important to remark that the base PHB/PCL formulation was obtained through reactive extrusion with DCP [16]. FESEM images also reveal presence of some HNTs in the fracture surface. The sample with 3 wt% unmodified HNTs shows lack of continuity due to presence of large size aggregates. This absence of continuity is produced by the lack of interactions between the highly hydrophilic HNTs and the highly hydrophobic surround matrix. This is reflected in FESEM images by the presence of a small gap between the HNTs aggregates and the surrounding matrix with a negative effect on overall mechanical properties as described previously. In fact, this lack of interaction is responsible for a stress concentration phenomenon which leads to reduced elongation due to poor material cohesion. This gap is not detectable for composites containing both silanized and caffeic acid-loaded HNTs due to the increase in hydrophobicity that these two treatments provide to HNTs which, in turn, positively contribute to particle dispersion and, subsequently, to improved mechanical properties. Surface treatments on HNTs do not only provide better dispersion but also small aggregate size which provide more cohesion to the material. The better dispersion of HNTs can be observed in Figure IV.8.8 which shows the elemental mapping of carbon, oxygen and silicon.

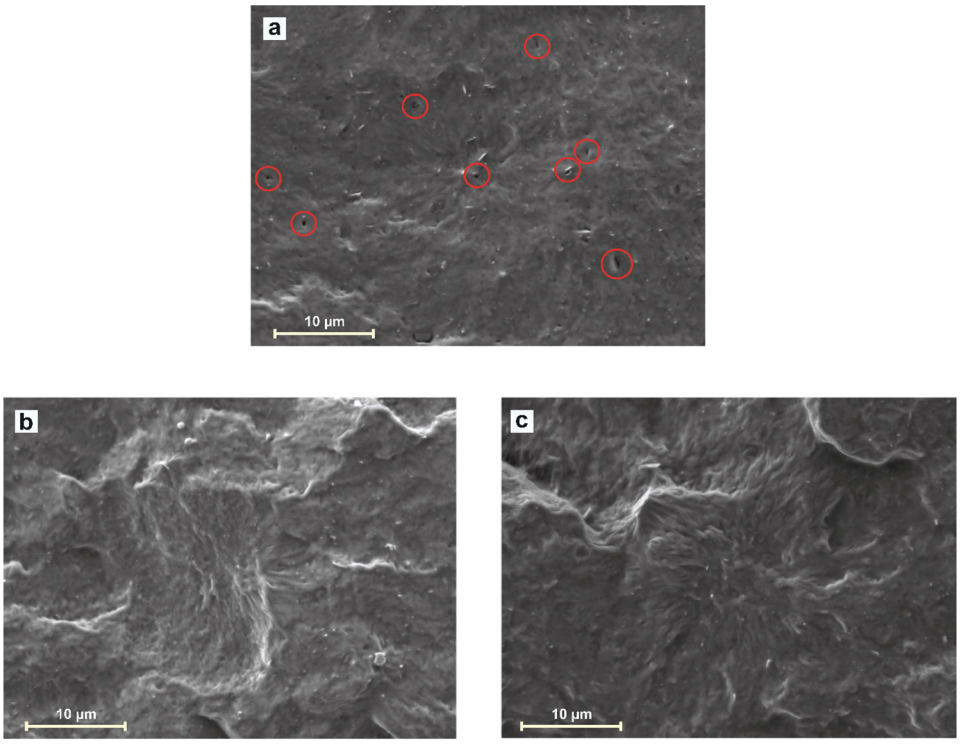

Figure IV.8.7. FESEM images of impact-fractured surfaces of PHB/PCL blend partially compatibilized by reactive extrusion with dicumyl peroxide (DCP) and 3 wt% HNTs: (a) unmodified HNTs; (b) silanized HNTs (HNT_{SIL}) and (c) caffeic acid-loaded HNTs (HNT_{CA}).

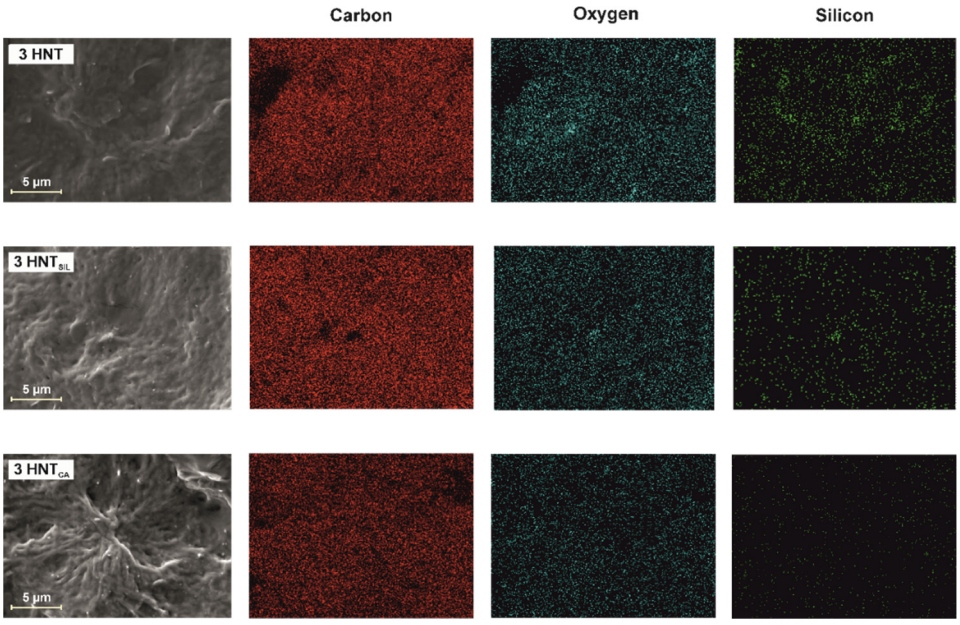

Figure IV.8.8. Elemental mapping of carbon, oxygen and silicon of impact-fractured surfaces of PHB/PCL blend partially compatibilized by reactive extrusion with dicumyl peroxide (DCP) and 3 wt% HNTs: (a) unmodified HNTs; (b) silanized HNTs (HNT_{SIL}) and (c) caffeic acid-loaded HNTs (HNT_{CA}).

CONCLUSIONS

Unmodified and chemically-modified (silanized and caffeic acid-loaded) halloysite nanotubes (HNTs) were successfully incorporated into PHB/PCL blends partially compatibilized by reactive extrusion with 1 phr dicumyl peroxide (DCP) and subsequent injection molding. Both silanization with (3-glycidyloxypropyl) trimethoxysilane and caffeic acid treatment, led to increased hydrophobicity in HNTs, which was particularly improved by the caffeic acid loading treatment. This increase in hydrophobicity had a positive effect on avoiding aggregate formation thus leading to a better particle dispersion as confirmed by FESEM-EDS. Mechanical characterization showed a remarkable increase in both mechanical resistant properties (tensile strength) and ductile properties (elongation at break) by using chemically-modified HNTs compared to unmodified HNTs. These results suggest the silanized and caffeic acid-loaded HNTs contribute to improve interactions with the polymer matrix since the high hydrophilic nature of unmodified HNTs does not allow good particle dispersion. In addition, it is worthy to note that PHB-based materials are high sensitive to thermal degradation as PHB degrades quickly over its melt point. Both chemically-modified HNTs lead to a decrease in the melt peak temperature of the PHB-rich phase (of about 5–6 °C) together with a delay of 5–6 °C in the onset degradation temperature. Therefore, the processing window is extended by 10 °C to 12 °C which is an important issue for PHB-based materials. As an overall conclusion, it is worthy to note the interesting properties that caffeic acid-loaded HNTs can give to PHB/PCL blend in terms of mechanical properties and thermal behavior.

ACKNOWLEDGEMENTS

This work was supported by the Ministry of Economy and Competitiveness (MINECO) [MAT2017-84909-C2-2-R]. D. Garcia-Garcia wants to thank the Spanish Ministry of Education, Culture and Sports for the financial support through a FPU grant [FPU13/06011].

REFERENCES

[1] Zhang M and Thomas NL. *Preparation and properties of polyhydroxybutyrate blended with different types of starch*. Journal of Applied Polymer Science, 2010. **116**(2):688-694.

[2] Godbole S, Gote S, Latkar M and Chakrabarti T. *Preparation and characterization of biodegradable poly-3-hydroxybutyrate–starch blend films*. Bioresource Technology, 2003. **86**(1):33-37.

[3] Garcia-Garcia D, Carbonell-Verdu A, Jordá-Vilaplana A, Balart R and Garcia-Sanoguera D. *Development and characterization of green composites from bio-based polyethylene and peanut shell*. Journal of Applied Polymer Science, 2016. **133**(37):43940.

[4] Choi JS and Park WH. *Effect of biodegradable plasticizers on thermal and mechanical properties of poly (3-hydroxybutyrate)*. Polymer Testing, 2004. **23**(4):455-460.

[5] Garcia-Garcia D, Fenollar O, Fombuena V, Lopez-Martinez J and Balart R. *Improvement of mechanical ductile properties of poly(3-hydroxybutyrate) by using vegetable oil derivatives*. Macromolecular Materials and Engineering, 2017. **302**(2):1600330.

[6] Zhang M and Thomas NL. *Blending polylactic acid with polyhydroxybutyrate: The effect on thermal, mechanical, and biodegradation properties*. Advances in Polymer Technology, 2011. **30**(2):67-79.

[7] Ma P, Hristova-Bogaerds DG, Lemstra PJ, Zhang Y and Wang S. *Toughening of PHBV/PBS and PHB/PBS blends via in situ compatibilization using dicumyl peroxide as a free-radical grafting initiator*. Macromolecular Materials and Engineering, 2012. **297**(5):402-410.

[8] Gassner F and Owen AJ. *Physical properties of poly(β-hydroxybutyrate)-poly(ε-caprolactone) blends*. Polymer, 1994. **35**(10):2233-2236.

[9] Lovera D, Márquez L, Balsamo V, Taddei A, Castelli C and Müller AJ. *Crystallization, morphology, and enzymatic degradation of polyhydroxybutyrate/polycaprolactone (PHB/PCL) blends*. Macromolecular Chemistry and Physics, 2007. **208**(9):924-937.

[10] Azuma Y, Yoshie N, Sakurai M, Inoue Y and Chûjô R. *Thermal behaviour and miscibility of poly(3-hydroxybutyrate)/poly(vinyl alcohol) blends*. Polymer, 1992. **33**(22):4763-4767.

[11] Olkhov AA, Vlasov SV, Iordanskii AL, Zaikov GE and Lobo VMM. *Water transport, structure features and mechanical behavior of biodegradable PHB/PVA blends*. Journal of Applied Polymer Science, 2003. **90**(6):1471-1476.

[12] Iulianelli GCV, David GS, dos Santos TN, Sebastião PJO and Tavares MIB. *Influence of TiO_2 nanoparticle on the thermal, morphological and molecular characteristics of PHB matrix.* Polymer Testing, 2018. **65**:156-162.

[13] Díez-Pascual AM and Díez-Vicente AL. *Poly(3-hydroxybutyrate)/ZnO bionanocomposites with improved mechanical, barrier and antibacterial properties*. International Journal of Molecular Sciences, 2014. **15**(6):10950-10973.

[14] Patrício PSO, Pereira FV, dos Santos MC, de Souza PP, Roa JPB and Orefice RL. *Increasing the elongation at break of polyhydroxybutyrate biopolymer: Effect of cellulose nanowhiskers on mechanical and thermal properties*. Journal of Applied Polymer Science, 2013. **127**(5):3613-3621.

[15] Garcia-Garcia D, Ferri JM, Boronat T, Lopez-Martinez J and Balart R. *Processing and characterization of binary poly (hydroxybutyrate) (PHB) and poly (caprolactone) (PCL) blends with improved impact properties*. Polymer Bulletin, 2016. **73**(12):3333-3350.

[16] Garcia-Garcia D, Rayón E, Carbonell-Verdu A, Lopez-Martinez J and Balart R. *Improvement of the compatibility between poly(3-hydroxybutyrate) and poly(ε-caprolactone) by reactive extrusion with dicumyl peroxide*. European Polymer Journal, 2017. **86**:41-57.

[17] Taguet A, Cassagnau P and Lopez-Cuesta JM. *Structuration, selective dispersion and compatibilizing effect of (nano)fillers in polymer blends*. Progress in Polymer Science, 2014. **39**(8):1526-1563.

[18] Wu D, Lin D, Zhang J, Zhou W, Zhang M, Zhang Y, Wang D and Lin B. *Selective localization of nanofillers: Effect on morphology and crystallization of PLA/PCL blends*. Macromolecular Chemistry and Physics, 2011. **212**(6):613-626.

[19] Hemmati F, Garmabi H and Modarress H. *Effects of organoclay on the compatibility and interfacial phenomena of PE/EVA blends with UCST phase behavior*. Polymer Composites, 2014. **35**(12):2329-2342.

[20] Chen RS, Ahmad S, Gan S, Ghani MHA and Salleh MN. *Effects of compatibilizer, compounding method, extrusion parameters, and nanofiller loading in clay-reinforced recycled HDPE/PET nanocomposites*. Journal of Applied Polymer Science, 2015. **132**(29):42287.

[21] Mofokeng JP and Luyt AS. *Dynamic mechanical properties of PLA/PHBV, PLA/PCL, PHBV/PCL blends and their nanocomposites with TiO_2 as nanofiller*. Thermochimica Acta, 2015. **613**:41-53.

[22] Vrsaljko D, Macut D and Kovačević V. *Potential role of nanofillers as compatibilizers in immiscible PLA/LDPE blends*. Journal of Applied Polymer Science, 2015. **132**(6):41414.

[23] Urquijo J, Aranburu N, Dagréou S, Guerrica-Echevarría G and Eguiazábal JI. *CNT-induced morphology and its effect on properties in PLA/PBAT-based nanocomposites*. European Polymer Journal, 2017. **93**:545-555.

[24] Lvov YM, Shchukin DG, Möhwald H and Price RR. *Halloysite clay nanotubes for controlled release of protective agents*. ACS Nano, 2008. **2**(5):814-820.

[25] Yuan P, Southon PD, Liu Z, Green MER, Hook JM, Antill SJ and Kepert CJ. *Functionalization of halloysite clay nanotubes by grafting with γ-aminopropyltriethoxysilane*. The Journal of Physical Chemistry C, 2008. **112**(40):15742-15751.

[26] Jafarzadeh S, Haddadi-Asl V and Roghani-Mamaqani H. *Nanofibers of poly(hydroxyethyl methacrylate)-grafted halloysite nanotubes and polycaprolactone by combination of RAFT polymerization and electrospinning*. Journal of Polymer Research, 2015. **22**(7):123.

[27] Torres E, Fombuena V, Vallés-Lluch A and Ellingham T. *Improvement of mechanical and biological properties of polycaprolactone loaded with hydroxyapatite and halloysite nanotubes*. Materials Science and Engineering: C, 2017. **75**:418-424.

[28] Kurczewska J, Cegłowski M, Messyasz B and Schroeder G. *Dendrimer-functionalized halloysite nanotubes for effective drug delivery*. Applied Clay Science, 2018. **153**:134-143.

[29] Pal P, Kundu MK, Malas A and Das CK. *Compatibilizing effect of halloysite nanotubes in polar-nonpolar hybrid system*. Journal of Applied Polymer Science, 2014. **131**(1):39587.

[30] Krishnaiah P, Ratnam CT and Manickam S. *Development of silane grafted halloysite nanotube reinforced polylactide nanocomposites for the enhancement of mechanical, thermal and dynamic-mechanical properties*. Applied Clay Science, 2017. **135**:583-595.

[31] Carli LN, Daitx TS, Soares GV, Crespo JS and Mauler RS. *The effects of silane coupling agents on the properties of PHBV/halloysite nanocomposites*. Applied Clay Science, 2014. **87**:311-319.

[32] Raman VS, Rooj S, Das A, Stöckelhuber KW, Simon F, Nando GB and Heinrich G. *Reinforcement of solution styrene butadiene rubber by silane functionalized halloysite nanotubes*. Journal of Macromolecular Science, Part A, 2013. **50**(11):1091-1106.

[33] Liu M, Guo B, Du M, Lei Y and Jia D. *Natural inorganic nanotubes reinforced epoxy resin nanocomposites*. Journal of Polymer Research, 2008. **15**(3):205-212.

[34] Baykal A, Amir MD, Günerb S and Sözeri H. *Preparation and characterization of SPION functionalized via caffeic acid*. Journal of Magnetism and Magnetic Materials, 2015. **395**:199-204.

[35] Garcia-Garcia D, Ferri JM, Ripoll L, Hidalgo M, Lopez-Martinez J and Balart R. *Characterization of selectively etched halloysite nanotubes by acid treatment*. Applied Surface Science, 2017. **422**:616-625.

[36] Hendessi S, Sevinis EB, Unal S, Cebeci FC, Menceloglu YZ and Unal H. *Antibacterial sustained-release coatings from halloysite nanotubes/waterborne polyurethanes*. Progress in Organic Coatings, 2016. **101**:253-261.

[37] Kurusu RS, Demarquette NR, Gauthier C and Chenal JM. *Effect of ageing and annealing on the mechanical behaviour and biodegradability of a poly(3-hydroxybutyrate) and poly(ethylene-co-methyl-acrylate-co-glycidyl-methacrylate) blend*. Polymer International, 2014. **63**(6):1085-1093.

[38] Arrieta MP, Samper MD, López J and Jiménez A. *Combined effect of poly(hydroxybutyrate) and plasticizers on polylactic acid properties for film intended for food packaging*. Journal of Polymers and the Environment, 2014. **22**(4):460-470.

[39] Simões CL, Viana JC and Cunha AM. *Mechanical properties of poly(ε-caprolactone) and poly (lactic acid) blends*. Journal of Applied Polymer Science, 2009. **112**(1):345-352.

[40] Wang Q, Zhang J and Wang A. *Alkali activation of halloysite for adsorption and release of ofloxacin*. Applied Surface Science, 2013. **287**:54-61.

[41] Pasbakhsh P, Ismail H, Fauzi MNA and Bakar AA. *EPDM/modified halloysite nanocomposites*. Applied Clay Science, 2010. **48**(3):405-413.

[42] Sun P, Liu G, Lv D, Dong X, Wu J and Wang D. *Effective activation of halloysite nanotubes by piranha solution for amine modification via silane coupling chemistry*. RSC Advances, 2015. **5**(65):52916-52925.

[43] Hillier S, Brydson R, Delbos E, Fraser T, Gray N, Pendlowski H, Phillips I, Robertson J and Wilson I. *Correlations among the mineralogical and physical properties of halloysite nanotubes (HNTs)*. Clay Minerals, 2016. **51**(3):325-350.

[44] Erdogan AR, Kaygusuz I and Kaynak C. *Influences of aminosilanization of halloysite nanotubes on the mechanical properties of polyamide-6 nanocomposites*. Polymer Composites, 2014. **35**(7):1350-1361.

[45] Sun P, Liu G, Lv D, Dong X, Wu J and Wang D. *Simultaneous improvement in strength, toughness, and thermal stability of epoxy/halloysite nanotubes composites by interfacial modification*. Journal of Applied Polymer Science, 2016. **133**(13):43249.

[46] Chow WS and Neoh SS. *Dynamic mechanical, thermal, and morphological properties of silane-treated montmorillonite reinforced polycarbonate nanocomposites*. Journal of Applied Polymer Science, 2009. **114**(6):3967-3975.

[47] Williams PAM, Baró ACG and Ferrer EG. *Study of the interaction of oxovanadium (IV) with a plant component (caffeic acid). Synthesis and characterization of a solid compound*. Polyhedron, 2002. **21**(20):1979-1984.

[48] Bischoff E, Daitx T, Simon D, Schrekker HS, Liberman SA and Mauler RS. *Organosilane-functionalized halloysite for high performance halloysite/heterophasic ethylene-propylene copolymer nanocomposites*. Applied Clay Science, 2015. **112**:68-74.

[49] Carli LN, Crespo JS and Mauler RS. *PHBV nanocomposites based on organomodified montmorillonite and halloysite: The effect of clay type on the morphology and thermal and mechanical properties*. Composites Part A: Applied Science and Manufacturing, 2011. **42**(11):1601-1608.

[50] Du M, Guo B and Jia D. *Thermal stability and flame retardant effects of halloysite nanotubes on poly(propylene)*. European Polymer Journal, 2006. **42**(6):1362-1369.

[51] Çakman G and Dilsiz N. *Preparation and physical, thermal properties of polycaprolactone/m-halloysite nanocomposite*. Journal of Multidisciplinary Engineering Science Studies, 2016. **2**(9):842-848.

[52] Terzopoulou Z, Papageorgiou DG, Papageorgiou GZ and Bikiaris DN. *Effect of surface functionalization of halloysite nanotubes on synthesis and thermal properties of poly(ε-caprolactone)*. Journal of Materials Science, 2018. **53**(9): 6519–6541.

[53] Liu M, Zhang Y and Zhou C. *Nanocomposites of halloysite and polylactide*. Applied Clay Science, 2013. **75**:52-59.

[54] Zhao H, Cui Z, Wang X, Turng LS and Peng X. *Processing and characterization of solid and microcellular poly(lactic acid)/polyhydroxybutyrate-valerate (PLA/PHBV) blends and PLA/PHBV/Clay nanocomposites*. Composites Part B: Engineering, 2013. **51**:79-91.

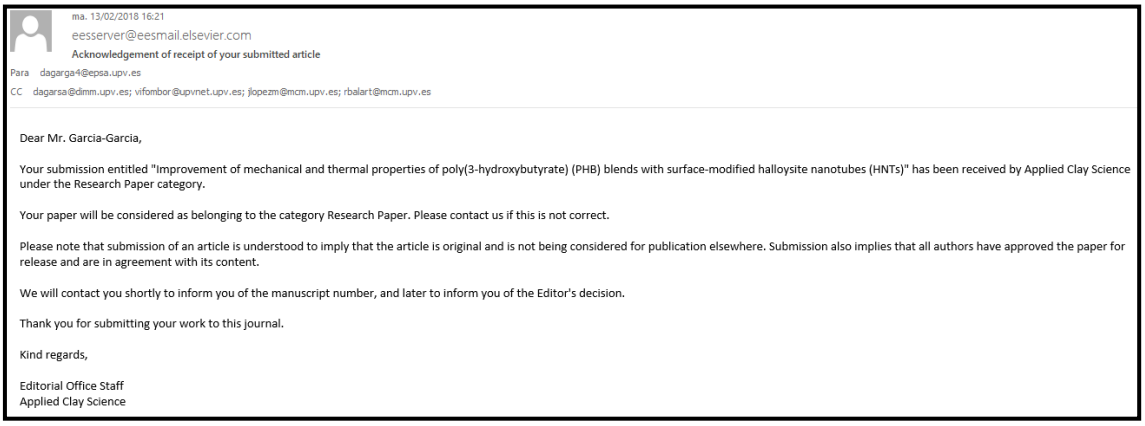

ma. 13/02/2018 16:21
eesserver@eesmail.elsevier.com
Acknowledgement of receipt of your submitted article
Para dagarga4@epsa.upv.es
CC dagarsa@dimm.upv.es; vifombor@upvnet.upv.es; jlopezm@mcm.upv.es; rbalart@mcm.upv.es

Dear Mr. Garcia-Garcia,

Your submission entitled "Improvement of mechanical and thermal properties of poly(3-hydroxybutyrate) (PHB) blends with surface-modified halloysite nanotubes (HNTs)" has been received by Applied Clay Science under the Research Paper category.

Your paper will be considered as belonging to the category Research Paper. Please contact us if this is not correct.

Please note that submission of an article is understood to imply that the article is original and is not being considered for publication elsewhere. Submission also implies that all authors have approved the paper for release and are in agreement with its content.

We will contact you shortly to inform you of the manuscript number, and later to inform you of the Editor's decision.

Thank you for submitting your work to this journal.

Kind regards,

Editorial Office Staff
Applied Clay Science

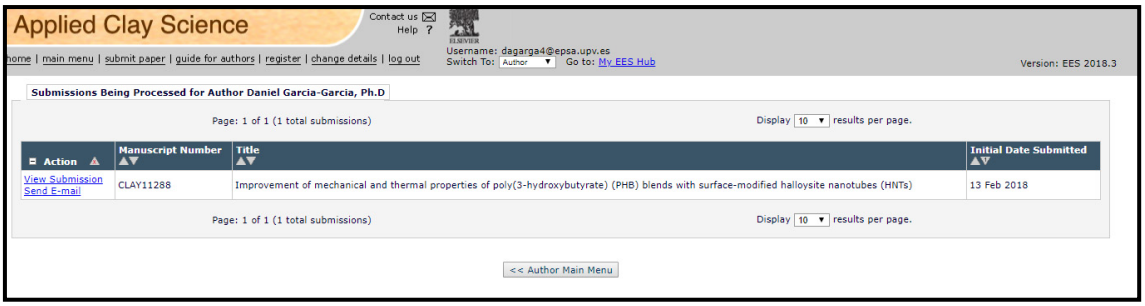

Applied Clay Science
Contact us
Help ?
home | main menu | submit paper | guide for authors | register | change details | log out
Username: dagarga4@epsa.upv.es
Switch To: Author Go to: My EES Hub
Version: EES 2018.3

Submissions Being Processed for Author Daniel Garcia-Garcia, Ph.D

Page: 1 of 1 (1 total submissions) Display 10 results per page.

Action	Manuscript Number	Title	Initial Date Submitted
View Submission Send E-mail	CLAY11288	Improvement of mechanical and thermal properties of poly(3-hydroxybutyrate) (PHB) blends with surface-modified halloysite nanotubes (HNTs)	13 Feb 2018

Page: 1 of 1 (1 total submissions) Display 10 results per page.

<< Author Main Menu

V. CONCLUSIONES

V.1. CONCLUSIONES PARCIALES

Tras el análisis de los resultados obtenidos y de acuerdo con los objetivos específicos planteados, las principales conclusiones de cada uno de los bloques en los que se ha dividido la presente tesis doctoral se resumen a continuación:

Plastificación

Los resultados obtenidos en este bloque evidencian, de forma global, la efectividad de los derivados de aceites vegetales como agentes plastificantes para el PHB.

De todos los derivados de aceites vegetales estudiados, se observó cómo el aceite de soja epoxidado (ESBO) fue el único que no demostró eficacia como plastificante del biopolímero, empeorando sus propiedades mecánicas.

El aceite de linaza epoxidado (ELO), el aceite de linaza maleinizado (MLO) y los ésteres de ácidos grasos epoxidados (EFAE) mejoraron las propiedades mecánicas dúctiles del PHB, incrementando su alargamiento a la rotura y su absorción de energía a impacto, y redujeron sus propiedades mecánicas resistentes, como la resistencia a tracción y el módulo elástico, obteniéndose formulaciones con una menor rigidez y fragilidad que el PHB puro. Esta mejora de la ductilidad del PHB se consiguió con la incorporación de pequeñas cantidades de plastificante, entre 5 y 10 phr.

La estabilidad térmica del PHB mejoró notablemente tras la incorporación de los derivados de aceites vegetales, observándose una reducción de su temperatura de fusión y un significativo aumento de su temperatura de inicio de degradación. Todo ello reduce el riesgo de degradación térmica del PHB y aumenta de forma considerable su ventana de procesado.

El análisis de los resultados demostró que el mejor equilibrio entre propiedades térmicas y mecánicas del PHB se obtiene tras la incorporación de 5 phr de EFAE, con el que se consiguió un incremento del 40 y del 109% del alargamiento a la rotura y de la absorción de energía a impacto con respecto al PHB puro respectivamente, así como un aumento de la ventana de procesado superior a 29 °C.

De forma general, los resultados obtenidos demostraron cómo la incorporación de pequeñas cantidades de derivados aceites vegetales permite reducir la fragilidad intrínseca y mejorar la estabilidad térmica del PHB, sin afectar a su biodegradabilidad, y todo ello de una forma eficiente, simple y económica.

Mezcla física en fundido o "*Blending*"

Los resultados obtenidos tras la incorporación de diferentes cantidades de PCL al PHB evidencian su efecto como modificador de la tenacidad, proporcionando una menor rigidez y una mayor ductilidad en las formulaciones obtenidas con respecto al PHB puro.

De las composiciones estudiadas, la más interesante para el desarrollo de la presente tesis fue la mezcla con un contenido del 25% en peso de PCL, con la cual se obtuvo un ligero aumento del alargamiento a la rotura y de la absorción de energía a impacto con respecto al PHB puro. Sin embargo, los cambios producidos en las propiedades mecánicas tras la incorporación de dicha cantidad de PCL al PHB no fueron significativos debido a la inmiscibilidad existente entre ambos polímeros.

La incorporación de un 25% en peso de PCL al PHB mejoró notablemente la temperatura de inicio de degradación del PHB puro, ampliándose así la ventana de procesado.

Mediante extrusión reactiva de la mezcla de PHB/PCL con peróxido de dicumilo (DCP) se obtuvo una mejora considerable de la compatibilidad entre ambos polímeros, lo cual quedó demostrado mediante FESEM y AFM.

El aumento de la compatibilidad entre ambos polímeros tras la extrusión reactiva mejoró notablemente las propiedades dúctiles de la mezcla, sin afectar de forma significativa a las propiedades resistentes y a la estabilidad térmica alcanzada en la mezcla sin compatibilizar.

En este caso, las mejores propiedades mecánicas se obtuvieron tras la incorporación de un 1 phr de DCP en el proceso de extrusión reactiva, incrementándose el alargamiento a la rotura y la absorción de energía a impacto en un 91 y un 231% respectivamente con respecto a la mezcla sin compatibilizar. Además, en dicha formulación también se observó un notable descenso de la cristalinidad.

Por tanto, la mezcla física de PHB con PCL compatibilizada con DCP permite la obtención de formulaciones con mayor ductilidad, mejor estabilidad térmica y menor coste que el PHB puro.

Incorporación de nanopartículas

Nanocristales de celulosa

Los resultados obtenidos en este bloque evidencian la viabilidad de las piñas de pino como materia prima para la extracción de nanocristales de celulosa (CNCs).

Se observó cómo el tiempo de hidrólisis influye de forma considerable en las propiedades físico-químicas y en el rendimiento de CNCs obtenidos. En este caso, los mejores resultados en cuanto a rendimiento, contenido de celulosa, relación de aspecto, cristalinidad y comportamiento térmico de los CNCs se obtuvieron con un tiempo de hidrólisis de 45 minutos.

Tras la incorporación de diferentes cantidades de CNCs en la mezcla de PHB/PCL se observó cómo la mejor dispersión de los mismos en la matriz se logró con un contenido del 3% en peso, observándose para dicha formulación una mejora de la adhesión interfacial entre ambos polímeros, que dio lugar a un aumento de la transparencia de los films, sin afectar significativamente a las propiedades mecánicas de la mezcla.

La presencia de CNCs en la mezcla de PHB/PCL disminuyó ligeramente su estabilidad térmica, debido a la baja estabilidad térmica de los CNCs, y aumentó su humectabilidad, debido al elevado carácter hidrofílico de los mismos.

Tras el estudio de degradación en compost, se observó cómo la presencia de CNCs en el film de PHB/PCL aumenta notablemente su velocidad de degradación, debido principalmente a la mayor hidrofilidad y al menor grado de cristalinidad obtenido en el film tras la incorporación de los CNCs.

Nanotubos de haloisita

Los resultados obtenidos tras el tratamiento de los nanotubos de haloisita (HNTs) con diferentes ácidos mostraron cómo el ácido acético fue el que dio lugar a un mayor aumento en las dimensiones del lumen de los HNTs sin afectar a su estabilidad estructural, permitiendo de esta forma mejorar significativamente su capacidad de almacenamiento de sustancias para su posterior liberación controlada.

Tras los tratamientos hidrofóbicos realizados a los HNTs, se observó que la mayor hidrofobicidad superficial se consiguió tras su tratamiento con ácido cafeico. Esta mayor hidrofobicidad de los HNTs dio lugar a un menor tamaño de los agregados.

Tras la incorporación de los HNTs sin tratar y tratados a la mezcla de PHB/PCL compatibilizada con DCP se observó que la formulación reforzada con HNTs tratados con

ácido cafeico presentaba una mejor dispersión del refuerzo en la matriz. Esta buena dispersión, unida al elevado carácter hidrofóbico alcanzado tras el tratamiento, mejoró la compatibilidad entre el refuerzo y la matriz, lo cual se vio reflejado en una mejora de la resistencia a tracción y del alargamiento a la rotura con respecto a las formulaciones reforzadas con HNTs sin tratar y con HNTs tratados con silano. Además, el alargamiento a la rotura obtenido en dicha formulación fue similar al de la mezcla de PHB/PCL compatibilizada con DCP sin reforzar.

Las propiedades térmicas de la mezcla de PHB/PCL compatibilizada se vieron afectadas por la presencia de HNTs, observándose una disminución de la temperatura de fusión y un aumento de la temperatura de inicio de degradación, lo cual aumenta la ventana de procesado de las formulaciones y reduce el riesgo de degradación térmica del PHB.

Por tanto, la incorporación de nanocargas en la mezcla física de PHB/PCL se consolida como alternativa eficaz para la modificación de propiedades con el fin de adaptar la formulación a diferentes aplicaciones como por ejemplo el envasado de alimentos.

V.2. CONCLUSIÓN GENERAL

Como conclusión general del presente trabajo, se puede indicar que la plastificación del PHB con derivados de aceites vegetales, la mezcla física con poli(ε-caprolactona) compatibilizada mediante extrusión reactiva con peróxido de dicumilo y la incorporación de nanocargas, como nanocristales de celulosa y nanotubos de haloisita, dan lugar a formulaciones totalmente biodegradables con propiedades mejoradas y con un menor coste que el PHB puro. Esto permite que las formulaciones basadas en PHB obtenidas mediante los sistemas de modificación empleados en la presente tesis resulten más competitivas a nivel industrial que el polímero puro, facilitando su incorporación en sectores como el del envase y embalaje o el sector médico.

VI. APÉNDICES

ÍNDICE DE FIGURAS

ÍNDICE DE TABLAS